Effect of Concrete Properties and Prestressing Steel Reinforcement Type on the Development Length in Pretensioned Concrete Railroad ties

KSU-21-4

March 2021

Dr. Amir F. Momeni, Civil Engineering, KSU
Dr. Robert J. Peterman, Civil Engineering, KSU
Dr. B. Terry Beck, Mechanical & Nuclear Engineering, KSU
Dr. Chih-Hang Wu, Industrial & Manufacturing Systems Engineering, KSU

Abstract

A study was conducted to determine the effect of different concrete properties and prestressing steel reinforcement type on the development length and flexural capacity of prestressed concrete railroad ties. Thirteen different 5.32-mm-diameter prestressing wires and six different strands (four 7-wire strands and two 3-wire strands) were used to fabricate 4-tendon pretensioned prisms with a square cross section. A consistent concrete mixture utilizing Type III cement and a water-to-cementitious ratio of 0.32 was used for all prisms. The prisms were detensioned at concrete compressive strengths of 3500 psi, 4500 psi, and 6000 psi. Load tests revealed that there is a large difference in the development length for different wire/strand types as well as with different concrete release strengths. Additionally, cyclic load tests revealed that there is also a significant difference in the bond performance of these reinforcement types under repeated loadings.

Corresponding Author: Dr. Robert J. Peterman (bob@ksu.edu)

U.S. Department of Transportation
Federal Railroad Administration

The contents of this report reflect the views of the authors, who are responsible for the facts and accuracy of the information presented herein. This document is disseminated in the interest of information exchange. The report is funded, partially or entirely, by a grant from the U.S. Department of Transportation's University Transportation Centers Program. However, the U.S. Government assumes no liability for the contents or use thereof.

METRIC/ENGLISH CONVERSION FACTORS

ENGLISH TO METRIC

LENGTH (APPROXIMATE)

1 inch (in)	=	2.5 centimeters (cm)
1 foot (ft)	=	30 centimeters (cm)
1 yard (yd)	=	0.9 meter (m)
1 mile (mi)	=	1.6 kilometers (km)

AREA (APPROXIMATE)

1 square inch (sq in, in^2)	=	6.5 square centimeters (cm^2)
1 square foot (sq ft, ft^2)	=	0.09 square meter (m^2)
1 square yard (sq yd, yd^2)	=	0.8 square meter (m^2)
1 square mile (sq mi, mi^2)	=	2.6 square kilometers (km^2)
1 acre = 0.4 hectare (he)	=	4,000 square meters (m^2)

MASS - WEIGHT (APPROXIMATE)

1 ounce (oz)	=	28 grams (gm)
1 pound (lb)	=	0.45 kilogram (kg)
1 short ton = 2,000 pounds (lb)	=	0.9 tonne (t)

VOLUME (APPROXIMATE)

1 teaspoon (tsp)	=	5 milliliters (ml)
1 tablespoon (tbsp)	=	15 milliliters (ml)
1 fluid ounce (fl oz)	=	30 milliliters (ml)
1 cup (c)	=	0.24 liter (l)
1 pint (pt)	=	0.47 liter (l)
1 quart (qt)	=	0.96 liter (l)
1 gallon (gal)	=	3.8 liters (l)
1 cubic foot (cu ft, ft^3)	=	0.03 cubic meter (m^3)
1 cubic yard (cu yd, yd^3)	=	0.76 cubic meter (m^3)

TEMPERATURE (EXACT)

[(x-32)(5/9)] °F = y °C

METRIC TO ENGLISH

LENGTH (APPROXIMATE)

1 millimeter (mm)	=	0.04 inch (in)
1 centimeter (cm)	=	0.4 inch (in)
1 meter (m)	=	3.3 feet (ft)
1 meter (m)	=	1.1 yards (yd)
1 kilometer (km)	=	0.6 mile (mi)

AREA (APPROXIMATE)

1 square centimeter (cm^2)	=	0.16 square inch (sq in, in^2)
1 square meter (m^2)	=	1.2 square yards (sq yd, yd^2)
1 square kilometer (km^2)	=	0.4 square mile (sq mi, mi^2)
10,000 square meters (m^2)	=	1 hectare (ha) = 2.5 acres

MASS - WEIGHT (APPROXIMATE)

1 gram (gm)	=	0.036 ounce (oz)
1 kilogram (kg)	=	2.2 pounds (lb)
1 tonne (t)	=	1,000 kilograms (kg)
	=	1.1 short tons

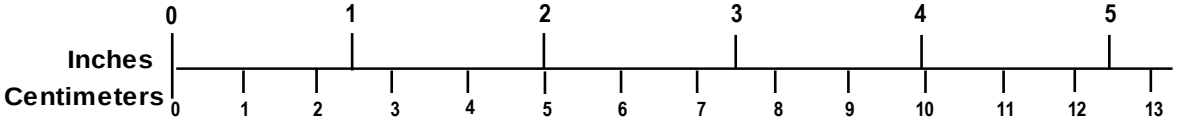
VOLUME (APPROXIMATE)

1 milliliter (ml)	=	0.03 fluid ounce (fl oz)
1 liter (l)	=	2.1 pints (pt)
1 liter (l)	=	1.06 quarts (qt)
1 liter (l)	=	0.26 gallon (gal)
1 cubic meter (m^3)	=	36 cubic feet (cu ft, ft^3)
1 cubic meter (m^3)	=	1.3 cubic yards (cu yd, yd^3)

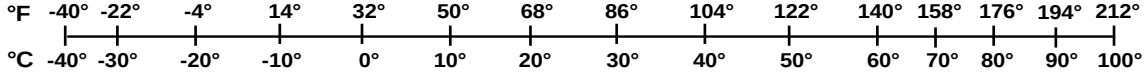
TEMPERATURE (EXACT)

[(9/5) y + 32] °C = x °F

QUICK INCH - CENTIMETER LENGTH CONVERSION



QUICK FAHRENHEIT - CELSIUS TEMPERATURE CONVERSION



For more exact and or other conversion factors, see NIST Miscellaneous Publication 286, Units of Weights and Measures. Price $2.50 SD Catalog No. C13 10286

Updated 6/17/98

Acknowledgements

The authors would like to thank the Federal Railroad Administration (FRA) for providing the majority of funding that made this research possible. Additionally, LB Foster/CXT Concrete Ties donated extensive resources, including all of the reinforcements, to help make the project a success. The researcher would also like to thank Drs. Hailing Yu and David Jeong at the John A. Volpe National Transportation Systems Center for their valuable suggestions and parallel analysis work. Finally, the authors wish to thank the Precast/Prestressed Concrete Institute (PCI) for establishing an industry advisory panel for the project, and the Kansas State University Transportation Center (K-State UTC) for graduate student tuition support.

Contents

Acknowledgements ii

Illustrations v

Tables xxiii

Executive Summary 1

1. Introduction 3
   1.1 Background 3
   1.2 Problem Description 3
   1.3 Objectives 4
   1.4 Scope 5
   1.5 Organization of the Report 6

2. Literature Review 7
   2.1 The Concrete Tie 7
   2.2 Transfer Length vs Development Length 8
   2.3 Modeling stress-strain curve for wires - Power Formula 12
   2.4 History of Development-Length Expressions 14
   2.5 Fatigue Behavior of Pretensioned Prestressed Concrete Members 21
   2.6 Conclusion 25

3. Methodology 26
   3.1 Phase I-Effect of Concrete Properties and Wire Indentation Types on the Development Length and Flexural Capacity of Pretensioned Concrete Crossties 26
   3.2 Phase II-Effect of Concrete Properties and Prestressing Strand Indentation Types on the Development Length and Flexural Capacity of Pretensioned Concrete Crossties Made With Three- and Seven-Wire Strands 43
   3.3 Phase III-Effect of Prestressing Wire Indentation Type on the Bond Performance and Flexural Capacity of Pretensioned Concrete Crossties Subjected to Cyclic Loading 51

4. Results 55
   4.1 Phase I-Effect of Concrete Properties and Wire-Indentation Types on Development Length and Flexural Capacity of Pretensioned Concrete Crossties 55
   4.2 Phase II-Effect of Concrete Properties and Prestressing Strand-Indentation Types on Development Length and Flexural Capacity of Pretensioned Concrete Crossties Made With Three- and Seven-Wire Strands 77
   4.3 Phase III-Effect of Prestressing Wire-Indentation Type on the Bond Performance and Flexural Capacity of Pretensioned Concrete Crossties Subjected to Cyclic Loading 88

5. Data Analysis and Model Development 104
   5.1 A Prediction Model for the Development Length of Wires Commonly Used in the Railroad Industry 104

6. Conclusions and Recommendations 126

6.1 RECOMMENDATIONS 127
7. References 128
Appendix A. Example of Strain Compatibility Analysis Used in This Study 133
Appendix B. Experimental Development Length Evaluation 140
Appendix C. Load vs Deflection Graphs and Picture of Failed Prisms 163
Prisms made with wires, 4500 psi concrete release strength and 6 in. slump 163
Prisms made with wires, 4500 psi concrete release strength and 3 in. slump 216
Prisms made with wires, 4500 psi concrete release strength and 9 in. slump 236
Prisms made with wires, 6000 psi concrete release strength and 6 in. slump 257
Prisms made with wires, 3500 psi concrete release strength and 6 in. slump 278
Prisms made with strands, 4500 psi concrete release strength and 6 in. slump 299
Prisms made with strands, 3500 psi concrete release strength and 6 in. slump 325
Prisms made with strands, 6000 psi concrete release strength and 6 in. slump 346
Prisms made with wires, 4500 psi concrete release strength and 6 in. slump tested cyclically 367

Illustrations

Figure 1. Transfer length and flexural-bond length [after: (Vazquez-Herrero, Martinez-Lage, Aquilar, & Martinez-Abella, 2013)] 11

Figure 2. Schematic of development-length test [after: (Kahn, Jason, & Reutlinger, 2002)] 20

Figure 3. Cross section of the pretensioned concrete prism (1 inch=25.4 mm) 27

Figure 4. Picture of all 13 types of wire used in production of test prisms [after: (Arnold, 2013)] 28

Figure 5. Close-up picture of wire indentation types [after: (Arnold, 2013)] 29

Figure 6. Load-test specimen nomenclature 31

Figure 7. Load case 1: prisms loaded at 20-in. embedment length 32

Figure 8. Load case 2: prisms loaded at 13-in. embedment length 32

Figure 9. Load case 3: prisms loaded at 16.5-in. embedment length 32

Figure 10. Load case 1: prisms loaded at 9.5-in. embedment length 33

Figure 11. Wire end-slip LVDT 34

Figure 12. Deflection LVDT 35

Figure 13. Actuator used to apply load on the prisms 36

Figure 14. Setup used for running the loading tests 37

Figure 15. The prism failed in shear-compression mode 38

Figure 16. The prism failed in shear-bond mode 39

Figure 17. The prism failed in pure-shear mode 40

Figure 18. The prism failed in concrete-compression mode 41

Figure 19. Horizontal-splitting mode where the prism split along the bottom row of prestress wires 42

Figure 20. Bond-failure mode with significant wire end-slip for the bottom row of prestress wire 43

Figure 21. Cross section of prisms made with strands of 3/8-in. diameter (1 inch=25.4 mm) 44

Figure 22. Cross section of prisms made with 5/16-in. diameter three-wire strand (1 inch=25.4 mm) 45

Figure 23. Sample of six strands with different indentation types and diameters [after: (Arnold, 2013)] 46

Figure 24. Close-up view of strands indentation types [after: (Arnold, 2013)] 47

Figure 25. Load case 1: prisms loaded at 28-in. embedment length 48

Figure 26. Load case 2: prisms loaded at 20-in. embedment length 48

Figure 27. Load case 3: prisms loaded at 16.5-in. embedment length 49

Figure 28. Load case 4: prisms loaded at 13-in. embedment length..... 49
Figure 29. Actuator used for conducting load tests on prisms containing strands 50
Figure 30. Schematic of test setup for cyclic loading test (1 inch=25.4 mm) 52
Figure 31. A picture of test setup used to run cyclic tests 52
Figure 32. Spreader beam used during the cyclic loading test 53
Figure 33. Load-deflection graphs for all 13 types of wire for 20-in. embedment length..... 56
Figure 34. Load-deflection graphs for all 13 types of wire for 16.5-in. embedment length..... 56
Figure 35. Load-deflection graphs for all 13 types of wire for 16.5-in. embedment length..... 57
Figure 36. Load-deflection graphs for all 13 types of wire for 9.5-in. embedment length..... 57
Figure 37. Prism under applied load at time of failure and self weight (WA-4500-6-1-L)..... 58
Figure 38. Maximum moment vs transfer length measured at time of de-tensioning for test with 20-in. embedment length 59
Figure 39. Maximum moment vs transfer length measured at time of de-tensioning for test with 16.5-in. embedment length 60
Figure 40. Maximum moment vs transfer length measured at time of de-tensioning for test with 13-in. embedment length 60
Figure 41. Maximum moment vs transfer length measured at time of de-tensioning for test with 9.5-in. embedment length 61
Figure 42. Maximum moment vs average transfer length for prisms made with WA and 3,500, 4,500 and 6,000 psi release strengths..... 66
Figure 43. Maximum moment vs average transfer length for prisms made with WE and 3,500, 4,500 and 6,000 psi release strengths..... 67
Figure 44. Maximum moment vs average transfer length for prisms made with WG and 3,500, 4,500 and 6,000 psi release strengths..... 67
Figure 45. Maximum moment vs average transfer length for prisms made with WH and 3,500, 4,500 and 6,000 psi release strengths..... 68
Figure 46. Maximum moment vs average transfer length for prisms made with WK and 3,500, 4,500 and 6,000 psi release strengths..... 68
Figure 47. Maximum moment vs average transfer length for prisms made with WA wire and concrete slumps of 3, 6, and 9 in. 73
Figure 48. Maximum moment vs average transfer length for prisms made with WE wire and concrete slumps of 3, 6, and 9 in. 73
Figure 49. Maximum moment vs average transfer length for prisms made with WG wire and concrete slumps of 3, 6, and 9 in. 74
Figure 50. Maximum moment vs average transfer length for prisms made with WH wire and concrete slumps of 3, 6, and 9 in. 74

Figure 51. Maximum moment vs average transfer length for prisms made with WK wire and concrete slumps of 3, 6, and 9 in. 75
Figure 52. Load-deflection graphs for all 5 types of strand for 28 in. embedment length 78
Figure 53. Load-deflection graphs for all 5 types of strand for 20 in. embedment length 79
Figure 54. Load-deflection graphs for all 5 types of strand for 16.5 in. embedment length 79
Figure 55. Load-deflection graphs for all 5 types of strand for 13 in. embedment length 80
Figure 56. Ratio of maximum experimental moment to nominal-moment capacity vs strand type for different embedment lengths 81
Figure 57. Max moment resisted vs embedment length for prisms made with SA strand 84
Figure 58. Max moment resisted vs embedment length for prisms made with SD strand 84
Figure 59. Max moment resisted vs embedment length for prisms made with SE strand..... 85
Figure 60. Max moment resisted vs embedment length for prisms made with SF strand..... 85
Figure 61. Max moment resisted vs embedment length for prisms made with SA strand 86
Figure 62. Load-deflection graphs of prisms after cyclic loading until failure 89
Figure 63. Load-deflection graphs for all 13 types of wire at 20-in. embedment length 89
Figure 64. Load-deflection graphs at different cycles for prism made with WH wire..... 91
Figure 65. Load-deflection graphs at different cycles for prism made with WD wire..... 92
Figure 66. Prism made with WH wire failed at 11,400th cycle of loading 93
Figure 67. Prism made with WD wire failed at 162,760th cycle of loading 94
Figure 68. Prism made with WH wire failed at 89,875th cycle of loading (repeated test)..... 95
Figure 69. Load-deflection graphs prior to cyclic loading and after cyclic loading until failure (prism made with WA wire) 96
Figure 70. Load-deflection graphs prior to cyclic loading and after cyclic loading until failure (prism made with WB wire) 96
Figure 71. Load-deflection graphs prior to cyclic loading and after cyclic loading until failure (prism made with WC wire) 97
Figure 72. Load-deflection graphs prior to cyclic loading and after cyclic loading until failure (prism made with WE wire)..... 97
Figure 73. Load-deflection graphs prior to cyclic loading and after cyclic loading until failure (prism made with WF wire)..... 98
Figure 74. Load-deflection graphs prior to cyclic loading and after cyclic loading until failure (prism made with WG wire) 98
Figure 75. Load-deflection graphs prior to cyclic loading and after cyclic loading until failure (prism made with WI wire)..... 99

Figure 76. Load-deflection graphs prior to cyclic loading and after cyclic loading until failure (prism made with WJ wire)..... 99

Figure 77. Load-deflection graphs prior to cyclic loading and after cyclic loading until failure (prism made with WK wire) 100

Figure 78. Load-deflection graphs prior to cyclic loading and after cyclic loading until failure (prism made with WL wire)..... 100

Figure 79. Load-deflection graphs prior to cyclic loading and after cyclic loading until failure (prism made with WM wire)..... 101

Figure 80. Compression mode of failure for prisms subjected to cyclic loading (prism made with WF) …… 102

Figure 81. Compression mode of failure for prisms subjected to cyclic loading (prism made with WB) ……103

Figure 82. Final dimensions of wire pull out test specimen [after: (Arnold, 2013)] 105

Figure 83. Ratio of resisted-moment to nominal-moment capacity of section tested versus embedment length..... 111

Figure 84. Graphical display of predicted development lengths using existing equations versus experimental development lengths 117

Figure 85. Graphical display of predicted development lengths using existing equations versus experimental development lengths 119

Figure 86 Predicted development lengths using developed mean equation versus experimental development lengths 122

Figure 87. Predicted developments lengths using Equation. 27 for different concrete release strengths versus experimental development lengths. 124

Figure 88 Stress and strain distribution across beam depth..... 134

Figure 89 Ratio of maximum experimental moment to nominal moment capacity versus embedment length for prisms made with WA wire and 4500 psi release strength..... 140

Figure 90 Ratio of maximum experimental moment to nominal moment capacity versus embedment length for prisms made with WB wire and 4500 psi release strength..... 141

Figure 91 Ratio of maximum experimental moment to nominal moment capacity versus embedment length for prisms made with WC wire and 4500 psi release strength..... 142

Figure 92 Ratio of maximum experimental moment to nominal moment capacity versus embedment length for prisms made with WD wire and 4500 psi release strength..... 143

Figure 93 Ratio of maximum experimental moment to nominal moment capacity versus embedment length for prisms made with WE wire and 4500 psi release strength 144

Figure 94 Ratio of maximum experimental moment to nominal moment capacity versus embedment length for prisms made with WF wire and 4500 psi release strength 145

Figure 95 Ratio of maximum experimental moment to nominal moment capacity versus embedment length for prisms made with WG wire and 4500 psi release strength..... 146

Figure 96 Ratio of maximum experimental moment to nominal moment capacity versus embedment length for prisms made with WH wire and 4500 psi release strength..... 147
Figure 97 Ratio of maximum experimental moment to nominal moment capacity versus embedment length for prisms made with WI wire and 4500 psi release strength 148
Figure 98 Ratio of maximum experimental moment to nominal moment capacity versus embedment length for prisms made with WJ wire and 4500 psi release strength..... 149
Figure 99 Ratio of maximum experimental moment to nominal moment capacity versus embedment length for prisms made with WK wire and 4500 psi release strength..... 150
Figure 100 Ratio of maximum experimental moment to nominal moment capacity versus embedment length for prisms made with WL wire and 4500 psi release strength 151
Figure 101 Ratio of maximum experimental moment to nominal moment capacity versus embedment length for prisms made with WM wire and 4500 psi release strength..... 152
Figure 102 Ratio of maximum experimental moment to nominal moment capacity versus embedment length for prisms made with WA wire and 3500 psi release strength..... 153
Figure 103 Ratio of maximum experimental moment to nominal moment capacity versus embedment length for prisms made with WE wire and 3500 psi release strength 154
Figure 104 Ratio of maximum experimental moment to nominal moment capacity versus embedment length for prisms made with WG wire and 3500 psi release strength..... 155
Figure 105 Ratio of maximum experimental moment to nominal moment capacity versus embedment length for prisms made with WH wire and 3500 psi release strength..... 156
Figure 106 Ratio of maximum experimental moment to nominal moment capacity versus embedment length for prisms made with WK wire and 3500 psi release strength..... 157
Figure 107 Ratio of maximum experimental moment to nominal moment capacity versus embedment length for prisms made with WA wire and 6000 psi release strength..... 158
Figure 108 Ratio of maximum experimental moment to nominal moment capacity versus embedment length for prisms made with WE wire and 6000 psi release strength 159
Figure 109 Ratio of maximum experimental moment to nominal moment capacity versus embedment length for prisms made with WG wire and 6000 psi release strength..... 160
Figure 110 Ratio of maximum experimental moment to nominal moment capacity versus embedment length for prisms made with WH wire and 6000 psi release strength..... 161
Figure 111 Ratio of maximum experimental moment to nominal moment capacity versus embedment length for prisms made with WK wire and 6000 psi release strength..... 162
Figure 112 Load vs Deflection and Wire End Slip WA-4500-6-1-L 164
Figure 113 Picture of Failed Prism WA-4500-6-1-L..... 164
Figure 114 Load Deflection and Wire End Slip WA-4500-6-1-S 165
Figure 115 Picture of Failed Prism WA-4500-6-1-S..... 165
Figure 116 Load Deflection and Wire End Slip WA-4500-6-2-L..... 166

Figure 117 Picture of Failed Prism WA-4500-6-2-L 166
Figure 118 Load Deflection and Wire End Slip WA-4500-6-2-S 167
Figure 119 Picture of Failed Prism WA-4500-6-2-S 167
Figure 120 Load Deflection and Wire End Slip WB-4500-6-1-L 168
Figure 121 Picture of Failed Prism WB-4500-6-1-L 168
Figure 122 Load Deflection and *Wire* End Slip WB-4500-6-1-S 169
Figure 123 Picture of Failed Prism WB-4500-6-1-S 169
Figure 124 Load Deflection and Wire End Slip WB-4500-6-2-L 170
Figure 125 Picture of Failed Prism WB-4500-6-2-L 170
Figure 126 Load Deflection and Wire End Slip WB-4500-6-2-S 171
Figure 127 Picture of Failed Prism WB-4500-6-2-S 171
Figure 128 Load Deflection and Wire End Slip WC-4500-6-1-L 172
Figure 129 Picture of Failed Prism WC-4500-6-1-L 172
Figure 130 Load Deflection and Wire End Slip WC-4500-6-1-S 173
Figure 131 Picture of Failed Prism WC-4500-6-1-S 173
Figure 132 Load Deflection and Wire End Slip WC-4500-6-2-L 174
Figure 133 Picture of Failed Prism WC-4500-6-2-L 174
Figure 134 Load Deflection and Wire End Slip WC-4500-6-2-S 175
Figure 135 Picture of Failed Prism WC-4500-6-2-S 175
Figure 136 Load Deflection and Wire End Slip WD-4500-6-1-L 176
Figure 137 Picture of Failed Prism WD-4500-6-1-L 176
Figure 138 Load Deflection and Wire End Slip WD-4500-6-1-S 177
Figure 139 Picture of Failed Prism WD-4500-6-1-S 177
Figure 140 Load Deflection and Wire End Slip WD-4500-6-2-L 178
Figure 141 Picture of Failed Prism WD-4500-6-2-L 178
Figure 142 Load Deflection and Wire End Slip WD-4500-6-2-S 179
Figure 143 Picture of Failed Prism WD-4500-6-2-S 179
Figure 144 Load Deflection and Wire End Slip WE-4500-6-1-L 180
Figure 145 Picture of Failed Prism WE-4500-6-1-L 180
Figure 146 Load Deflection and Wire End Slip WE-4500-6-1-S 181
Figure 147 Picture of Failed Prism WE-4500-6-1-S 181
Figure 148 Load Deflection and Wire End Slip WE-4500-6-2-L 182

Figure 149 Picture of Failed Prism WE-4500-6-2-L 182
Figure 150 Load Deflection and Wire End Slip WE-4500-6-2-S 183
Figure 151 Picture of Failed Prism WE-4500-6-2-S 183
Figure 152 Load Deflection and Wire End Slip WF-4500-6-1-L 184
Figure 153 Picture of Failed Prism WF-4500-6-1-L 184
Figure 154 Load Deflection and Wire End Slip WF-4500-6-1-S 185
Figure 155 Picture of Failed Prism WF-4500-6-1-S 185
Figure 156 Load Deflection and Wire End Slip WF-4500-6-2-L 186
Figure 157 Picture of Failed Prism WF-4500-6-2-L 186
Figure 158 Load Deflection and Wire End Slip WF-4500-6-2-S 187
Figure 159 Picture of Failed Prism WF-4500-6-2-S 187
Figure 160 Load Deflection and Wire End Slip WG-4500-6-1-L 188
Figure 161 Picture of Failed Prism WG-4500-6-1-L 188
Figure 162 Load Deflection and Wire End Slip WG-4500-6-1-S 189
Figure 163 Picture of Failed Prism WG-4500-6-1-S 189
Figure 164 Load Deflection and Wire End Slip WG-4500-6-2-L 190
Figure 165 Picture of Failed Prism WG-4500-6-2-L 190
Figure 166 Load Deflection and Wire End Slip WG-4500-6-2-S 191
Figure 167 Picture of Failed Prism WG-4500-6-2-S 191
Figure 168 Load Deflection and Wire End Slip WH-4500-6-1-L 192
Figure 169 Picture of Failed Prism WH-4500-6-1-L 192
Figure 170 Load Deflection and Wire End Slip WH-4500-6-1-S 193
Figure 171 Picture of Failed Prism WH-4500-6-1-S 193
Figure 172 Load Deflection and Wire End Slip WH-4500-6-2-L 194
Figure 173 Picture of Failed Prism WH-4500-6-2-L 194
Figure 174 Load Deflection and Wire End Slip WH-4500-6-2-S 195
Figure 175 Picture of Failed Prism WH-4500-6-2-S 195
Figure 176 Load Deflection and Wire End Slip WI-4500-6-1-L 196
Figure 177 Picture of Failed Prism WI-4500-6-1-L 196
Figure 178 Load Deflection and Wire End Slip WI-4500-6-1-S 197
Figure 179 Picture of Failed Prism WI-4500-6-1-S 197
Figure 180 Load Deflection and Wire End Slip WI-4500-6-2-L 198

Figure 181 Picture of Failed Prism WI-4500-6-2-L 198
Figure 182 Load Deflection and Wire End Slip WI-4500-6-2-S 199
Figure 183 Picture of Failed Prism WI-4500-6-2-S 199
Figure 184 Load Deflection and Wire End Slip WJ-4500-6-1-L 200
Figure 185 Picture of Failed Prism WJ-4500-6-1-L 200
Figure 186 Load Deflection and Wire End Slip WJ-4500-6-1-S 201
Figure 187 Picture of Failed Prism WJ-4500-6-1-S 201
Figure 188 Load Deflection and Wire End Slip WJ-4500-6-2-L 202
Figure 189 Picture of Failed Prism WJ-4500-6-2-L 202
Figure 190 Load Deflection and Wire End Slip WJ-4500-6-2-S 203
Figure 191 Picture of Failed Prism WJ-4500-6-2-S 203
Figure 192 Load Deflection and Wire End Slip WK-4500-6-1-L 204
Figure 193 Picture of Failed Prism WK-4500-6-1-L 204
Figure 194 Load Deflection and Wire End Slip WK-4500-6-1-S 205
Figure 195 Picture of Failed Prism WK-4500-6-1-S 205
Figure 196 Load Deflection and Wire End Slip WK-4500-6-2-L 206
Figure 197 Picture of Failed Prism WK-4500-6-2-L 206
Figure 198 Load Deflection and Wire End Slip WK-4500-6-2-S 207
Figure 199 Picture of Failed Prism WK-4500-6-2-S 207
Figure 200 Load Deflection and Wire End Slip WL-4500-6-1-L 208
Figure 201 Picture of Failed Prism WL-4500-6-1-L 208
Figure 202 Load Deflection and Wire End Slip WL-4500-6-1-S 209
Figure 203 Picture of Failed Prism WL-4500-6-1-S 209
Figure 204 Load Deflection and Wire End Slip WL-4500-6-2-L 210
Figure 205 Picture of Failed Prism WL-4500-6-2-L 210
Figure 206 Load Deflection and Wire End Slip WL-4500-6-2-S 211
Figure 207 Picture of Failed Prism WL-4500-6-2-S 211
Figure 208 Load Deflection and Wire End Slip WM-4500-6-1-L 212
Figure 209 Picture of Failed Prism WM-4500-6-1-L 212
Figure 210 Load Deflection and Wire End Slip WM-4500-6-1-S 213
Figure 211 Picture of Failed Prism WM-4500-6-1-S 213
Figure 212 Load Deflection and Wire End Slip WM-4500-6-2-L 214

Figure 213 Picture of Failed Prism WM-4500-6-2-L 214
Figure 214 Load Deflection and Wire End Slip WM-4500-6-2-S 215
Figure 215 Picture of Failed Prism WM-4500-6-2-S 215
Figure 218 Load Deflection and Wire End Slip WA-4500-3-1-S 217
Figure 219 Picture of Failed Prism WA-4500-3-1-S 217
Figure 220 Load Deflection and Wire End Slip WA-4500-3-2-L 218
Figure 221 Picture of Failed Prism WA-4500-3-2-L 218
Figure 222 Load Deflection and Wire End Slip WA-4500-3-2-S 219
Figure 223 Picture of Failed Prism WA-4500-3-2-S 219
Figure 224 Load Deflection and Wire End Slip WE-4500-3-1-L 220
Figure 225 Picture of Failed Prism WE-4500-3-1-L 220
Figure 226 Load Deflection and Wire End Slip WE-4500-3-1-S 221
Figure 227 Picture of Failed Prism WE-4500-3-1-S 221
Figure 228 Load Deflection and Wire End Slip WE-4500-3-2-L 222
Figure 229 Picture of Failed Prism WE-4500-3-2-L 222
Figure 230 Picture of Failed Prism WE-4500-3-2-S 223
Figure 231 Load Deflection and Wire End Slip WG-4500-3-1-L 224
Figure 232 Picture of Failed Prism WG-4500-3-1-L 224
Figure 233 Load Deflection and Wire End Slip WG-4500-3-1-S 225
Figure 234 Picture of Failed Prism WG-4500-3-1-S 225
Figure 235 Load Deflection and Wire End Slip WG-4500-3-2-L 226
Figure 236 Picture of Failed Prism WG-4500-3-2-L 226
Figure 237Load Deflection and Wire End Slip WG-4500-3-2-S 227
Figure 238 Picture of Failed Prism WG-4500-3-2-S 227
Figure 239 Load Deflection and Wire End Slip WH-4500-3-1-L 228
Figure 240 Picture of Failed Prism WH-4500-3-1-L 228
Figure 241 Load Deflection and Wire End Slip WH-4500-3-1-S 229
Figure 242 Picture of Failed Prism WH-4500-3-2-L 230
Figure 243 Picture of Failed Prism WH-4500-3-2-S 231
Figure 244 Load Deflection and Wire End Slip WK-4500-3-1-L 232
Figure 245 Picture of Failed Prism WK-4500-3-1-L 232
Figure 246 Load Deflection and Wire End Slip WK-4500-3-1-S 233

Figure 247 Picture of Failed Prism WK-4500-3-1-S 233
Figure 248 Load Deflection and Wire End Slip WK-4500-3-2-L 234
Figure 249 Picture of Failed Prism WK-4500-3-2-L 234
Figure 250 Load Deflection and Wire End Slip WK-4500-3-2-S 235
Figure 251 Picture of Failed Prism WK-4500-3-2-S 235
Figure 252 Figure 144 Load Deflection and Wire End Slip WA-4500-9-1-L 237
Figure 253 Picture of Failed Prism WA-4500-9-1-L 237
Figure 254 Load Deflection and Wire End Slip WA-4500-9-1-S 238
Figure 255 Picture of Failed Prism WA-4500-9-1-S 238
Figure 256 Load Deflection and Wire End Slip WA-4500-9-2-L 239
Figure 257 Picture of Failed Prism WA-4500-9-2-L 239
Figure 258 Load Deflection and Wire End Slip WA-4500-9-2-S 240
Figure 259 Picture of Failed Prism WA-4500-9-2-S 240
Figure 260 Load Deflection and Wire End Slip WE-4500-9-1-L 241
Figure 261 Picture of Failed Prism WE-4500-9-1-L 241
Figure 262 Load Deflection and Wire End Slip WE-4500-9-1-S 242
Figure 263 Picture of Failed Prism WE-4500-9-1-S 242
Figure 264 Load Deflection and Wire End Slip WE-4500-9-2-L 243
Figure 265 Picture of Failed Prism WE-4500-9-2-L 243
Figure 266 Load Deflection and Wire End Slip WE-4500-9-2-S 244
Figure 267 Picture of Failed Prism WE-4500-9-2-S 244
Figure 268 Load Deflection and Wire End Slip WG-4500-9-1-L 245
Figure 269 Picture of Failed Prism WG-4500-9-1-L 245
Figure 270 Load Deflection and Wire End Slip WG-4500-9-1-S 246
Figure 271 Picture of Failed Prism WG-4500-9-1-S 246
Figure 272 Load Deflection and Wire End Slip WG-4500-9-2-L 247
Figure 273 Picture of Failed Prism WG-4500-9-2-L 247
Figure 274 Load Deflection and Wire End Slip WG-4500-9-2-S 248
Figure 275 Picture of Failed Prism WG-4500-9-2-S 248
Figure 276 Load Deflection and Wire End Slip WH-4500-9-1-L 249
Figure 277 Picture of Failed Prism WH-4500-9-1-L 249
Figure 278 Load Deflection and Wire End Slip WH-4500-9-1-S 250

Figure 279 Picture of Failed Prism WH-4500-9-1-S 250
Figure 280 Load Deflection and Wire End Slip WH-4500-9-2-L 251
Figure 281 Picture of Failed Prism WH-4500-9-2-L 251
Figure 282 Load Deflection and Wire End Slip WH-4500-9-2-S 252
Figure 283 Picture of Failed Prism WH-4500-9-2-S 252
Figure 284 Load Deflection and Wire End Slip WK-4500-9-1-L 253
Figure 285 Picture of Failed Prism WK-4500-9-1-L 253
Figure 286 Load Deflection and Wire End Slip WK-4500-9-1-S 254
Figure 287 Picture of Failed Prism WK-4500-9-1-S 254
Figure 288 Load Deflection and Wire End Slip WK-4500-9-2-L 255
Figure 289 Picture of Failed Prism WK-4500-9-2-L 255
Figure 290 Load Deflection and Wire End Slip WK-4500-9-2-S 256
Figure 291 Picture of Failed Prism WK-4500-9-2-S 256
Figure 292 Load Deflection and Wire End Slip WA-6000-6-1-L 258
Figure 293 Picture of Failed Prism WA-6000-6-1-L 258
Figure 294 Load Deflection and Wire End Slip WA-6000-6-1-S 259
Figure 295 Picture of Failed Prism WA-6000-6-1-S 259
Figure 296 Load Deflection and Wire End Slip WA-6000-6-2-L 260
Figure 297 Picture of Failed Prism WA-6000-6-2-L 260
Figure 298 Load Deflection and Wire End Slip WA-6000-6-2-S 261
Figure 299 Picture of Failed Prism WA-6000-6-2-S 261
Figure 300 Load Deflection and Wire End Slip WE-6000-6-1-L 262
Figure 301 Load Deflection and Wire End Slip WE-6000-6-1-S 263
Figure 302 Picture of Failed Prism WE-6000-6-1-S 263
Figure 303 Load Deflection and Wire End Slip WE-6000-6-2-L 264
Figure 304 Picture of Failed Prism WE-6000-6-2-L 264
Figure 305 Load Deflection and Wire End Slip WE-6000-6-2-S 265
Figure 306 Picture of Failed Prism WE-6000-6-2-S 265
Figure 307 Load Deflection and Wire End Slip WG-6000-6-1-L 266
Figure 308 Picture of Failed Prism WG-6000-6-1-L 266
Figure 309 Load Deflection and Wire End Slip WG-6000-6-1-S 267
Figure 310 Picture of Failed Prism WG-6000-6-1-S 267

Figure 311 Load Deflection and Wire End Slip WG-6000-6-2-L 268
Figure 312 Picture of Failed Prism WG-6000-6-2-L 268
Figure 313 Load Deflection and Wire End Slip WG-6000-6-2-S 269
Figure 314 Picture of Failed Prism WG-6000-6-2-S 269
Figure 315 Load Deflection and Wire End Slip WH-6000-6-1-L 270
Figure 316 Picture of Failed Prism WH-6000-6-1-L 270
Figure 317 Load Deflection and Wire End Slip WH-6000-6-1-S 271
Figure 318 Picture of Failed Prism WH-6000-6-1-S 271
Figure 319 Load Deflection and Wire End Slip WH-6000-6-2-L 272
Figure 320 Picture of Failed Prism WH-6000-6-2-L 272
Figure 321 Load Deflection and Wire End Slip WH-6000-6-2-S 273
Figure 322 Picture of Failed Prism WH-6000-6-2-S 273
Figure 323 Load Deflection and Wire End Slip WK-6000-6-1-L 274
Figure 324 Picture of Failed Prism WK-6000-6-1-L 274
Figure 325 Load Deflection and Wire End Slip WK-6000-6-1-S 275
Figure 326 Picture of Failed Prism WK-6000-6-1-S 275
Figure 327 Load Deflection and Wire End Slip WK-6000-6-2-L 276
Figure 328 Picture of Failed Prism WK-6000-6-2-L 276
Figure 329 Load Deflection and Wire End Slip WK-6000-6-2-S 277
Figure 330 Picture of Failed Prism WK-6000-6-2-S 277
Figure 331 Load Deflection and Wire End Slip WA-3500-6-1-L 279
Figure 332 Picture of Failed Prism WA-3500-6-1-L 279
Figure 333 Load Deflection and Wire End Slip WA-3500-6-1-S 280
Figure 334 Picture of Failed Prism WA-3500-6-1-S 280
Figure 335 Load Deflection and Wire End Slip WA-3500-6-2-L 281
Figure 336 Picture of Failed Prism WA-3500-6-2-L 281
Figure 337 Load Deflection and Wire End Slip WA-3500-6-2-S 282
Figure 338 Load vs Deflection and Wire End Slip WE-3500-6-1-L 283
Figure 339 Picture of Failed Prism for WE-3500-6-1-L 283
Figure 340 Load vs Deflection and Wire End Slip WE-3500-6-1-S 284
Figure 341 Picture of Failed Prism for WE-3500-6-1-S 284
Figure 342 Load vs Deflection and Wire End Slip WE-3500-6-2-L 285

Figure 343 Picture of Failed Prism for WE-3500-6-2-L 285
Figure 344 Load vs Deflection and Wire End Slip WE-3500-6-2-S 286
Figure 345 Picture of Failed Prism for WE-3500-6-2-S 286
Figure 346 Load vs Deflection and Wire End Slip WG-3500-6-1-L 287
Figure 347 Picture of Failed Prism for WG-3500-6-1-L 287
Figure 348 Load vs Deflection and Wire End Slip WG-3500-6-1-S 288
Figure 349 Picture of Failed Prism for WG-3500-6-1-S 288
Figure 350 Picture of Failed Prism for WG-3500-6-2-L 289
Figure 351 Load vs Deflection and Wire End Slip WG-3500-6-2-S 290
Figure 352 Picture of Failed Prism for WG-3500-6-2-S 290
Figure 353 Load vs Deflection and Wire End Slip WH-3500-6-1-L 291
Figure 354 Picture of Failed Prism for WH-3500-6-1-L 291
Figure 355 Load vs Deflection and Wire End Slip WH-3500-6-1-S 292
Figure 356 Picture of Failed Prism for WH-3500-6-1-S 292
Figure 357 Load vs Deflection and Wire End Slip WH-3500-6-2-L 293
Figure 358 Picture of Failed Prism for WH-3500-6-2-L 293
Figure 359 Load vs Deflection and Wire End Slip WH-3500-6-2-S 294
Figure 360 Picture of Failed Prism for WH-3500-6-2-S 294
Figure 361 Load vs Deflection and Wire End Slip WK-3500-6-1-L 295
Figure 362 Picture of Failed Prism for WK-3500-6-1-L 295
Figure 363 Load vs Deflection and Wire End Slip WK-3500-6-1-S 296
Figure 364 Picture of Failed Prism for WK-3500-6-1-S 296
Figure 365 Load vs Deflection and Wire End Slip WK-3500-6-2-L 297
Figure 366 Picture of Failed Prism for WK-3500-6-2-L 297
Figure 367 Load vs Deflection and Wire End Slip WK-3500-6-2-S 298
Figure 368 Picture of Failed Prism for WK-3500-6-2-S 298
Figure 369 Load vs Deflection and Strand End Slip SA-4500-6-1-L 300
Figure 370 Picture of Failed Prism for SA-4500-6-1-L 300
Figure 371 Load vs Deflection and Strand End Slip SA-4500-6-1-L-2nd 301
Figure 372 Picture of Failed Prism for SA-4500-6-1-L-2nd 301
Figure 373 Load vs Deflection and Strand End Slip SA-4500-6-2-L 302
Figure 374 Picture of Failed Prism for SA-4500-6-2-L 302

Figure 375 Load vs Deflection and Strand End Slip SA-4500-6-3-L 303
Figure 376 Picture of Failed Prism for SA-4500-6-3-L 303
Figure 377 Load vs Deflection and Strand End Slip SA-4500-6-3-S 304
Figure 378 Picture of Failed Prism for SA-4500-6-3-S 304
Figure 379 Load vs Deflection and Strand End Slip SB-4500-6-1-L 305
Figure 380 Picture of Failed Prism for SB-4500-6-1-L 305
Figure 381 Load vs Deflection and Strand End Slip SB-4500-6-1-L-2nd 306
Figure 382 Picture of Failed Prism for SB-4500-6-1-L-2nd 306
Figure 383 Load vs Deflection and Strand End Slip SB-4500-6-2-L 307
Figure 384 Picture of Failed Prism for SB-4500-6-2-L 307
Figure 385 Load vs Deflection and Strand End Slip (SB-4500-6-3-L) 308
Figure 386 Picture of Failed Prism for SB-4500-6-3-L 308
Figure 387 Load vs Deflection and Strand End Slip SB-4500-6-3-S 309
Figure 388 Picture of Failed Prism for SB-4500-6-3-S 309
Figure 389 Load vs Deflection and Strand End Slip SD-4500-6-1-L 310
Figure 390 Picture of Failed Prism for SD-4500-6-1-L 310
Figure 391 Load vs Deflection and Strand End Slip SD-4500-6-1-L-2nd 311
Figure 392 Picture of Failed Prism for SD-4500-6-1-L-2nd 311
Figure 393 Load vs Deflection and Strand End Slip SD-4500-6-2-L 312
Figure 394 Picture of Failed Prism for SD-4500-6-2-L 312
Figure 395 Load vs Deflection and Strand End Slip SD-4500-6-3-L 313
Figure 396 Picture of Failed Prism for SD-4500-6-3-L 313
Figure 397 Load vs Deflection and Strand End Slip SD-4500-6-3-S 314
Figure 398 Picture of Failed Prism for SD-4500-6-3-S 314
Figure 399 Load vs Deflection and Strand End Slip SE-4500-6-1-L 315
Figure 400 Picture of Failed Prism for SE-4500-6-1-L 315
Figure 401 Load vs Deflection and Strand End Slip SE-4500-6-1-L-2nd 316
Figure 402 Picture of Failed Prism for SE-4500-6-1-L-2nd 316
Figure 403 Load vs Deflection and Strand End Slip SE-4500-6-2-L 317
Figure 404 Picture of Failed Prism for SE-4500-6-2-L 317
Figure 405 Picture of Failed Prism for SE-4500-6-3-L 318
Figure 406 Load vs Deflection and Strand End Slip SE-4500-6-3-S 319

Figure 407 Picture of Failed Prism for SE-4500-6-3-S 319
Figure 408 Load vs Deflection and Strand End Slip SF-4500-6-1-L 320
Figure 409 Picture of Failed Prism for SF-4500-6-1-L 320
Figure 410 Load vs Deflection and Strand End Slip SF-4500-6-1-L-2nd 321
Figure 411 Picture of Failed Prism for SF-4500-6-1-L 2nd 321
Figure 412 Load vs Deflection and Strand End Slip SF-4500-6-2-L 322
Figure 413 Picture of Failed Prism for SF-4500-6-2-L 322
Figure 414 Load vs Deflection and Strand End Slip SF-4500-6-3-L 323
Figure 415 Picture of Failed Prism for SF-4500-6-3-L 323
Figure 416 Load vs Deflection and Strand End Slip SF-4500-6-3-S 324
Figure 417 Picture of Failed Prism for SF-4500-6-3-S 324
Figure 418 Load vs Deflection and Strand End Slip SA-3500-6-1-L 326
Figure 419 Picture of Failed Prism for SA-3500-6-1-L 326
Figure 420 Picture of Failed Prism for SA-3500-6-1-L-2nd 327
Figure 421 Load vs Deflection and Strand End Slip SA-3500-6-2-L 328
Figure 422 Picture of Failed Prism for SA-3500-6-2-L 328
Figure 423 Load vs Deflection and Strand End Slip SA-3500-6-3-L 329
Figure 424 Picture of Failed Prism for SA-3500-6-3-L 329
Figure 425 Load vs Deflection and Strand End Slip SA-3500-6-3-S 330
Figure 426 Picture of Failed Prism for SA-3500-6-3-S 330
Figure 427 Load vs Deflection and Strand End Slip SD-3500-6-1-L 331
Figure 428 Picture of Failed Prism for SD-3500-6-1-L 331
Figure 429 Load vs Deflection and Strand End Slip SD-3500-6-1-L-2nd 332
Figure 430 Picture of Failed Prism for SD-3500-6-1-L-2nd 332
Figure 431 Load vs Deflection and Strand End Slip SA-3500-6-2-L 333
Figure 432 Picture of Failed Prism for SD-3500-6-2-L 333
Figure 433vLoad vs Deflection and Strand End Slip SA-3500-6-3-L 334
Figure 434 Picture of Failed Prism for SD-3500-6-3-L 334
Figure 435 Load vs Deflection and Strand End Slip SD-3500-6-3-S 335
Figure 436 Picture of Failed Prism for SD-3500-6-3-S 335
Figure 437 Load vs Deflection and Strand End Slip SE-3500-6-1-L 336
Figure 438 Picture of Failed Prism for SE-3500-6-1-L 336

Figure 439 Load vs Deflection and Strand End Slip SE-3500-6-1-L-2nd 337
Figure 440 Picture of Failed Prism for SE-3500-6-1-L-2nd 337
Figure 441 Load vs Deflection and Strand End Slip SE-3500-6-2-L 338
Figure 442 Picture of Failed Prism for SE-3500-6-2-L 338
Figure 443 Load vs Deflection and Strand End Slip SE-3500-6-3-L 339
Figure 444 Figure 338 Picture of Failed Prism for SE-3500-6-3-L 339
Figure 445 Picture of Failed Prism for SE-3500-6-3-S 340
Figure 446 Load vs Deflection and Strand End Slip SF-3500-6-1-L 341
Figure 447 Picture of Failed Prism for SF-3500-6-1-L 341
Figure 448 Load vs Deflection and Strand End Slip SF-3500-6-1-L-2nd 342
Figure 449 Picture of Failed Prism for SF-3500-6-1-L-2nd 342
Figure 450 Load vs Deflection and Strand End Slip SF-3500-6-2-L 343
Figure 451 Picture of Failed Prism for SF-3500-6-2-L 343
Figure 452 Picture of Failed Prism for SF-3500-6-3-L 344
Figure 453 Load vs Deflection and Strand End Slip SF-3500-6-3-S 345
Figure 454 Picture of Failed Prism for SF-3500-6-3-S 345
Figure 455 Load vs Deflection and Strand End Slip SA-6000-6-1-L 347
Figure 456 Picture of Failed Prism for SA-6000-6-1-L 347
Figure 457 Load vs Deflection and Strand End Slip SA-6000-6-1-L-2nd 348
Figure 458 Picture of Failed Prism for SA-6000-6-1-L-2nd 348
Figure 459 Load vs Deflection and Strand End Slip SA-6000-6-2-L 349
Figure 460 Picture of Failed Prism for SA-6000-6-2-L 349
Figure 461 Load vs Deflection and Strand End Slip SA-6000-6-3-L 350
Figure 462 Picture of Failed Prism for SA-6000-6-3-L 350
Figure 463 Load vs Deflection and Strand End Slip SA-6000-6-3-S 351
Figure 464 Picture of Failed Prism for SA-6000-6-3-S 351
Figure 465 Load vs Deflection and Strand End Slip SD-6000-6-1-L 352
Figure 466 Picture of Failed Prism for SD-6000-6-1-L 352
Figure 467 Load vs Deflection and Strand End Slip SD-6000-1-L-2nd 353
Figure 468 Picture of Failed Prism for SD-6000-6-1-L-2nd 353
Figure 469 Load vs Deflection and Strand End Slip SD-6000-6-2-L 354
Figure 470 Picture of Failed Prism for SD-6000-6-2-L 354

Figure 471 Load vs Deflection and Strand End Slip SA-6000-6-3-L 355
Figure 472 Picture of Failed Prism for SD-6000-6-3-L 355
Figure 473 Load vs Deflection and Strand End Slip SD-6000-6-3-S 356
Figure 474 Picture of Failed Prism for SD-6000-6-3-S 356
Figure 475 Load vs Deflection and Strand End Slip SE-6000-6-1-L 357
Figure 476 Picture of Failed Prism for SE-6000-6-1-L 357
Figure 477 Load vs Deflection and Strand End Slip SE-6000-6-1-L-2nd 358
Figure 478 Picture of Failed Prism for SE-6000-6-1-L-2nd 358
Figure 479 Picture of Failed Prism for SE-6000-6-2-L 359
Figure 480 Load vs Deflection and Strand End Slip SE-6000-6-3-L 360
Figure 481 Picture of Failed Prism for SE-6000-6-3-L 360
Figure 482 Load vs Deflection and Strand End Slip SE-6000-6-3-S 361
Figure 483 Picture of Failed Prism for SE-6000-6-3-S 361
Figure 484 Load vs Deflection and Strand End Slip SF-6000-6-1-L 362
Figure 485 Picture of Failed Prism for SF-6000-6-1-L 362
Figure 486 Load vs Deflection and Strand End Slip SF-6000-6-1-L-2nd 363
Figure 487 Picture of Failed Prism for SF-6000-6-1-L-2nd 363
Figure 488 Load vs Deflection and Strand End Slip SF-6000-6-2-L 364
Figure 489 Picture of Failed Prism for SF-6000-6-2-L 364
Figure 490 Load vs Deflection and Strand End Slip SF-6000-6-3-L 365
Figure 491 Picture of Failed Prism for SF-6000-6-3-L 365
Figure 492 Picture of Failed Prism for SF-6000-6-3-S 366
Figure 493 Load vs Deflection WA-4500-6 368
Figure 494 Picture of Failed Prism for WA-4500-6-3-Cyclic 368
Figure 495 Load vs Deflection WB-4500-6 369
Figure 496 Picture of Failed Prism for WB-4500-6-3-Cyclic 369
Figure 497 Load vs Deflection WC-4500-6 370
Figure 498 Picture of Failed Prism for WC-4500-6-3-Cyclic 370
Figure 499 Picture of Failed Prism for WD-4500-6-3-Cyclic 371
Figure 500 Load vs Deflection WE-4500-6 372
Figure 501 Picture of Failed Prism for WE-4500-6-3-Cyclic 372
Figure 502 Load vs Deflection WF-4500-6 373

Figure 503 Picture of Failed Prism for WF-4500-6-3-Cyclic 373
Figure 504 Load vs Deflection WG-4500-6 374
Figure 505 Picture of Failed Prism for WG-4500-6-3-Cyclic 374
Figure 506 Picture of Failed Prism for WH-4500-6-3-Cyclic 375
Figure 507 Load vs Deflection WI-4500-6 376
Figure 508 Picture of Failed Prism for WI-4500-6-3-Cyclic 376
Figure 509 Load vs Deflection WJ-4500-6 377
Figure 510 Picture of Failed Prism for WJ-4500-6-3-Cyclic 377
Figure 511 Load vs Deflection WK-4500-6 378
Figure 512 Picture of Failed Prism for WK-4500-6-3-Cyclic 378
Figure 513 Load vs Deflection WL-4500-6 379
Figure 514 Picture of Failed Prism for WL-4500-6-3-Cyclic 379
Figure 515 Load vs Deflection WM-4500-6 380
Figure 516 Picture of Failed Prism for WM-4500-6-3-Cyclic 380

Tables

Table 1. Mechanical properties of each wires obtained from laboratory tests [after: (Chen, 2016)] 13

Table 2. Basic indent geometrical features [after: (Haynes, Wu, Beck, Bodapati, & Peterman, 2014)] 30

Table 3. Loading steps and load rates for running monotonic load tests on prisms made with wires 37

Table 4. Mechanical properties of strands used in this study 46

Table 5 Loading steps and load rates in tests on prisms manufactured with strands 51

Table 6 Loading steps and load rates for cyclic test 54

Table 7 Transfer lengths determined at time of de-tensioning at each prism end for prisms with 4500 psi concrete-release strength (Bodapati, et al., 2013) 55

Table 8. Results from load tests of two identical prisms for each wire type and 4,500 psi release strength 62

Table 9 Development-length estimations for each end tested 64

Table 10 Transfer lengths determined at the time of de-tensioning at tested prism ends for prisms with 3,500 psi concrete-release strength (Bodapati, et al., 2013) 65

Table 11 Transfer lengths determined at time of de-tensioning at tested prism ends for prisms with 4,500 psi concrete-release strength (Bodapati, et al., 2013) 65

Table 12 Transfer lengths determined at time of de-tensioning at tested prism ends for prisms with 6,000 psi concrete-release strength (Bodapati, et al., 2013) 66

Table 13. Results from load tests of two identical prisms for each wire type and different concrete-release strengths 70

Table 14 Transfer lengths determined at time of de-tensioning at prism ends for prisms with 3-in. concrete slump (Bodapati, et al., 2013) 72

Table 15 Transfer lengths determined at time of de-tensioning at prism ends for prisms with 6-in. concrete slump (Bodapati, et al., 2013) 72

Table 16 Transfer lengths determined at time of de-tensioning at prism ends for prisms with 9-in. concrete slump (Bodapati, et al., 2013) 72

Table 17. Results from load tests of two identical prisms for each wire type and different concrete slumps 76

Table 18. Average transfer lengths at the time of de-tensioning for prisms made with concrete release strength of 4,500 psi and different strands 77

Table 19 Properties of prisms manufactured with different strands and their nominal- moment capacity 81

Table 20. Results from load tests of three identical prisms for each strand type and 4,500 psi release strength 82

Table 21. Range of development length for each type of strand 83

Table 22. Results from load tests of three identical prisms for each strand type and different release strengths 87

Table 23. Comparison between maximum-moment capacities obtained from cyclic loading and monotonic loading at 20 in. from prism end. 90

Table 24. Matrix of wire pull-out testing program [after: (Arnold, 2013)] 104

Table 25. As-received wires, average pullout force at 0.10 in. end slip [after: (Arnold, 2013)] 106

Table 26. Pea strain values (microstrain) determined for each end of prisms with 4500 psi release strength before load testing and at the time of de-tensioning 107

Table 27. Peak strain values (microstrain) determined for each end of prisms with 3500 psi release strength before load testing and at the time of de-tensioning 108

Table 28. Peak strain values (microstrain) determined for each end of prisms with 6000 psi release strength before load testing and at the time of de-tensioning 108

Table 29. Initial and total losses in percentage for ends of prisms with 4,500 psi release strength 109

Table 30. Initial and total losses in percentage for ends of prisms with 3,500 psi release strength 109

Table 31. Initial and total losses in percentage for ends of prisms with 6,000 psi release strength 109

Table 32. Resisted-moment and nominal-moment capacity calculated for each end of prisms with 4,500 psi release strength (EL=embedment length) 112

Table 33. Ratio of resisted moment to nominal moment capacity calculated for each end of prisms tested (EL=embedment length) 112

Table 34 Resisted-moment and nominal nominal-moment capacity calculated for each end of prisms with 3,500 psi release strength (EL=embedment length)..... 113

Table 35 Ratio of resisted resisted-moment to nominal nominal-moment capacity calculated for each end of prisms tested (EL=embedment length)..... 113

Table 36. Resisted-moment and nominal-moment capacity calculated for each end of prisms with 6,000 psi release strength (EL=embedment length) 113

Table 37 Ratio of resisted resisted-moment to nominal nominal-moment capacity calculated for each end of prisms tested (EL= embedment length)..... 114

Table 38. Development lengths evaluated, transfer lengths and ratio of development length to transfer length for prisms made with different wires and concrete-release strength 115

Table 39. Predicted development lengths and experimental development lengths 116

Table 40. Predicted development lengths and experimental development lengths 118

Table 41. Statistical parameters for development-length model 120

Table 42. Predicted development lengths using developed mean model and experimental development lengths 121

Table 43 Predicted development lengths versus experimental development lengths..... 125

Executive Summary

This report summarizes work that is part of a larger project funded by the FRA titled "Quantifying the Effect of Prestressing Steel and Concrete Variables on the Transfer Length in Pretensioned Concrete Crossties." The project has the following Major Research Tasks:

Laboratory Phase

1) Pre-tensioned Concrete Prism Tests
2) Un-tensioned Pullout Tests with Mortar
3) Tensioned Pullout Tests with Concrete
4) Precise Measurements of the Reinforcement and Indent Geometry
5) Performing Load Tests on the Pre-Tensioned Concrete Prisms

Plant Phase

6) Automated Device for Transfer Length Measurement
7) Measuring Transfer Lengths of Concrete Crossties at the Plant
8) Un-tensioned Pullout Tests with Concrete

Joint Research Activities

9) Evaluation of Ties Installed in Track

The work presented herein specifically covers task (5) "Performing Load Tests on the Pre-Tensioned Concrete Prisms".

A study was conducted to determine the effect of different concrete properties and prestressing steel indentation types on development length and flexural capacity of pretensioned members. Wires and strands commonly used in the manufacturing of prestressed concrete railroad ties worldwide were selected for the study. Thirteen different 5.32-mm-diameter prestressing wire types and six different strands (four, seven-wire strands and two, three-wire strands) were used to cast prisms with a square cross section. The ratio of concrete to prestressed steel in the test prism's cross section was representable of typical concrete railroad ties. Thus, geometrical and mechanical properties of test prisms were representative of actual ties in the railroad industry.

To understand the effect of concrete-release strengths and slumps on development length, all parameters were kept constant in the prisms except concrete-release strength and slump. To manufacture prisms with different release strengths, all four wires/strands were pulled and de-tensioned gradually when the concrete compressive strength reached 3500 (24.13 MPa), 4500 (31.03 MPa), and 6000 (41.37 MPa) psi. To determine the effect of different slumps on development length, prisms with different slumps of 3 in. (7.6 cm), 6 in. (15.2 cm), and 9 in.

(22.9 cm) were manufactured and all other parameters were kept constant in prisms. All prisms were tested in three-point bending at different spans to obtain estimations of development length based on type of reinforcement, concrete-release strength, and concrete slump. Lastly, a design equation was developed based on experimental data for prediction of development length.

In the last phase of load tests, cyclic-loading tests were conducted on the prisms manufactured with wires to evaluate the bond performance of wires with different indentation types under cyclic loading.

A total of 210 load tests, including 14 cyclic tests, were conducted. The monotonic-load tests revealed a large difference in the development length of pretensioned concrete members manufactured with different wire/strand types and different concrete-release strengths. Also, the cyclic-load tests revealed a significant difference in bond performance of different wire types under cyclic loading compared to monotonic loading.

1. Introduction

1.1 Background

The first major utilization of prestressed concrete ties in North America was in 1966 (Hanna, 1979). But initial interest for their use in the United States and Canada in the late 1960s rapidly vanished when early designs did not perform well. During the 1970s, the American Rail Engineers and Maintenance Association (AREMA) improved specifications, which resulted in concrete ties with higher flexural-moment capacities. Higher tie-bending moments were achieved by initiating use of indented prestressing steel and elastic fasteners with iron shoulders cast into the tie to deliver positive gauge control (White, 1984).

The main tasks of railroad ties as an integral part of railroad tracks include preventing rails from any lateral or longitudinal displacements. Thus, their main function is stabilization of rails (Yu & Jeong, 2014). Use of prestressed concrete railroad ties is growing in the United States as the railroad industry is becoming more efficient. Records to date show that pretensioned concrete crossties have produced a more economical design and better structural behavior, which improves overall stability and performance of the railroad track (Lu Z. , Boothby, Bakis, & Nanni). Prestressed concrete railroad crossties have indicated many desirable features over wood crossties. These include long life expectancy, environmental friendliness, and reduction in fuel consumption of trains. Considering these advantages, many track owners are switching from wood crossties to prestressed concrete crossties (Bodapati, et al., 2013).

1.2 Problem Description

The bond between prestressing steel and concrete is a crucial factor contributing to the integrity of pretensioned concrete members (Russel & Burns, 1993). This is different from post-tensioned members, where total compressive force is fully transferred to the concrete cross section by means of end anchorage and bearing plates (Ghosh & Fintel, 1986). In pretensioned, prestressed concrete crossties, transfer length (Lt) is the length required to transfer the prestressed force from prestressing steel to the concrete. Loading a pretensioned member to its ultimate flexural capacity requires a secondary length beyond the transfer length in order to develop the prestressing steel stress from the effective prestress to stress at nominal flexural capacity. This secondary bond length is called flexural bond length, and the development length (Ld) is the sum of the transfer length and flexural bond length. Transfer and development length of pretensioned concrete crossties are of the most important parameters in design of pretensioned concrete members (Ghosh & Fintel, 1986). Transfer and development length of pretensioned concrete crossties are important parameters in the design of pretensioned concrete members. Thus, as design for ultimate capacity under external loads is approached, the concept of development length should be applied. Not providing sufficient development length for prestressing steel causes the pretensioned member to fail by bond rather than by flexural. Bond failures take place in three stages:

1. Tendon slippage, with the surrounding concrete, initiates at the time flexural cracks occur.
2. Bond slip propagates along the entire development length.

3. Mechanical interlock between the wire surface and surrounding concrete is destroyed (Ghosh & Fintel, 1986).

The transfer of prestress force from prestress tendons to concrete at a consistent length and the achievement of nominal-moment capacity over a predictable development length are important requirements to the performance of pretensioned concrete members (Logan, March-April 1997).

Concerns arose with the development length equation for seven-wire strands recommended by Building Code Requirements for Structural Concrete (ACI 318-95) and Commentary, and the American Association of State Highway and Transportation Officials 1998 (AASHTO), as several bond failures of pretenstioned members have been observed since the approval of the equation. Martin and Scott concluded the equation was not conservative and described the bond failure of a pretensioned member in a load test as 85 percent of nominal-moment capacity (1976). Also, Talat and Paul described a failure in bond in a pretensioned concrete beam which violated the standards given by ACI 318-95 and AASHTO equation (1977). After observance of all of these test results, the Federal Highway Administration (FHWA) required the development length calculated by ACI equation to be increased by 60 percent, and many tests were then started to determine actual transfer and development length of strands in pretensioned concrete (Logan, March-April 1997). At the time of this study, uncertainties about the development length of smooth prestressing strands in pretensioned, prestressed concrete members still exist.

Moreover, behavior of different types of indented strands and prestressing wires under monotonic and cyclic loading was essentially undocumented. Fatigue is the process of increasing internal structural deterioration in a material under cycles of repetitive stresses. Crack growth and fracture of steel or concrete may occur if the stress quantities are adequately large. A significant number of researchers have studied the fatigue behavior of prestressed concrete beams while developing experimental techniques. These studies were mainly conducted to assess the fatigue strength of prestressed concrete beams. There is a little knowledge on how to predict the growth in deflection and crack widths based on the constituent materials properties for prestressed concrete beams (Balaguru, 1981). The need for this knowledge is growing as utilization of prestressed concrete increases in different structures such as bridges and railroad ties. Kaar noted the bond between prestressing steel and surrounding concrete is typically adequate for uncracked, pretensioned, prestressed members subjected to monotonic or cyclic loading. However, for pretensioned crossties subjected to cyclic loading that produce large bending moments in end regions of the member, large transfer lengths of the prestressed tendon can reduce the prestressed force and thus the cracking moment. In this situation, early bond failure of the pretensioned member is probable under cyclic loading with a crack in or near the transfer length (1975).

1.3 Objectives

Load tests were conducted on pretensioned concrete prisms cast with 13 different 5.32-mm-diameter prestressing wire types and six different strands (four, seven-wire strands and two, three-wire strands) used in the manufacturing of pretensioned concrete railroad ties worldwide. The tests were specifically designed to evaluate development length and bonding performance of these different reinforcements. The prestressing wires were denoted “WA” through “WM,” and indentation types included smooth, spiral, chevron, diamond, and two-dot and four-dot.

In the second phase of the research, a study was conducted to determine the effect of concrete-release strength and slump on development length and flexural capacity of members utilizing five different 5.32-mm-diameter prestressing wires commonly used in the manufacturing of prestressed concrete railroad ties worldwide. To understand the effect of concrete-release strength and slump on development length, all prisms were identical except for wire type, compressive strength at the time of de-tensioning, and slump.

In the last phase of the bond performance studies, the tests were specifically designed to evaluate the bond performance of wires with different indentation type under cyclic loading.

1.4 Scope

Prestressing wires used in this study were denoted "WA" through "WM," and indentation types included smooth, spiral, chevron, diamond, and two-dot and four-dot. Four wires were embedded into each concrete prism, which had a 3.5-in. (88.9-mm) x 3.5-in. (88.9-mm)-square cross section. The wires were initially tensioned to 7,000 pounds (31.14 KN) and gradually de-tensioned when t concrete compressive strength reached 3,500 (24.13 MPa), 4500 (31.03 MPa), and 6,000 (41.37 MPa) psi. A consistent concrete mixture with Type III cement, a water-cement ratio of 0.32, was used for all prisms.

Prisms were tested in three-point bending at different spans to obtain estimations of the development length of each type of reinforcement. Two identical 69-in.-long (175.3-cm) prisms were load-tested at both ends for each reinforcement type evaluated. First, prisms were tested at 20 in. (50.8-cm) from one end and 13 in. (33-cm) from the other end. Whereas, the second prisms were loaded at 16.5 in. (41.9-cm) from one end and 9.5 in. (24.1-cm) from the other end. Thus, a total of 52 load tests (13 wire types x four tests each) were conducted in this study.

During each test, a concentrated load with the rate of 300 lb/min (1334 N/min) was applied at mid-span until failure occurred. Values of load, mid-span deflection, and wire end-slip were continuously monitored and recorded. Plots of load-vs-deflection were then compared for prisms with each wire type and span. Maximum experimental moment was also calculated for each test.

The same test procedure was used to evaluate the effect of concrete-release strength and slump on development length and flexural capacity of prisms made with wires.

For prisms fabricated with strands, prisms were loaded in three-point bending to determine the effect of strand-indentation types and concrete-release strengths on the ultimate-bond characteristics of pretensioned ties. Two out of three testing prisms were tested at only one end, and one was tested at both ends.

To Compare the behavior of different wires under cyclic loading with monotonic loading, for each type of wire, one 69-in.-long (175.3-cm) prism was tested in four-point bending under the cyclic load, and one in three-point bending under monotonic load at a 20-in. (50.8-cm) embedment length. For cyclic load tests, the prisms were supported by two rollers spanning 45 in. (114.3 cm), and the load was applied on a spreader beam set on the top of the test prism. The prism setup and loading configuration were symmetric, and load was applied to the prism from spreader beam to two bearings spaced 15 in. (38.1 cm) apart. During each test, a concentrated load with the rate of 250 lb/min (1112 N/min) was applied until two cracks were observed at the maximum- moment region on the test prisms (region between two bearings).

Once cracks were observed, the load was held constant for three minutes at the cracking load. After this, the load started to cycle between 400 lb (1779 N) to 4,000 lb (17790 N), at a frequency of 3 Hz. The test was designed to go through 200,000 cycles. For prisms able to finish 200,000 cycles of load, the procedure was to unload to zero and start loading the prism at the rate of 250 lb/min (1112 N/min) until the prism failed. Values of load, mid-span deflection, and wires' end-slip were continuously monitored and recorded during each test.

1.5 Organization of the Report

This report is organized into seven chapters. Following Chapter 1, Chapter 2 includes a literature review of work conducted on pretensioned, prestressed concrete members in the past. Chapter 3 includes methods used for running the load tests and experimental program. Chapter 4 includes results of loading tests from different phases of the research project. In Chapter 5, models are developed based on experimental data to predict development length of pretensioned members made with different wires and concrete-release strengths. Conclusions and recommendations are offered in Chapter 6. Lastly, references are in Chapter 7.

2. Literature Review

2.1 The Concrete Tie

2.1.1 Background

Competition among varying modes of transportation is leading the railroad industry to strive for improvements. Railroads are expected to increase the tonnage they can transport via railway tracks. Increasing demands on the railroad tracks require railroads with high-quality engineering track systems. Utilization of concrete ties is being put into place for the advancement of railroad tracks. Earlier utilization of a major number of concrete ties in North America include the Florida East Coast, AMTRAK, and CN Rail. Burlington Northern Railway was one of the largest initial users of concrete ties, installing 150,000 prestressed concrete ties in 1986 (Buekett, 1987). Use of concrete ties in recent years in the United States has increased. This is explained by the better consistency in product quality that can be reached by use of concrete, the natural suitability of concrete ties for use with continuously welded rails, and the necessity for better performance of track systems at high-speed operations. Concrete ties can lead to desirable structural and economical designs and can improve the overall stability of the railroad track (Hanna, 1986).

Initial interest for utilization of concrete ties in the United States and Canada in the late 1960s rapidly vanished when early designs did not perform well. This was due to multiple causes: a fastening system which was weak against lateral loads, ties with insufficient flexural moment capacity, a weak bond existing between prestressing steels and the surrounding concrete, pull-out and corrosion of the fastenings, and the difficulty involved in fastenings maintenance in icy ballast. During the 1970s, the American Rail Engineers and Maintenance Association (AREMA) improved specifications, which resulted in concrete ties with higher flexural-moment capacities. Higher tie-bending moments were achieved by initiating use of indented prestressing steel and elastic fasteners with steel shoulders cast into the tie to deliver positive gauge control (White, 1984).

2.1.2 Concrete tie vs wood tie (advantages of concrete tie)

The main benefits from utilization of concrete ties are to significantly reduce maintenance costs and to avoid frequent interruption of traffic for maintenance purposes. Savings obtained from lower maintenance costs may not justify the larger capital investment in concrete tie tracks. However, other maintenance costs such as diverting or interrupting traffic are significant and should be considered. Moreover, life expectancy under service loads for concrete ties is longer than that of wood ties. Another factor that improves economical behavior of tracks using concrete ties is the possibility of energy savings due to less rolling resistance. The stiffer track structure resulting from concrete ties provides a lower rolling resistance and an improved ride quality, along with higher safety compared to wood ties.

Interest in use of concrete ties is increasing in the U.S. railroad industry. This growth can be explained by consistency in product quality, low annual cost, and outstanding performance. Records to date not only show concrete ties are economically and technically reasonable, but

they provide an excellent track system that guarantees high performance and safety (Hanna, 1986).

2.2 Transfer Length vs Development Length

In pretensioned, prestressed concrete, prestress force transfers by bond to the concrete, the length required from pretensioned member end to the point the member is at its ultimate flexural capacity is called development length. Development length consists of two lengths:

1) Transfer length,L_t, is the minimum length from member end required to transfer effective prestress tension, f_{pe}, from prestressing steel to the concrete through bond.
2) Flexural bond length, L_{fb}, is a distance beyond the transfer length required for the prestressing steel to reach a tension stress equal to its ultimate-limit state, f_{ps}.

Transfer length can be determined from strain distribution along the length of the member in pretensioned members after transfer of prestress force. Two methods measure the strains: 1) strain distribution on the prestressing steel, and 2) strain distribution on the concrete surface along the line of prestressing steel. However, there are drawbacks to the first method since the strain gauges may be damaged during concrete casting and also at the time of prestress steel de-tensioning. Moreover, installation of strain gauges on the steel may lower adequate bonding between concrete and steel (Si, et al., 2013).

2.2.1 Analytical models to calculate transfer length

Bond can be defined as a property that tightly holds the embedded steels to prevent them from sliding longitudinally along the concrete member (Vazquez-Herrero, Martinez-Lage, & Martinez-Abella, 2013).

Guyon recommended a formula that relates transfer length proportionally to prestressing draw-in and is inversely proportional to initial prestressing strand stress (1953):

$$l_t = \alpha . \delta . {E_p}/{f_{pi}} \qquad \text{(Equation. 1)}$$

where E_p is the modulus of elasticity of the prestressing strand,

δ is the strand draw-in,

and α is the Guyon coefficient which reflects a profile of stress distribution of the concrete in the transfer length ($\alpha = 2$ for a constant bond stress, $\alpha = 3$ for a linear distribution of the bond stress).

To estimate transfer length, another equation was proposed by Balaz, using the same variables (1993):

$$l_t = 2 . \alpha . {E_p}/{[f_{pi}(1 - b)]} \qquad \text{(Equation. 2)}$$

where b is an experimental variable between zero and one, dependent on concrete type and prestressing strand.

Assuming prestressing stress follows Hooke's law, value of strand draw-in immediately after transfer can be estimated by Equation 3:

$$\delta = \int_0^{l_t} [\frac{f_{pi} - \sigma_p(x)}{E_p}] \, dx - \int_0^{l_t} \varepsilon_c(x) dx \qquad \text{(Equation. 3)}$$

where $\varepsilon_c\ (x)$ is the instantaneous longitudinal strain of the concrete surrounding prestressing steel because of prestress release at x (positive compressive strain)

$\sigma_p(x)$ is the prestressing reinforcement stress after transfer at the cross section located at a distance x from the end.

f_{pi} is the prestressing strand stress immediately before transfer (Vazquez-Herrero, Martinez-Lage, & Martinez-Abella, 2013).

2.2.2 Existing experimental methods to measure transfer length

Three common experimental techniques are currently being used to determine transfer length. These are based on the following measurements: 1) prestressing steel end-slip measurements, 2) longitudinal strain profile of the concrete surface, and 3) prestressing reinforcement stress (or force).

1) The first technique is based on the Guyon theory, which relates transfer length to prestressing steel end-slip (δ) during prestress transfer. Guyon proposed the following equation from a theoretical analysis (1953).

$$L_t = {\alpha . \delta}/{\varepsilon_{pi}} \qquad \text{(Equation. 4)}$$

- In this equation, L_t is the transfer length.
- δ is the prestressing reinforcement end-slip at the free end of the pretensioned concrete member.
- ε_{pi} is the initial prestressing reinforcement strain.
- The α coefficient represents the shape of the bond stress distribution over transfer length ($\alpha = 2$ for uniform bond stress distribution and $\alpha = 3$ for linear descending bond stress distribution).

2) The second method focuses on analysis of strain profiles of the concrete surface after prestress transfer versus distance from the member free end. Recent systems have been enabled to measure concrete surface strains and calculate transfer length (Wu, Zhao, Beck, & Peterman, 2011). However, strain gauges are typically attached along the sides of the pretensioned member prior to de-tensioning. After release, compressive strains in the concrete along the length of the member are measured through strain gauges. These strains' profiles increase until they reach a plateau. Transfer length can be determined from the concrete surface strains' profile (Mahmoud, Rizkalla, & Zaghloul, 1999) by

using the slope-intercept method (Deatherage, Burdette, & Chew, 1994), or by the 95% average maximum strain (AMS) method (Russel & Burns, 1996). Smoothing techniques are normally implemented for these profiles (Lu Z. , Boothby, Bakis, & Nanni, 2000).

3) The third method is to determine the prestressing steel stress (or force) profile. The strain in prestressing steel is measured through the attachment of electrical-resistance strain gauges to the surface of the prestressing steel. Strain measurements at the prestressing steel surface can be converted to stress by applying the modulus of elasticity of prestressing steel. Using this method, a stress profile for prestress force in reinforcement is attained and the transfer length is the distance from the member end to the point that prestress force reaches the plateau (Marti-Vargas, Caro, & Serna, 2013). However, the attachment of strain gages to the prestressing tendons serves to eliminate bond with the surrounding concrete in the vicinity of the gages, and theoretically results in longer-than-normal transfer length values being determined when this method is employed.

2.2.3 Hoyer effect

When a straight tendon is pulled, its diameter decreases due to Poisson effect, and as the stress is removed, the tendon returns to its original diameter. The lateral expansion and regain in the steel's diameter, which causes radial forces, improves the bond strength (in the sense of prestress force transfer to the concrete) and contributes to transferring the force from the prestressing tendon to the concrete. This enhancement in bond strength and transfer of prestress force is referred to as the Hoyer effect (Briere, Harries, Kasan, & Hager, 2013).

Due to the Hoyer effect at the ends of members, wedging of the prestressing steel occurs, which improves the bond capacity. The opposite effect happens in the flexural bond length when the member is under service loads. Under service loads, friction between the prestressing cable and concrete reduces due to reduced contact between the concrete and cable. Reduced contact is the result of decreased diameter of the cable due to the Poisson effect. The result is reduced bond. In those sections of pretensioned member, where the prestress force goes beyond the initial value f_{pi}, tensile hoop stresses of concrete are barely created. Due to the Hoyer effect, the bond capacity between the concrete and steel in the transfer length is larger than that occurring in the flexural-bond length, which causes the slope of the pretensioning force in the transfer length to be steeper than the slope of pretensioning force of the cable in the flexural-bond length. For this reason, structural concrete requirements propose a bilinear model for prestress force in the development length, with a steeper line for the transfer length than for the flexural-bond length. Figure 1 shows the transfer length and the flexural-bond length (Vazquez-Herrero, Martinez-Lage, Aquilar, & Martinez-Abella, 2013).

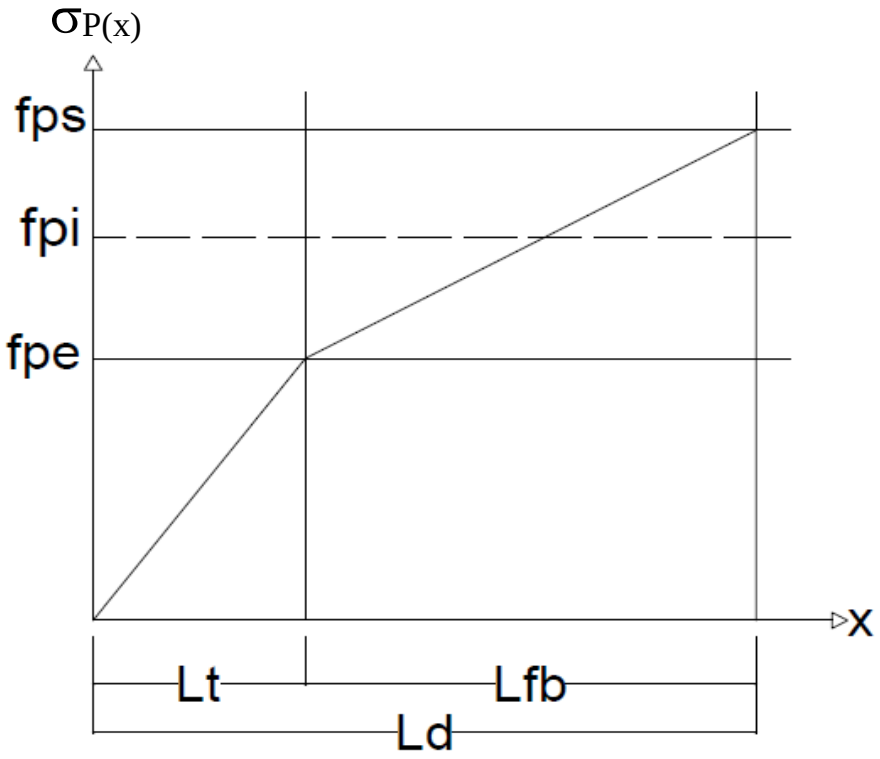


Figure 1. Transfer length and flexural-bond length [after: (Vazquez-Herrero, Martinez-Lage, Aquilar, & Martinez-Abella, 2013)]

Various experimental methods exist for characterizing bond behavior of pretensioned steels:

- Tests measure transfer length through manufacturing and application of pretensioned elements with prestressing steel at the center of the section.
- Tests determine development length by manufacturing and flexural-load testing of to-scale pretensioned, prestressed beams with eccentric prestressing.
- Tests on samples define bond behavior of pretensioned strands, which can be categorized as follows:

-Pull-out tests, in which a sample is made with concrete around a strand with or without previous tension, and after the concrete hardens, the tension is increased from one end of the sample.

-Push-in testing, in which a sample is made with a strand that had been previously stressed at a determined tension and surrounded by concrete, and after the concrete is hardened, the test is executed by slowly reducing pretensioning force on the upper end, which creates a gradient of the pretensioning force along the bonded length of the sample.

-Tests combine pull-out and push-in methods (Vazquez-Herrero, Martinez-Lage, Aquilar, & Martinez-Abella, 2013).

In recent years, a large number of experimental tests were conducted in many laboratories around the United States to characterize the bond behavior of prestressing strands by running three types of tests: large block pull-out tests (also known as Moustafa pull-out tests) (Logan, March-April 1997), Post-Tensioning Institute (PTI) bond tests (Post-Tensioning Inistitute, 1996), and North American Strand Producers (NASPs) bond tests (Ramirez & Russel, 2007). Results from different laboratories were then compared to assess the reproducibility of each test. Also, a Comparison was made between results of each test, and transfer and development lengths determined by manufacturing and testing of rectangular section beams and AASHTO beams. The study indicated the NASP bond test is the most reproducible. The NASP bond test is also the most descriptive of bonding behavior of prestressing strands (Vazquez-Herrero, Martinez-Lage, Aquilar, & Martinez-Abella, 2013).

2.3 Modeling stress-strain curve for wires - Power Formula

The stress-strain behavior of 5.32-mm-diameter prestressing wires was modeled by Chen at Kansas State University (Chen, 2016). This work resulted in an improved Power Formula that accurately represents both the linear and post-yield behavior of the wires. This formula used to calculate section nominal-moment capacity of prism ends as opposed to using the PCI prestressing steel stress-strain curve. The design-oriented Power Formula gives more accurate stress-strain curves for wires as opposed to the PCI prestressing steel stress-strain curve, which was originally developed to model the stress-strain curve for seven-wire strands. The design power formula was developed to model the stress-strain curve for wires with ultimate tensile strength (f_{pu}) of 250 ksi to 300 ksi (1,723.7 to 2,068.4 MPa). Test results showed the minimum elongation limit of 4% strain is appropriate (Chen, 2016). Also, ultimate tensile strength (f_{pu}) and Young's modulus (E_p) of each wire were determined through laboratory tests at Kansas State University (Chen, 2016). It should be noted that for WA, WC, and WK wires, values of ultimate tensile strength (f_{pu}) and Young's modulus (E_p) were obtained from manufacturer Mill Certs. The following steps were taken to calculate the stress in prestressing wires (f_{ps}) using the design-oriented power formula:

1) Having ultimate tensile strength (f_{pu}) and Modulus of Elasticity (E_p) of each wire from either laboratory tests or manufacturer Mill Certs, Kf_{py}, $f_{py}$and constant Q were calculated using the following equations:

$$Kf_{py} = 1.1607 f_{pu} - 60.0118 \quad \text{(Equation. 5)}$$

$$f_{py} = 1.0017 f_{pu} - 25.7794 \quad \text{(Equation. 6)}$$

$$Q = \frac{f_{pu} - Kf_{py}}{\varepsilon_{pu} E_p - Kf_{py}} \quad \text{(Equation. 7)}$$

2) Setting f_{ps} and f_{py} equal, the power formula should be solved for R^* by these iterations:

$$f_{ps} = \varepsilon_{py} E_p \left[Q + \frac{1-Q}{\left(1+\left(\frac{\varepsilon_{py} E_p}{K f_{py}}\right)^R\right)^{1/R}} \right] \quad \text{(Equation. 8)}$$

In Equation. 8, ε_{py}, the yield strain, is equal to 0.01 and values of Kf_{py}, f_{py} and constant Q were calculated by Equation. 5, Equation. 6 and Equation. 7, respectively. Substituting all values in Equation. 8 and solving the equation for R by iterations, parameter R can be determined.

Plugging R, wire's Young's modulus (E_p), total strain in prestressing wire (ε_{ps}), calculated Kf_{py} and constant of Q into the power formula, stress in prestressing wire (f_{ps}) can be computed.

$$f_{ps} = \varepsilon_{ps} E_p \left[Q + \frac{1-Q}{\left(1+\left(\frac{\varepsilon_{ps} E_p}{K f_{py}}\right)^R\right)^{1/R}} \right]$$

In calculation of nominal-moment capacity of prism sections, stress in prestressing wires (f_{ps}) was calculated using the above steps. Young's modulus and ultimate tensile strength of each wire obtained from laboratory tests and Mill Certs are summarized in the Table 1.

Table 1. Mechanical properties of each wires obtained from laboratory tests [after: (Chen, 2016)]

Wire type	Average Young's modulus (ksi)	Average ultimate tensile strength (ksi)
[WA]	29700	295.5
[WB]	29418	296.0
[WC]	28400	287.0
[WD]	29763	281.5
[WE]	29057	281.7
[WF]	28778	279.4
[WG]	28889	267.5
[WH]	30882	290.4
[WI]	29254	282.3
[WJ]	28298	285.2
[WK]	29430	283.0
[WL]	29696	284.1
[WM]	29721	287.0

2.4 History of Development-Length Expressions

2.4.1 (AASHTO, 1998)/ (ACI 318R-02, 2002)

Development length equation of

$$L_d = (f_{ps} - \frac{2}{3} f_{se}) d_b \qquad \text{(Equation. 9)}$$

was originally derived by ACI Committee 323, at the time to be included in the 1963 ACI Building Code. AASHTO adopted the equation in 1973. The majority of data used to develop this equation was from tests conducted at the Portland Cement Association (PCA) by Hanson and Kaar (1959). Hanson and Kaar explained that in a pretensioned member, flexural cracks occur and as the load increases, flexural cracks progress from the point of maximum stress toward transfer length (1959). A bond slip will happen if the flexural cracks reach to the end of transfer length. They conducted tests on 47 pretensioned rectangular beams and calculated minimum embedment length required to reach the breaking strength of Grade 250 strands of 1/4, 3/8, and 1/2 in. (6.4, 9.5 and 12.7 mm) diameters.

2.4.2 (Talat & Paul, September-October 1977)

Talat & Paul recommended a more conservative equation for prediction of development length after they witnessed a bond failure following adoption of the current code (1977).

$$L_d = 1.5 \frac{f_{si}}{f'_{ci}} - 4.6 + 1.25(f_{ps} - f_{se}) d_b \qquad \text{(Equation. 10)}$$

where f_{si} (ksi) is stress in the strand immediately after transfer,

f'_{ci} (ksi) is concrete compressive strength at transfer, limited to 8 ksi (55.2 MPa).

f_{ps}(ksi) is stress in the prestressing steel at ultimate strength.

d_b (in) is the diameter of the prestressing reinforcement

f_{se} (ksi) is the stress in the reinforcement after all prestress losses

Results from development-length evaluations in 1986 at North Carolina State University (NCSU) indicated considerably larger development lengths for uncoated, pretensioned strands than predicted by the ACI equation. Results from the NCSU study and the higher pretensioning stresses in current precast practices led the Federal Highway Administration (FHWA) to question the development-length equation in ACI/AASHTO. In October 1988, FHWA applied the following restrictions to use of seven-wire strands in bridges:

1) 0.6 -in. (15.2-mm) strands should not be used in pretensioned concrete members.
2) Center-to-center spacing of strands should be at least four times the nominal strand's diameter.
3) Development length of strands with 9/16-in. (14.3-mm) diameter and less, should be increased by 60% after being calculated by the ACI/AASHTO equation.

The FHWA, requiring a 60% increase in development lengths obtained from current code, initiated many research projects. These were the origin of several new strand-development-length expressions (Buckner, March-April 1995).

2.4.3 (Mitchel, Cook, Khan, & Tham, May-June 1993)

The development-length expression in ACI/AASHTO is based on test data from (Hanson & Kaar, 1959) and (Kaar, LaFraugh, & Mass, 1963). There is concern about the current transfer and development-length expression since it was developed based on some standards that may not be applicable to current practices. In earlier studies by (Hanson & Kaar, 1959) and (Kaar, LaFraugh, & Mass, 1963) the code expression based on a strand with ultimate strength of 250 ksi (1720 MPa), which was pulled to $0.7f_{pu}$ in the bed, was used. Also, concrete strengths were significantly lower compared to high-strength concretes being used in current practices, and tests have been conducted on strands with diameters larger than 0.5 in. (12.7 mm). Thus, the ACI/AASHTO expression is questionable, since in current practice, a large amount of low-relaxation strand with f_{pu} of 270 ksi (1860 MPa) is used with higher bed stresses up to ($0.8f_{pu}$). In addition, another parameter that affects transfer and development lengths is high-strength concrete.

Prisms were fabricated with different 28-day compressive strengths of concrete(f_c'), different sizes of strands d_b, and different concrete-release strengths (f_{ci}'). These were then load- tested at different embedment lengths in three-point and four-point bending. Values of (f_c') included 4500 (31 MPa), 6240 (43 MPa), 9430 (65 MPa), 10880 (75 MPa), and 12900 (89MPa) psi. Strands utilized in fabrication of prisms had diameters of 3/8 (9.5 mm), 1/2 (12.7 mm), and 0.62 (15.7 mm) in. Values of targeted release strengths were 3000 (21 MPa), 3975 (27 MPa), 6950 (48 MPa), 7225 (50 MPa), and 7310 (50 MPa) psi.

Load tests were conducted at different embedment lengths on prisms with different concrete and strand properties. Following expression as a modification to the ACI Code, the development-length equation was proposed by Mitchel, Cook, Khan, & Tham in ksi and in. units (1993):

$$L_d = 0.033 f_{pi} d_b \sqrt{\frac{3}{f_{ci}'}} + (f_{ps} - f_{se}) d_b \sqrt{\frac{4.5}{f_c'}} \qquad \text{(Equation. 11)}$$

The proposed expression reflects the effect of concrete compressive strength both at transfer and service on the development length of pretensioned concrete members. The first term of this expression represents transfer length. From this equation, the following is concluded:

1) An increase in compressive strength of concrete at the time of de-tensioning(f_{ci}') decreases transfer length.
2) An increase in compressive strength of concrete(f_c') decreases flexural-bond length. Thus, strand development length decreases.

2.4.4 Purdue University tests (Abdalla, Ramirez, & Lee, 1993)

Full-scale AASHTO bridge girders and box beams with fully bonded and debonded strands were load-tested. Fully bonded girders failed at two-thirds to three-quarters of their nominal-moment capacities at an embedment length equal to 1.2 times of the calculated development length from

the ACI/AASHTO equation. Specimens achieved their nominal- moment capacity at 1.8 times the calculated development length from the ACI/AASHTO equation. This led to the conclusion that flexural controls, 1.7 times the calculated development length from the ACI/AASHTO equation, would be adequate to develop sufficient bond between concrete and prestressing strands.

2.4.5 (Deatherage, Burdette, & Chew, January-February 1994)

After an FHWA memorandum in 1988 limiting use of certain sizes of seven-wire strand in pretensioned concrete girders, this PCI-funded project was initiated to evaluate the effect of various seven-wire strand diameter sizes on transfer and development lengths of pretensioned concrete members. Strands in test specimens included 1/2 in. (13 mm), 1/2 in. special (13.3 mm), 9/16 in. (14 mm), and 0.6 in. (15 mm) diameters.

All pretensioned beams were 31 ft. (9.45 m) long and all prestressing steel utilized was seven-wire, low-relaxation strand with ultimate strength (f_{pu}) of 270 ksi (1860 MPa). Two specimens were fabricated for each diameter of strand.

Forty load tests were conducted on 20 test specimens using a hydraulic actuator. Deflection and strand end-slip were measured using LVDT and mounted dial gauges on the bottom strands. Bending moments were calculated from applied load on the simply supported beam. Average of cracking moments (M_{cr})was approximately 66 % of maximum experimental moment.

Development length, evaluated from monotonic load tests to failure, indicated the ACI/AASHTO provisions for prediction of development length are slightly unconservative. Results of a number of other studies and a study done by Deatherage, Burdette, & Chew, showed a flexural-bond length approximately 42 % larger than the flexural-bond length calculated by the ACI/AASHTO expression (1994). Twenty, full-scale AASHTO Type II girders were tested and the University of Tennessee at Knoxville (UTK) proposed the following expression for development length:

$$L_d = \frac{f_{si} d_b}{3} + 1.5(f_{ps} - f_{se}) d_b \qquad \text{(Equation. 12)}$$

In the proposed equation, transfer length was increased by replacing f_{si} with f_{se}. Hence, development length was increased as well. Also, development length was increased through increasing flexural-bond length by 50 %.

2.4.6 (Buckner, March-April 1995)

In 1988, research conducted at North Carolina State University showed larger development lengths compared to those calculated based on AASHTO equation, and because of the incompatibility between the strand used in the research resulting in AASHTO equation and the strand currently in use, the Federal Highway Administration (FHWA 1988), in a memorandum, forbade use of 15-mm (0.6-in)-diameter strand in pretensioned members. Furthermore, center-to-center spacing was limited to not less than four times the strand's diameter. The FHWA memorandum also required an increase of 60% in development length of fully bonded strands in pretensioned members. Buckner proposed a new equation for calculation of transfer and development length after considering all previous research since the 1988 FHWA memorandum

(1994, 1995). Buckner proposed a conservative equation for transfer and development length. The transfer length equation was:

$$l_t = {f_{si} d_b}/{3} \quad \text{(Equation. 13)}$$

and Buckner's equation for development length was as follows:

$$l_d = l_t + \lambda \left(f_{ps} - f_{se}\right) d_b \quad \text{(Equation. 14)}$$

where f_{si} (ksi) is stress in the strand immediately after transfer,

f_{ps} (ksi) is the stress in prestressing reinforcement at the nominal strength

f_{se} (ksi) is the stress in the reinforcement after all prestress losses

d_b(in) is the diameter of the prestressing reinforcement

l_t (in) is the transfer length, and

λ was calculated as $1.0 \leq [\lambda = \left(0.6 + 40\varepsilon_{ps}\right)] \leq 2.0$

where ε_{ps} is strain in the prestressing steel at nominal strength of the section.

In May 1996, after reviewing the most recent research and conducting their own research program, the FHWA changed the memorandum of 1988 to allow use of 15-mm (0.6-in.)-diameter strand in pretensioned members. Permissible center-to-center spacing for 15 mm (0.6 in.) and the diameter of the strands was 50.8 mm (2 in). The 60% increase in development length was still maintained.

2.4.7 (Lane, 1998)

Lane proposed a new FHWA equation for transfer and development length. The transfer-length expression was written as follows (1998):

$$l_t = {4 f_{pt} d_b}\Big/{f_c'} - 21 \quad \text{(Equation. 15)}$$

where f_{pt} (ksi) is stress in the prestressing strand immediately before transfer

f_c' (ksi) is the concrete compressive strength, limited to 10 ksi (69.0 MPa), and

d_b (in) is the diameter of the prestressing reinforcement

Lane's equation for the development length was written as follows:

$$l_d = l_t + [6.4 \frac{(f_{su} - f_{se}) d_b}{f_c'} + 26] \quad \text{(Equation. 16)}$$

where f_{su}(ksi) is stress in the prestressing steel at ultimate strength.

f_{se} (ksi) is the stress in the reinforcement after all prestress losses, and

l_t (in) is the transfer length (Lane, 1998).

2.4.8 (Lu Z. , Boothby, Bakis, & Nanni, March-April 2000)

Lu Z., Boothby, Bakis, & Nanni conducted experiments on 42 pretensioned prisms manufactured with FRP tendons and seven-wire steel strands (2000). From these 42 prisms, 12 prisms were fabricated with seven-wire prestressing steel and 10 prisms were manufactured for each of three FRP tendon materials. All prisms had one tendon. Two prisms were manufactured with concentrically placed tendons for the purpose of transfer-length measurement, and 40 rectangular prisms were fabricated with prestressing tendons placed eccentrically. Prisms made with FRP tendons had 3.5-in. x 7-in. rectangular cross sections and were 10 ft long. No transverse reinforcement was provided for the specimens.

The concrete mix used for prism fabrication contained 750 lb/yd3 of Type III Portland cement, and 131 lb/yd3 of fly ash with a water-to-cementitious materials ratio of 0.36. Compressive strength of the concrete at the time of de-tensioning was 5570 psi (38.4 MPa). FRPs used in the specimens included lead-line tendons (CL), an indented tendon with spirals over the length of tendons, Technora tendons (AT), aramid yarns twisted spirally around straight yarns to enhance bond strength of tendons, and a non-commercial tendon (CS) produced only for this study. Its purpose is to be used as a reference in this or any future studies.

Development lengths were determined through three-point, bending-load tests. A hydraulic jack was used to conduct the load test and apply load on prisms at different embedment lengths. Using a linear variable differential transformer (LVDT), the prestressing tendon end-slip was measured. Various embedment lengths were obtained by applying the load at different distances from the prism end.

For each test at different embedment lengths, force in the prestressing tendon was calculated using the flexural model of a pretensioned concrete beam. This procedure is explained in detail by (Lu Z. , 1998). A graph was plotted for force in the tendon at failure versus embedment length of the test for different embedment lengths. For all embedment lengths tested in this study, all prisms failed in bond or concrete crushing. Thus, a linear trend appeared that as embedment length increases, force in the tendon increases as well. The least embedment length where a flexural mode of failure occurred was considered as the development length for that FRP tendon and f_{ps} was calculated from the flexural model. The calculated f_{ps} was plugged into the development-length models proposed by (AASHTO, 1998), (ACI 318-99, 1999), (Deatherage, Burdette, & Chew, 1994), (Cousins, Johnson, & Zia, July-August 1990), (Shahawy, Issa, & Batchelor, May-June 1992), (Buckner, March-April 1995), (Mitchel, Cook, Khan, & Tham, May-June 1993), and (Mahmoud, Rizkalla, & Zaghloul, July-August 1999) and comparisons were made. All mentioned development-length models are discussed in this chapter.

Development length can be conservatively estimated for FRP tendons by the modified ACI formula for FRP tendons (Lu Z. , Boothby, Bakis, & Nanni, March-April 2000):

$$L_d = \frac{1}{3} f_{se} d_b + \frac{3}{4}(f_r - f_{se}) d_b \qquad \text{(Equation. 17)}$$

d_b =Diameter of tendon

f_r =Rupture strength of tendon

f_{se} =Effective prestress of tendon

Using this ACI-modified model, development lengths for FRP tendons were closer to experimental results in this study. Test results by Lu Z. , Boothby, Bakis, & Nanni indicated that despite the variation in FRP and steel properties, maximum development lengths evaluated were approximately equal for all three types of FRP materials and steel strands experimented on in this study (2000). Moreover, substituting FRP strand rupture (f_r) for strand stress at nominal strength (f_{ps}), the ACI equation predicts conservative development lengths. Models developed to predict development length of steel tendons did not provide good development length predictions for FRP tendons and overestimated FRP development lengths. The reason for this was higher bond stresses of FRP tendons compared to steel tendons (Lu Z. , Boothby, Bakis, & Nanni, March-April 2000).

2.4.9 (Peterman, Ramirez, & Olek, September-October 2000)

In a study conducted by Peterman, Ramirez, & Olek, development lengths of members manufactured with semi-light-weight concrete were evaluated rather than members manufactured with normal-weight concrete (2000).

Twelve pretensioned beams, including six, single-strand and six, multiple-strand beams, were load-tested to evaluate development length. The prestressing tendons were fully bonded, straight tendons. Specimens were loaded incrementally by a hydraulic actuator until failure. The shortest embedment length where a flexural failure was observed was considered as the development length. Whereas, a bond failure indicated an insufficient bond between prestressing steel and concrete, and that development length was larger than the tested embedment length.

Each single-strand concrete member was used to conduct two loading tests at both its ends. Transverse reinforcement was provided only in the central region of the beams to ensure this region would not be damaged after conducting the first load-test on beams. All prestressed specimens in this study had concrete compressive strength of 7,000 psi (48 MPa). The single-strand beams were manufactured with an 8-in. x 12-in. (200 x 305-mm) rectangular cross section, and prestressing steel depth (d_p) of 10 in. (225 mm). Strands used in fabrication of single-strand beams were from two different manufacturers. Beams were load-tested using a hydraulic actuator and values of load, deflection, and strand-slip at the applied load were continuously recorded. To understand the effect of multiple strands on development length, full-scale beams were load-tested in addition to single-strand beams. Multiple-strand members had five strands at the bottom of a T-shaped section. Overall section depth was 21 in. (535 mm) and width of the compression flange was 36 in. (915 mm). Contrary to single-strand beams tested at both ends, multiple-strand beams were tested only at one end.

Load tests were conducted on single-strand beams at an embedment length equal to predicted development length by an AASHTO design equation. In all cases, the maximum experimental moment was larger than the nominal-moment capacity of the section. Twelve load tests on single-strand concrete members showed that ACI and AASHTO development-length equations of $L_d = (f_{ps} - \frac{2}{3} f_{se}) d_b$ can be used to predict development length of pretensioned members fabricated with semi-light- weight concrete (SLW).

Load tests on multiple-strand beams showed that developing a flexure-shear crack prior to failure will result in a shift in maximum tensile stress in strand from the maximum-moment section toward the beam end.

2.4.10 (Kahn, Jason, & Reutlinger, 2002)

Kahn, Jason, & Reutlinger conducted a study to determine development length of 15-mm.(0.6-in)-diameter strand in pretensioned beams (2002). To determine minimum prestressing reinforcement development length, each pretensioned prism was simply supported and a point -load was applied at an assessed embedment length from one end, as shown in Figure 2.

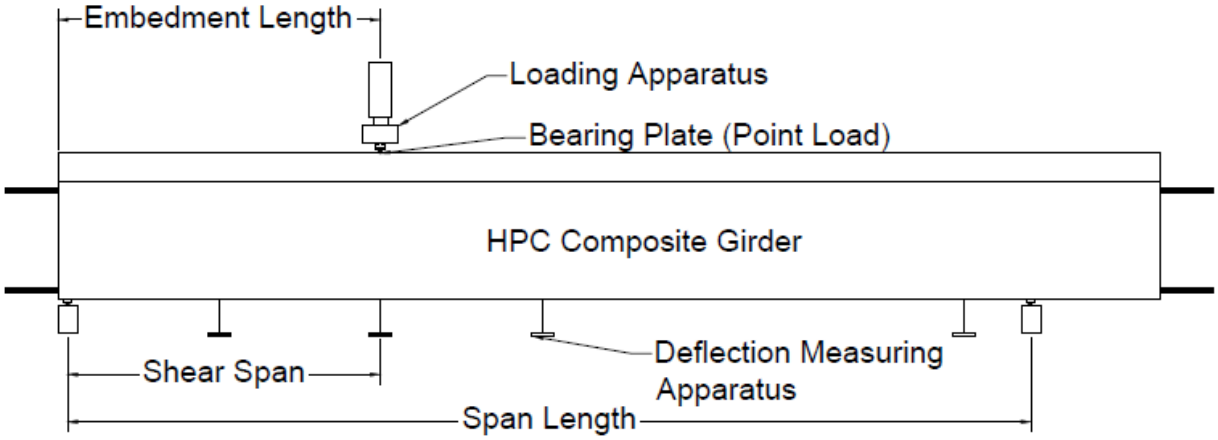


Figure 2. Schematic of development-length test [after: (Kahn, Jason, & Reutlinger, 2002)]

The embedment length was changed after one end of the pretensioned beam was tested. The minimum embedment length at which the beam failed in a flexural mode, while its capacity was higher than calculated nominal-moment capacity and bond slip, was less than the 2 mm defined as development length.

All beams were loaded uniformly in small displacement increments of about 2 mm. Loading tests were stopped once the beam failed in either a shear/bond or flexural mode. Shear/bond failures were obvious when large diagonal cracks occurred, when the end-slip of bottom strands was larger than 6 mm, and when slip kept increasing with no increase in load- carrying capacity. Flexural failures included ductile behavior and yielding of the prestressing reinforcement. The tests were stopped when the concrete crushed at 0.003 strain (Kahn, Jason, & Reutlinger, 2002).

2.4.11 Florida Department of Transportation (FDOT) proposal for development length

The FDOT conducted tests for three separate studies on development length of strands. These included tests of 17 AASHTO Type II girders with composite slabs, seven solid and hollowed slabs, and members simulating piles embedded in an in-situ concrete cap. Based on results from these tests, FDOT proposed the following expression to AASHTO Committee T-10:

$$L_d = \frac{\frac{f_{si} d_b}{3} + (f_{ps} - f_{se}) d_b}{(k_b \mu_{ave})} \qquad \text{(Equation. 18)}$$

where μ_{ave} equals 250 psi (1.73 MPa) and k_b is a dimensionless constant equal to

$$\begin{cases} k_b = 8 \; for \; piles \; embedded \; in \; a \; concrete \; footing \\ k_b = 4 \; for \; slabs \; and \; slender \; members \\ k_b = 2 \; if \; the \; calculated \; development - length \; to \; member - depth \; ratio \\ (using \; k_b = 4) is \; less \; than \; or \; equal \; to \; 3 \end{cases}$$

The FDOT expression led to approximately the same result as ACI/AASHTO. The difference was that the FDOT equation increased the value of the development length by 100 % for deep members and decreased the value by 50 % for embedded piles (Buckner, March-April 1995).

2.4.12 McGill University proposal

Twenty-two, single-strand, rectangular concrete members were tested and researchers at McGill University proposed an equation for strand-development length as a function of compressive strength of concrete. The equation is Comparable to the ACI/AASHTO expression, except it is multiplied by the terms reflecting concrete compressive strength. The following is the equation proposed by McGill University:

$$L_d = 0.33 f_{si} d_b \sqrt{\frac{3}{f'_{ci}}} + (f_{ps} - f_{se}) d_b \sqrt{\frac{4.5}{f'_c}} \qquad \text{(Equation. 19)}$$

This equation agrees well with test data from McGill University, but it does not agree well with data from other studies (Buckner, March-April 1995).

2.4.13 Strand development by UTA criteria

The UTA study recommended an equation of

$$L_t = f_{se} \frac{d_b}{2} \qquad \text{(Equation. 20)}$$

for transfer length, which gives a transfer length 50 % larger than that calculated by the current ACI/AASHTO equation. The UTA concluded that in order to have fully developed seven-wire strands, cracks in the transfer zone should be prevented. Instead of checking the development length, design standards were set to prevent concrete cracking in the transfer zone of concrete members (Russel & Burns, 1993). This conclusion included all sizes of pretensioned strands — both fully bonded and debonded. Some cases questioned the validity of this criterion. For instance, Hanson & Kaar conducted tests on pretensioned concrete members and several of their specimens had bond failure in a lower-moment rather than nominal-moment capacity, without cracks in the transfer length of the specimens (1959).

2.5 Fatigue Behavior of Pretensioned Prestressed Concrete Members

Fatigue is a process of growing life-long internal structural deterioration in a material under cycles of repetitive stresses. Crack growth and fracture of steel or concrete may occur if stress quantities are adequately large. A significant number of researchers have studied fatigue behavior of prestressed concrete beams and developed experimental techniques. These studies were mainly conducted to assess fatigue strength of prestressed concrete beams. ACI committee 215 developed broad recommendations based on experimental findings to the design of

reinforced and prestressed concrete beams for fatigue behavior. However, there is little knowledge on how to predict growth in deflection and crack widths, based on constituent materials properties for prestressed concrete beams. Yet the need for this knowledge is increasing, as utilization of prestressed concrete is increasing in different structures such as bridges and railroad ties. Change in the amount of stresses in concrete and reinforcing and prestressing steel, and progress in deflection and crack size of a prestressed concrete beam under cyclic loading can be mainly attributed to —

a) cyclic creep of the concrete in the compression zone, and

b) continuous reduction of stiffness of concrete in the tension zone (Balaguru, 1981).

a) Cyclic creep of concrete

Whaley and Neville have studied creep deformations of concrete subjected to cyclic compressive stresses. They have indicated that repetitive variation of compressive stresses from σ_{max} to σ_{min} causes larger creep strain than conditions where σ_{max} is kept constant. This means creep strain of concrete is a major factor in progress of deflections and crack sizes. Concrete, cyclic creep deformations in the compression zone will increase average tensile stress of steel similar to static creep deformations. According to Whaley and Neville's experimental data, cyclic creep strain can be defined as the sum of two strain elements: a mean-strain element and a cyclic-strain element. The mean-strain element is the creep due to static-mean stress σ_m. The cyclic-strain element depends on both the mean stress σ_m and the stress range. Whaley and Neville proposed a predictive equation for the cyclic creep strain as follows (Whaley & Neville, September 1973):

$$\epsilon_c = 129\sigma_m(1 + 3.87\Delta)t^{1/3} \qquad \text{(Equation. 21)}$$

where ϵ_c is the cyclic creep in $10^6\ {}^{in.}/_{in.}$

Δ is the stress range defined as a ratio of the compressive strength ${(\sigma_{max} - \sigma_{min})}/{f_c'}$.

σ_m is the mean stress defined as ${(\sigma_{max} + \sigma_{min})}/{2f_c'}$.

t is the time from the start of loading in hours.

Frequency of the cyclic load by which tests were conducted was 585 cycles per minute. In order to make the given predictive equation for the cyclic creep strain independent of the loading frequency, the following equation was proposed:

$$\epsilon_c = 129\sigma_m t^{1/3} + 17.8\sigma_m \Delta N^{1/3} \qquad \text{(Equation. 22)}$$

In this equation, N is the number of cycles rather than the time.

Having knowledge of maximum and minimum stress, number of loading cycles, and load frequency, creep strain can be calculated employing Equation. 22.

Whaley and Neville noted the model may be more accurate for values of $\sigma_m < 0.45$. This restriction is not limiting for most of the cases, since maximum working stress is typically

smaller than$0.4f_c'$. However, Equation. 22 accuracy decreases if maximum compressive stresses are greater than $0.45f_c'$ (Whaley & Neville, September 1973).

b) Reduction in stiffness contribution of tension-zone concrete

When reinforced concrete beams are under cyclic loading, an increase in the damage rate of bond between steel and concrete has been observed. The growing damage means a progressive increase in crack sizes, reduction in the concrete contribution to the tension between cracks, and an increase in deflection. The contribution of concrete in the tension zone between the flexural cracks for a beam under static service loads can be predicted by the empirical formula in the ACI Code:

$$I_{eff} = I_{cr} + (\frac{{M_{cr}}^3}{{M_a}^3})(I_g - I_{cr}) \leq I_g \qquad \text{(Equation. 23)}$$

where I_{eff}, I_{cr}, and $I_g$are the effective, cracked, and gross moment of inertia.

$M_a$is the maximum applied moment along the beam.

M_{cr} is the cracking moment, which can be calculated by the $M_{cr} = {I_g f_r}/{y_t}$equation; $f_r$is the modulus of rupture of concrete and y_t is the distance between the neutral axis and extreme tension fiber (Balaguru, 1981).

Using proper values of M_{cr} and $I_{cr}$for the ACI equation, researchers applied the ACI equation for prestressed concrete beams as well. Since concrete between the cracks and surrounding prestressing steel suffers from tensile fatigue under cyclic loading, its modulus of rupture, f_r decreases as the number of cycles increases. The relation between modulus of rupture at first cycle, $f_{r,}$ and modulus of rupture after N number of cycles $f_{r,N,}$ can be expressed as:

$$f_{r,N} = f_r(1 - \frac{log_{10}N}{13}) \qquad \text{(Equation. 24)}$$

If Equation. 24 is used to obtain the cracking moment, M_{cr}, as the number of cycles increases, M_{cr} decreases. Thus, average stiffness of the beam expressed by I_{eff} also decreases with the number of cycles. This method was used to consider the effect of reduction in concrete tension stiffness due to tensile cracking and bond loss (Balaguru, Analysis of Prestressed Concrete Beams for Fatigue Loading, 1981).

2.5.1 Effects of the constitutive materials properties in a prestressed concrete beam on the fatigue behavior

Fluctuations in prestressing steel stress due to opening and closing of the cracks under cyclic loading warns for potential fatigue failure. Effects of the main material properties in a prestressed concrete beam, which have effects on fatigue behavior, can be summarized as follows:

2.5.1.1. Concrete:

It is generally accepted that fatigue strength of concrete in compression, tension, or flexural for a life of 10,000,000 cycles, is half of the static ultimate strength.

2.5.1.2. Reinforcing steel (bars):

Stress range, bar size, geometry of deformation, bending, and welding characteristics are primary factors affecting fatigue strength of deformed bars. Fatigue life is generally unaffected by yield and tensile strengths of reinforcing bars, and decreases little with increasing bar size. Various limitations have been proposed by different design codes for stress range in reinforcing steel under cyclic loading.

2.5.1.3. Prestressing Steel:

Fatigue strength of prestressing steel is dependent on stress range, form of prestressing steel (wire, strand, or bar), and bond quality. Stress range is the most important factor in prediction of fatigue strength, and primarily depends on loading range and prestress levels. ACI committee 215 recommends stress range for prestressed steel under 2,000,000 cycles of load or less, at a minimum stress level up to 60% of tensile strength, f_{pu}, shall not increase to stresses greater than $0.7f_{pu}$ for strand or bars, and $0.72f_{pu}$ for wires (El Shahawi & Batchelor, 1986).

The bond between prestressing steel and surrounding concrete is adequate for uncracked, pretensioned, prestressed members subjected to static or cyclic loading. Although, for pretensioned crossties subjected to cyclic loading producing large bending moments in end regions of the member, large transfer lengths of the prestress tendon can reduce the prestress force, thus reducing the cracking moment. In this situation, cracking may occur. Early bond failure of the pretensioned member is probable to happen under cyclic loading in a member with a crack in or near the transfer length. Studies have shown that resistance to bond loss or prestressing steel slippage is dependent on the embedment length for members under static load. In a study done by Kaar and Hanson, fatigue test results from railroad crossties made with smooth seven-wire strand of 3/8-in. diameter showed the following:

1) A crosstie is able to resist three million cycles of severe loading, opening an existing crack of more than 0.001 in., if the crosstie is loaded in a distance greater than 2.2 times the strand transfer length for smooth strand. This end distance is not practical for railroad crossties.
2) A crosstie is able to resist three million cycles of less-severe loading, opening an existing crack of only 0.001 in., if the crosstie is loaded in a distance greater than 1.2 times the strand transfer length for smooth strand (Kaar P. , 1975).

Since manufacturing reinforced concrete members is easier than prestressed concrete members, reinforced concrete members have been the main focus in the study of fatigue behavior rather than prestressed concrete members. Contrary to reinforced concrete, prestressed concrete members are susceptible to prestressing steel fatigue failures under the high prestressing steel stress range. ACI 440.2R-02 limits service steel stress to 0.8 of yield stress ($0.8f_y$), where large prestressing steel stress range levels can be expected when limits are applied to a prestressed concrete member. AASHTO (1988) limits the strand stress range to 69 MPa (10 ksi) for

prestressed members with harped strand, and 124 MPa (18 ksi) for members with straight strand (Larson, Peterman, & Rasheed, 2005).

2.6 Conclusion

At present, 5.32-mm-diameter wires and strands with smaller diameters (smaller than 0.5 in.) are the primary prestressing steels utilized in manufacturing of prestressed concrete railroad ties. Development length is an important concept in design of pretensioned concrete railroad ties. However, there have been very few studies on the development length of prestressing wires. In this research project, pretensioned prisms fabricated with 5.32-mm-diameter prestressing wires were commonly used in the manufacture of railroad ties and load tests conducted on them to evaluate development length of different wires. Also, prisms with strands with a diameter of less than 0.5 in. (3/8 and 5/16 in.) were fabricated and load tests were conducted on them as well. It should be noted that all prisms were manufactured by Naga Narendra Bodapoti, graduate student at Kansas State University. The ratio of concrete to prestress steel in the test prism's cross section was representable of typical concrete railroad ties. Thus, geometrical and mechanical properties of test prisms were representative of actual ties in the railroad industry. Currently, very little knowledge exists about the development length of wires. To fulfill the need of the railroad industry for quantifying the development length of these commonly used wires, load tests were conducted on prisms, and a model was developed to predict the development length of wires in pretensioned concrete ties.

3. Methodology

3.1 Phase I-Effect of Concrete Properties and Wire Indentation Types on the Development Length and Flexural Capacity of Pretensioned Concrete Crossties

3.1.1 Experimental program

Load tests were conducted on pretensioned concrete prisms cast with 13 different 5.32-mm-diameter prestressing wire types used in the manufacture of pretensioned concrete railroad ties worldwide. The tests were specifically designed to evaluate development lengths of these different reinforcements. The prestressing wires were denoted "WA" through "WM" and indentation types included smooth, spiral, chevron, diamond, and two-dot and four-dot. Four wires were embedded into each concrete prism, which had a 3.5-in. (88.9-mm) x 3.5-in. (88.9 - mm) square cross section. The wires were initially tensioned to 7,000 pounds (31.14 KN) and gradually detensioned when the concrete compressive strength reached 4500 psi (31.03 MPa). A consistent concrete mixture with Type III cement, water-cement ratio of 0.32 and a 6-in. slump was used for all prisms. All prisms load-tested in this study were fabricated by Naga Narendra Bodapati, with the purpose of determining the effect of concrete properties and prestressing steel indentation types on the transfer length of pretensioned concrete members. It should be noted that prestressing tendons were all gradually detensioned rather than flame cut.

Additional tests were conducted to determine the effect of concrete-release strength on development length and flexural capacity of members utilizing five of the wires in this study. These included two chevron-indented wires with different indent depths, one spiral-indented wire, one dot-indented wire, and one smooth wire (with no surface indentation). A consistent concrete mixture was used for the manufacture of all test specimens, and the different release strengths were obtained by allowing the specimens to cure for different amounts of time prior to de-tensioning. Each prismatic specimen (prism) had a 3.5-in. (88.9-mm) x 3.5-in. (88.9-mm) square cross section with four wires arranged symmetrically. The prisms were identical except for wire type and compressive strength at the time of de-tensioning. Two prisms, each having different concrete- release strengths, were tested with each of the five wire types. Development lengths, determined by subsequent load testing of the prisms, were then compared for each type of wire on the basis of release strength. Two identical prisms for each of three different release strengths were tested for each wire type to estimate the development length. All four wires were each initially tensioned to 7,000 pounds (31.14 KN), and then de-tensioned gradually when the concrete compressive strength reached 3,500 (24.13 MPa), 4,500 (31.03 MPa), and 6,000 (41.37 MPa) psi. Precise de-tensioning strengths were ensured by testing 4-in.-diameter (101.6-mm) x 8-in.-long (203.2-mm) compression-strength cylinders that had been temperature-match-cured.

Another group of load tests was conducted on prisms to determine the effect of concrete slump on development length and flexural capacity of members utilizing five of the wires in this study. These included two chevron-indented wires with different indent depths, one spiral-indented wire, one dot-indented wire, and one smooth wire (with no surface indentation). The concrete properties were the same for the manufacture of all test specimens except concrete slump. Each prismatic specimen (prism) had a 3.5-in. (88.9- mm) x 3.5-in. (88.9-mm) square cross section

with four wires arranged symmetrically. The prisms were identical except for wire type and concrete slump. Concrete-release strength was 4,500 (31.03 MPa) psi for all prisms. Figure 3 shows the geometry of the prisms' cross section made with wires.

.

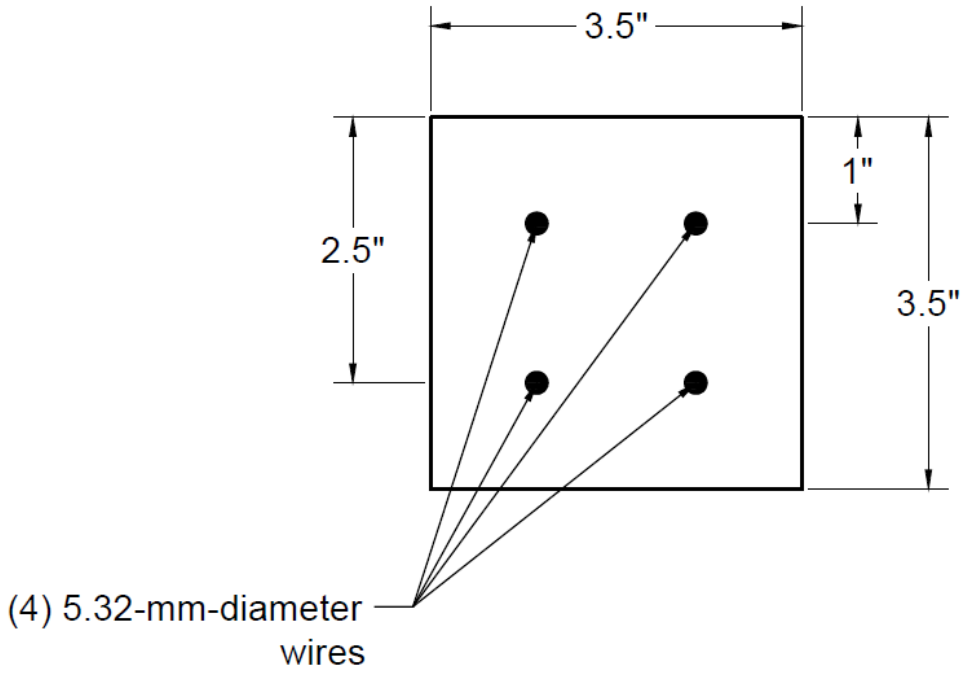


Figure 3. Cross section of the pretensioned concrete prism (1 inch=25.4 mm)

Concrete mix

For this study, a consistent concrete mixture of Type III cement with a water-cement ratio of 0.32 was used for all prisms. In order to produce mixes similar to those currently being used by prestress crosstie manufacturers, a mix design that gained high, early compressive strength was selected. Oven-dried materials were used in manufacturing all prisms to obtain consistency in mixture proportions.

Prestress wire

Thirteen types of 5.32-mm-diameter prestress wires commonly used worldwide in manufacturing concrete crossties were obtained (Zhao, Murphy, Peterman, Beck, & Wu, Winter 2012) and utilized for fabrication of test prisms. These prestress wires were generically named from "WA" to "WM," and indentation types included smooth, spiral, chevron, diamond, two-dot, and four-dot. Geometrical properties of all wire indents were quantified according to ASTM A-881 (2010) and values are tabulated in Table 2. Note that "WA" is smooth wire and has no indentation. Also, for spiral wires "WC" and "WE," there was no nominal length of the indent (Haynes, Wu, Beck, Bodapati, & Peterman, 2014). Figure 4 and Figure 5 show pictures of all types of wires used in production of test prisms, and a close-up view of their indentation types.

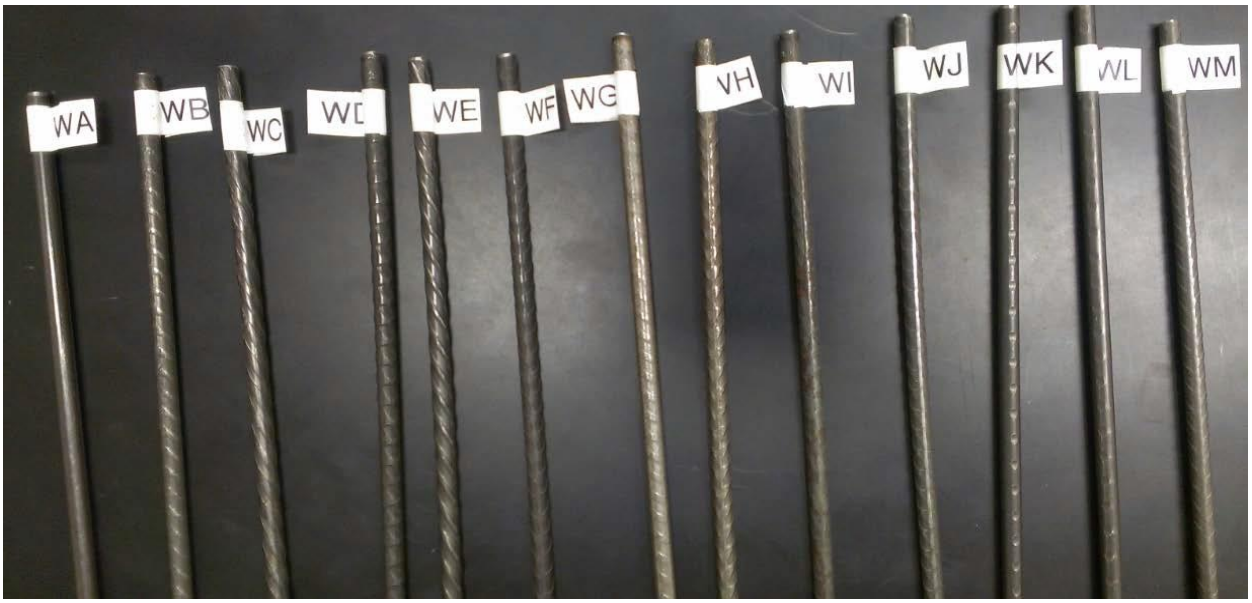


Figure 4. Picture of all 13 types of wire used in production of test prisms [after: (Arnold, 2013)]

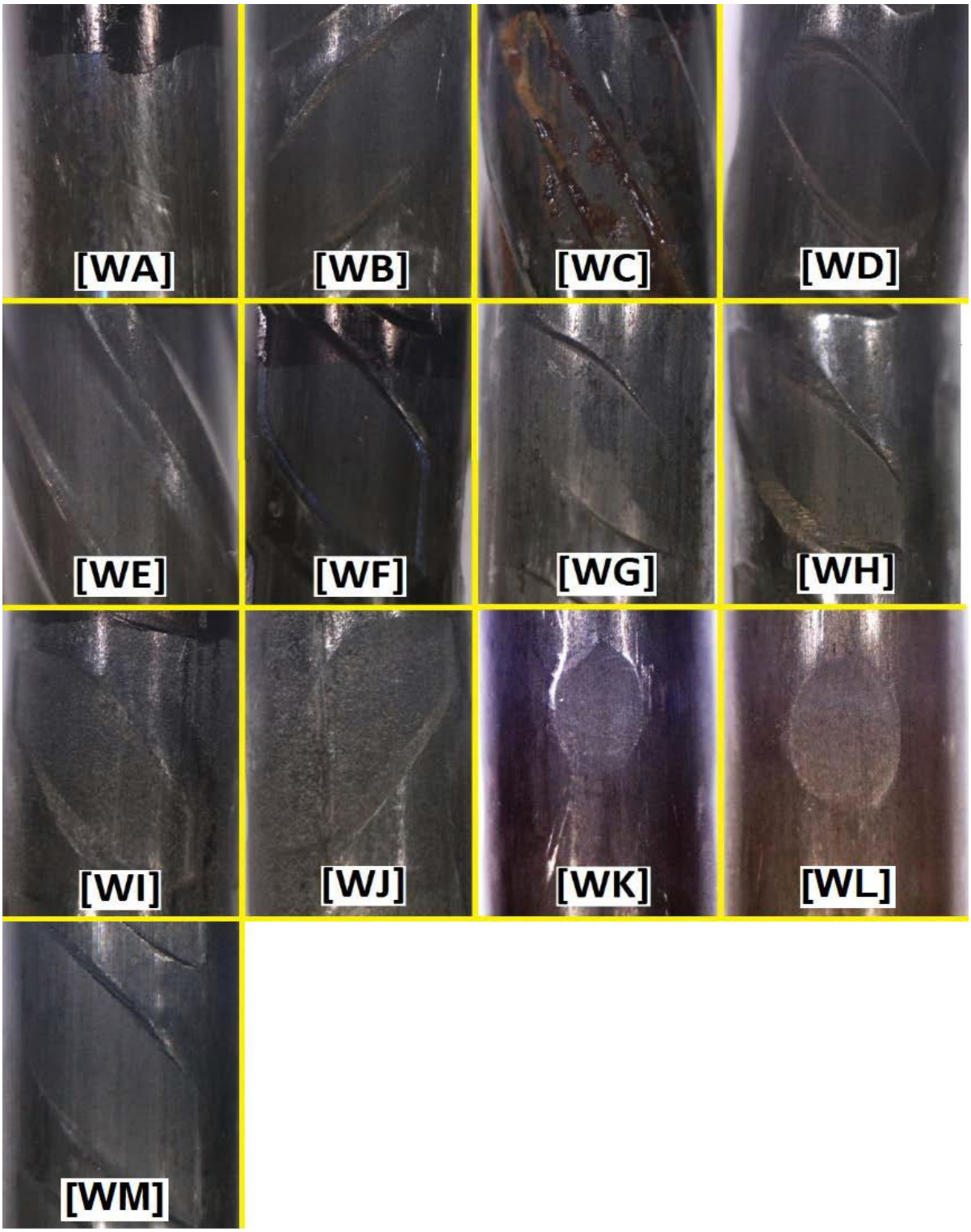


Figure 5. Close-up picture of wire indentation types [after: (Arnold, 2013)]

Table 2. Basic indent geometrical features [after: (Haynes, Wu, Beck, Bodapati, & Peterman, 2014)]

Wire type	Average depth (mm)	Average width (mm)	Average edge wall angle (deg)
WA	0.000	0.000	0.0
WB	0.146	4.191	23.6
WC	0.176	3.932	29.3
WD	0.167	4.097	17.9
WE	0.259	6.164	15.1
WF	0.192	4.143	32.6
WG	0.100	3.629	25.7
WH	0.186	4.078	14.2
WI	0.141	4.157	10.6
WJ	0.164	4.445	10.2
WK	0.132	2.860	8.0
WL	0.124	2.826	7.7
WM	0.126	4.097	21.8

Research variables

To understand the effect of wire-indentation types on development length, all parameters in test prisms were kept constant except type of wire. Thus, the only variable in test prisms was type of wire. Two identical prisms for each of 13 types of wire were tested to estimate the development length. For all these prisms, each prestress wire was initially pulled to 7,000 pounds (31.14 KN) and was gradually de-tensioned when the compressive strength of concrete reached 4500 psi (31.03 MPa). To understand the effect of concrete-release strengths on development length, for WA, WE, WG, WH, and WK wires, prisms with the same wire and concrete properties — but different release strengths of 3500 (24.13 MPa), 4500 (31.03 MPa), and 6000 (41.37 MPa) psi — were manufactured as well. Also, to examine the effect of concrete slump on development length and flexural capacity of prisms for WA, WE, WG, WH, and WK wires, prisms with concrete slumps of 3 in. (7.6 cm), 6 in. (15.2 cm), and 9 in. (22.9 cm) were fabricated for each type of wire. It should be noted all prisms were fabricated by graduate student, Naga Bodapati, during 2011, 2012 and 2013.

Nomenclature

A nomenclature was developed to easily identify the main properties of test specimens in this study. Figure 6 shows the nomenclature of a typical test prism to clarify the naming system used throughout this study.

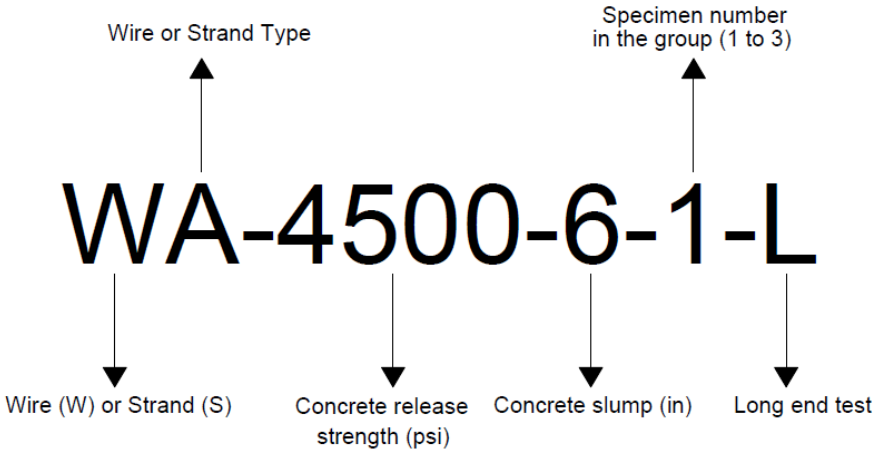


Figure 6. Load-test specimen nomenclature

3.1.2 Testing configuration

All prisms were tested in three-point bending at different spans to obtain estimations of the development length based on wire type, concrete-release strength, and concrete slump. Each prism was loaded on both ends. First, prisms were tested at 20 in. (50.8 cm) from one end and 13 in. (33.02 cm) from the other end, whereas the second prisms were loaded at 16.5 in. (41.9 cm) from one end and 9.5 in. (24.13 cm) from the other end. Prisms were set up on two roller supports with center-to-center distance of rollers equal to 38 in. (96.52 cm), 24 in. (60.96 cm), 31 in. (78.74 cm), and 17 in. (43.18 cm) for tests with embedment lengths of 20 in. (96.52 cm), 13 in. (33.02 cm), 16.5 in. (41.9 cm), and 9.5in. (24.13 cm) from beam end, respectively. Figure 7 to Figure 10 show schematics of test setups for all load cases.

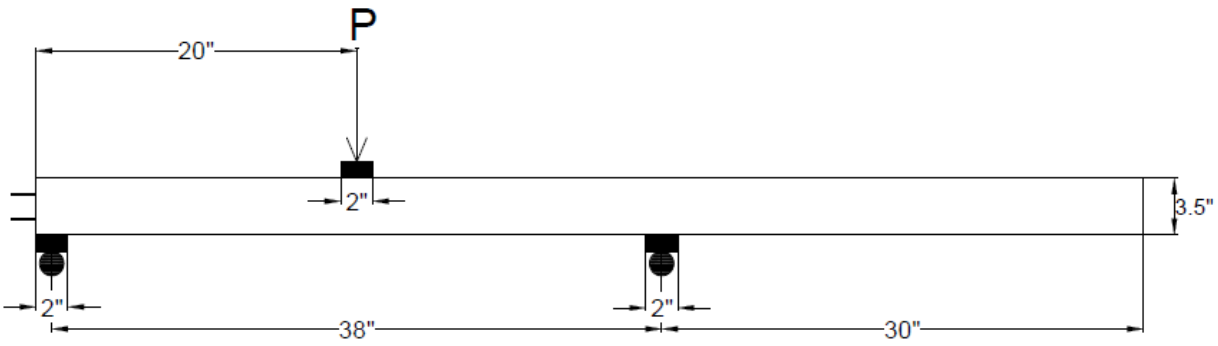


Figure 7. Load case 1: prisms loaded at 20-in. embedment length

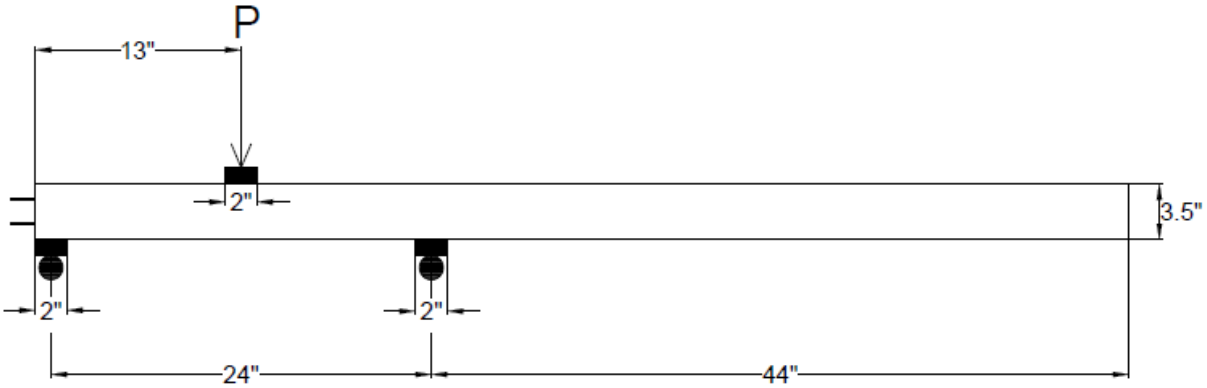


Figure 8. Load case 2: prisms loaded at 13-in. embedment length

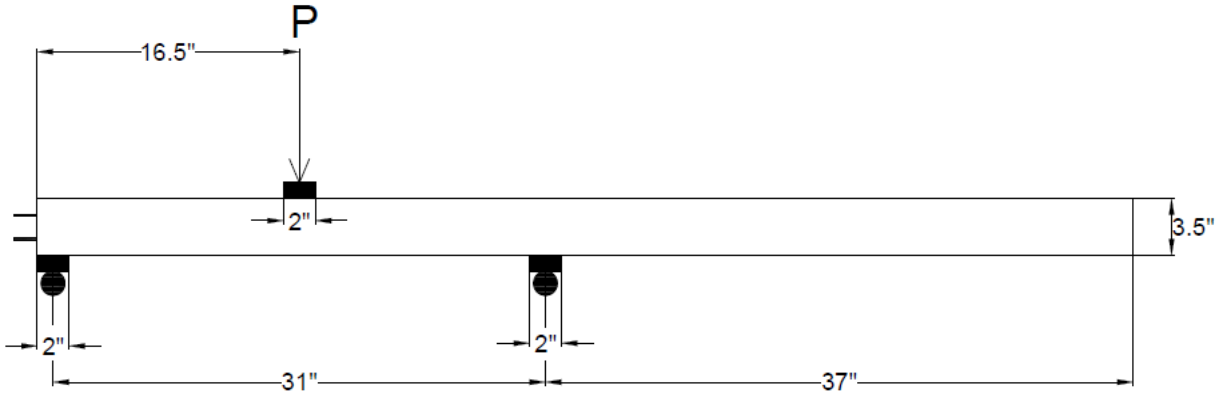


Figure 9. Load case 3: prisms loaded at 16.5-in. embedment length

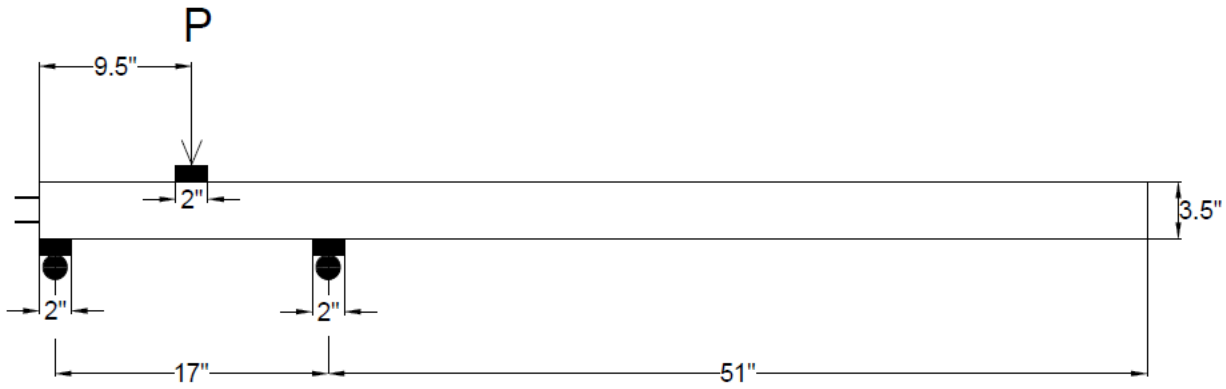


Figure 10. Load case 1: prisms loaded at 9.5-in. embedment length

Transfer lengths were determined from changes in concrete surface strain for each end of each prism before load testing. Brass points were inserted on both sides along the length of prisms at mid-height at the time of casting. They were longitudinally spaced at 1-in. (2.54-mm), center-to-center intervals. Starting from 0.5 in. (12.7 mm) from prism end, brass inserts were installed on both sides of the prism at a 34-in. (86.4-cm) length. Prior to releasing the prestressing steel, the distance between brass points was measured with accuracy of 0.0001 in. (0.00254 mm) using a Whittemore gage with gage length of 8 in. (203.2 mm). This reading is the base for subsequent readings in order to calculate concrete surface strains. Another reading was conducted after de-tensioning to calculate surface strains at the time of de-tensioning. A program was developed that incorporated a least-square algorithm to determine transfer length from the concrete surface strain data (Zhao W. , et al., 2013). Readings prior to de-tensioning and after de-tensioning were conducted by Naga Bodapoti, and transfer lengths were determined based on calculated surface strains. Transfer lengths presented throughout this report are those at the time of de-tensioning determined by Naga Narendra Bodapati (Bodapati, et al., 2013).

During each test, a concentrated load with the rate of 300 lb/min (1334 N/min) was applied at mid-span until the prism failed. Values of load, mid-span deflection, and all wires' end-slip were continuously monitored and recorded. Also, the corresponding load for the first observed crack and type of failure was documented for each test. Using linear variable differential transformers (LVDTs), mid-span deflection and wires' end-slip were measured.



Figure 11. Wire end-slip LVDT

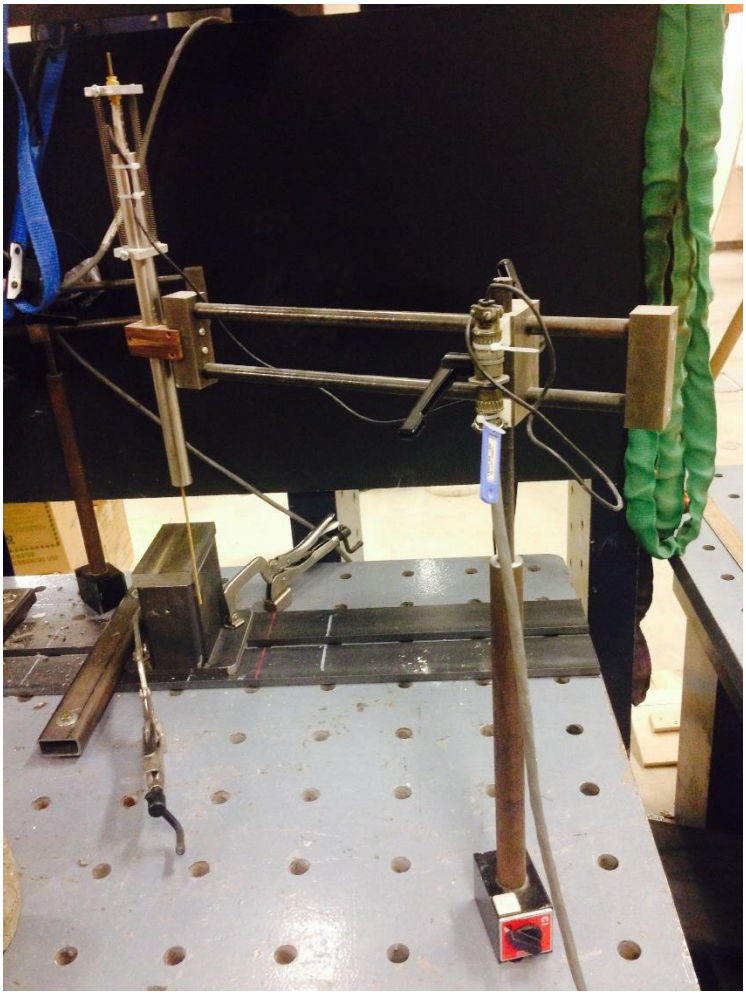


Figure 12. Deflection LVDT

Load was applied to the prisms using an MTS hydraulic actuator controlled by an MTS FlexTest digital servo-hydraulic controller. The load was applied through a 2-in (50.8-mm)-wide metal plate that was grouted to the top surface to eliminate any surface anomalies and rotations. The actuator was able to apply a concentrate load up to 22,000 lbs. (97.86 KN). Figure 13 shows a picture of the actuator used in loading tests.

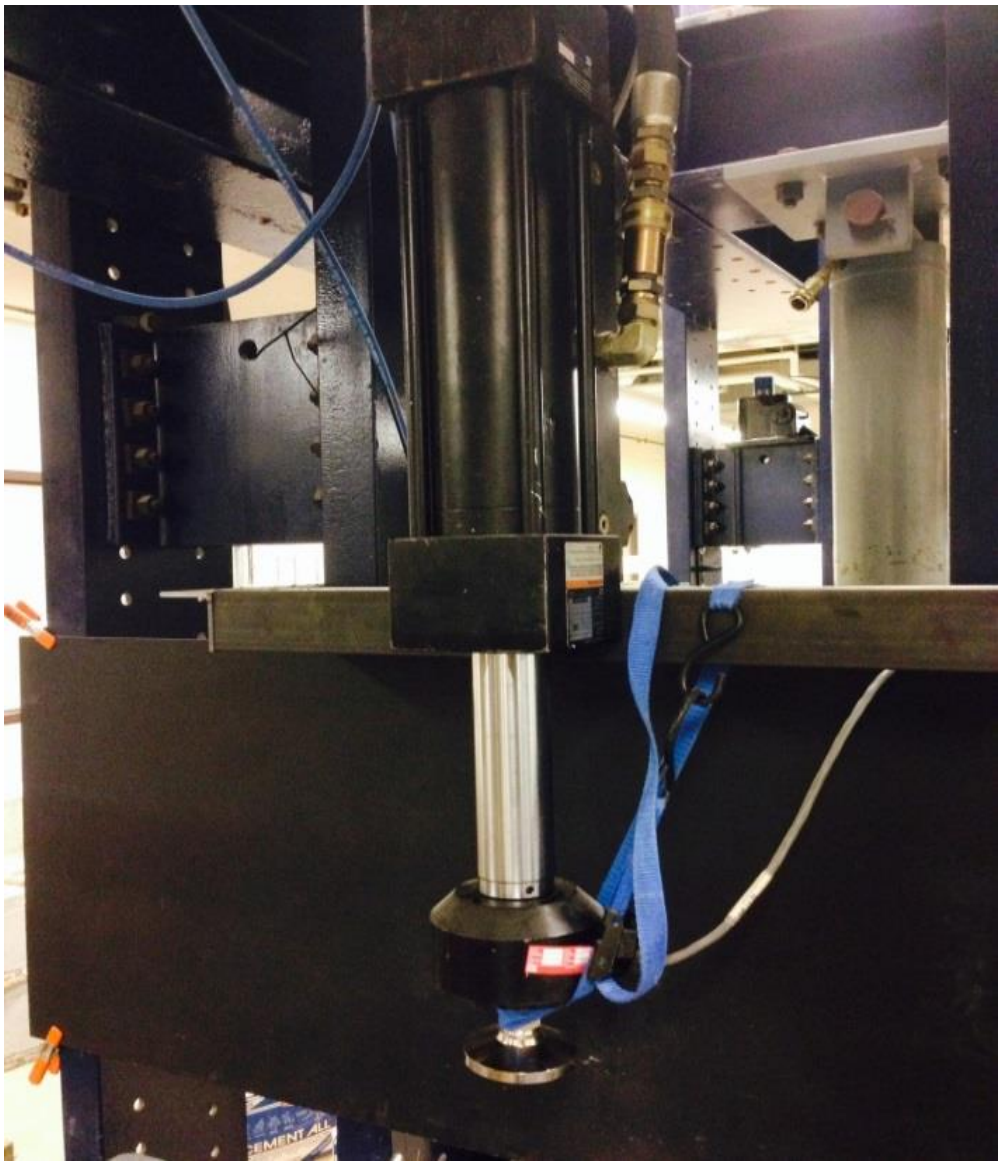


Figure 13. Actuator used to apply load on the prisms

Two LVDTs, one on each side of the prism, were used to measure mid-span deflection. Mid-span deflection at a given load was then taken as the average of the two LVDT readings. The prism supports and LVDT setup were affixed to a large structural steel base positioned under the actuator. Figure 14 shows a picture of the setup used to conduct the load tests.

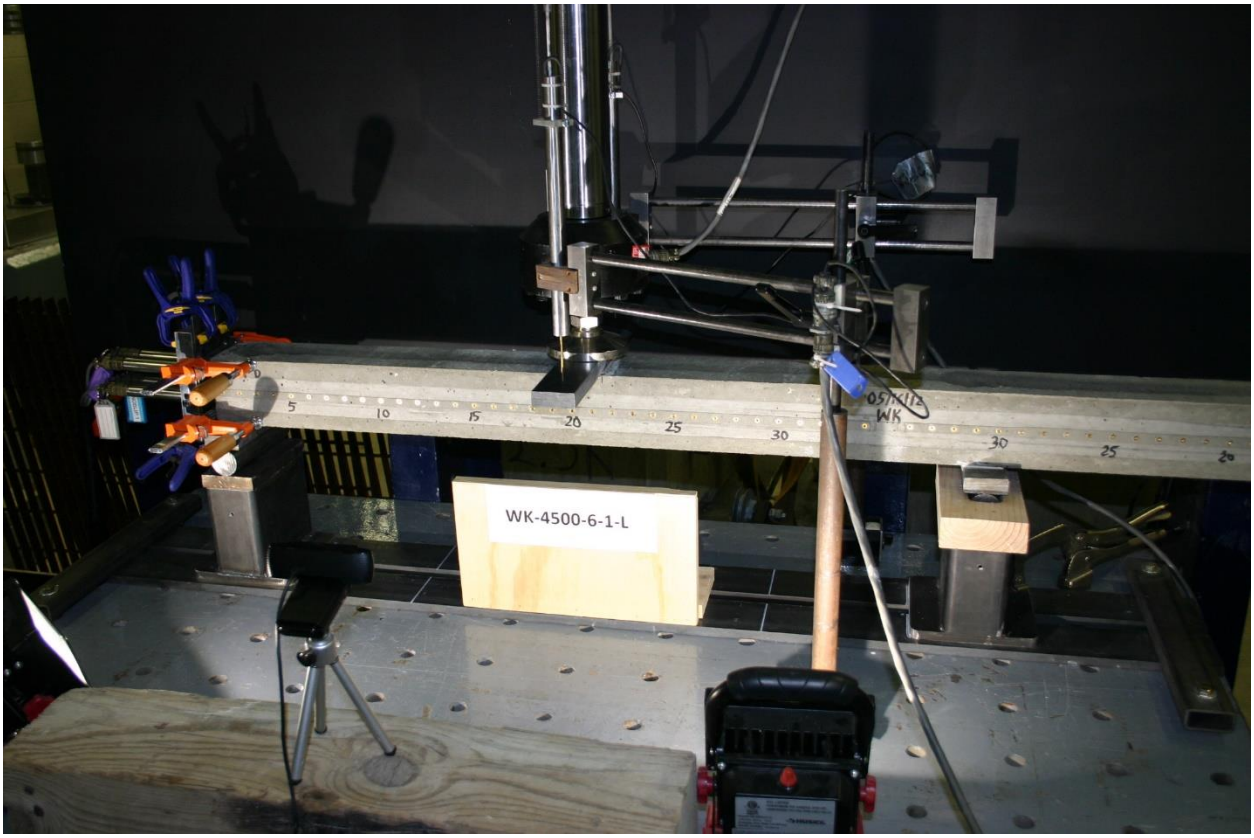


Figure 14. Setup used for running the loading tests

MTS Multi-Purpose TestWare (MPT) software was programmed to apply the load at a uniform rate of 300 lb/min (1334 N/min) and increase until the first crack was observed. When the first crack was observed, the operator paused the test and the load was held constant at this load (the load where the first crack was observed) for 10 minutes. Accurate determination of the cracking load was enabled by illuminating the side of the prism surface with two flood lights (refer to Figure 14). After the 10-minutes hold period was completed, the load was increased uniformly until the prism failed. Depending on the loading span, test length was between 25 to 50 minutes. Table 3 shows the procedure for running load tests on prisms made with wires.

Table 3. Loading steps and load rates for running monotonic load tests on prisms made with wires

Loading steps	Load rate
Load until one crack is observed	300 lb/min
Hold for 10 minutes	0
Load to failure	300 lb/min

During the testing, different failure types were observed. These are described below, and images related to each type of failure are shown in Figure 15 to Figure 20 and described below:

1) Shear-compression failure – A diagonal shear crack initiates at the tip of a pre-existing flexural crack, and the diagonal crack advances upwards to the point where the concrete fails by compression. A typical shear-compression failure is shown in Figure 15.
2) Shear-bond failure – A shear diagonal crack intersects the bottom tendon row and causes a loss in bond as indicated by wire slippage prior to failure. A shear-bond failure is shown in Figure 16.
3) Pure shear – A wide diagonal crack occurs very suddenly along the shear span without prior wire slippage. Figure 17 shows a pure-shear failure in a tested prism.
4) Concrete-compression failure – Flexural cracks initiate from the bottom and grow vertically until the concrete can no longer withstand the compression demand and fails by direct crushing. A compression mode of failure is shown in Figure 18.
5) Horizontal-splitting failure – A horizontal crack initiates and propagates along the bottom row of wires and causes a sudden total bond loss. A typical horizontal- splitting failure is shown in Figure 19.
6) Bond failure – After the initiation of flexural cracking, the prestressing tendons cannot withstand the increased tensile demand and slip with respect to the surrounding concrete occurs. With additional applied load, the tendons continue to slip and allow the cracks to open to a point where no further load can be supported. Figure 20 shows a picture of a bond-failure mode.

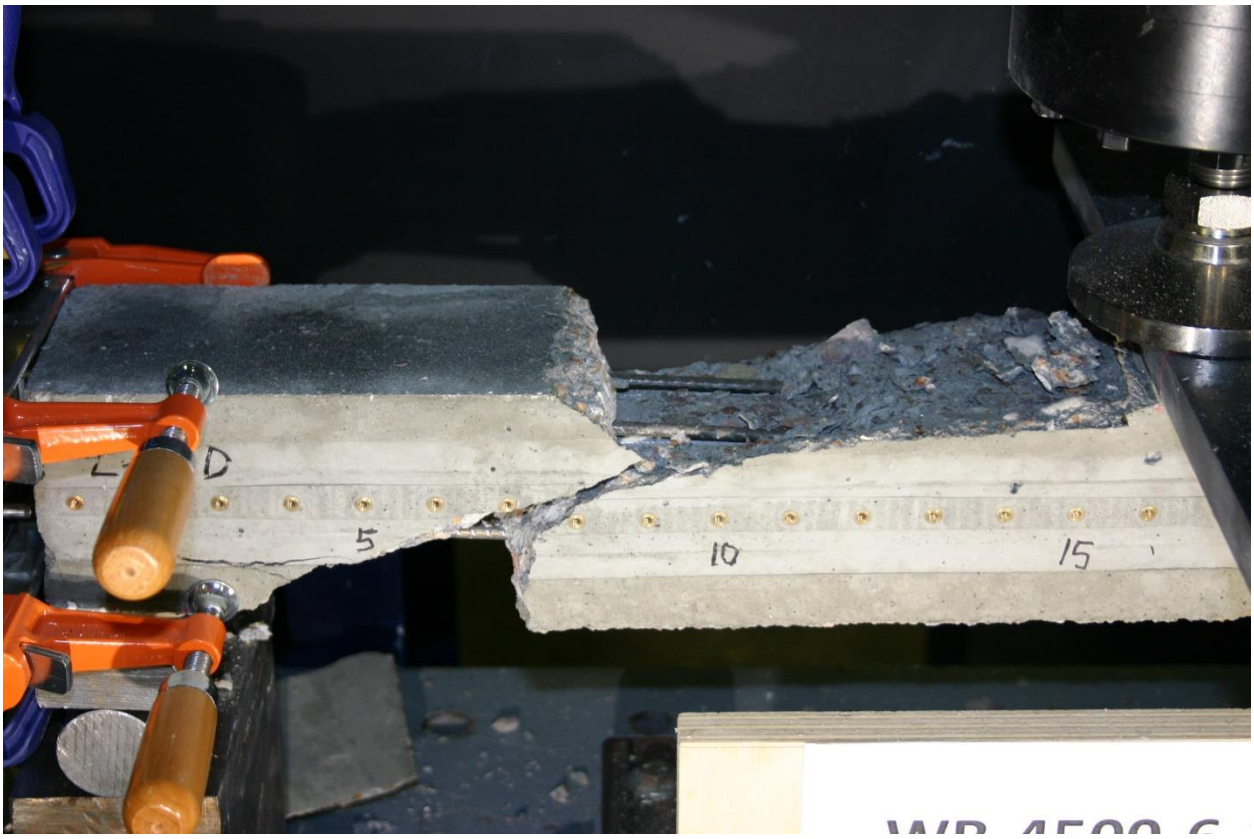


Figure 15. The prism failed in shear-compression mode

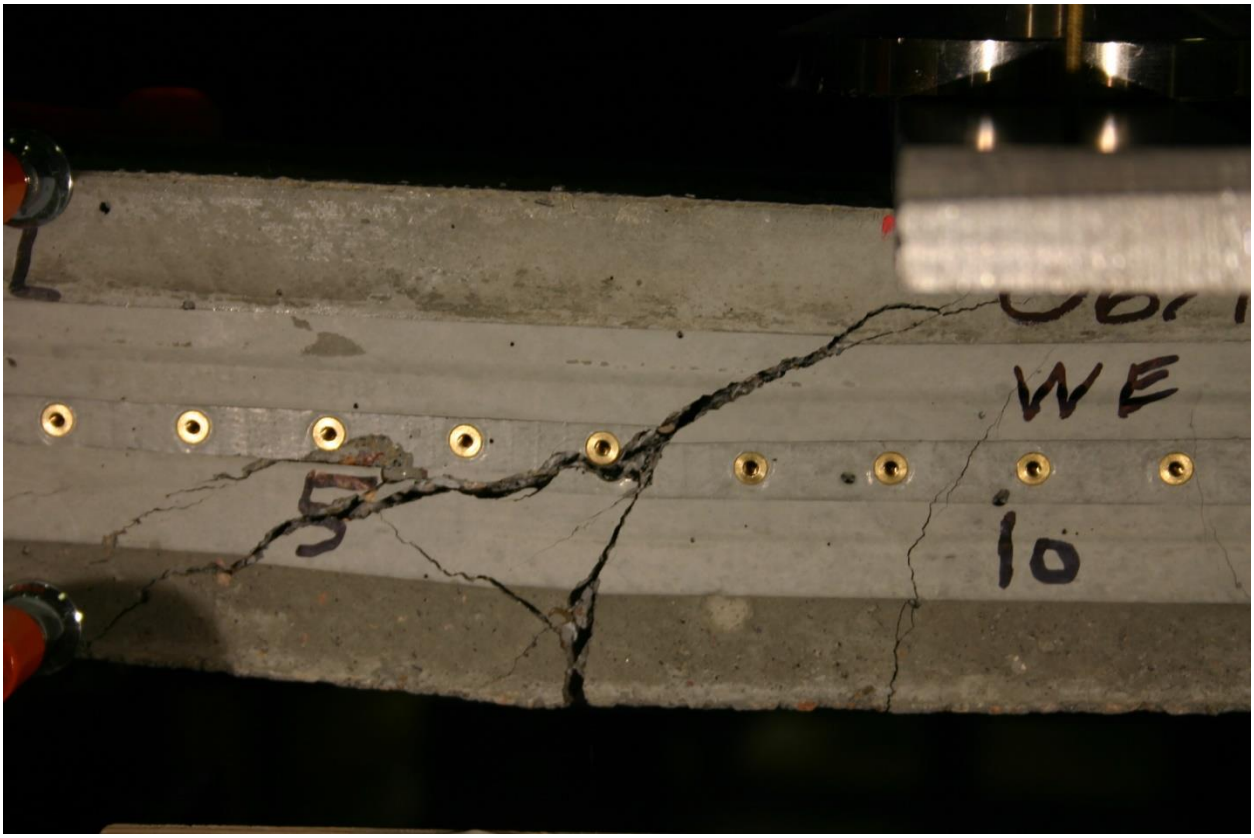


Figure 16. The prism failed in shear-bond mode

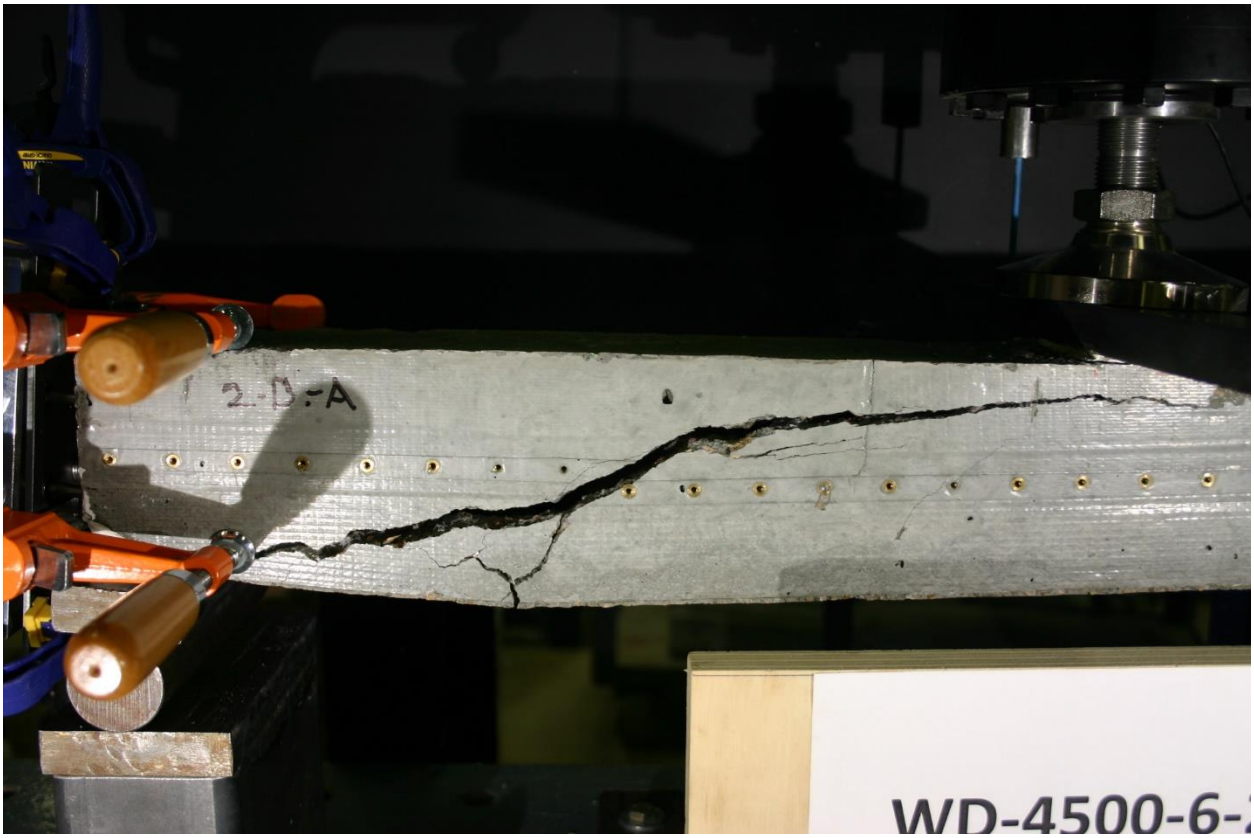


Figure 17. The prism failed in pure-shear mode

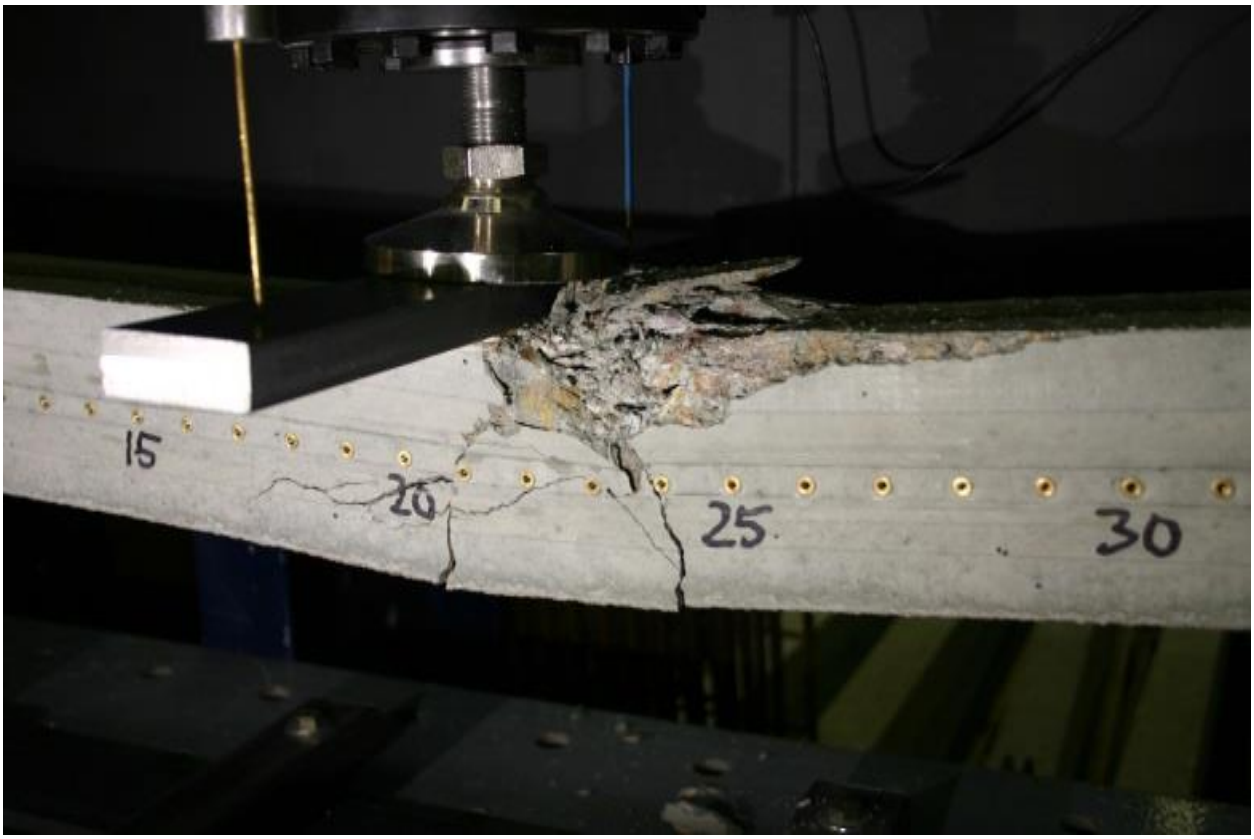


Figure 18. The prism failed in concrete-compression mode



Figure 19. Horizontal-splitting mode where the prism split along the bottom row of prestress wires

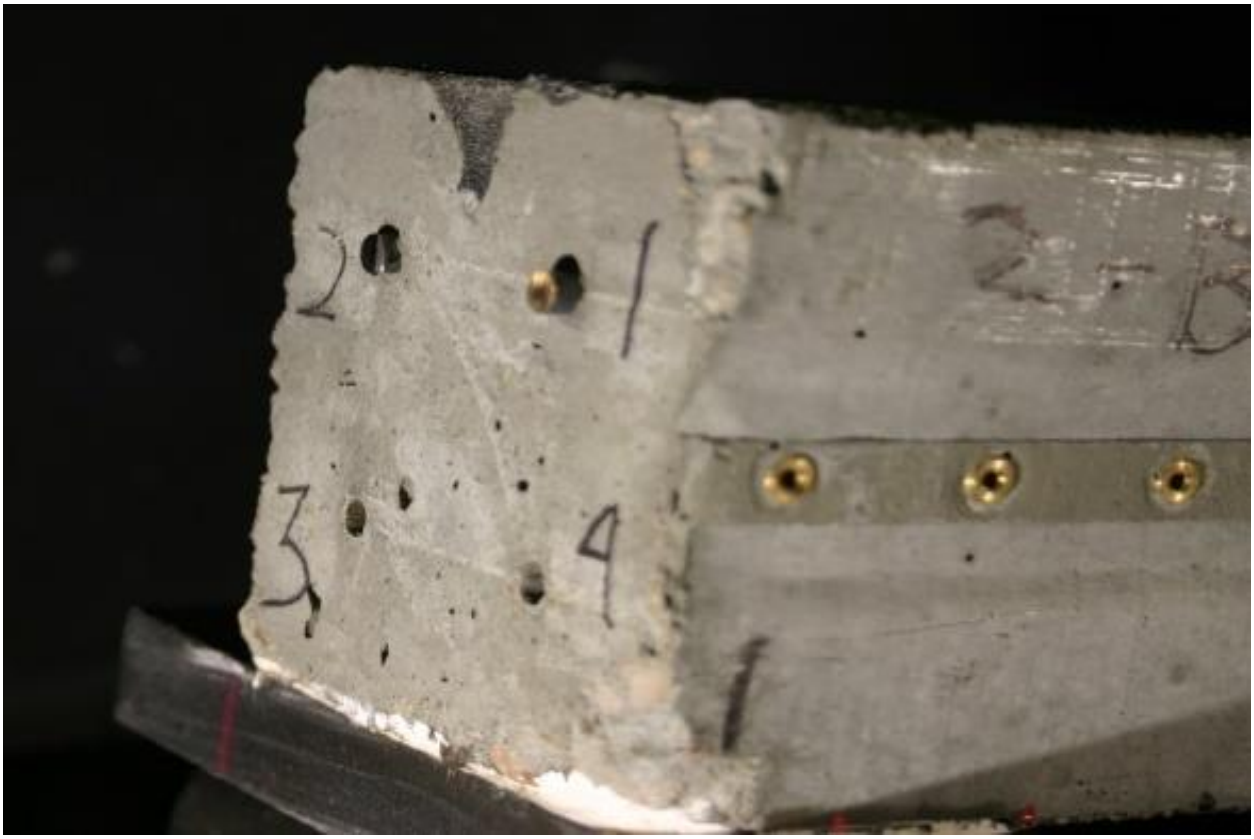


Figure 20. Bond-failure mode with significant wire end-slip for the bottom row of prestress wire

3.2 Phase II-Effect of Concrete Properties and Prestressing Strand Indentation Types on the Development Length and Flexural Capacity of Pretensioned Concrete Crossties Made with Three- and Seven-Wire Strands

3.2.1 Experimental program

Pretensioned concrete prisms made with six different prestressing strand types (four, seven-wire strands and two, three-wire strands) were load-tested to failure in order to understand the effect of strand-indentation type on development length and bonding performance of these different reinforcements. The prestressing strands were denoted "SA" through "SF." SA and SC were smooth strands while the other four were indented strands. All strands utilized in manufacturing of prisms had diameters of 3/8 in. (9.52 mm), except the SC strand which had a 5/16-in. (7.94-mm) diameter. Among all types of strands, SC and SF were the only three-wire strands, and the remaining strands were all seven-wire strands. For SA, SB, SD, SE, and SF strands, four strands were embedded into each concrete prism, which had a 5.5-in. (139.7-mm) x 5.5-in. (139.7-mm)-square cross section, while the prisms made with SC had four strands embedded into each concrete prism, but a square section of 4.5 in. (114.3 mm) x 4.5 in. (114.3 mm). The strands were

tensioned and gradually detensioned when the concrete compressive strength reached 4,500 psi (31.03 MPa).

Additional tests were conducted on pretensioned members made with five different strands (three, seven-wire strands and two, three-wire strands) to determine the effect of concrete-release strength on development length and flexural capacity of members. Five strands named SA, SC, SD, SE, and SF were utilized in prism manufacturing. All strands had diameters of 3/8 in. (9.52 mm) except SC, which had a diameter of 5/16 in. (7.94 mm). Different release strengths were obtained by allowing the specimens to cure for different amounts of time prior to de-tensioning. For SA, SD, SE, and SF strands, each prismatic specimen (prism) had a 5.5-in. (139.7-mm) x 5.5- in. (139.7 mm)-square cross section with four strands arranged symmetrically. However, prisms made with SC strand had a 4.5-in. (114.3-mm) x 4.5-in. (114.3-mm)-square cross section with four strands arranged symmetrically. The prisms were identical except for strand type and compressive strength of concrete at the time of de-tensioning. All four strands were pulled and detensioned gradually when the concrete-compressive strength reached 3,500 (24.13 MPa), 4,500 (31.03 MPa), and 6,000 (41.37 MPa) psi. Precise de-tensioning strengths were ensured by testing 4-in.-diameter (101.6-mm) x 8-in.-long (203.2-mm) compression-strength cylinders that were temperature- match-cured. All prisms load tested in this study were fabricated by Naga Narendra Bodapati, with the purpose of determining the effect of concrete properties and prestressing steel indentation types on transfer length of pretensioned concrete members. Figure 21 and Figure 22 show schematics of the prisms' cross sections and arrangement of the strands.

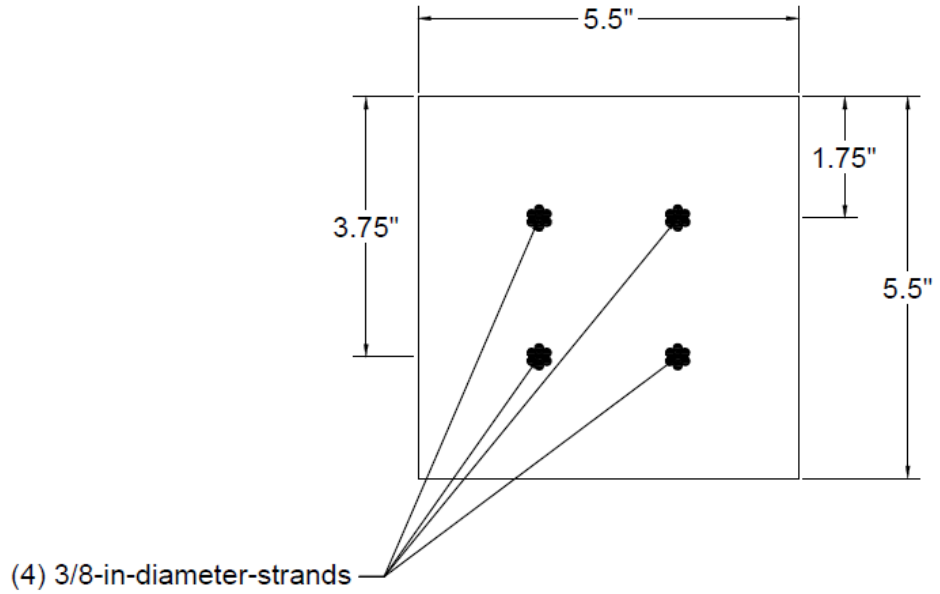


Figure 21. Cross section of prisms made with strands of 3/8-in. diameter (1 inch=25.4 mm)

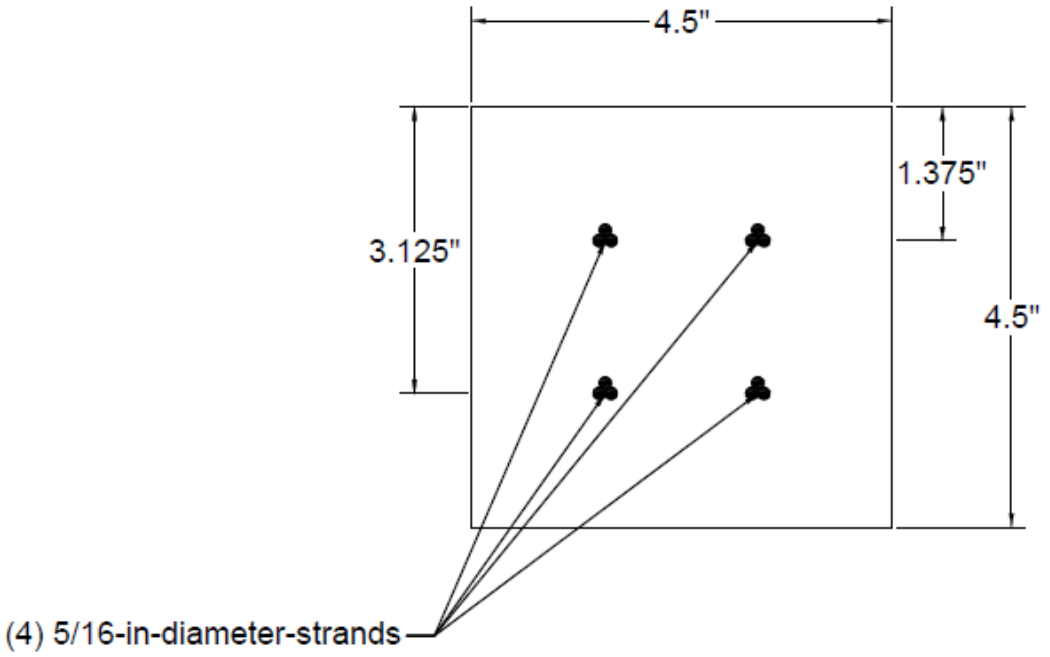


Figure 22. Cross section of prisms made with 5/16-in. diameter three-wire strand (1 inch=25.4 mm)

Concrete mix

For this study, a consistent concrete mixture with Type III cement, water-cement ratio of 0.32, and 6-in. slump was used for all test specimens. Mix design used was similar to mix being currently used by prestress crosstie producers — a mix which gains high, early compressive strength. To attain consistency in mixture proportioning, oven-dried materials were used.

Prestress strand

Six different types of strand were used in manufacturing the test prisms. Strands were named generically SA, SB, SC, SD, SE, and SF, and were all indented except SA (no surface indentation). Table 4 shows mechanical properties of all strands used in the prisms.

Table 4. Mechanical properties of strands used in this study

Strand type	Actual area (in)	Breaking load (lb)	Yield load at 1% extension (lb)	Elongation (%)	Modulus of elasticity (ksi)
SA	0.0846	23661	22206	5.21	29000
SB	0.0854	23793	21831	5.47	29000
SC	0.0582	15871	14485	5.47	29000
SD	0.0855	22998	20705	3.50	28282
SE	0.0825	23069	21210	4.78	28110
SF	0.0650	18550		6.20	28555

Figure 23 and shows the six strands used in the test prisms while Figure 24 shows a close-up view of their indentation patterns.



Figure 23. Sample of six strands with different indentation types and diameters [after: (Arnold, 2013)]

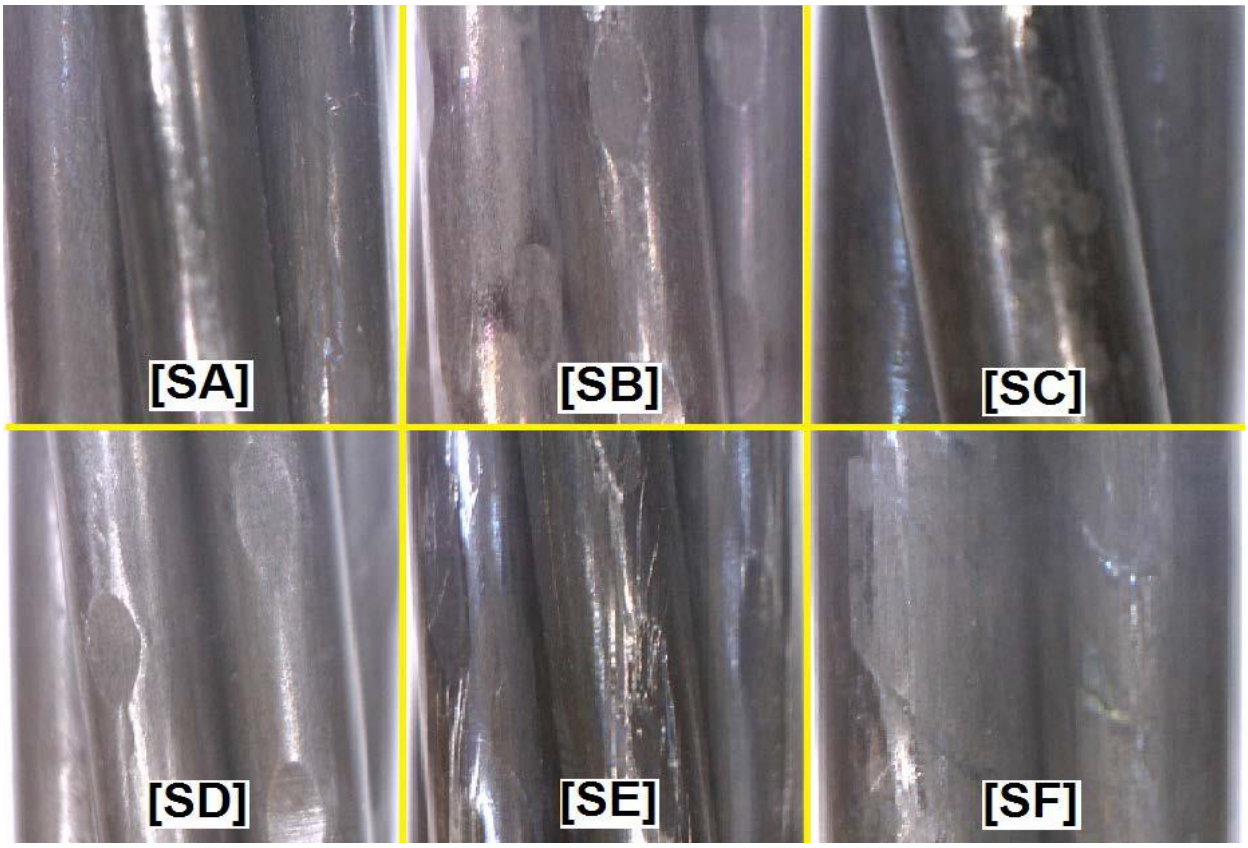


Figure 24. Close-up view of strands indentation types [after: (Arnold, 2013)]

Research variables

To understand the effect of prestressing strand-indentation type on development length of pretensioned members, all other parameters were kept constant in the prisms except strand type. Also, to evaluate the effect of concrete-release strengths on development length and flexural capacity of pretensioned members, prisms with different concrete-release strengths were manufactured and all other parameters were kept constant in prisms for each strand type.

3.2.2 Testing configuration

Three-point bending load tests were conducted at different assessed embedment lengths on prisms to obtain estimations of the development length based on strand type and concrete-release strength. Three identical prisms were tested for each type of strand and concrete-release strength. First prisms were tested at 28 in. (71.12 cm) from prism end, while second prisms were tested at 20 in. (50.8 cm) from prism end. Having load tests at 16.5 in. (41.9 cm) from the third prism end and 13 in. (33.02 cm) from the other end of prism, the third prisms were tested at both ends. Pretensioned beams were set up on two roller supports with center-to-center distance of rollers equal to 54 in. (137.16 cm), 38 in. (96.52 cm), 31 in. (78.74 cm), and 24 in. (60.96 cm) for tests with embedment lengths of 28 in. (71.12 cm), 20 in. (50.8 cm), 16.5 in. (41.9 cm), and 13in. (33.02 cm). Figure 25 to Figure 28 show schematics of test setups for all load cases.

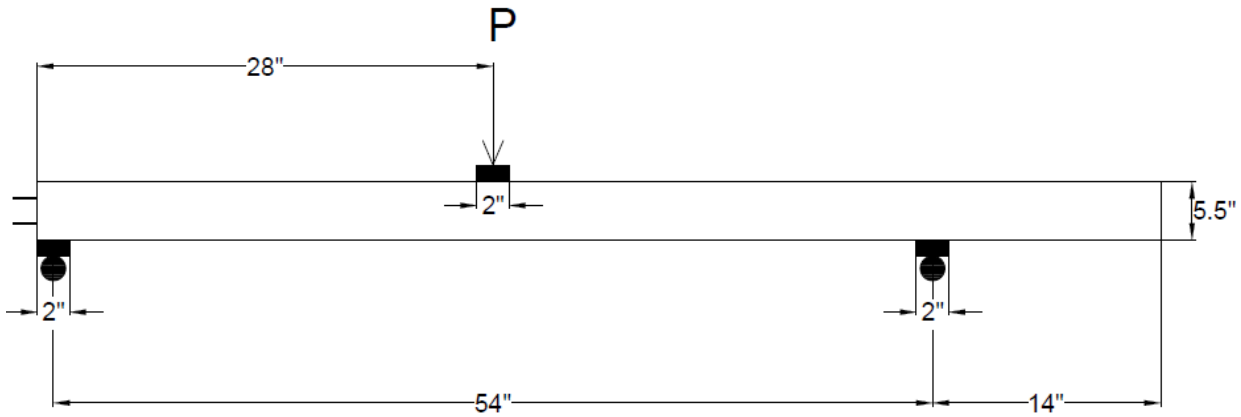


Figure 25. Load case 1: prisms loaded at 28-in. embedment length

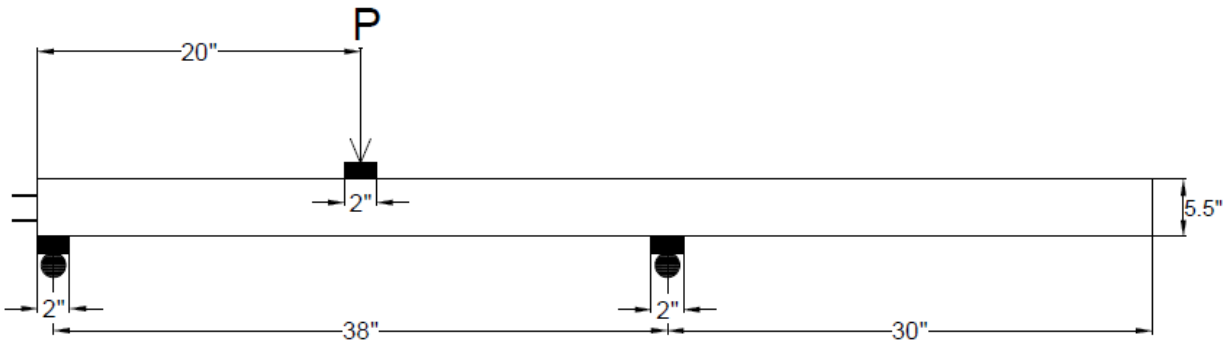


Figure 26. Load case 2: prisms loaded at 20-in. embedment length

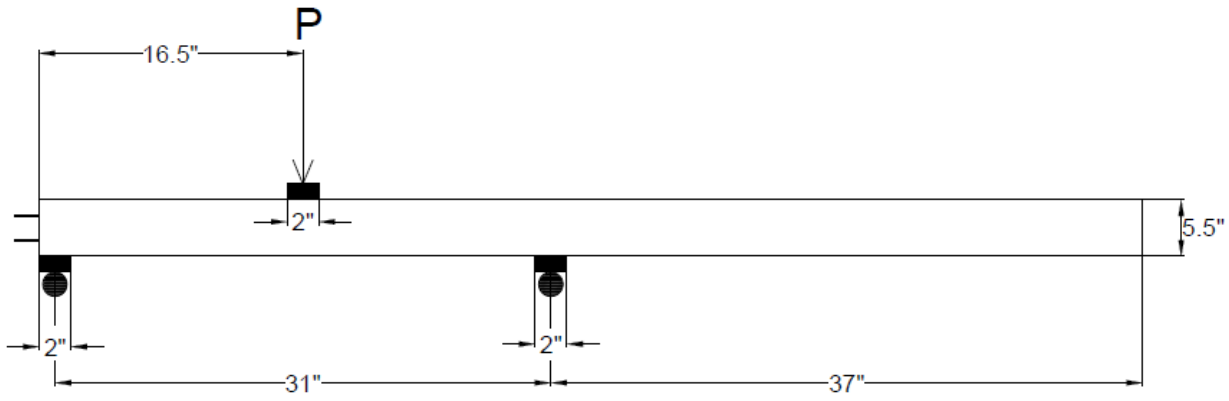


Figure 27. Load case 3: prisms loaded at 16.5-in. embedment length

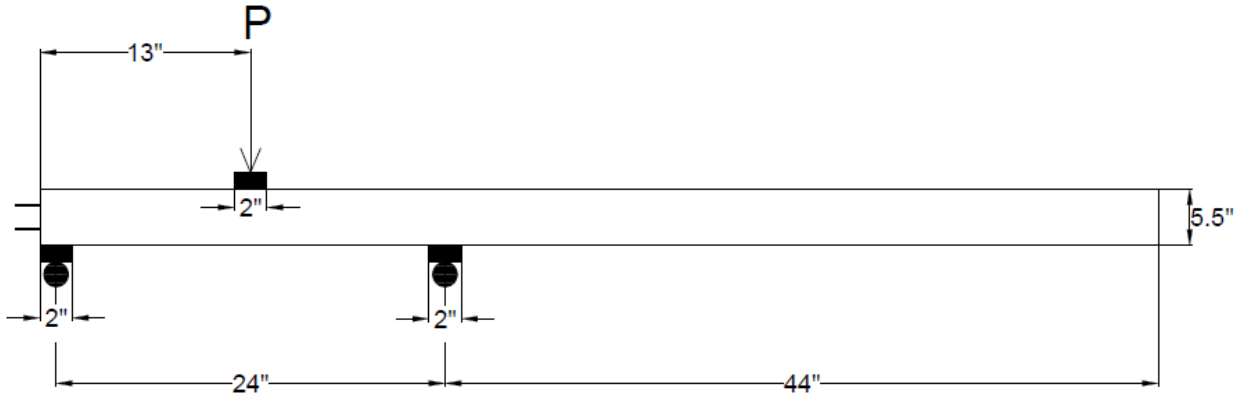


Figure 28. Load case 4: prisms loaded at 13-in. embedment length

During each test, for beams with a 5.5-in. x 5.5-in. (139.7-mm x 139.7-mm) section, a concentrate load with the rate of 900 lb/min (4003 N/min) was applied at mid-span until prism failure happened. Values of load, mid-span deflection and all strands' end-slip were constantly monitored and recorded. Loading rate for smaller prisms of 4.5-in. x 4.5-in. (114.3-mm x 114.3-mm) sections was 500 lb/min (2224 N/min). The load corresponding to the first observed crack-and-failure type was documented for each test. Linear variable differential transformers (LVDTs) were used to measure mid-span deflection and strands' end-slip (refer to Figure 11 and Figure 12).

MTS Multi-Purpose TestWare (MPT) software was used for the load application on the prism, and the actuator applied load on a 2-in (50.8-mm)-width metal plate that was grouted on top of the prism to avoid any displacements and rotations. The actuator used to conduct loading tests was able to apply a concentrate load up to 50,000 lbs (222.41 KN). Figure 29 shows the actuator used for running the load tests on prisms with strands.



Figure 29. Actuator used for conducting load tests on prisms containing strands

The applied load was increased until the first crack occurred. Once the first crack was initiated, the operator paused the test and the load was held constant at that same load for 10 minutes.

Precise determination of the cracking load was assisted by illuminating the side of the prism surface with two flood lights (refer to Figure 14). Once the 10-minute holding period was completed, load was increased uniformly until the prism failed. The total length of each test was between 25 and 50 minutes, depending on the loaded span length. Table 5 shows the procedure for running load tests on 4.5-in. x 4.5-in. (114.3-mm x 114.3-mm) and 5.5-in. x 5.5-in. (139.7-mm x 139.7-mm) prisms.

Table 5 Loading steps and load rates in tests on prisms manufactured with strands

	5.5 in X 5.5 in prisms	4.5 in X 4.5 in prisms
Loading step	**Load rate**	**Load rate**
Load until one crack is observed	900 lb/min	500 lb/min
Hold for 10 minutes	0	0
Load to failure	900 lb/min	500 lb/min

3.3 Phase III-Effect of Prestressing Wire Indentation Type on the Bond Performance and Flexural Capacity of Pretensioned Concrete Crossties Subjected to Cyclic Loading

3.3.1 Experimental program

Thirteen types of prestressing wire with different indentations were utilized in the manufacturing of pretensioned test prisms. For each type of wire, one prism was tested monotonically, and one prism was tested cyclically, thus 26 prisms were evaluated experimentally. All prisms had a 3.5-in. (88.9-mm) x 3.5-in (88.9-mm)-square cross section, a 69-in. (175.3-cm) length and four wires of 5.32-mm-diameter symmetrically embedded in concrete. Figure 3 shows a schematic of the prism cross section and arrangement of the wires.

Concrete mix

For this study, a consistent concrete mixture with Type III cement, water-cement ratio of 0.32, and 6-in. slump was used for all prisms.

Prestress wire

All 13 types of wire in this study (WA to WM) were utilized by Naga Bodapoti to fabricate prisms for this phase of study. Geometrical properties of all wire indents were quantified according to ASTM A-881 (2010) and values are tabulated in Table 2.

Research variables

To understand the effect of wire-indentation type on the resistance of pretensioned concrete ties to cyclic loading, all parameters in test prisms were kept constant except type of wire. Thus, the only variable in test prisms was type of wire. One prism for each of 13 types of wire was tested to evaluate the fatigue behavior of pretensioned ties made with different wires. For all these prisms, each prestress wire was initially pulled to 7,000 pounds (31.14 KN) and was gradually detensioned when the compressive strength of concrete reached 4,500 psi (31.03 MPa).

3.3.2 Testing configuration

Prisms were tested in cyclic loading to understand the effect of wire-indentation type on fatigue resistance and propagation of cracks under the cyclic loading. For each type of wire, a 69-in.-long prism was tested in four-point bending under the cyclic load. The prisms were supported by two rollers spanning 45 in. (114.3 cm), and load was applied on a spreader beam set on the top of the test prism. The prism setup and loading configuration were symmetric, and the load was applied to the prism from the spreader beam to two bearings spaced 15 in. (38.1 cm) apart. Figure 30 shows the schematic of the test setup, and Figure 31 shows a picture of the test setup. Figure 32 shows the spreader beam used to apply the load to the beam.

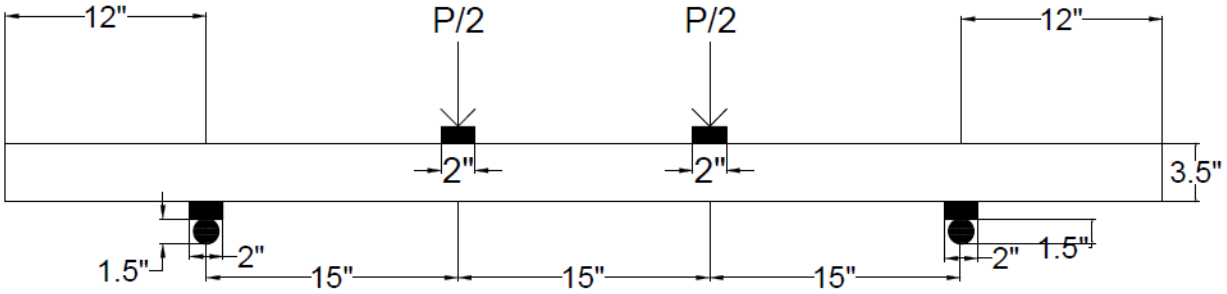


Figure 30. Schematic of test setup for cyclic loading test (1 inch=25.4 mm)

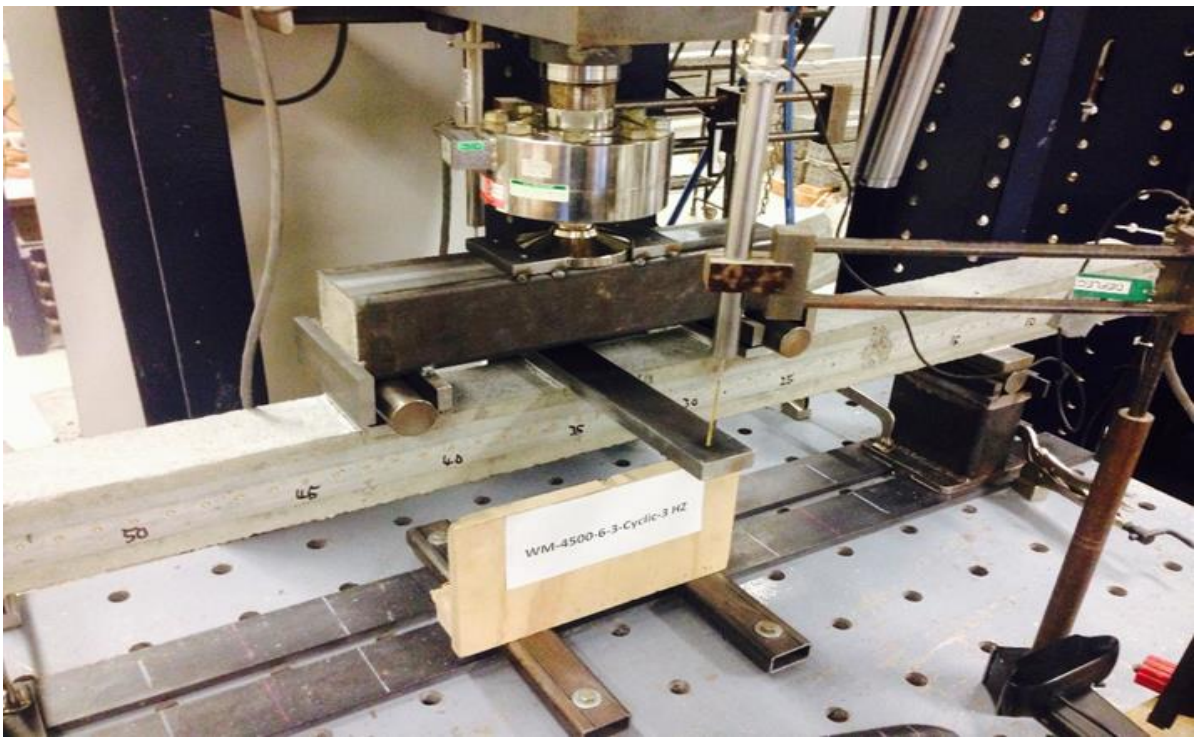


Figure 31. A picture of test setup used to run cyclic tests



Figure 32. Spreader beam used during the cyclic loading test

During each cyclic test, a concentrated load with the rate of 250 lb/min (1110 N/min) was applied until two cracks were observed at the maximum-moment region on the test prisms (region between two bearings). Once cracks were observed, the load was held constant for three minutes at the cracking load. After holding the load constant for three minutes, the load started to be increased to 4,000 lb (17790 N), and then stated to cycle between 400 lb (1780 N) to 4,000 lb (17790 N) with the frequency of 3 Hz. The test was designed to go through 200,000 cycles and interlock limits were assigned to the program to stop the test in case of prism failure under cyclic loading. For prisms able to finish 200,000 cycles of load, the procedure was to unload to zero and start loading the prism at the rate of 250 lb/min (1110 N/min) until the prism failed. Values of load, mid-span deflection, and wires' end-slip were continuously monitored and recorded during each test. Using linear variable differential transformers (LVDTs), mid-span deflection and wires' end-slip were measured. Three-point bending load tests were conducted for prisms under monotonic load. Pretensioned prisms were tested at 20 in. (50.8 cm) from prism end where they were set up on two roller supports with center-to-center distance of rollers equal to 38 in. (96.52 cm) for a test with embedment length of 20 in. (50.8 cm). Figure 7 shows a schematic of test setup for a 20-in. (50.8 cm) embedment length.

Table 6 shows the procedure for running cyclic load tests.

Table 6 Loading steps and load rates for cyclic test

Loading steps	Load rate
Load until two cracks are observed	250 lb/min
Hold for 3 minutes	0
Increase load to 4000 lb	250 lb/min
Cycle load between 400 to 4000 lb	3 Hertz
Load to failure	250 lb/min

4. Results

4.1 Phase I-Effect of Concrete Properties and Wire-Indentation Types on Development Length and Flexural Capacity of Pretensioned Concrete Crossties

4.1.1 Effect of wire-indentation types on development length

All prisms were fabricated by Naga Narendra Bodapoti and transfer lengths for each end of each prism were determined at the time of de-tensioning. In this chapter, transfer lengths presented are all transfer lengths at the time of de-tensioning and were determined by graduate student, Naga Bodapati. Table 7 shows values of transfer lengths determined for prism ends related to 20-in. (50.8-cm), 16.5-in. (41.9-cm), 13-in. (33.02-cm), and 9.5-in. (24.13-cm) loading locations. Note the last column is the average transfer length of six ends and not the average of four transfer lengths in the Table 7.

Table 7 Transfer lengths determined at time of de-tensioning at each prism end for prisms with 4500 psi concrete-release strength (Bodapati, et al., 2013)

Wire Designation	Indentation Type	T.L determined end tested @ 20 (in.)	T.L determined end tested @ 16.5 (in.)	T.L determined end tested @ 13 (in.)	T.L determined end tested @ 9.5 (in.)	Average T.L (in)
WA	**smooth**	16.4	17.9	14.4	15.6	16.3
WB	**chevron**	10.9	12.8	10.4	12	11.6
WC	**spiral**	8.5	10.8	8.5	8.6	8.8
WD	**chevron**	10.8	11.4	10.5	10.3	11.1
WE	**spiral**	7.2	8	6.8	7.9	7.4
WF	**diamond**	8.6	7.9	9.3	9.3	8.5
WG	**chevron**	11.6	11.6	11.6	12.6	11.8
WH	**chevron**	7.4	7.5	6.5	7.9	7.5
WI	**chevron**	9.8	10.5	10.3	9.4	10.1
WJ	**chevron**	8.6	8	8.5	11	9.0
WK	**4-dot**	14.2	14	14.9	13.7	14.0
WL	**2-dot**	19.1	18.1	18.5	20.3	18.7
WM	**chevron**	10.8	11	10.4	11.9	11.0

Tests of different specimens resulted in different modes of failure. Specimens with large- wire end-slip failed in bond, indicating the bond between wires and concrete is not fully developed, or in the other words, development length was larger than the tested embedment length. Bond failures were evidenced by large-wire slippage and no concrete split-cracking.

Recorded force and deflection data for each test were used to construct force versus deflection graphs. Plotted graphs of force versus mid-span deflection for all types of wire were combined on one single chart, and four separate charts were created for four loading spans. Comparison of

behavior of prisms manufactured with different wires under the point load was better understood through the combination of load-deflection graphs on one chart. Figure 33 to Figure 36 show load-deflection graphs for all types of wire for each embedment length.

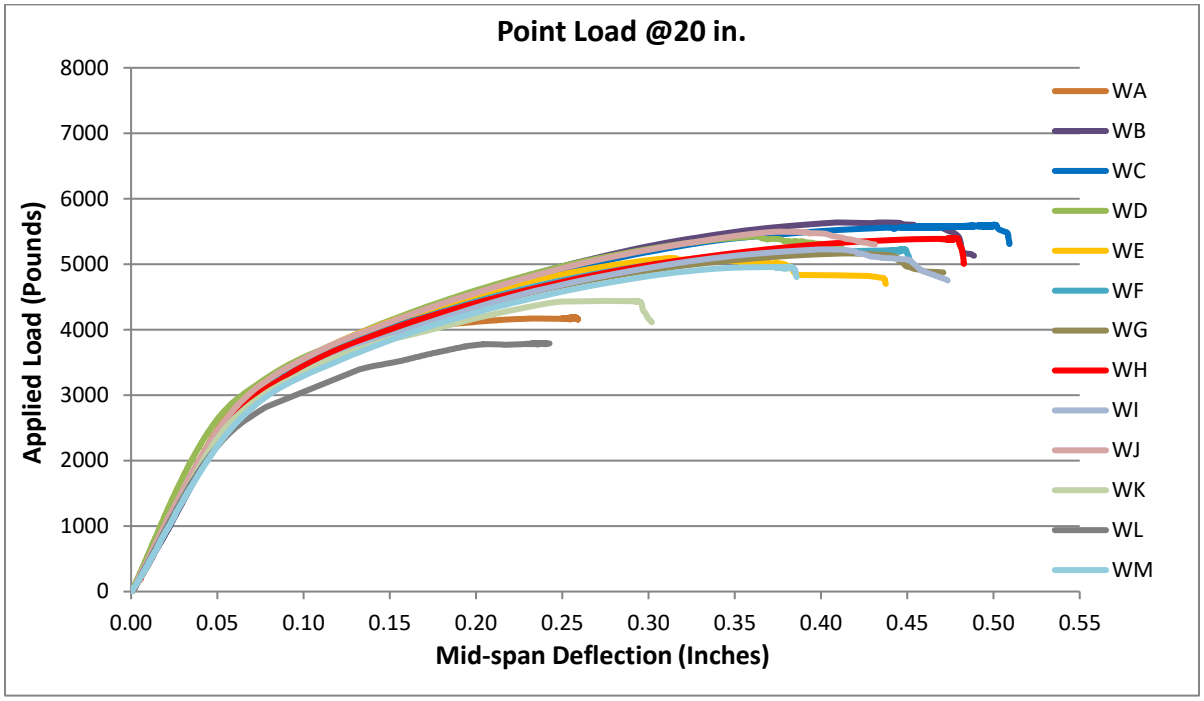


Figure 33. Load-deflection graphs for all 13 types of wire for 20-in. embedment length

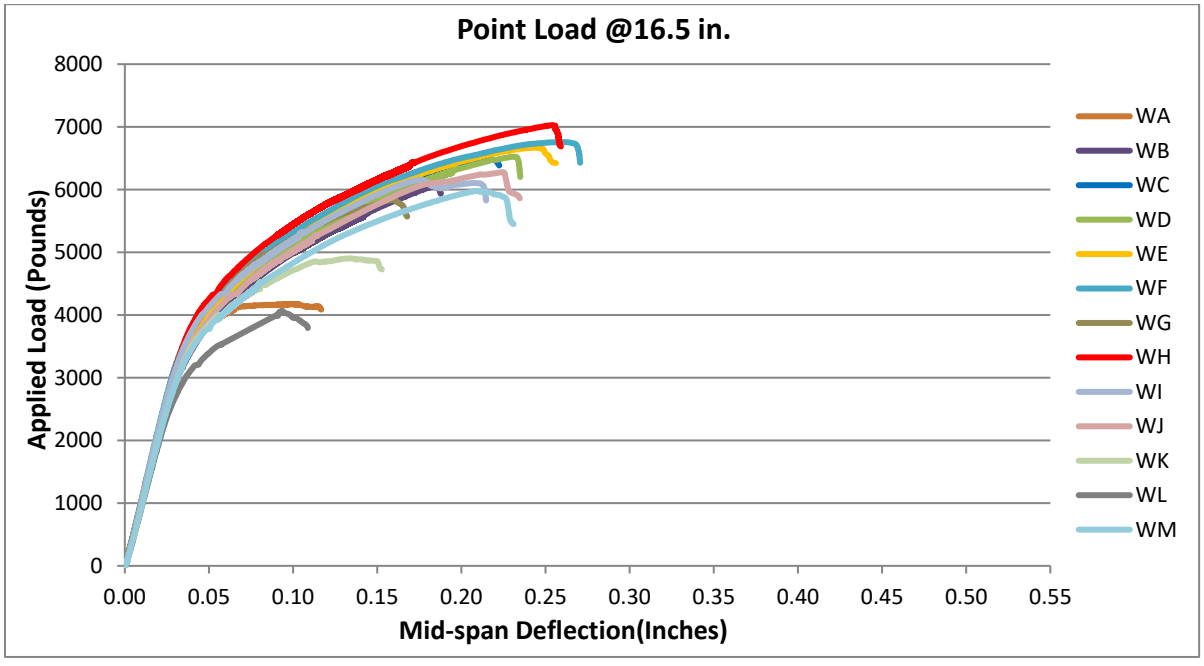


Figure 34. Load-deflection graphs for all 13 types of wire for 16.5-in. embedment length

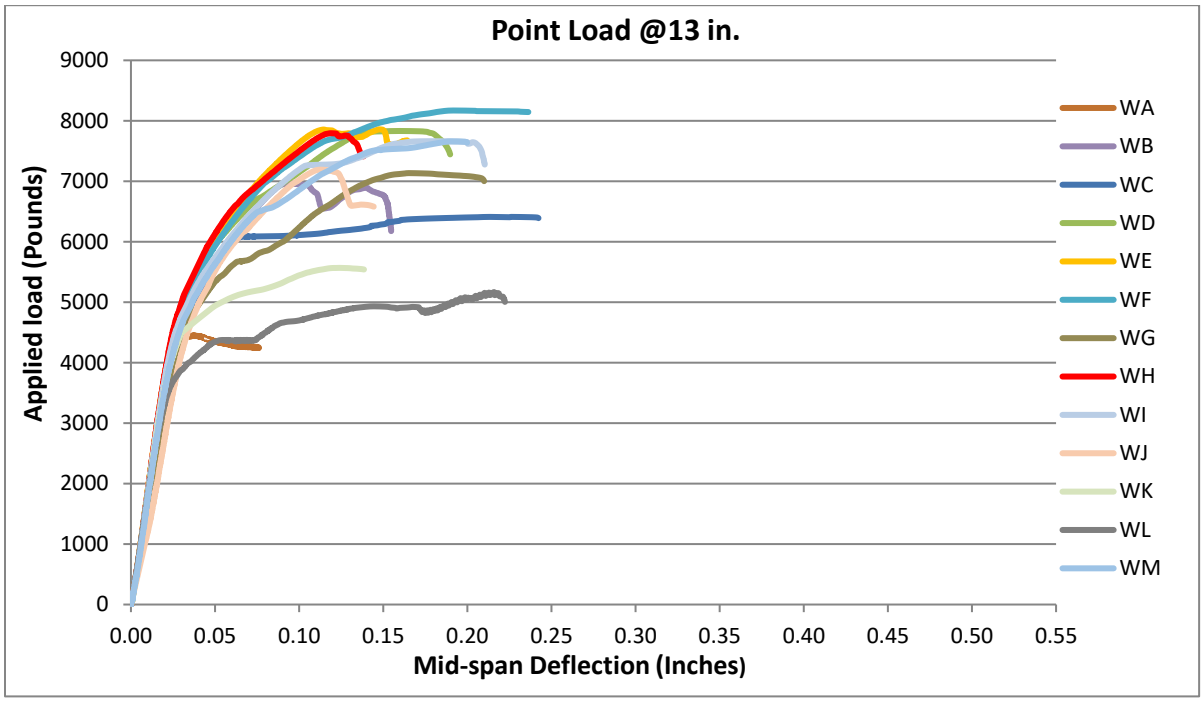


Figure 35. Load-deflection graphs for all 13 types of wire for 16.5-in. embedment length

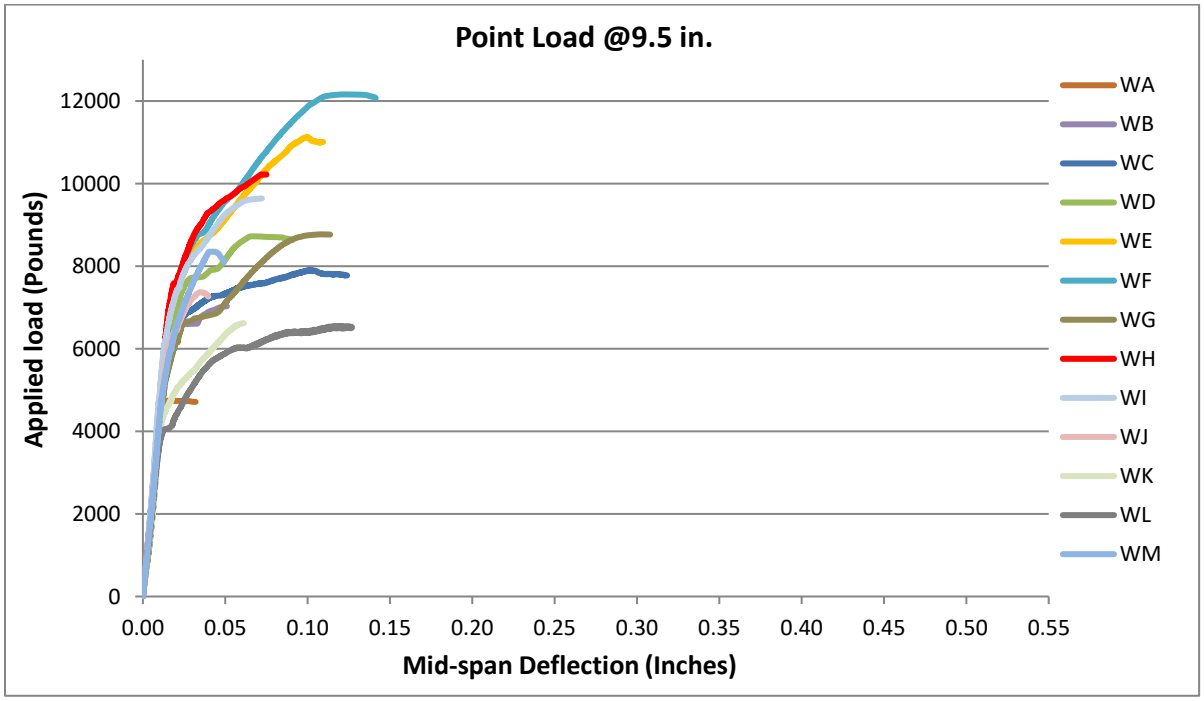


Figure 36. Load-deflection graphs for all 13 types of wire for 9.5-in. embedment length

Maximum load each prism was able to resist was used to calculate the maximum experimental moment (M_{exp}). M_{exp} was calculated under the failure load and prism self-weight. A loading diagram and calculation of M_{exp} is presented below:

Calculating M_{exp} for WA-4500-6-1-L (embedment length=20 in.), prism failed at 4100 lb:

$$Weight\ of\ concrete\ was\ assumed\ to\ be\ 145\ lb/ft^3.$$

$$Thus, self\ weight\ of\ (145\ x\ 3.5\ x\ 3.5)/12^3\ =\ 1.03\ lb/in\ \ was\ used\ in\ calculation\ of\ M_{exp}.$$

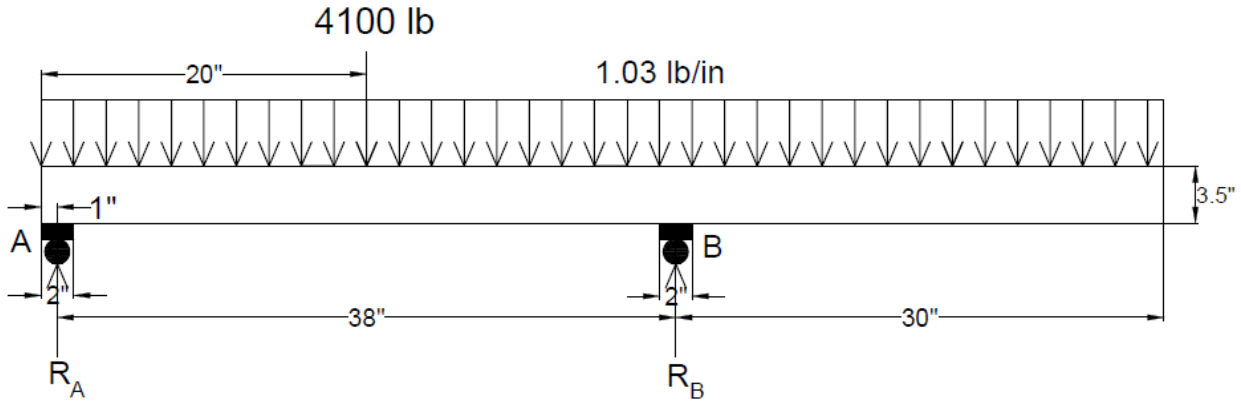


Figure 37. Prism under applied load at time of failure and self weight (WA-4500-6-1-L)

$$\sum M_A = 0 = 4100 \times 19 + 68 \times 1.03 \times 34 - 1.03 \times 1 \times 0.5 - R_B \times 38$$

$$R_B = 2112.6\ lb$$

$$\sum F_Y = 0 = 4100 + 69 \times 1.03 - 2112.6 - R_A$$

$$R_A = 2058.5\ lb$$

$$\sum M_{mid-span} = 2058.5 \times 19 - 20 \times 1.03 \times 10 = 38905.5\ lb - in = 3.24\ kip - ft$$

Next, an additional set of graphs was constructed for maximum experimental moment versus transfer length (calculated before loading tests) for all four different loading spans. Also, nominal-moment capacity (M_n) of prisms was calculated through analysis of pretensioned concrete beams. A strain compatibility-analysis was conducted by assuming the stress-strain diagram from the PCI Design handbook (2010).

In this analysis, compressive strength (f'c) of 12000 psi (82.73 MPa) and release strength (f'ci) of 4500 psi (31.02 MPa) was used for concrete. The horizontal line on the charts shows the

nominal-moment capacity obtained by strain compatibility of the prism cross section. Thus, all 52 loading tests' results are shown in four charts in terms of maximum-moment capacity versus transfer length. Figure 38 to Figure 41 show results for different loading spans.

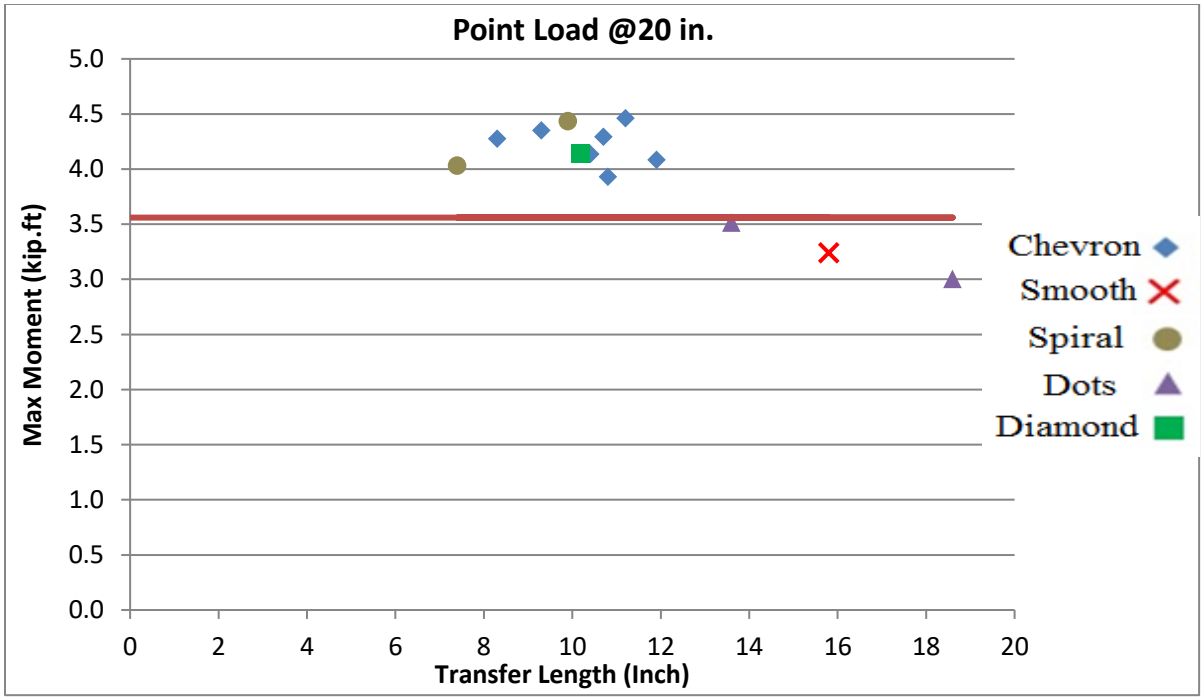


Figure 38. Maximum moment vs transfer length measured at time of de-tensioning for test with 20-in. embedment length

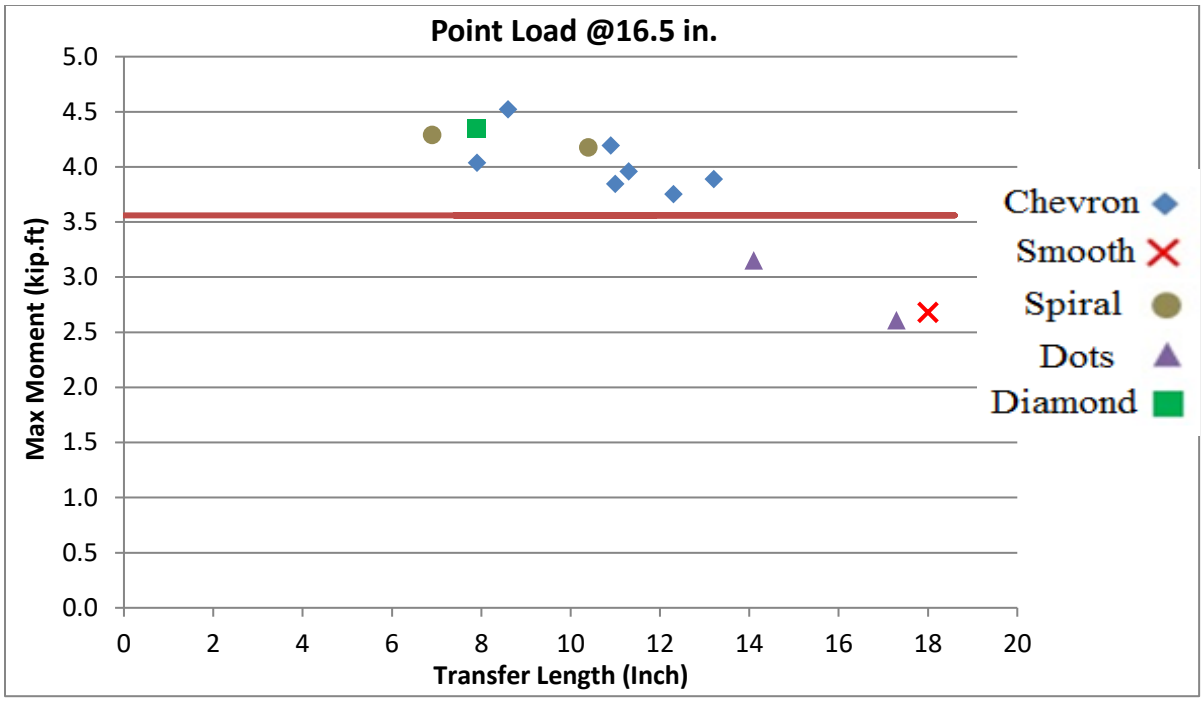


Figure 39. Maximum moment vs transfer length measured at time of de-tensioning for test with 16.5-in. embedment length

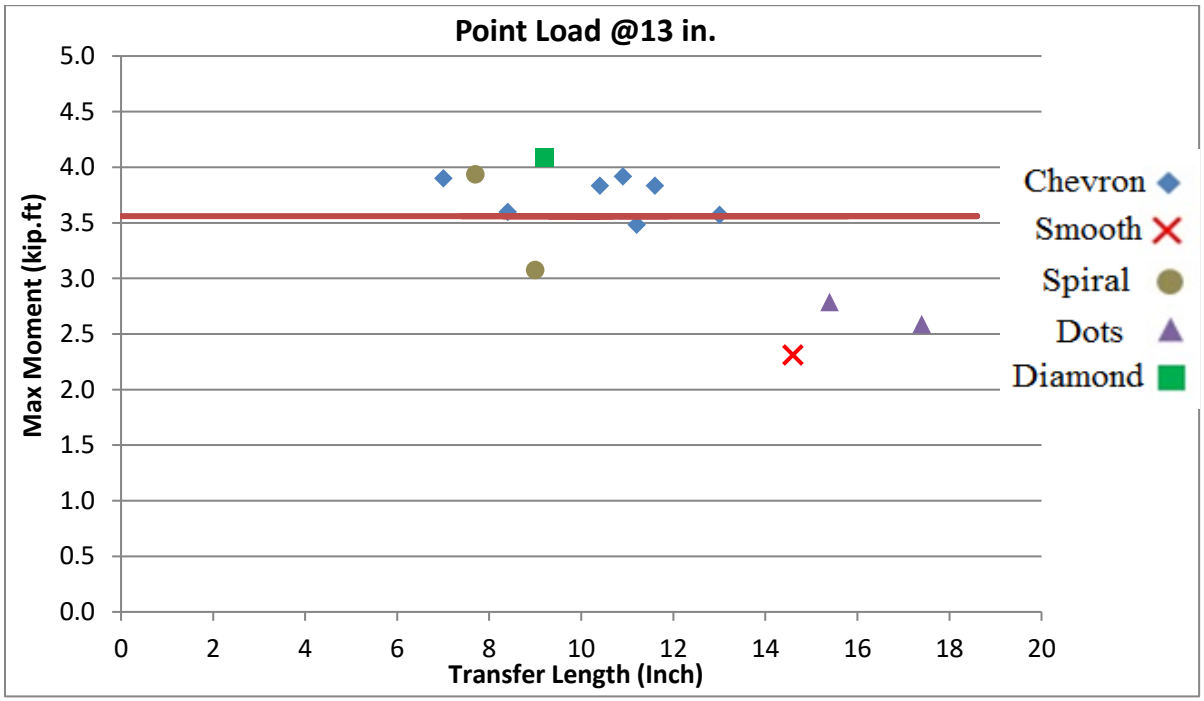


Figure 40. Maximum moment vs transfer length measured at time of de-tensioning for test with 13-in. embedment length

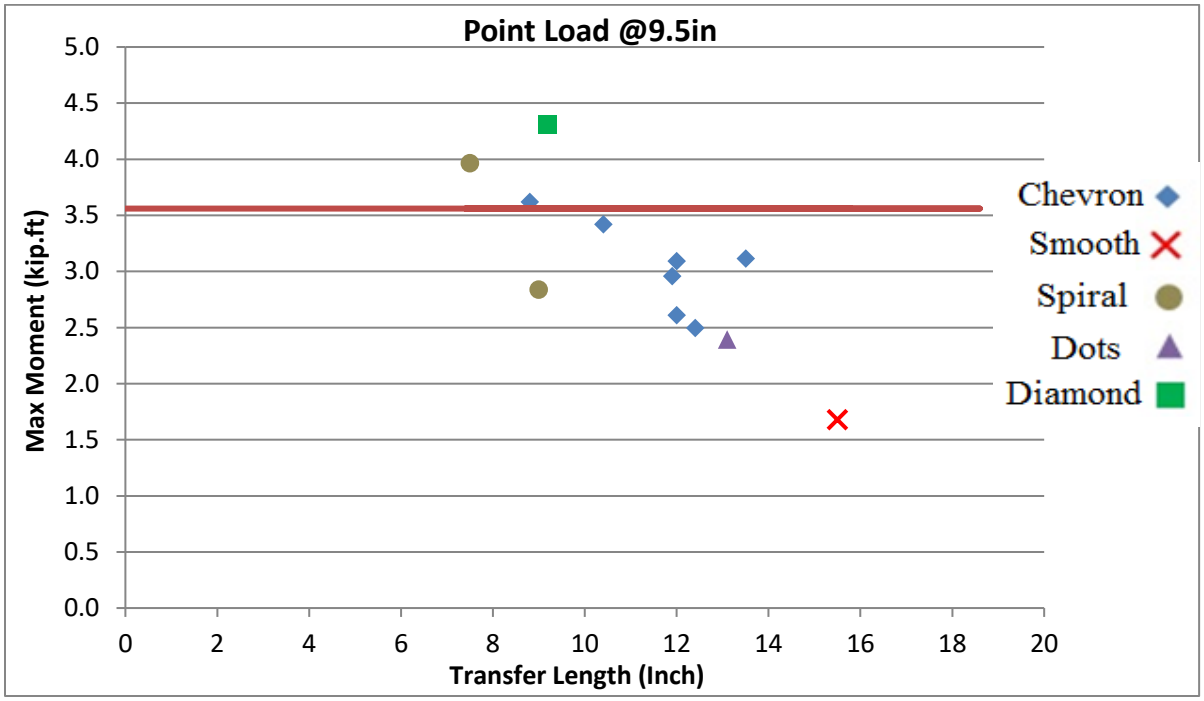


Figure 41. Maximum moment vs transfer length measured at time of de-tensioning for test with 9.5-in. embedment length

In these charts, prisms were categorized according to their wire type in order to obtain estimations for development length based on wire type. Wires were categorized into five groups of chevron indentation, smooth (no surface indentation), spiral, dots, and diamond shape. Each point on these graphs represents maximum moment resisted by the prism versus the transfer length corresponding to the end of the beam that was tested. Table 8 shows results obtained in each load test at prism ends. The last column of Table 8 is the ratio of maximum experimental moment to nominal-moment capacity of that end. Nominal-moment capacity for each end was calculated precisely through strain -compatibility analysis explained in Chapter 5.

Table 8. Results from load tests of two identical prisms for each wire type and 4,500 psi release strength

Beam Designation	Embedment Length (in)	Failure Load (lb)	Mode of Failure	Mexp/Mn
WA-4500-6-1-L	20	4100	Compression	0.91
WA-4500-6-1-S	13	4615	Bond	0.64
WA-4500-6-2-L	16.5	4179	Shear-Bond	0.73
WA-4500-6-2-S	9.5	4743	Bond	0.46
WB-4500-6-1-L	20	5642	Shear-Compression	1.22
WB-4500-6-1-S	13	6963	Shear-Bond	0.96
WB-4500-6-2-L	16.5	6054	Shear-Compression	1.07
WB-4500-6-2-S	9.5	7049	Shear-Bond	0.68
WC-4500-6-1-L	20	5606	Compression	1.28
WC-4500-6-1-S	13	6143	Shear-Bond	0.87
WC-4500-6-2-L	16.5	6495	Compression	1.14
WC-4500-6-2-S	9.5	8012	Shear-Bond	0.80
WD-4500-6-1-L	20	5426	Shear-Compression	1.23
WD-4500-6-1-S	13	7833	Shear-Bond	1.11
WD-4500-6-2-L	16.5	6525	Shear	1.10
WD-4500-6-2-S	9.5	8729	Shear-Bond	0.83
WE-4500-6-1-L	20	5095	Compression	1.15
WE-4500-6-1-S	13	7861	Shear-Compression	1.12
WE-4500-6-2-L	16.5	6670	Shear-Bond	1.21
WE-4500-6-2-S	9.5	11,191	Bond	1.11
WF-4500-6-1-L	20	5235	Shear-Compression	1.18
WF-4500-6-1-S	13	8175	Shear-Bond	1.18
WF-4500-6-2-L	16.5	6758	Shear-Bond	1.23
WF-4500-6-2-S	9.5	12,163	Shear-Bond	1.22
WG-4500-6-1-L	20	5165	Compression	1.20
WG-4500-6-1-S	13	7138	Shear-Bond	1.06
WG-4500-6-2-L	16.5	5842	Shear-Compression	1.09
WG-4500-6-2-S	9.5	8791	Shear-Bond	0.87
WH-4500-6-1-L	20	5404	Shear-Compression	1.19
WH-4500-6-1-S	13	7798	Shear-Compression	1.09
WH-4500-6-2-L	16.5	7031	Shear-Compression	1.14
WH-4500-6-2-S	9.5	10,222	Shear-Bond	0.91
WI-4500-6-1-L	20	5230	Shear-Compression	1.22
WI-4500-6-1-S	13	7663	Shear-Bond	1.11
WI-4500-6-2-L	16.5	6158	Shear-Bond	1.11
WI-4500-6-2-S	9.5	9653	Shear-Bond	0.96
WJ-4500-6-1-L	20	5500	Compression	1.21
WJ-4500-6-1-S	13	7192	Shear-Bond	1.00
WJ-4500-6-2-L	16.5	6279	Shear-Bond	1.12
WJ-4500-6-2-S	9.5	7371	Shear-Compression	0.72
WK-4500-6-1-L	20	4443	Shear-Bond	1.03
WK-4500-6-1-S	13	5567	Shear-Bond	0.81
WK-4500-6-2-L	16.5	4908	Shear-Bond	0.89
WK-4500-6-2-S	9.5	6753	Shear-Bond	0.67
WL-4500-6-1-L	20	3799	Compression	0.89
WL-4500-6-1-S	13	5170	Shear-Bond	0.74
WL-4500-6-2-L	16.5	4066	Compression	0.73
WL-4500-6-2-S	9.5	6634	Bond	0.67
WM-4500-6-1-L	20	4968	Compression	1.10
WM-4500-6-1-S	13	7664	Bond	1.08
WM-4500-6-2-L	16.5	5983	Shear-Compression	1.08
WM-4500-6-2-S	9.5	8355	Shear-Bond	0.84

Discussion of results

As can be seen in presented load-deflection graphs for different loading spans, ultimate loads resisted by prisms were the highest when loading span was the smallest. However, mid-span deflections were the smallest when loading span was 9.5 in. (24.13 cm) from the prism end. Load-deflection graphs presented in the Results section show some important properties of these pretensioned concrete test prisms:

1) Prior to initial crack, all prisms exhibited the same linear behavior and linear parts of loading graphs laid on each other. This shows all prisms had the same flexural rigidity (EI).
2) Different prestressing wire types made a big difference in reserve capacity (capacity beyond the cracking load) of the prisms. Some failed with a slight increase in load beyond the cracking load, showing minor reserve capacity.
3) Prisms made with smooth wire (WA) showed no reserve capacity in some cases and failed right after occurrence of initial crack.

To understand and Compare the capacity of these pretensioned concrete prisms when loaded at different locations (i.e. having different embedment lengths), maximum experimental moments were calculated based on the maximum load resisted by prisms in each test.

As noted previously, development length is the sum of transfer length and flexural-bond length. Prisms were load-tested in different spans to obtain estimations for development length based on wire indentation. In this experiment, loading span decreased from 20 in. (96.52 cm) to 9.5 in. (24.13 cm) from the prism end to note any change in moment capacity. Any considerable reduction in maximum moment with reduction in loading span means the wires were not fully developed at that location.

Since development length is larger than transfer length, in estimations of development length, previous knowledge of transfer length should be considered. Having this in mind, development lengths for different wire types can be estimated as follows:

1) As can be seen in Figure 38 to Figure 41, maximum moment of prisms with chevron wires (WB, WD, WG, WH, WI, WJ, and WM) starts to decrease when the loading span decreases from 16.5 in. (41.9 cm) to 13in. (33.02 cm), and maximum moment starts to decrease even more rapidly when the loading span reduces to 9.5 in. (24.13 cm) from the prism end. This estimates development length between 13 in. (33.02 cm) to 16.5 in. (41.9 cm).
2) Looking at graphs indicates the maximum moment for prisms manufactured with smooth wire keeps decreasing as the loading span decreases, meaning the loading point falls into the development length for all four embedment lengths. Thus, development length for the smooth wire is larger than 20 in. (50.8 cm).
3) Results were quite different for different indentation depths of spirals. The spiral with deeper indentation (WE) showed no abrupt reduction in maximum moment with reduction in loading span, indicating a development length of smaller than 9.5 in. (24.13 cm). However, the spiral with shallower indentation (WC) showed a significant reduction in moment capacity when the loading span was reduced from 16.5 in. (41.9

cm) to 13 in. (33.02 cm), indicating a development length between 13 in. (33.02 cm) to 16.5 in. (41.9 cm).

4) From figures plotted, it can be seen the development length for dot-indented wires is larger than 20 in. (41.9 cm).

5) Graphs show consistent-moment capacity for prisms with diamond-shaped indentation (WF), and no significant reduction in moment capacity can be seen as the loading span changes. This estimates a development length which is slightly larger than transfer length, indicating an exceptional flexural-bond development.

Also, development-length estimations are made for each type of wire and documented as a range in Table 9. When maximum experimental moment for each test was larger than nominal-moment capacity obtained from strain-compatibility analysis, the wire was assumed to be fully developed at that location. This means any point above the horizontal line in Figure 38 to Figure 41 represents a prism with fully developed wires. Table 9 is generated based on results presented in Figure 38 through Figure 41.

Table 9 Development-length estimations for each end tested

		Achieved Nominal-Moment Capacity (Mn)					
Wire Label	**Average Lt (in)**	**at 20 in.**	**at 16.5 in.**	**at 13 in.**	**at 9.5 in.**	**Ld Range (in)**	**Ld/Lt**
WA	16.3	No	No	No	No	>20	>1.23
WB	11.6	Yes	Yes	No	No	13-16.5	1.12-1.42
WC	8.8	Yes	Yes	No	No	13-16.5	1.48-1.87
WD	11.1	Yes	Yes	Yes	No	9.5-13	1-1.17
WE	7.4	Yes	Yes	Yes	Yes	<9.5	<1.28
WF	8.5	Yes	Yes	Yes	Yes	<9.5	<1.12
WG	11.8	Yes	Yes	Yes	No	9.5-13	1-1.10
WH	7.5	Yes	Yes	Yes	Yes	<9.5	<1.26
WI	10.1	Yes	Yes	Yes	No	9.5-13	1-1.29
WJ	9	Yes	Yes	Yes	No	9.5-13	1.05-1.44
WK	14	No	No	No	No	20>	>1.43
WL	18.7	No	No	No	No	20>	>1.07
WM	11	Yes	Yes	Yes	No	9.5-13	1-1.18

In this table, when maximum experimental moment was larger than nominal-moment capacity obtained from analysis, the word “Yes” was used to show the nominal-moment capacity was achieved and development length was shorter than loading span. In the last column of this table, ratio of development length to transfer length is calculated to estimate development length as a percentage of transfer length.

4.1.2 Effect of concrete-release strengths on development length

For prisms with different concrete-release strengths, maximum experimental moment (M_{exp}) by each prism was determined from the maximum applied load by equilibrium of forces and the following figures were generated. Figure 42 through Figure 46 plot the maximum experimental moments for each wire type, as a function of the average transfer length at the time of de-tensioning (Bodapati, et al., 2013), for the same wire and release strength, as well as the embedment lengths. Values of determined transfer lengths at the time of de-tensioning (Bodapati, et al., 2013) for each type of wire and three different concrete-release strengths are summarized in Table 10 to

Table 12. Note the last column shows average transfer lengths of six ends and not the average of four transfer lengths in the table.

Table 10 Transfer lengths determined at the time of de-tensioning at tested prism ends for prisms with 3,500 psi concrete-release strength (Bodapati, et al., 2013)

3500 psi Concrete-Release Strength						
Wire designation	Indentation type	T.L determined end tested @ 20 (in.)	T.L determined end tested @ 16.5 (in.)	T.L determined end tested @ 13 (in.)	T.L determined end tested @ 9.5 (in.)	Average T.L (in)
WA	smooth	19.8	20.4	21.4	21.5	21.4
WE	spiral	8.6	11.3	11.1	9.8	10.5
WG	chevron	13.9	13.8	12.8	14.4	13.8
WH	chevron	9.9	10.4	10.0	10.3	11.2
WK	4-dot	17.5	19.0	16.7	16.6	17.7

Table 11 Transfer lengths determined at time of de-tensioning at tested prism ends for prisms with 4,500 psi concrete-release strength (Bodapati, et al., 2013)

4500 psi Concrete-Release Strength						
Wire designation	Indentation type	T.L determined end tested @ 20 (in.)	T.L determined end tested @ 16.5 (in.)	T.L determined end tested @ 13 (in.)	T.L determined end tested @ 9.5 (in.)	Average T.L (in)
WA	smooth	16.4	17.9	14.4	15.6	16.3
WE	spiral	7.2	8.0	6.8	7.9	7.4
WG	chevron	11.6	11.6	11.6	12.6	11.8
WH	chevron	7.4	7.5	6.5	7.9	7.5

WK	**4-dot**	14.2	14.0	14.9	13.7	14.0

Table 12 Transfer lengths determined at time of de-tensioning at tested prism ends for prisms with 6,000 psi concrete-release strength (Bodapati, et al., 2013)

6000 psi Concrete-Release Strength						
Wire designation	**Indentation type**	**T.L determined end tested @ 20 (in.)**	**T.L determined end tested @ 16.5 (in.)**	**T.L determined end tested @ 13 (in.)**	**T.L determined end tested @ 9.5 (in.)**	**Average T.L (in)**
WA	**smooth**	14.2	13.3	13.5	14.3	13.5
WE	**spiral**	7.5	7.5	8.3	5.1	7.1
WG	**chevron**	9.7	10.3	10.9	8.5	9.8
WH	**chevron**	6.6	8.4	8.0	6.8	7.3
WK	**4-dot**	10.5	10	11.4	10.5	11.1

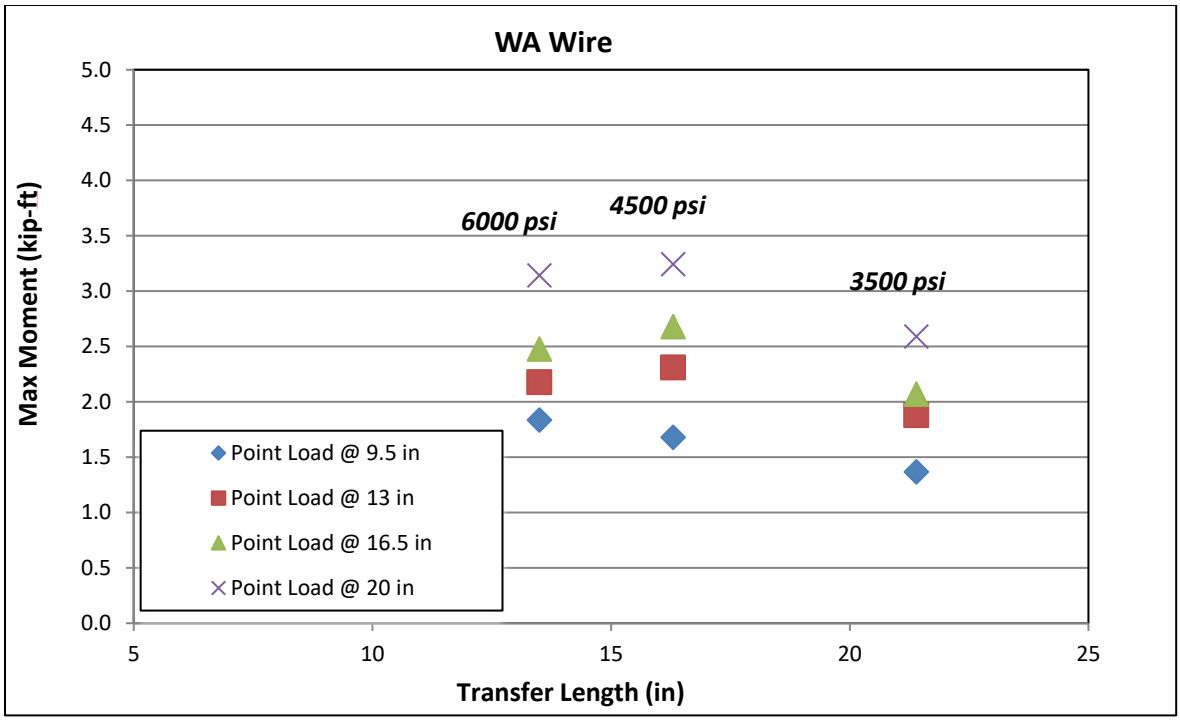


Figure 42. Maximum moment vs average transfer length for prisms made with WA and 3,500, 4,500 and 6,000 psi release strengths

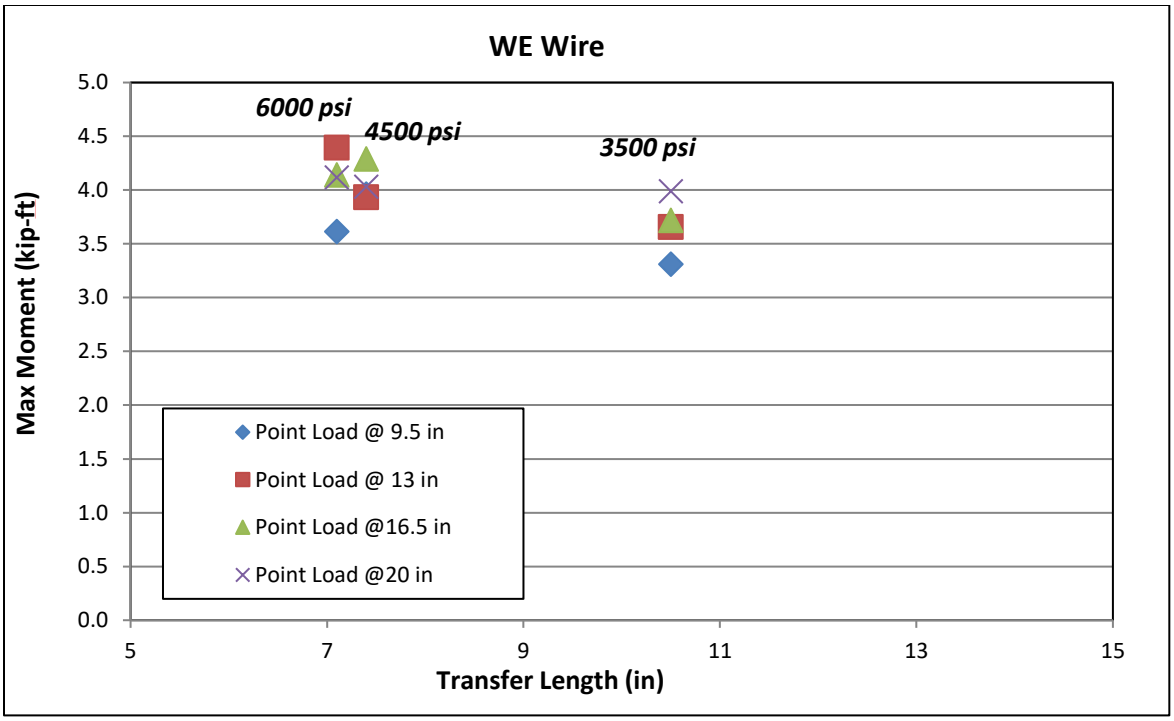


Figure 43. Maximum moment vs average transfer length for prisms made with WE and 3,500, 4,500 and 6,000 psi release strengths

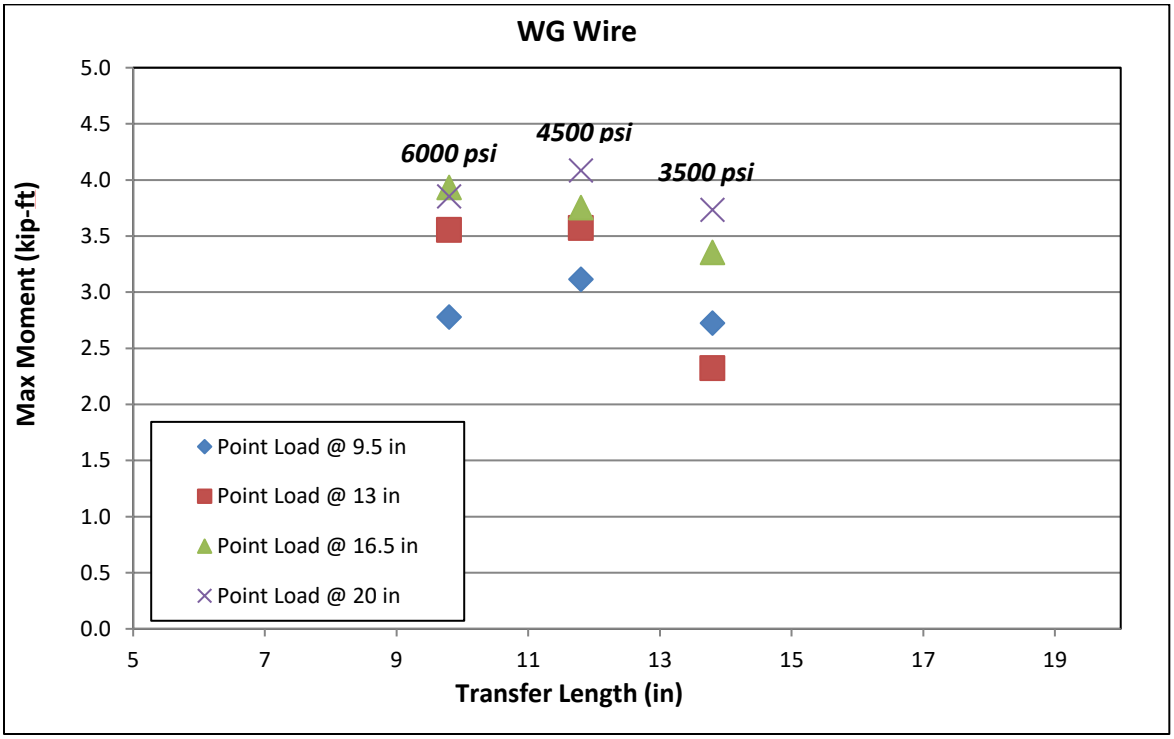


Figure 44. Maximum moment vs average transfer length for prisms made with WG and 3,500, 4,500 and 6,000 psi release strengths.

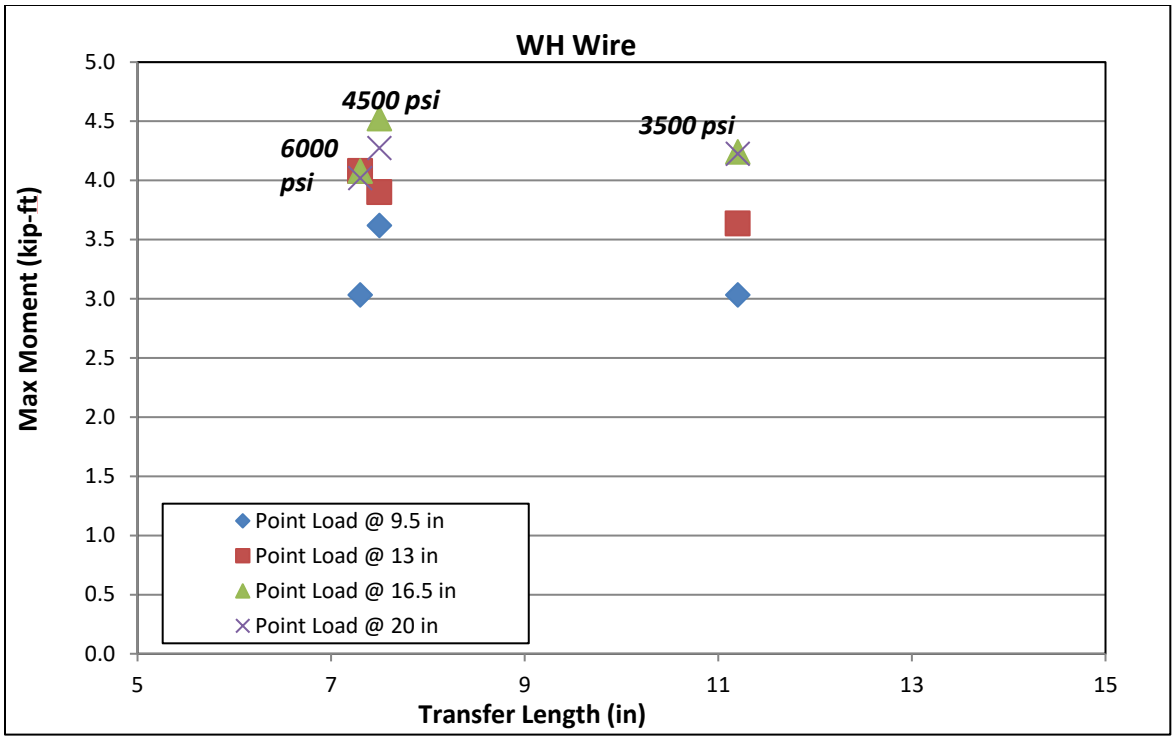


Figure 45. Maximum moment vs average transfer length for prisms made with WH and 3,500, 4,500 and 6,000 psi release strengths.

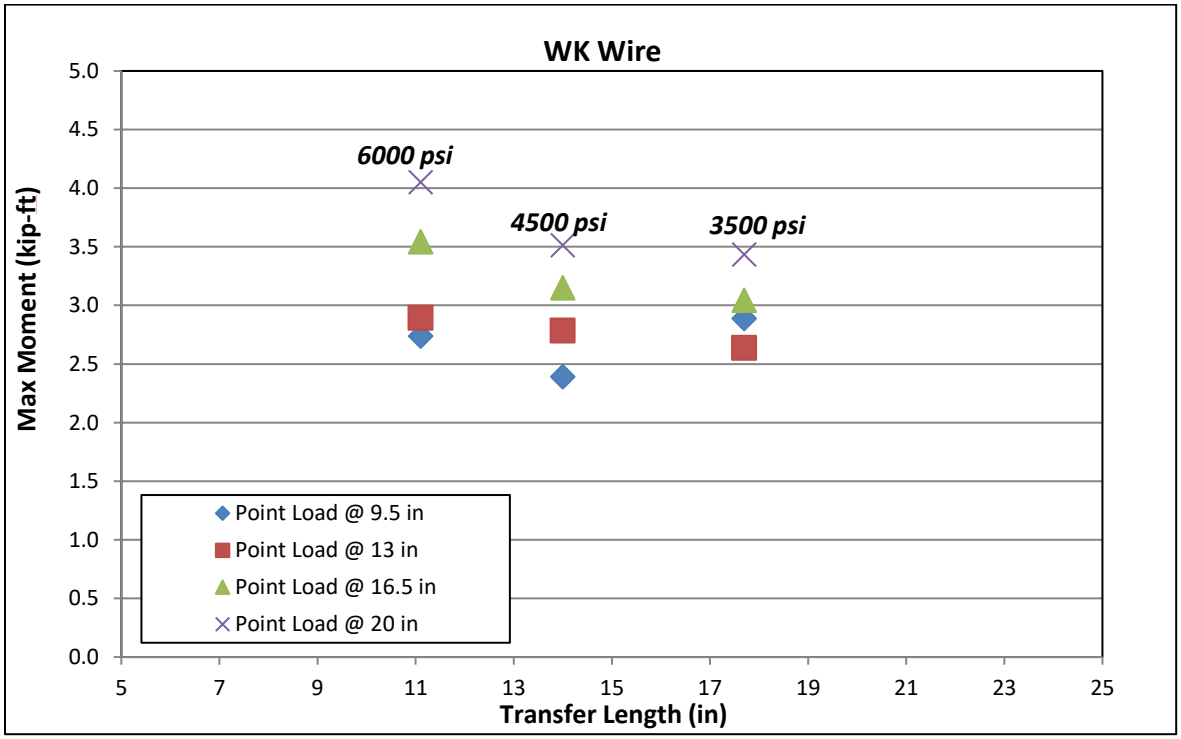


Figure 46. Maximum moment vs average transfer length for prisms made with WK and 3,500, 4,500 and 6,000 psi release strengths.

Table 13 shows results obtained in each load test at prism ends for prisms with 3500 and 6,000 psi concrete-release strengths. The last column of Table 13 is the ratio of maximum experimental moment to nominal-moment capacity of that end. Nominal-moment capacity for each end was calculated precisely through strain-compatibility analysis explained in Chapter 5. Note that test results from prisms manufactured with 4,500 psi release strength are in Table 8.

Table 13. Results from load tests of two identical prisms for each wire type and different concrete-release strengths

Beam designation	Embedment length (in)	Failure load (lb)	Mode of failure	Mexp/Mn
WA-3500-6-1-L	20	3275	Shear-Compression	0.72
WA-3500-6-1-S	13	3750	Shear-Bond	0.53
WA-3500-6-2-L	16.5	3234	Shear-Bond	0.59
WA-3500-6-2-S	9.5	3860	Bond	0.39
WE-3500-6-1-L	20	5042	Shear-Bond	1.14
WE-3500-6-1-S	13	7306	Shear-Bond	1.23
WE-3500-6-2-L	16.5	5785	Shear-Compression	1.13
WE-3500-6-2-S	9.5	9350	Bond	1.00
WG-3500-6-1-L	20	4720	Compression	1.13
WG-3500-6-1-S	13	4639	Shear-Bond	1.03
WG-3500-6-2-L	16.5	5222	Shear-Compression	1.15
WG-3500-6-2-S	9.5	7690	Shear-Bond	0.80
WH-3500-6-1-L	20	5341	Compression	1.19
WH-3500-6-1-S	13	7268	Shear-Bond	1.01
WH-3500-6-2-L	16.5	6596	Shear-Bond	1.16
WH-3500-6-2-S	9.5	8562	Shear-Bond	0.81
WK-3500-6-1-L	20	4343	Shear-Bond	0.83
WK-3500-6-1-S	13	5271	Shear-Bond	0.75
WK-3500-6-2-L	16.5	4744	Shear-Compression	0.83
WK-3500-6-2-S	9.5	8160	Bond	0.85
WA-6000-6-1-L	20	3973	Bond	0.87
WA-6000-6-1-S	13	4348	Shear-Bond	0.62
WA-6000-6-2-L	16.5	3865	Shear-Bond	0.67
WA-6000-6-2-S	9.5	5182	Bond	0.50
WE-6000-6-1-L	20	5206	Compression	1.14
WE-6000-6-1-S	13	8783	Compression	1.23
WE-6000-6-2-L	16.5	6442	Compression	1.13
WE-6000-6-2-S	9.5	10,201	Shear-Bond	1.00
WG-6000-6-1-L	20	4873	Compression	1.13
WG-6000-6-1-S	13	7100	Shear-Compression	1.03
WG-6000-6-2-L	16.5	6119	Shear-Compression	1.15
WG-6000-6-2-S	9.5	7845	Shear-Bond	0.80
WH-6000-6-1-L	20	5081	Shear-Compression	1.11
WH-6000-6-1-S	13	8153	Shear	1.13
WH-6000-6-2-L	16.5	6346	Compression	1.14
WH-6000-6-2-S	9.5	8567	Shear-Bond	0.84
WK-6000-6-1-L	20	5124	Compression	1.18
WK-6000-6-1-S	13	5758	Shear-Bond	0.82
WK-6000-6-2-L	16.5	5516	Shear-Bond	1.00
WK-6000-6-2-S	9.5	7736	Shear-Bond	0.78

Discussion of results

Results shown in Figure 42 to Figure 46 are categorized according to wire type in order to make Comparisons between the different concrete-release strengths possible. Loading tests were conducted with four different loading spans to obtain estimations of development length. Any reduction in maximum moment caused by a reduction in embedment length means the prestress force is not fully developed, and the section was not at its maximum capacity.

Comparing results presented in the above figures led to the following findings:

1) For all types of wires except spiral-indented (WE) and chevron-indented (WH), transfer lengths for prisms with 6,000 (41.37 MPa) psi release strength were significantly shorter than transfer lengths for prisms with 4,500 (31.02 MPa) psi release strength; and transfer lengths were the largest for prisms with 3,500 (24.13 MPa) psi release strength. For wire types WE and WH, the average transfer lengths at 6000 psi (41.37 MPa) were only slightly shorter than the average transfer lengths at 4500 psi (31.02 MPa).
2) Comparing maximum experimental moments for different release strengths and embedment lengths for each type of wire shows that for wires with light or no indentations (WK and WA), there was a general trend where maximum experimental moment increased as release strength increased. This is likely due to the fact that for these wires, the tested length often was located within the transfer length.
3) For the better-bonding wires with more pronounced indentations (WE, WG, and WH), there was little difference in the moment capacities with increasing concrete-release strength. This is likely because the tests were conducted after the prisms were more than a year old, and the concrete compressive strength of all specimens at the time of testing was essentially the same.

4.1.3 Effect of concrete slump on development length

For prisms with different concrete slump, maximum experimental moment resisted by each prism was determined from maximum applied load by equilibrium of forces, and the following figures were generated. Figure 47 through Figure 51 plot the maximum experimental moments for each wire type, as a function of the average transfer length at the time of de-tensioning (for the same wire and concrete slump) (Bodapati, et al., 2013), as well as the embedment length. Values of determined transfer lengths at the time of de-tensioning for each type of wire and three different concrete slumps are summarized in

Table 14 to Table 16. Note the last column is the average transfer length for six ends and not the average of four transfer lengths in the table.

Table 14 Transfer lengths determined at time of de-tensioning at prism ends for prisms with 3-in. concrete slump (Bodapati, et al., 2013)

3 in. Slump and 4500 psi Concrete-Release Strength					
Wire designation	T.L determined end tested @ 20 (in.)	T.L determined end tested @ 16.5 (in.)	T.L determined end tested @ 13 (in.)	T.L determined end tested @ 9.5 (in.)	Average T.L (in)
WA	15.1	15.0	15.5	16.0	16.1
WE	6.4	7.0	8.9	8.3	8.3
WG	12.5	11.0	12.9	12.0	11.8
WH	8.7	21.0	10.8	9.3	11.2
WK	13.3	14.0	12.5	13.4	14.0

Table 15 Transfer lengths determined at time of de-tensioning at prism ends for prisms with 6-in. concrete slump (Bodapati, et al., 2013)

6 in. Slump and 4500 psi Concrete-Release Strength					
Wire designation	T.L determined end tested @ 20 (in.)	T.L determined end tested @ 16.5 (in.)	T.L determined end tested @ 13 (in.)	T.L determined end tested @ 9.5 (in.)	Average T.L (in)
WA	16.4	18.0	14.4	15.6	16.3
WE	7.2	8.0	6.8	7.9	7.4
WG	11.6	12.0	11.6	12.6	11.8
WH	7.4	8.0	6.5	7.9	7.5
WK	14.2	14.0	14.9	13.7	14.0

Table 16 Transfer lengths determined at time of de-tensioning at prism ends for prisms with 9-in. concrete slump (Bodapati, et al., 2013)

9 in. Slump and 4500 psi Concrete-Release Strength					
Wire designation	T.L determined end tested @ 20 (in.)	T.L determined end tested @ 16.5 (in.)	T.L determined end tested @ 13 (in.)	T.L determined end tested @ 9.5 (in.)	Average T.L (in)
WA	17.1	17.0	15.8	17.9	16.9
WE	8.3	10.0	8.6	10.3	9.3
WG	13.3	12.9	13.0	14.2	13.3
WH	8.7	8.9	10.8	10.4	9.2
WK	15.5	17.1	14.2	16.4	15.2

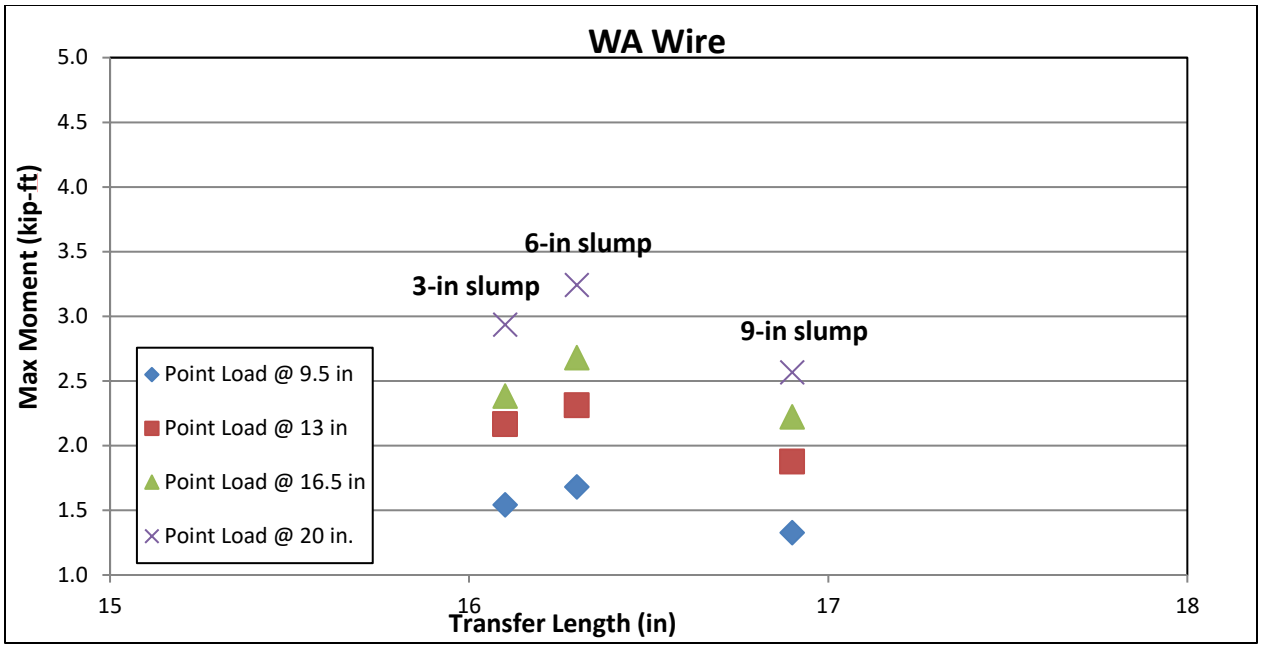


Figure 47. Maximum moment vs average transfer length for prisms made with WA wire and concrete slumps of 3, 6, and 9 in.

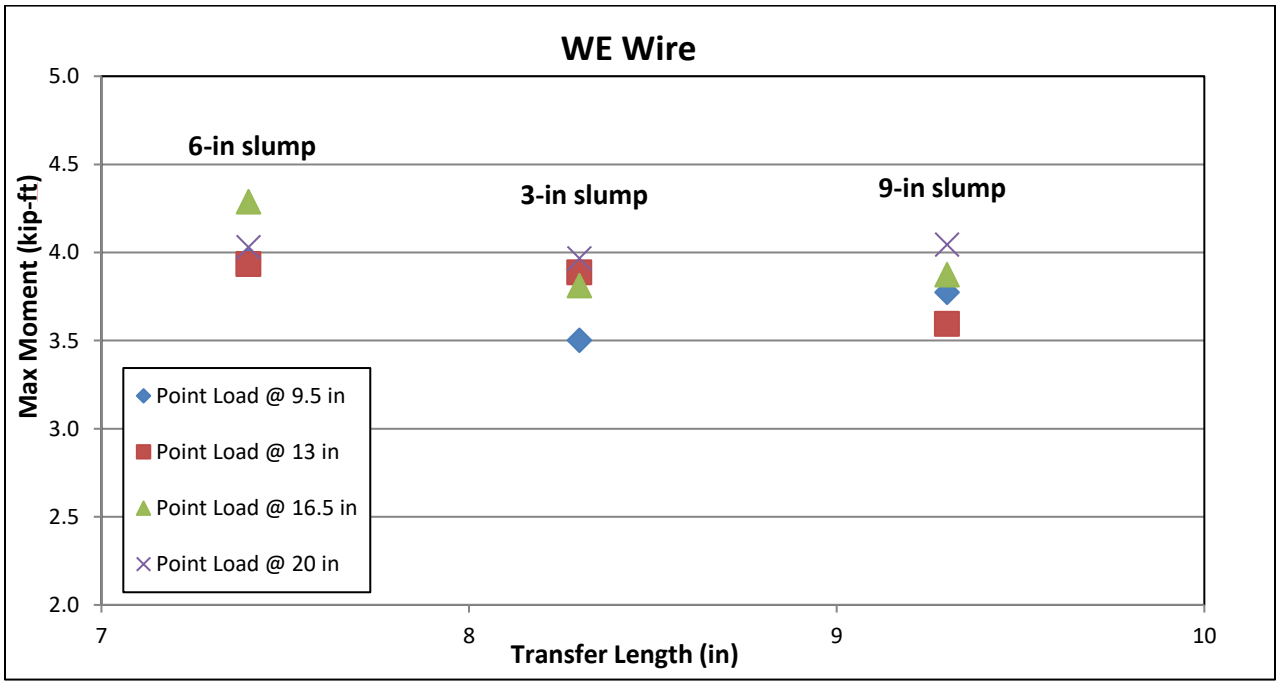


Figure 48. Maximum moment vs average transfer length for prisms made with WE wire and concrete slumps of 3, 6, and 9 in.

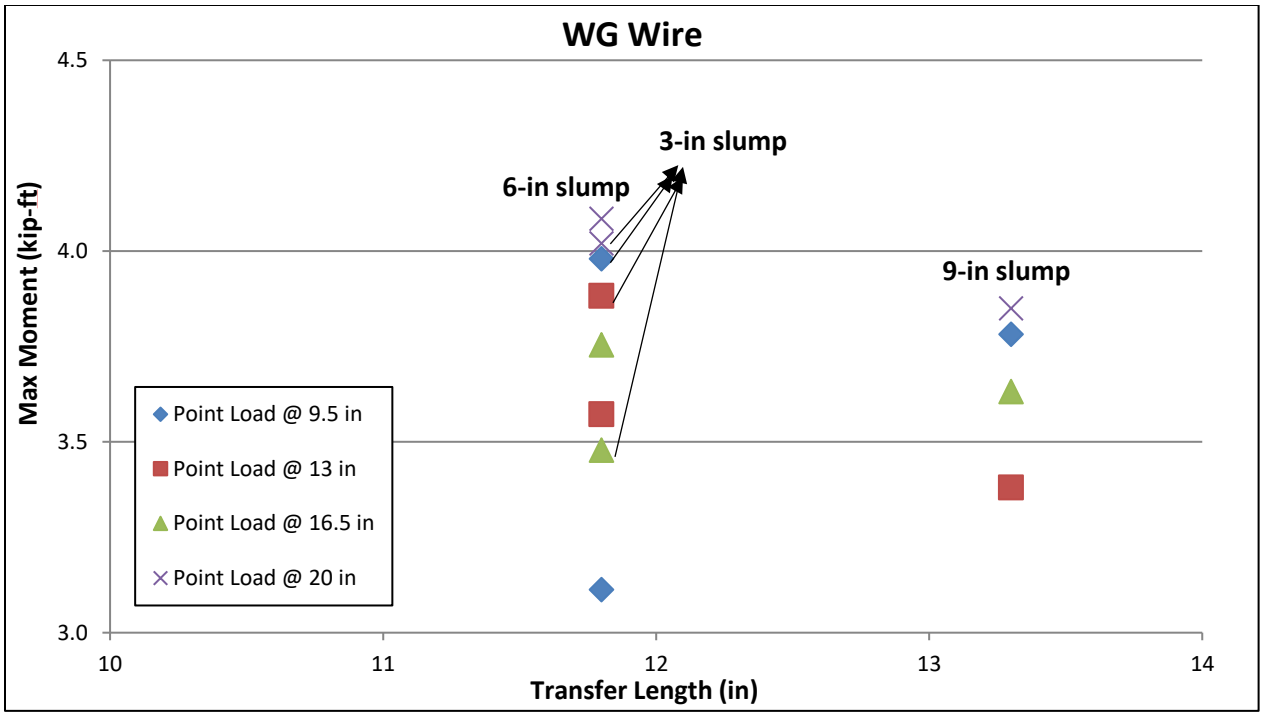


Figure 49. Maximum moment vs average transfer length for prisms made with WG wire and concrete slumps of 3, 6, and 9 in.

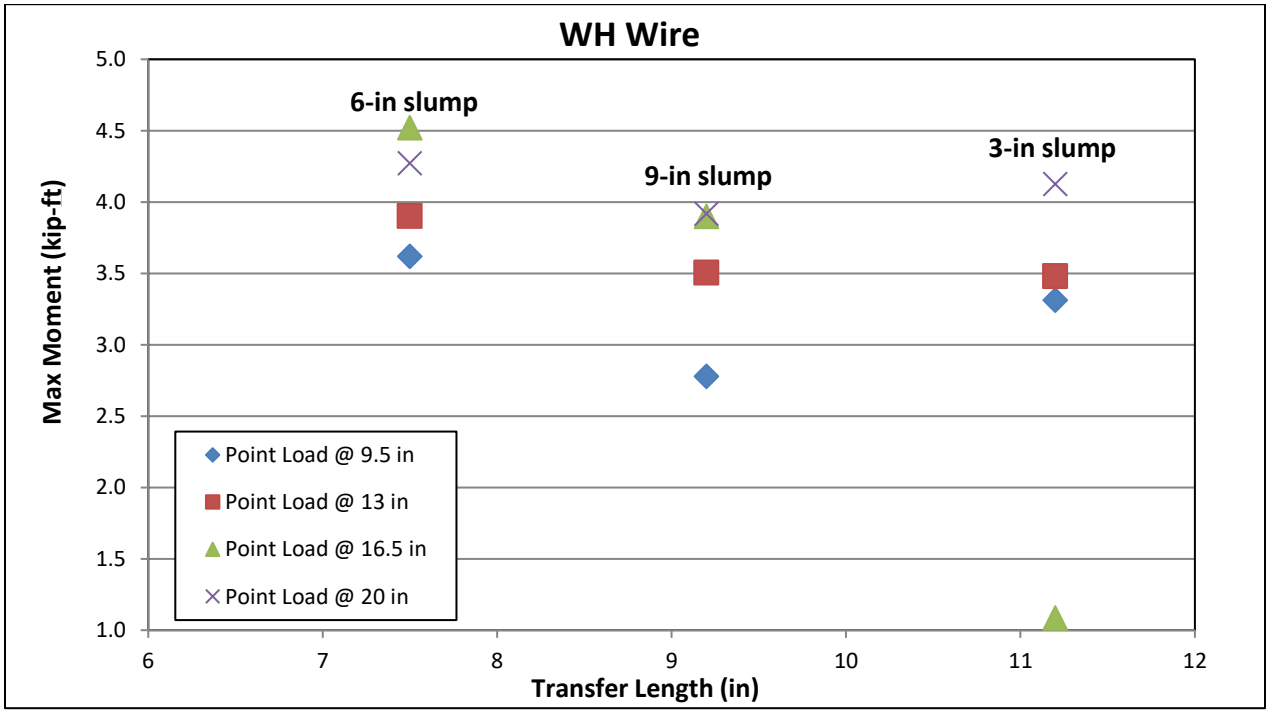


Figure 50. Maximum moment vs average transfer length for prisms made with WH wire and concrete slumps of 3, 6, and 9 in.

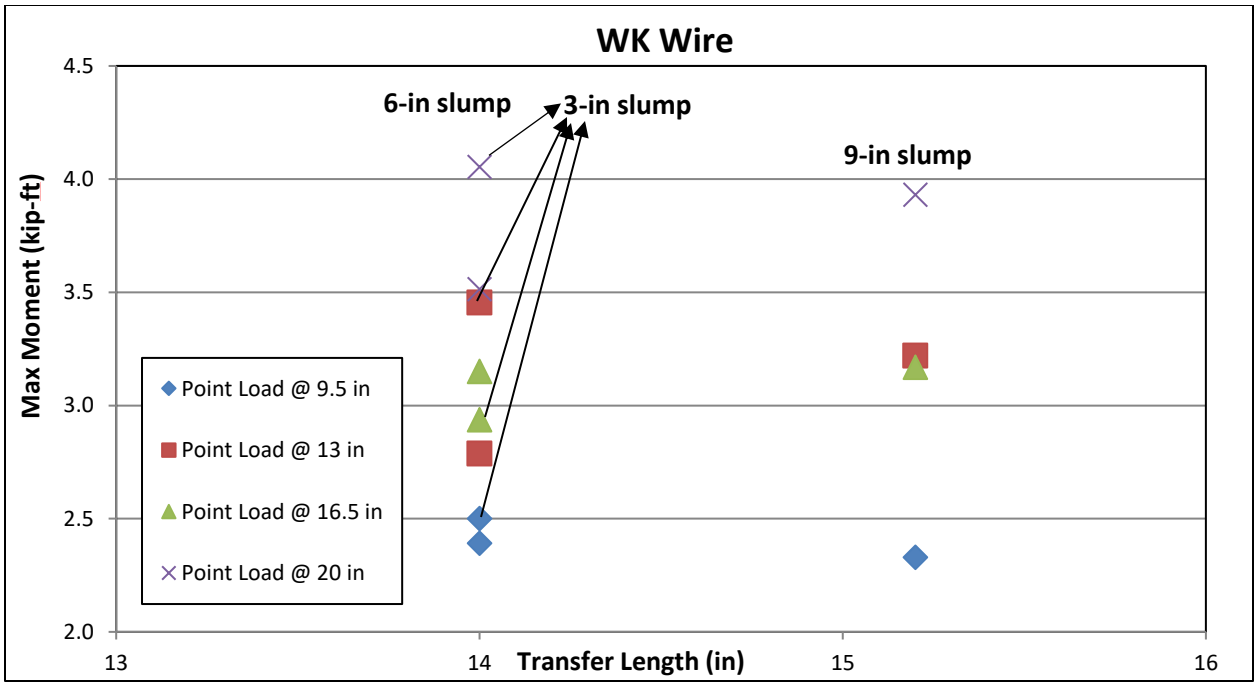


Figure 51. Maximum moment vs average transfer length for prisms made with WK wire and concrete slumps of 3, 6, and 9 in.

Table 17 shows results obtained in each load test at prism ends for prisms with 3-in. and 9-in. concrete slump. Note that test results from prisms manufactured with 6-in. concrete slump are in Table 8.

Table 17. Results from load tests of two identical prisms for each wire type and different concrete slumps

Beam designation	Embedment length (in)	Failure load (lb)	Mode of failure
WA-4500-3-1-L	20	3713	Bond
WA-4500-3-1-S	13	4403	Bond
WA-4500-3-2-L	16.5	3722	Shear-Bond
WA-4500-3-2-S	9.5	4509	Bond
WE-4500-3-1-L	20	5017	Shear-Compression
WE-4500-3-1-S	13	7848	Shear-Compression
WE-4500-3-2-L	16.5	5934	Shear-Compression
WE-4500-3-2-S	9.5	10,042	Shear
WG-4500-3-1-L	20	5083	Shear-Bond
WG-4500-3-1-S	13	7838	Shear-Bond
WG-4500-3-2-L	16.5	5417	Horizontal Splitting
WG-4500-3-2-S	9.5	11,391	Shear-Bond
WH-4500-3-1-L	20	5218	Shear-Compression
WH-4500-3-1-S	13	7035	Shear-Bond
WH-4500-3-2-L	16.5	1715	Prism had cracks (flawed)
WH-4500-3-2-S	9.5	9509	Shear-Bond
WK-4500-3-1-L	20	5126	Shear-Bond
WK-4500-3-1-S	13	6981	Shear-Bond
WK-4500-3-2-L	16.5	4578	Shear-Bond
WK-4500-3-2-S	9.5	7214	Shear-Bond
WA-4500-9-1-L	20	3246	Bond
WA-4500-9-1-S	13	3825	Bond
WA-4500-9-2-L	16.5	3472	Shear-Bond
WA-4500-9-2-S	9.5	3901	Bond
WE-4500-9-1-L	20	5116	Shear-Compression
WE-4500-9-1-S	13	7262	Shear
WE-4500-9-2-L	16.5	6030	Shear-Compression
WE-4500-9-2-S	9.5	10,812	Bond
WG-4500-9-1-L	20	4868	Shear-Bond
WG-4500-9-1-S	13	6834	Bond
WG-4500-9-2-L	16.5	5654	Shear-Compression
WG-4500-9-2-S	9.5	10,833	Bond
WH-4500-9-1-L	20	4954	Compression
WH-4500-9-1-S	13	7085	Shear
WH-4500-9-2-L	16.5	6071	Compression
WH-4500-9-2-S	9.5	8002	Shear
WK-4500-9-1-L	20	4970	Shear-Bond
WK-4500-9-1-S	13	6514	Bond
WK-4500-9-2-L	16.5	4938	Shear
WK-4500-9-2-S	9.5	6731	Bond

Discussion of results

Results shown in Figure 47 to Figure 51 are categorized according to wire type in order to make Comparisons between different concrete slumps possible. Loading tests were conducted with four different loading spans to obtain estimations of development length. Comparing results presented in the above figures leads to the following findings:

1) For all types of wires except WH, prisms with concrete slump of 9 in. had the largest transfer lengths compared to prisms with 3- or 6-in. slump.
2) Prisms made with WG and WK wires had equal average transfer lengths for concrete mixes with 3- and 6-in. slump.
3) No general correlation between concrete slump and development length, and flexural capacity of prisms can be seen.

4.2 Phase II-Effect of Concrete Properties and Prestressing Strand-Indentation Types on Development Length and Flexural Capacity of Pretensioned Concrete Crossties Made with Three- and Seven-Wire Strands

4.2.1 Effect of strand diameter and indentation type on development length

Transfer lengths were determined at the time of de-tensioning by Naga Narendra Bodapati for both ends of all three prisms. Average values of six, determined transfer lengths are reported in the following table for all strand types.

Table 18. Average transfer lengths at the time of de-tensioning for prisms made with concrete release strength of 4,500 psi and different strands

Average transfer length (in)	
SA	11.6
SB	16.3
SD	15.8
SE	19.0
SF	12.5
SC	13.8

Load testing of different specimens resulted in different modes of failure. Specimens with large-strand end-slip failed in bond, indicating the bond between strands and concrete was not fully developed, or in the other words, development length was larger than the tested embedment length. Bond failures were evidenced by large-strand slippage and no concrete split-cracking.

The recorded force and deflection data for each test were used to construct force versus deflection graphs. Plotted graphs of force versus mid-span deflection for SA, SB, SD, and SE

strands were combined on one single chart, and four separate charts were created for four loading spans. Comparison of behavior of prisms manufactured with different strands under the point load was better understood through combination of load-deflection graphs on one chart. Figure 52 to Figure 55 show load-deflection graphs for SA, SB, SD, and SE strands for each embedment length.

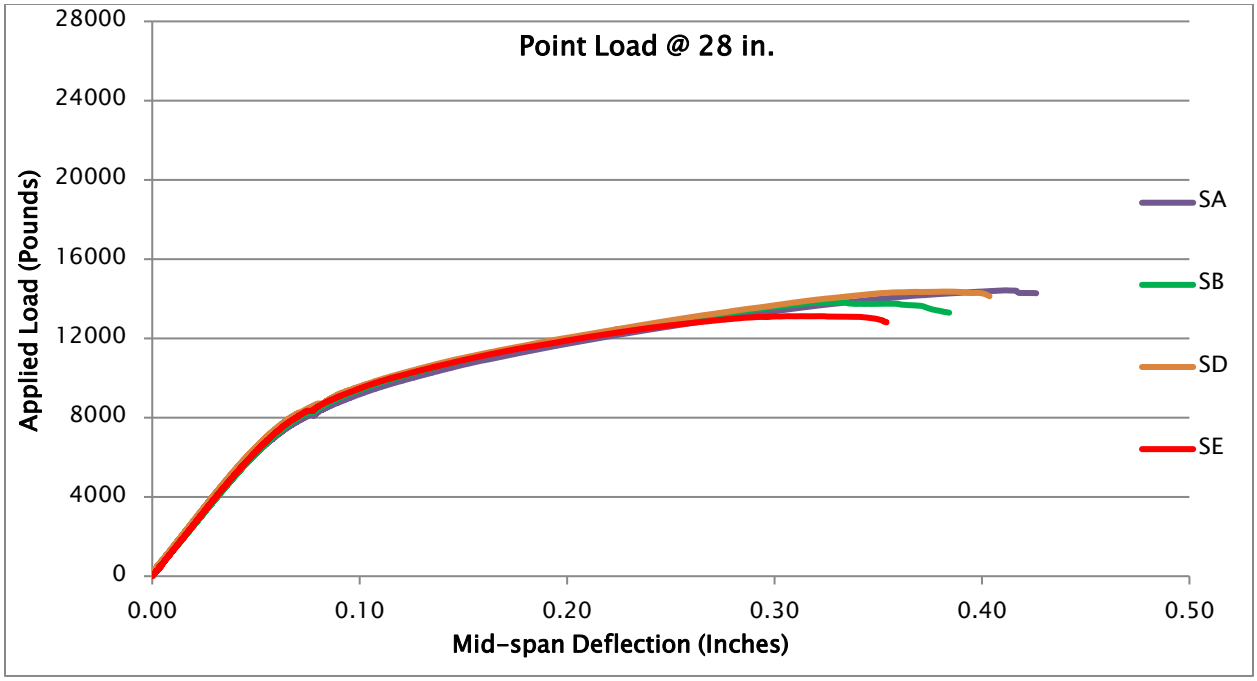


Figure 52. Load-deflection graphs for all 5 types of strand for 28 in. embedment length

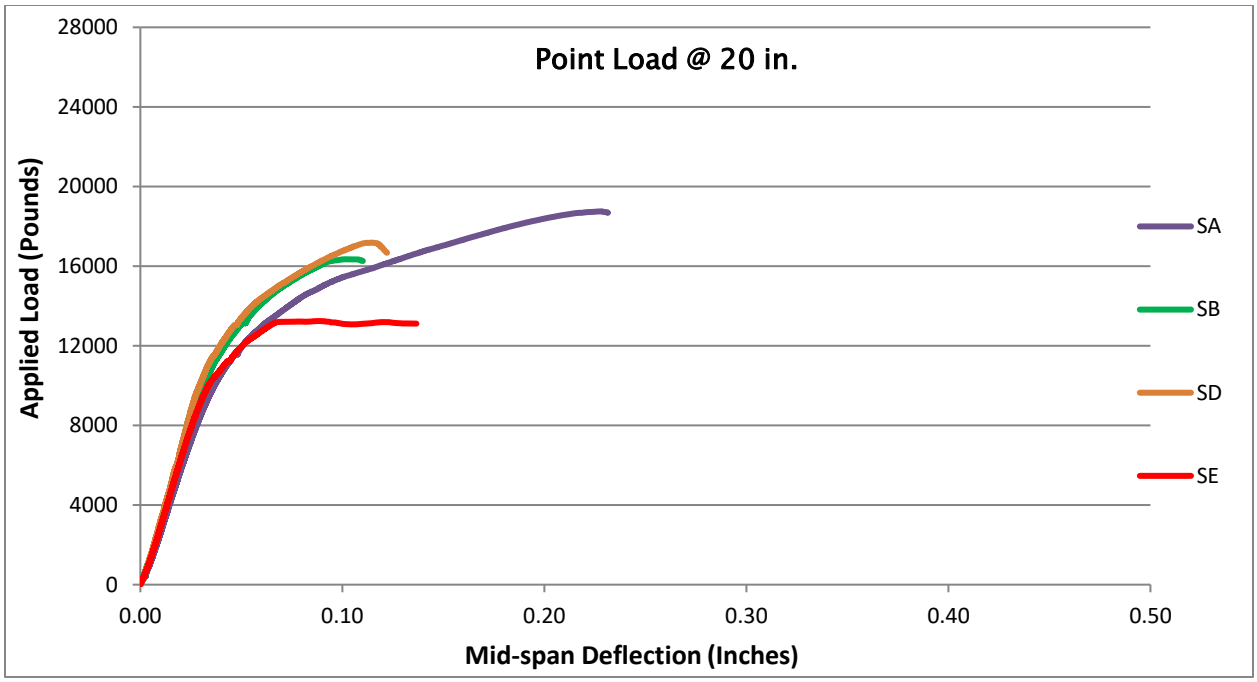


Figure 53. Load-deflection graphs for all 5 types of strand for 20 in. embedment length

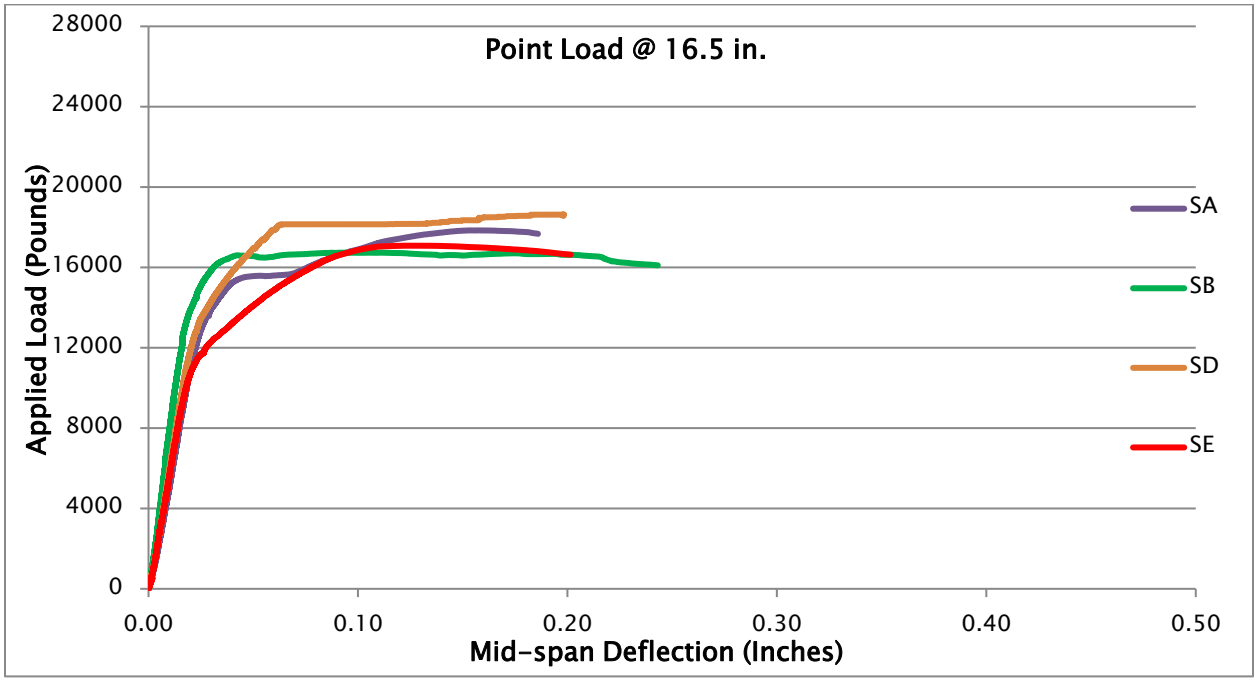


Figure 54. Load-deflection graphs for all 5 types of strand for 16.5 in. embedment length

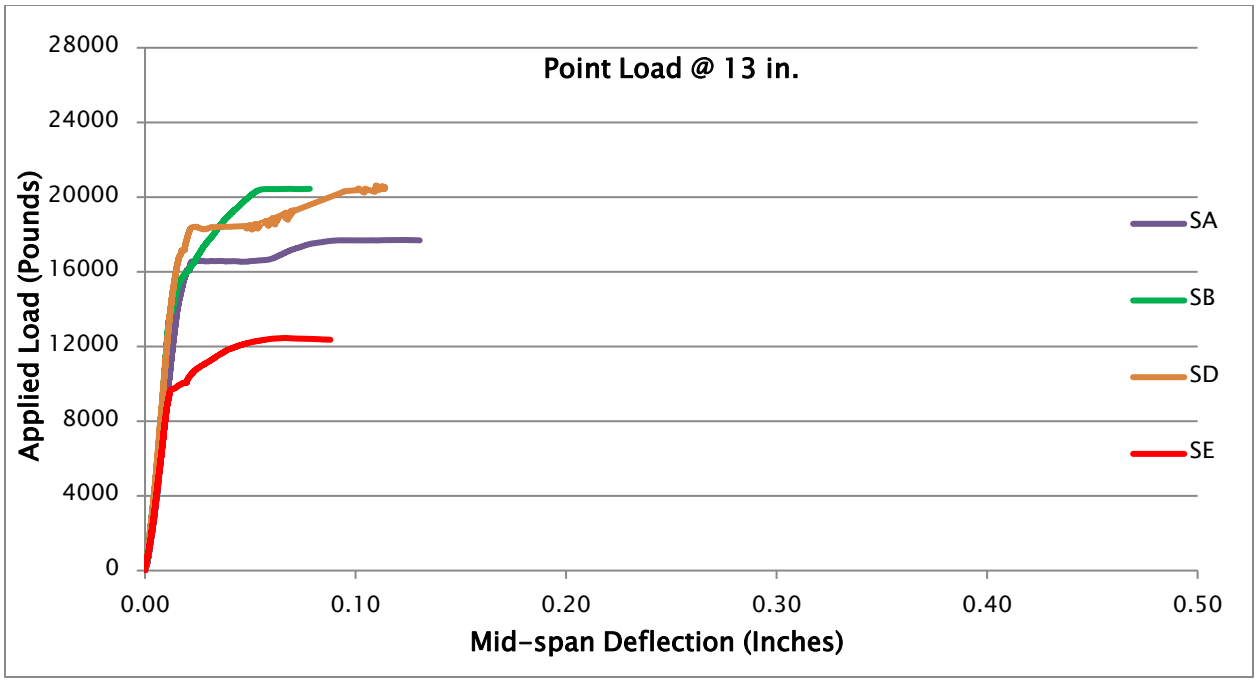


Figure 55. Load-deflection graphs for all 5 types of strand for 13 in. embedment length

The maximum load each prism was able to resist was used to calculate the maximum experimental moment (M_{exp}). Then, another group of graphs was constructed for ratio of maximum experimental moment to nominal-moment capacity versus strand type. Nominal-moment capacity (M_n) of prisms was calculated through analysis of pretensioned concrete beams. A strain-compatibility analysis was conducted by assuming the stress-strain diagram from the PCI Design Handbook (2010). In this analysis, compressive strength (f'_c) of 12,000 psi (82.73 MPa) was used for concrete. Strand cross-sectional area used in analysis was 0.085 in^2 (54.8 mm^2) for SA, SB, SD, and SE strands, whereas strand areas used in analysis of prisms manufactured with SF and SC strands were 0.065 in^2 (41.9 mm^2) and 0.058 in^2 (37.4 mm^2), respectively. Concrete surface strain values were measured at both ends of all three prisms before load testing, and an average of the six peak strain values were used to calculate prestress losses. Multiplying average peak strain by the Modulus of Elasticity of strands and knowing that strands were tensioned to 75 percent of their ultimate strength, total prestress losses were calculated. Table 19 shows the nominal-moment capacity of prisms manufactured with different strands.

Table 19 Properties of prisms manufactured with different strands and their nominal-moment capacity

Strand type	Strand diameter (in)	Strand area (in2)	Prestress loss (%)	Cross section	f'c (psi)	Mn (k-ft)
SA	0.375	0.085	28.4	5.5 in x 5.5 in	12000	13.26
SB	0.375	0.085	28.4	5.5 in x 5.5 in	12000	13.26
SD	0.375	0.085	28.4	5.5 in x 5.5 in	12000	13.26
SE	0.375	0.085	28.4	5.5 in x 5.5 in	12000	13.26
SF	0.375	0.065	22.7	5.5 in x 5.5 in	12000	11.38
SC	0.3125	0.058	29.9	4.5 in x 4.5 in	12000	8.48

In Figure 56, ratios of maximum experimental moment to nominal-moment capacity ($\frac{M_{exp}}{M_n}$), were calculated for all tests and plotted versus strand type for different embedment lengths. The horizontal line on the chart shows $\frac{M_{exp}}{M_n} = 1$, when $\frac{M_{exp}}{M_n}$ in a test is greater or equal to 1, the strand is developed at that embedment length. All 24 loading-test results are shown in Figure 56.

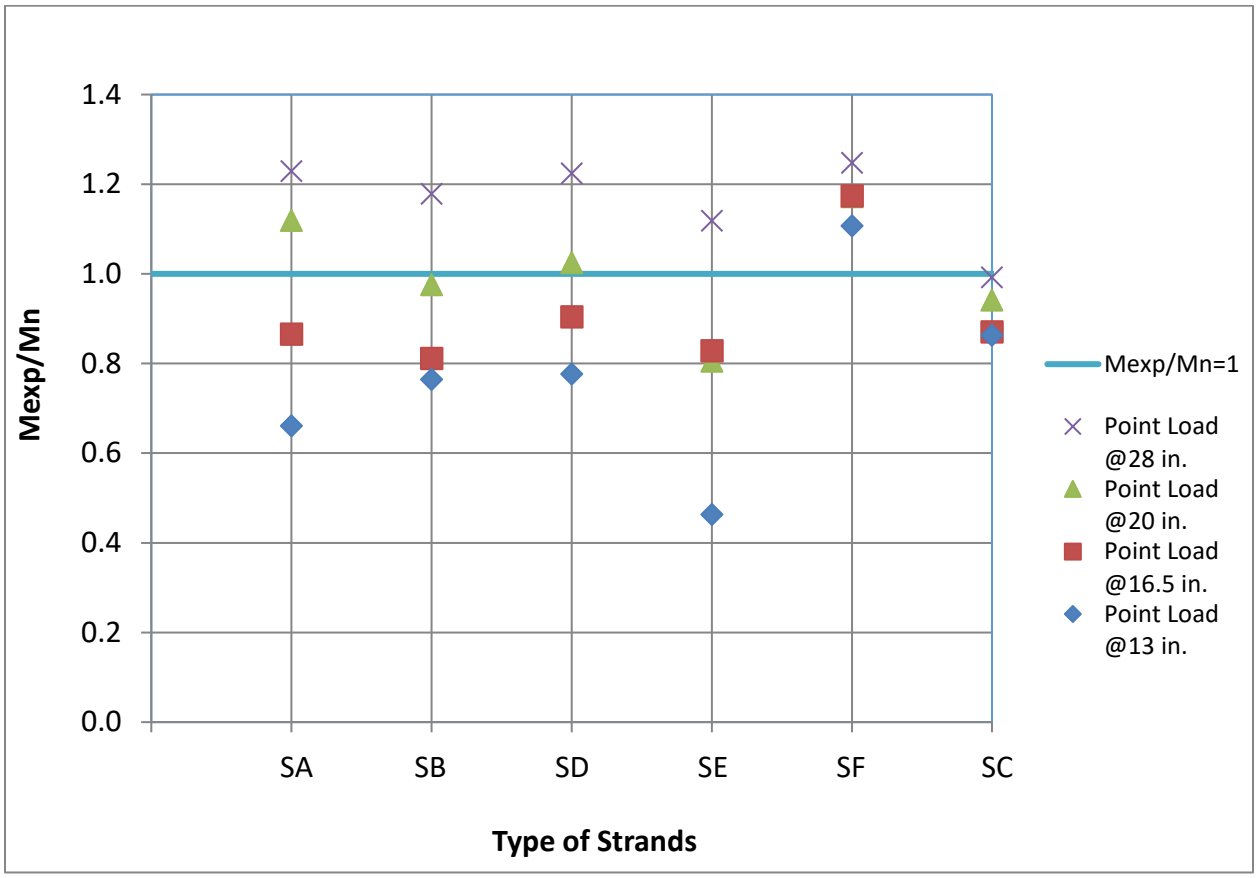


Figure 56. Ratio of maximum experimental moment to nominal-moment capacity vs strand type for different embedment lengths

Table 20 shows results obtained in each load test at prism ends. The last column of Table 20 is the ratio of maximum experimental moment to nominal-moment capacity of that end. Nominal-moment capacity for each end was calculated by strain-compatibility analysis using the PCI Design Handbook (2010) stress-strain diagram for prestressing strand.

Table 20. Results from load tests of three identical prisms for each strand type and 4,500 psi release strength

Beam designation	Embedment length (in)	Failure load (lb)	Mode of failure	Mexp/Mn
SA-4500-6-1-L	20	18,755	Shear-Bond	1.12
SA-4500-6-2-L	28	14,428	Shear-Compression	1.23
SA-4500-6-3-L	16.5	17,847	Shear-Compression	0.87
SA-4500-6-3-S	13	17,704	Shear-Bond	0.66
SB-4500-6-1-L	20	16,351	Shear-Compression	0.98
SB-4500-6-2-L	28	13,832	Compression	1.18
SB-4500-6-3-L	16.5	16,738	Shear-Compression	0.81
SB-4500-6-3-S	13	20,451	Shear-Bond	0.76
SD-4500-6-1-L	20	17,182	Shear-Bond	1.03
SD-4500-6-2-L	28	14,368	Shear-Compression	1.22
SD-4500-6-3-L	16.5	18,649	Shear-Compression	0.90
SD-4500-6-3-S	13	20,785	Shear-Bond	0.78
SE-4500-6-1-L	20	13,500	Shear-Compression	0.81
SE-4500-6-2-L	28	13,126	Shear-Compression	1.12
SE-4500-6-3-L	16.5	17,084	Bond	0.83
SE-4500-6-3-S	13	12,459	Shear-Bond	0.46
SF-4500-6-1-L	20	16,861	Shear-Bond	1.17
SF-4500-6-2-L	28	12,561	Shear-Compression	1.25
SF-4500-6-3-L	16.5	20,764	Shear-Compression	1.17
SF-4500-6-3-S	13	25,372	Bond	1.11
SC-4500-6-1-L	28	7438	Shear-Compression	0.99
SC-4500-6-2-L	20	10,090	Shear-Compression	0.94
SC-4500-6-3-L	16.5	11,487	Shear-Bond	0.87
SC-4500-6-3-S	13	14,755	Shear-Bond	0.86

Discussion of results

As can be seen from the presented load-deflection graphs for different loading spans, ultimate loads resisted by prisms were the highest when loading span was the smallest. However, mid-span deflections were the smallest when loading span was 13 in. (33 cm) from the prism end. Load-deflection graphs presented in the Results section show some important properties of these pretensioned concrete test prisms:

1) Prior to initial crack, all prisms exhibited the same linear behavior, and the linear parts of loading graphs were essentially identical. This shows all prisms had the same initial flexural stiffness (EI).
2) Prisms made with smooth strand (SA) showed much higher reserve capacity compared to prisms made with smooth wire (WA), and did not fail right after occurrence of the first crack.
3) As the embedment lengths decrease, load-deflection graphs for different strands scatters more considerably, showing more different capacities at end regions.

To understand and compare the capacity of these pretensioned concrete prisms at different end locations, maximum experimental moments were calculated based on the maximum load resisted by prisms in each test. Prisms were load-tested in different spans to obtain estimations for development length based on strand-indentation type. In this experiment, embedment lengths decreased from 28 in. (71.1 cm) to 13 in. (33 cm) from the prism end to determine the change in moment capacity. Any considerable reduction in maximum moment with reduction in embedment length indicates the strand was not fully developed at that location.

Also, development-length estimations were made for each type of strand and documented as a range in Table 21. When maximum experimental moment for each test was larger than nominal-moment capacity obtained from strain-compatibility analysis, the strand was assumed to be fully developed at that location. This means any point above the horizontal line in Figure 56 represents a prism with a fully developed strand. Table 21 was generated based on results presented in Figure 56.

Table 21. Range of development length for each type of strand

Strand type	Lt (in)	@ 28 in.	@ 20 in.	@ 16.5 in.	@ 13 in.	Ld Range (in)	Ld/Lt
SA	11.6	Yes	Yes	No	No	16.5-20	1.42-1.72
SB	16.3	Yes	No	No	No	20-28	1.23-1.72
SD	15.8	Yes	Yes	No	No	20-28	1.26-1.77
SE	19	Yes	No	No	No	20-28	1.05-1.47
SF	12.5	Yes	Yes	Yes	Yes	<13	<1.6
SC	13.8	No	No	No	No	>28	>2.03

In this table, when maximum experimental moment was larger than nominal-moment capacity obtained from analysis, the word “Yes” was used to show nominal-moment capacity was achieved, and development length was shorter than embedment length. In the last column of this table, ratio of development length to transfer length was calculated to estimate development length as a percentage of transfer length.

For prisms with different concrete-release strengths, maximum experimental moment resisted by each prism was determined from the maximum applied load by an equilibrium of forces, and the following figures were generated. Figure 57 through Figure 61 plot the maximum experimental

moments for each strand type versus assessed embedment lengths for different concrete-release strengths.

4.2.2 *Effect of concrete-release strength on development length of pretensioned members made with strands*

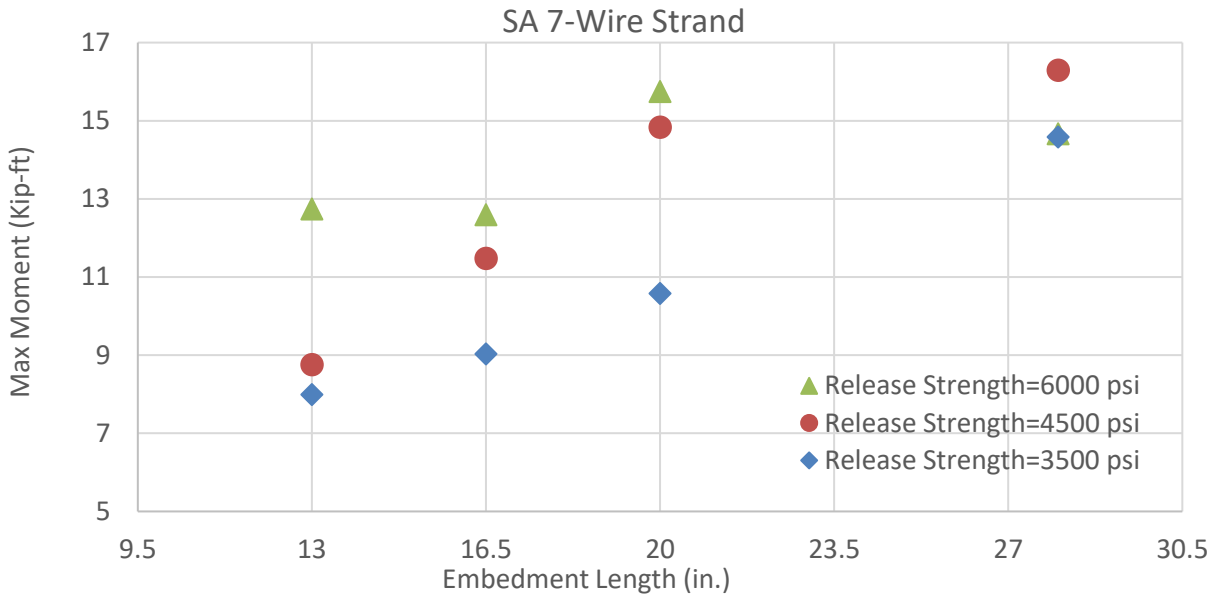


Figure 57. Max moment resisted vs embedment length for prisms made with SA strand

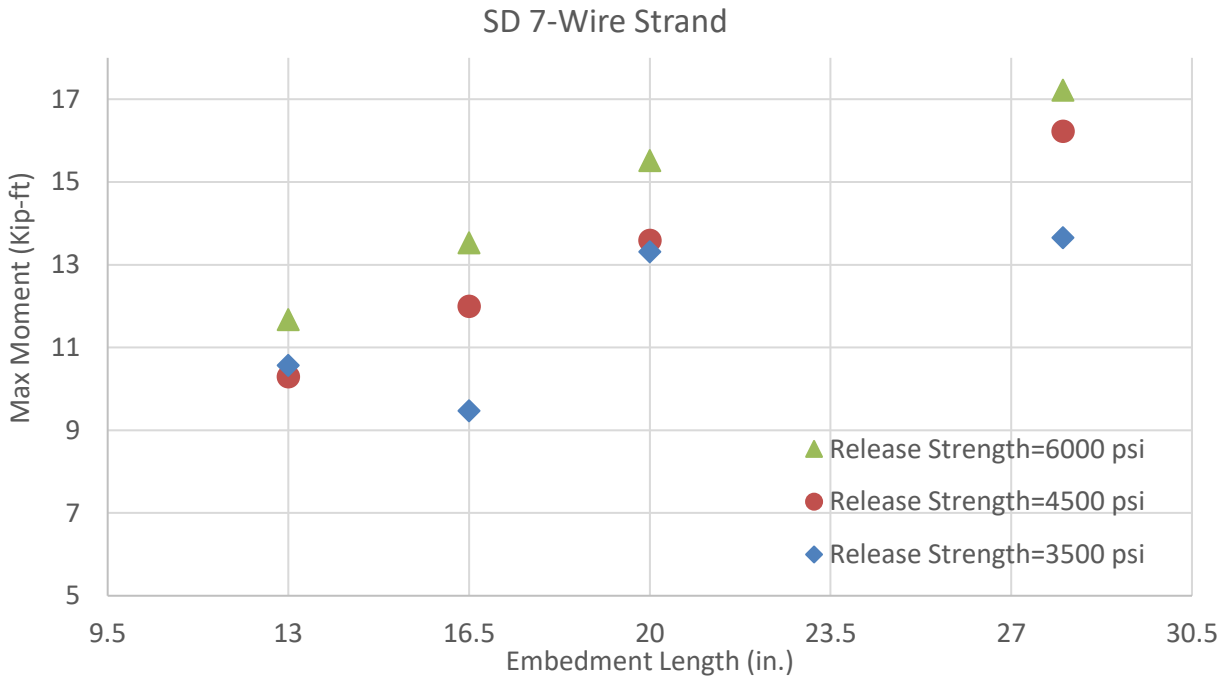


Figure 58. Max moment resisted vs embedment length for prisms made with SD strand

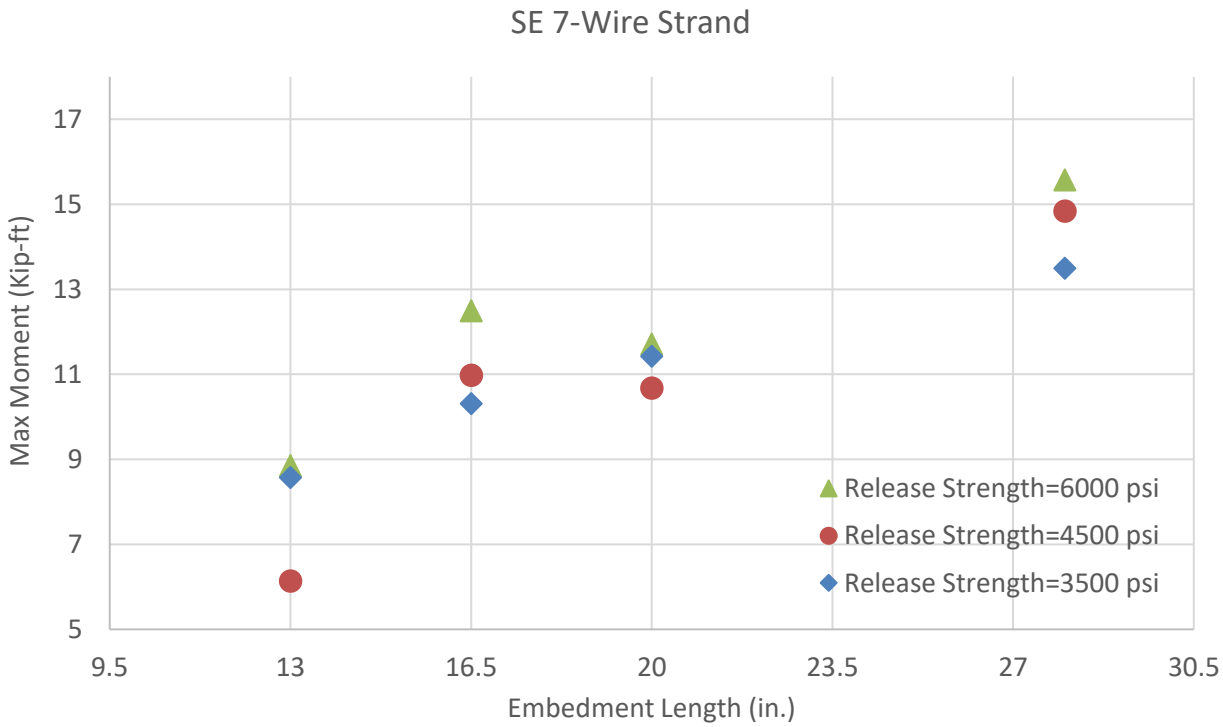


Figure 59. Max moment resisted vs embedment length for prisms made with SE strand

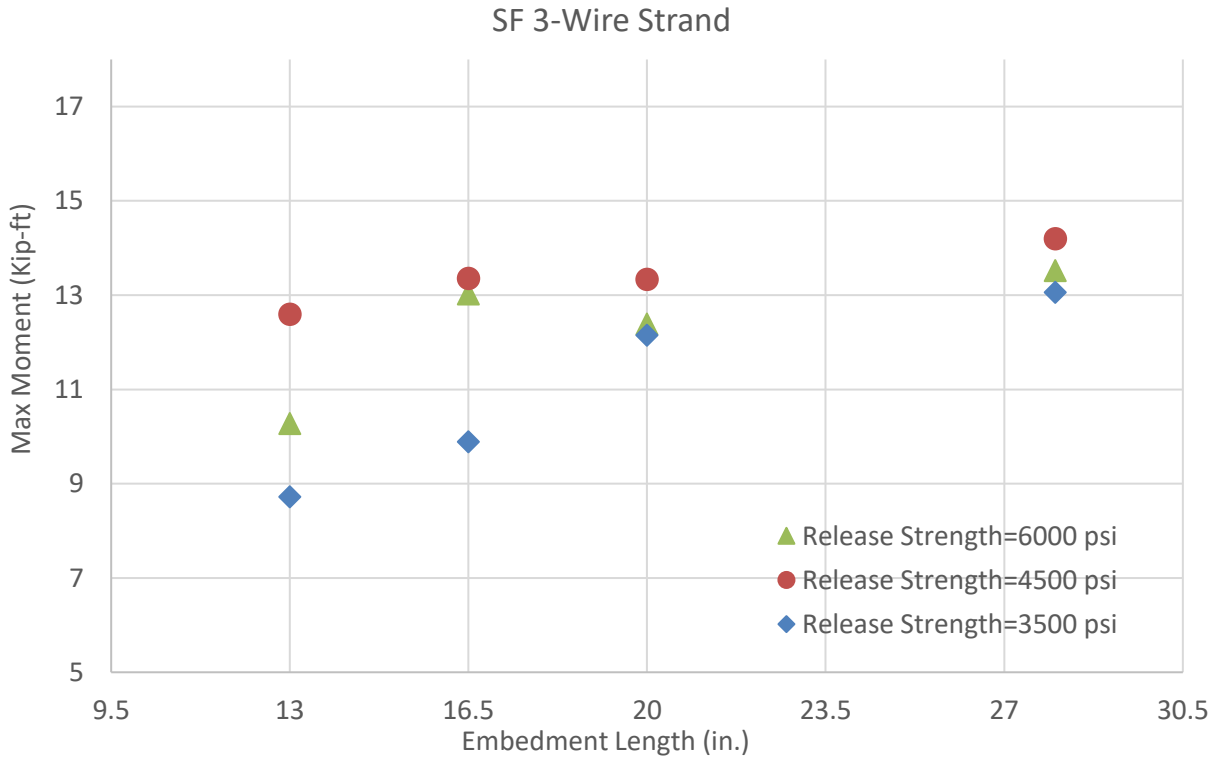


Figure 60. Max moment resisted vs embedment length for prisms made with SF strand

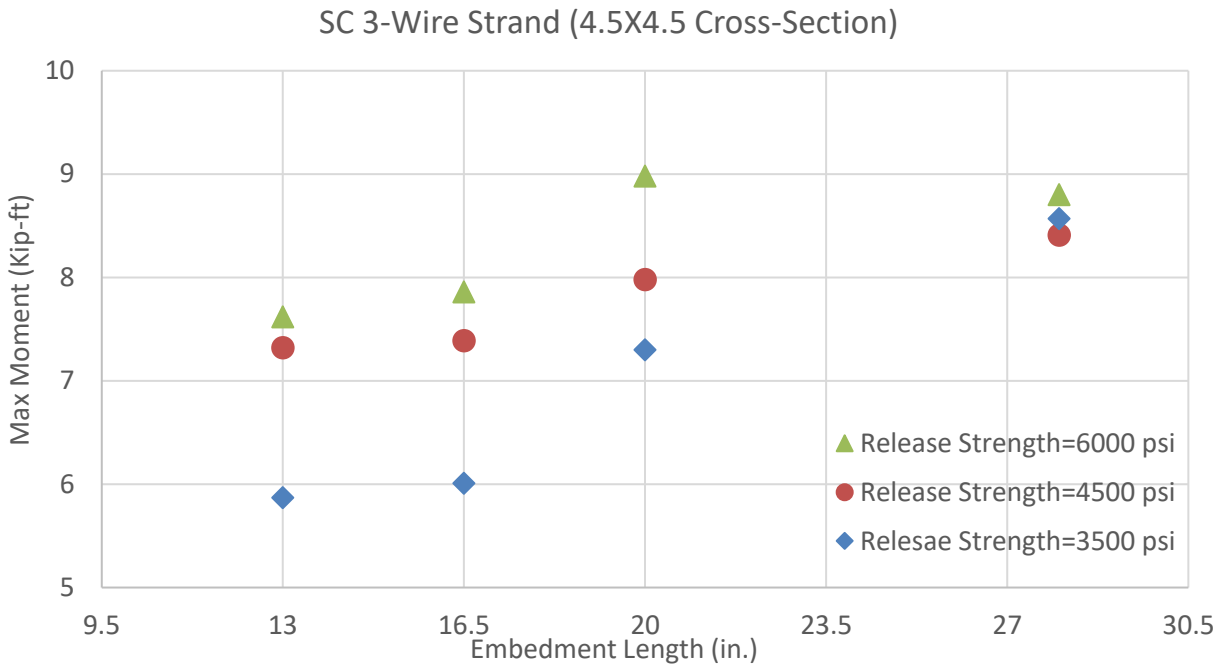


Figure 61. Max moment resisted vs embedment length for prisms made with SA strand

Table 22 shows results obtained in each load test at prism ends. The last column of Table 22 is the ratio of maximum experimental moment to nominal-moment capacity of that end. Nominal-moment capacity for each end was calculated by strain-compatibility analysis using the PCI Design Handbook (2010) stress-strain diagram for prestressing strand.

Table 22. Results from load tests of three identical prisms for each strand type and different release strengths

Beam designation	Embedment length (in)	Failure load (lb)	Mode of failure	Mexp/Mn
SA-3500-6-1-L	20	13,380	Shear-Compression	0.80
SA-3500-6-2-L	28	12,904	Shear-Compression	1.10
SA-3500-6-3-L	16.5	14,051	Shear-Compression	0.68
SA-3500-6-3-S	13	16,156	Shear-Bond	0.60
SD-3500-6-1-L	20	16,826	Bond	1.00
SD-3500-6-2-L	28	12,072	Shear-Compression	1.03
SD-3500-6-3-L	16.5	14,735	Shear-Compression	0.71
SD-3500-6-3-S	13	21,330	Shear-Bond	0.80
SE-3500-6-1-L	20	14,442	Bond	0.86
SE-3500-6-2-L	28	11,928	Shear-Compression	1.02
SE-3500-6-3-L	16.5	16,034	Bond	0.78
SE-3500-6-3-S	13	17,315	Bond	0.65
SF-3500-6-1-L	20	15,357	Shear-Compression	1.07
SF-3500-6-2-L	28	11,548	Compression	1.15
SF-3500-6-3-L	16.5	15,365	Shear	0.87
SF-3500-6-3-S	13	17,624	Shear-Bond	0.77
SC-3500-6-1-L	28	7578	Shear-Compression	1.01
SC-3500-6-2-L	20	9235	Shear-Compression	0.86
SC-3500-6-3-L	16.5	9359	Shear-Compression	0.71
SC-3500-6-3-S	13	11,869	Shear-Bond	0.69
SA-6000-6-1-L	20	21,257	Shear-Compression	1.19
SA-6000-6-2-L	28	12,980	Shear-Compression	1.11
SA-6000-6-3-L	16.5	19,578	Shear-Bond	0.95
SA-6000-6-3-S	13	25,668	Bond	0.96
SD-6000-6-1-L	20	19,617	Shear-Compression	1.17
SD-6000-6-2-L	28	15,243	Shear-Compression	1.30
SD-6000-6-3-L	16.5	21,019	Compression	1.02
SD-6000-6-3-S	13	23,529	Shear-Compression	0.88
SE-6000-6-1-L	20	14,808	Shear-Compression	0.88
SE-6000-6-2-L	28	13,775	Shear-Compression	1.17
SE-6000-6-3-L	16.5	19,411	Bond	0.94
SE-6000-6-3-S	13	17,888	Bond	0.67
SF-6000-6-1-L	20	15,668	Shear-Compression	1.09
SF-6000-6-2-L	28	11,960	Shear-Compression	1.19
SF-6000-6-3-L	16.5	20,245	Shear-Compression	1.14
SF-6000-6-3-S	13	20,745	Shear-Bond	0.90
SC-6000-6-1-L	28	7784	Compression	1.04
SC-6000-6-2-L	20	11,346	Shear-Compression	1.06
SC-6000-6-3-L	16.5	12,228	Compression	0.93
SC-6000-6-3-S	13	15,364	Bond	0.90

Discussion of results

Results presented in Figure 57 to Figure 61 are categorized according to strand type in order to Compare the moment capacities for different concrete-release strengths. Loading tests were run with four different loading spans to estimate development lengths. Any considerable reduction in maximum experimental moment resisted by a prism with a reduction in embedment length means the strand force was not fully developed and the section was not at its maximum capacity.

The following findings can be concluded from the above figures:

1) For all seven-wire strands, there was a general trend where the maximum experimental moment increased as release strength increased.
2) For SF, a three-wire indented strand with a diameter of 3/8 in., maximum experimental moment resisted by prisms with 4,500 psi release strength was slightly higher than prisms with 6,000 psi, and prisms with 3,500 psi had the lowest moment capacity at any assessed embedment length.
3) For SC, a smooth three-wire strand with a diameter of 5/16, there was a general trend where the maximum experimental moment increased as release strength increased.

4.3 Phase III-Effect of Prestressing Wire-Indentation Type on the Bond Performance and Flexural Capacity of Pretensioned Concrete Crossties Subjected to Cyclic Loading

Pretensioned prisms made with 13 types of wire with different indentation types were load-tested cyclically using the test configuration presented in Figure 30 and Figure 31. Eleven out of 13 prisms were able to resist 200,000 cycles of loading and unloading, while two prisms failed under cyclic load. For prisms able to complete the cyclic loading, the load was removed and then they were monotonically loaded to failure and maximum experimental-moment capacity was calculated for each prism. Maximum experimental-moment capacity for prisms which have gone through cyclic load was then compared with maximum experimental-moment capacity of prisms loaded monotonically to failure without having experienced the cyclic load prior to failure.

For prisms loaded monotonically (no cyclic loading prior to failure), the embedment length was 20 inches (fully transferred prestressing force). This comparison was done to determine if some moment-capacity reduction occurred due to the cyclic loading. Figure 62 shows graphs of load versus mid-span deflection for all types of prisms after cyclic loading, whereas Figure 63 shows graphs of load versus mid-span deflection for all prisms subjected to single monotonic loading.

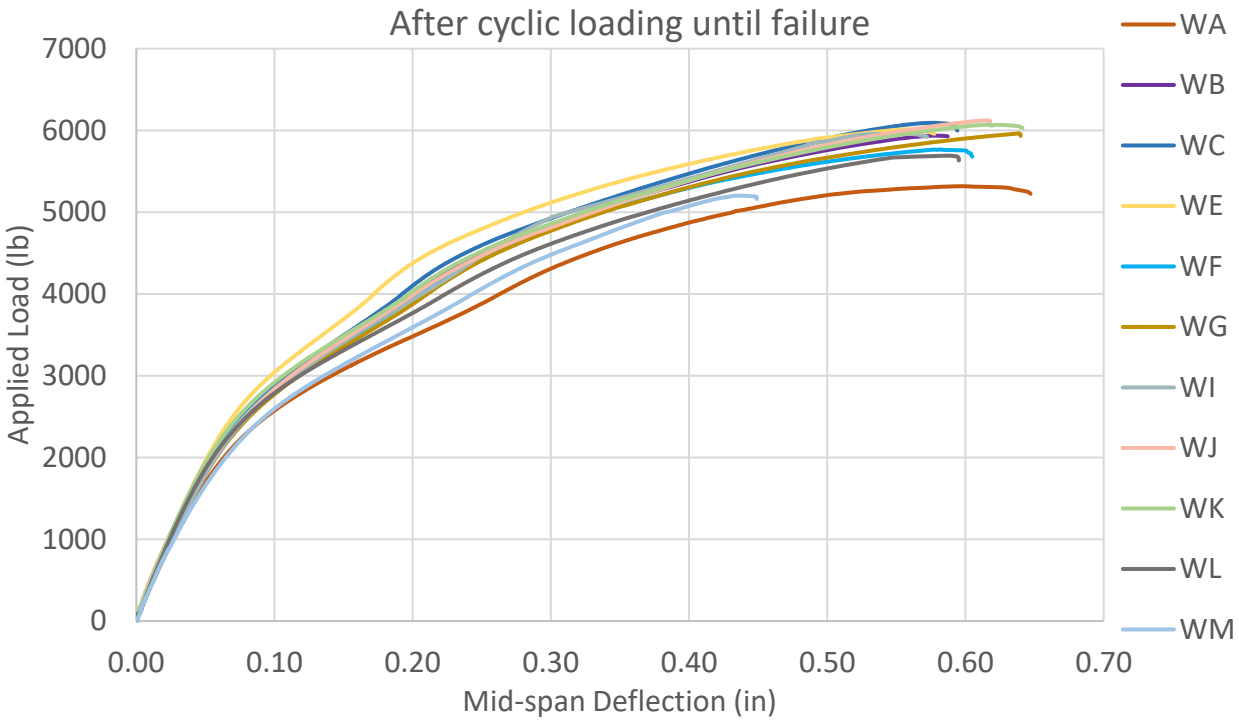


Figure 62. Load-deflection graphs of prisms after cyclic loading until failure

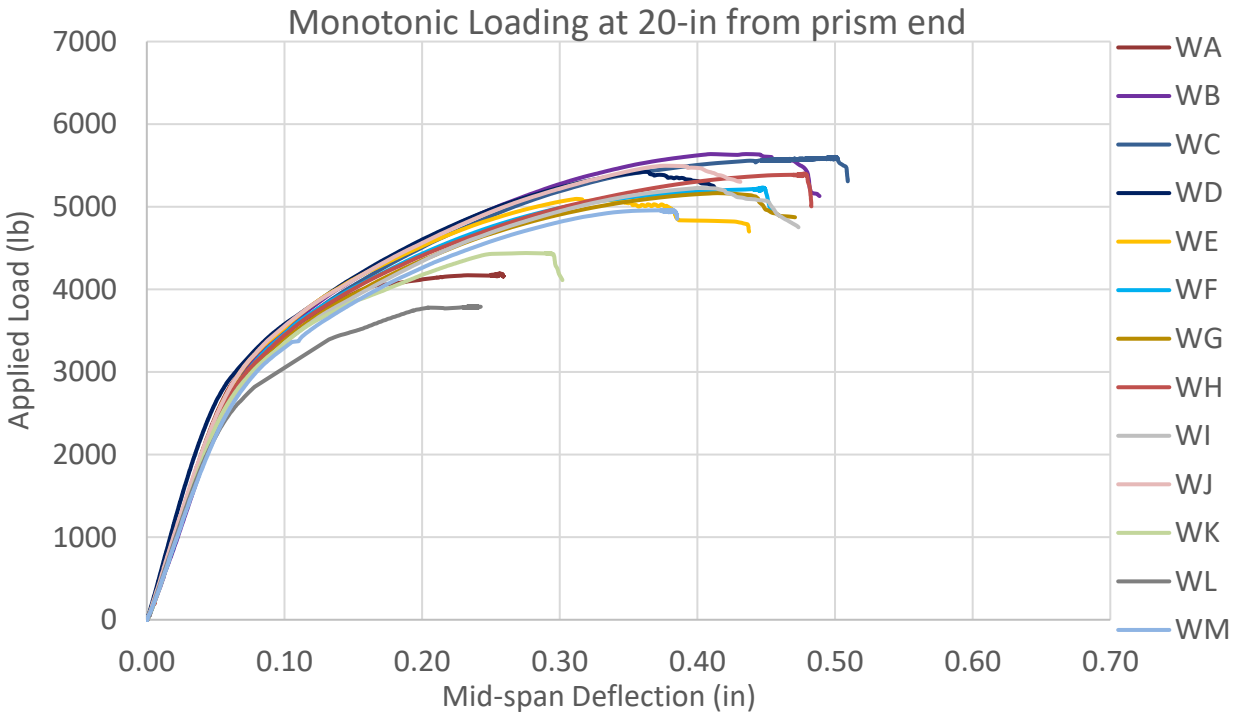


Figure 63. Load-deflection graphs for all 13 types of wire at 20-in. embedment length

Maximum load resisted by prisms having gone through 200,000 cycles of loading and by prisms only loaded monotonically were then selected to compare maximum experimental moment. Table 23 Compares the moment capacity of two similar prisms, one loaded monotonically at embedment length of 20 in. and the other loaded until failure after having the prism experience 200,000 cycles of load at a frequency of 3 Hz.

Table 23. Comparison between maximum-moment capacities obtained from cyclic loading and monotonic loading at 20 in. from prism end.

	M1=Moment Cyclic Load (k-ft)	M2=Moment @ 20 in. from Prism End (k-ft)	M1/M2 (%)
WA	*3.340*	*3.242*	*103.0*
WB	*3.727*	*4.463*	*83.5*
WC	*3.823*	*4.434*	*86.2*
WD	*failed @ 162760 cycle*	*4.292*	.....
WE	*3.776*	*4.030*	*93.7*
WF	*3.621*	*4.141*	*87.5*
WG	*3.743*	*4.085*	*91.6*
WH	*failed @ 114505 cycle*	*4.274*	.....
WI	*3.742*	*4.137*	*90.5*
WJ	*3.845*	*4.350*	*88.4*
WK	*3.811*	*3.514*	*108.5*
WL	*3.573*	*3.004*	*118.9*
WM	*3.270*	*3.929*	*83.2*

Results from monotonic and cyclic loading tests show that for all prisms, except those made with lightly indented wires (WA, WK, and WL), moment capacity of a section after cyclic loading decreases compared to the identical section loaded monotonically until failure. The reason for the lower-moment capacity of prisms tested in cyclic loading is unknown but may be attributed to the lack of confinement in the maximum-moment region (region between loading points), which could allow an earlier compression failure.

However, for wire with no surface indentation and lightly indented wires (WA, WK, and WL), the maximum experimental moment calculated for prisms in after cyclic-loading was higher than maximum experimental moment calculated for the identical prisms in a monotonic-loading test. The reason for lower-moment capacities for lightly indented wires under monotonic load may be due to the smaller embedment length of 20 in. from prism end. Thus, the prism was not at its maximum capacity at 20 in. from prism end and failed at lower loads. In the cyclic-loading test, embedment length was 27 in. (68.58 cm) and wires were more developed compared to the monotonic-loading test. Accordingly, no wire end-slip was observed during cyclic testing.

Prisms made with WH and WD wires (chevron-indented) failed under cyclic loading and were not able to resist 200,000 cycles of load. Graphs of load vs mid-span deflection were plotted for each prism at different cycles to see any gradual effect of bond loss or softening of the beams due to cycles of loading and unloading. Figure 64 and Figure 65 show graphs of load vs mid-span deflection at different cycles, and also the nearest cycle to failure.

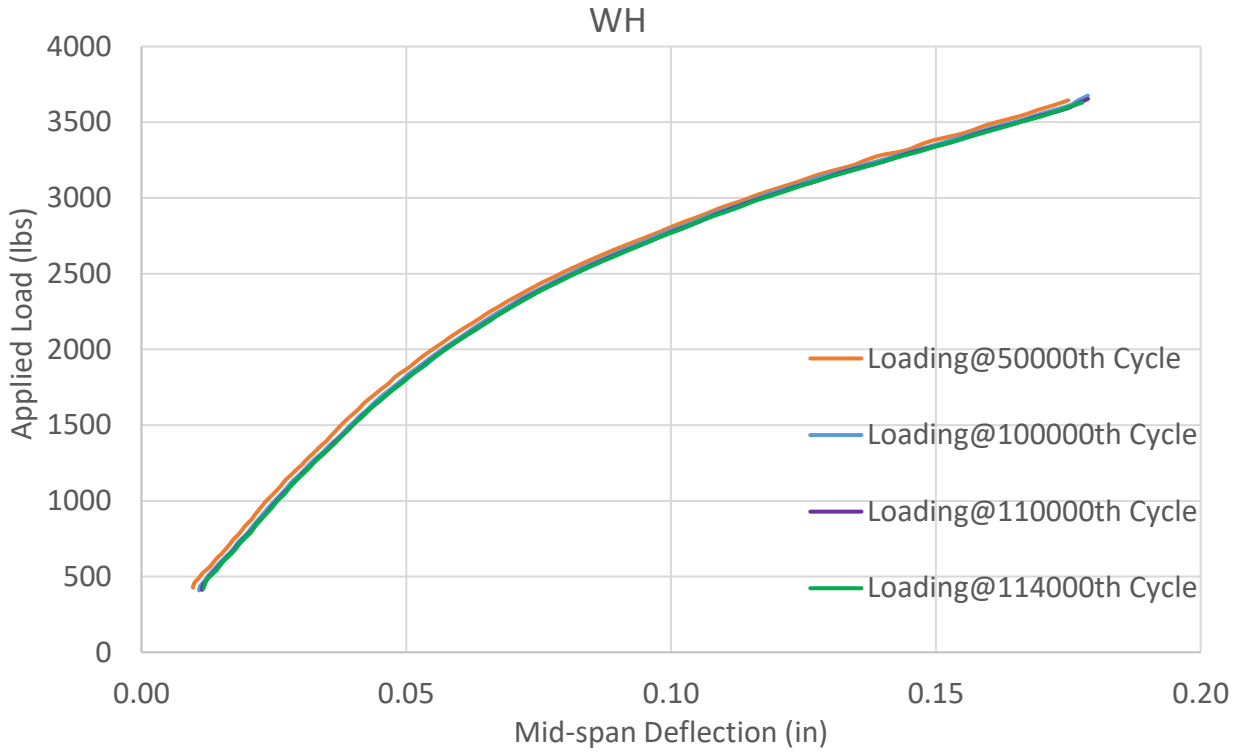


Figure 64. Load-deflection graphs at different cycles for prism made with WH wire

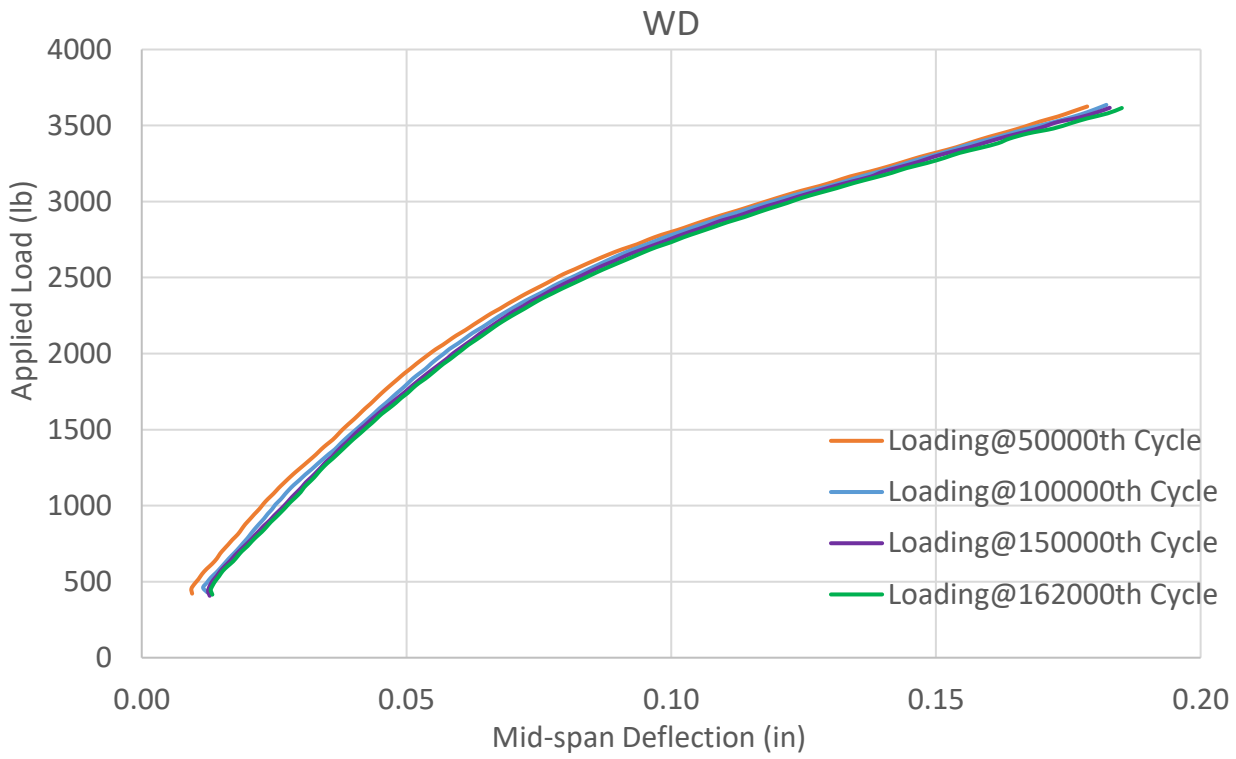


Figure 65. Load-deflection graphs at different cycles for prism made with WD wire

Prisms made with WH wire failed at the 114,505th cycle and the last cycle plotted in Figure 64 is the 114,000th cycle. As can be seen, no gradual bond loss or beam softening occurred over 114,000 cycles of load since all curves are nearly identical. This means that fatigue took place suddenly and not over thousands of cycles. A failure without warning can cause dangerous outcomes and should be avoided in structures. To gain higher confidence about the findings obtained for WH wire, the same cyclic-loading test was repeated for an identical prism made with WH wire. Once again, the prism manufactured with WH wire failed under the cyclic load without warning, but this time at the 89,875th cycle. Note that wire WH has a deep-indent profile with low-edge wall angle compared to other wires tested (refer to Table 2.)

Also, the prism made with WD wire failed under cyclic loading at the 162,760th cycle. Figure 65 shows load vs mid-span deflection relationship at different cycles, and also the nearest recorded cycle to the point at which failure occurred. From Figure 65, it can be seen there was no gradual softening as cycles of loading and unloading was being applied on the beam. This observation indicated once again that fatigue failure in the pretensioned prism occurred rapidly and without warning. Unfortunately, all prisms fabricated with WD wire were load-tested and repeating a cyclic-load test on a prism made with WD wire was not possible. Figure 66, Figure 67, and 68 show pictures of failed prisms under cyclic loading.

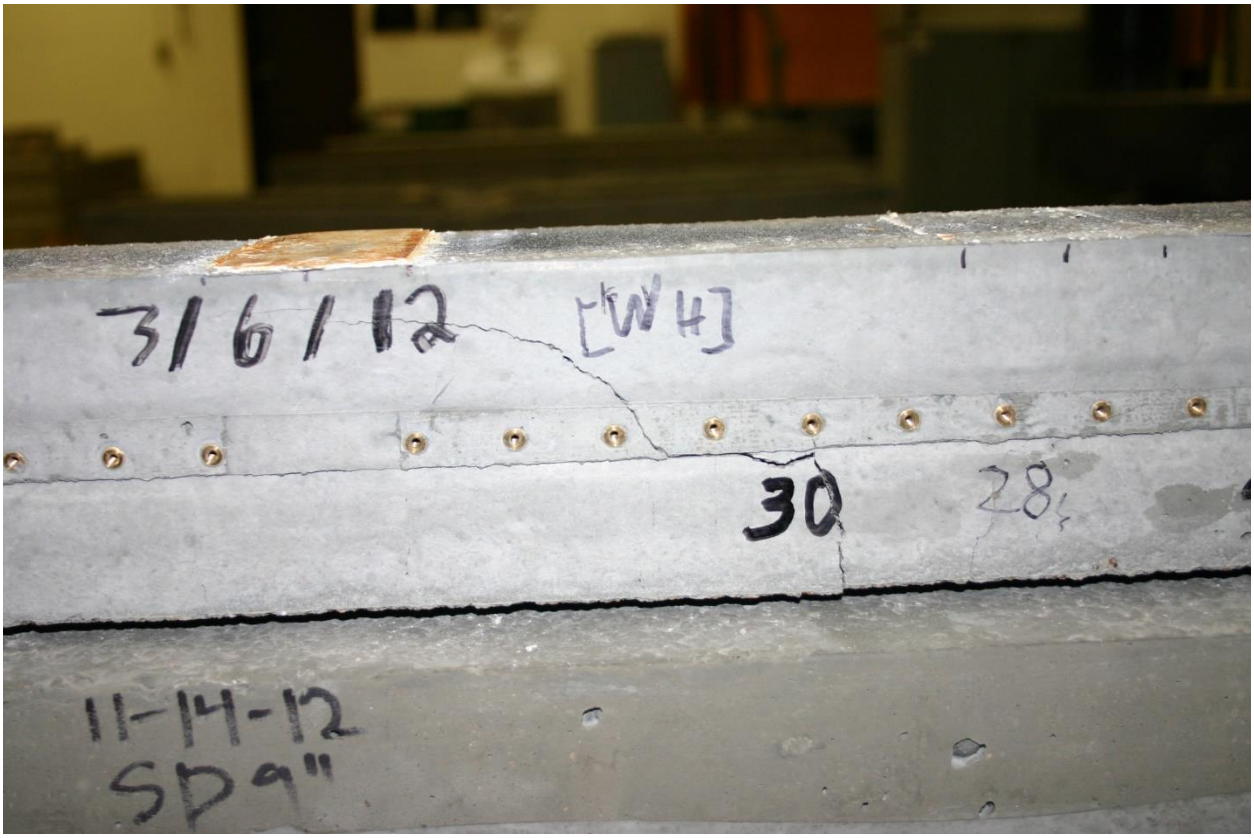


Figure 66. Prism made with WH wire failed at 11,400th cycle of loading

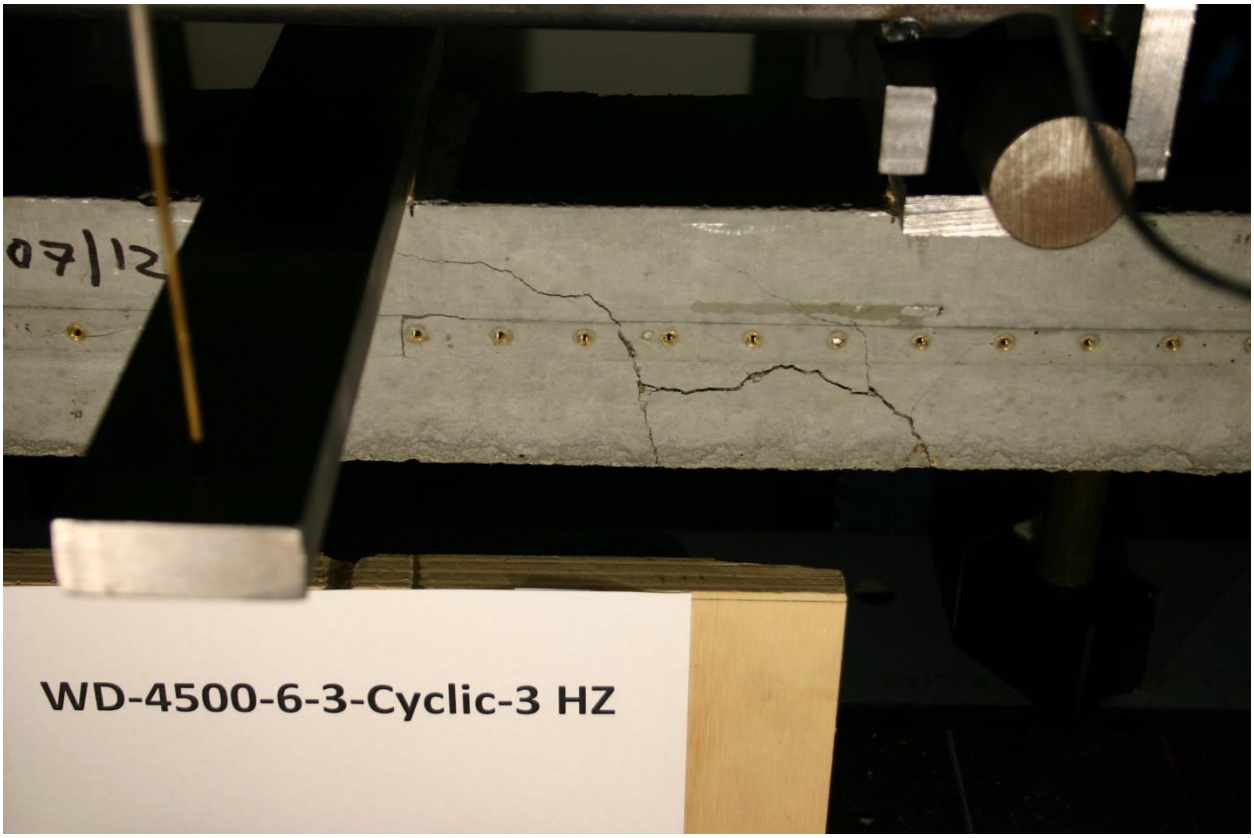


Figure 67. Prism made with WD wire failed at 162,760th cycle of loading



Figure 68. Prism made with WH wire failed at 89,875th cycle of loading (repeated test)

Also, for prisms tested cyclically, load-vs-deflection graphs were plotted before cyclic loading (loading from 0 to 4,000 lbs) and after cyclic loading until failure, and then compared for prisms with each wire type to see any change in behavior and rigidity of pretensioned sections. Figure 69 to Figure 79 show behavior of prisms that survived under 200,000 cycles of load.

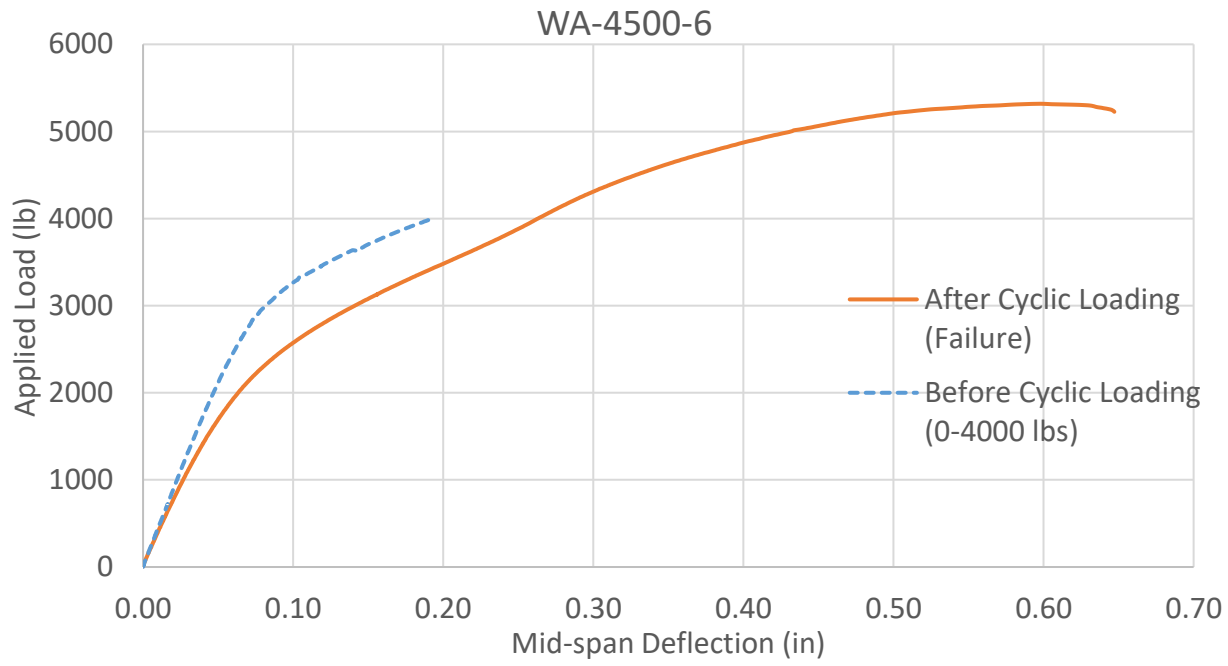


Figure 69. Load-deflection graphs prior to cyclic loading and after cyclic loading until failure (prism made with WA wire)

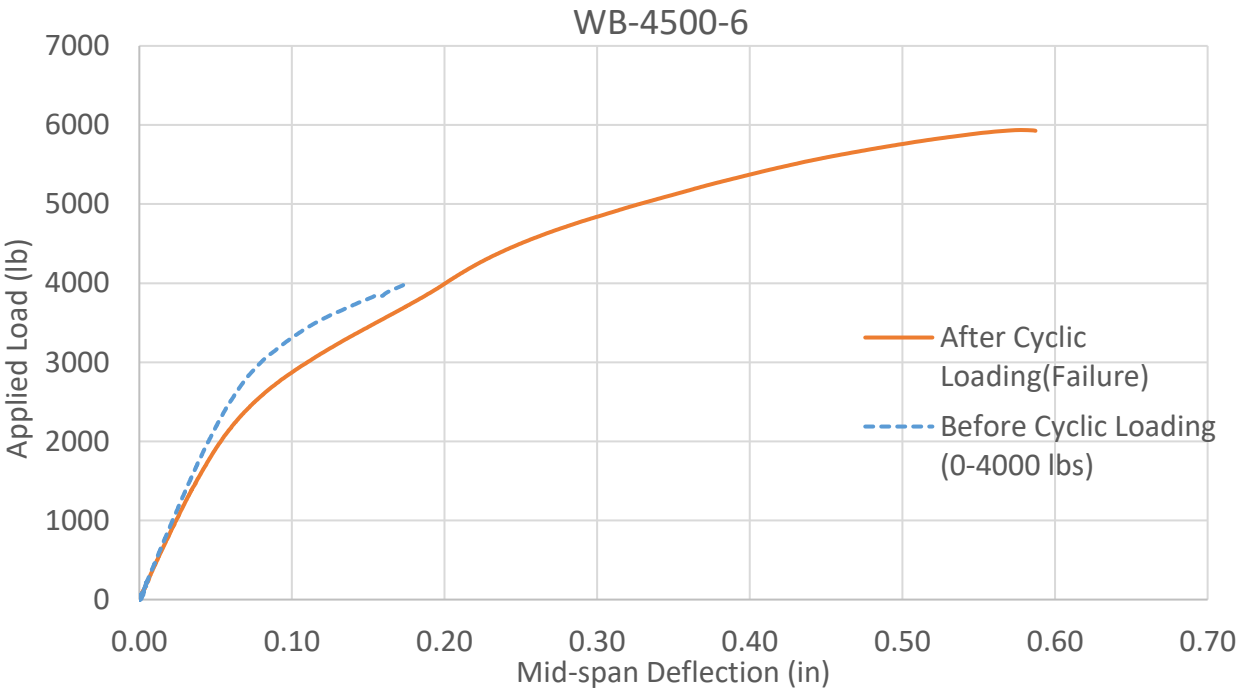


Figure 70. Load-deflection graphs prior to cyclic loading and after cyclic loading until failure (prism made with WB wire)

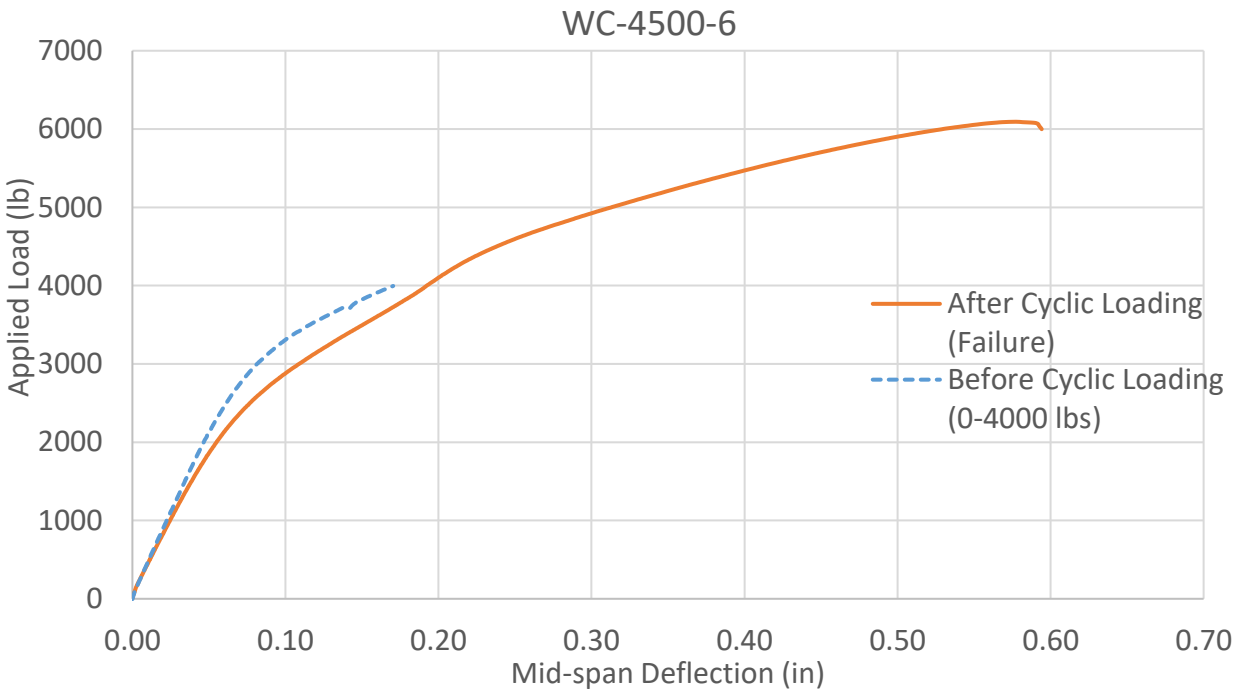


Figure 71. Load-deflection graphs prior to cyclic loading and after cyclic loading until failure (prism made with WC wire)

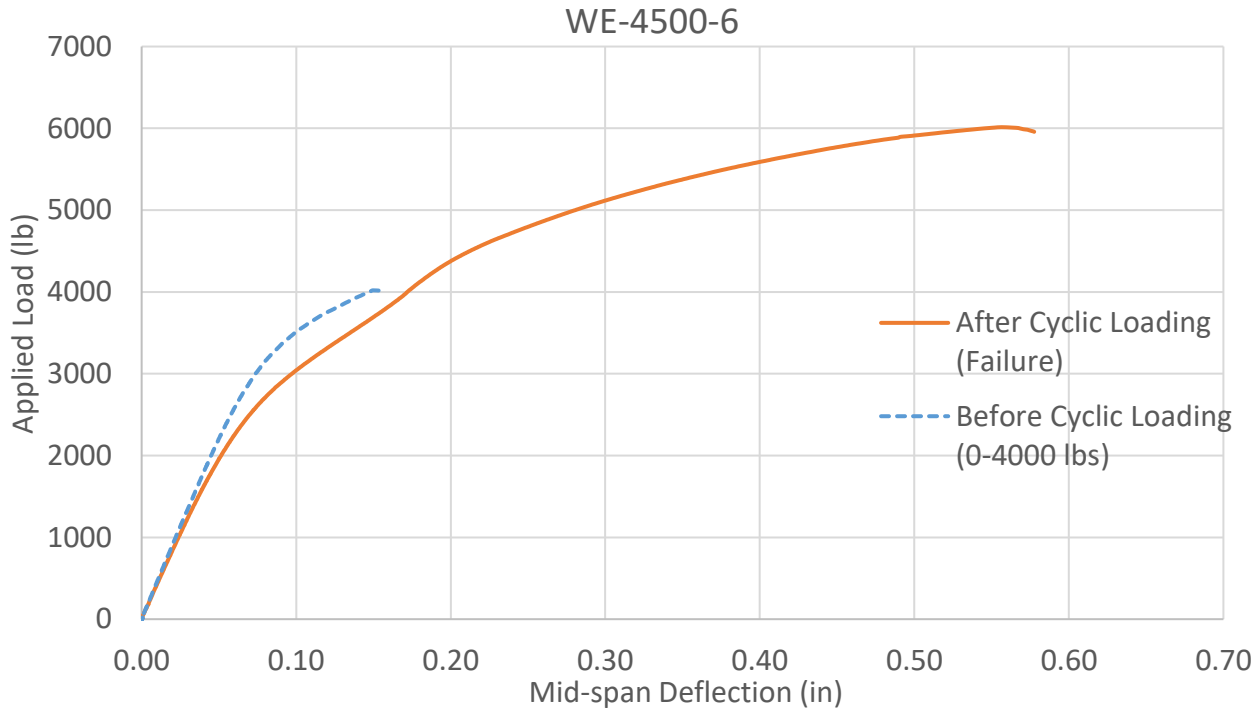


Figure 72. Load-deflection graphs prior to cyclic loading and after cyclic loading until failure (prism made with WE wire)

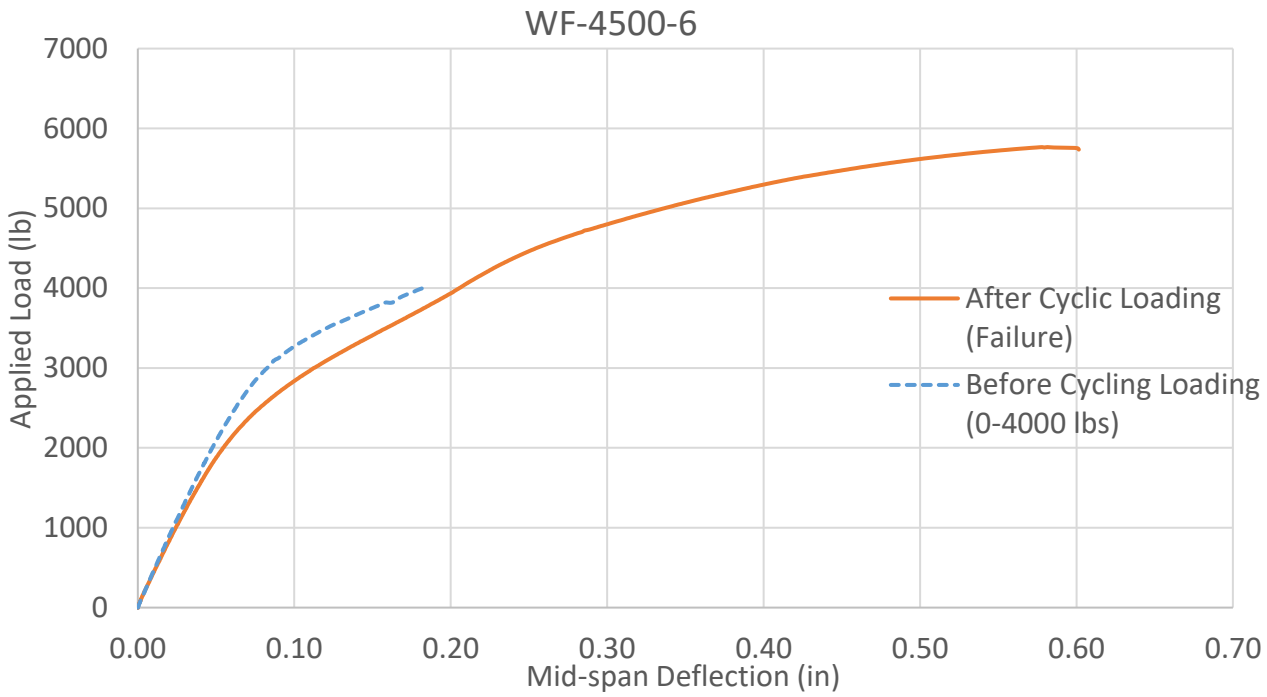


Figure 73. Load-deflection graphs prior to cyclic loading and after cyclic loading until failure (prism made with WF wire)

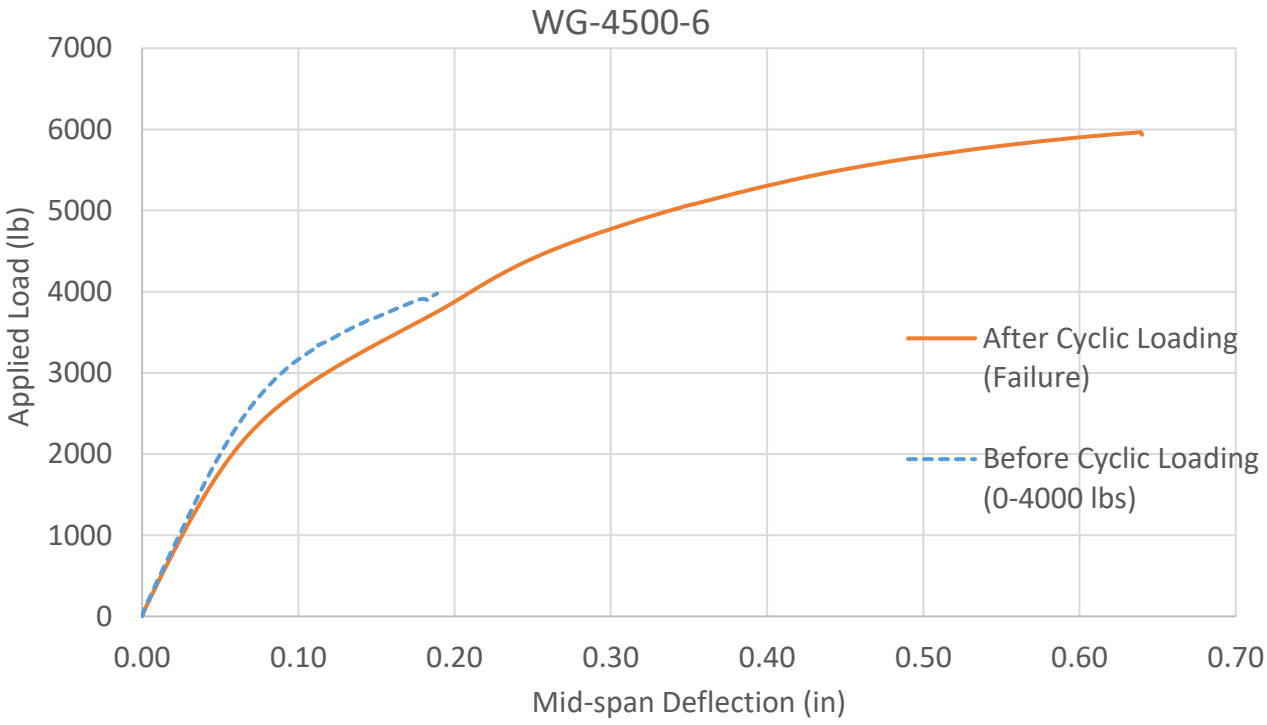


Figure 74. Load-deflection graphs prior to cyclic loading and after cyclic loading until failure (prism made with WG wire)

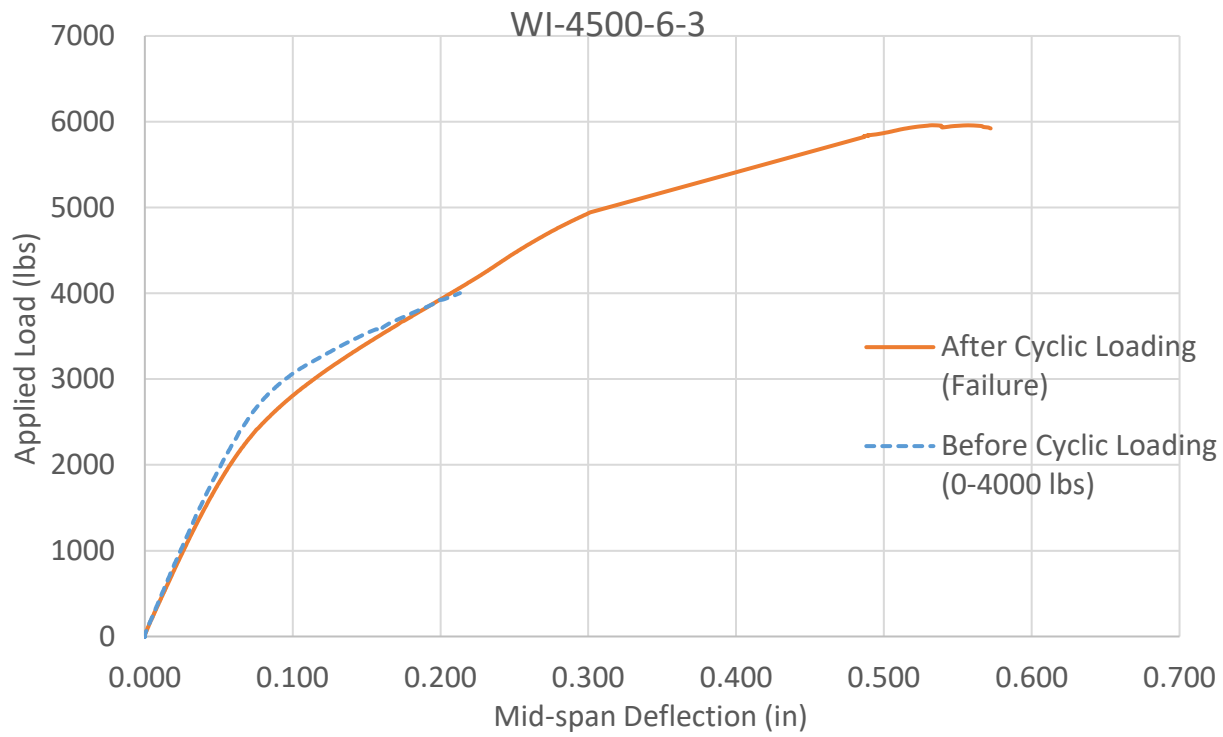


Figure 75. Load-deflection graphs prior to cyclic loading and after cyclic loading until failure (prism made with WI wire)

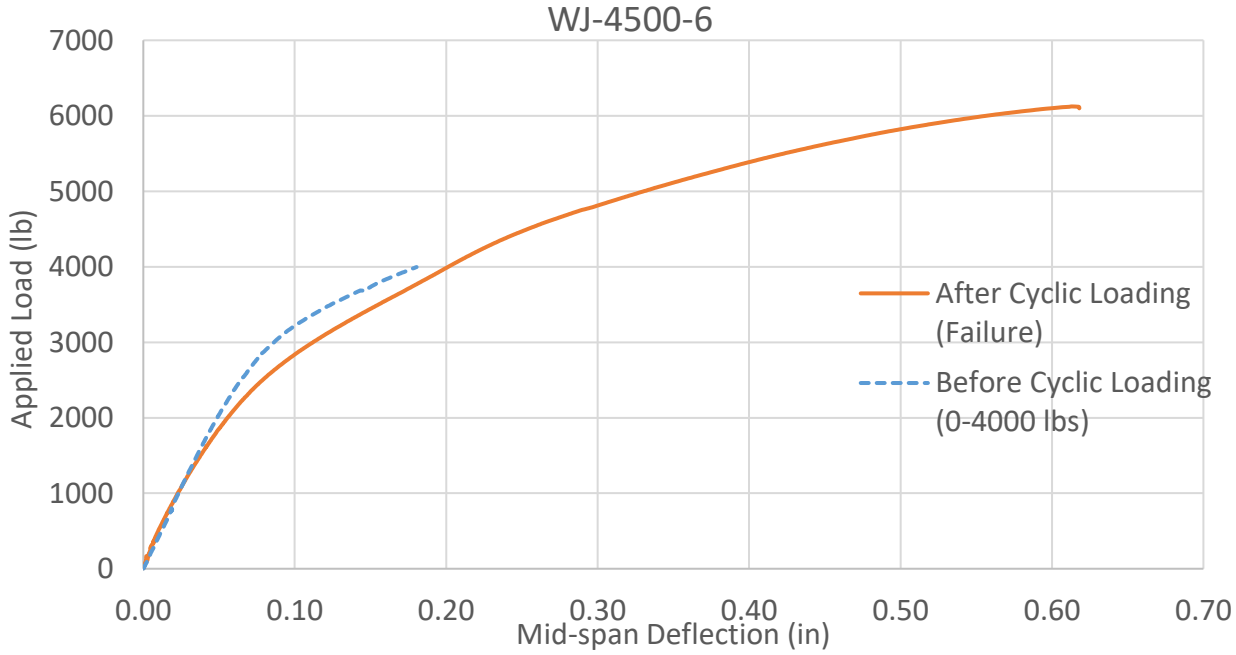


Figure 76. Load-deflection graphs prior to cyclic loading and after cyclic loading until failure (prism made with WJ wire)

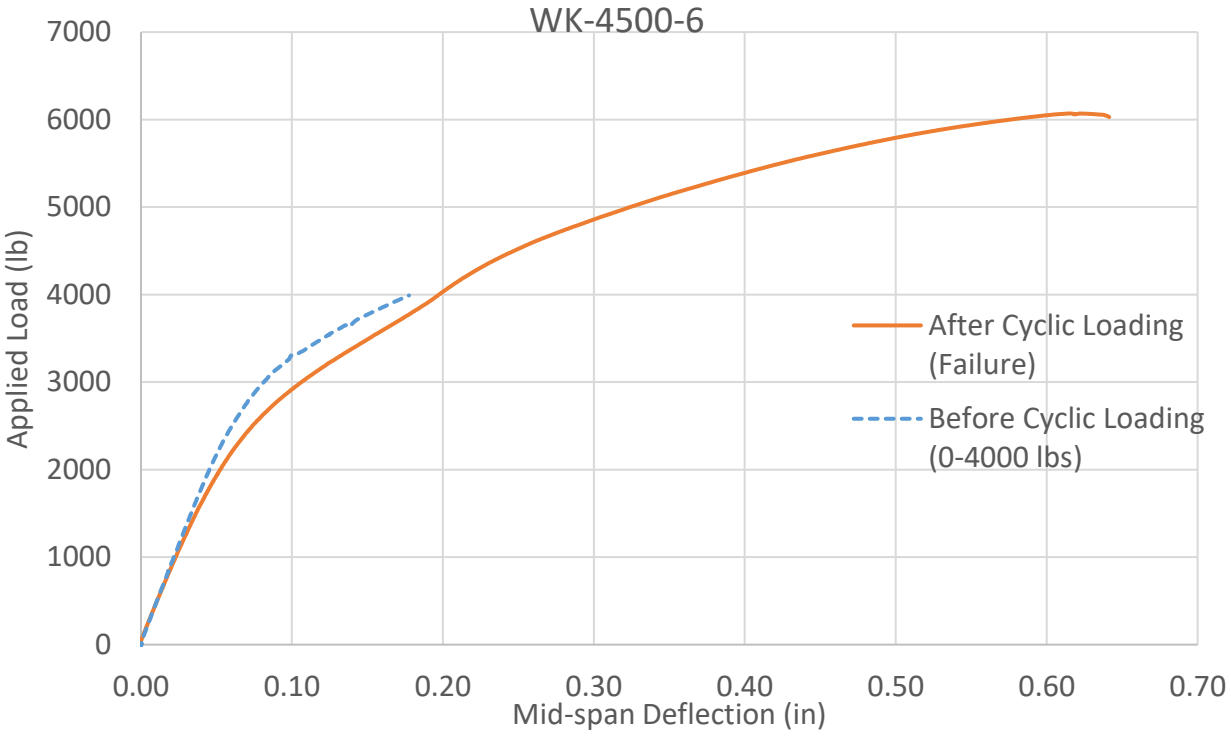


Figure 77. Load-deflection graphs prior to cyclic loading and after cyclic loading until failure (prism made with WK wire)

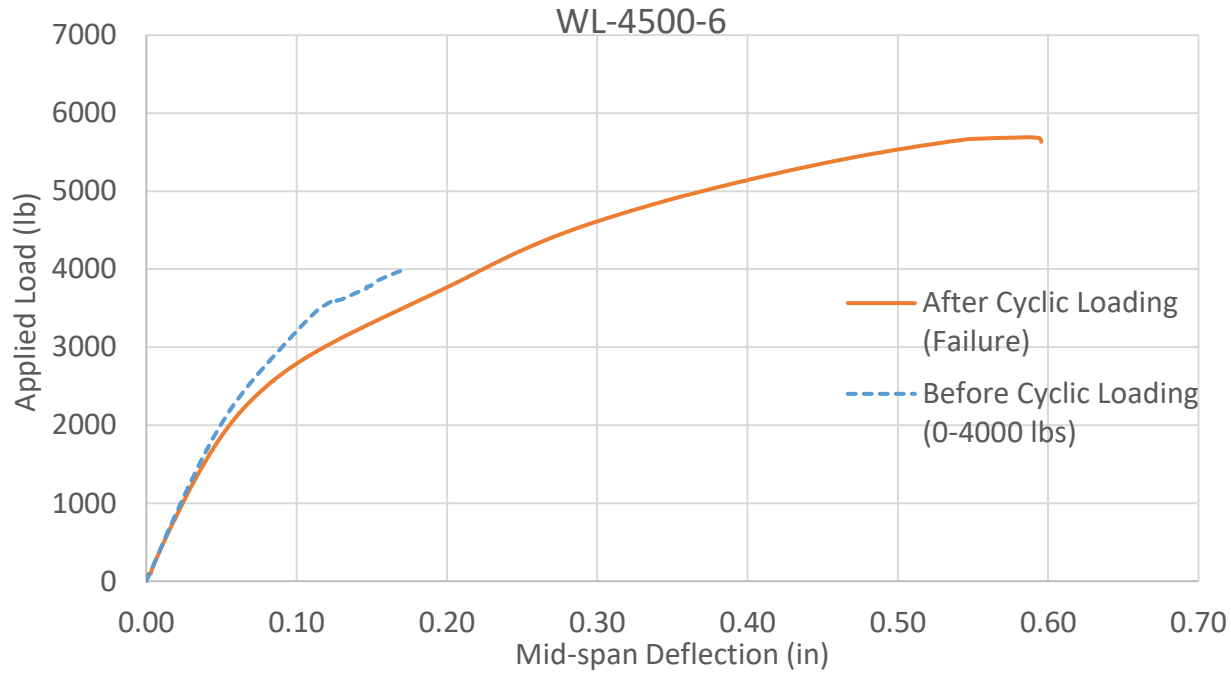


Figure 78. Load-deflection graphs prior to cyclic loading and after cyclic loading until failure (prism made with WL wire)

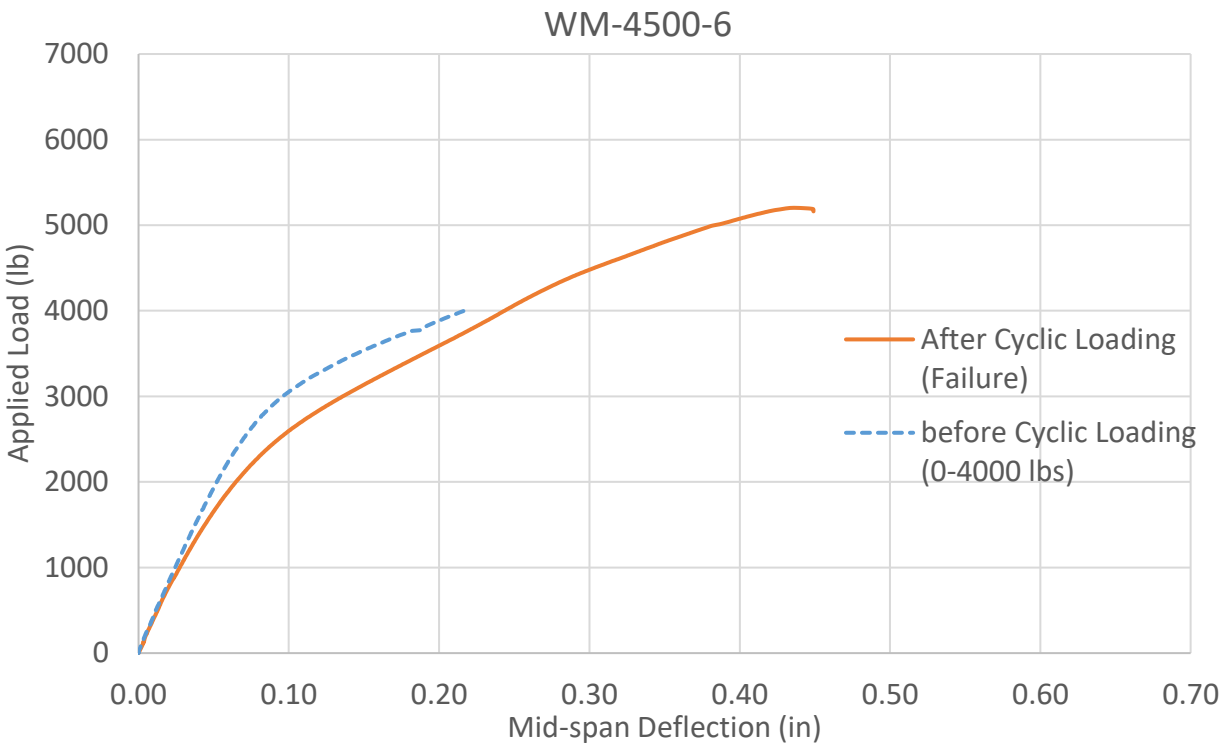


Figure 79. Load-deflection graphs prior to cyclic loading and after cyclic loading until failure (prism made with WM wire)

From Figure 69 to Figure 79, it can be seen that, prior to cyclic loading, the prisms are stiffer, and the load-deflection graph is always above the graph for identical prism after cyclic loading. However, after experiencing cyclic loading, for loads beyond the cracking load, the section which has been subjected to cyclic loading will "stiffen up" and its graph is essentially the continuation of the graph before cyclic loading. Same results were observed for all prisms made with different wires.

For prisms able to finish 200,000 cycles of load, compression mode of failure was the only observed mode of failure, and all prisms except those made with lightly indented wires (WA, WK, and WL) showed lower-moment capacities in cyclic-load testing than monotonic-load testing. Figure 80 and Figure 81 show compression mode of failure for prisms made with WF and WB wires.

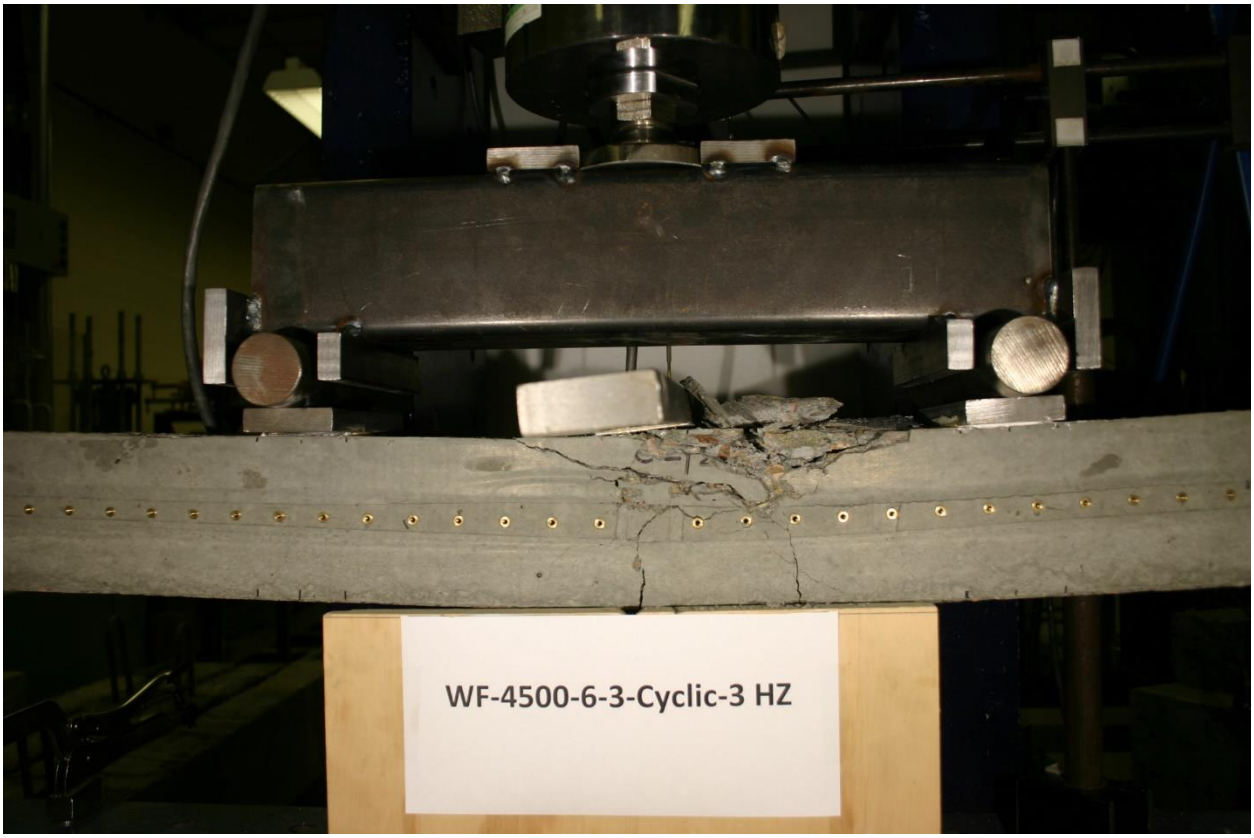


Figure 80. Compression mode of failure for prisms subjected to cyclic loading (prism made with WF)

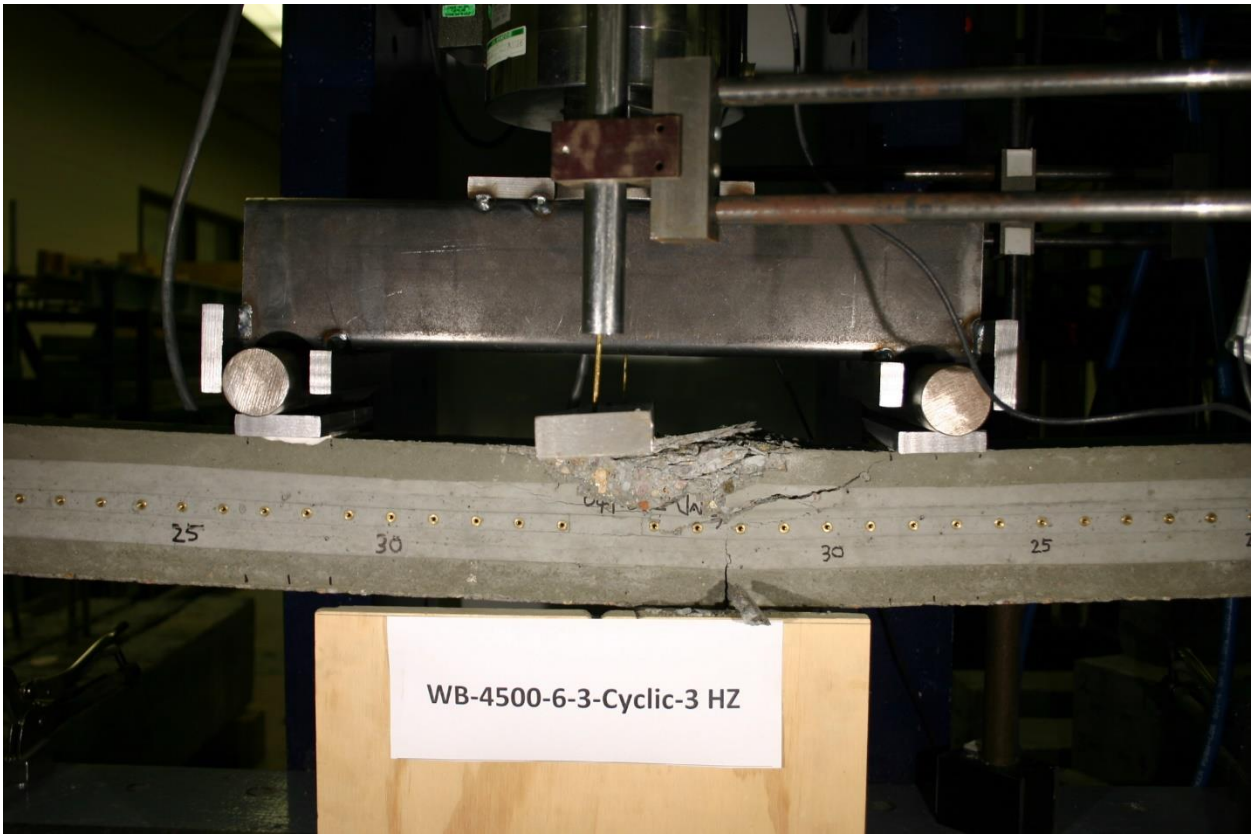


Figure 81. Compression mode of failure for prisms subjected to cyclic loading (prism made with WB)

5. Data Analysis and Model Development

5.1 A Prediction Model for the Development Length of Wires Commonly Used in the Railroad Industry

Among different concrete properties and prestressing wire properties evaluated, wire-indentation type and compressive strength of concrete at release time showed the biggest impact on development length. In a study done by a former graduate student (Arnold, 2013) at Kansas State University, un-tensioned pull-out tests were conducted for all 13 wires and pull-out force was measured at 0.10 in. end-slip in each test. For each type of wire, six un-tensioned pull-out tests were conducted and maximum pull-out forces at a free-end slip less than or equal to 0.10 in. were averaged. It is generally accepted that pull-out values are a good indicator of bond performance of prestressing wires, and the test has since been adopted as the ASTM A1096 test procedure. Table 24 shows wire types and their indentation type, number of transfer-length measurements for each wire type, and number of un-tensioned pull-out tests conducted for each wire type.

Table 24. Matrix of wire pull-out testing program [after: (Arnold, 2013)]

Wire Identification	Indentation Type	Number of test specimens	
		Transfer Lengths (no of ends)	As-received un-tensioned pullouts
[WA]	smooth	6	6
[WB]	chevron	6	6
[WC]	spiral	6	6
[WD]	chevron	6	6
[WE]	spiral	6	6
[WF]	diamond	6	6
[WG]	chevron	6	6
[WH]	chevron	6	6
[WI]	chevron	6	6
[WJ]	chevron	6	6
[WK]	4-dot	6	6
[WL]	2-dot	6	6
[WM]	chevron	6	6
Total		78	78

Wire pull-out test specimens had dimensions of 4-in.-outer-diameter steel tube, 1/8-in. wall thickness, and 8-in. height. A 6 x 6 x 3/16-in. steel plate (3/16-in. thick) was welded to the

bottom of the specimen. Across the height of steel tube, two, 1-in. bond breakers were installed at the top and the bottom of the tube, creating 6-in. bond length. The top bond breaker was projected for 1 in. from the top mortar surface. Figure 82 shows a schematic of the wire pull out test setup (Arnold, 2013).

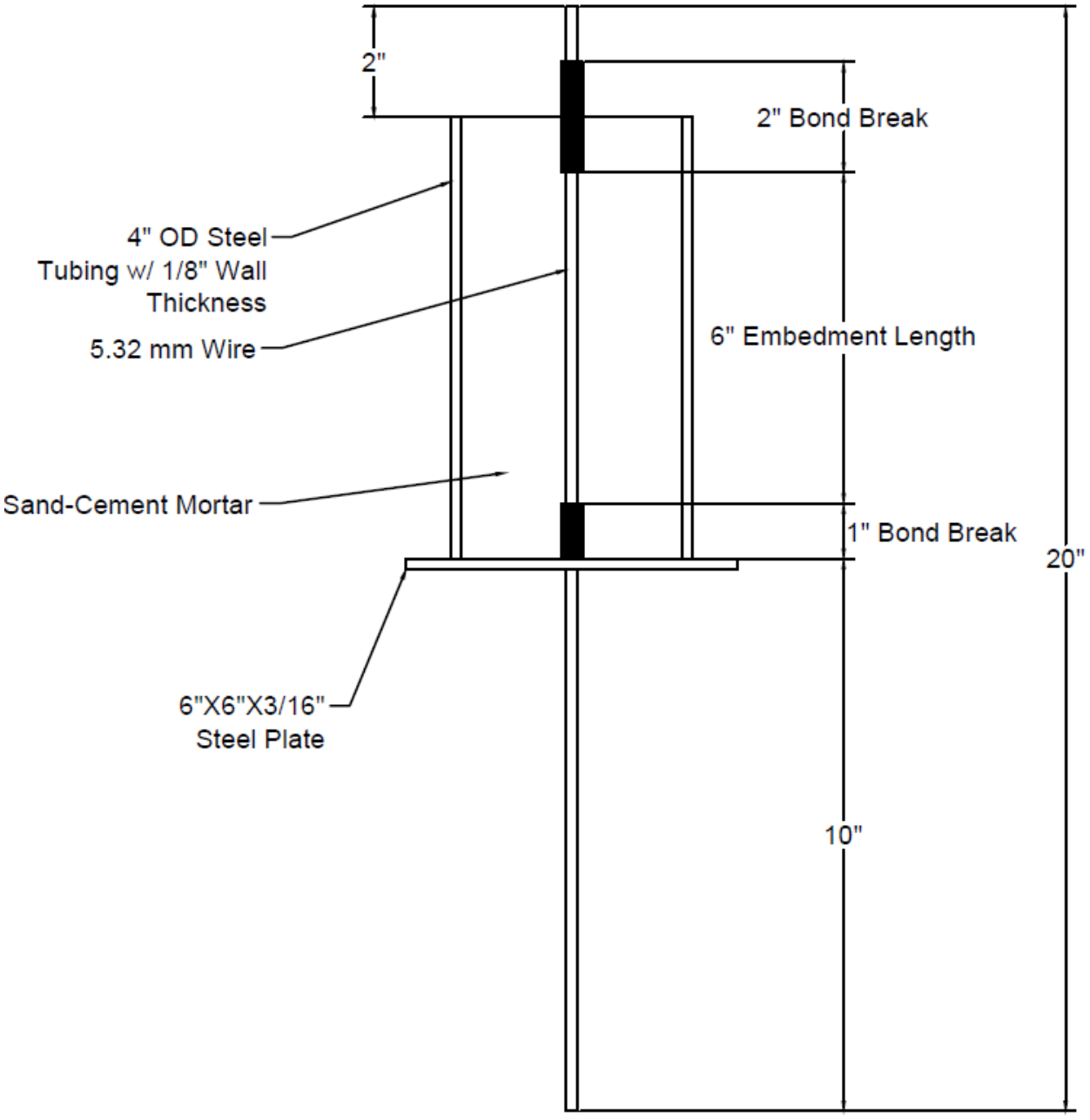


Figure 82. Final dimensions of wire pull out test specimen [after: (Arnold, 2013)]

A mortar mixture with water-to-cement ratio (w/c) of 0.427, and sand-to-cement ratio of (s/c) of 2.0, was used for all test specimens. Type III cement was used in manufacture of all specimens.

Pull-out tests were conducted when the mortar cube strength reached 4,500 psi and were completed before cube strength reached 5,000 psi. The load was applied to the bottom of the specimen at the rate of 2,000 lbs/min for all tests. During each test, the applied load was continuously recorded and wire end-slip at the top end of the specimen was recorded using an LVDT. Results from un-tensioned pull-out tests are summarized in Table 25 (Arnold, 2013).

Table 25. As-received wires, average pullout force at 0.10 in. end slip [after: (Arnold, 2013)]

As-received pull-out test results 4-in. diameter, 6-in. bond length, Ottawa sand pull-out force at 0.10-in. end-slip			
Wire identification	**Avg. pull-out force (lbf)**	**Std. dev (lbf)**	**C.V. (%)**
[WA]	378	32	8.5
[WB]	6473	563	8.7
[WC]	7663	969	12.6
[WD]	5302	300	5.7
[WE]	7817	487	6.2
[WF]	7993	441	5.5
[WG]	5469	388	7.1
[WH]	7270	462	6.4
[WI]	6439	498	7.7
[WJ]	6814	591	8.7
[WK]	3434	347	10.1
[WL]	2067	323	15.6

Load tests were conducted on pretensioned, prestressed prisms and development lengths were evaluated. For each type of wire and concrete-release strength, two identical prisms were load-tested at each end with different embedment lengths. In evaluation of development lengths, it was assumed prestressing wires were developed at a distance from the prism end to point load, if the maximum moment resisted by the prism was larger than calculated nominal-moment capacity of the section using the strain-compatibility method of analysis. To calculate nominal-moment capacity of each section, actual-section dimensions, initial and total prestress losses, accurate compressive strength of concrete, and stress-strain curves particular to each wire were used. Prior to running the load tests, dimensions of the prism's cross section and depth of prestress wires from the top of the section were measured for each end of the prism.

5.1.1 Initial and total prestress losses

Initial and total prestress losses were calculated using concrete-surface strain values at the time of de-tensioning and before load testing, respectively. Peak strain values (microstrain) at the time of de-tensioning were determined by Naga Bodapoti. Table 26 through Table 28 show the peak microstrain values determined for each prism end. Brass points were inserted on both sides along the length of prisms at mid-height. They were longitudinally spaced at 1-in. (2.54-mm), center-

to-center intervals. Starting from 0.5 in. (12.7 mm) from prism end, brass inserts were installed on both sides of the prism at a 34-in. (86.4-cm) length. Prior to releasing the prestressing steel, the distance between brass points was measured with accuracy of 0.0001 in. (0.00254 mm) using a Whittemore gage with gage length of 8 in. (203.2 mm). This reading is the base for subsequent readings in order to calculate concrete surface strains. Another reading was conducted after de-tensioning to calculate surface strains at the time of de-tensioning. A program was developed that incorporated a least-square algorithm to determine transfer length from the concrete surface strain data (Zhao W. , et al., 2013). Readings prior to de-tensioning and after de-tensioning were conducted by Naga Bodapoti, and transfer lengths were determined based on calculated surface strains.

Table 26. Peak strain values (microstrain) determined for each end of prisms with 4500 psi release strength before load testing and at the time of de-tensioning

	Prism 1		Prism 2		Prism 1		Prism 2	
	Max microstrain before testing		Max microstrain before testing		Max microstrain at de-tensioning		Max microstrain at de-tensioning	
RS = 4500 psi and Slump=6 in.	Avg Live End	Avg Dead End	Avg Live End	Avg Dead End	Avg Live End	Avg Dead End	Avg Live End	Avg Dead End
WA	1800	1900	1900	1900	780	850	940	940
WB	1900	1900	2000	2000	850	840	940	920
WC	1850	1900	1800	1850	730	750	800	810
WD	1800	1900	1780	1800	740	800	730	740
WE	1850	1900	1870	1900	740	770	850	850
WF	2100	2000	1950	2000	980	900	980	980
WG	1900	1900	1950	1920	880	900	950	940
WH	1800	1900	1880	1800	660	720	900	850
WI	2000	2080	1950	2000	1000	1040	900	980
WJ	1850	1850	1850	1850	840	800	870	880
WK	1950	1900	1940	1950	950	950	1000	1000
WL	1950	1950	2050	2000	910	900	1080	1040
WM	2050	2020	2020	2000	850	850	860	880

Table 27. Peak strain values (microstrain) determined for each end of prisms with 3500 psi release strength before load testing and at the time of de-tensioning

	Prism 1		Prism 2		Prism 1		Prism 2	
	Max microstrain before testing		Max microstrain before testing		Max microstrain at de-tensioning		Max microstrain at de-tensioning	
RS = 3500 psi and Slump=6 in.	Avg Live End	Avg Dead End	Avg Live End	Avg Dead End	Avg Live End	Avg Dead End	Avg Live End	Avg Dead End
WA	1950	1980	2000	2050	1000	980	1070	1050
WE	1950	2050	2050	2100	880	900	950	980
WG	2100	2070	1900	1980	960	940	900	920
WH	2050	2000	2000	1960	1060	1070	1080	1060
WK	2100	2100	2100	2100	1050	1075	1175	1150

Table 28. Peak strain values (microstrain) determined for each end of prisms with 6000 psi release strength before load testing and at the time of de-tensioning

	Prism 1		Prism 2		Prism 1		Prism 2	
	Max microstrain before testing		Max microstrain before testing		Max microstrain at de-tensioning		Max microstrain at de-tensioning	
RS = 6000 psi and Slump=6 in.	Avg Live End	Avg Dead End	Avg Live End	Avg Dead End	Avg Live End	Avg Dead End	Avg Live End	Avg Dead End
WA	1660	1780	1660	1600	640	700	640	630
WE	1750	1750	1680	1770	690	700	640	720
WG	1730	1720	1630	1700	720	700	700	730
WH	1730	1730	1700	1700	730	720	710	730
WK	1780	1770	1660	1690	670	670	650	660

Using Hooke's Law, maximum microstrain measured for each end of the prism was multiplied by Young's modulus of prestressing steel (E_{ps}) to calculate prestress loss. Exact values of Young's modulus for each wire type were obtained from laboratory tests done by (Chen, 2016), except for WA, WC, and WK wires whose Young's modulus and ultimate tensile-strength values were obtained from mill certs (refer to Table 1). Losses in percentage were a fraction of prestress loss to jacking stress in the prestressed steel. Each wire was pulled to 7,000 lb and had a cross section of 0.0344 in^2. Thus, the jacking stress in each wire was $f_{pi} = \frac{7000}{0.0344} = 203.4\ ksi$. Initial and total prestress losses used in the analysis of the prism sections were the average of losses calculated for both ends of each prism.

Table 29. Initial and total losses in percentage for ends of prisms with 4,500 psi release strength

	Prism 1		Prism 2	
RS = 4500 psi and Slump=6 in.	Total Losses (%)	Initial Losses (%)	Total Losses (%)	Initial Losses (%)
WA	27.13	11.95	27.87	13.79
WB	27.60	12.28	29.06	13.51
WC	26.30	10.38	25.60	11.29
WD	27.19	11.32	26.31	10.80
WE	26.91	10.83	27.05	12.20
WF	29.13	13.36	28.07	13.93
WG	27.11	12.70	27.61	13.48
WH	28.21	10.52	28.06	13.34
WI	29.47	14.74	28.53	13.58
WJ	25.85	11.46	25.85	12.23
WK	27.98	13.81	28.27	14.53
WL	28.60	13.27	29.70	15.54
WM	29.87	12.48	29.50	12.77

Table 30. Initial and total losses in percentage for ends of prisms with 3,500 psi release strength

	Prism 1		Prism 2	
RS =3500 psi and Slump=6 in.	Total Losses (%)	Initial Losses (%)	Total Losses (%)	Initial Losses (%)
WA	28.82	14.52	29.70	15.55
WE	28.70	12.77	29.77	13.85
WG	29.75	13.55	27.68	12.98
WH	30.88	16.24	30.20	16.32
WK	30.52	15.44	30.52	16.90

Table 31. Initial and total losses in percentage for ends of prisms with 6,000 psi release strength

	Prism 1		Prism 2	
RS = 6000 psi and Slump=6 in.	Total Losses (%)	Initial Losses (%)	Total Losses (%)	Initial Losses (%)
WA	25.23	9.83	23.91	9.31
WE	25.11	9.97	24.75	9.76
WG	24.61	10.13	23.75	10.20
WH	26.38	11.06	25.93	10.98
WK	25.80	9.74	24.34	9.52

5.1.2 Modeling stress-strain curve-Power Formula

The design "power formula" for wires was improved by (Chen, 2016) and used to calculate section nominal-moment capacity of prism ends as opposed to using the PCI (2010) prestressing steel stress-strain curve.

5.1.3 Compressive strength of concrete

4 (in) x 8 (in) cylinders were manufactured with the same concrete mix used in prism fabrication and tested according to ASTM C39/C39M to attain concrete compressive strength. The average of the three compressive strength tests indicated a compressive strength of 12,000 psi (82.73 MPa).

A macro-enabled program was developed in Microsoft Excel to calculate the nominal-moment capacity (M_n) of each section using measured dimensions, prestress losses, evaluated concrete compressive strength, and the stress-strain curve developed particular to each wire. Maximum resisted moment for each end tested was calculated under maximum resisted load and prism self-weight. A hand calculation for analysis of section capacity using the strain-compatibility method appears in Appendix-A. In the next step, the ratio of resisted-moment to nominal-moment capacity (M_{exp}/M_n) was calculated. When $M_{exp}/M_n \geq 1$, it is assumed that wires are developed at that embedment length tested. M_{exp}/M_n versus embedment lengths were plotted and the equation corresponding to the trend line, which passes through all four points (four load tests), was attained. Note that embedment lengths tested were 9.5, 13, 16.5, and 20 in. Figure 83 shows a plot of M_{exp}/M_n versus embedment lengths, and the trend line passing through the scattered points for prisms made with WA wire and concrete release strength of 4,500 psi.

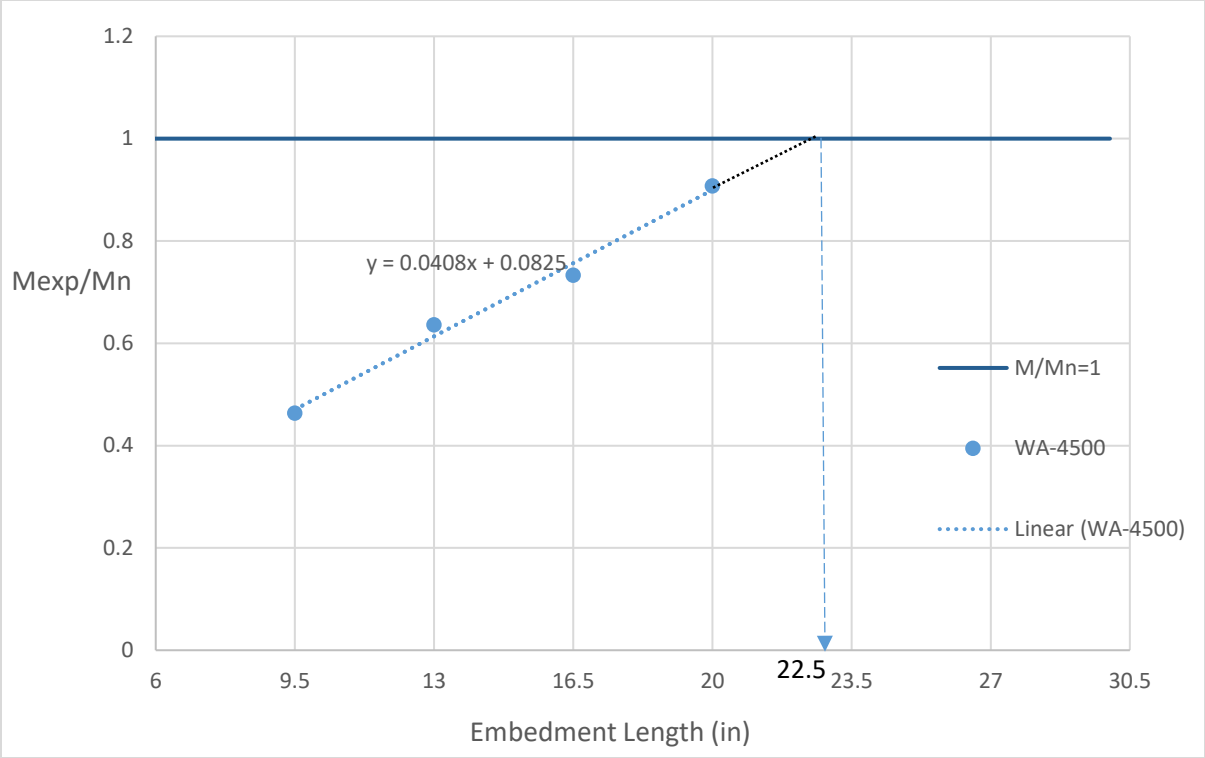


Figure 83. Ratio of resisted-moment to nominal-moment capacity of section tested versus embedment length

As can be seen in Figure 83, a linear trend appears as the embedment length increases the ratio of resisted-moment to nominal-moment capacity increases as well. Prisms manufactured with WA wire and concrete-release strength of 4,500 psi were not fully developed, even at 20-in. embedment length, since resisted-moment was smaller than nominal-moment capacity calculated through the analysis. By setting the trend-line equation equal to one, development length can be determined. For cases where $M_{exp}/M_n > 1$ for all four different embedment lengths, development length can be considered to be equal to the shortest embedment length tested. Experimental moments, nominal-moment capacities and their ratio calculated for all prism ends are summarized in Table 32 to Table 37. All experimental development lengths were determined with the same described method and graphs are presented in Appendix-B.

Table 32. Resisted-moment and nominal-moment capacity calculated for each end of prisms with 4,500 psi release strength (EL=embedment length)

	Resisted moment (Mexp) (k-ft)				Calculated nominal moment (Mn) (k-ft)			
RS = 4500 psi and Slump=6 in.	EL=20 in	EL=16.5 in	EL=13 in	EL=9.5 in	EL=20 in	EL=16.5 in	EL=13 in	EL=9.5 in
WA	3.24	2.68	2.31	1.68	3.57	3.66	3.63	3.63
WB	4.46	3.89	3.48	2.50	3.66	3.65	3.64	3.65
WC	4.43	4.18	3.07	2.84	3.48	3.68	3.53	3.56
WD	4.29	4.20	3.92	3.09	3.49	3.81	3.52	3.74
WE	4.03	4.29	3.93	3.96	3.50	3.56	3.51	3.56
WF	4.14	4.35	4.09	4.31	3.50	3.53	3.47	3.53
WG	4.09	3.75	3.57	3.11	3.41	3.43	3.38	3.59
WH	4.27	4.52	3.90	3.62	3.60	3.97	3.57	3.96
WI	4.14	3.96	3.83	3.42	3.40	3.58	3.46	3.58
WJ	4.35	4.04	3.60	2.61	3.61	3.61	3.61	3.61
WK	3.51	3.15	2.79	2.39	3.42	3.56	3.45	3.56
WL	3.00	2.61	2.59	2.35	3.39	3.58	3.50	3.49
WM	3.93	3.84	3.84	2.96	3.57	3.57	3.54	3.52

Table 33. Ratio of resisted moment to nominal moment capacity calculated for each end of prisms tested (EL=embedment length)

	Mexp/Mn			
RS = 4500 psi and Slump=6 in.	EL=20 in	EL=16.5 in	EL=13 in	EL=9.5 in
WA	0.91	0.73	0.64	0.46
WB	1.22	1.07	0.96	0.68
WC	1.28	1.14	0.87	0.80
WD	1.23	1.10	1.11	0.83
WE	1.15	1.21	1.12	1.11
WF	1.18	1.23	1.18	1.22
WG	1.20	1.09	1.06	0.87
WH	1.19	1.14	1.09	0.91
WI	1.22	1.11	1.11	0.96
WJ	1.21	1.12	1.00	0.72
WK	1.03	0.89	0.81	0.67
WL	0.89	0.73	0.74	0.67
WM	1.10	1.08	1.08	0.84

Table 34 Resisted-moment and nominal nominal-moment capacity calculated for each end of prisms with 3,500 psi release strength (EL=embedment length)

	Resisted moment (Mexp) (k-ft)				Calculated nominal moment (Mn) (k-ft)			
RS = 3500 psi and Slump=6 in.	EL=20 in	EL=16.5 in	EL=13 in	EL=9.5 in	EL=20 in	EL=16.5 in	EL=13 in	EL=9.5 in
WA	2.59	2.07	1.88	1.37	3.59	3.52	3.53	3.52
WE	3.99	3.72	3.66	3.31	3.41	3.56	3.49	3.54
WG	3.73	3.35	2.32	2.72	3.44	3.38	3.42	3.54
WH	4.22	4.24	3.64	3.03	3.55	3.64	3.60	3.75
WK	3.43	3.04	2.64	2.89	3.51	3.67	3.53	3.40

Table 35 Ratio of resisted resisted-moment to nominal nominal-moment capacity calculated for each end of prisms tested (EL=embedment length)

	Mexp/Mn			
RS = 3500 psi and Slump=6 in.	EL=20 in	EL=16.5 in	EL=13 in	EL=9.5 in
WA	0.72	0.59	0.53	0.39
WE	1.17	1.04	1.05	0.94
WG	1.08	0.99	0.68	0.77
WH	1.19	1.16	1.01	0.81
WK	0.98	0.83	0.75	0.85

Table 36. Resisted-moment and nominal-moment capacity calculated for each end of prisms with 6,000 psi release strength (EL=embedment length)

	Resisted moment (Mexp) (k-ft)				Calculated nominal moment (Mn) (k-ft)			
RS = 6000 psi and Slump=6 in.	EL=20 in	EL=16.5 in	EL=13 in	EL=9.5 in	EL=20 in	EL=16.5 in	EL=13 in	EL=9.5 in
WA	3.14	2.48	2.18	1.84	3.59	3.72	3.54	3.69
WE	4.12	4.14	4.39	3.61	3.63	3.66	3.57	3.60
WG	3.85	3.93	3.55	2.78	3.42	3.43	3.45	3.46
WH	4.02	4.08	4.08	3.03	3.62	3.59	3.62	3.62
WK	4.05	3.54	2.90	2.74	3.44	3.56	3.55	3.53

Table 37 Ratio of resisted resisted-moment to nominal nominal-moment capacity calculated for each end of prisms tested (EL= embedment length)

	Mexp/Mn			
RS = 6000 psi and Slump=6 in.	**EL=20 in**	**EL=16.5 in**	**EL=13 in**	**EL=9.5 in**
WA	0.87	0.67	0.62	0.50
WE	1.14	1.13	1.23	1.00
WG	1.13	1.15	1.03	0.80
WH	1.11	1.14	1.13	0.84
WK	1.18	1.00	0.82	0.78

Development lengths for all different prisms were determined and summarized in Table 38. It was previously noted that, among all parameters studied in this project, wire pull-out values and concrete compressive strength at the time of de-tensioning were the primary parameters affecting development length of pretensioned, prestressed prisms. Transfer lengths at the time of de-tensioning (Bodapati, et al., 2013) and ratio of development length to transfer length are summarized in the following table as well.

Table 38. Development lengths evaluated, transfer lengths and ratio of development length to transfer length for prisms made with different wires and concrete-release strength

Row number	Wire type	Concrete release strength (ksi)	Average pull out force (kip)	Experimental Ld (in)	Lt (in) at de-tensioning	Ld/Lt
1	WA	3741	378	29.4	21.4	1.37
2		4664	378	22.5	16.3	1.38
3		6128	378	23.7	13.5	1.76
4	WE	3486	7817	11.4	10.5	1.09
5		4650	7817	9.5	7.4	1.28
6		6020	7817	9.5	7.1	1.34
7	WG	3561	5469	16.5	13.8	1.20
8		4697	5469	11.9	11.8	1.01
9		5825	5469	12.5	9.8	1.28
10	WH	3614	7270	13	11.2	1.16
11		4695	7270	11.3	7.5	1.51
12		6059	7270	11.4	7.3	1.56
13	WK	3528	3434	20.5	17.7	1.16
14		4572	3434	19.3	14	1.38
15		5857	3434	16.5	11.1	1.49
16	WB	4453	6473	14.3	11.6	1.23
17	WC	4701	7663	14.7	8.8	1.67
18	WD	4400	5302	11.6	11.1	1.05
19	WF	4466	7993	9.5	8.5	1.12
20	WI	4547	6439	10.4	10.1	1.03
21	WJ	4521	6814	13	9	1.44
22	WL	4476	2067	25.3	18.7	1.35
23	WM	4506	6879	11.9	9.8	1.21

Development length expressions proposed by other researchers noted in the literature review of this report were used to predict development length of wires with different indentations (AASHTO, 1998) (ACI 318R-02, 2002) (Abdalla, Ramirez, & Lee, 1993) (Buckner, March-April 1995) (Deatherage, Burdette, & Chew, January-February 1994) (Lane, 1998) (Mitchel, Cook, Khan, & Tham, May-June 1993) (Talat & Paul, September-October 1977) (FDOT). All expressions noted in literature review were originally proposed to predict development length of strands. Since there is very little knowledge on development length prediction of wires, proposed equations for strand development length were used to determine wire development lengths and Comparisons were made between models and experimental development lengths. Table 39 Compares predicted development lengths for different wires and concrete release strengths with

experimental development lengths. Note that in Table 39, none of expressions used to predict development length incorporates concrete properties ($f'_{ci}\ and\ f'_c$).

Table 39. Predicted development lengths and experimental development lengths

Wire type	Concrete Release Strength (psi)	ACI/AASHTO	Abdalla, Ramirez, & Lee	Deatherage, Burdette, & Chew	Buckner	FDOT Proposal for Development Length	Experimental Ld (in)
WA	3741	31.8	54.0	46.8	35.9	35.9	29.4
	4664	31.5	53.6	46.1	35.4	35.4	22.5
	6128	31.1	52.9	44.8	34.6	34.6	23.7
WE	3486	30.5	51.8	44.8	34.6	34.6	11.4
	4650	30.1	51.1	43.8	33.9	33.9	9.5
	6020	29.7	50.6	42.8	33.3	33.3	9.5
WG	3561	28.6	48.5	41.8	32.6	32.6	16.5
	4697	28.3	48.1	41.2	32.2	32.2	11.9
	5825	27.7	47.0	39.5	31.1	31.1	12.5
WH	3614	31.5	53.5	46.6	35.8	35.8	13
	4695	31.1	52.8	45.5	35.1	35.1	11.3
	6059	30.7	52.2	44.6	34.4	34.4	11.4
WK	3528	30.8	52.3	45.6	35.1	35.1	20.5
	4572	30.4	51.6	44.5	34.4	34.4	19.3
	5857	29.9	50.8	43.0	33.4	33.4	16.5
WB	4453	31.7	53.9	46.5	35.7	35.7	14.3
WC	4701	30.5	51.8	44.1	34.2	34.2	14.7
WD	4400	29.9	50.9	43.5	33.7	33.7	11.6
WF	4466	30.1	51.2	44.2	34.2	34.2	9.5
WI	4547	30.5	51.8	44.8	34.6	34.6	10.4
WJ	4521	30.4	51.7	44.0	34.1	34.1	13
WL	4476	30.6	52.1	45.1	34.8	34.8	25.3
WM	4506	31.0	52.8	45.8	35.3	35.3	11.9

As it can be seen from Table 39, development lengths predicted were larger than experimental development lengths. Moreover, since proposed equations do not include the effect of concrete compressive strength at time of de-tensioning and prestressing steel indentation type, there is not significant variation in predicted development lengths for different wires and concrete release strengths. Predicted development lengths versus experimental development lengths are plotted in Figure 84.

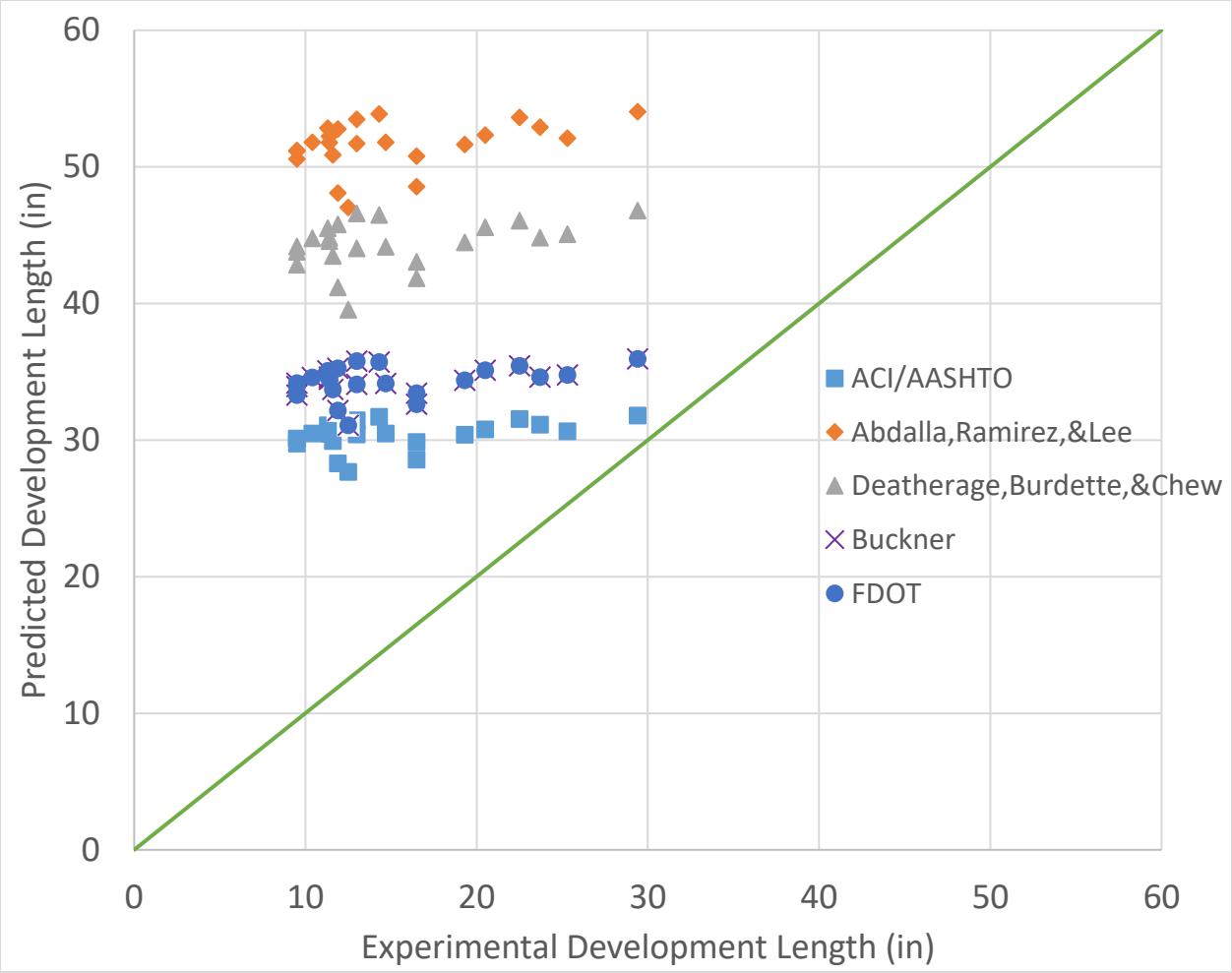


Figure 84. Graphical display of predicted development lengths using existing equations versus experimental development lengths

As it can be seen from Figure 84 predicted development lengths scattered above unity line and predicted development lengths were much larger than experimental development lengths. Note that proposed equations by Buckner March-April 1995, Deatherage, Burdette, & Chew, January-February 1994, Building Code Requirements for Structural Concrete (ACI 318-02) And Commentary (ACI 318R-02), Abdalla, Ramirez, & Lee, 1993 and FDOT do not consider compressive strength of concrete at time of de-tensioning and wire indentation type. Thus, predicted development lengths did not correlate well with experimental development lengths.

Also, comparisons were made between models incorporating concrete properties (f'_{ci} and f'_c) in development length predictions and experimental development lengths.

Table 40. Predicted development lengths and experimental development lengths

Wire type	Concrete Release Strength (psi)	Talalat & Paul	Mitchel, Cook, Khan, & Tham	Lane	Experimental Ld (in)
WA	3741	22.6	25.9	30.8	29.4
	4664	22.0	24.3	30.5	22.5
	6128	20.9	22.3	30.1	23.7
WE	3486	20.9	25.5	30.1	11.4
	4650	20.1	23.4	29.7	9.5
	6020	19.3	21.6	29.4	9.5
WG	3561	18.5	24.2	29.0	16.5
	4697	17.9	22.2	28.8	11.9
	5825	16.5	20.4	28.2	12.5
WH	3614	22.4	26.0	30.7	13
	4695	21.5	24.0	30.3	11.3
	6059	20.7	22.3	30.0	11.4
WK	3528	21.6	25.8	30.3	20.5
	4572	20.6	23.7	29.9	19.3
	5857	19.5	21.8	29.4	16.5
WB	4453	22.3	24.7	30.7	14.3
WC	4701	20.4	23.4	29.8	14.7
WD	4400	19.8	23.6	29.6	11.6
WF	4466	20.4	23.8	29.8	9.5
WI	4547	20.9	23.9	30.1	10.4
WJ	4521	20.3	23.6	29.8	13
WL	4476	21.1	24.1	30.2	25.3
WM	4506	21.7	24.4	30.4	11.9

As it can be seen Table 40, although, these models incorporate the effect of compressive strength of concrete at time of de-tensioning(f'_{ci}), development length predictions were poor and there was a big difference between predicted development lengths and experimental development lengths. Wires with different indentation types showed significant difference in bond performance in load tests. The major neglected factor in these equations was wire indentation type which was the main source of error in development length predictions. Figure 85 Compares development lengths predicted and experimental development lengths.

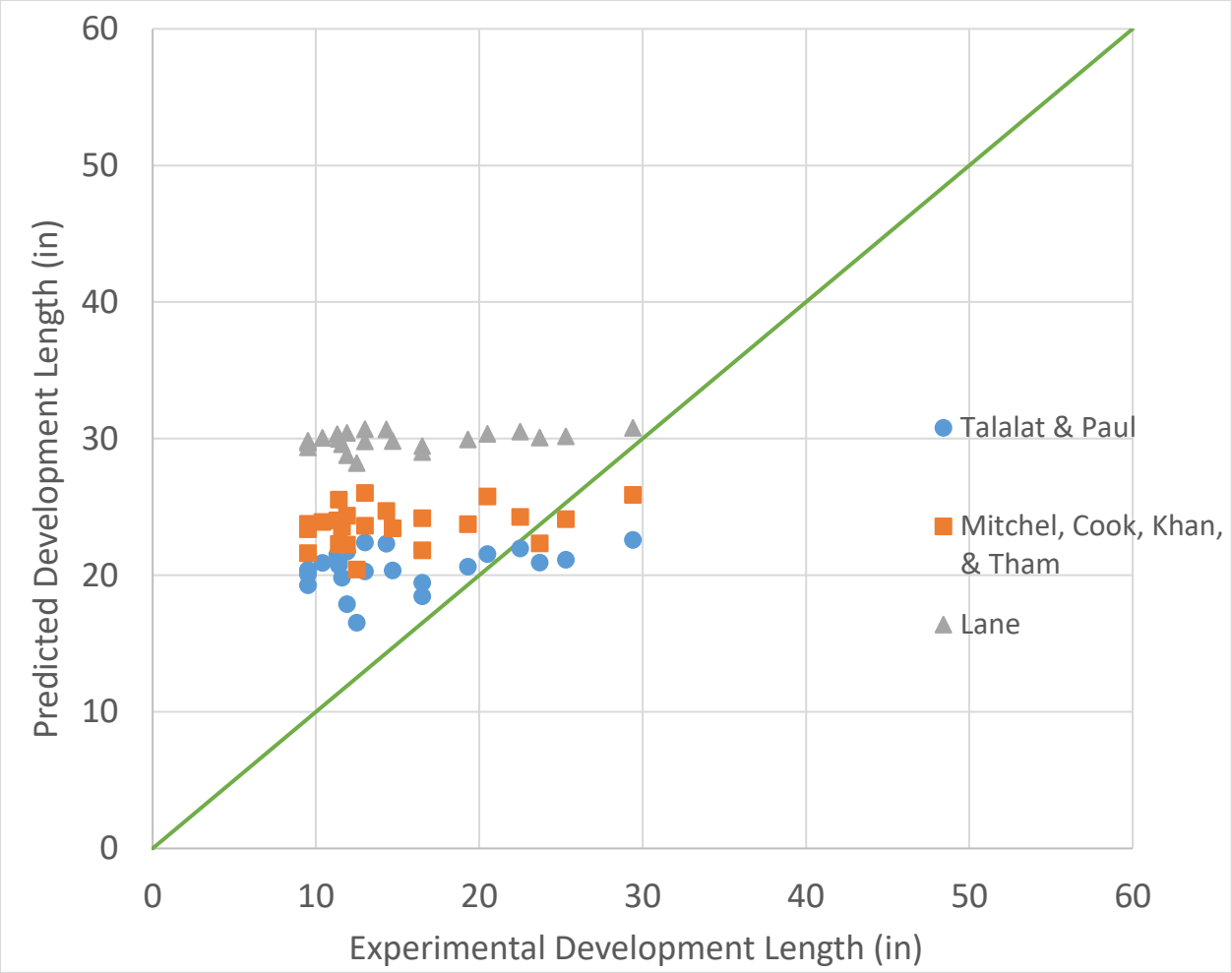


Figure 85. Graphical display of predicted development lengths using existing equations versus experimental development lengths

As it can be seen in Figure 85 , there was a big error in prediction of development lengths for wires using proposed equations by Talalat & Paul 1977, Mitchel, Cook, Khan, and Tham 1993, and Lane 1998.

From Figure 84 and Figure 85, it was understood that current equation in the ACI/AASHTO Code and equations proposed by other researchers to predict development length were not able to predict development length of wires accurately. This was mainly due excluding the effect of wire indentation type and concrete release strength from development length determination. In this study, experimental tests were conducted, and development lengths were evaluated for prisms made with different wires and concrete release strengths. A statistical model was developed using 14 out of 23 data sets (60 percent of data sets) as training data, and nine data sets (40 percent of data sets) as validation for the model. Data sets from row numbers 1 to 14 were used as training data, and the rest were used as validation for the model. Models with 80 percent training data sets and 20 percent validation data sets were developed as well. However, more accurate models resulted from models developed with 60 percent training data sets and 40 percent validation data sets. Multiple-variable linear and multiple-variable nonlinear regressions

were run in Microsoft Excel 2013, and the best model was selected. Multiple-variable nonlinear regressions predicted development lengths with higher accuracy for training data (high R^2 and low absolute errors). However, they had larger absolute errors in development-length predictions of validation data sets compared to linear models. Thus, nonlinear models resulted in overfitting of training data. The best model was picked based on the highest R^2. A development-length equation for design of pretensioned concrete members proposed based on wire pull out values obtained according to ASTM A1096 and concrete release-strength(f'_{ci}). The best-fit model (mean equation) obtained from statistical analysis was as follows:

$$L_d = 31.75 - 1.25(f'_{ci}) - 2.02(A1096) \qquad \text{(Equation. 25)}$$

where L_d is predicted development length (in).

f'_{ci} is compressive strength of concrete at the time of de-tensioning (ksi).

$A1096$ is pull out force values for each wire type according to ASTM A1096 standard (kip).

Statistical parameters of this equation are presented in Table 41.

Table 41. Statistical parameters for development-length model

Regression statistics	
Multiple R	0.968
R square	0.936
Adjusted R square	0.925
Standard error	1.699
Observations	14

	Coefficients	Standard deviation	t Stat	P-value
Intercept	31.75	2.36	13.46	0.000
X Variable 1	-1.25	0.47	-2.66	0.022
X Variable 2	-2.02	0.16	-12.39	0.000

As it can be seen in the Table 41, Coefficient of Determination $R^2 = 0.936$ and the P-value for all parameters is less than 0.05. It should be noted that X Variable 1 and X variable 2, refer to f'_{ci} and $A1096$ respectively.

Equation. 25 was used to predict development lengths based on pull-out force values ASTM A1096 and concrete-release strengths (f'_{ci}). Table 42 shows predicted development lengths, and experimental development lengths for different wires and concrete release strengths.

Table 42. Predicted development lengths using developed mean model and experimental development lengths

Wire type	Concrete release strength (psi)	Experimental Ld (in)	Predicted Ld (in)
WA	3.741	29.4	26.3
	4.664	22.5	25.2
	6.128	23.7	23.3
WE	3.486	11.4	11.6
	4.650	9.5	10.2
	6.020	9.5	8.5
WG	3.561	16.5	16.3
	4.697	11.9	14.8
	5.825	12.5	13.4
WH	3.614	13	12.6
	4.695	11.3	11.2
	6.059	11.4	9.5
WK	3.528	20.5	20.4
	4.572	19.3	19.1
	5.857	16.5	17.5
WB	4.453	14.3	13.1
WC	4.701	14.7	10.4
WD	4.400	11.6	15.6
WF	4.466	9.5	10.0
WI	4.547	10.4	13.1
WJ	4.521	13	12.4
WL	4.476	25.3	22.0
WM	4.506	11.9	12.2

Predicted development lengths using Equation. 25 and experimental development lengths were plotted against each other to have a graphical display of model accuracy.

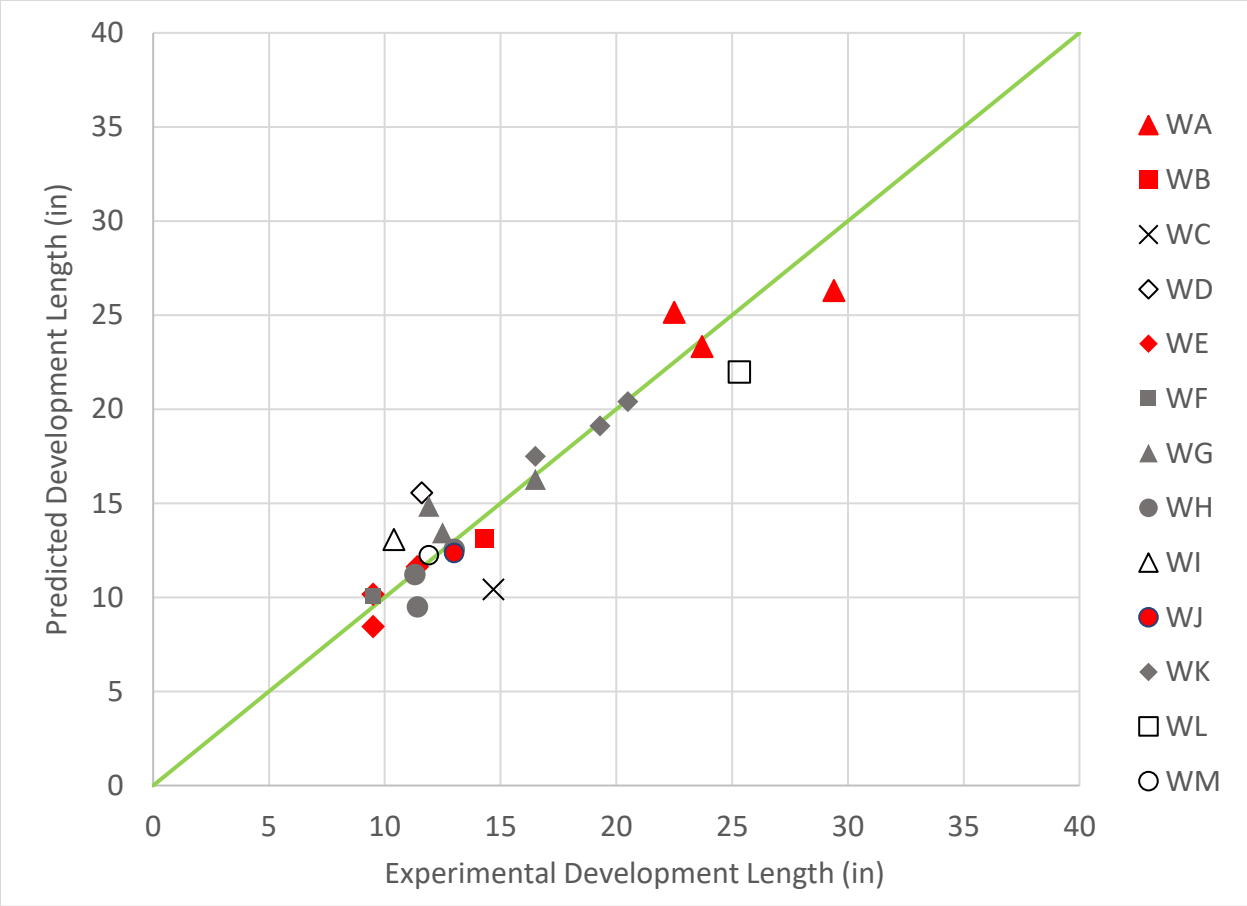


Figure 86 Predicted development lengths using developed mean equation versus experimental development lengths

As it can be seen in Figure 86, data points were located on or near unity line, indicating predicted development lengths correlated well to experimental development lengths.

To develop a design equation, Tolerance Factor Method described in (ACI Committee 214, 2010) was used. The design model was developed for a 90% confidence level of 10% fractal using Tolerance Factor Method. The upper tolerance limit on the 10% fractal of the development length was obtained from the following equation:

$$L_{d-0.10} = \bar{L_d} + Ks_c \qquad \text{(Equation. 26)}$$

where $\bar{L_d}$ is development length predicted by best fit model.

K is a factor for one-sided tolerance limits on the 10% fractal value. Values of K can be found in Table 9.2 of ACI 214.4R-10 (ACI Committee 214, 2010).

s_c is standard deviation of the sample.

23 development lengths were determined through experiments in this study. Thus, sample size was 23 (n=23). From Table 9.2 of ACI 214.4R-10, K-factor value of 1.73 was obtained through interpolation for 90% confidence level and sample size of 23. Standard deviation for the

intercept (2.36 in.) (refer to Table 41) substituted in Equation. 26 to develop design equation for development length prediction. Design equation proposed for development length is written as follows:

$$L_d = 35 - \frac{(A1096\ value)}{500} - \frac{f'_{ci}}{800} \qquad \text{(Equation. 27)}$$

where

TL = Transfer length in inches

f'_{ci} = Concrete compressive strength at de-tensioning in psi

A1096 value = ASTM A1096 pullout value (6-specimen average) in pounds

Predicted development lengths using **Error! Reference source not found.** were plotted against A1096 values for different concrete release strengths (3500, 4500, and 6000 psi). Also, experimental development lengths were plotted on the same chart in order to Compare experimental development lengths with predicted development lengths using **Error! Reference source not found.**. Figure 87 shows predicted developments lengths using proposed design equation for different concrete release strengths versus experimental development lengths.

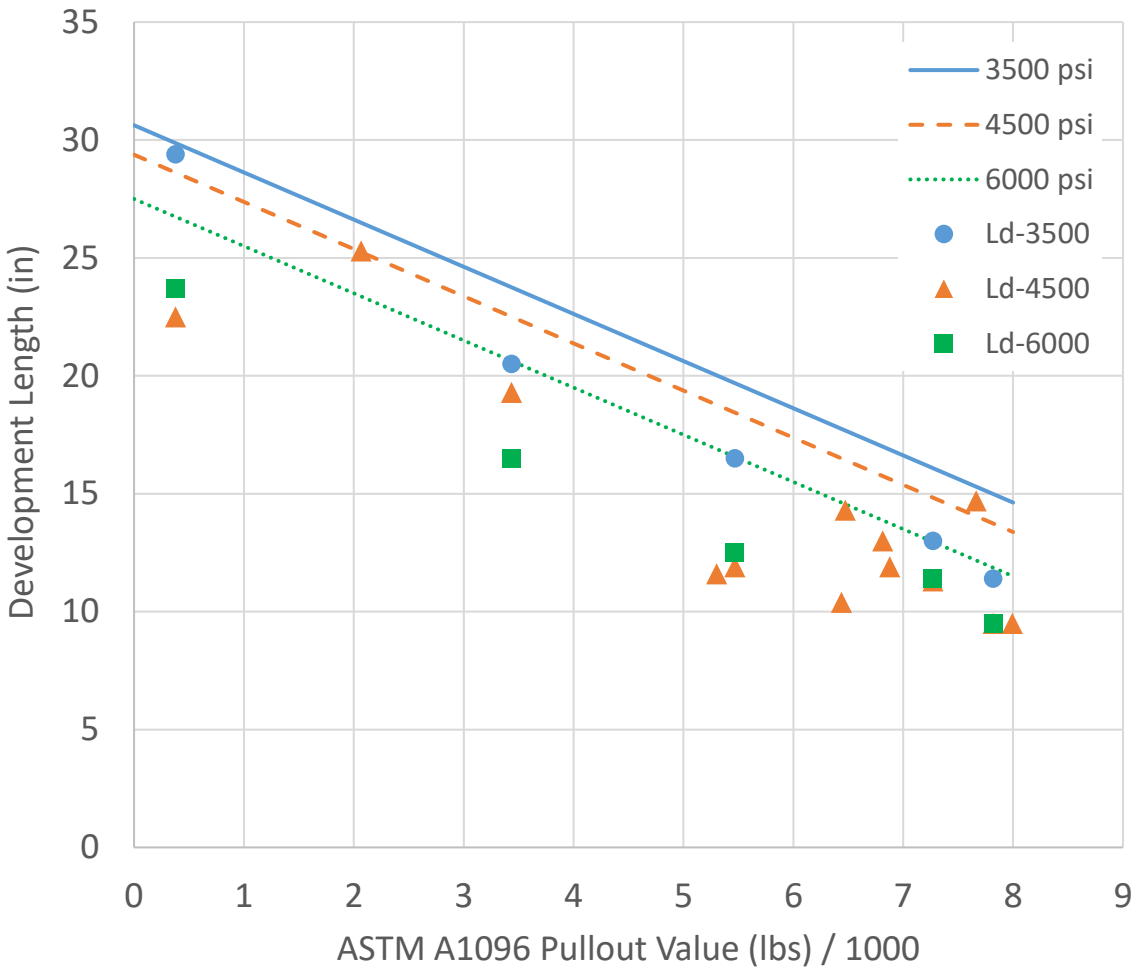


Figure 87. Predicted developments lengths using Error! Reference source not found. **for different concrete release strengths versus experimental development lengths.**

From Figure 87, it can be seen that 21 out of 23 experimental development lengths were below predicted development lengths using design equation and those 2 remaining were adjacent to predicted values. Table 43 shows predicted development lengths using **Error! Reference source not found.**, experimental development lengths, and error resulted from prediction.

Table 43 Predicted development lengths versus experimental development lengths

Wire type	Concrete release strength (ksi)	Average pull out force (kip)	Experimental Ld (in)	Predicted Ld (in)	Predicted-Experimental (in)
WA	3.741	0.378	29.4	29.6	0.2
	4.664	0.378	22.5	28.4	5.9
	6.128	0.378	23.7	26.6	2.9
WE	3.486	7.817	11.4	15.0	3.6
	4.65	7.817	9.5	13.6	4.1
	6.02	7.817	9.5	11.8	2.3
WG	3.561	5.469	16.5	19.6	3.1
	4.697	5.469	11.9	18.2	6.3
	5.825	5.469	12.5	16.8	4.3
WH	3.614	7.27	13	15.9	2.9
	4.695	7.27	11.3	14.6	3.3
	6.059	7.27	11.4	12.9	1.5
WK	3.528	3.434	20.5	23.7	3.2
	4.572	3.434	19.3	22.4	3.1
	5.857	3.434	16.5	20.8	4.3
WB	4.453	6.473	14.3	16.5	2.2
WC	4.701	7.663	14.7	13.8	-0.9
WD	4.4	5.302	11.6	18.9	7.3
WF	4.466	7.993	9.5	13.4	3.9
WI	4.547	6.439	10.4	16.4	6.0
WJ	4.521	6.814	13	15.7	2.7
WL	4.476	2.067	25.3	25.3	0.0
WM	4.506	6.879	11.9	15.6	3.7

6. Conclusions and Recommendations

Experimental results from load tests on pretensioned, prestressed concrete prisms indicated that both indentation type and concrete strength at de-tensioning have a large impact on development length and flexural capacity of these members. Load-testing of pretensioned prisms made with different wires and concrete-release strengths showed that development length was between 1.01 to 1.76 times the transfer lengths at de-tensioning (refer to Table 38). The difference between development length and transfer length, flexural bond length(L_{fb}), was smallest for the pretensioned member manufactured with WG wire, and largest for the pretensioned member manufactured with WA wire (smooth wire) (refer to Table 38).

Results from load-testing of pretensioned, prestressed ties manufactured with different concrete-release strengths indicated that although the concrete-compressive strength at de-tensioning had a significant effect on transfer lengths of most wire types, it had less effect on long-term moment capacity of sections utilizing prestressing wires with deep indent patterns.

For wires with light or no indentations (WK and WA), there was a general trend where maximum experimental moment increased as release strength increased. This is likely due to the fact that for these wires, the tested length often was located within the transfer length.

For the better-bonding wires with more pronounced indentations (WE, WG, and WH), however, there was little difference in the maximum moment capacities with increasing concrete-release strength. This is likely because the tests were conducted after the prisms were more than a year old, and the concrete compressive strength of all specimens at the time of testing was the same.

Based on research findings in this study, a development-length expression was proposed based on concrete-release strength (f'_{ci}) and ASTM A-1096 pull-out values to predict development length in pretensioned concrete members fabricated with wires. This design model covers a wide range of prestressing indentation types and concrete-release strengths and can be used as criteria in design of pretensioned concrete members fabricated with wires. It should be noted, however, that the specimens in this study utilized one concrete mixture that was representative of mixes used in the manufacture of concrete railroad ties and had a long-term compressive strength of approximately 12,000 psi. Therefore, development lengths may be longer for other concrete mixtures that have significantly-lower compressive strengths.

Additional load tests were conducted on pretensioned, prestressed prisms fabricated with three-wire and seven-wire strands. Prisms made with smooth strand (strand without indents on its surface), contrary to prisms made with smooth wires, showed much higher reserve capacity and did not fail immediately after crack occurrence. In these experiment, embedment lengths were varied from 13 in. (33 cm) to 28 in. (71.1 cm).

Load tests showed that surface indents in strands had a significant impact on development length and flexural capacity of pretensioned members, and prisms made with different strand-indentation types behave differently under load. Also, load tests were conducted on pretensioned, prestressed prisms made with different concrete-release strengths to understand the effect of concrete-release strength on development length and flexural capacity of pretensioned members made with strands. Results indicated that high release strengths generally increase flexural capacity of pretensioned prisms for all strands except SF, while prisms with 4,500 psi release-

strength showed higher capacity than 6000 psi release. This could be due different concrete ages in specimens at the time of load testing since prisms with SF strands and 4500 psi release strength were manufactured a year before other specimens. Development lengths for prisms manufactured with strands were shorter than predicted by current design codes. All strands were fully developed at a distance less than two times the transfer length from the prism end, except prisms made with SC strand (refer to Table 21). SC strand is a 5/16-in-diameter (7.9 mm), three-wire smooth strand whose development length exceeded two times its transfer length.

In the last phase of the project, pretensioned prisms made with wires were cyclically-loaded to evaluate the bond performance of wires under repeated loading. Conclusions from cyclic-load testing are as follows:

1) Fatigue failure due to splitting along the wire lines in pretensioned, prestressed members can occur suddenly and without warning if no transverse reinforcement is provided.
2) Pretensioned prisms made with wires with deep indents are more likely to fail under cyclic loading presumably due to increased splitting demand they impart to the surrounding concrete.
3) Although prisms made with WH wires had short transfer and development lengths, they did not perform well under cyclic loading and failed prior to reaching 200,000 cycles.
4) Prisms made with lightly-indented wires had higher moment capacities in cyclic-load tests than in monotonic load tests. This is likely due to the fact that the cyclic-loading tests had a longer embedment length and the wires were not fully developed in the monotonic load tests.

6.1 RECOMMENDATIONS

1) The development-length expression for 5.32-mm-diameter prestressing wires was proposed as $L_d = 35 - 2(A1096) - 1.25(f'_{ci})$. This expression covers a wide range of wire-indentation types and concrete-release strengths. The model is based on 92 flexural tests on prisms utilizing 13 different prestressing wires and a concrete mixture similar to one used by a current railroad tie producer. The equation is based on a 90% confidence level on a 10% fractal and should be conservative for prestressed concrete members utilizing concrete mixtures with similar long-term compressive strengths. It is therefore recommended that this equation be adopted for determining the nominal moment capacity of concrete railroad ties with similar reinforcements.
2) In lieu of using the proposed design equation, the load-testing procedure documented in this report can be successfully used with a variety of embedment lengths to determine development length for a particular concrete mixture and release strength.

7. References

AASHTO. (1998). *American Association of State Highway and Transportation Officials.* Washington, DC: Standard Specifications for Highway Bridges, LRFD. US Customery Units, Second Edition.

Abdalla, O. A., Ramirez, J. A., & Lee, R. H. (1993). *Strand Debonding in Pretensioned Beams-Precast Prestressed Concrete Bridges With Debonded Strands-Simply Supported Tests-Part 2, Final Report.* FHWA/INDOTJHRP-92.

ACI 318-99. (1999). *Building Code Requirements for Reinforced Concrete.* Farmington Hills, MI: American Concrete Inistitute.

ACI 318R-02. (2002). *Building Code Requirements for Structural Concrete (ACI 318-02) and Commentary (ACI 318R-02).* Farmington Hill, MI: American Concrete Institute.

ACI Committee 214. (2010). *Guide for Obtaining Cores and Interpreting Compressive Strength Results.* Farmington Hills, MI: American Concrete Institute.

Arnold, M. L. (2013). *Un-tensioned Pull-Out Tests to Predict the Bond Quality of Different Prestressing Reinforcements Used in Concrete Railroad Ties.* Manhattan, KS: Kansas State University.

ASTM Standard A881 Standard Specification for Steel Wire, Indented, Low Relaxation for Prestressed Concrete Railroad Ties. (2010). *ASTM Standard*. West Conshohocken, PA, USA: ASTM International. doi:10.1520/A0881-A0881M-10

Balaguru, P.N. (1981). Analysis of Prestressed Concrete Beams for Fatigue Loading. *Prestressed Concrete Institute*, 70-94.

Balaz, G. (1993, March-April). Transfer Length of Prestressing Strand as a Function of Strand Draw-in and Initial Prestress. *PCI*, 86-93.

Barsom, J. M., & Rolfe, S. T. (1999). *Fracture and Fatigue Control in Structures: Applications of Fracture Mechanics (Astm Manual Series).* Philadelphia, PA: Astm Intl.

Beck, B., Zhao , W., Peterman, R., Wu, C.-H., Holste, J., Bodapati, N., & Lee, G. (2013). Effect of Surface-Strain Sampling Interval on the Reliability of Pretensioned Concrete Railroad Tie Transfer Length Measurements. *PCI Convention and National Bridge Conference.* Washington D.C.

Bodapati, N. B., Zhao, W., Peterman , R. J., Wu, C.-H., Beck, B., Haynes, M., & Holste, J. R. (2013). Influence of Indented Wire Geometry and Concrete Parameters on the Transfer Length in Prestressed Concrete Crossties. *Joint Rail Conference.*

Bodapati, N., Peterman, R. J., Beck, B. T., & Wu, C.-H. (2014). Effect of Concrete Properties on Transfer Lengths in Concrete RailRoad Ties. *Joint Rail Conference*.

Bodapati, N., Peterman, R. J., Zhao, W., Beck, B., Wu, C.-H., Holste, J., . . . Schweiger, R. (2013). Transfer-Length Measurements on Concrete Railroad Ties Fabricated with 15 Different Prestressing Reinforcements. *PCI Convention and National Bridge Conference.* Grapevine, TX.

Bodapati, N., Peterman, R. J., Zhao, W., Beck, B., Wu, C.-H., Holste, J., . . . Schweiger, R. (2014). Long-Term Transfer-Length Measurements on Pretensioned Concrete RailRoad Ties. *PCI Convention and National Bridge Conference.* Washington D.C.

Briere, V., Harries, K., Kasan, J., & Hager, C. (2013). Dilation Behavior of Seven-wire Prestressing Strand-The Hoyer Effect. *Construction and Building Materials* , 650-658.

Buckner, C. (March-April 1995). A Review of Strand Development Length for Pretensioned Concrete. *PCI*, 84-105.

Buekett, J. (1987). Concrete Ties in Modern Track. *Railway Track and Structures*, 32-35.

Chen, Y.-S. (2016). *Testing and Modeling Tensile Stress-Strain Curve for Prestressing Wires in Railroad Ties.* Manhattan, KS: Master of Science Report, Kansas State University.

Cousins, T. E., Johnson, D., & Zia, P. (July-August 1990). Transfer and Development Length of Epoxy Coated and Uncoated Prestressing Strands. *PCI*, 92-103.

Deatherage, H. J., Burdette, E. G., & Chew, C. K. (January-February 1994). Development Length and Lateral Spacing Requirements of Prestressing Strand for Prestressed Concrete Bridge Girders. *PCI*, 70-83.

El Shahawi, M., & Batchelor, B. (1986). Fatigue of Partially Prestressed Concrete. *Journal of Structural Engineering*, 524-537.

Fisher, J. M., & Van De Pas, J. P. (2002). New Fatigue Provisions for the Design of Crane Runway Girders. *Engineering Journal of American Instititute of Steel Construction*, 65-73.

Ghosh, S., & Fintel, M. (1986). Development Length of Prestressing Strands, Including Debonded Strands, and Allowable Concrete Stresses in Pretensioned Members. *PCI JOURNAL*, 38-57.

Guyon, Y. (1953). Prestressed Concrete. *John Wiley and Sons*.

Hanna, A. (1986). Concrete Ties for U.S Railroads-an Update. *Concrete in Transportation*, 267-286.

Hanson, N. W., & Kaar, P. H. (1959). Flexural Bond Tests of Pretesnioned Prestressed Beams . *ACI Journal*, 783-803.

Haynes, M., Wu, C.-H., Beck, B., Bodapati, N., & Peterman, R. J. (2014). Prestressing Steel Reinforcement Wire Measurement Protocol. *Joint Rail Conference.* Colorado Spring.

Kaar, P. (1975). Bond Fatigue Tests of Beams Simulating Pretensioned Concrete Crossties. *PCI*, 65-80.

Kaar, P., LaFraugh, R. W., & Mass, M. A. (1963). Influence of Concrete Strength on Strand Transfer Length. *PCI*, 47-67.

Kahn, L. F., Jason, C. D., & Reutlinger, C. G. (2002). Transfer and Development Length of 15-mm Strand in High Performance Concrete Girders. *Journal of Structural Engineering*, 913-921.

Lane, S. N. (1998). *A New Development Length Equation for Pretensioned Strands in Bridge Beams and Piles.* Washington, DC: Federal Highway Administration .

Larson, K. H., Peterman, R. J., & Rasheed, H. A. (2005). Strength-Fatigue Behavior of Fiber Reinforced Polymer Strengthened Prestressed Concrete T-Beams. *Journal of Composites for Construction*, 313-326.

Logan, D. R. (March-April 1997). Acceptance Criteria for Bond Quality of Strand for Pretensioned Prestressed Concrete Applications. *PCI*, 52-90.

Lu, Z. (1998). *Flexure Performance of Fiber Reinforced Polymer Prestressing Tendons* . The Pennsylvania State University, University Park, PA: M.S Report.

Lu, Z., Boothby, T. E., Bakis, C. E., & Nanni, A. (March-April 2000). Trasnfer and Development Lengths of FRP Prestressing Tendons. *PCI*, 84-95.

Madugula, M. K. (1991). Design against fatigue and fracture in steel structures. An overview. *International Symposium on Fatigue and Fracture in Steel and Concrete Structures*, 1261-1276.

Mahmoud, Z. I., Rizkalla, S. H., & Zaghloul, E. R. (July-August 1999). Transfer and Development Lengths of Carbon Fiber Reinforced Polymer Prestressing Reinforcement . *ACI Structural Journal*, 594-602.

Martin, L., & Scott, N. (August 1976). Development of Prestressing Strand in Pretensioned Members. *ACI*, 453-456.

Marti-Vargas, J., Caro, L., & Serna, P. (2013). Experimental Technique for Measuring the Long-term Transfer Length in Prestressed Concrete. *Strain An International Journal for Experimental Mechanics*, 125-134.

Mitchel, D., Cook, W. D., Khan, A. A., & Tham, T. (May-June 1993). Influence of High Strength Concrete on Transfer and Development Length of Pretensioning Strand . *PCI*, 52-66.

PCI DESIGN HANDBOOK Precast and Prestressed Concrete. (2010). Chicago: PCI.

Peterman, R. J., Ramirez, J. A., & Olek, J. (September-October 2000). Influence of Flexure-Shear Cracking on Strand Development Length in Prestressed Concrete Members. *PCI*, 76-94.

Post-Tensioning Inistitute. (1996). *PTI.Recommendations for Prestressed Rock and Soil anchors (Revised 1996).* Phoenix: Post-Tensioning Inistitute.

Ramirez, J., & Russel, B. W. (2007). *Transfer, Development, and Splice Length for Strand/Reinforcement in High-Strength Concrete.* West Lafayette (IN Purdue University.

Rasheed, H. A. (2014). *Strengthening Design of Reinforced Concrete with FRP*. Boca Raton: CRC Press.

Russel, B. W., & Burns, N. H. (1993). *Design Guidelines for Transfer, Development and Debonding of Large Diameter Seven Wire Strands in Pretensioned Concrete Girders.* Center for Transportation Research Bureau of Engineering Research The University of Texas at Austin.

Russel, B. W., & Burns, N. H. (1996). Measured Transfer Lengths of 0.5 and 0.6 in. Strands in Pretensioned Concrete. *PCI*, 44-65.

Shahawy, M. A., Issa, M., & Batchelor, B. (May-June 1992). Strand Transfer Lengths in Full Scale AASHTO Prestressed Concrete Girders. *PCI*, 84-96.

Si, N., Young, C., Byung, H., Ji, S., Soobong, S., & Myung, K. (2013). Bond Characteristics and Transfer Length of Prestressing Strand in Pretensioned Concrete Structures. *VIII International Conference on Fracture Mechanics of Concrete and Concrete Structures.* Toledo, Spain: IA-FraMCoS.

Talat, M., & Paul, Z. (September-October 1977). Development Length of Prestressing Strands. *PCI*, 54-65.

Vazquez-Herrero, C., Martinez-Lage, I., & Martinez-Abella, F. (2013). Transfer Length in Pretensioned Prestressed Concrete Structures Composed of High Performance Lightweight and Normal-Weight Concrete. *Engineering Structures*, 983-992.

Vazquez-Herrero, C., Martinez-Lage, I., Aquilar, G., & Martinez-Abella, F. (2013). Evaluation of Strand Bond Properties along the Transfer Length of Prestressed Lightweight Concrete Members. *Engineering Structures*, 1048-1058.

Whaley, C. P., & Neville, A. M. (September 1973). *Non-Elastic Deformation of Concrete Under Cyclic Compression.* London.

White, J. (1984). Concrete Ties for North America. *Modern Railroads*, 44-47.

Wu, C. H., Zhao, W., Beck, T., & Peterman, R. (2011). Optical Sensor Developments for Measuring the Surface Strains in Prestressed Concrete Members. *Strain 47*, 376-386.

Yu, H., & Jeong, D. Y. (2014). Bond between Smooth Prestressing Wires and Concrete: Finite Element Model and Transfer Length Analysis for Pretensioned Concrete Crossties. *ASCE Structures Congress*, (pp. 797-812).

Zhao, W., Beck, B., Peterman , B., Wu, C.-H., Bodapati, N., & Lee, G. (2014). Reliable Transfer Length Assessment For Real-Time Monitoring Of Railroad Cross-Tie Production. *Joint Rail Conference* . Colorado Spring, CO.

Zhao, W., Beck, B., Peterman, R., Murphy, R., Wu, C.-H., & Lee, G. (2013). A Direct Comparison of the Traditional Method and A New Approach in Determining 220 Transfer Lengths in Prestressed Concrete Railroad Ties. *Joint Rail Conference* . Knoxville, TN.

Zhao, W., Beck, B., Peterman, R., Wu, C.-h., Lee, G., & Bodapati, N. (2013). Determining Transfer Length In Pre-Tensioned Concrete Railroad Ties: Is Anew Evaluation Method Needed? *ASME Rail Transportation Division Fall Technical Conference.* Altoona, PA.

Zhao, W., Murphy, R. L., Peterman, R. J., Beck, B., & Wu, C.-H. (2013, March). A Non-Contact Inspection Method to Determine the Transfer Length in Pre-tensioned Concrete Railroad Ties. *ASCE Journal of Engineering Mechanics, 139*(3), 256-263.

Zhao, W., Murphy, R. L., Peterman, R. J., Beck, B., & Wu, C.-H. (Winter 2012). Development of A Laster Speckle Imaging Device to Determine the Transfer Length in Pretensioned Concrete Members. *PCI*, 135-143.

Appendix A.
Example of Strain Compatibility Analysis Used in This Study

Calculating nominal moment capacity of prism WA-4500-6-1 at its dead end (prism end tested at 20 in. embedment length):

Properties of the cross section and materials are as follows:

$$f_{pu} = 295.5\ ksi$$

$$E_{ps} = 29700\ ksi$$

$$Wire\ Dia = \frac{5.32mm}{25.4} = 0.2094\ in$$

$$wire\ cross-sectional\ area = \pi \times \frac{0.2094^2}{4} = 0.0344\ in^2$$

$$d_{p1} = 1.0312\ in$$

$$d_{p2} = 2.4375\ in$$

$$f_c' = 12\ ksi$$

$$section\ width = b = 3.625\ in$$

$$section\ height = h = 3.5625\ in$$

$$cross\ section\ area = A = 12.9141\ in^2$$

$$section\ moment\ of\ inertia = I = \frac{bh^3}{12} = 13.6581\ in^4$$

$$y_b = \frac{h}{2} = 1.7812\ in$$

$$y_t = \frac{h}{2} = 1.7812\ in$$

Calculating prestress loss:

$$strain\ measured\ for\ the\ prism = 1850 \times 10^{-6}$$

$$Prestress\ loss = 1850 \times 10^{-6} \times E_{ps} = 1850 \times 10^{-6} \times 29700 = 54.945\ ksi$$

$$each\ wire\ was\ pulled\ to\ 7000\ lbs => f_{pi} = \frac{7000}{0.0344} = 203.2\ ksi$$

$$Total\ prestress\ loss\ (\%) = \frac{54.945}{203.2} \times 100 = 27\ \%$$

Prestressing wire cross-sectional area and its eccentricity:

$$top\ row\ of\ prestress\ wires => A_{ps1} = 2 \times \pi \times \frac{0.2094^2}{4} = 0.0689\ \ in^2$$

$$bottom\ row\ of\ prestress\ wires => A_{ps2} = 2 \times \pi \times \frac{0.2094^2}{4} = 0.0689\ \ in^2$$

$$e_1 = 1.0312 - 1.7812 = -0.75\ in$$

$$e_2 = 2.4375 - 1.7812 = 0.6563\ in$$

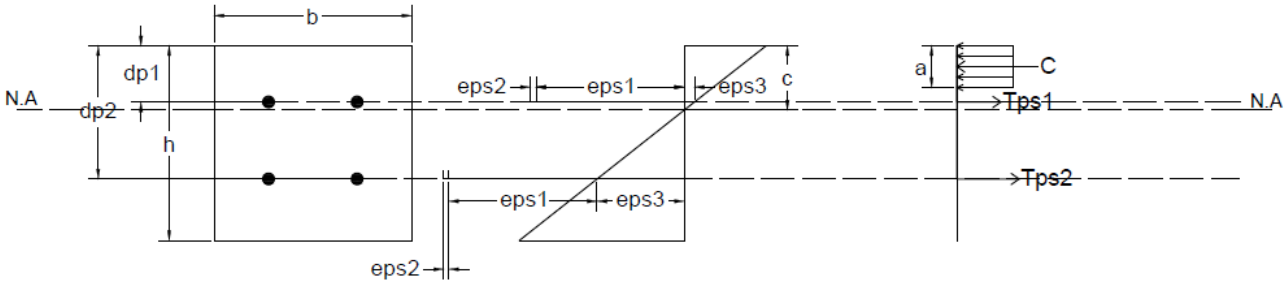


Figure 88 Stress and strain distribution across beam depth

Calculating strains in top and bottom rows of prestressing wires:

$$top\ row\ strains = \varepsilon_{ps1} = \varepsilon_1 + \varepsilon_2 + \varepsilon_3$$

$$f_{pe} = 203.2 \times \left(1 - \frac{27}{100}\right) = 148.3\ ksi$$

$$\varepsilon_1 = \frac{f_{pe}}{E_{ps}} = \frac{148.3}{29700} = 0.00499$$

$$E_c = 57\sqrt{f_c'} = 57 \times \sqrt{12000} = 6244.037\ ksi$$

$$\varepsilon_2 = \frac{p_e}{A_c E_c} + \frac{p_e e^2}{I_c E_c} = \frac{148.3 \times 0.0689}{12.9141 \times 6244.073} + \frac{148.3 \times 0.0689 \times (-0.75^2)}{13.6581 \times 6244.037} = 0.00019$$

Try c=1 in:

$$\varepsilon_3 = 0.003 \times \frac{d_{p1} - c}{c} = 0.003 \times \frac{1.0312 - c}{c} = 0.00009$$

$$top\ row\ strains = \varepsilon_{ps1} = 0.00499 + 0.00019 + 0.00009 = 0.0053$$

$$bottom\ row\ strains = \varepsilon_{ps2} = \varepsilon_1 + \varepsilon_2 + \varepsilon_3$$

$$\varepsilon_1 = \frac{f_{pe}}{E_{ps}} = \frac{148.3}{29700} = 0.00499$$

$$\varepsilon_2 = \frac{p_e}{A_c E_c} + \frac{p_e e^2}{I_c E_c} = \frac{148.3 \times 0.0689}{12.9141 \times 6244.073} + \frac{148.3 \times 0.0689 \times (0.6563^2)}{13.6581 \times 6244.037} = 0.00018$$

$$\varepsilon_3 = 0.003 \times \frac{d_{p2} - c}{c} = 0.003 \times \frac{2.4375 - c}{c} = 0.0043$$

$$bottom\ row\ strains = \varepsilon_{ps2} = 0.00499 + 0.00018 + 0.0043 = 0.0095$$

The following steps were taken to calculate the stress in pre-stressing wires (f_{ps}) using design-oriented Power Formula:

1) Substituting the ultimate tensile strength (f_{pu}) and Young's modulus (E_p) of each wire into Equation. 5, Equation. 6, and Equation. 7, Kf_{py}, $f_{py}$and constant Q can be calculated.

$$Kf_{py} = 1.1607 f_{pu} - 60.0118 \qquad \text{(Equation. 5)}$$

$$f_{py} = 1.0017 f_{pu} - 25.7794 \qquad \text{(Equation. 6)}$$

$$Q = \frac{f_{pu} - Kf_{py}}{\varepsilon_{pu} E_p - Kf_{py}} \qquad \text{(Equation. 7)}$$

$$\varepsilon_{pu} = 0.04$$

$$Kf_{py} = 1.1607 \times 295.5 - 60.0118 = 282.97\ ksi$$

$$f_{py} = 1.0017 \times 295.5 - 25.7794 = 270.22\ ksi$$

$$Q = \frac{295.5 - 282.97}{0.04 \times 29700 - 282.97} = 0.0138$$

2) The other constant R will be solved by iterations using the "Power Formula" when $f_{ps} = f_{py}$.

$$f_{ps} = \varepsilon_{py} E_p \left[Q + \frac{1 - Q}{\left(1 + \left(\frac{\varepsilon_{py} E_p}{Kf_{py}}\right)^R\right)^{1/R}} \right] \qquad \text{(Equation. 8)}$$

ε_{py} is the yield strain of 0.01.

Kf_{py} is from Equation. 5.

f_{py} is from (Equation. 6).

Q is from (Equation. 7).

$$270.22 = 29700 \times 0.01 \left[0.0138 + \frac{1 - 0.0138}{\left(1 + \left(\frac{0.01 \times 29700}{282.97}\right)^R\right)^{1/R}} \right]$$

Doing iterations to solve for R➔ $R = 10.0791$

3) Substituting R, ε_{ps} and calculated constants of Q in the Power Formula, stress in pre-stressing wire (f_{ps}) can be determined. Note that ε_{ps} is the total strain in prestressing wires.

$$f_{ps1} = 29700 \times 0.0053\left[0.0138 + \frac{1 - 0.0138}{\left(1 + \left(\frac{0.0053 \times 29700}{282.97}\right)^{10.0791}\right)^{1/10.0791}}\right] = 156.8\ ksi$$

$$f_{ps2} = 29700 \times 0.0095\left[0.0138 + \frac{1 - 0.0138}{\left(1 + \left(\frac{0.0095 \times 29700}{282.97}\right)^{10.0791}\right)^{1/10.0791}}\right] = 263.8\ ksi$$

Summing forces across beam depth in horizontal direction:

$$\sum F_x = 0$$

$$C_c = T_{ps1} + T_{ps2}$$

$$0.85 \times f_c' \times \beta_1 \times c \times b = A_{ps1} \times f_{ps1} + A_{ps2} \times f_{ps2}$$

$$0.85 \times 12 \times 0.65 \times 1 \times 3.625 = 0.0689 \times 156.8 + 0.0689 \times 263.8$$

$$24.034 \neq 28.98 => T \neq C$$

Equilibrium of forces across beam depth is not satisfied.

After iterating for value of c, c=1.13 in. is chosen:

Calculating strains in top and bottom rows of prestressing wires:

$$top\ row\ strains = \varepsilon_{ps1} = \varepsilon_1 + \varepsilon_2 + \varepsilon_3$$

$$f_{pe} = 203.2 \times \left(1 - \frac{27}{100}\right) = 148.3\ ksi$$

$$\varepsilon_1 = \frac{f_{pe}}{E_{ps}} = \frac{148.3}{29700} = 0.00499$$

$$E_c = 57\sqrt{f_c'} = 57 \times \sqrt{12000} = 6244.037\ ksi$$

$$\varepsilon_2 = \frac{p_e}{A_c E_c} + \frac{p_e e^2}{I_c E_c} = \frac{148.3 \times 0.0689}{12.9141 \times 6244.073} + \frac{148.3 \times 0.0689 \times (-0.75^2)}{13.6581 \times 6244.037} = 0.00019$$

Try c=1.13 in:

$$\varepsilon_3 = 0.003 \times \frac{d_{p1} - c}{c} = 0.003 \times \frac{1.0312 - c}{c} = -.00026$$

$$top\ row\ strains = \varepsilon_{ps1} = 0.00499 + 0.00019 - 0.00026 = 0.0049$$

$$bottom\ row\ strains = \varepsilon_{ps2} = \varepsilon_1 + \varepsilon_2 + \varepsilon_3$$

$$\varepsilon_1 = \frac{f_{pe}}{E_{ps}} = \frac{148.3}{29700} = 0.00499$$

$$\varepsilon_2 = \frac{p_e}{A_c E_c} + \frac{p_e e^2}{I_c E_c} = \frac{148.3 \times 0.0689}{12.9141 \times 6244.073} + \frac{148.3 \times 0.0689 \times (0.6563^2)}{13.6581 \times 6244.037} = 0.00018$$

$$\varepsilon_3 = 0.003 \times \frac{d_{p2} - c}{c} = 0.003 \times \frac{2.4375 - c}{c} = 0.0035$$

$$bottom\ row\ strains = \varepsilon_{ps2} = 0.00499 + 0.00018 + 0.0035 = 0.0086$$

The following steps were taken to calculate the stress in pre-stressing wires (f_{ps}) using design-oriented Power Formula:

1) Substituting the ultimate tensile strength (f_{pu}) and Young's modulus (E_p) of each wire into Equation. 5, Equation. 6, and Equation. 7, Kf_{py}, $f_{py}$and constant Q can be calculated.

$$\varepsilon_{pu} = 0.04$$

$$Kf_{py} = 1.1607 \times 295.5 - 60.0118 = 282.97\ ksi$$

$$f_{py} = 1.0017 \times 295.5 - 25.7794 = 270.22\ ksi$$

$$Q = \frac{295.5 - 282.97}{0.04 \times 29700 - 282.97} = 0.0138$$

2) The other constant R will be solved by iterations using the "Power Formula" when $f_{ps} = f_{py}$.

$$f_{ps} = \varepsilon_{py} E_p \left[Q + \frac{1-Q}{\left(1 + \left(\frac{\varepsilon_{py} E_p}{Kf_{py}}\right)^R\right)^{1/R}} \right] \qquad \text{(Equation. 8)}$$

ε_{py} is the yield strain of 0.01.

Kf_{py} is from Equation. 5.

f_{py} is from (Equation. 6).

Q is from (Equation. 7).

$$270.22 = 29700 \times 0.01\left[0.0138 + \frac{1 - 0.0138}{\left(1 + \left(\frac{0.01 \times 29700}{282.97}\right)^{R}\right)^{1/R}}\right]$$

Doing iterations to solve for R➔ $R = 10.0791$

3) Substituting R, ε_{ps} and calculated constants of Q in the Power Formula, stress in pre-stressing wire (f_{ps}) can be determined. Note that ε_{ps} is the total strain in prestressing wires.

$$f_{ps1} = 29700 \times 0.0049\left[0.0138 + \frac{1 - 0.0138}{\left(1 + \left(\frac{0.0049 \times 29700}{282.97}\right)^{10.0791}\right)^{1/10.0791}}\right] = 146.3\ ksi$$

$$f_{ps2} = 29700 \times 0.0086\left[0.0138 + \frac{1 - 0.0138}{\left(1 + \left(\frac{0.0086 \times 29700}{282.97}\right)^{10.0791}\right)^{1/10.0791}}\right] = 248.9\ ksi$$

Summing forces across beam depth in horizontal direction:

$$\sum F_x = 0$$

$$C_c = T_{ps1} + T_{ps2}$$

$$0.85 \times f_c' \times \beta_1 \times c \times b = A_{ps1} \times f_{ps1} + A_{ps2} \times f_{ps2}$$

$$0.85 \times 12 \times 0.65 \times 1.13 \times 3.625 = 0.0689 \times 146.3 + 0.0689 \times 248.9$$

$T - C = 0$➔ Depth of neutral axis=c=1.13 in

Taking moment about concrete compression force:

$$M_n = A_{ps1} \times f_{ps1} \times (d_{p1} - \frac{\beta_1 c}{2}) + A_{ps2} \times f_{ps2} \times (d_{p2} - \frac{\beta_1 c}{2})$$

$$M_n = 0.0689 \times 146.3 \times \left(1.0312 - \frac{0.65 \times 1.13}{2}\right)$$
$$+ 0.0689 \times 248.9 \times \left(2.4375 - \frac{0.65 \times 1.13}{2}\right) = 42.2\ kip - in = 3.52\ kip - ft$$

Appendix B.
Experimental Development Length Evaluation

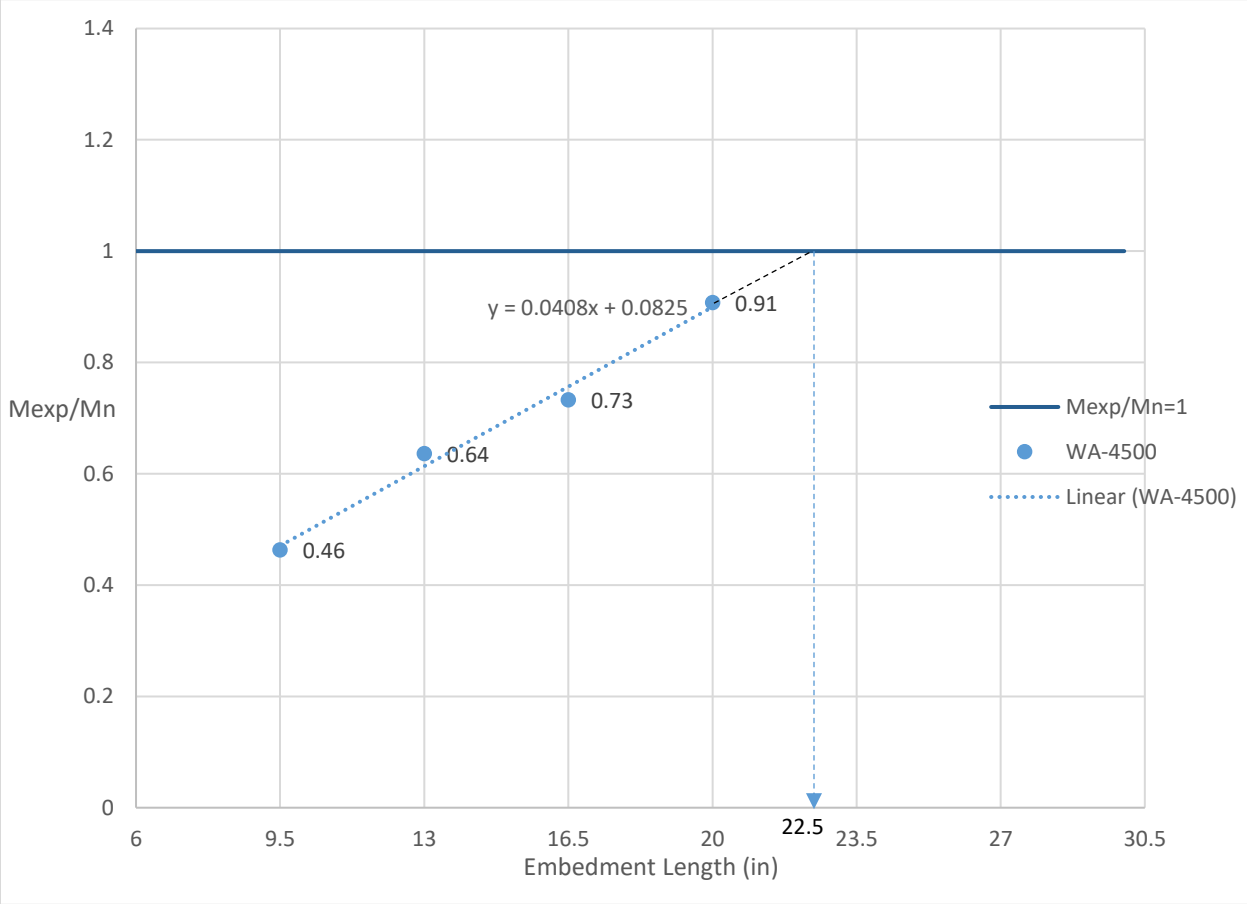


Figure 89 Ratio of maximum experimental moment to nominal moment capacity versus embedment length for prisms made with WA wire and 4500 psi release strength

$y = 0.0408x + 0.0825$

$1 = 0.0408D.L + 0.0825 ==> D.L = 22.5\ in.$

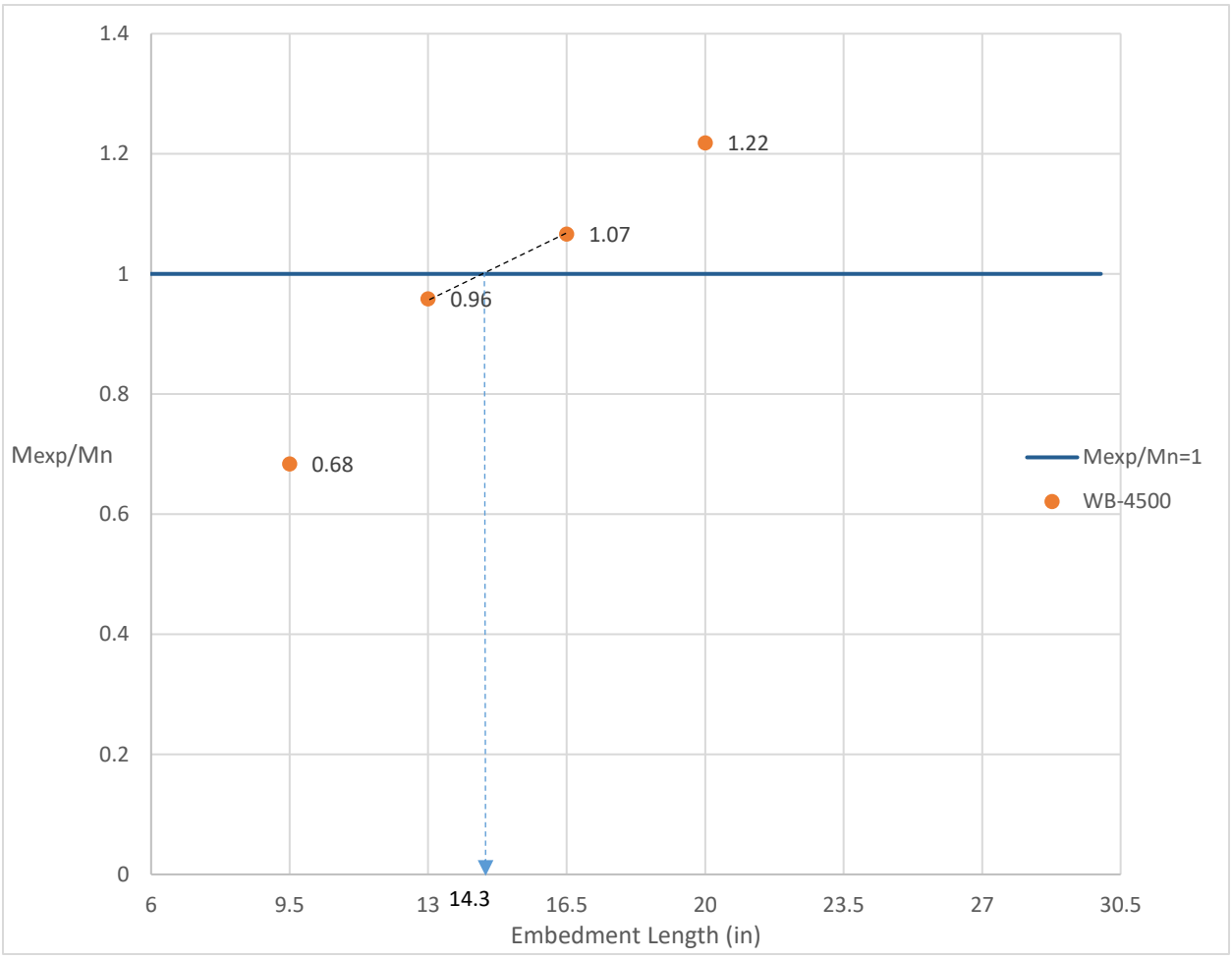


Figure 90 Ratio of maximum experimental moment to nominal moment capacity versus embedment length for prisms made with WB wire and 4500 psi release strength

$$y = \frac{1.07 - 0.96}{16.5 - 13} \times (x - 13) + 0.96$$

$$y = 0.031(x - 13) + 0.96$$

$$1 = 0.031(D.L - 13) + 0.96 ==> D.L = 14.3\ in.$$

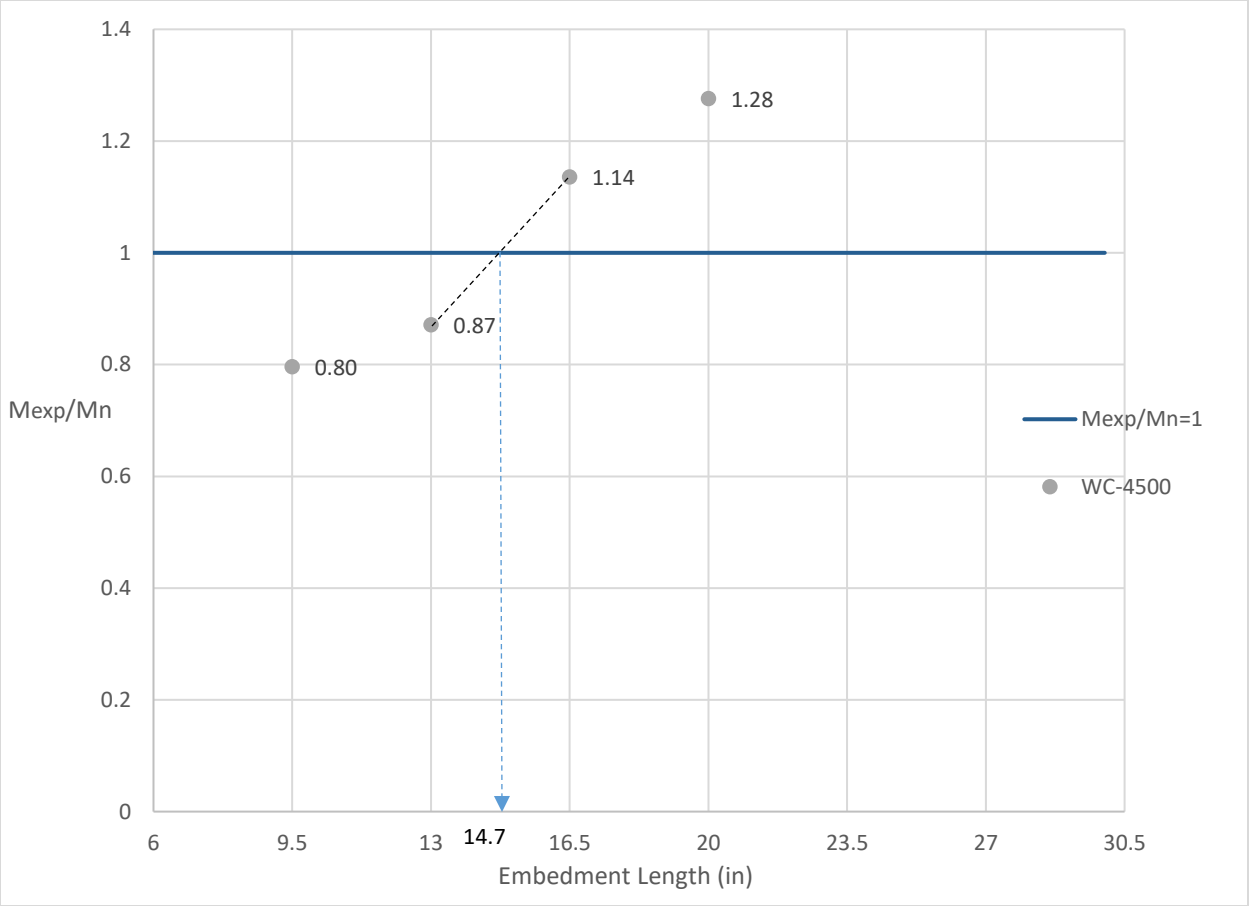


Figure 91 Ratio of maximum experimental moment to nominal moment capacity versus embedment length for prisms made with WC wire and 4500 psi release strength

$$y = \frac{1.14 - 0.87}{16.5 - 13} \times (x - 13) + 0.87$$

$$y = 0.077(x - 13) + 0.87$$

$$1 = 0.077(D.L - 13) + 0.87 ==> D.L = 14.7\ in.$$

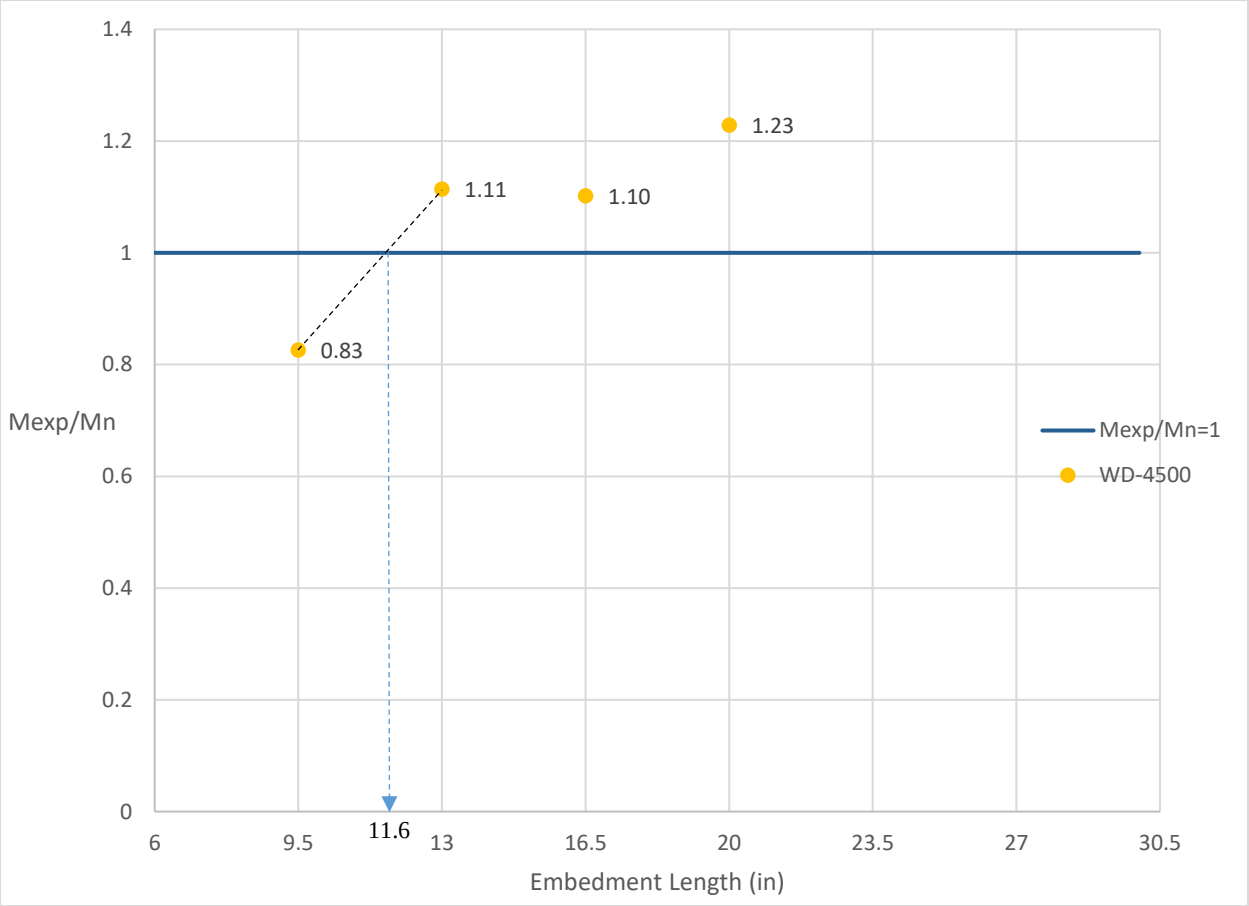


Figure 92 Ratio of maximum experimental moment to nominal moment capacity versus embedment length for prisms made with WD wire and 4500 psi release strength

$$y = \frac{1.11 - 0.83}{13 - 9.5} \times (x - 9.5) + 0.83$$

$$y = 0.08(x - 9.5) + 0.83$$

$$1 = 0.08(D.L - 9.5) + 0.83 ==> D.L = 11.6\ in.$$

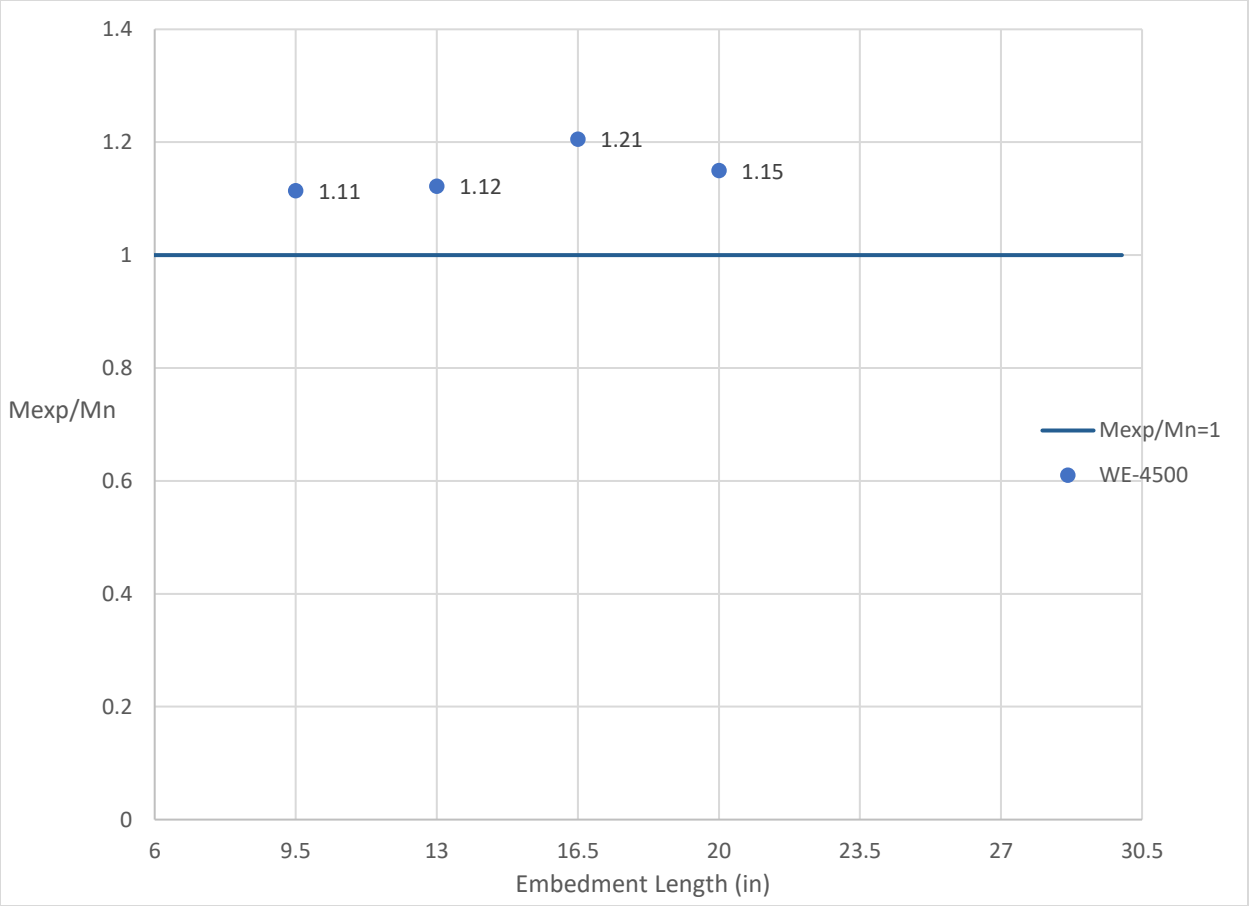


Figure 93 Ratio of maximum experimental moment to nominal moment capacity versus embedment length for prisms made with WE wire and 4500 psi release strength

Mexp/Mn>1 for all load cases➔Development length=9.5 in.

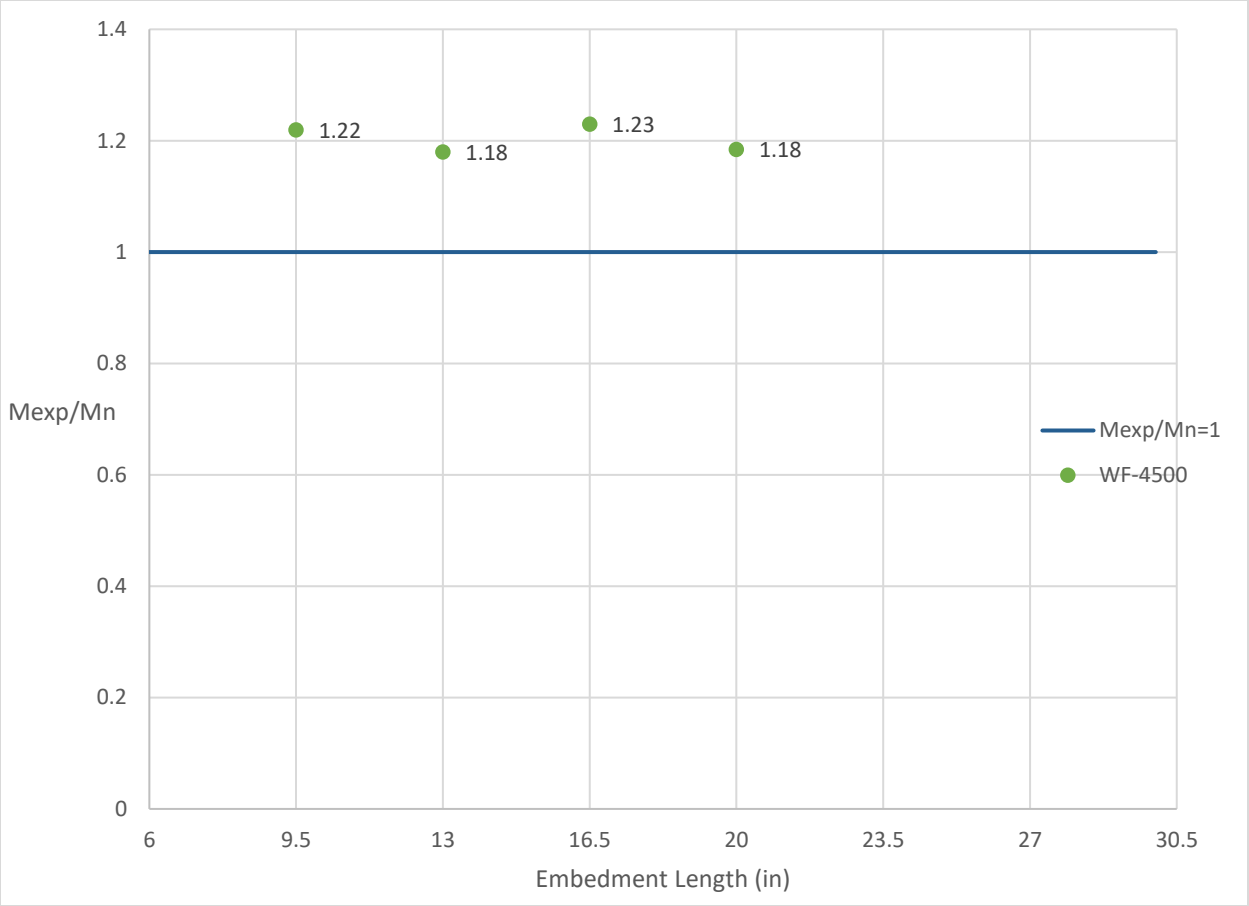


Figure 94 Ratio of maximum experimental moment to nominal moment capacity versus embedment length for prisms made with WF wire and 4500 psi release strength

Mexp/Mn>1 for all load cases➔Development length=9.5 in.

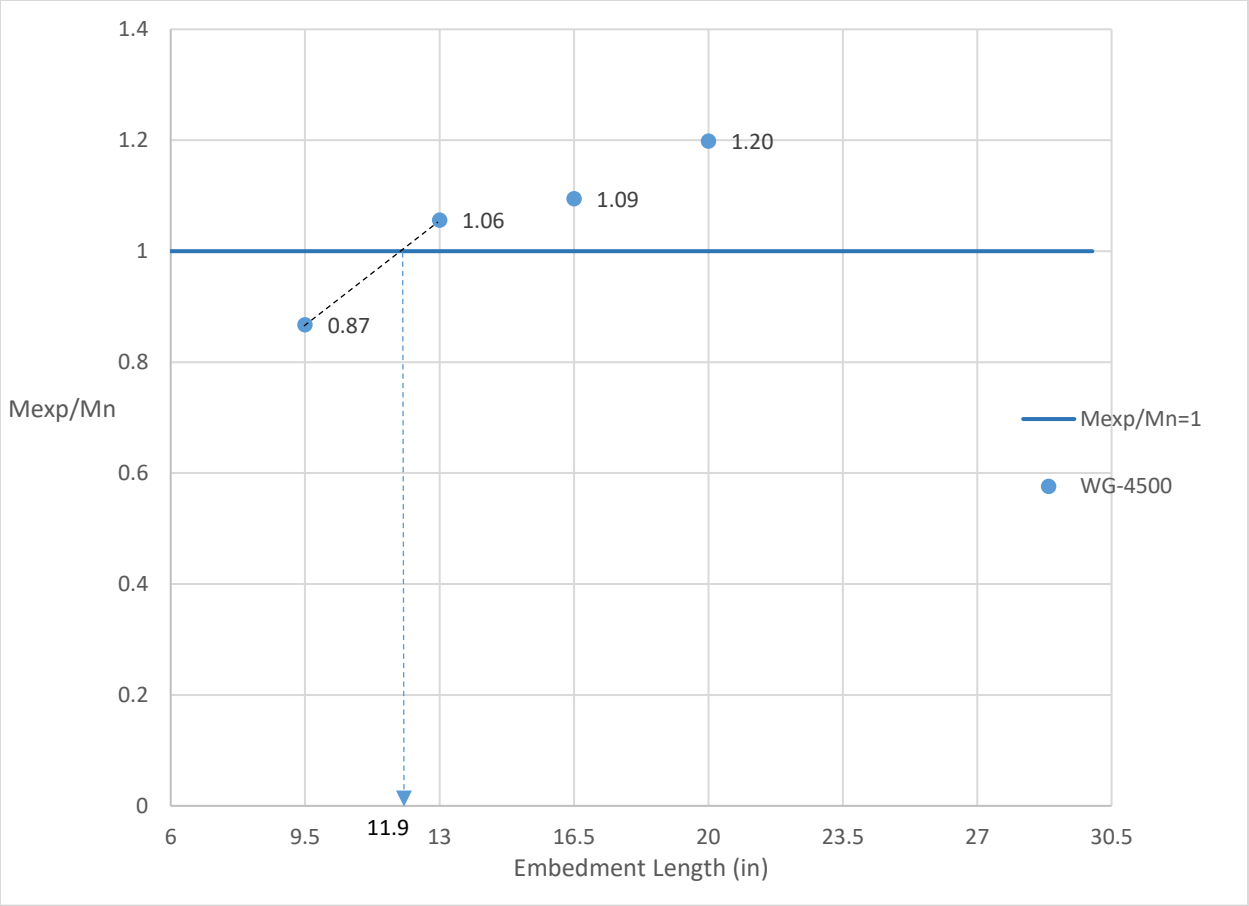


Figure 95 Ratio of maximum experimental moment to nominal moment capacity versus embedment length for prisms made with WG wire and 4500 psi release strength

$$y = \frac{1.06 - 0.87}{13 - 9.5} \times (x - 9.5) + 0.87$$

$$y = 0.054(x - 9.5) + 0.87$$

$$1 = 0.054(D.L - 9.5) + 0.87 ==> D.L = 11.9\ in.$$

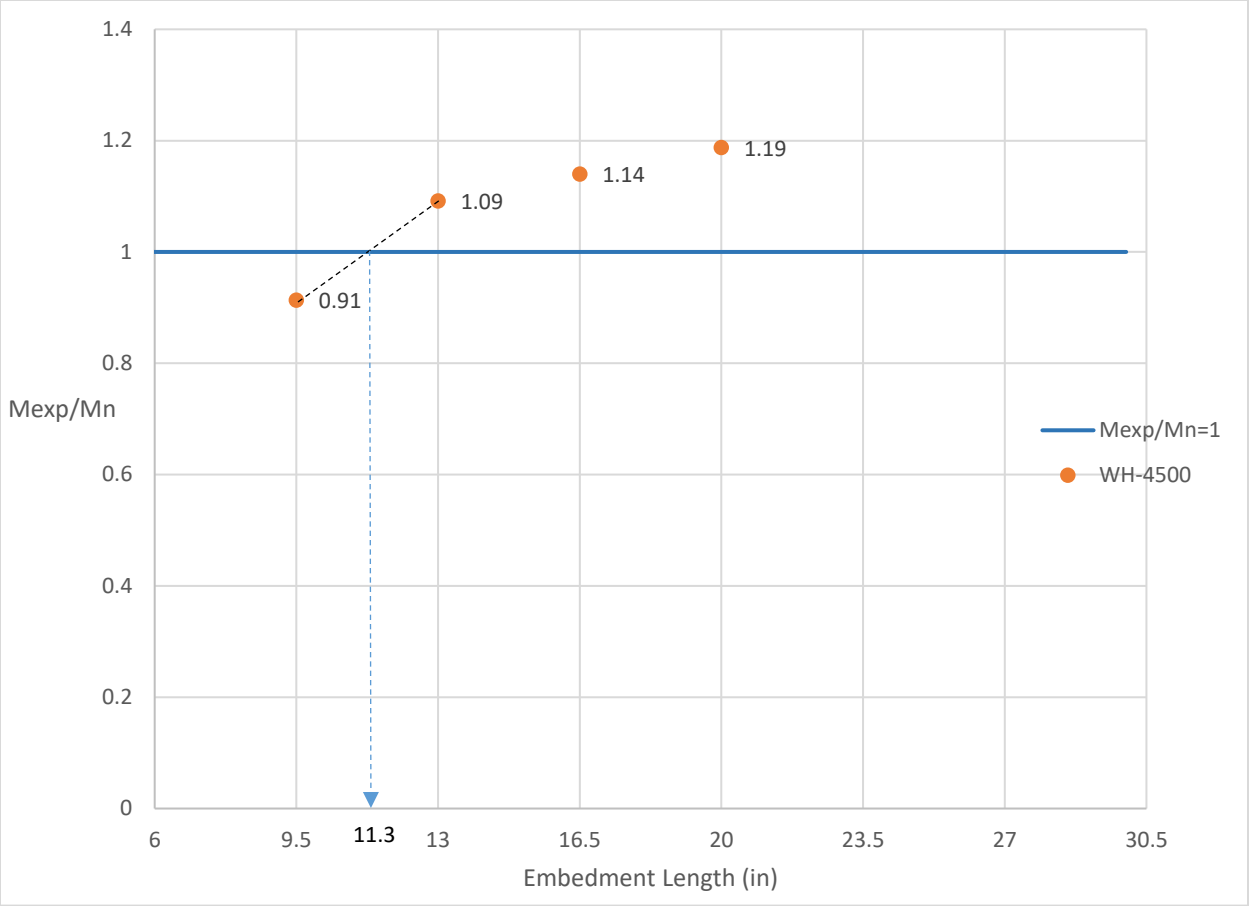


Figure 96 Ratio of maximum experimental moment to nominal moment capacity versus embedment length for prisms made with WH wire and 4500 psi release strength

$$y = \frac{1.09 - 0.91}{13 - 9.5} \times (x - 9.5) + 0.91$$

$$y = 0.051(x - 9.5) + 0.91$$

$$1 = 0.051(D.L - 9.5) + 0.91 ==> D.L = 11.3\ in.$$

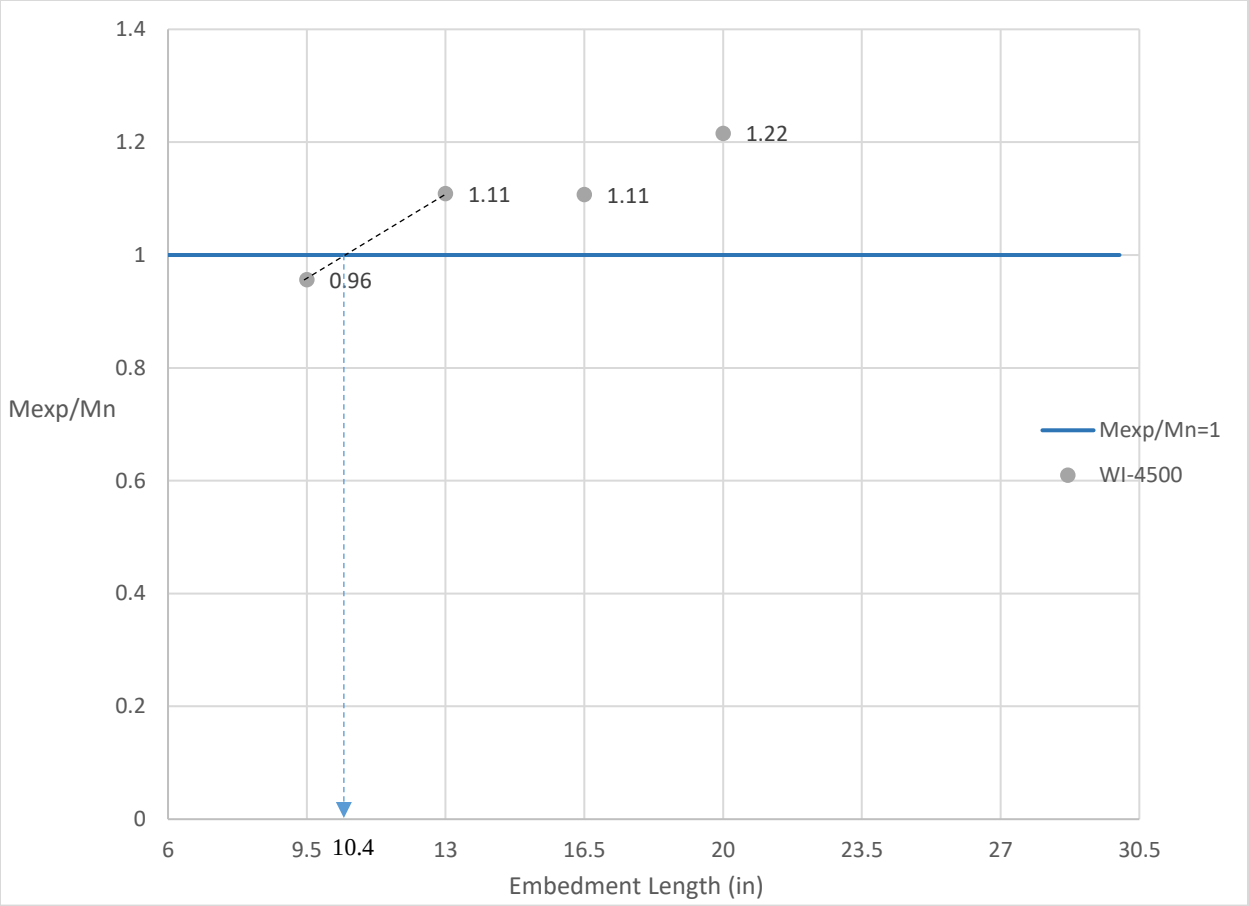


Figure 97 Ratio of maximum experimental moment to nominal moment capacity versus embedment length for prisms made with WI wire and 4500 psi release strength

$$y = \frac{1.11 - 0.96}{13 - 9.5} \times (x - 9.5) + 0.96$$

$$y = 0.043(x - 9.5) + 0.96$$

$$1 = 0.043(D.L - 9.5) + 0.96 ==> D.L = 10.4\ in.$$

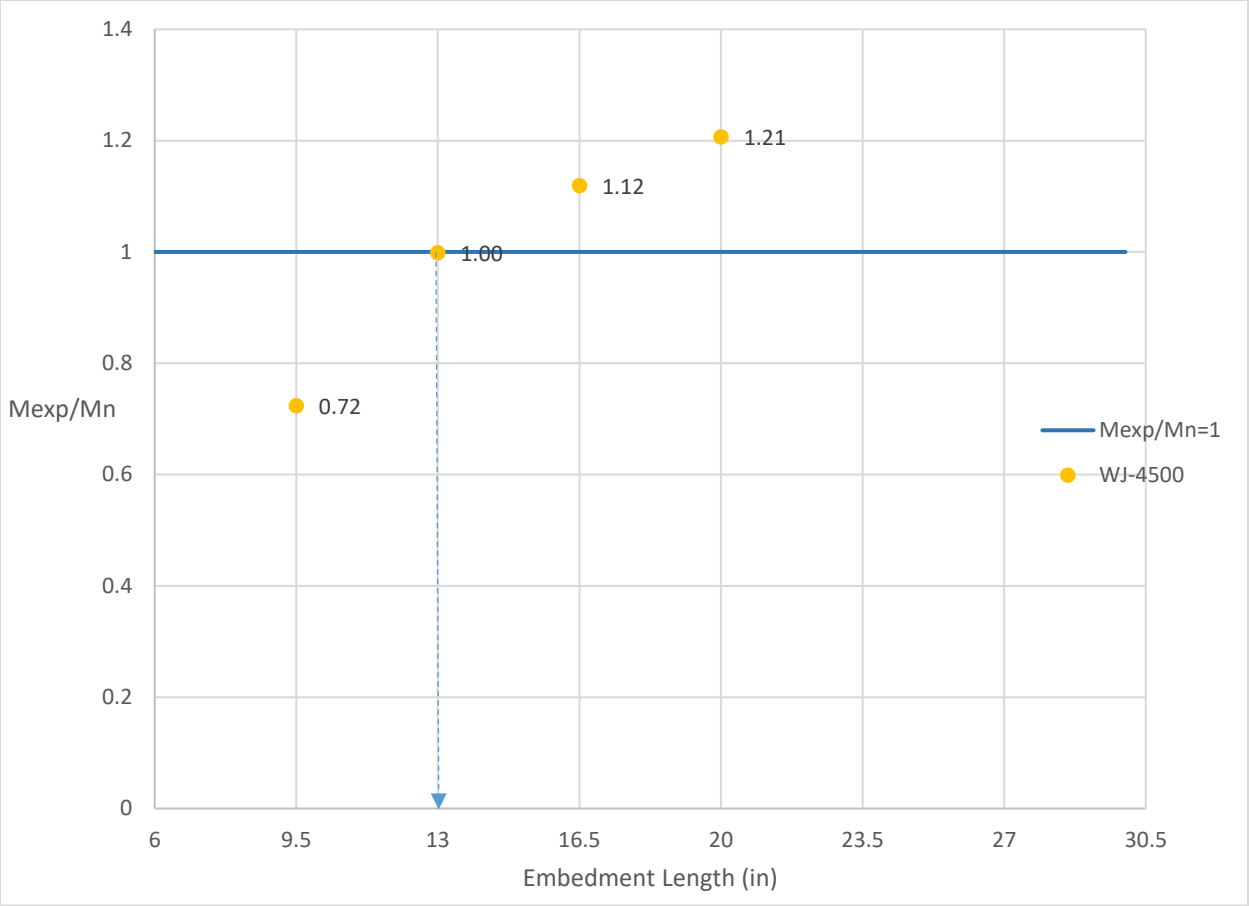


Figure 98 Ratio of maximum experimental moment to nominal moment capacity versus embedment length for prisms made with WJ wire and 4500 psi release strength

Development Length=13 in.

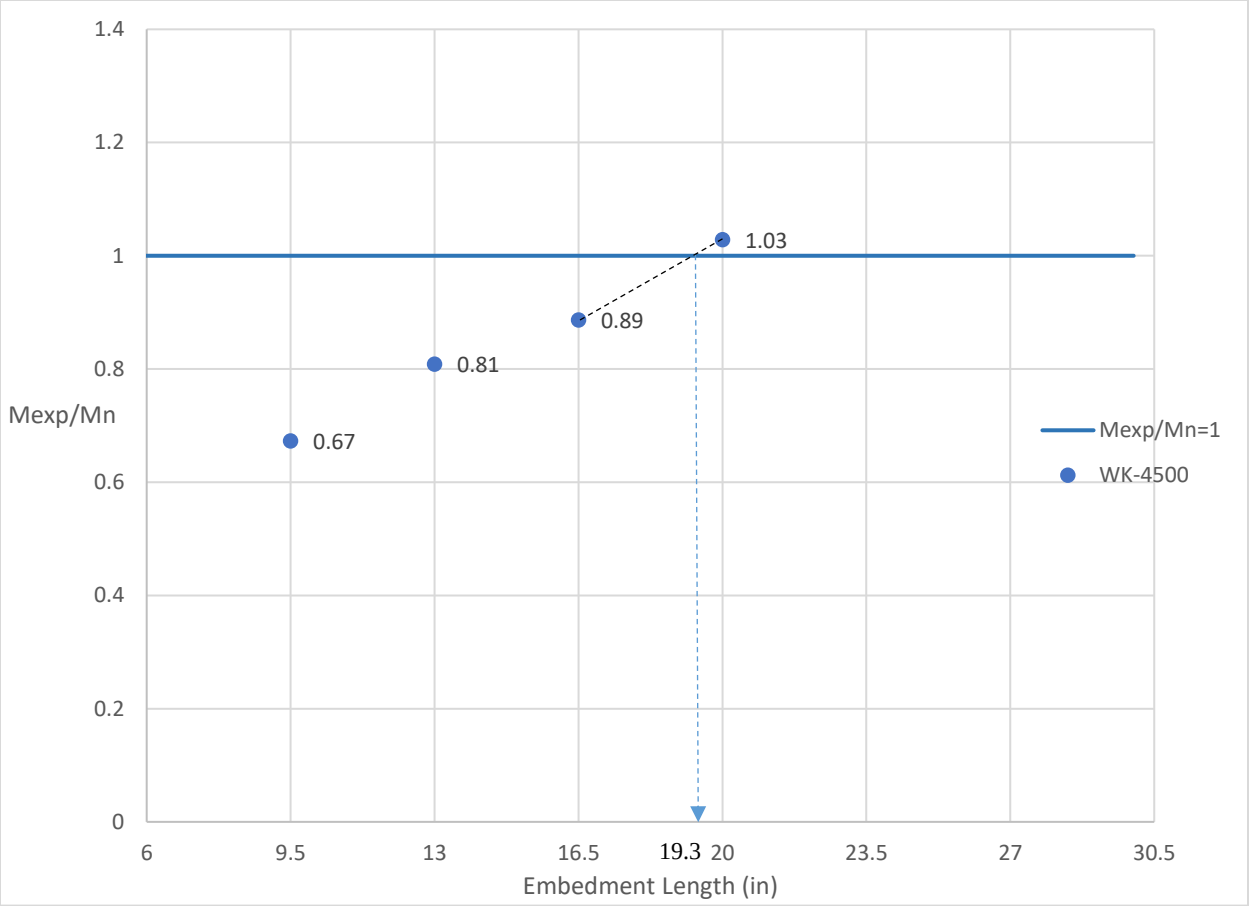


Figure 99 Ratio of maximum experimental moment to nominal moment capacity versus embedment length for prisms made with WK wire and 4500 psi release strength

$$y = \frac{1.03 - 0.89}{20 - 16.5} \times (x - 16.5) + 0.89$$

$$y = 0.04(x - 16.5) + 0.89$$

$$1 = 0.04(D.L - 16.5) + 0.89 ==> D.L = 19.3\ in.$$

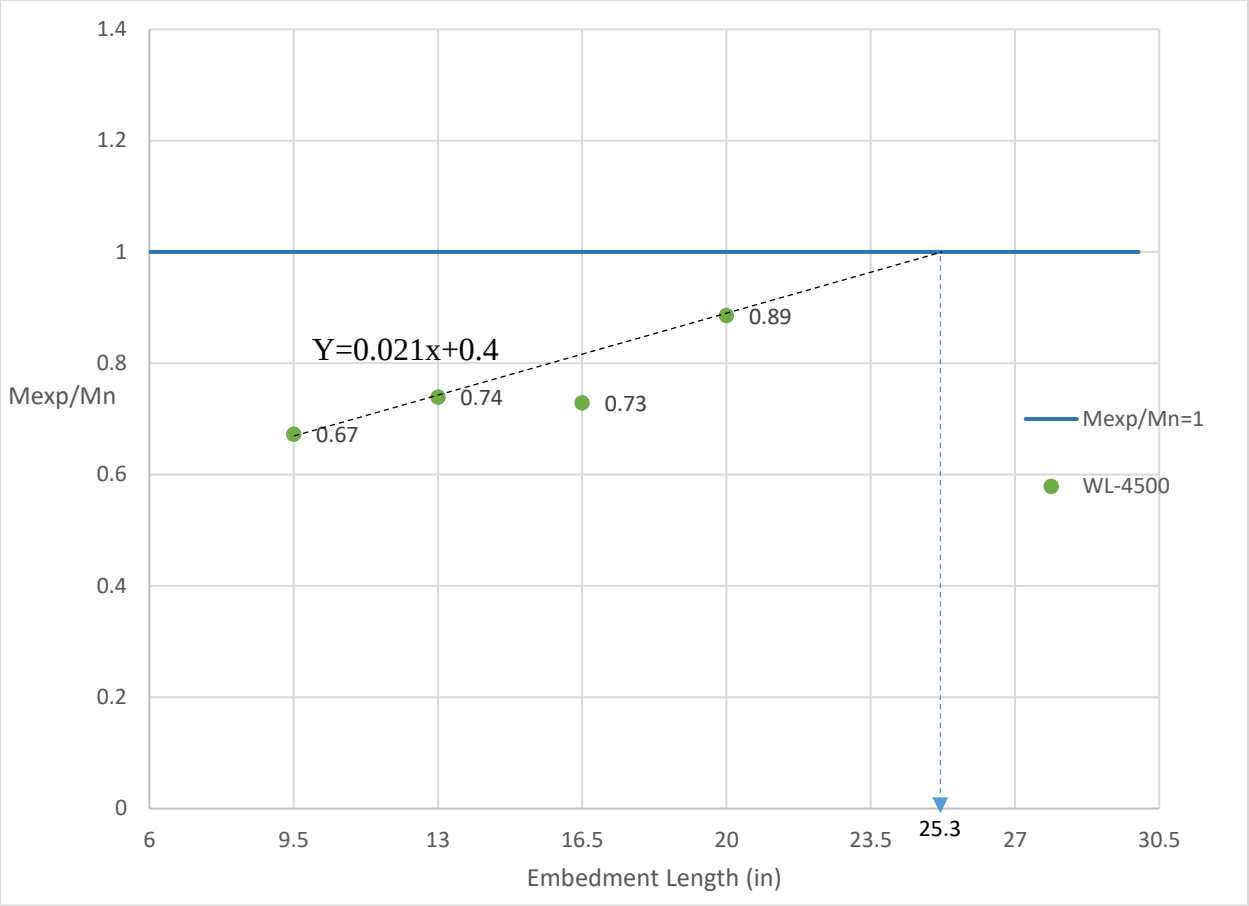


Figure 100 Ratio of maximum experimental moment to nominal moment capacity versus embedment length for prisms made with WL wire and 4500 psi release strength

Trend line for three points:

$y = 0.021x + 0.468$

$1 = 0.021D.L + 0.468 ==> D.L = 25.3\ in.$

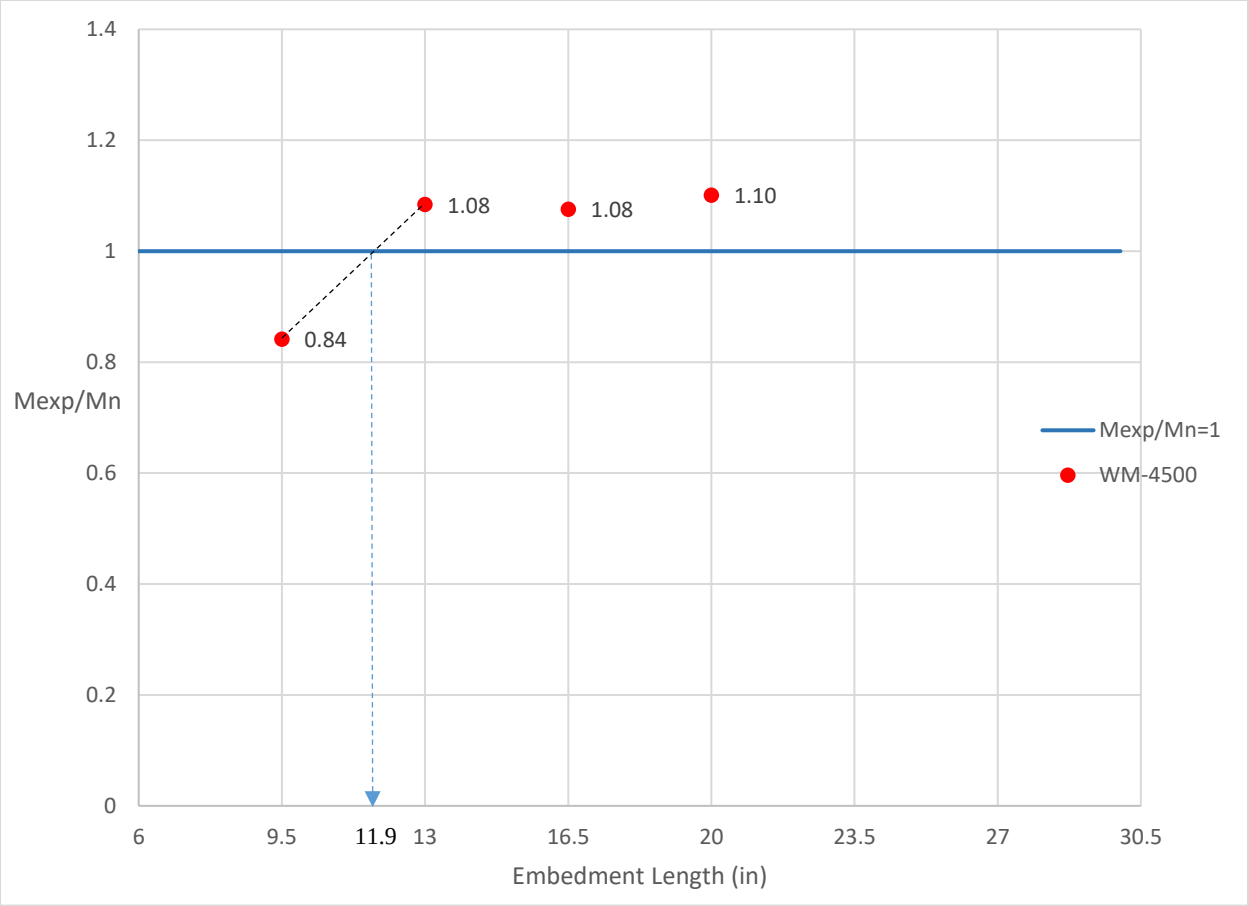


Figure 101 Ratio of maximum experimental moment to nominal moment capacity versus embedment length for prisms made with WM wire and 4500 psi release strength

$$y = \frac{1.08 - 0.84}{13 - 9.5} \times (x - 9.5) + 0.84$$

$$y = 0.068(x - 9.5) + 0.84$$

$$1 = 0.068(D.L - 9.5) + 0.84 ==> D.L = 11.9\ in.$$

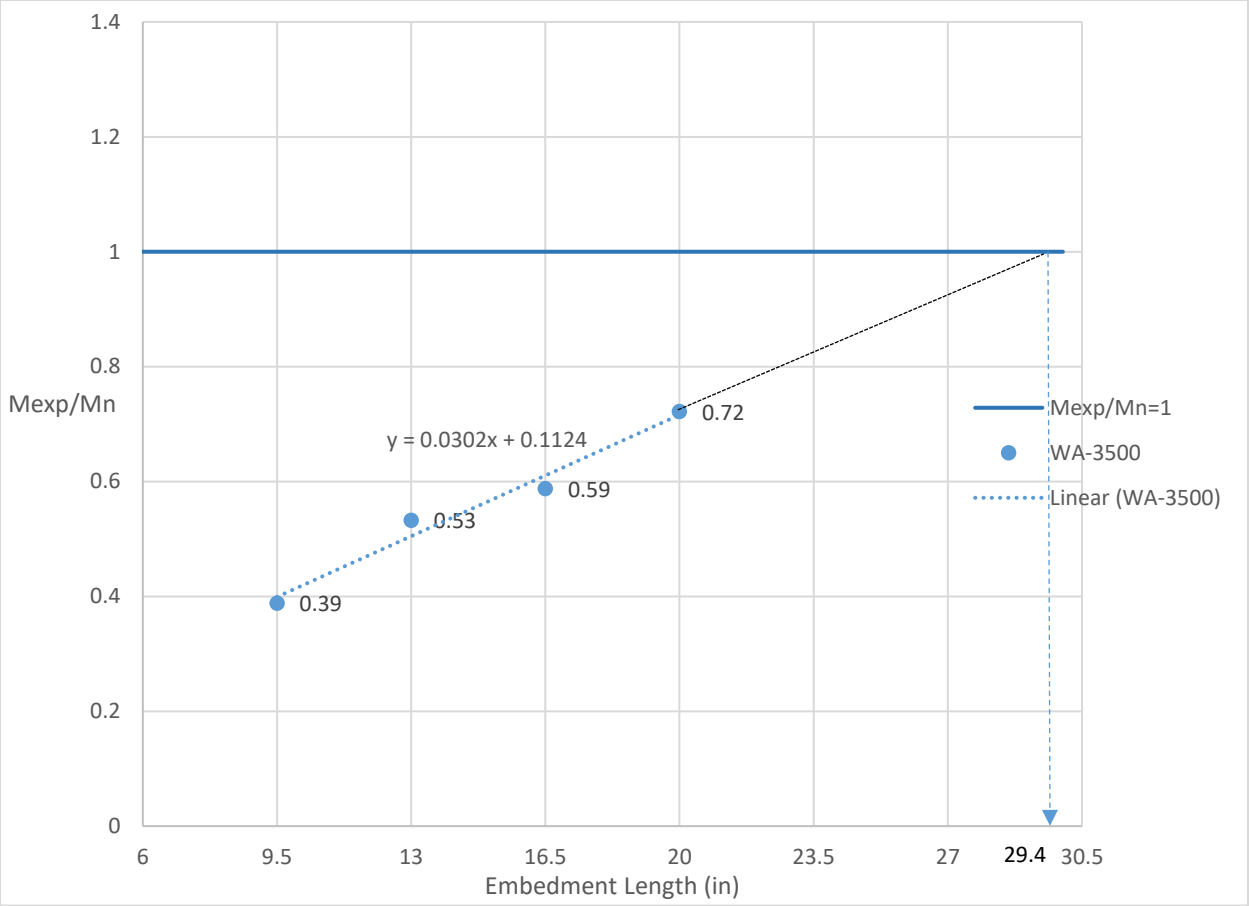


Figure 102 Ratio of maximum experimental moment to nominal moment capacity versus embedment length for prisms made with WA wire and 3500 psi release strength

$1 = 0.0302D.L + 0.1124 ==> D.L = 29.4$

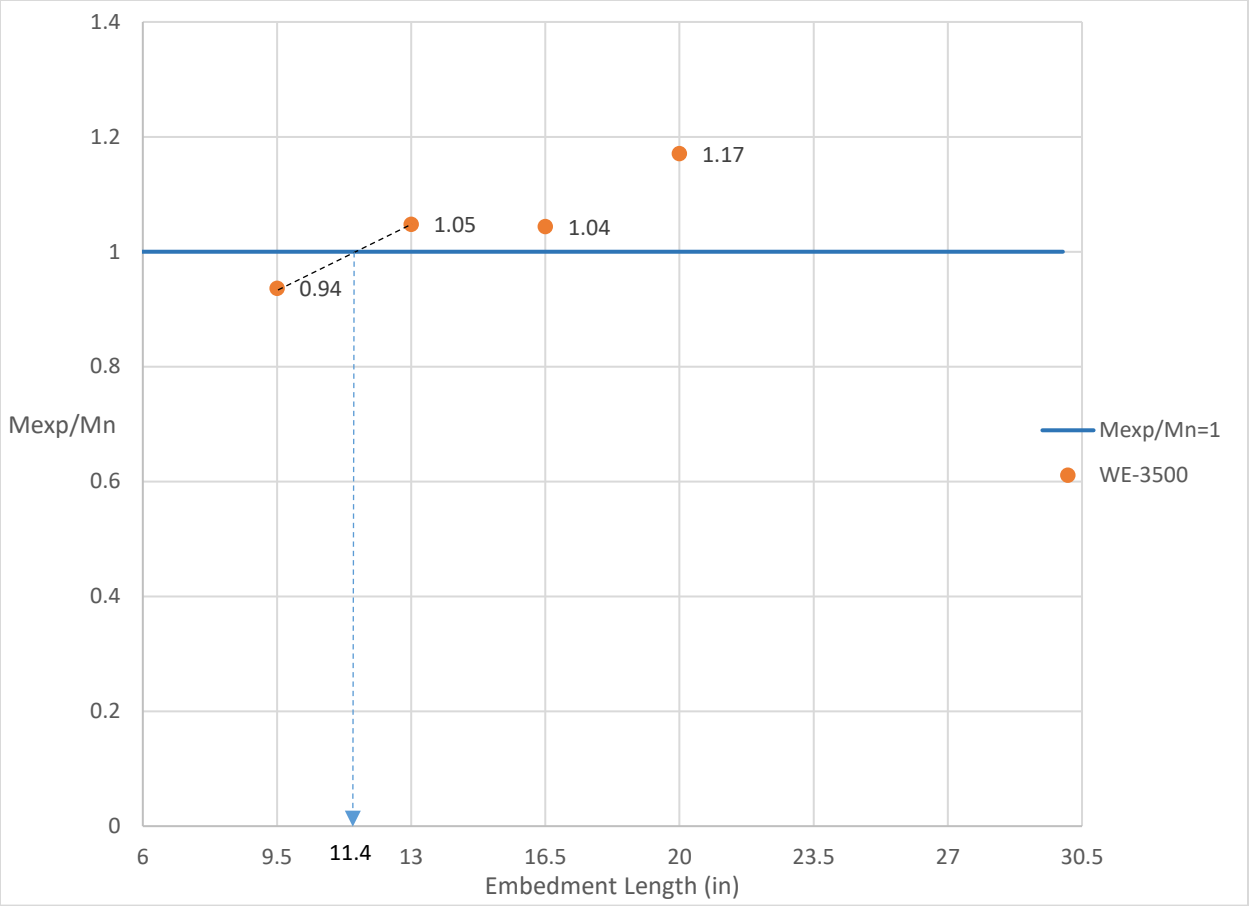


Figure 103 Ratio of maximum experimental moment to nominal moment capacity versus embedment length for prisms made with WE wire and 3500 psi release strength

$$y = \frac{1.05 - 0.94}{13 - 9.5} \times (x - 9.5) + 0.94$$

$$y = 0.031(x - 9.5) + 0.94$$

$$1 = 0.031(D.L - 9.5) + 0.94 ==> D.L = 11.4\ in.$$

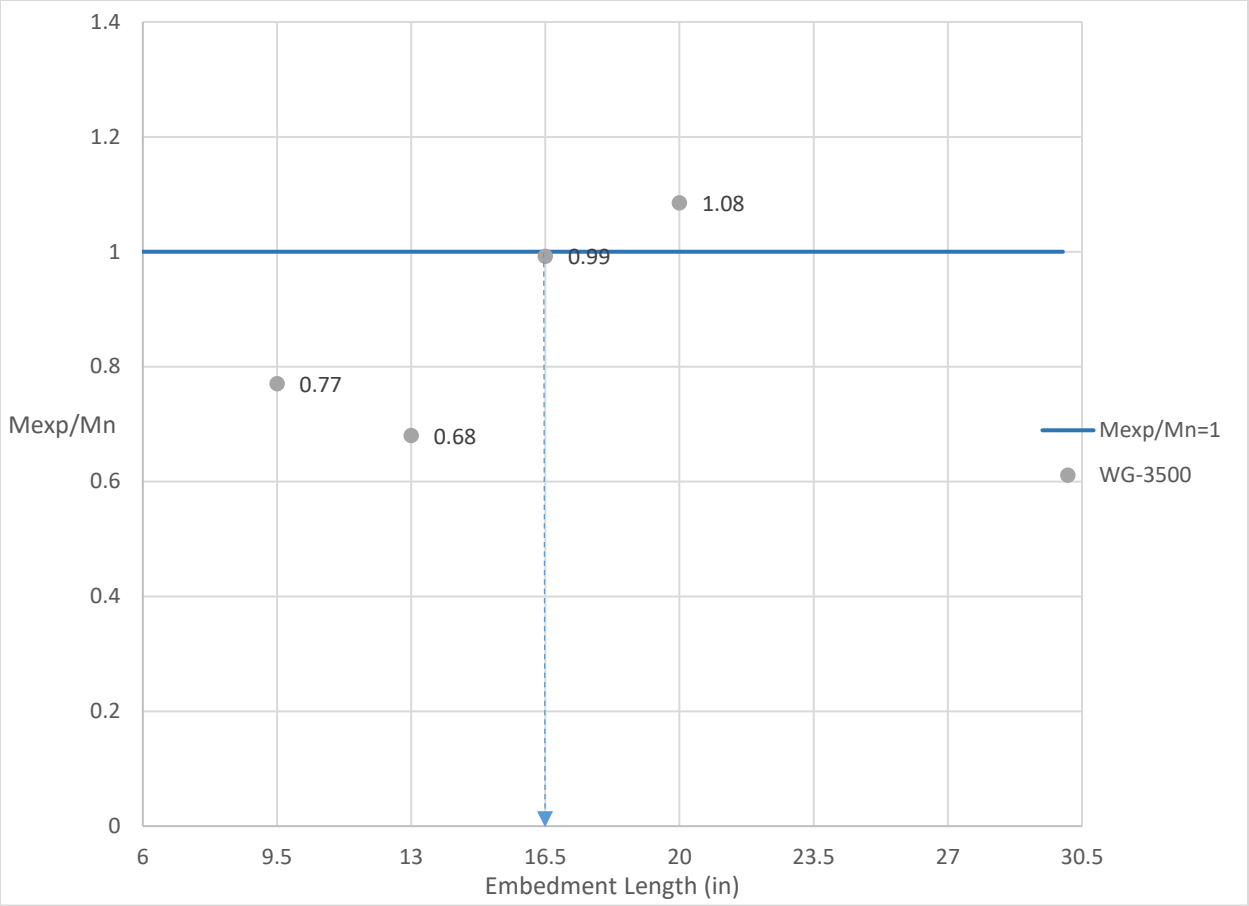


Figure 104 Ratio of maximum experimental moment to nominal moment capacity versus embedment length for prisms made with WG wire and 3500 psi release strength

Development Length=16.5 in.

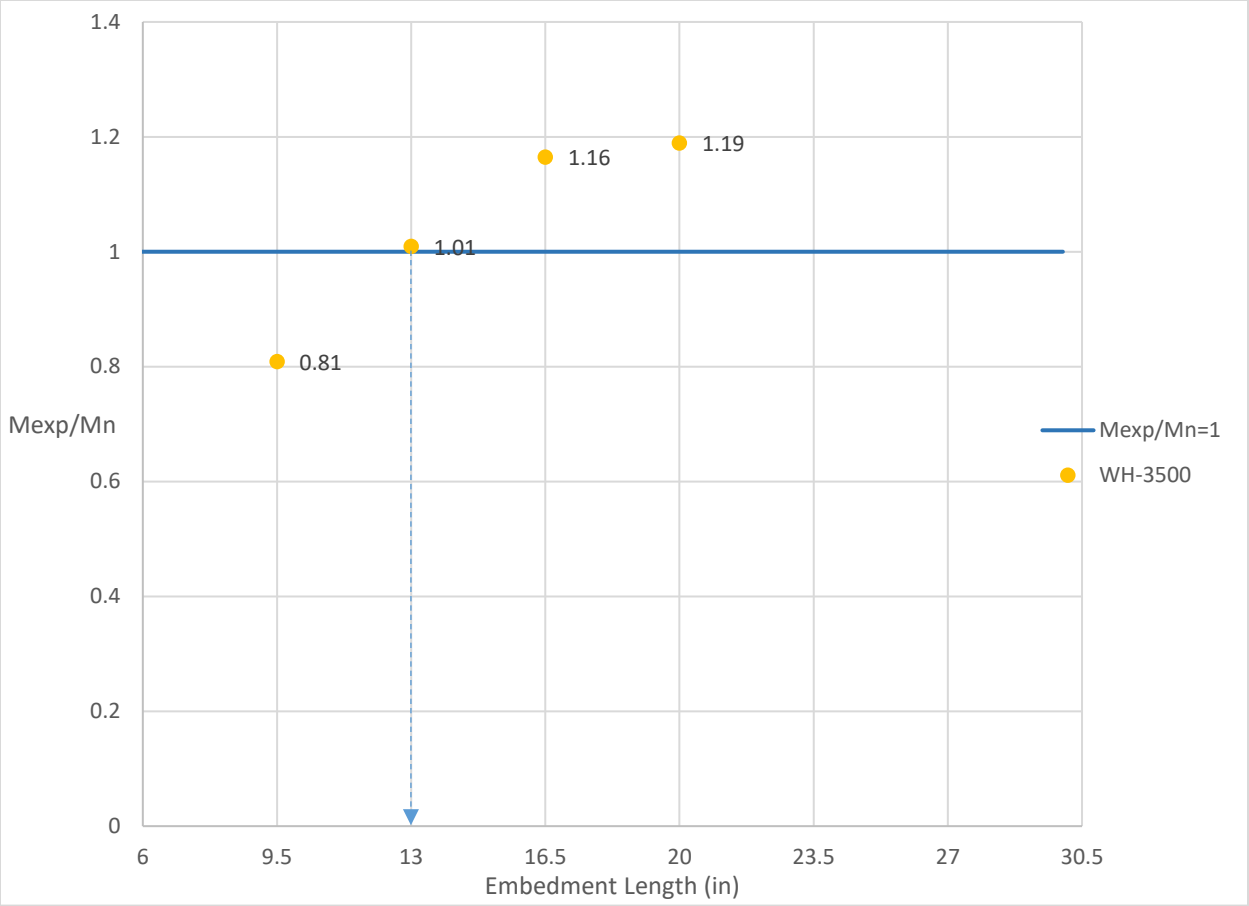


Figure 105 Ratio of maximum experimental moment to nominal moment capacity versus embedment length for prisms made with WH wire and 3500 psi release strength

Development Length=13 in.

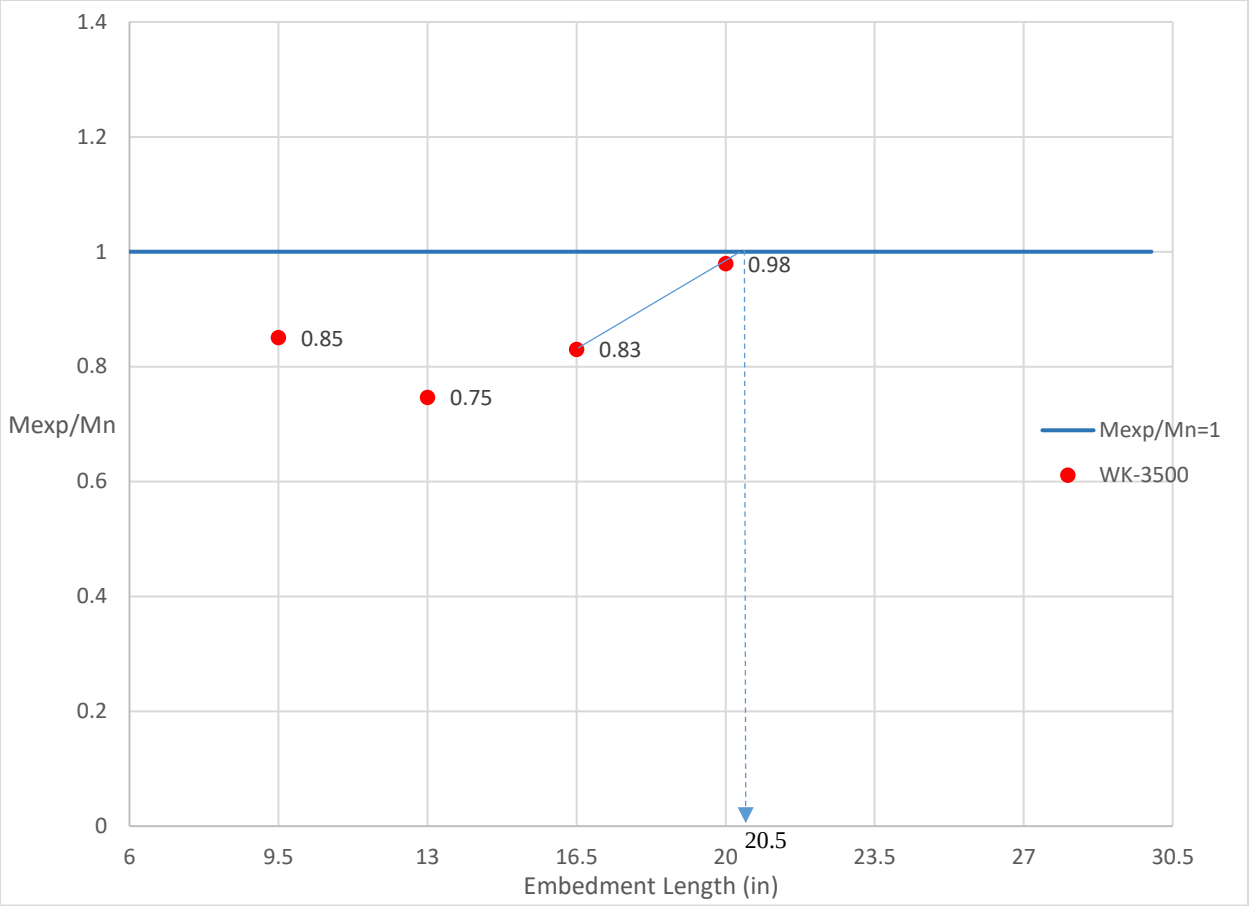


Figure 106 Ratio of maximum experimental moment to nominal moment capacity versus embedment length for prisms made with WK wire and 3500 psi release strength

$$y = \frac{0.98 - 0.83}{20 - 16.5} \times (x - 16.5) + 0.83$$

$$y = 0.043(x - 16.5) + 0.83$$

$$1 = 0.043(D.L - 16.5) + 0.83 ==> D.L = 20.5\ in.$$

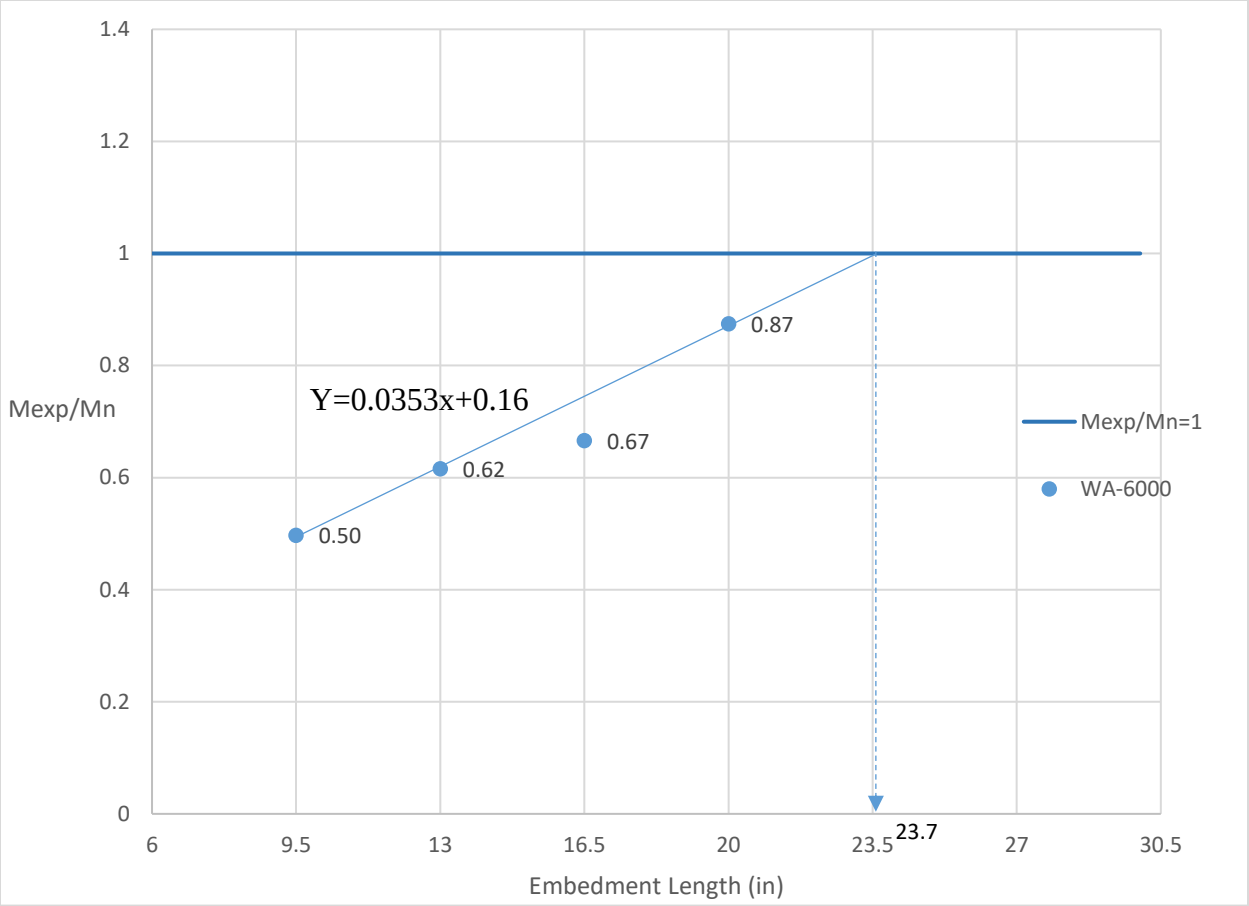


Figure 107 Ratio of maximum experimental moment to nominal moment capacity versus embedment length for prisms made with WA wire and 6000 psi release strength

Trend line for three points:

$y = 0.0353x + 0.1632$

$1 = 0.0353D.L + 0.1632 ==> D.L = 23.7\ in.$

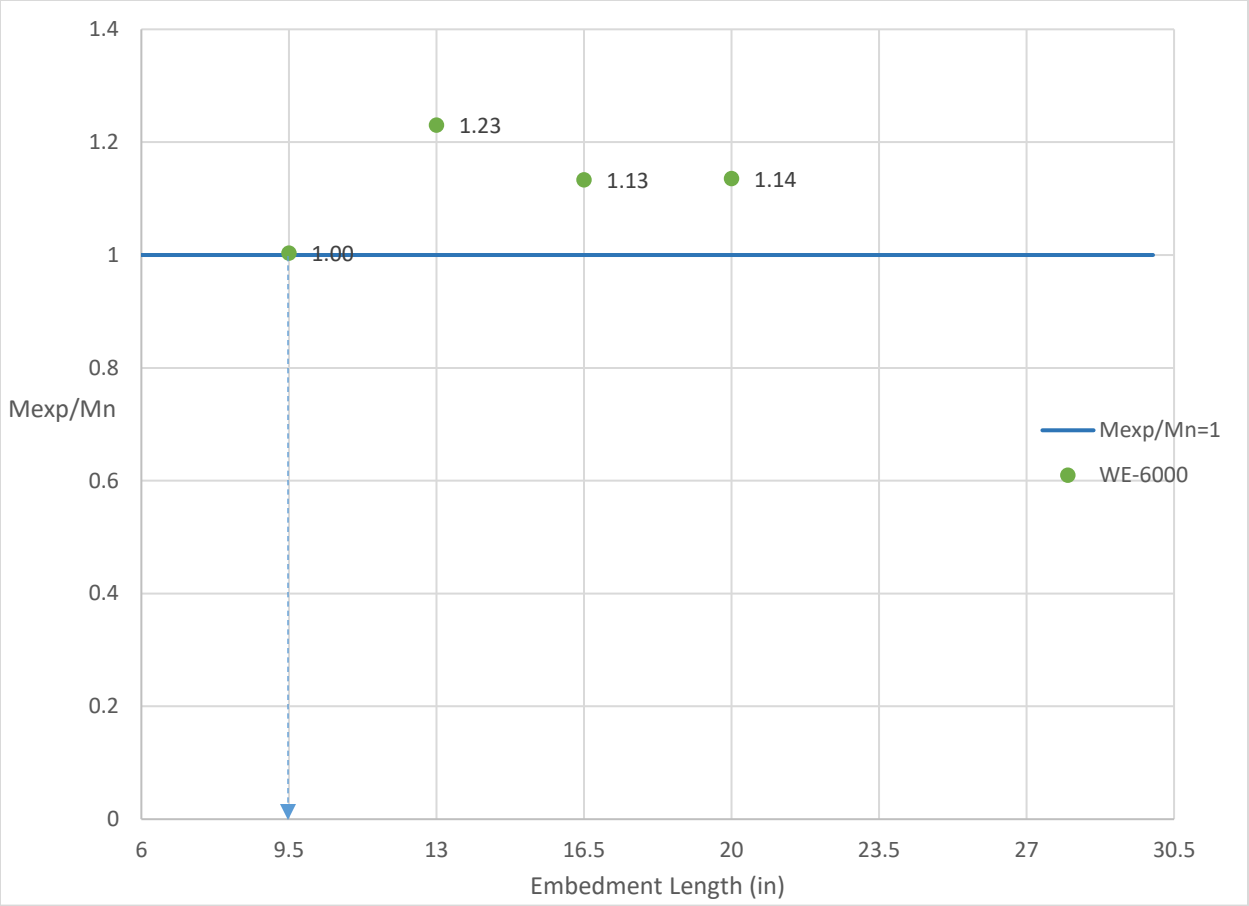


Figure 108 Ratio of maximum experimental moment to nominal moment capacity versus embedment length for prisms made with WE wire and 6000 psi release strength

Mexp/Mn>1 for all load cases➔Development length=9.5 in.

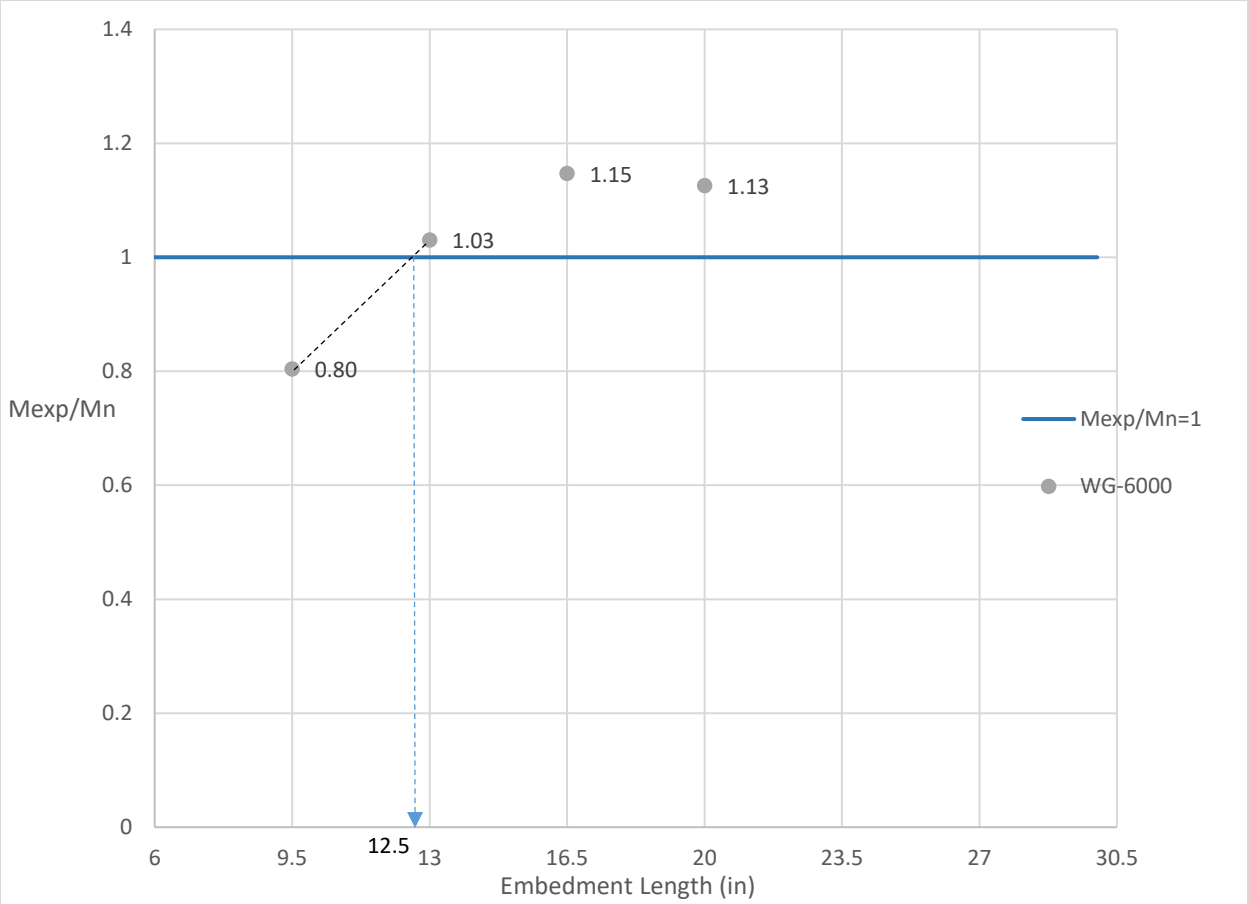


Figure 109 Ratio of maximum experimental moment to nominal moment capacity versus embedment length for prisms made with WG wire and 6000 psi release strength

$$y = \frac{1.03 - 0.80}{13 - 9.5} \times (x - 9.5) + 0.80$$

$$y = 0.043(x - 9.5) + 0.80$$

$$1 = 0.066(D.L - 9.5) + 0.80 ==> D.L = 12.5\ in.$$

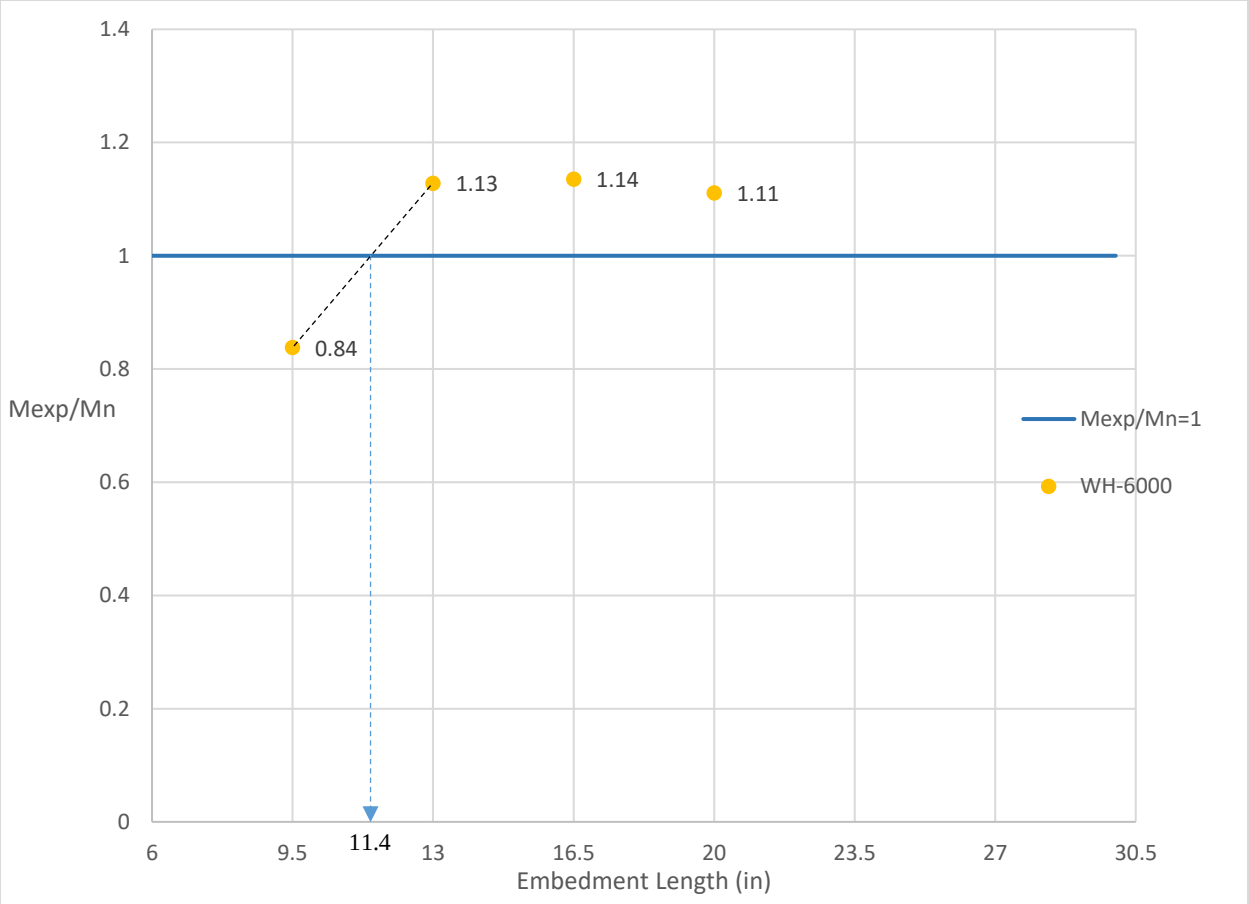


Figure 110 Ratio of maximum experimental moment to nominal moment capacity versus embedment length for prisms made with WH wire and 6000 psi release strength

$$y = \frac{1.13 - 0.84}{13 - 9.5} \times (x - 9.5) + 0.84$$

$$y = 0.083(x - 9.5) + 0.84$$

$$1 = 0.083(D.L - 9.5) + 0.84 ==> D.L = 11.4\ in.$$

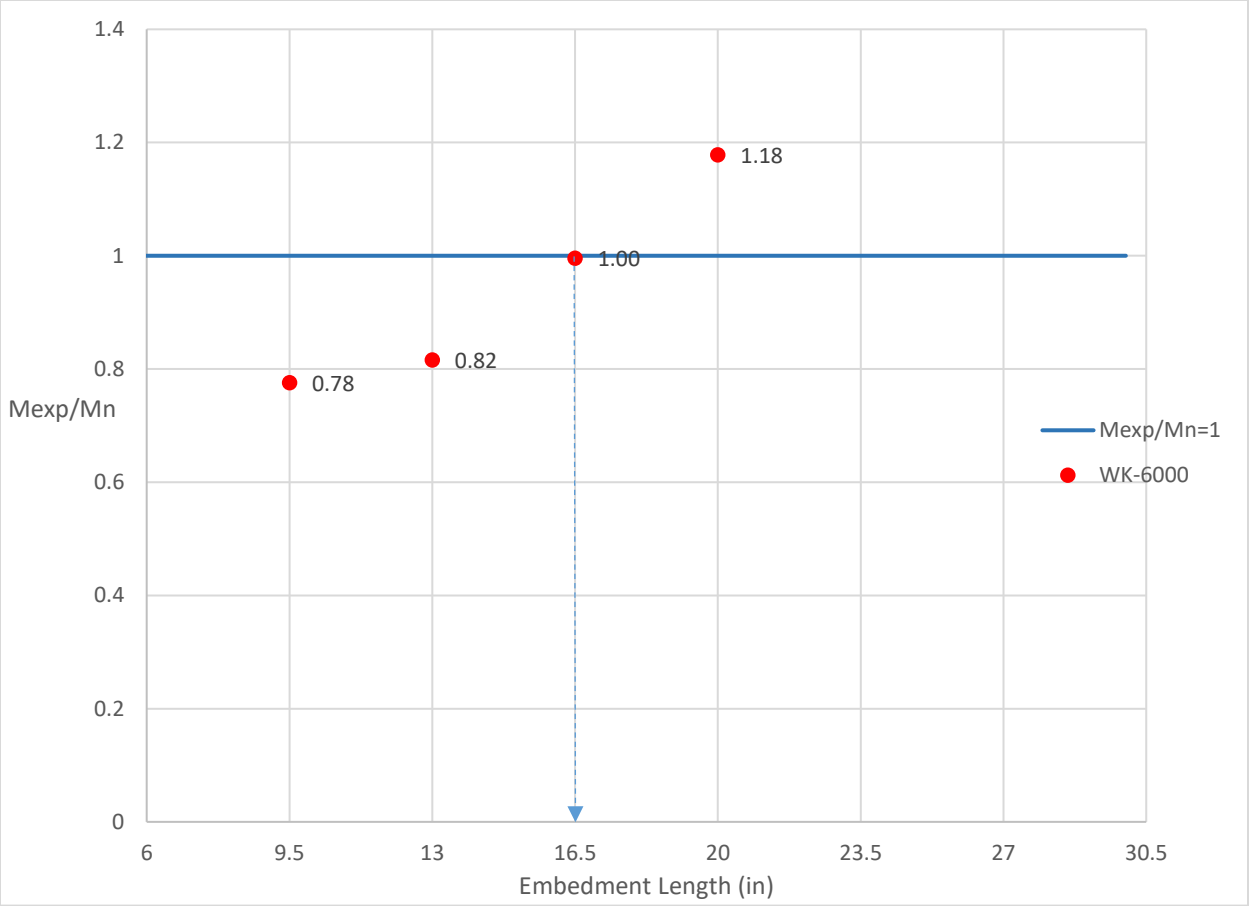


Figure 111 Ratio of maximum experimental moment to nominal moment capacity versus embedment length for prisms made with WK wire and 6000 psi release strength

Development Length=16.5 in.

Appendix C.
Load vs Deflection Graphs and Picture of Failed Prisms

Prisms made with wires, 4500 psi concrete release strength and 6 in. slump

Beam Identification	WA-4500-6-1-L
Wire Type:	WA
Embedment Length:	20 in
Release Strength:	4500 psi
Slump:	6 in

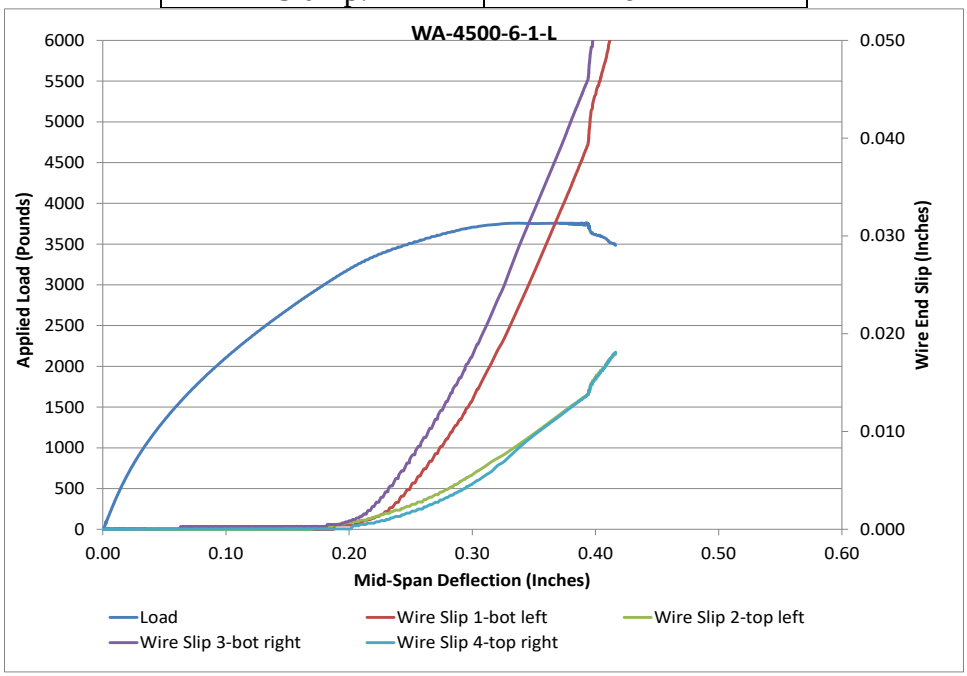


Figure 112 Load vs Deflection and Wire End Slip WA-4500-6-1-L

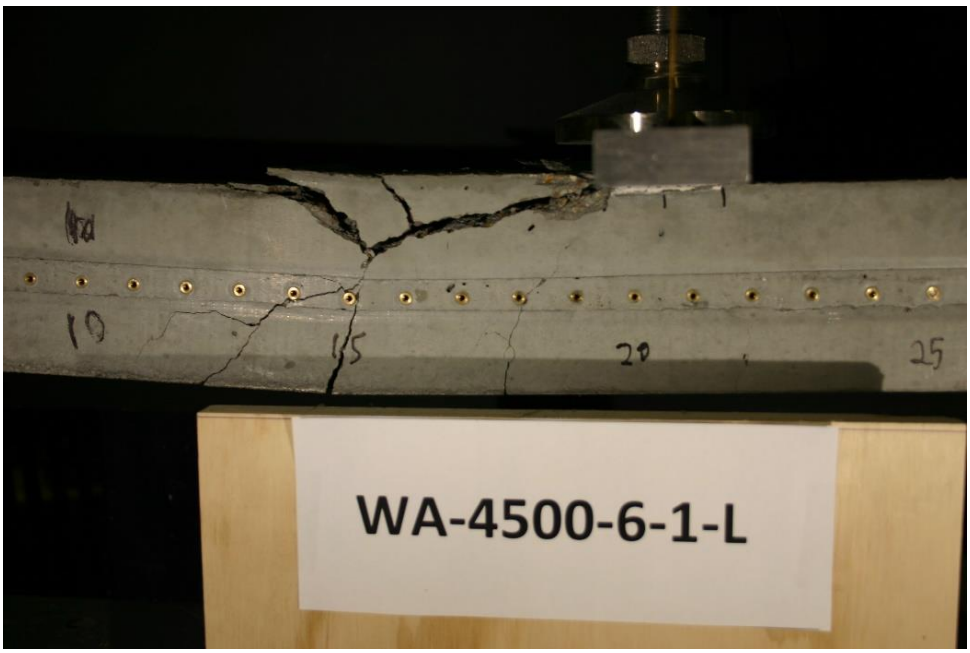


Figure 113 Picture of Failed Prism WA-4500-6-1-L

Beam Identification	WA-4500-6-1-S
Wire Type:	WA
Embedment Length:	13 in
Release Strength:	4500 psi
Slump:	6 in

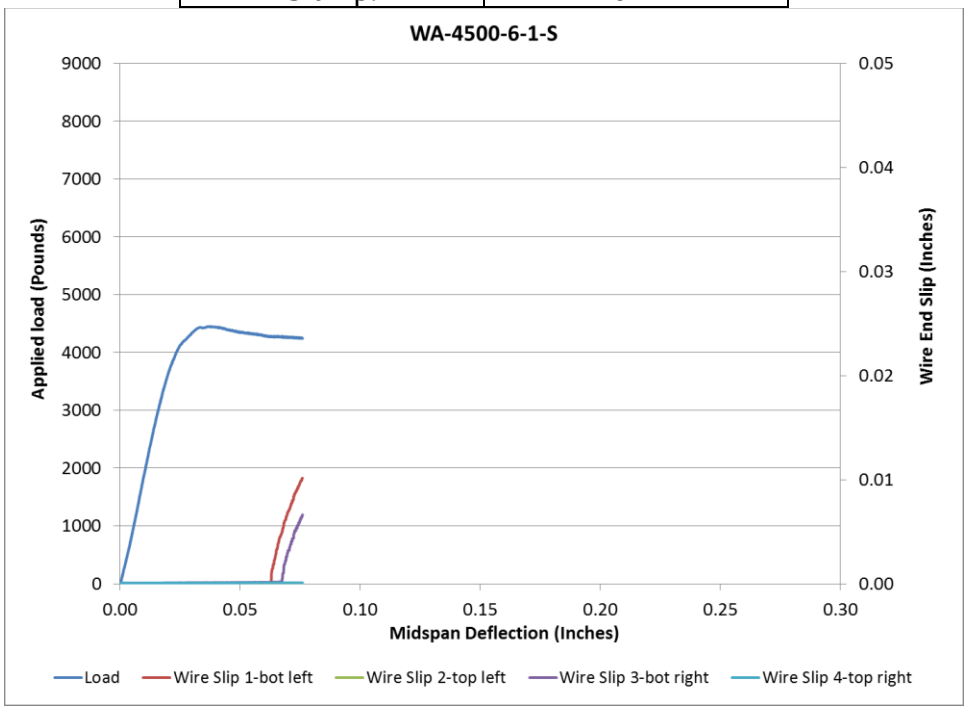


Figure 114 Load Deflection and Wire End Slip WA-4500-6-1-S

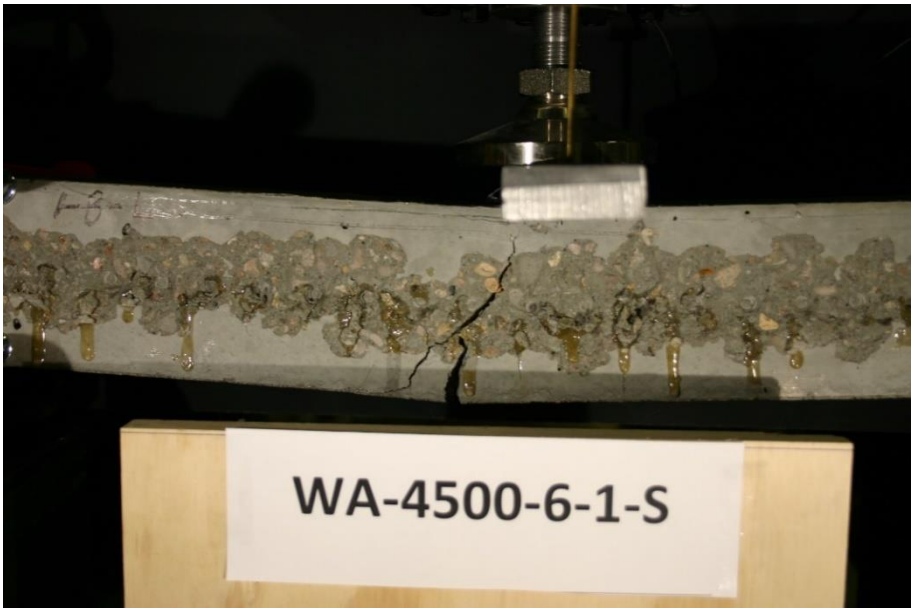


Figure 115 Picture of Failed Prism WA-4500-6-1-S

Beam Identification	WA-4500-6-2-L
Wire Type:	WA
Embedment Length:	16.5 in
Release Strength:	4500 psi
Slump:	6 in

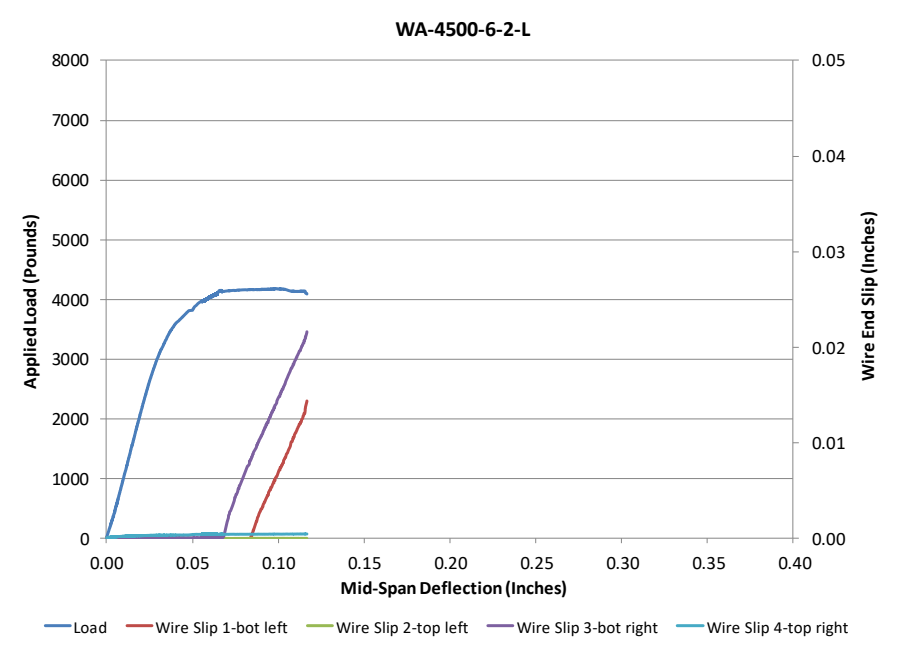


Figure 116 Load Deflection and Wire End Slip WA-4500-6-2-L

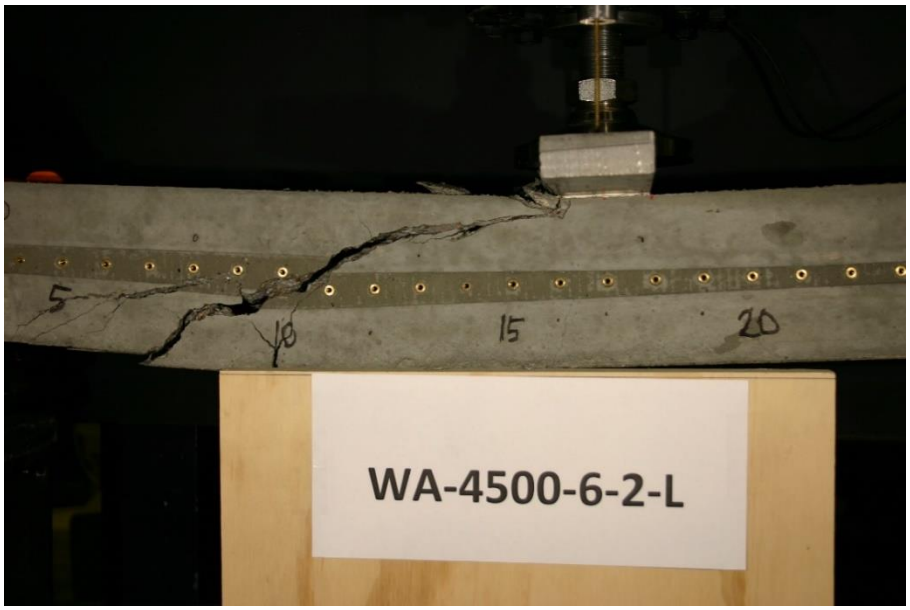


Figure 117 Picture of Failed Prism WA-4500-6-2-L

Beam Identification	WA-4500-6-2-S
Wire Type:	WA
Embedment Length:	9.5 in
Release Strength:	4500 psi
Slump:	6 in

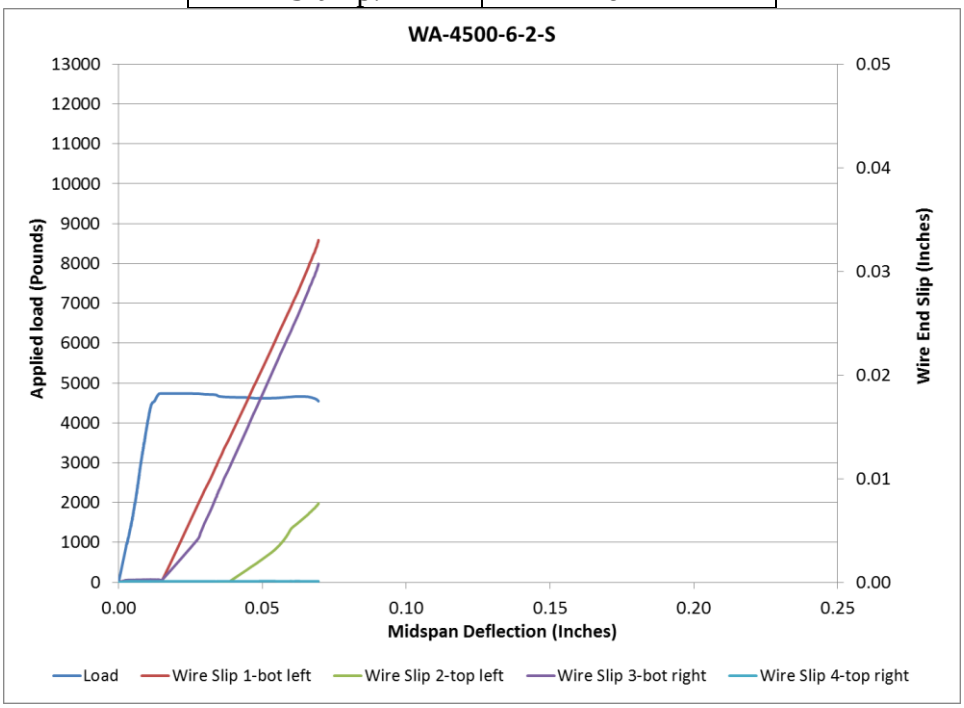


Figure 118 Load Deflection and Wire End Slip WA-4500-6-2-S

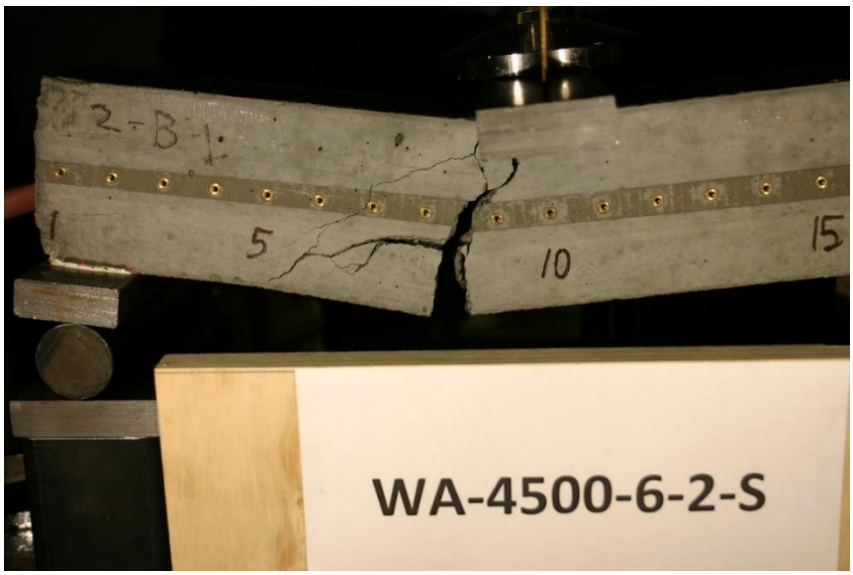


Figure 119 Picture of Failed Prism WA-4500-6-2-S

Beam Identification	WB-4500-6-1-L
Wire Type:	WB
Embedment Length:	20 in
Release Strength:	4500 psi
Slump:	6 in

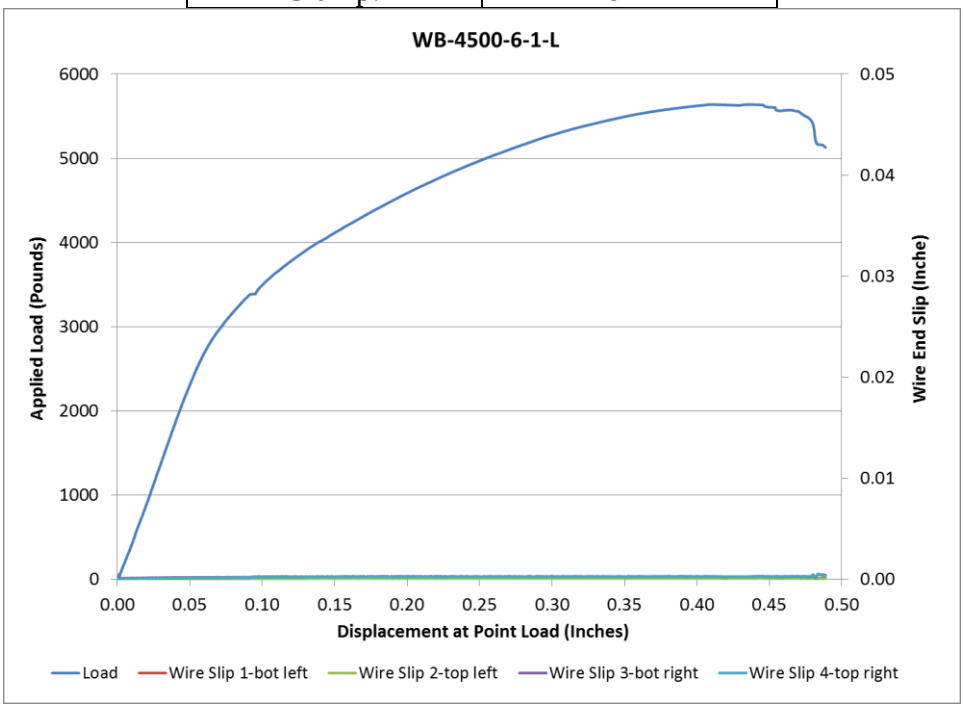


Figure 120 Load Deflection and Wire End Slip WB-4500-6-1-L

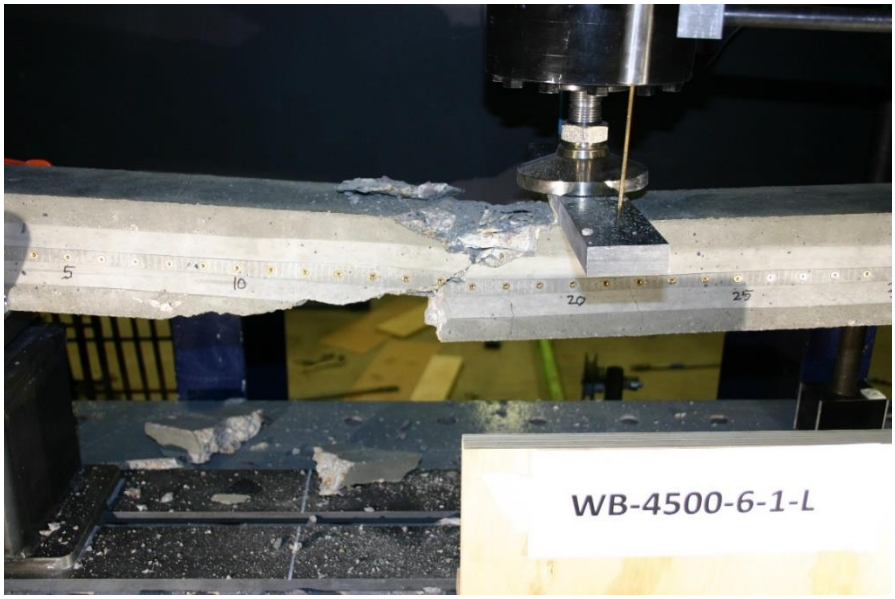


Figure 121 Picture of Failed Prism WB-4500-6-1-L

Beam Identification	WB-4500-6-1-S
Wire Type:	WB
Embedment Length:	13 in
Release Strength:	4500 psi
Slump:	6 in

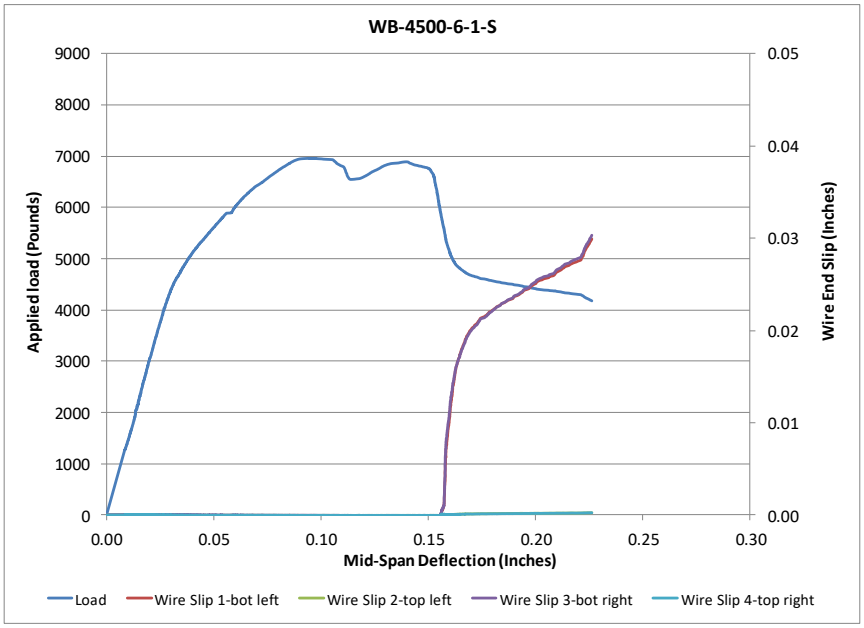


Figure 122 Load Deflection and *Wire* End Slip WB-4500-6-1-S

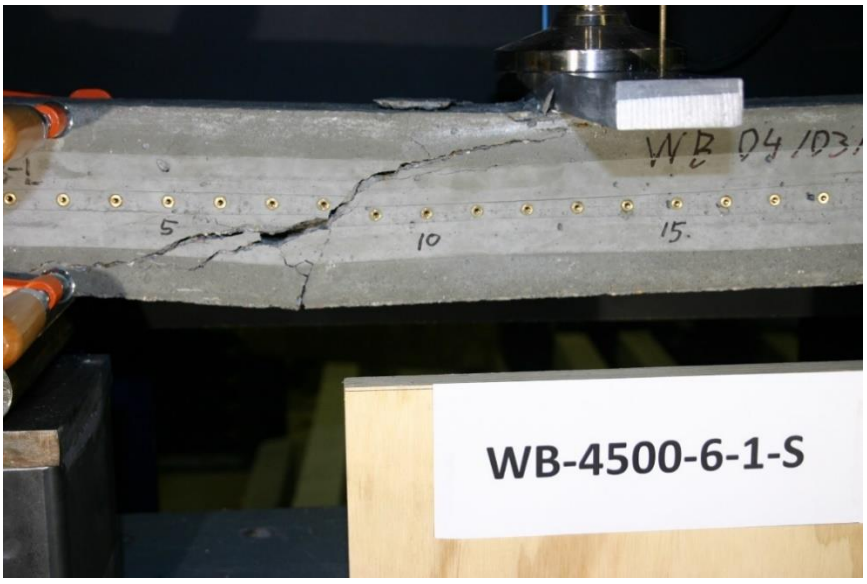


Figure 123 Picture of Failed Prism WB-4500-6-1-S

Beam Identification	WB-4500-6-2-L
Wire Type:	WB
Embedment Length:	16.5 in
Release Strength:	4500 psi
Slump:	6 in

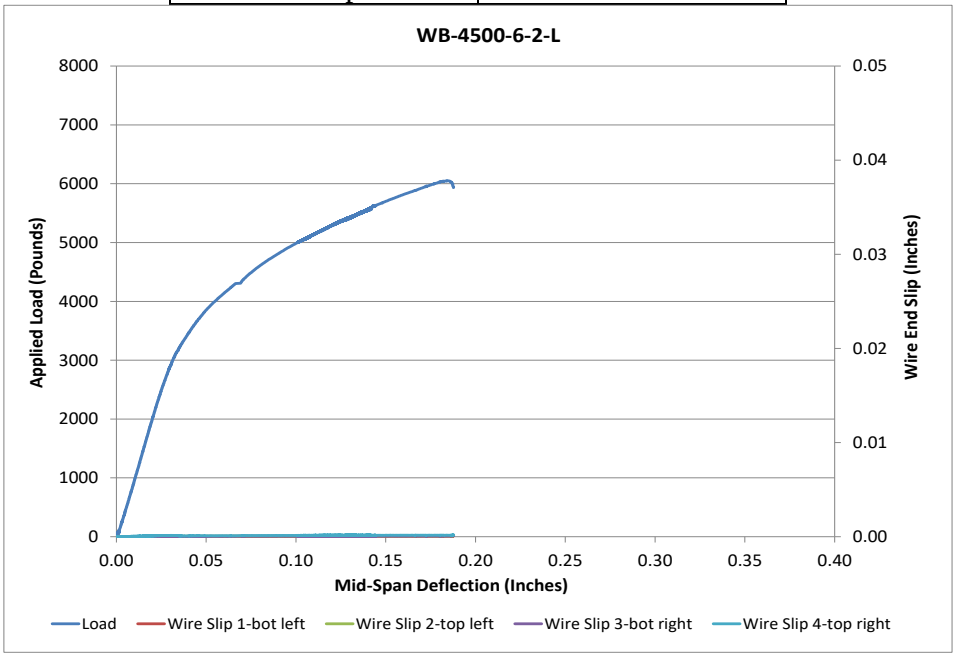


Figure 124 Load Deflection and Wire End Slip WB-4500-6-2-L

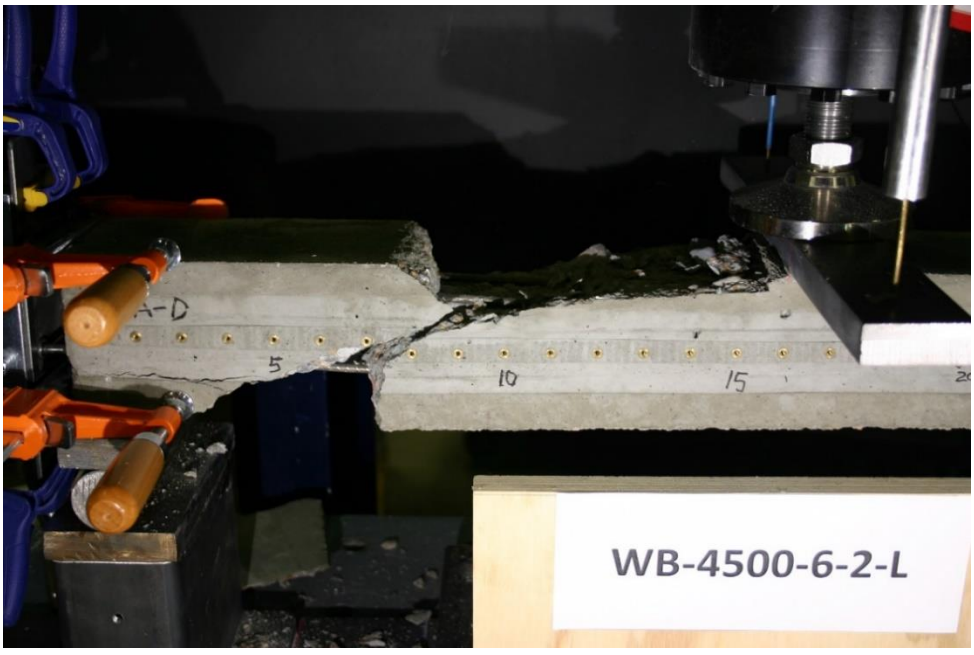


Figure 125 Picture of Failed Prism WB-4500-6-2-L

Beam Identification	WB-4500-6-2-S
Wire Type:	WB
Embedment Length:	9.5 in
Release Strength:	4500 psi
Slump:	6 in

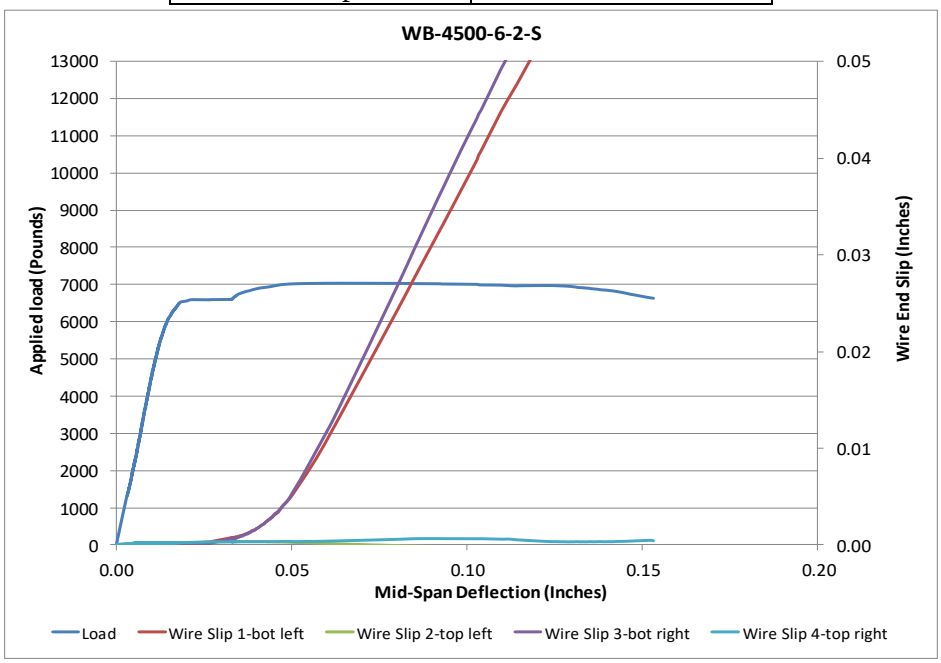


Figure 126 Load Deflection and Wire End Slip WB-4500-6-2-S

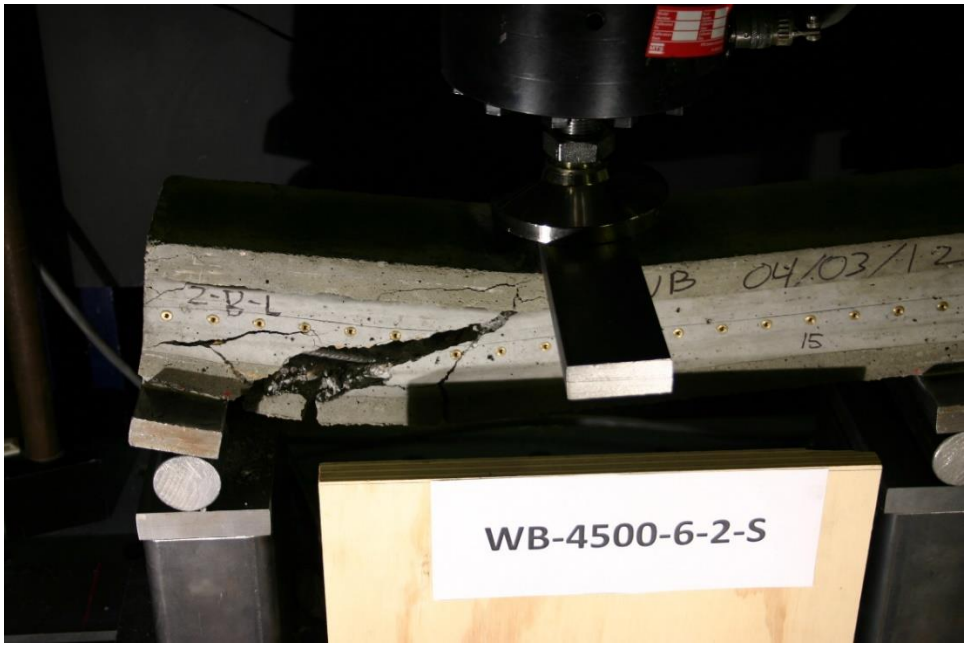


Figure 127 Picture of Failed Prism WB-4500-6-2-S

Beam Identification	WC-4500-6-1-L
Wire Type:	WC
Embedment Length:	20 in
Release Strength:	4500 psi
Slump:	6 in

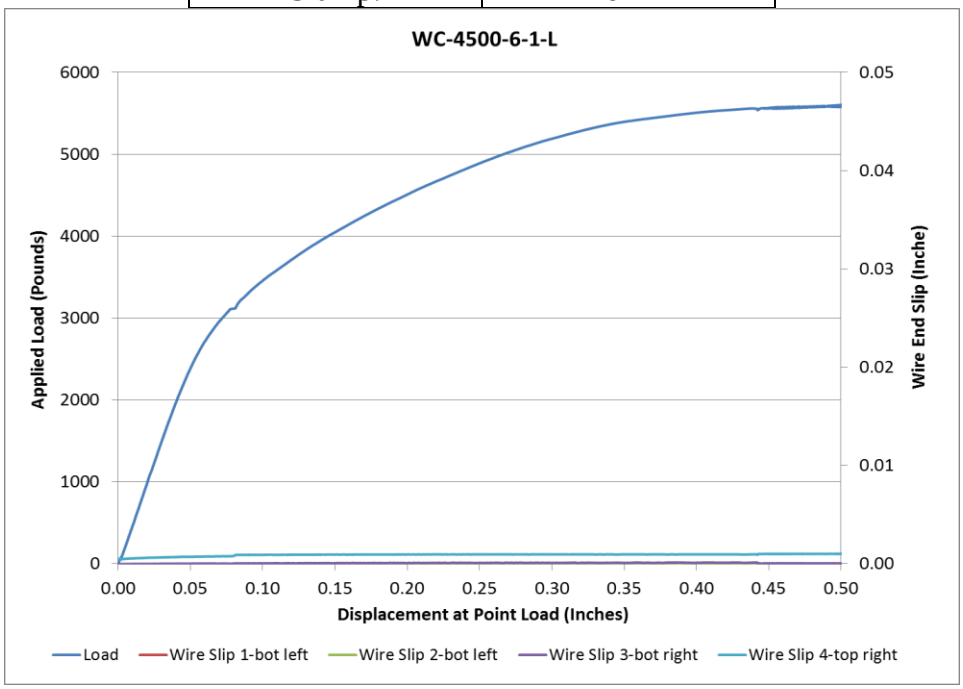


Figure 128 Load Deflection and Wire End Slip WC-4500-6-1-L

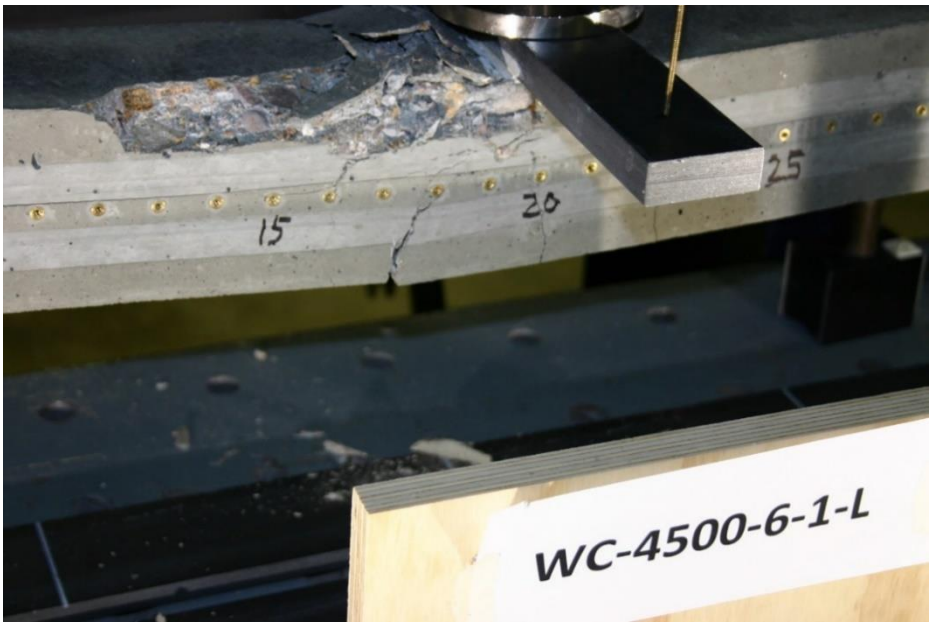


Figure 129 Picture of Failed Prism WC-4500-6-1-L

Beam Identification	WC-4500-6-1-S
Wire Type:	WC
Embedment Length:	13 in
Release Strength:	4500 psi
Slump:	6 in

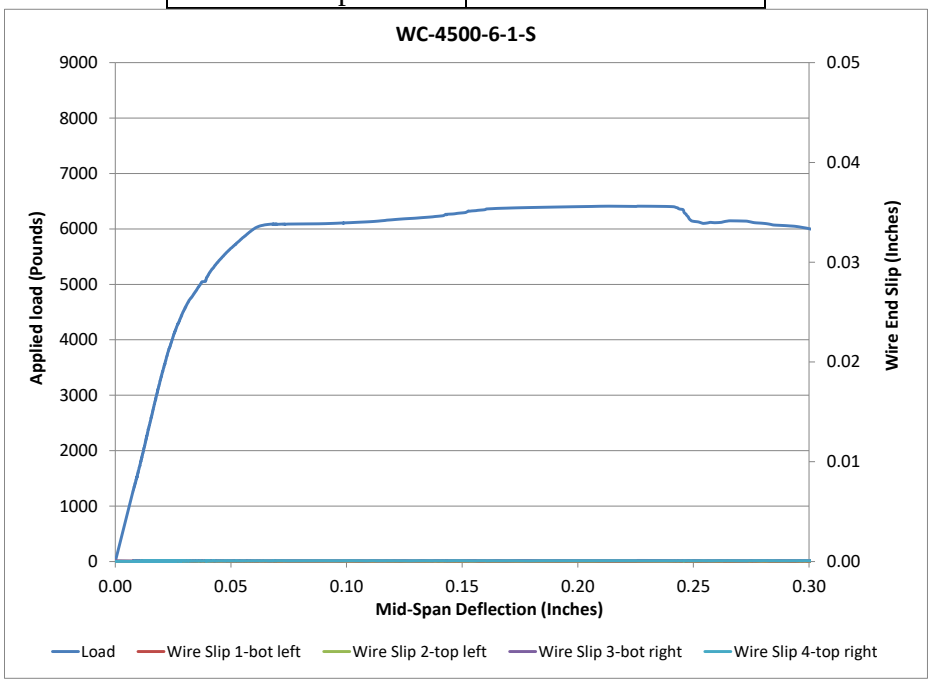


Figure 130 Load Deflection and Wire End Slip WC-4500-6-1-S

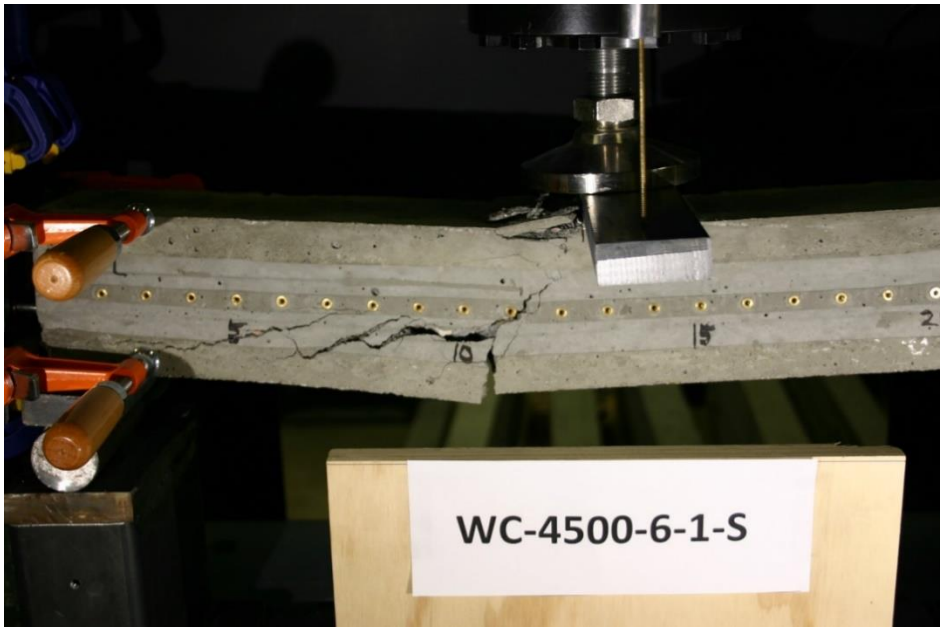


Figure 131 Picture of Failed Prism WC-4500-6-1-S

Beam Identification	WC-4500-6-2-L
Wire Type:	WC
Embedment Length:	16.5 in
Release Strength:	4500 psi
Slump:	6 in

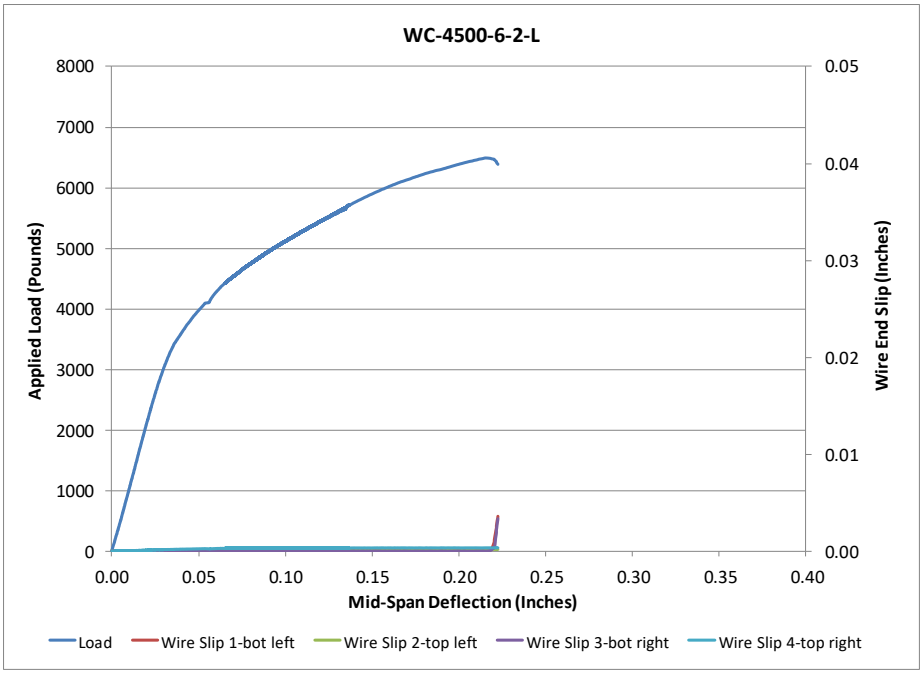


Figure 132 Load Deflection and Wire End Slip WC-4500-6-2-L

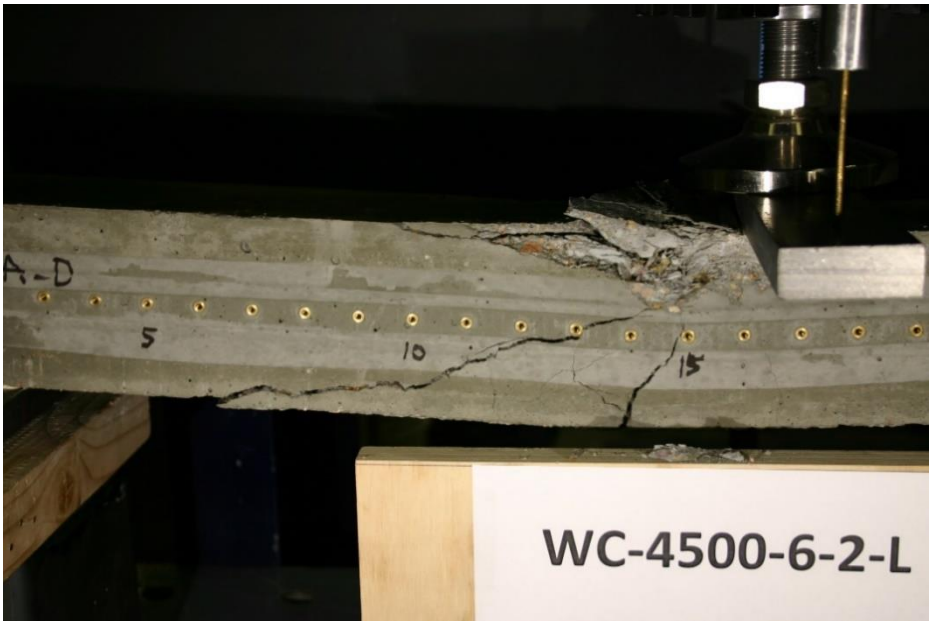


Figure 133 Picture of Failed Prism WC-4500-6-2-L

Beam Identification	WC-4500-6-2-S
Wire Type:	WC
Embedment Length:	9.5 in
Release Strength:	4500 psi
Slump:	6 in

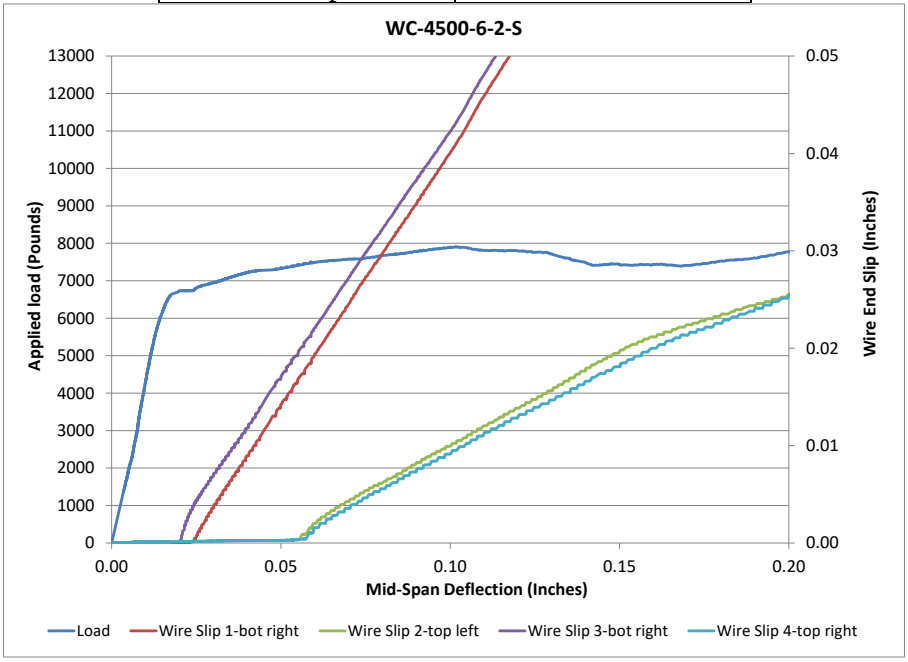


Figure 134 Load Deflection and Wire End Slip WC-4500-6-2-S

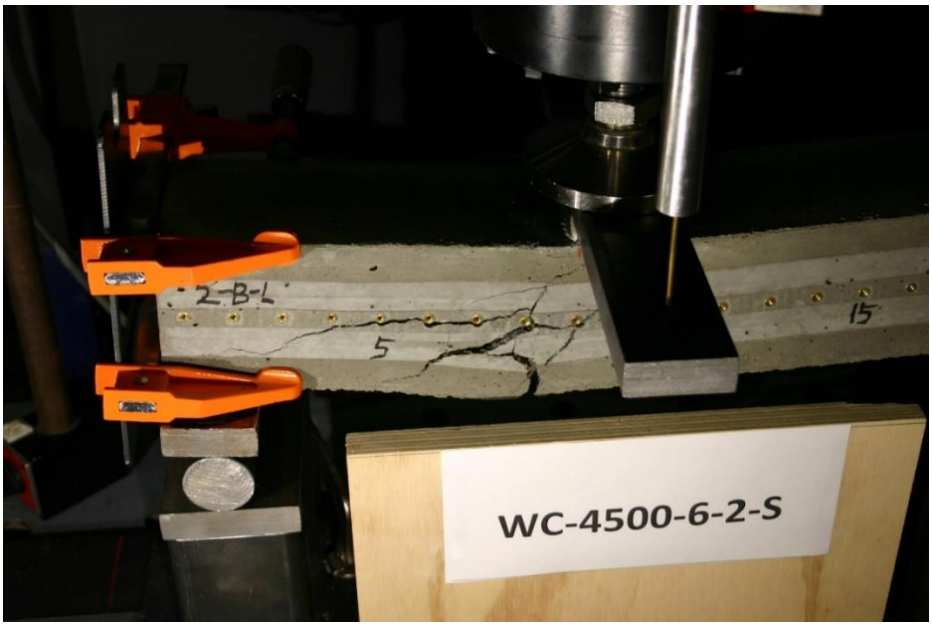


Figure 135 Picture of Failed Prism WC-4500-6-2-S

Beam Identification	WD-4500-6-1-L
Wire Type:	WD
Embedment Length:	20 in
Release Strength:	4500 psi
Slump:	6 in

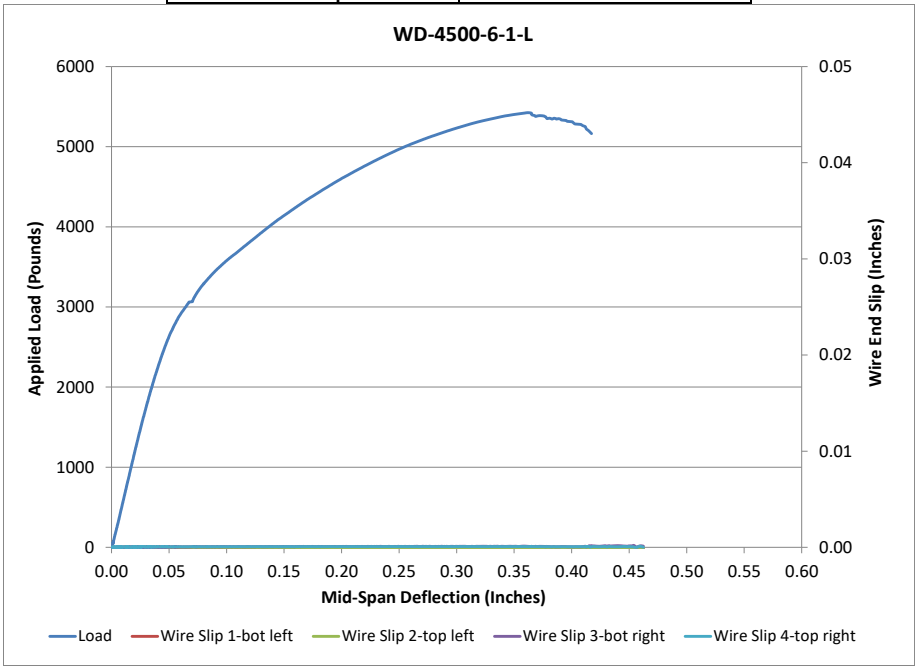


Figure 136 Load Deflection and Wire End Slip WD-4500-6-1-L

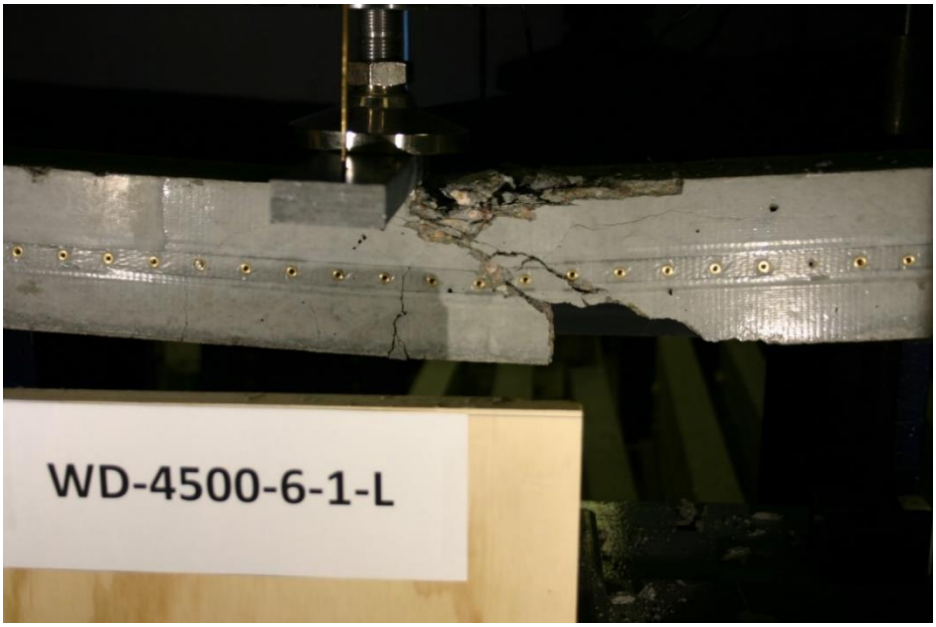


Figure 137 Picture of Failed Prism WD-4500-6-1-L

Beam Identification	WD-4500-6-1-S
Wire Type:	WD
Embedment Length:	13 in
Release Strength:	4500 psi
Slump:	6 in

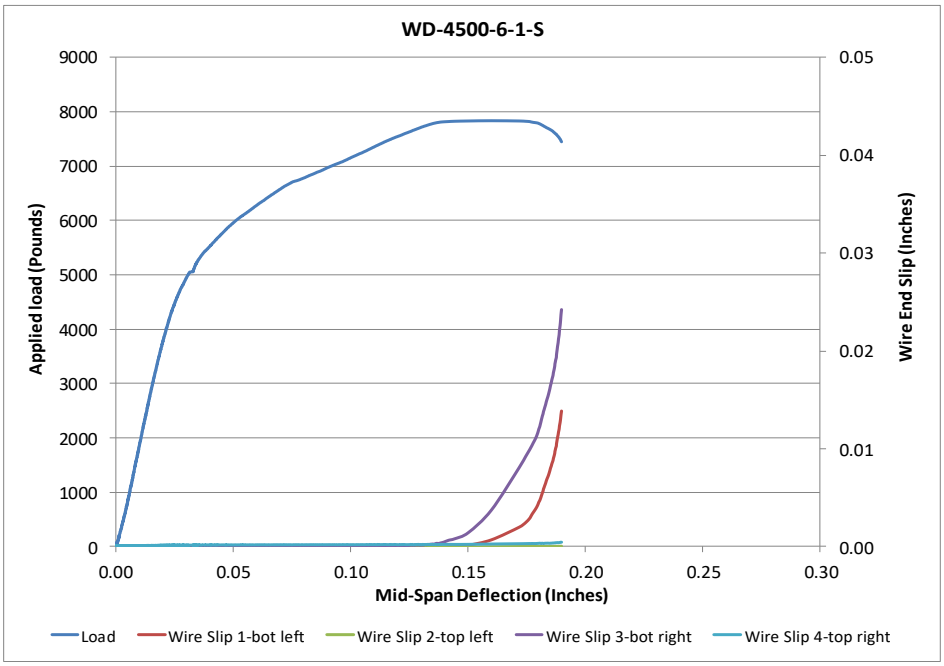


Figure 138 Load Deflection and Wire End Slip WD-4500-6-1-S



Figure 139 Picture of Failed Prism WD-4500-6-1-S

Beam Identification	WD-4500-6-2-L
Wire Type:	WD
Embedment Length:	16.5 in
Release Strength:	4500 psi
Slump:	6 in

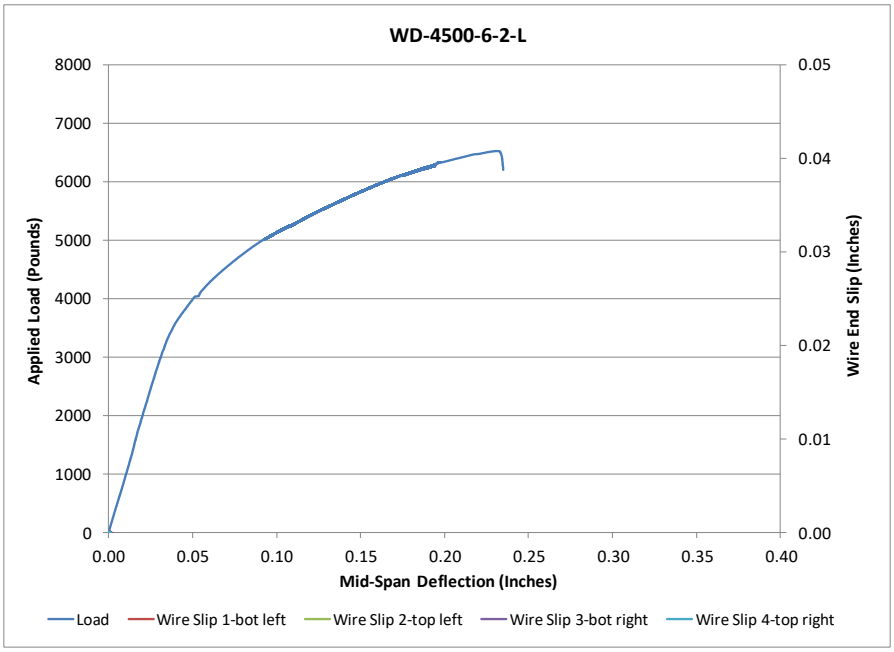


Figure 140 Load Deflection and Wire End Slip WD-4500-6-2-L

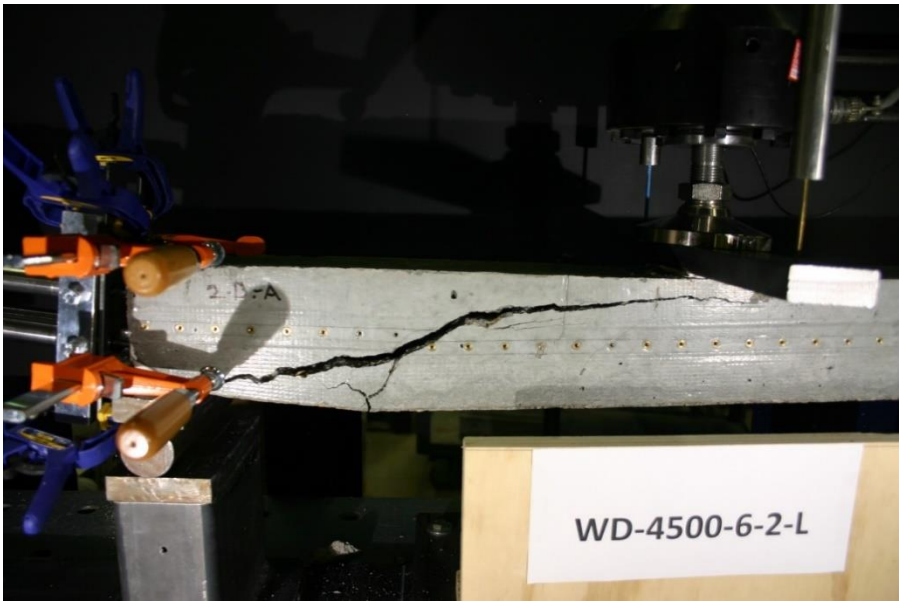


Figure 141 Picture of Failed Prism WD-4500-6-2-L

Beam Identification	WD-4500-6-2-S
Wire Type:	WD
Embedment Length:	9.5 in
Release Strength:	4500 psi
Slump:	6 in

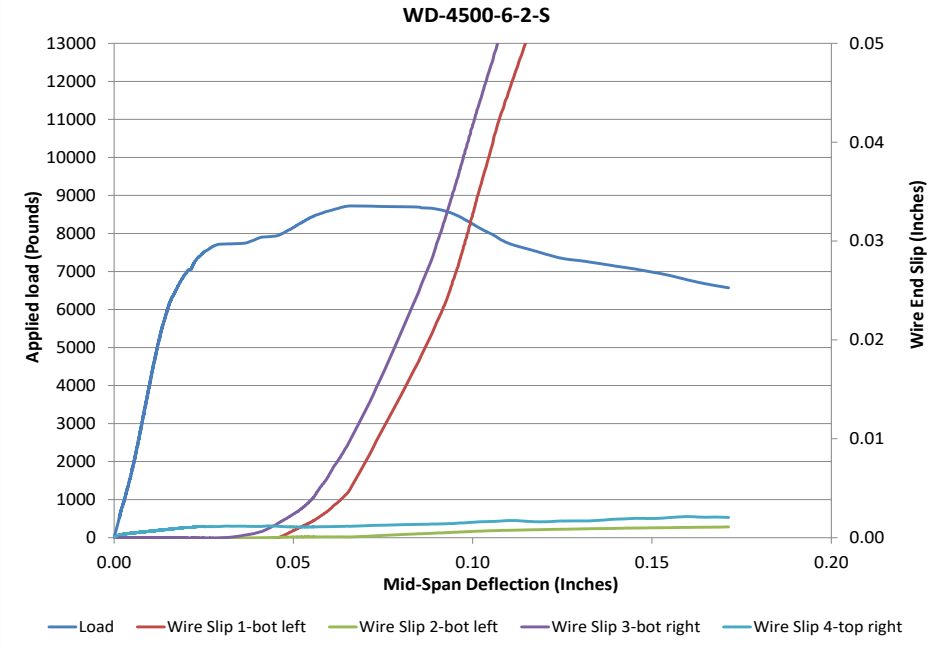


Figure 142 Load Deflection and Wire End Slip WD-4500-6-2-S

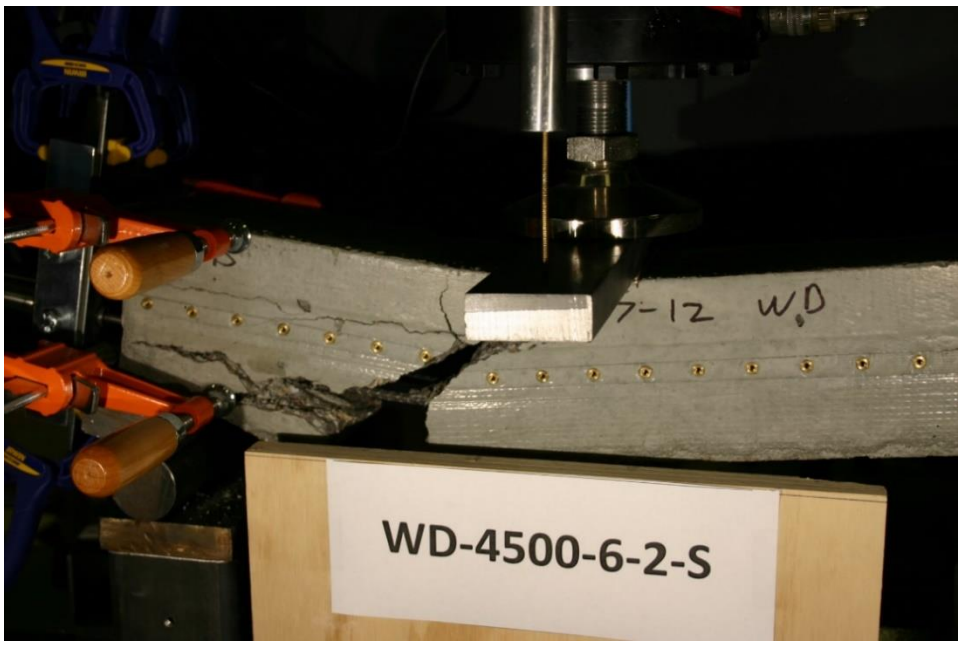


Figure 143 Picture of Failed Prism WD-4500-6-2-S

Beam Identification	WE-4500-6-1-L
Wire Type:	WE
Embedment Length:	20 in
Release Strength:	4500 psi
Slump:	6 in

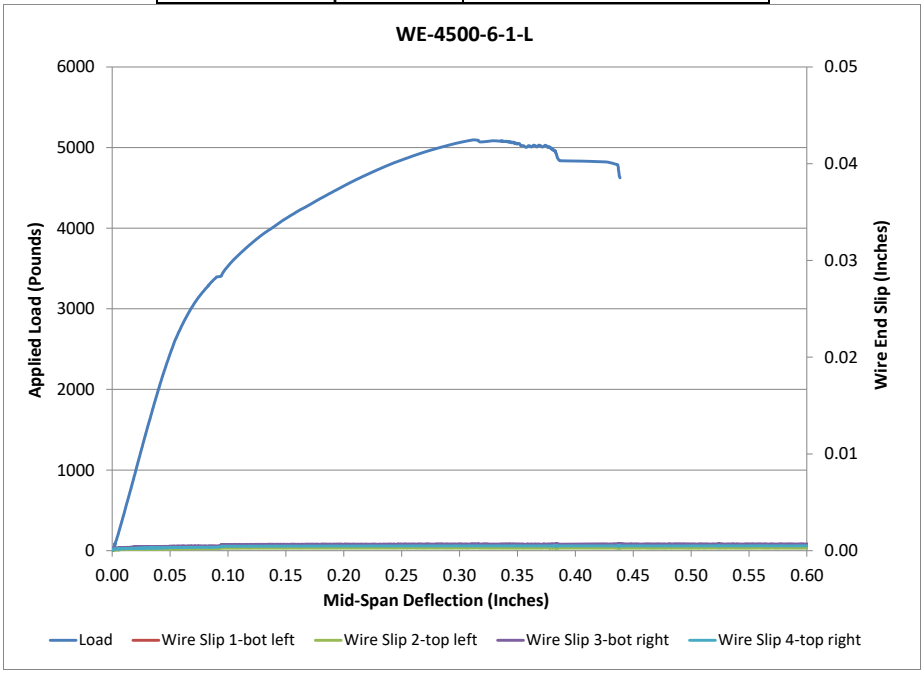


Figure 144 Load Deflection and Wire End Slip WE-4500-6-1-L



Figure 145 Picture of Failed Prism WE-4500-6-1-L

Beam Identification	WE-4500-6-1-S
Wire Type:	WE
Embedment Length:	13 in
Release Strength:	4500 psi
Slump:	6 in

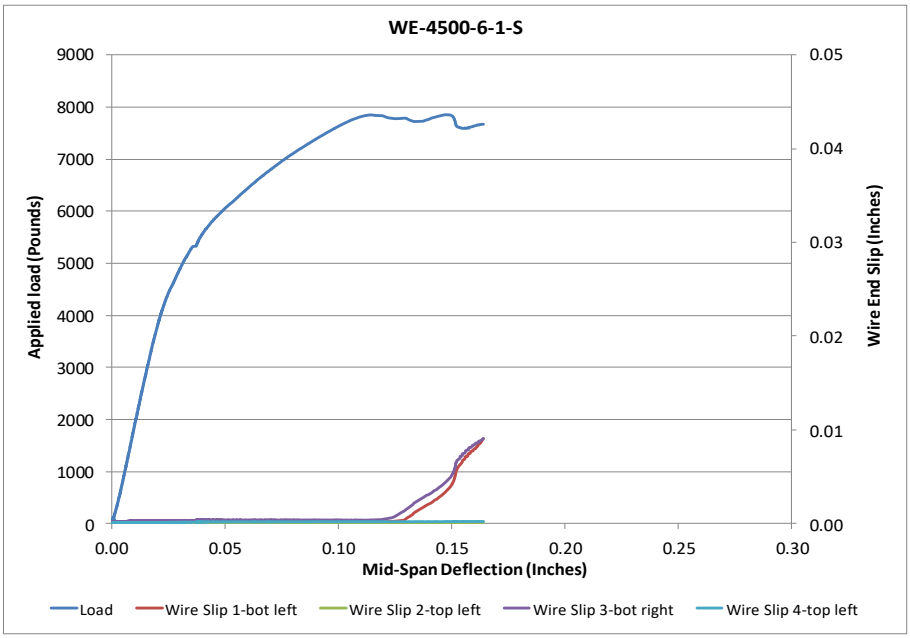


Figure 146 Load Deflection and Wire End Slip WE-4500-6-1-S



Figure 147 Picture of Failed Prism WE-4500-6-1-S

Beam Identification	WE-4500-6-2-L
Wire Type:	WE
Embedment Length:	16.5 in
Release Strength:	4500 psi
Slump:	6 in

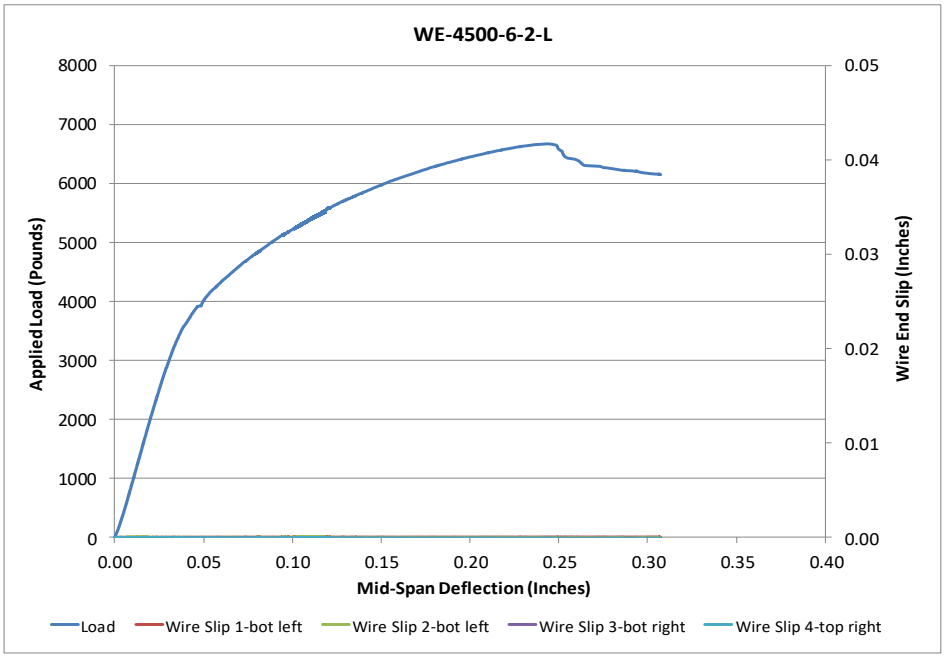


Figure 148 Load Deflection and Wire End Slip WE-4500-6-2-L



Figure 149 Picture of Failed Prism WE-4500-6-2-L

Beam Identification	WE-4500-6-2-S
Wire Type:	WE
Embedment Length:	9.5 in
Release Strength:	4500 psi
Slump:	6 in

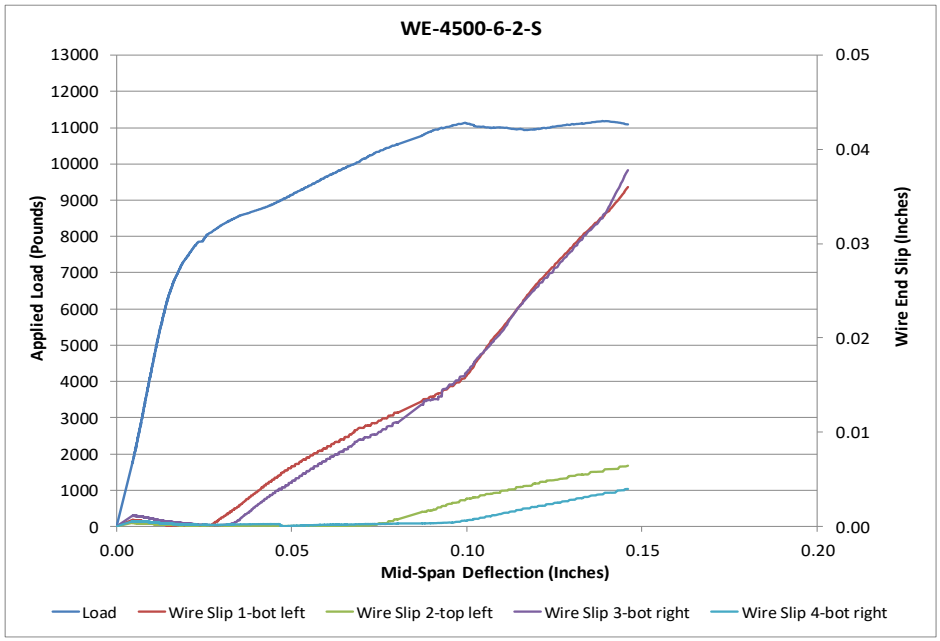


Figure 150 Load Deflection and Wire End Slip WE-4500-6-2-S



Figure 151 Picture of Failed Prism WE-4500-6-2-S

Beam Identification	WF-4500-6-1-L
Wire Type:	WF
Embedment Length:	20 in
Release Strength:	4500 psi
Slump:	6 in

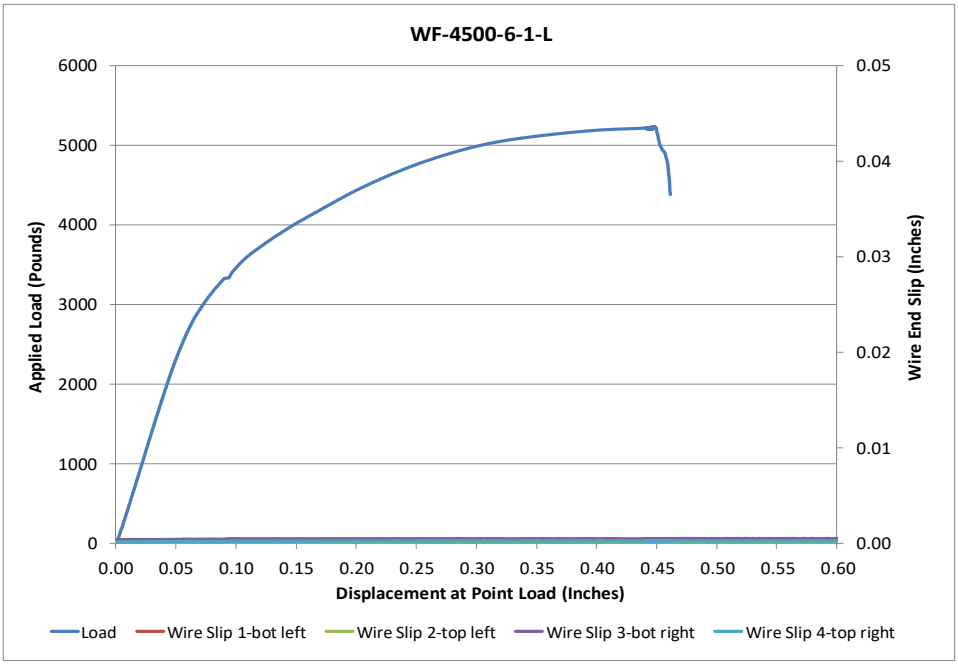


Figure 152 Load Deflection and Wire End Slip WF-4500-6-1-L

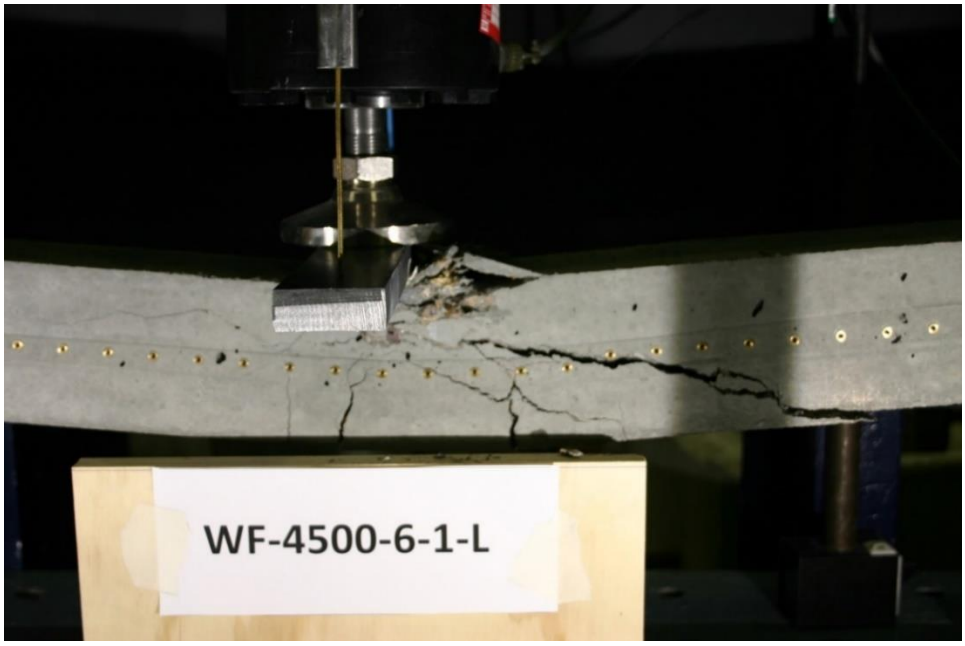


Figure 153 Picture of Failed Prism WF-4500-6-1-L

Beam Identification	WF-4500-6-1-S
Wire Type:	WF
Embedment Length:	13 in
Release Strength:	4500 psi
Slump:	6 in

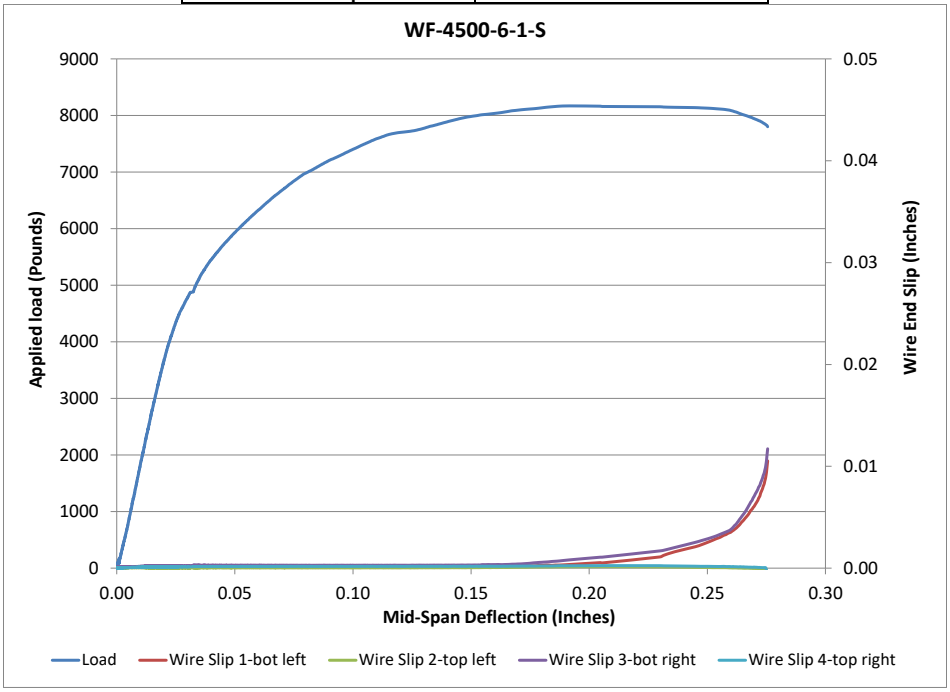


Figure 154 Load Deflection and Wire End Slip WF-4500-6-1-S



Figure 155 Picture of Failed Prism WF-4500-6-1-S

Beam Identification	WF-4500-6-2-L
Wire Type:	WF
Embedment Length:	16.5 in
Release Strength:	4500 psi
Slump:	6 in

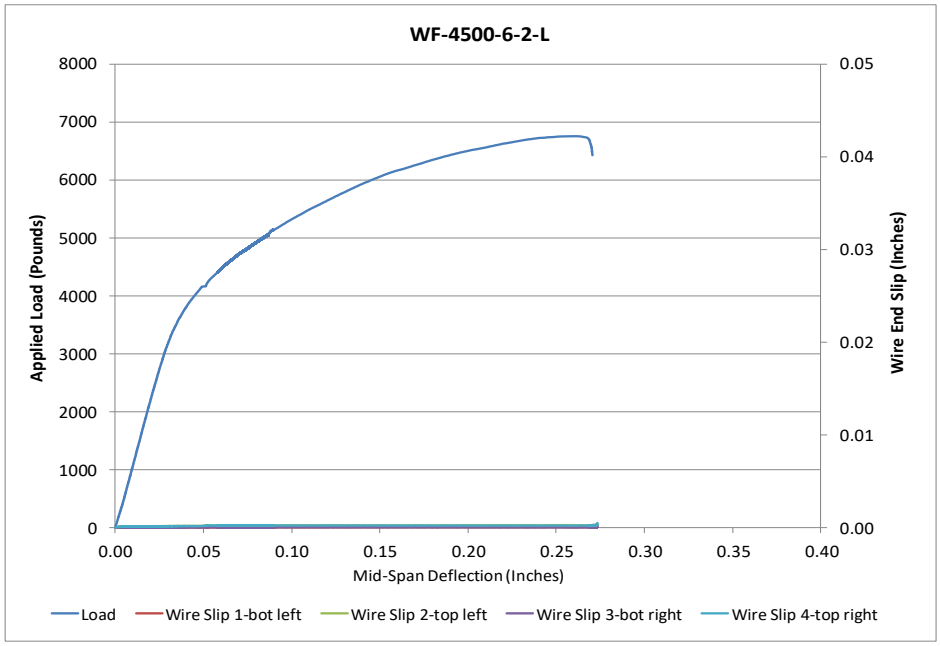


Figure 156 Load Deflection and Wire End Slip WF-4500-6-2-L

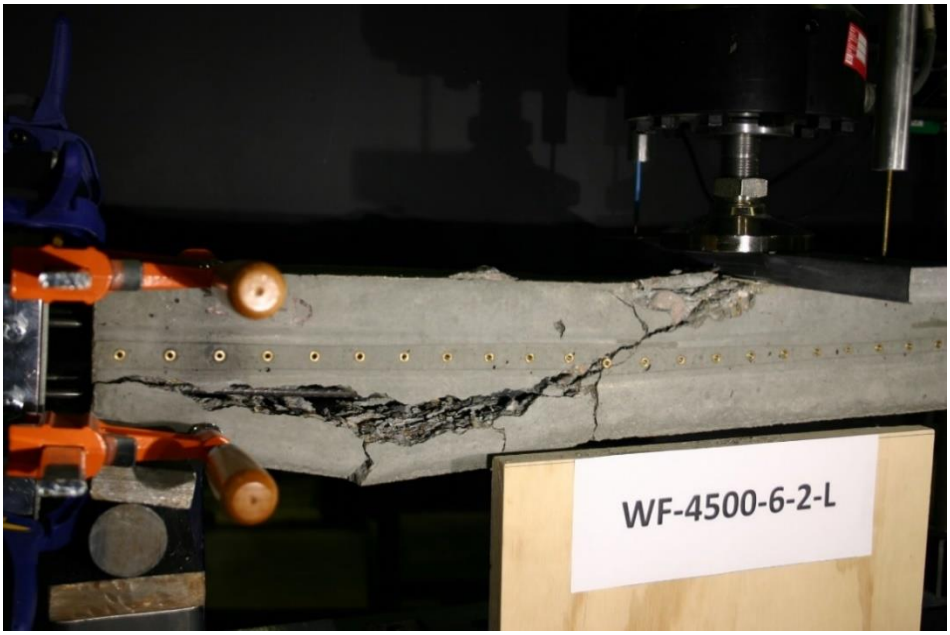


Figure 157 Picture of Failed Prism WF-4500-6-2-L

Beam Identification	WF-4500-6-2-S
Wire Type:	WF
Embedment Length:	9.5 in
Release Strength:	4500 psi
Slump:	6 in

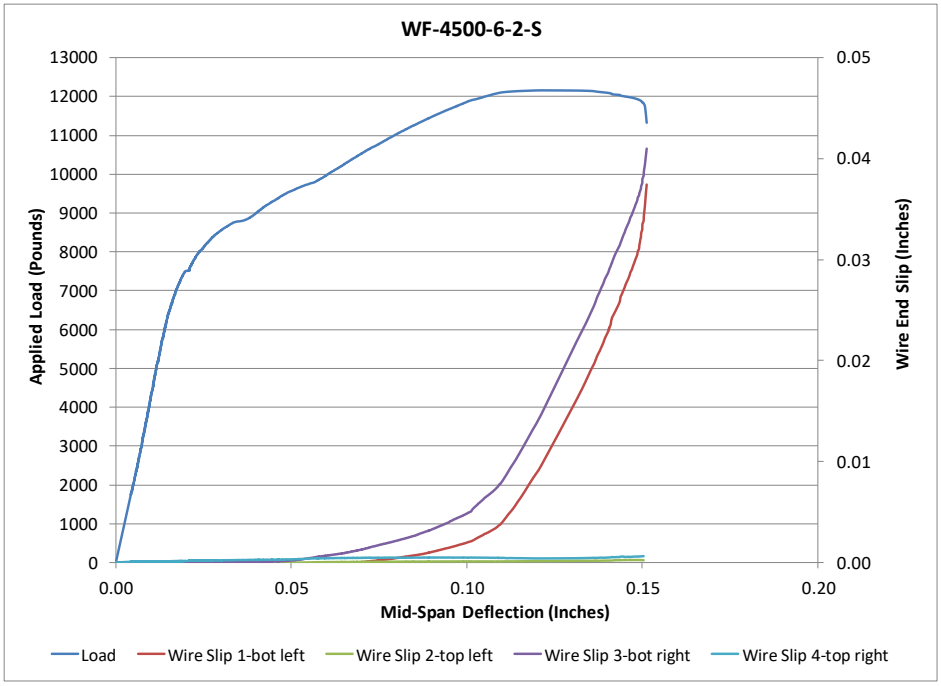


Figure 158 Load Deflection and Wire End Slip WF-4500-6-2-S



Figure 159 Picture of Failed Prism WF-4500-6-2-S

Beam Identification	WG-4500-6-1-L
Wire Type:	WG
Embedment Length:	20 in
Release Strength:	4500 psi
Slump:	6 in

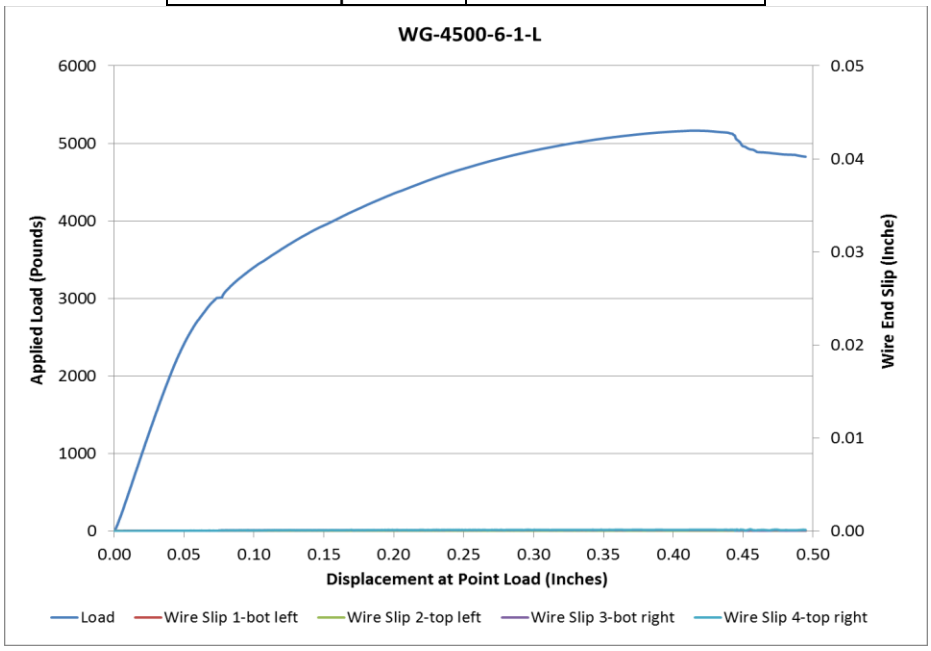


Figure 160 Load Deflection and Wire End Slip WG-4500-6-1-L

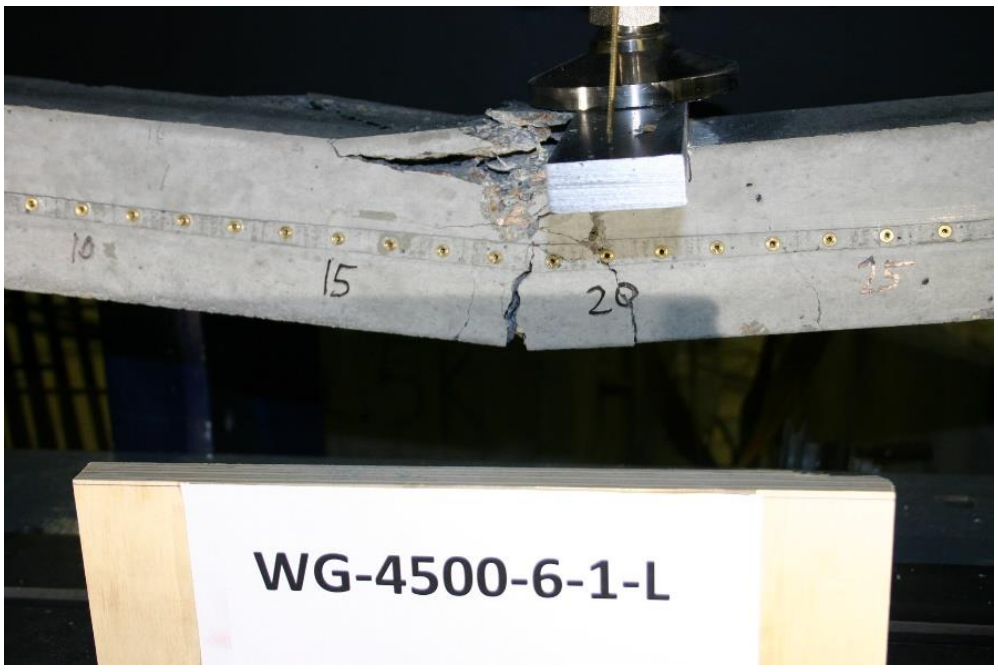


Figure 161 Picture of Failed Prism WG-4500-6-1-L

Beam Identification	WG-4500-6-1-S
Wire Type:	WG
Embedment Length:	13 in
Release Strength:	4500 psi
Slump:	6 in

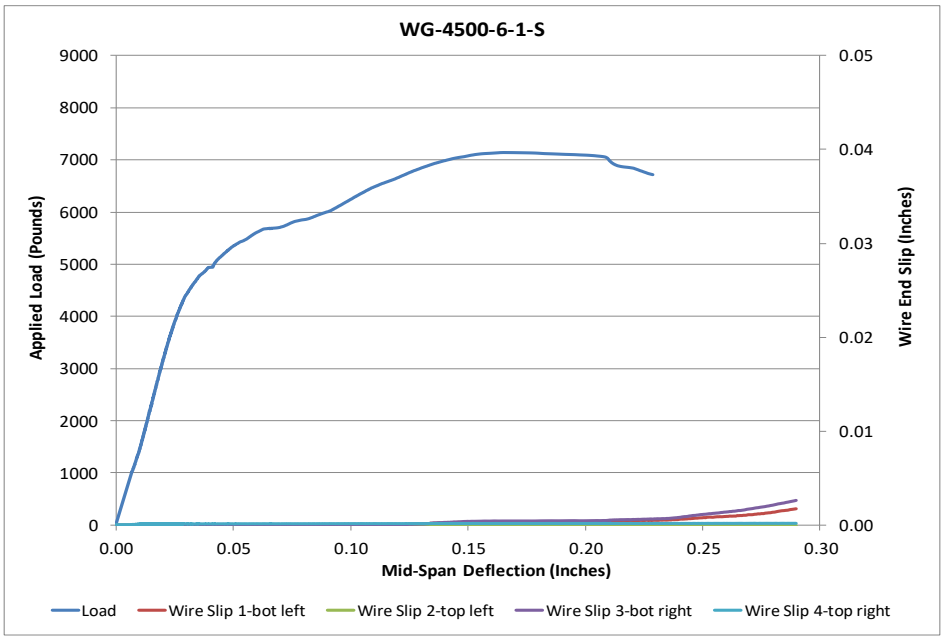


Figure 162 Load Deflection and Wire End Slip WG-4500-6-1-S

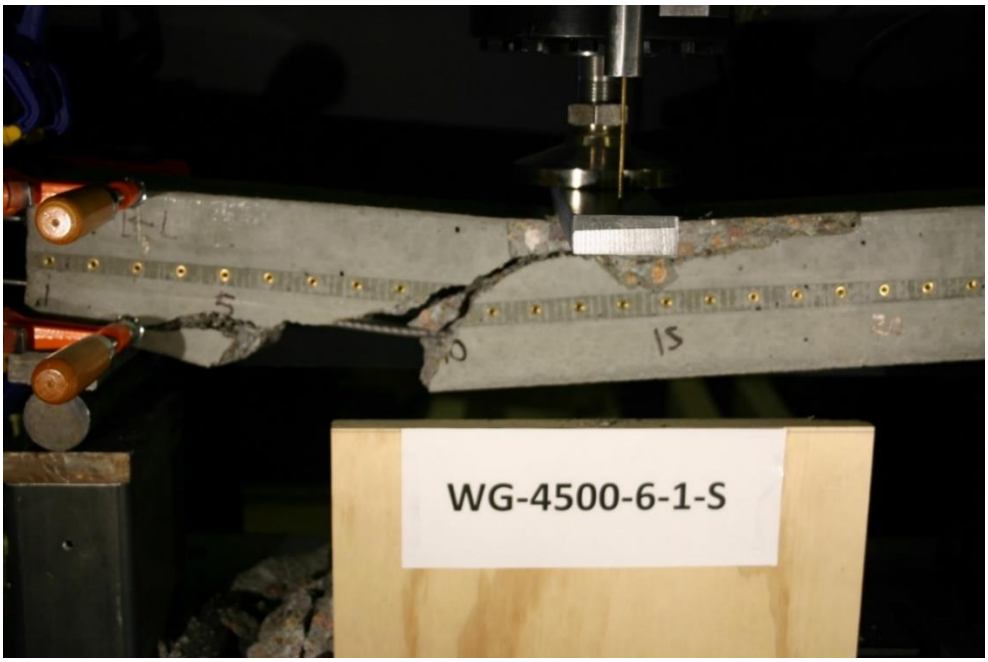


Figure 163 Picture of Failed Prism WG-4500-6-1-S

Beam Identification	WG-4500-6-2-L
Wire Type:	WG
Embedment Length:	16.5 in
Release Strength:	4500 psi
Slump:	6 in

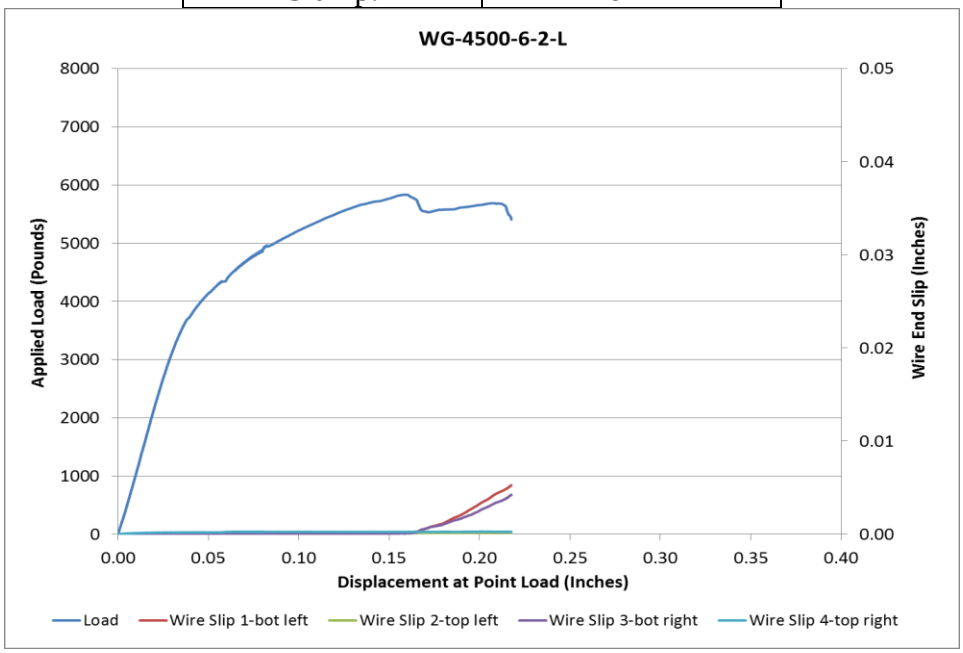


Figure 164 Load Deflection and Wire End Slip WG-4500-6-2-L

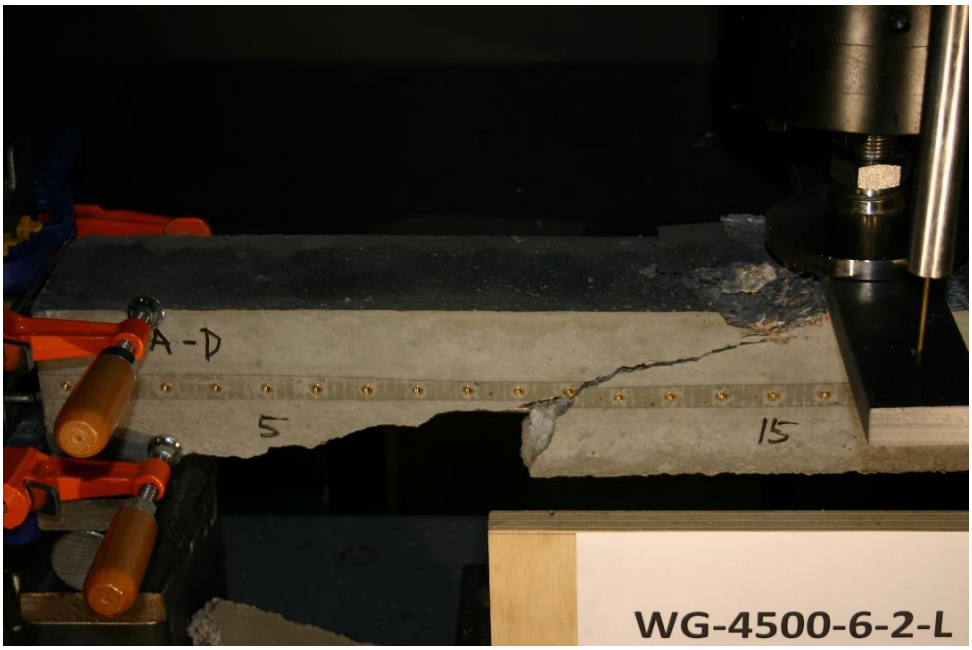


Figure 165 Picture of Failed Prism WG-4500-6-2-L

Beam Identification	WG-4500-6-2-S
Wire Type:	WG
Embedment Length:	9.5 in
Release Strength:	4500 psi
Slump:	6 in

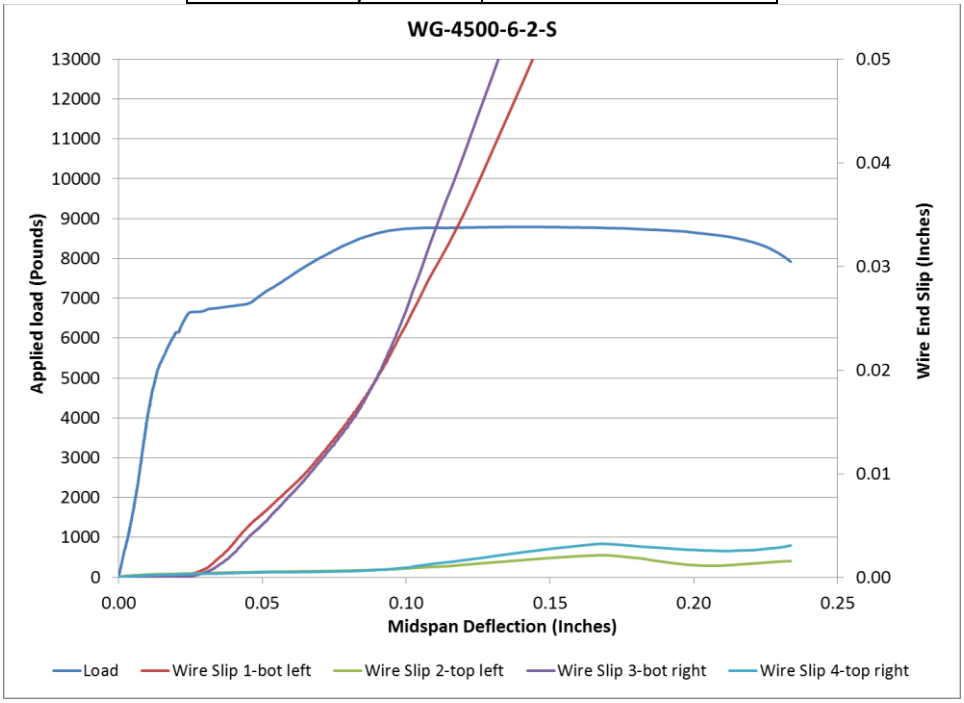


Figure 166 Load Deflection and Wire End Slip WG-4500-6-2-S

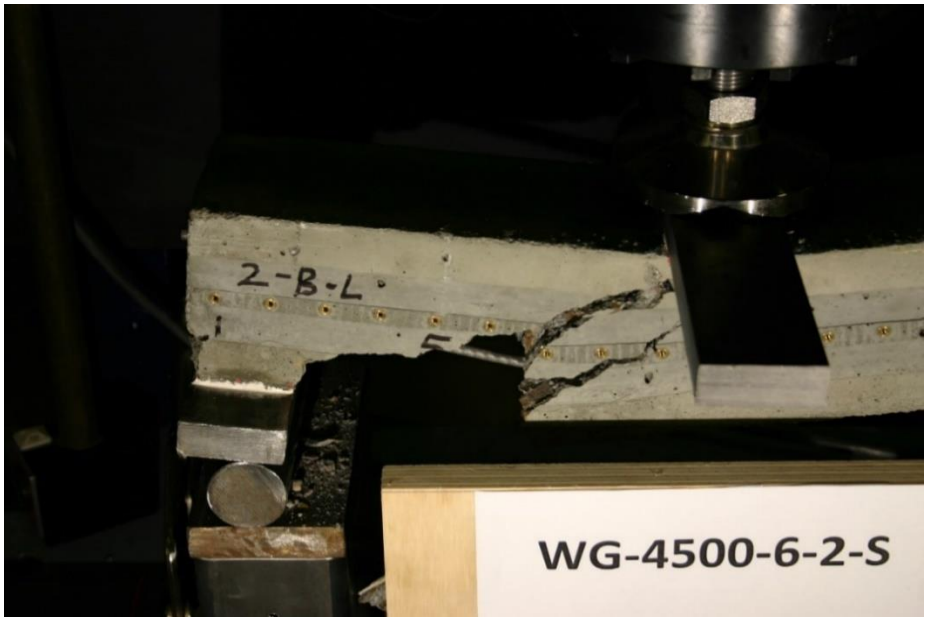


Figure 167 Picture of Failed Prism WG-4500-6-2-S

Beam Identification	WH-4500-6-1-L
Wire Type:	WH
Embedment Length:	20 in
Release Strength:	4500 psi
Slump:	6 in

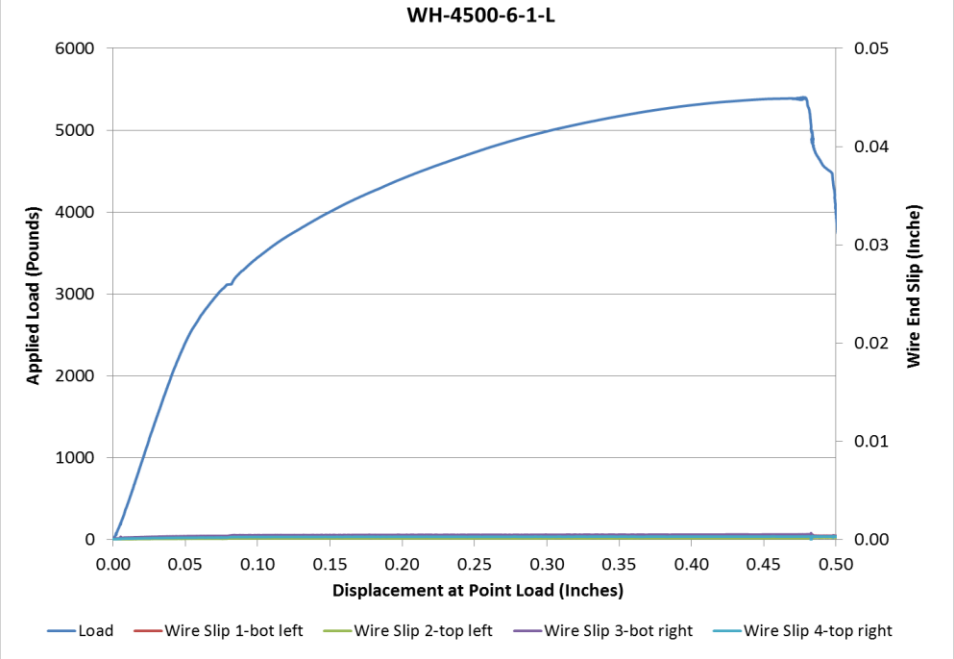


Figure 168 Load Deflection and Wire End Slip WH-4500-6-1-L

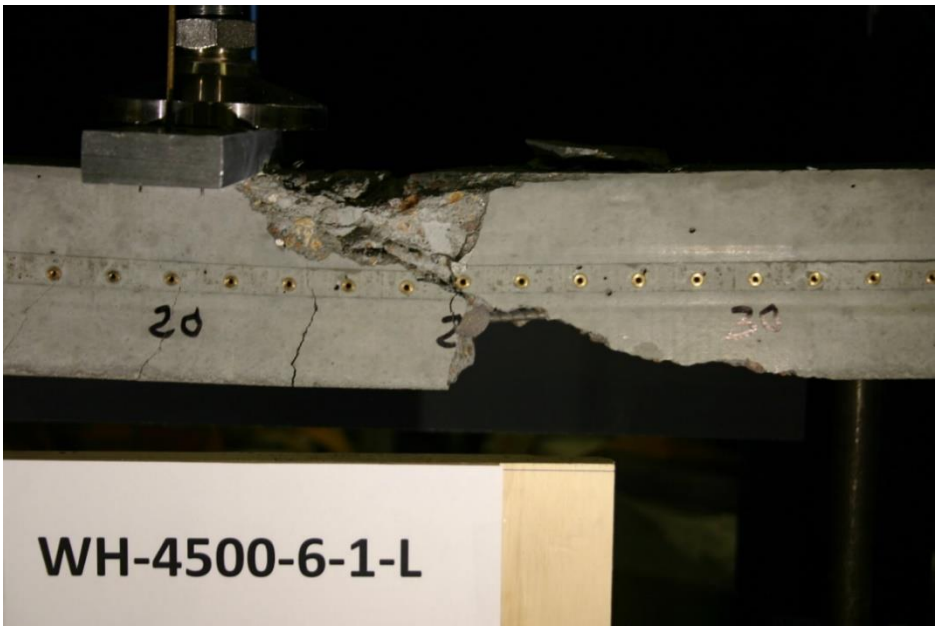


Figure 169 Picture of Failed Prism WH-4500-6-1-L

Beam Identification	WH-4500-6-1-S
Wire Type:	WH
Embedment Length:	13 in
Release Strength:	4500 psi
Slump:	6 in

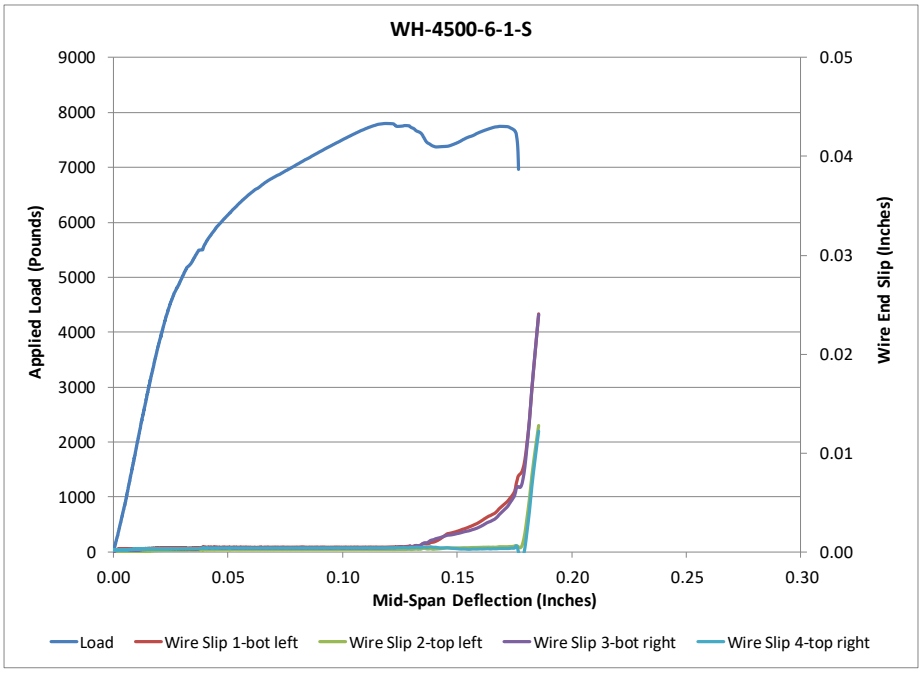


Figure 170 Load Deflection and Wire End Slip WH-4500-6-1-S



Figure 171 Picture of Failed Prism WH-4500-6-1-S

Beam Identification	WH-4500-6-2-L
Wire Type:	WH
Embedment Length:	16.5 in
Release Strength:	4500 psi
Slump:	6 in

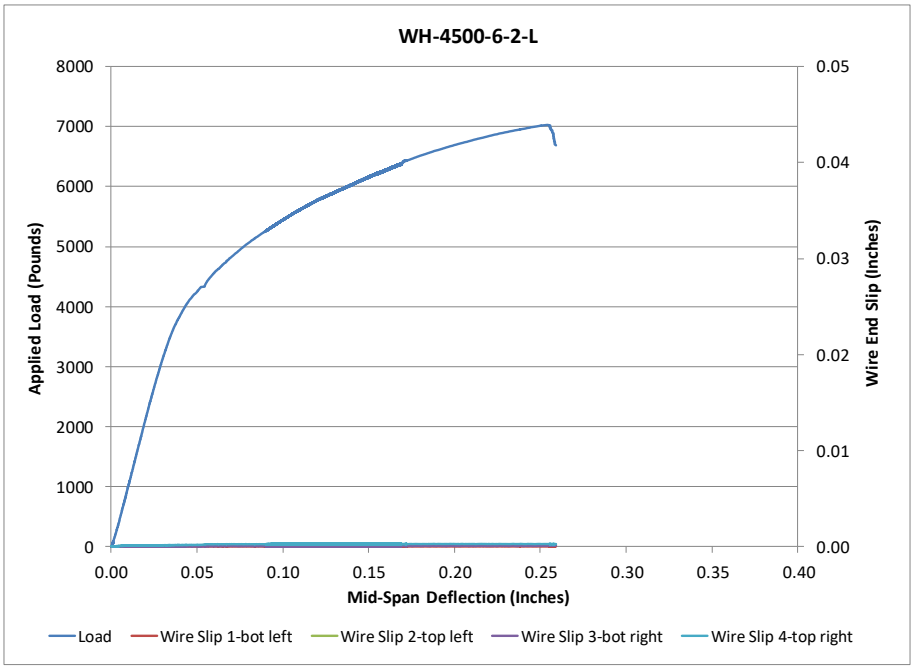


Figure 172 Load Deflection and Wire End Slip WH-4500-6-2-L



Figure 173 Picture of Failed Prism WH-4500-6-2-L

Beam Identification	WH-4500-6-2-S
Wire Type:	WH
Embedment Length:	9.5 in
Release Strength:	4500 psi
Slump:	6 in

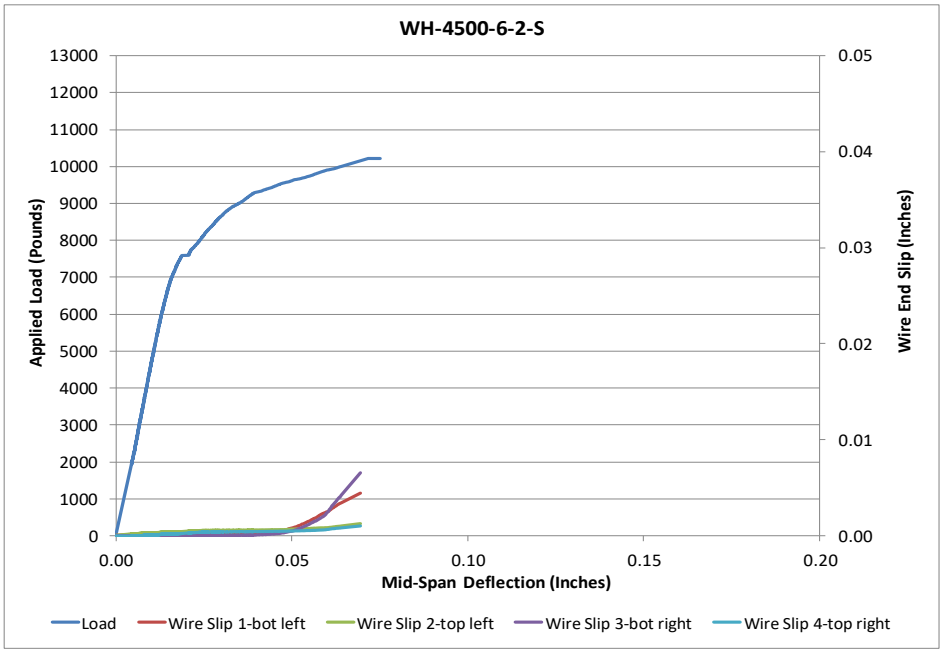


Figure 174 Load Deflection and Wire End Slip WH-4500-6-2-S

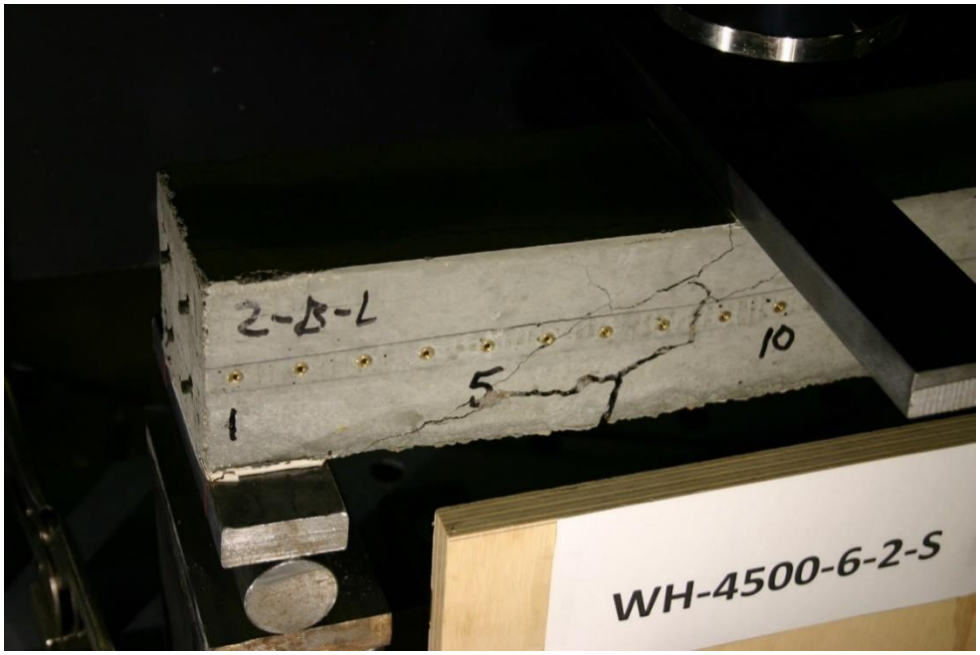


Figure 175 Picture of Failed Prism WH-4500-6-2-S

Beam Identification	WI-4500-6-1-L
Wire Type:	WI
Embedment Length:	20 in
Release Strength:	4500 psi
Slump:	6 in

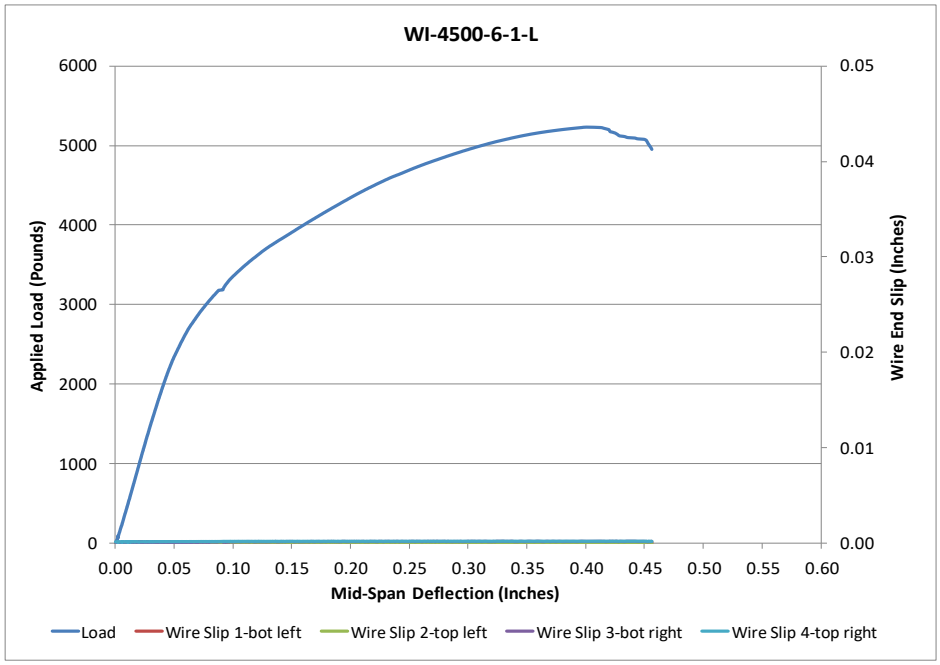


Figure 176 Load Deflection and Wire End Slip WI-4500-6-1-L



Figure 177 Picture of Failed Prism WI-4500-6-1-L

Beam Identification	WI-4500-6-1-S
Wire Type:	WI
Embedment Length:	13 in
Release Strength:	4500 psi
Slump:	6 in

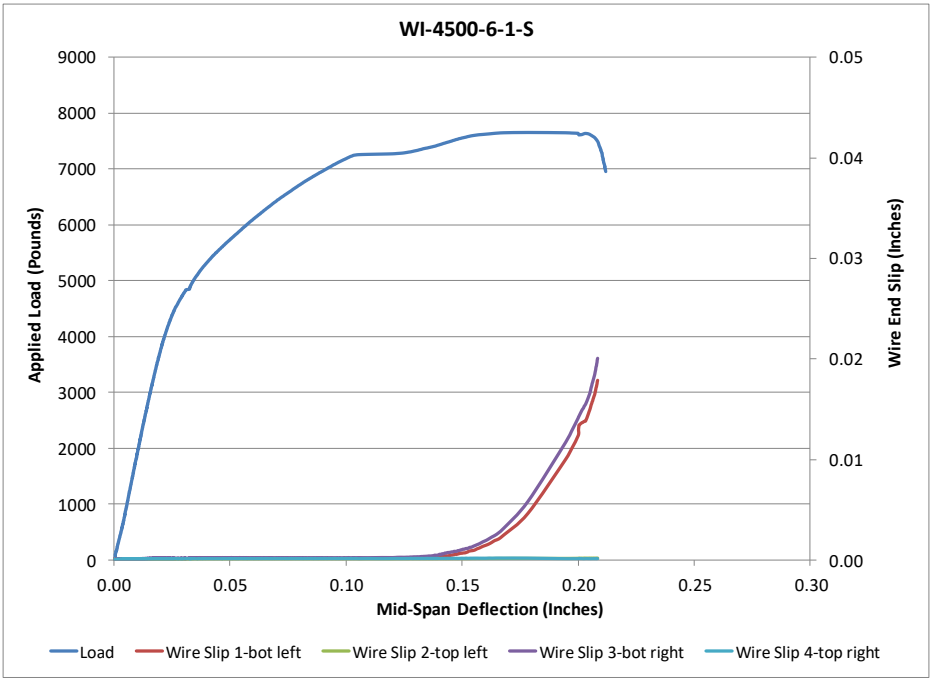


Figure 178 Load Deflection and Wire End Slip WI-4500-6-1-S

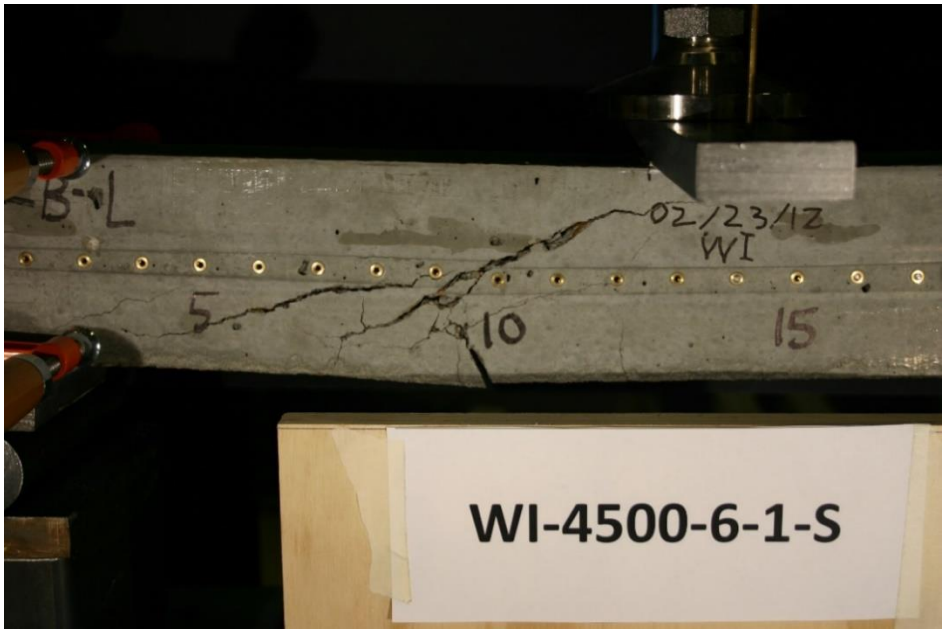


Figure 179 Picture of Failed Prism WI-4500-6-1-S

Beam Identification	WI-4500-6-2-L
Wire Type:	WI
Embedment Length:	16.5 in
Release Strength:	4500 psi
Slump:	6 in

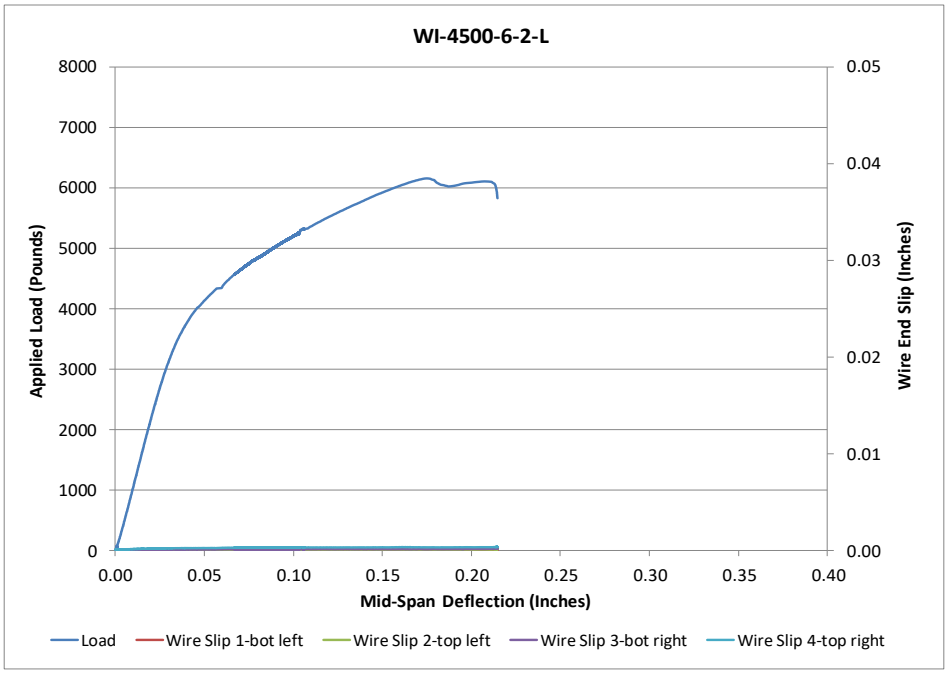


Figure 180 Load Deflection and Wire End Slip WI-4500-6-2-L



Figure 181 Picture of Failed Prism WI-4500-6-2-L

Beam Identification	WI-4500-6-2-S
Wire Type:	WI
Embedment Length:	9.5 in
Release Strength:	4500 psi
Slump:	6 in

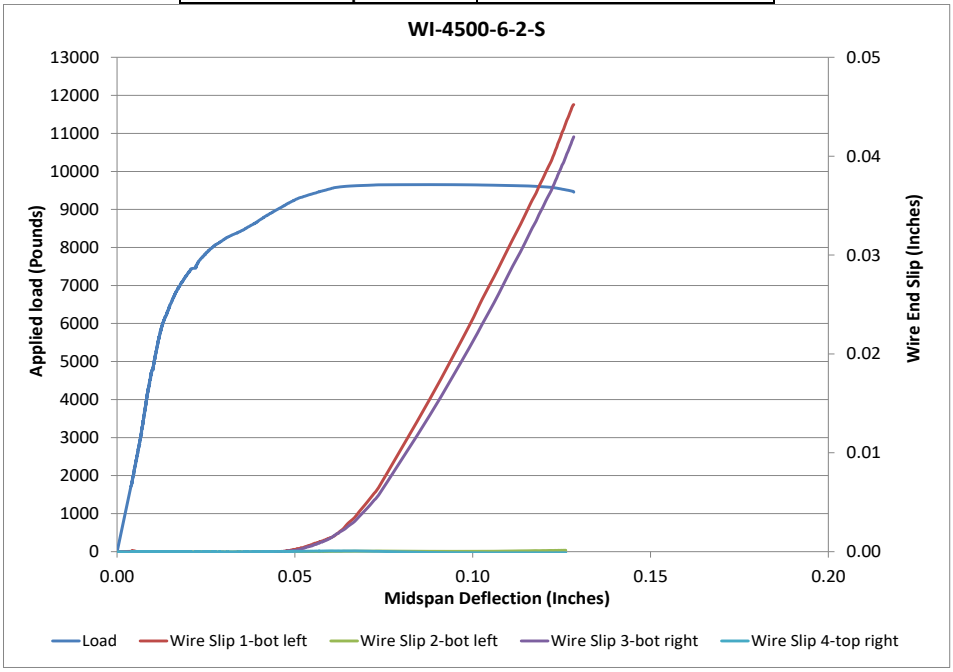


Figure 182 Load Deflection and Wire End Slip WI-4500-6-2-S



Figure 183 Picture of Failed Prism WI-4500-6-2-S

Beam Identification	WJ-4500-6-1-L
Wire Type:	WJ
Embedment Length:	20 in
Release Strength:	4500 psi
Slump:	6 in

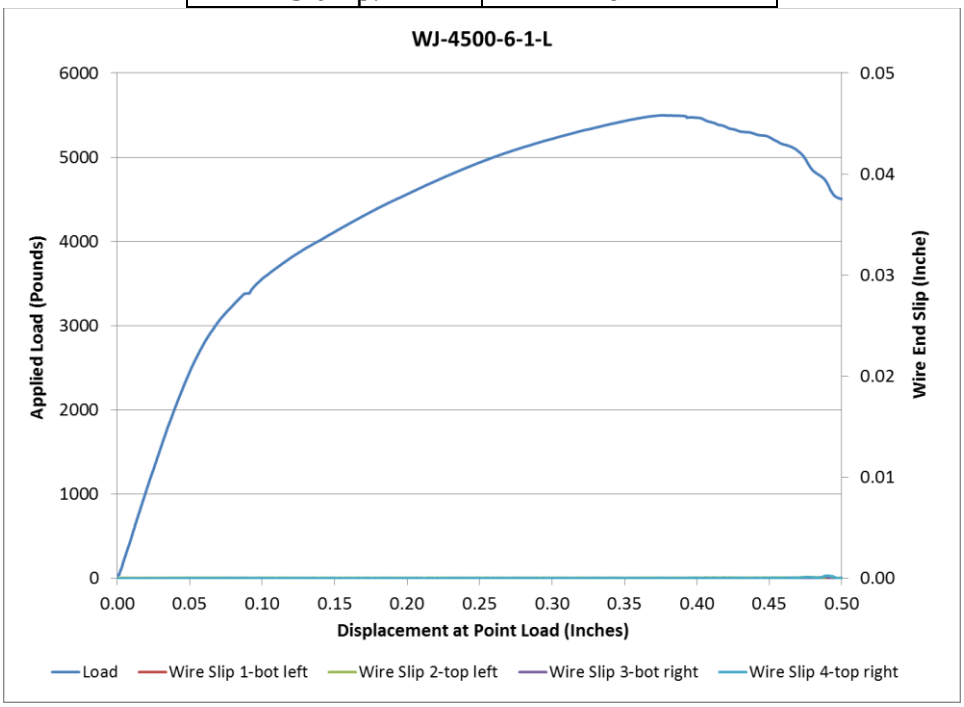


Figure 184 Load Deflection and Wire End Slip WJ-4500-6-1-L

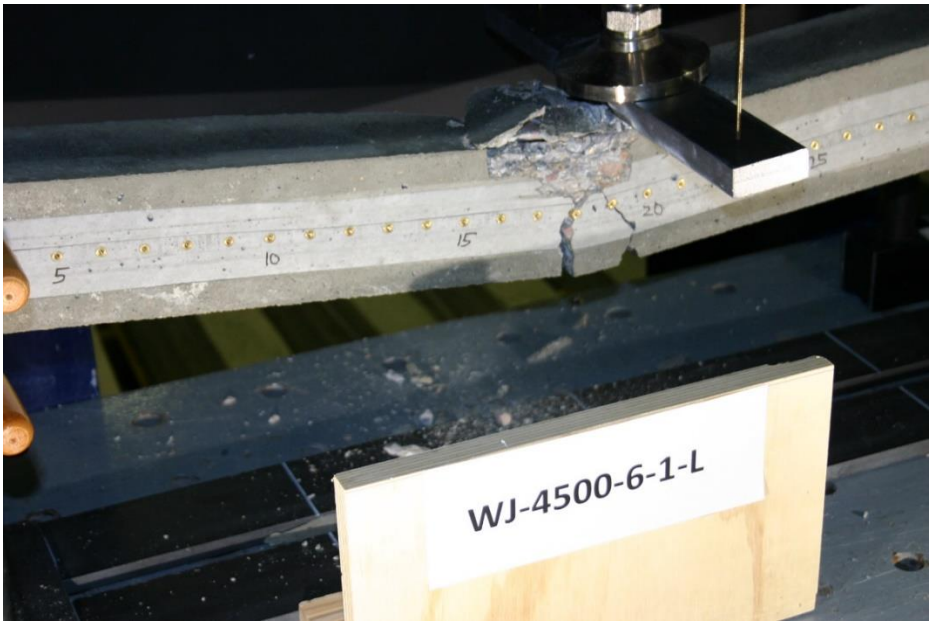


Figure 185 Picture of Failed Prism WJ-4500-6-1-L

Beam Identification	WJ-4500-6-1-S
Wire Type:	WJ
Embedment Length:	13 in
Release Strength:	4500 psi
Slump:	6 in

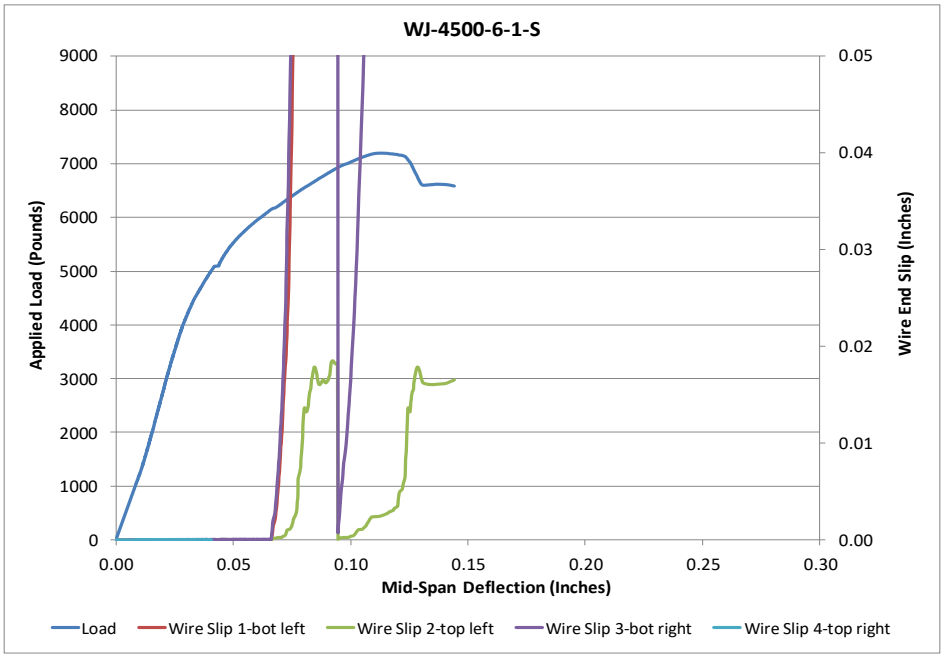


Figure 186 Load Deflection and Wire End Slip WJ-4500-6-1-S



Figure 187 Picture of Failed Prism WJ-4500-6-1-S

Beam Identification	WJ-4500-6-2-L
Wire Type:	WJ
Embedment Length:	16.5 in
Release Strength:	4500 psi
Slump:	6 in

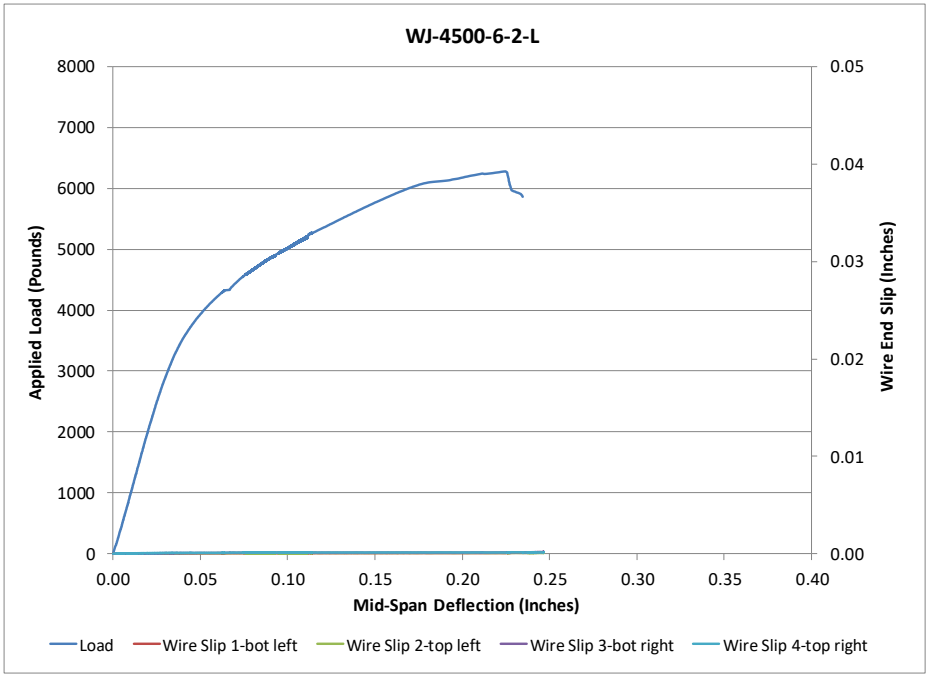


Figure 188 Load Deflection and Wire End Slip WJ-4500-6-2-L

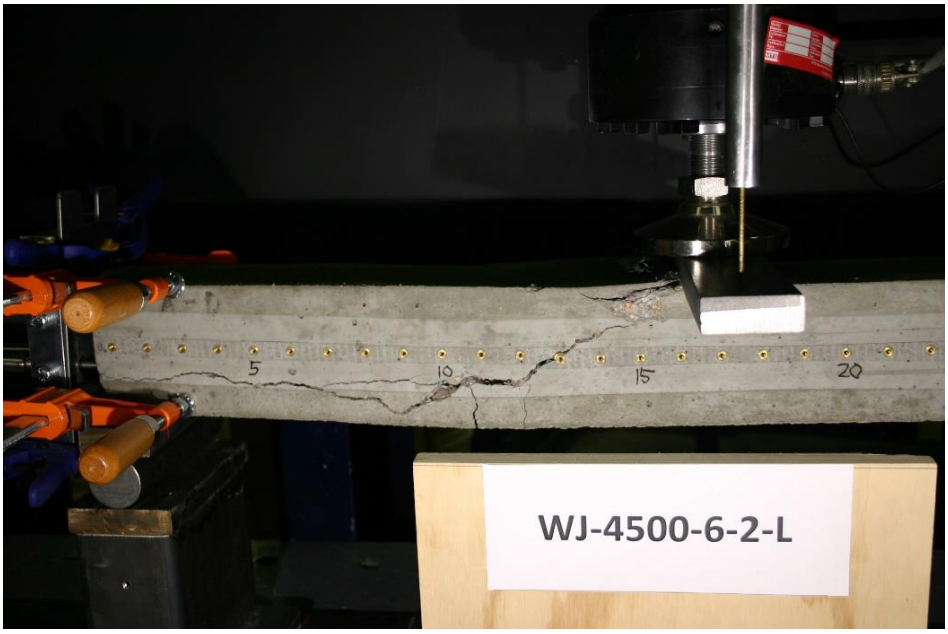


Figure 189 Picture of Failed Prism WJ-4500-6-2-L

Beam Identification	WJ-4500-6-2-S
Wire Type:	WJ
Embedment Length:	9.5 in
Release Strength:	4500 psi
Slump:	6 in

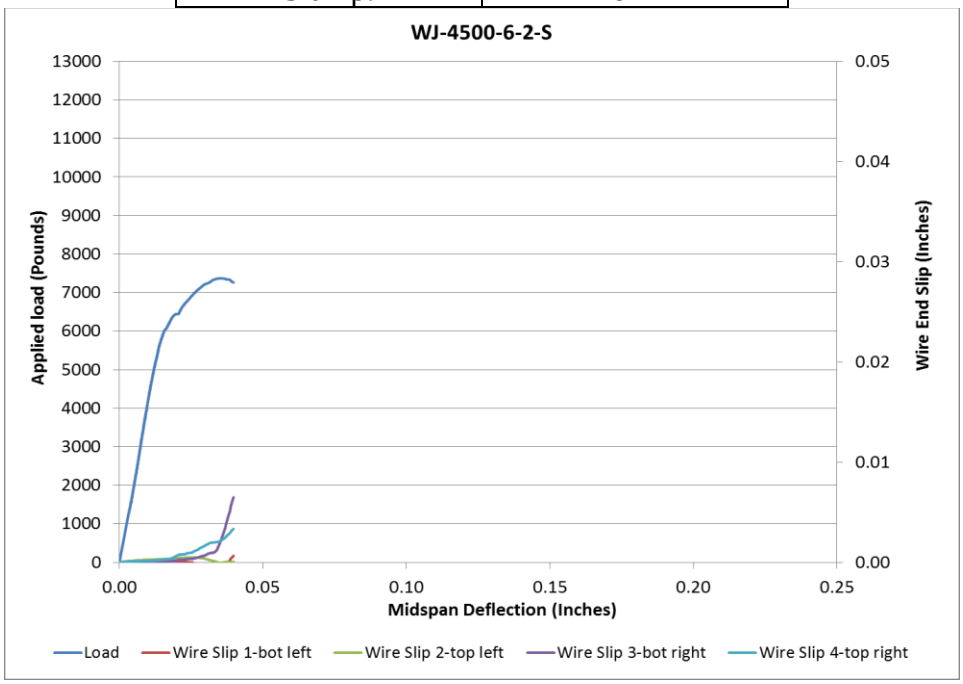


Figure 190 Load Deflection and Wire End Slip WJ-4500-6-2-S

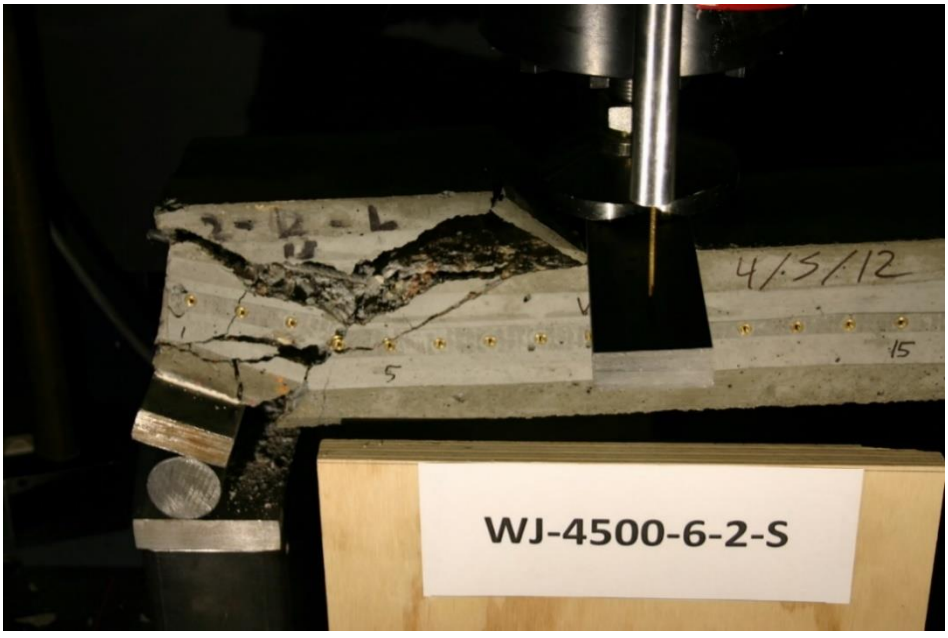


Figure 191 Picture of Failed Prism WJ-4500-6-2-S

Beam Identification	WK-4500-6-1-L
Wire Type:	WK
Embedment Length:	20 in
Release Strength:	4500 psi
Slump:	6 in

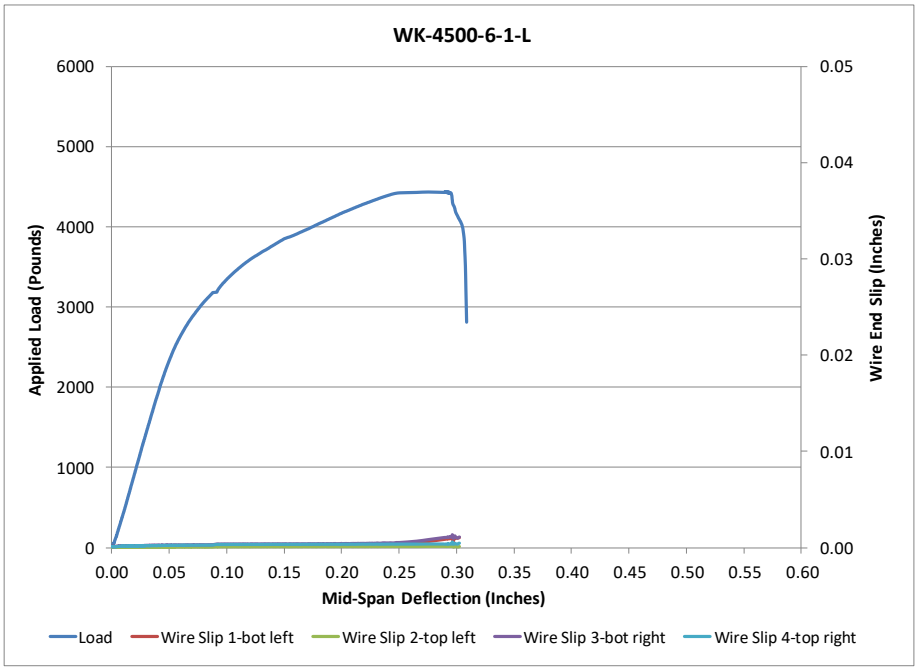


Figure 192 Load Deflection and Wire End Slip WK-4500-6-1-L

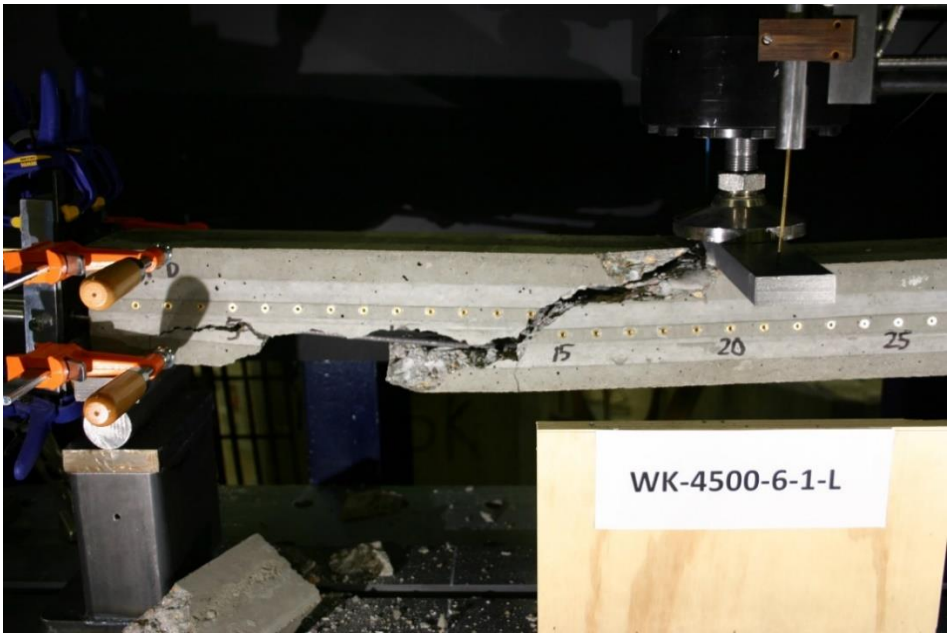


Figure 193 Picture of Failed Prism WK-4500-6-1-L

Beam Identification	WK-4500-6-1-S
Wire Type:	WK
Embedment Length:	13 in
Release Strength:	4500 psi
Slump:	6 in

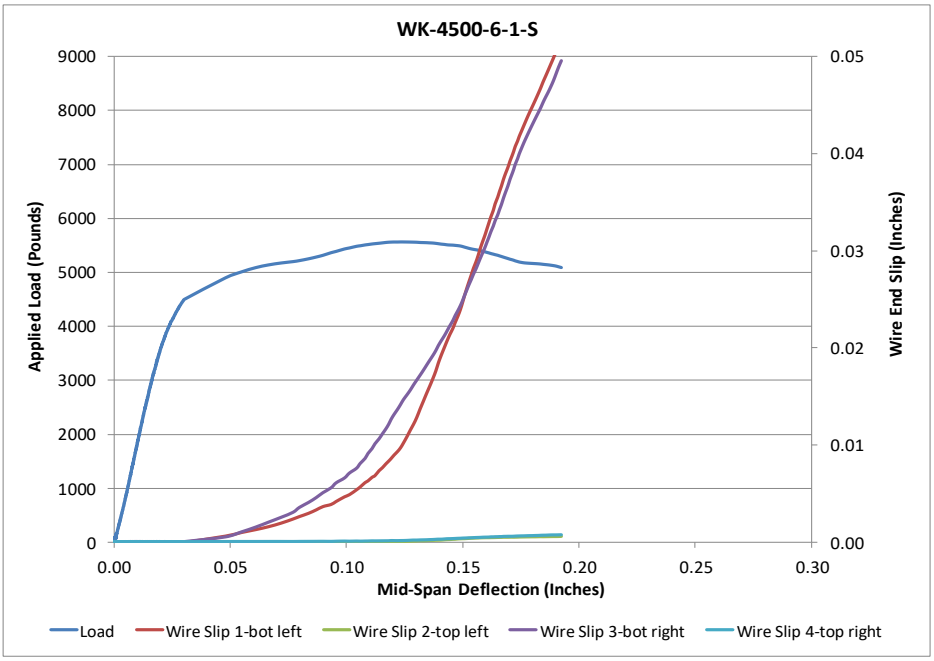


Figure 194 Load Deflection and Wire End Slip WK-4500-6-1-S

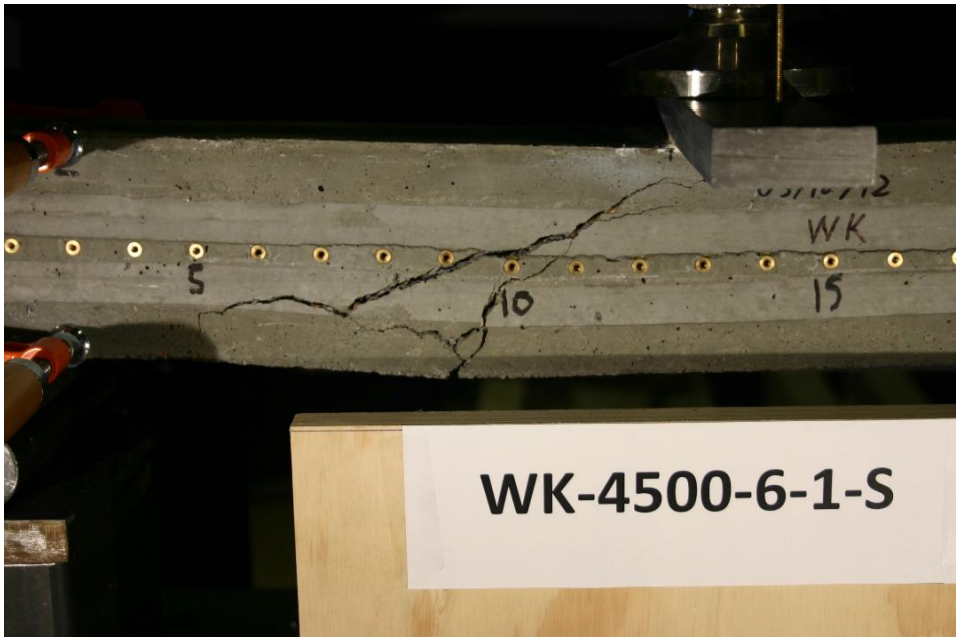


Figure 195 Picture of Failed Prism WK-4500-6-1-S

Beam Identification	WK-4500-6-2-L
Wire Type:	WK
Embedment Length:	16.5 in
Release Strength:	4500 psi
Slump:	6 in

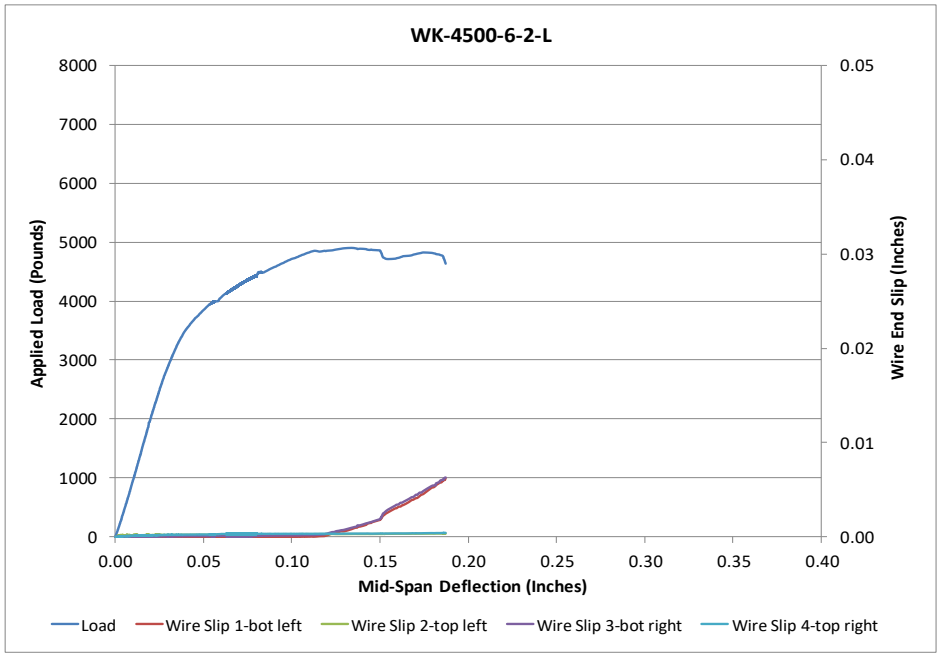


Figure 196 Load Deflection and Wire End Slip WK-4500-6-2-L



Figure 197 Picture of Failed Prism WK-4500-6-2-L

Beam Identification	WK-4500-6-2-S
Wire Type:	WK
Embedment Length:	9.5 in
Release Strength:	4500 psi
Slump:	6 in

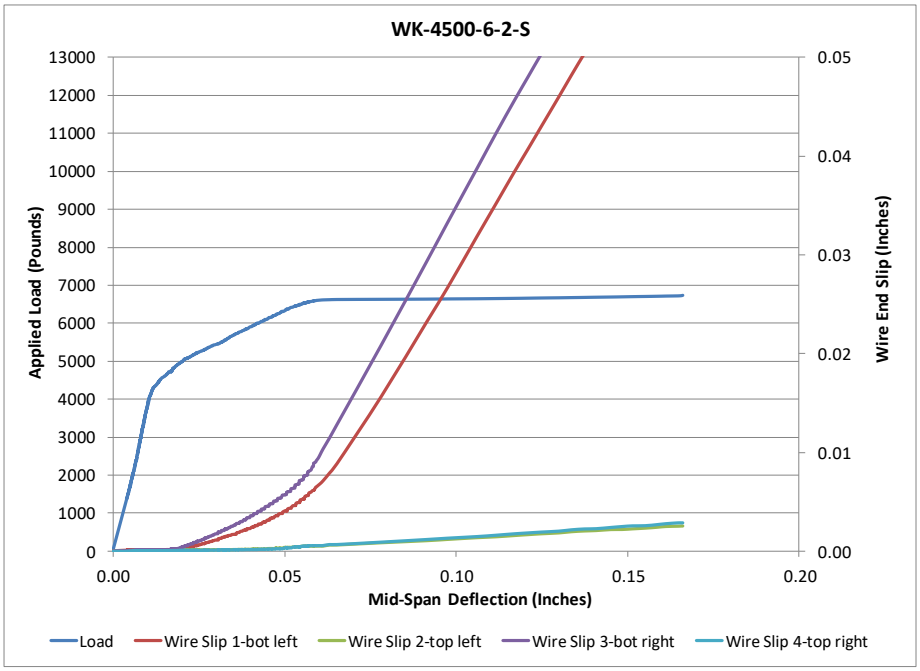


Figure 198 Load Deflection and Wire End Slip WK-4500-6-2-S

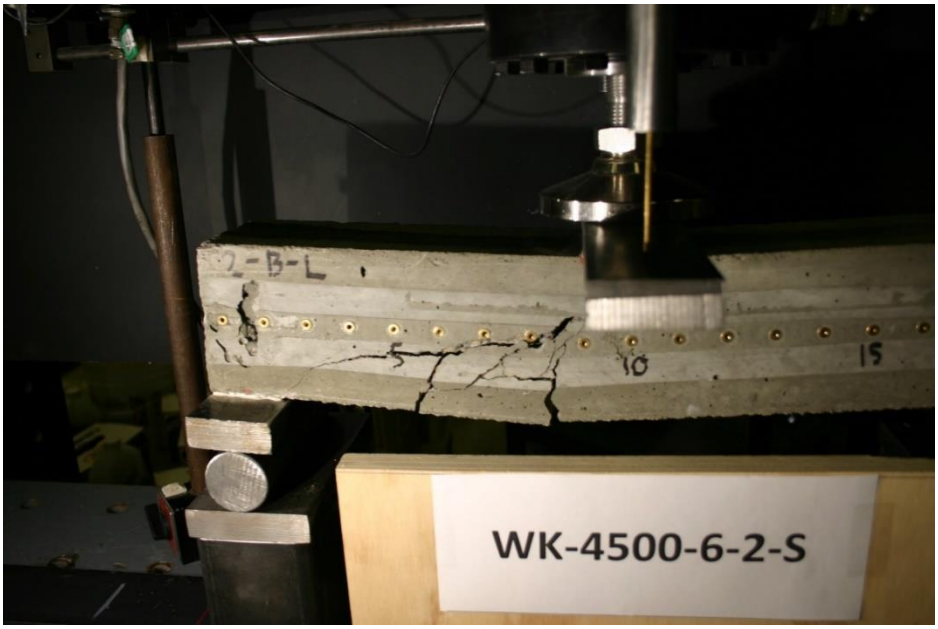


Figure 199 Picture of Failed Prism WK-4500-6-2-S

Beam Identification	WL-4500-6-1-L
Wire Type:	WL
Embedment Length:	20 in
Release Strength:	4500 psi
Slump:	6 in

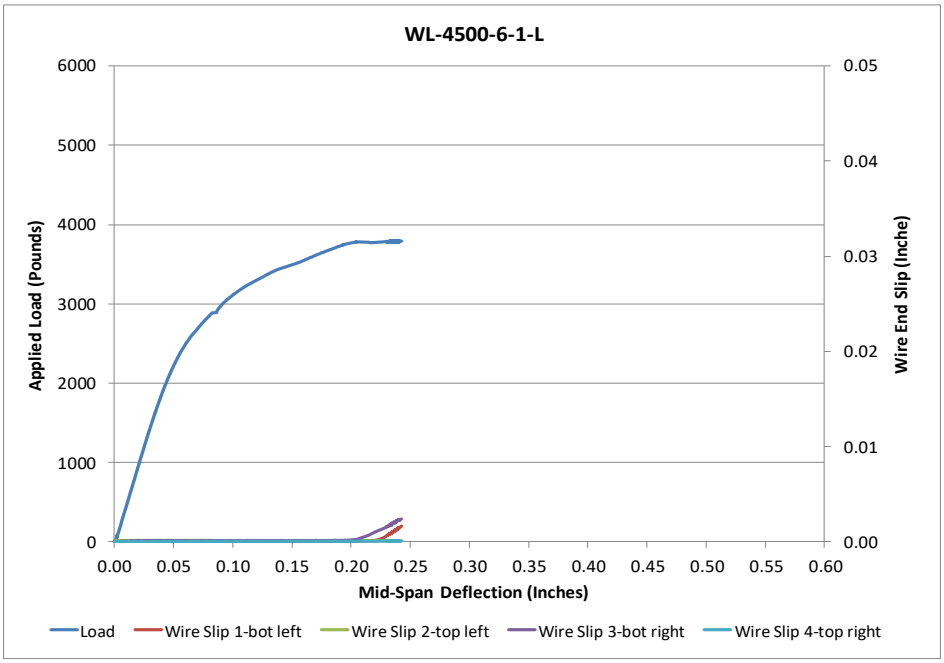


Figure 200 Load Deflection and Wire End Slip WL-4500-6-1-L



Figure 201 Picture of Failed Prism WL-4500-6-1-L

Beam Identification	WL-4500-6-1-S
Wire Type:	WL
Embedment Length:	13 in
Release Strength:	4500 psi
Slump:	6 in

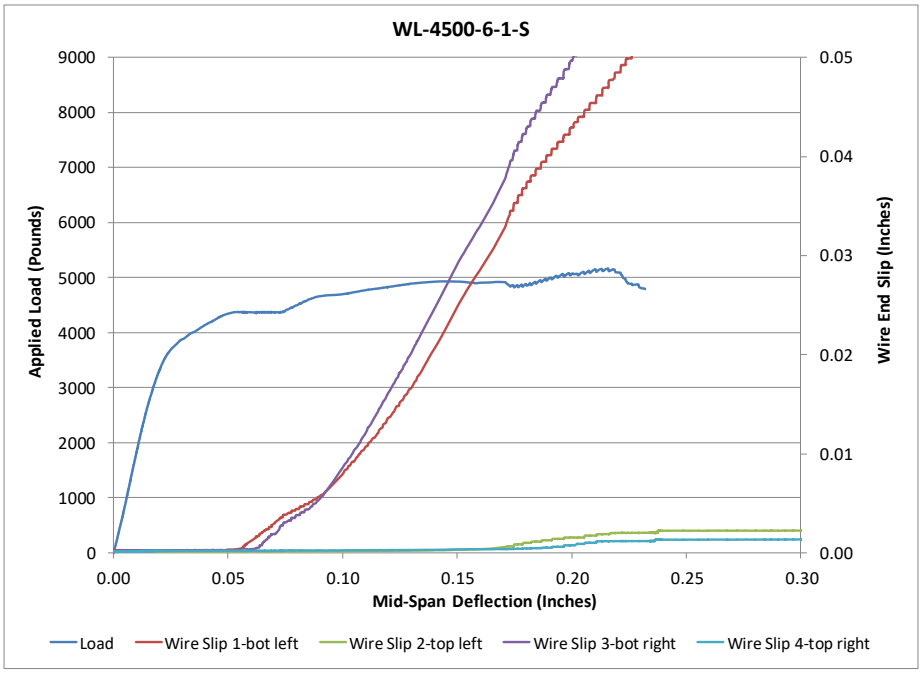


Figure 202 Load Deflection and Wire End Slip WL-4500-6-1-S



Figure 203 Picture of Failed Prism WL-4500-6-1-S

Beam Identification	WL-4500-6-2-L
Wire Type:	WL
Embedment Length:	16.5 in
Release Strength:	4500 psi
Slump:	6 in

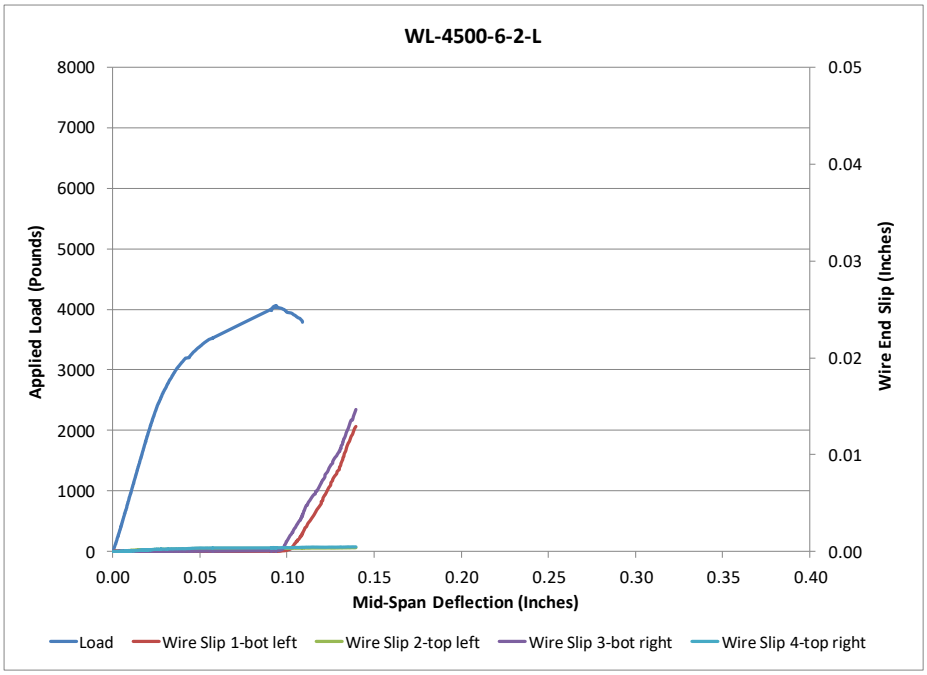


Figure 204 Load Deflection and Wire End Slip WL-4500-6-2-L



Figure 205 Picture of Failed Prism WL-4500-6-2-L

Beam Identification	WL-4500-6-2-S
Wire Type:	WL
Embedment Length:	9.5 in
Release Strength:	4500 psi
Slump:	6 in

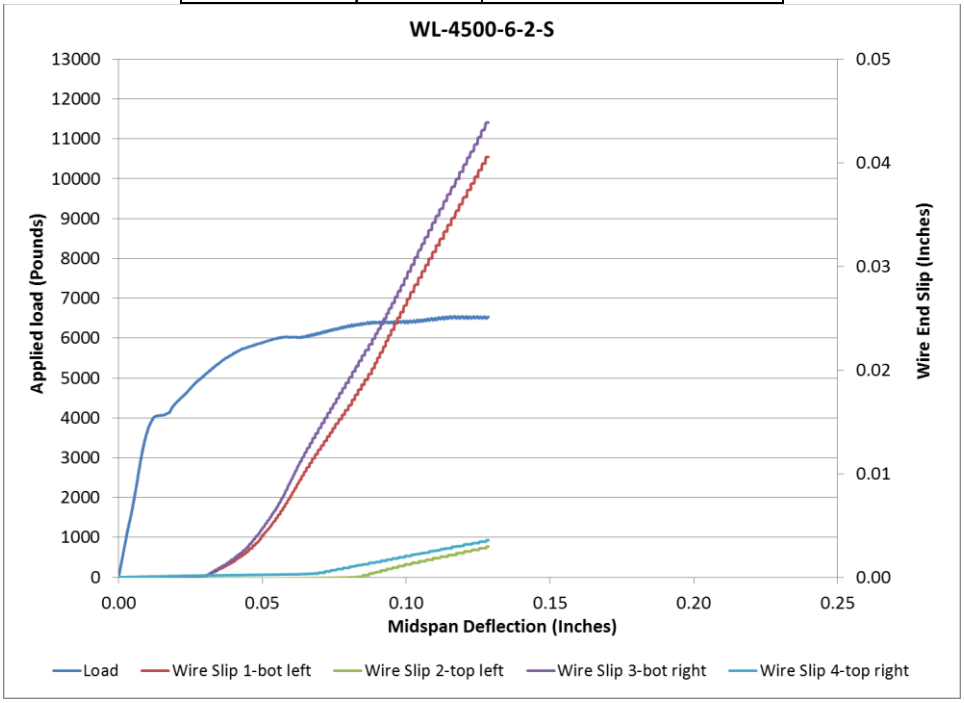


Figure 206 Load Deflection and Wire End Slip WL-4500-6-2-S

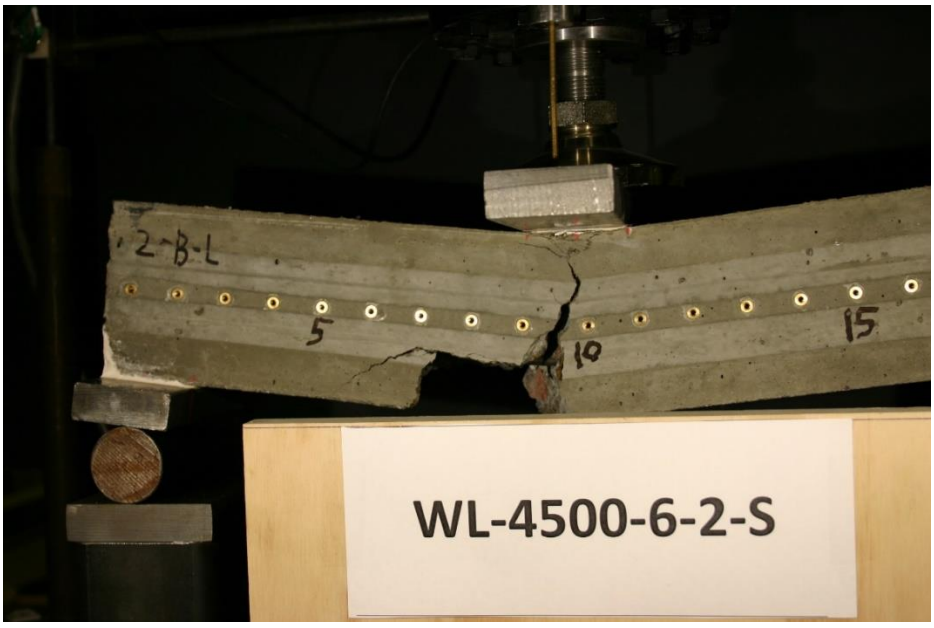


Figure 207 Picture of Failed Prism WL-4500-6-2-S

Beam Identification	WM-4500-6-1-L
Wire Type:	WM
Embedment Length:	20 in
Release Strength:	4500 psi
Slump:	6 in

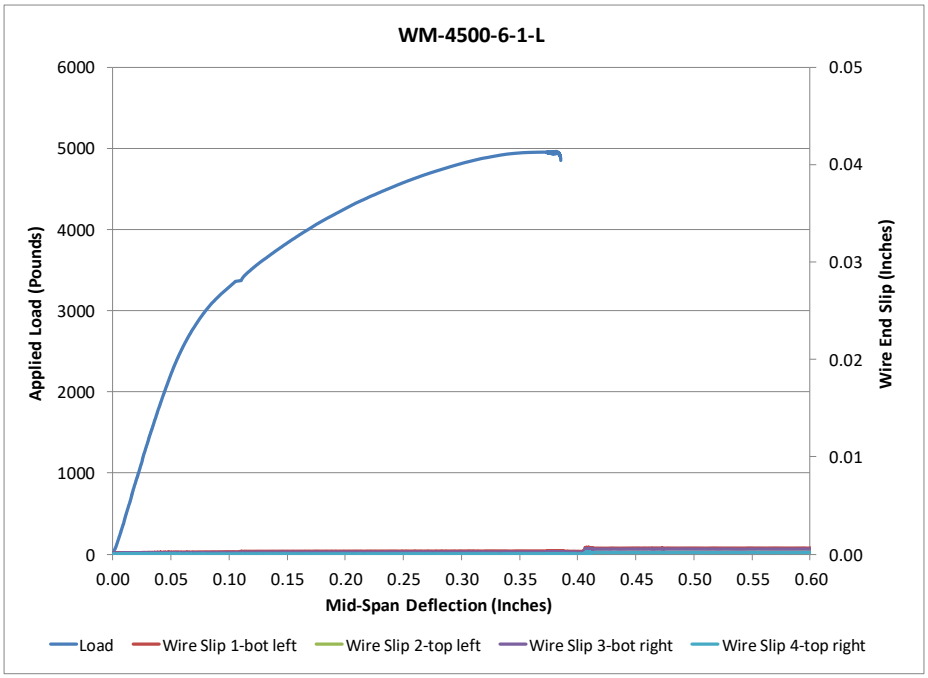


Figure 208 Load Deflection and Wire End Slip WM-4500-6-1-L

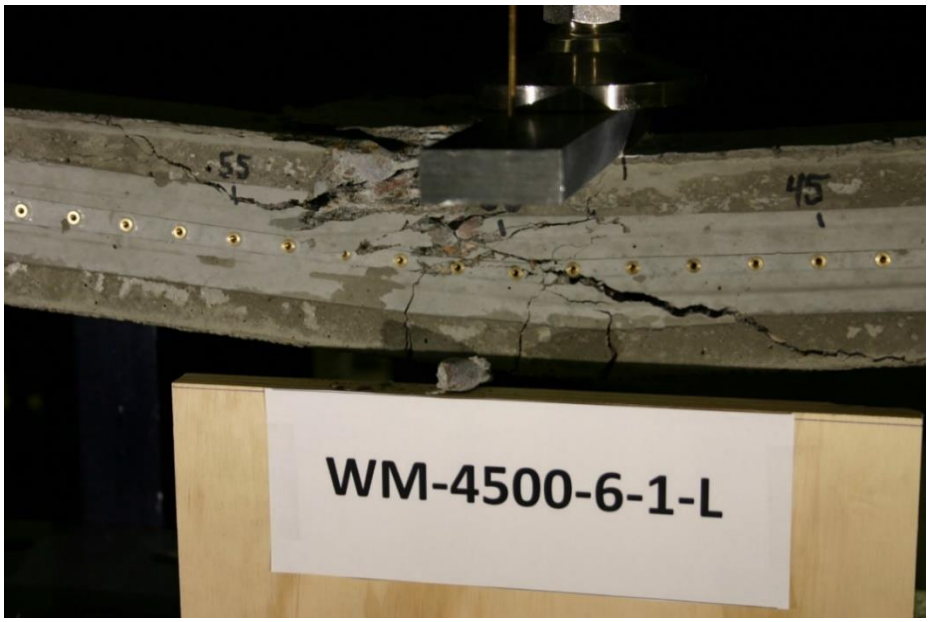


Figure 209 Picture of Failed Prism WM-4500-6-1-L

Beam Identification	WM-4500-6-1-S
Wire Type:	WM
Embedment Length:	13 in
Release Strength:	4500 psi
Slump:	6 in

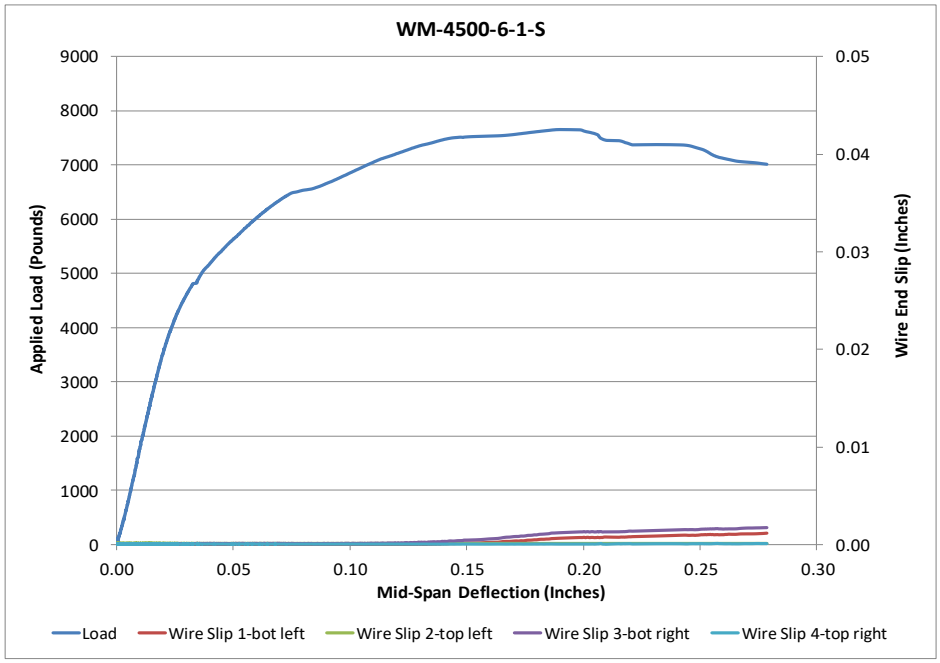


Figure 210 Load Deflection and Wire End Slip WM-4500-6-1-S



Figure 211 Picture of Failed Prism WM-4500-6-1-S

Beam Identification	WM-4500-6-2-L
Wire Type:	WM
Embedment Length:	16.5 in
Release Strength:	4500 psi
Slump:	6 in

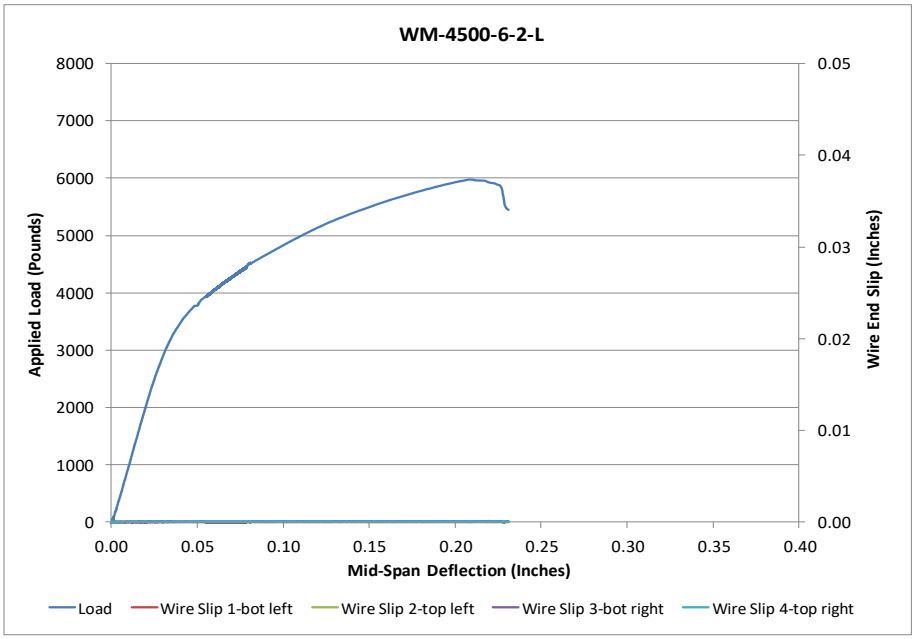


Figure 212 Load Deflection and Wire End Slip WM-4500-6-2-L

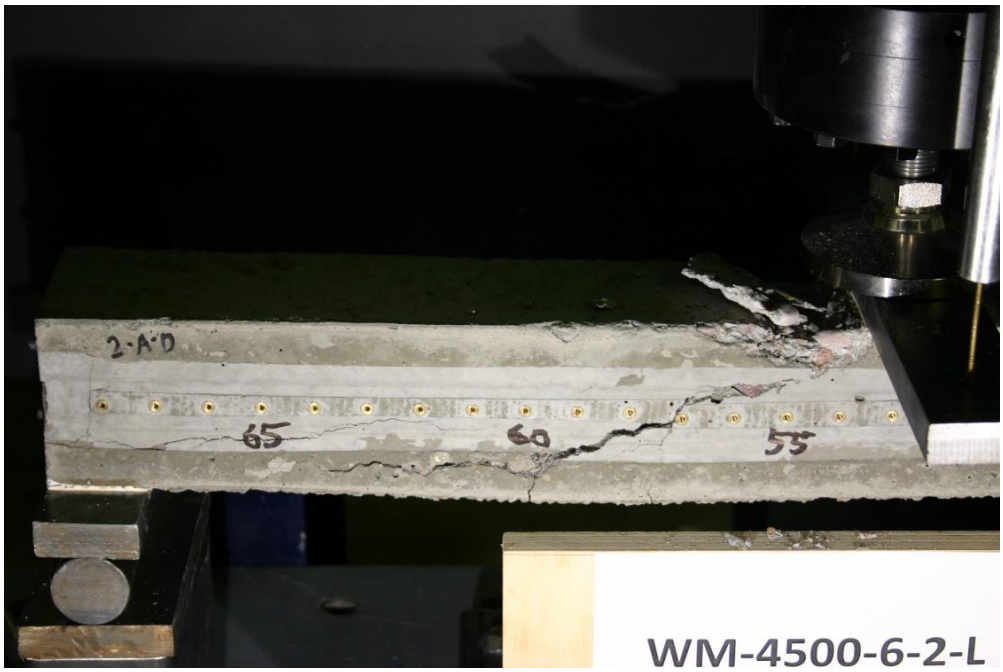


Figure 213 Picture of Failed Prism WM-4500-6-2-L

Beam Identification	WM-4500-6-2-S
Wire Type:	WM
Embedment Length:	9.5 in
Release Strength:	4500 psi
Slump:	6 in

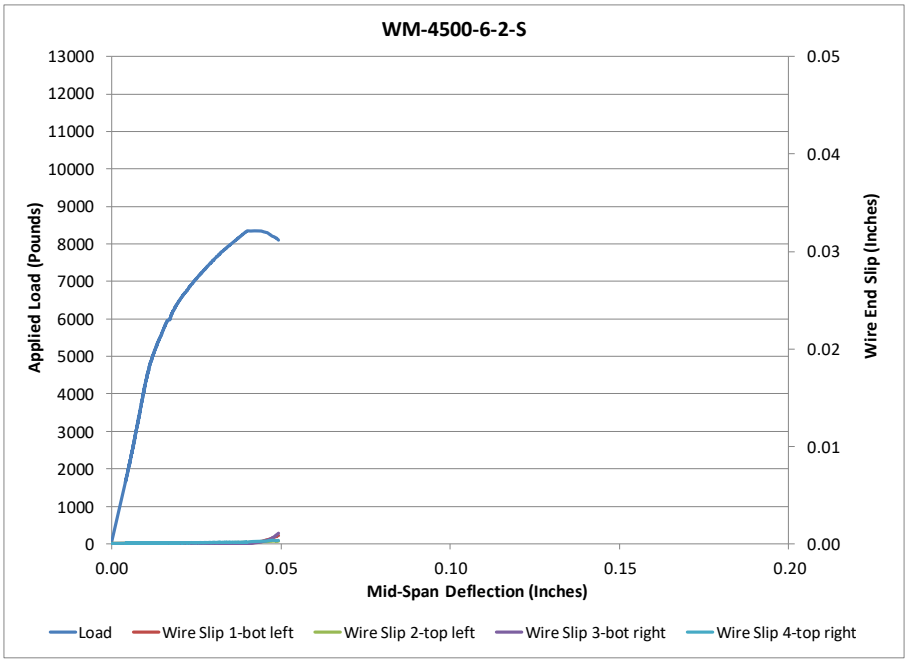


Figure 214 Load Deflection and Wire End Slip WM-4500-6-2-S

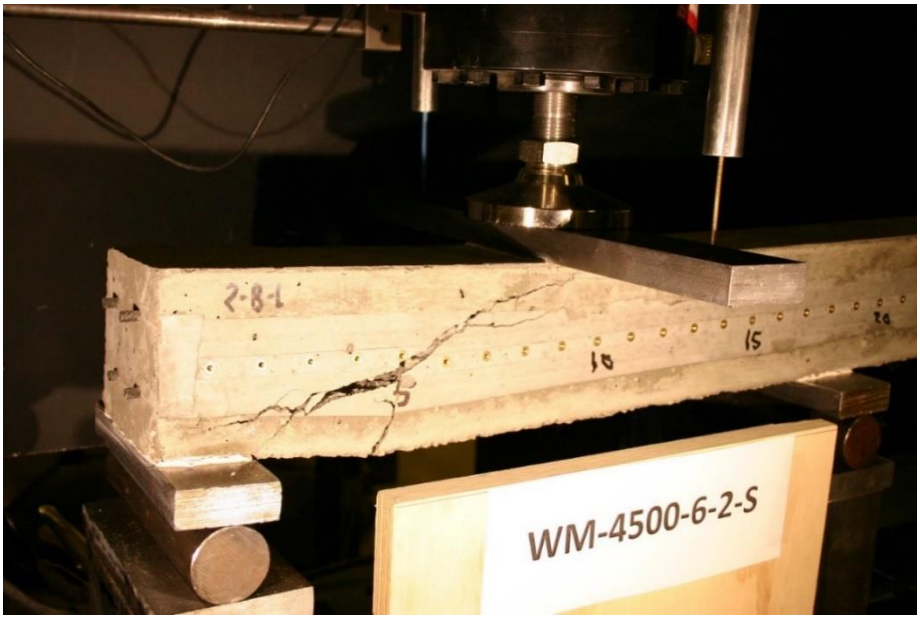


Figure 215 Picture of Failed Prism WM-4500-6-2-S

Prisms made with wires, 4500 psi concrete release strength and 3 in. slump

Beam Identification	WA-4500-3-1-S
Wire Type:	WA
Embedment Length:	13 in
Release Strength:	4500 psi
Slump:	3 in

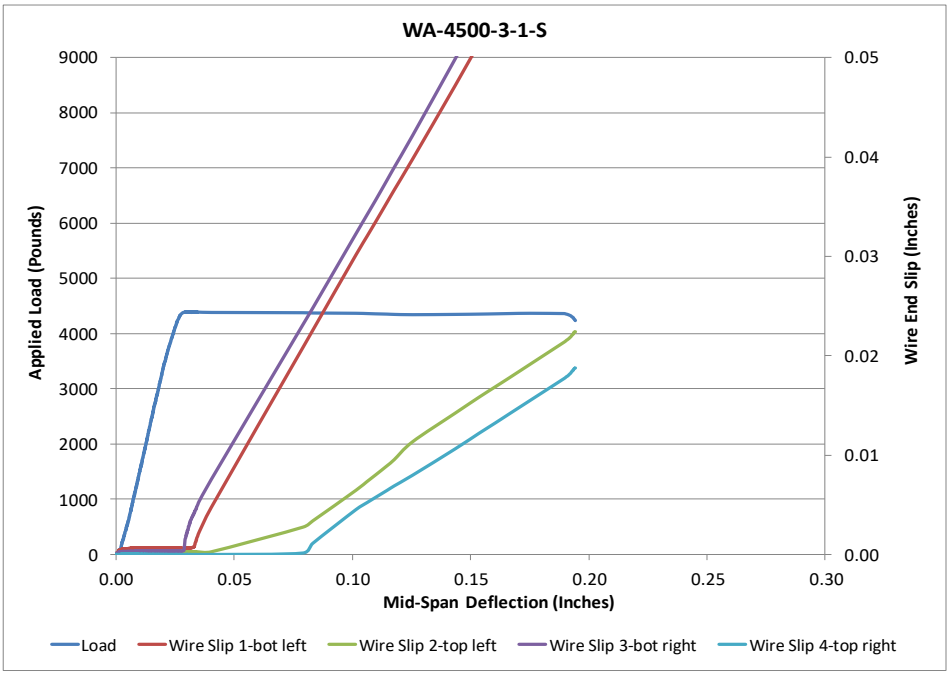


Figure 216 Load Deflection and Wire End Slip WA-4500-3-1-S

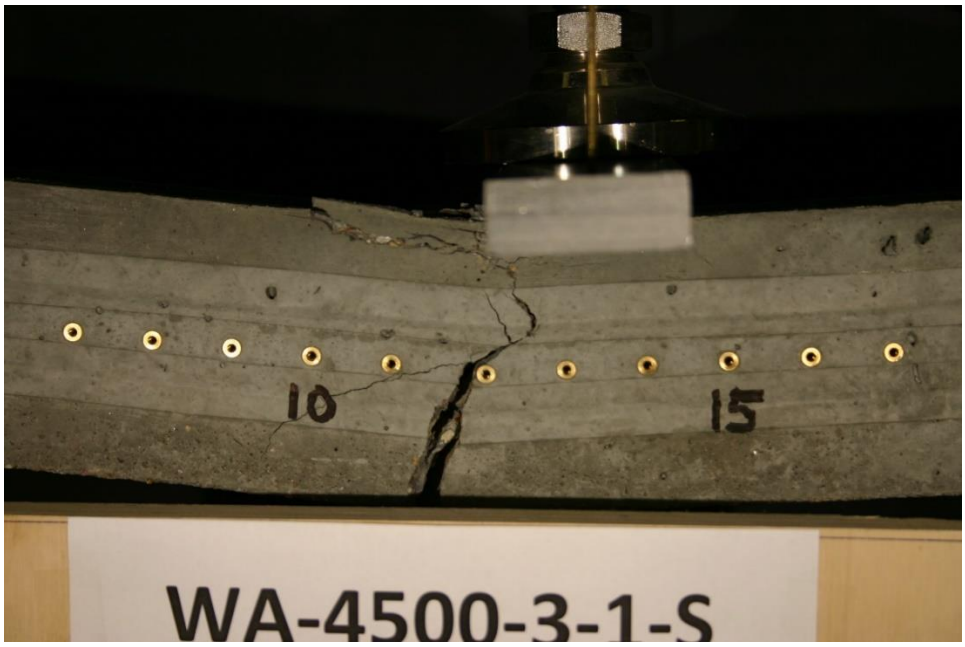


Figure 217 Picture of Failed Prism WA-4500-3-1-S

Beam Identification	WA-4500-3-2-L
Wire Type:	WA
Embedment Length:	16.5 in
Release Strength:	4500 psi
Slump:	3 in

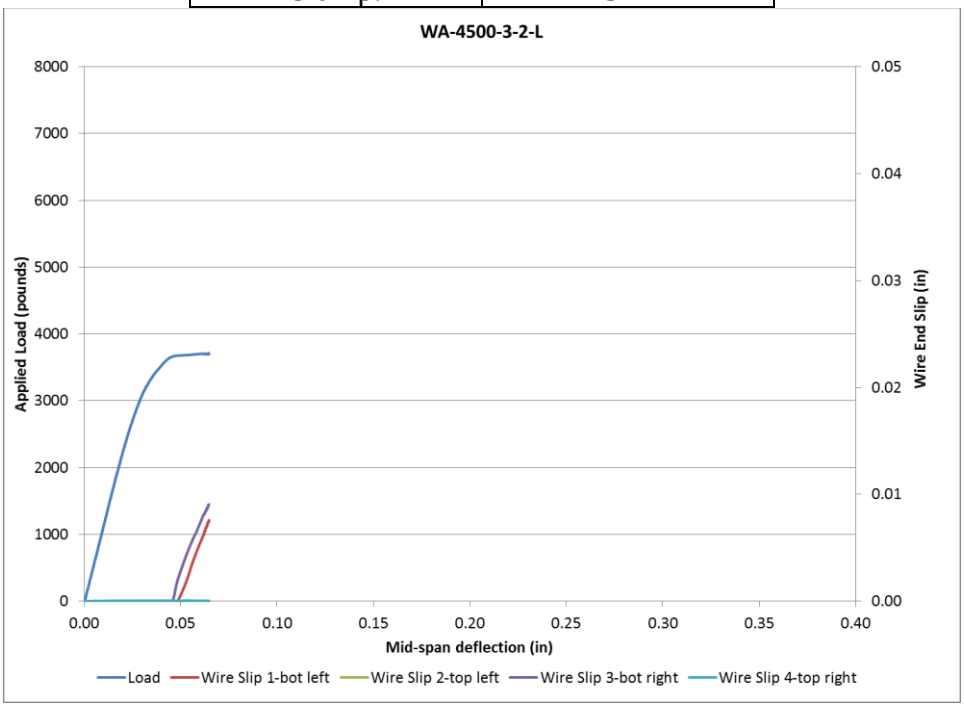


Figure 218 Load Deflection and Wire End Slip WA-4500-3-2-L

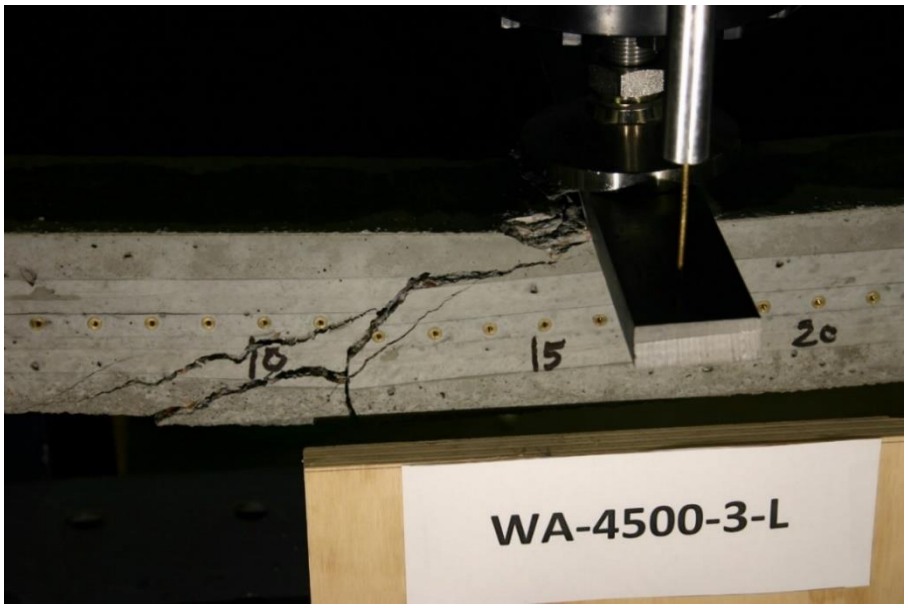


Figure 219 Picture of Failed Prism WA-4500-3-2-L

Beam Identification	WA-4500-3-2-S
Wire Type:	WA
Embedment Length:	9.5 in
Release Strength:	4500 psi
Slump:	3 in

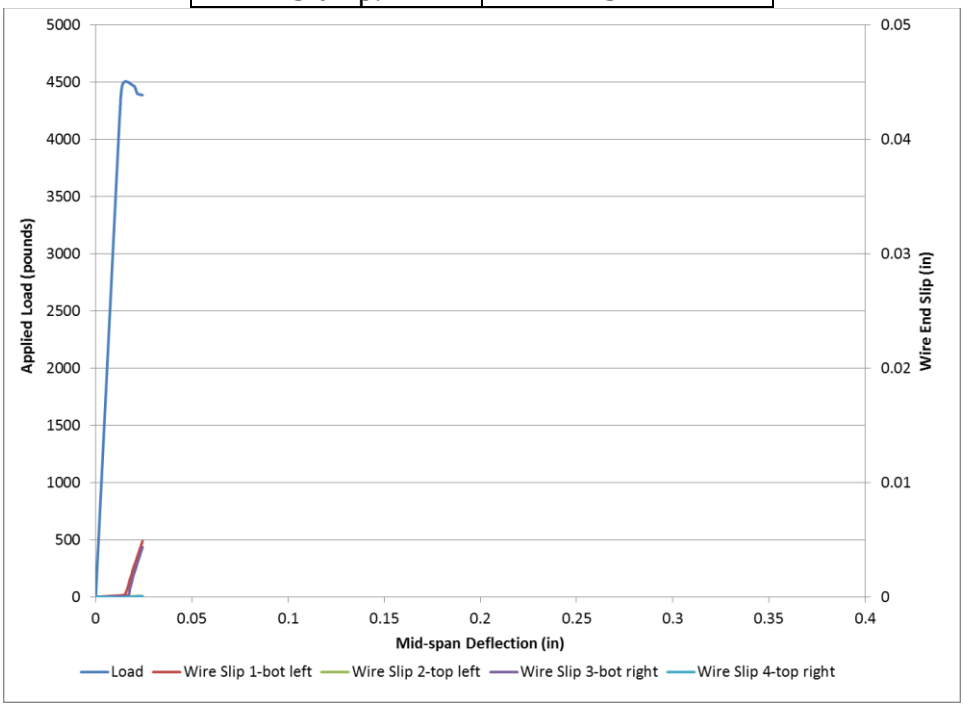


Figure 220 Load Deflection and Wire End Slip WA-4500-3-2-S

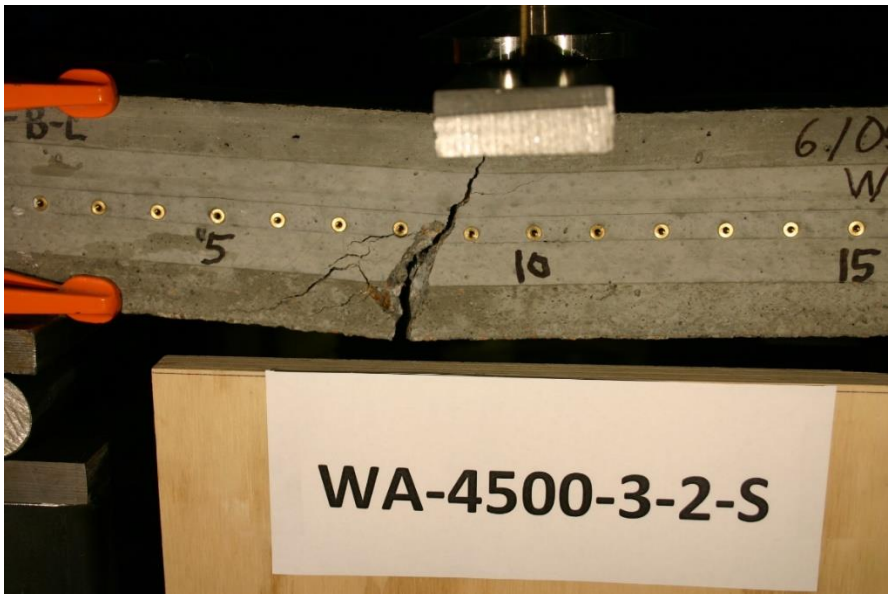


Figure 221 Picture of Failed Prism WA-4500-3-2-S

Beam Identification	WE-4500-3-1-L
Wire Type:	WE
Embedment Length:	20 in
Release Strength:	4500 psi
Slump:	3 in

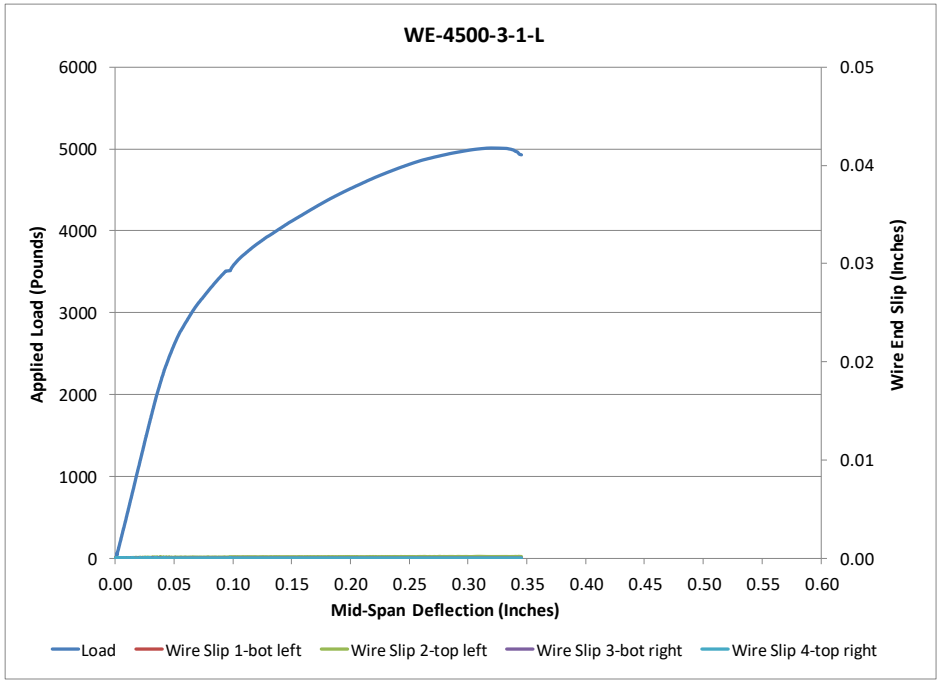


Figure 222 Load Deflection and Wire End Slip WE-4500-3-1-L

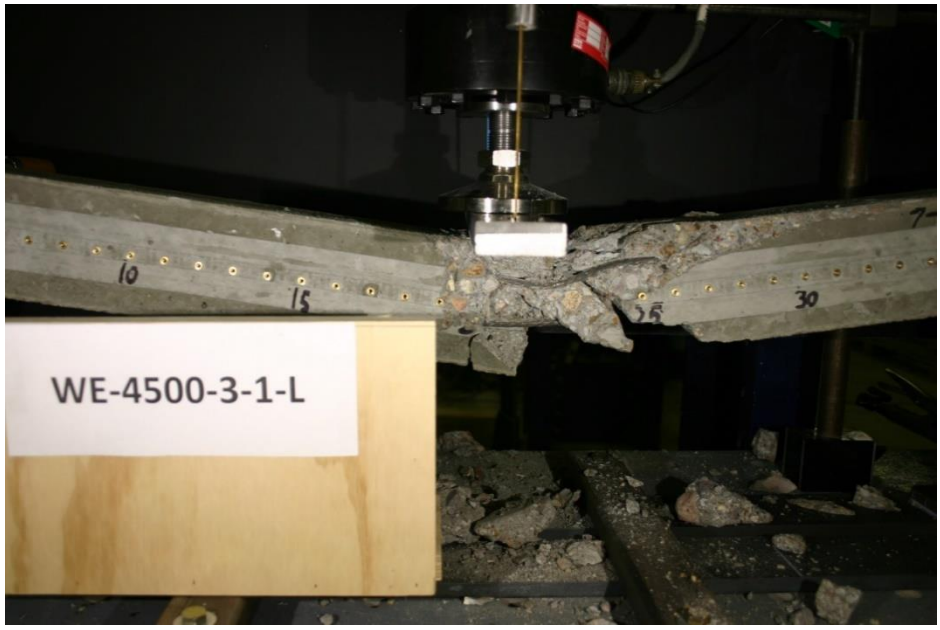


Figure 223 Picture of Failed Prism WE-4500-3-1-L

Beam Identification	WE-4500-3-1-S
Wire Type:	WE
Embedment Length:	13 in
Release Strength:	4500 psi
Slump:	3 in

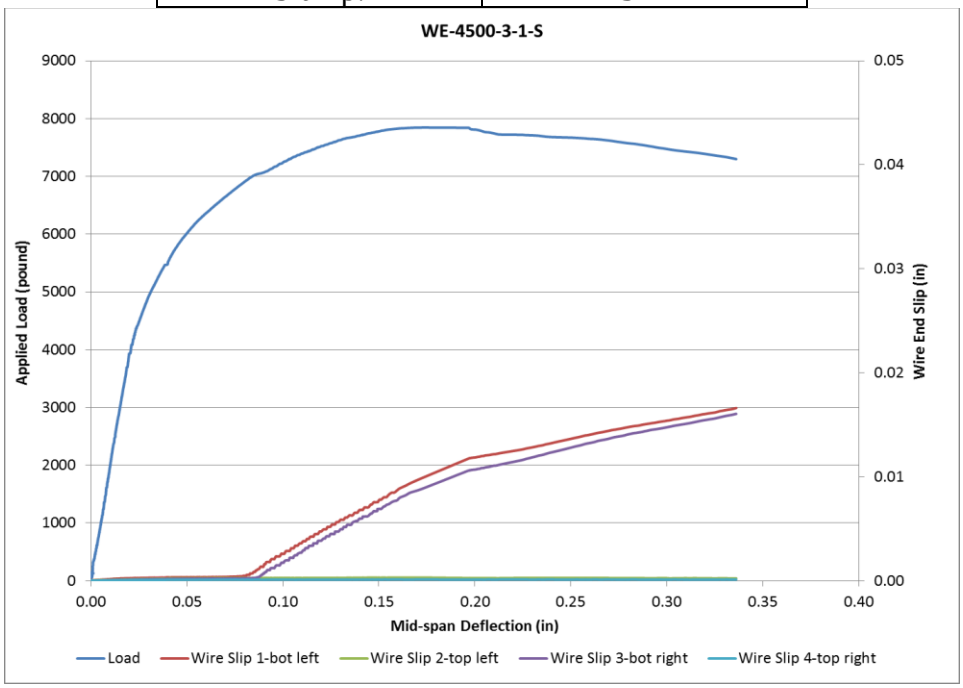


Figure 224 Load Deflection and Wire End Slip WE-4500-3-1-S



Figure 225 Picture of Failed Prism WE-4500-3-1-S

Beam Identification	WE-4500-3-2-L
Wire Type:	WE
Embedment Length:	16.5 in
Release Strength:	4500 psi
Slump:	3 in

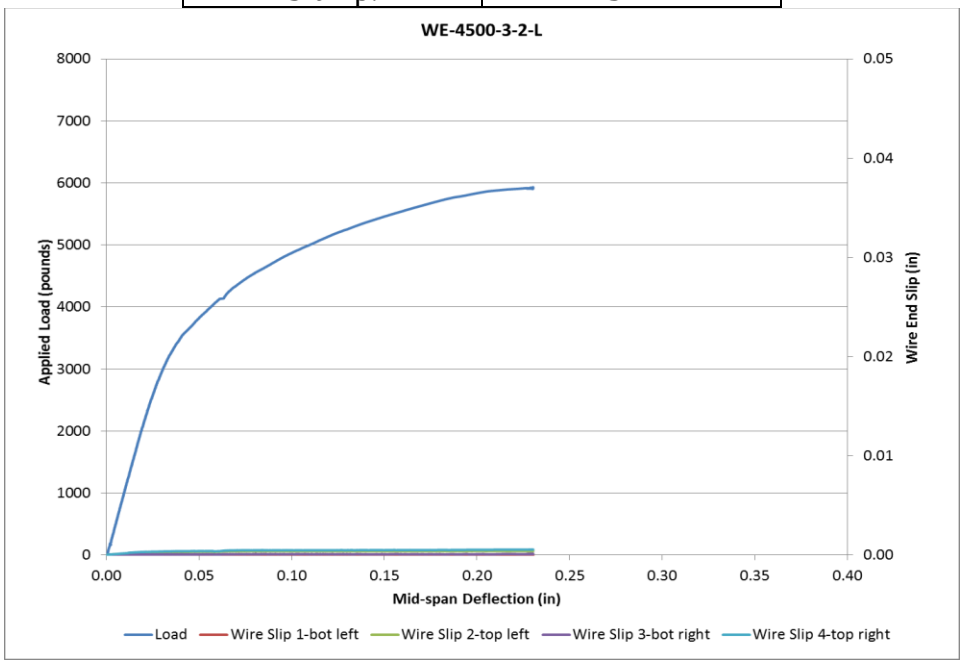


Figure 226 Load Deflection and Wire End Slip WE-4500-3-2-L

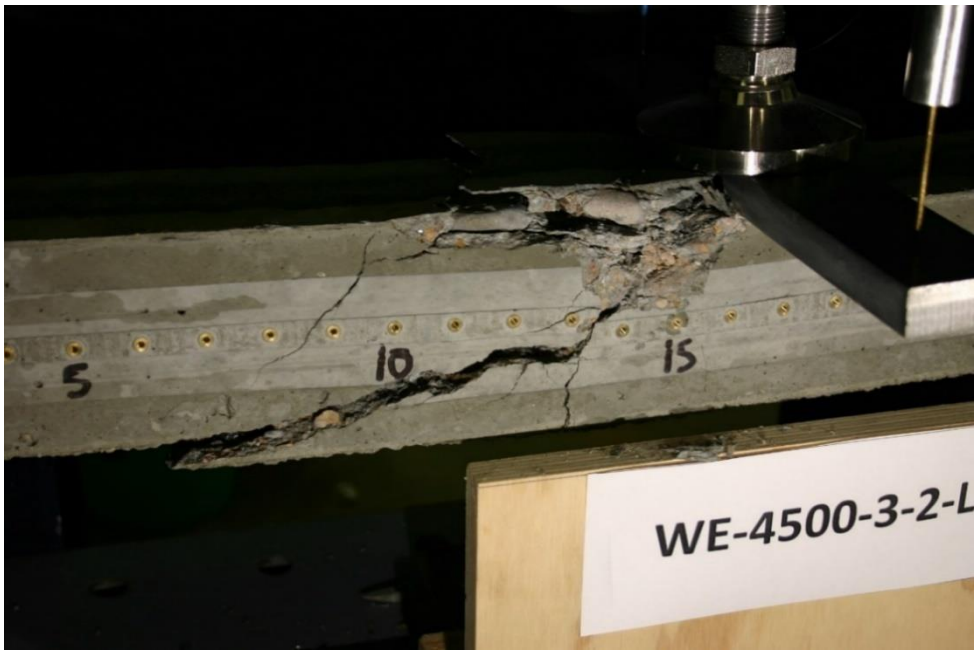


Figure 227 Picture of Failed Prism WE-4500-3-2-L

Beam Identification	WE-4500-3-2-S
Wire Type:	WE
Embedment Length:	9.5 in
Release Strength:	4500 psi
Slump:	3 in

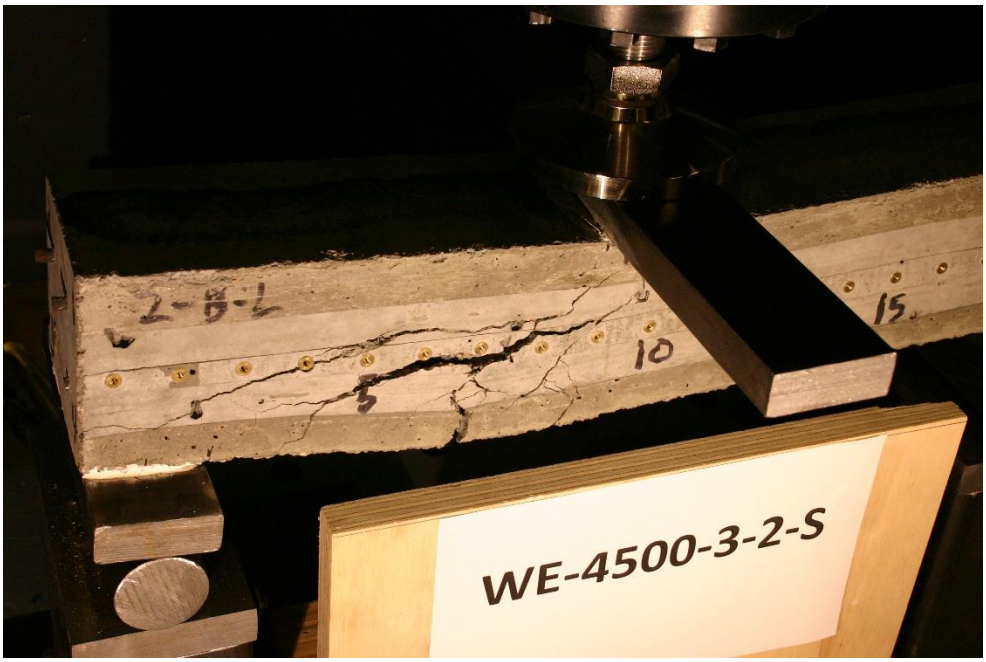


Figure 228 Picture of Failed Prism WE-4500-3-2-S

Beam Identification	WG-4500-3-1-L
Wire Type:	WG
Embedment Length:	20 in
Release Strength:	4500 psi
Slump:	3 in

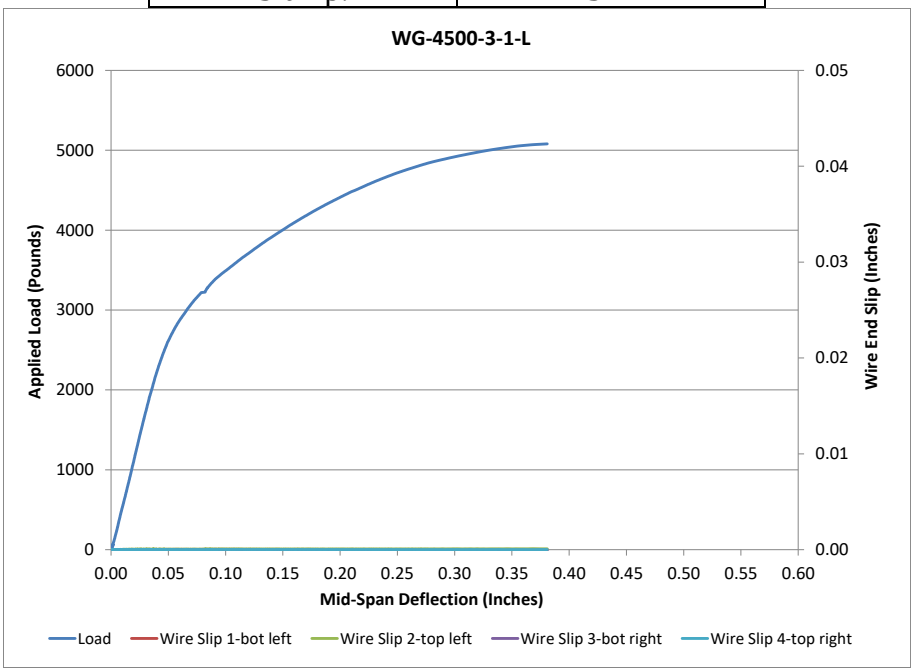


Figure 229 Load Deflection and Wire End Slip WG-4500-3-1-L

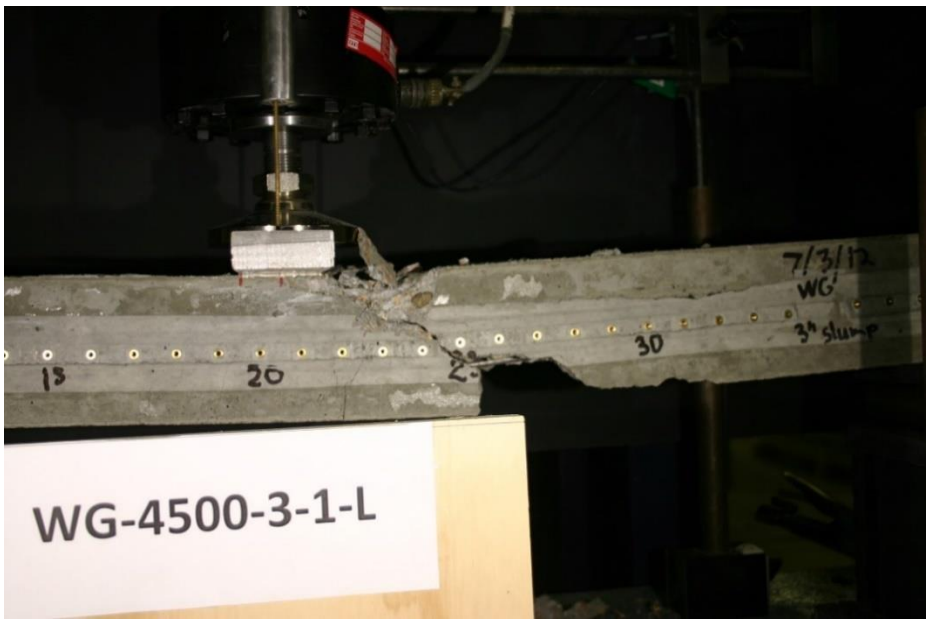


Figure 230 Picture of Failed Prism WG-4500-3-1-L

Beam Identification	WG-4500-3-1-S
Wire Type:	WG
Embedment Length:	13 in
Release Strength:	4500 psi
Slump:	3 in

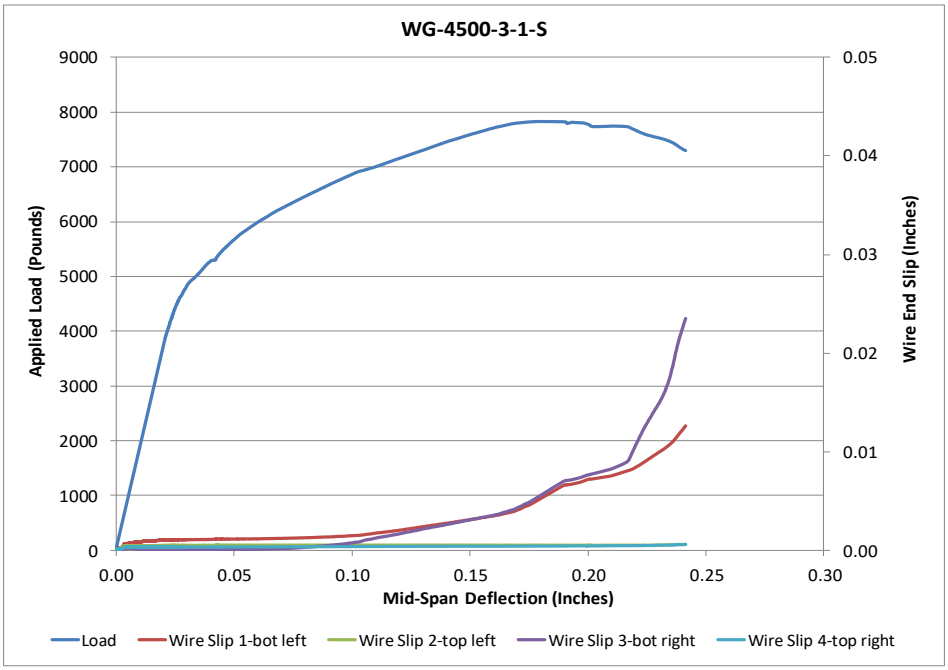


Figure 231 Load Deflection and Wire End Slip WG-4500-3-1-S



Figure 232 Picture of Failed Prism WG-4500-3-1-S

Beam Identification	WG-4500-3-2-L
Wire Type:	WG
Embedment Length:	16.5 in
Release Strength:	4500 psi
Slump:	3 in

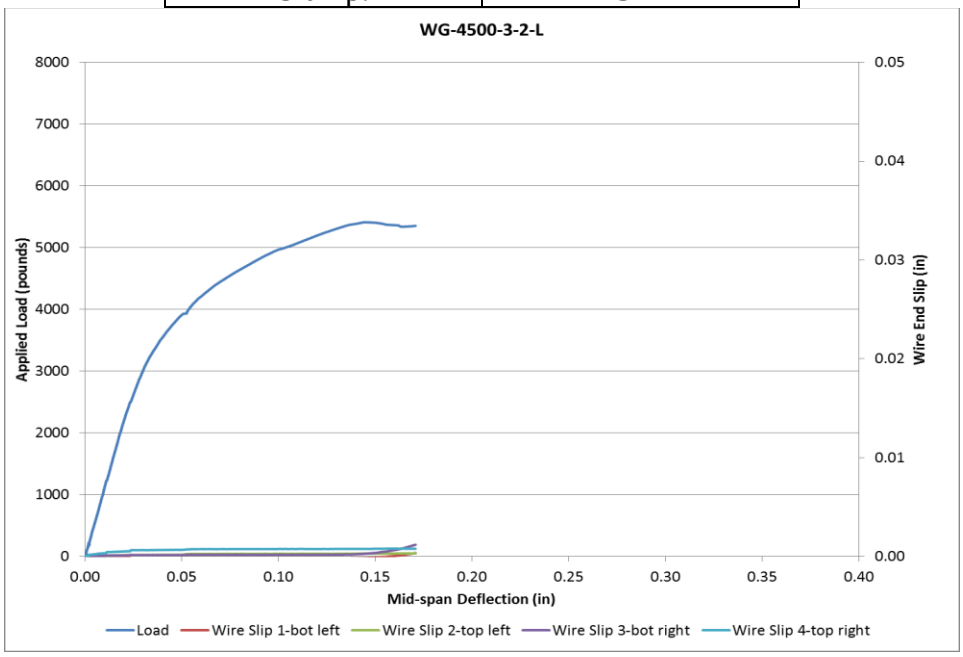


Figure 233 Load Deflection and Wire End Slip WG-4500-3-2-L

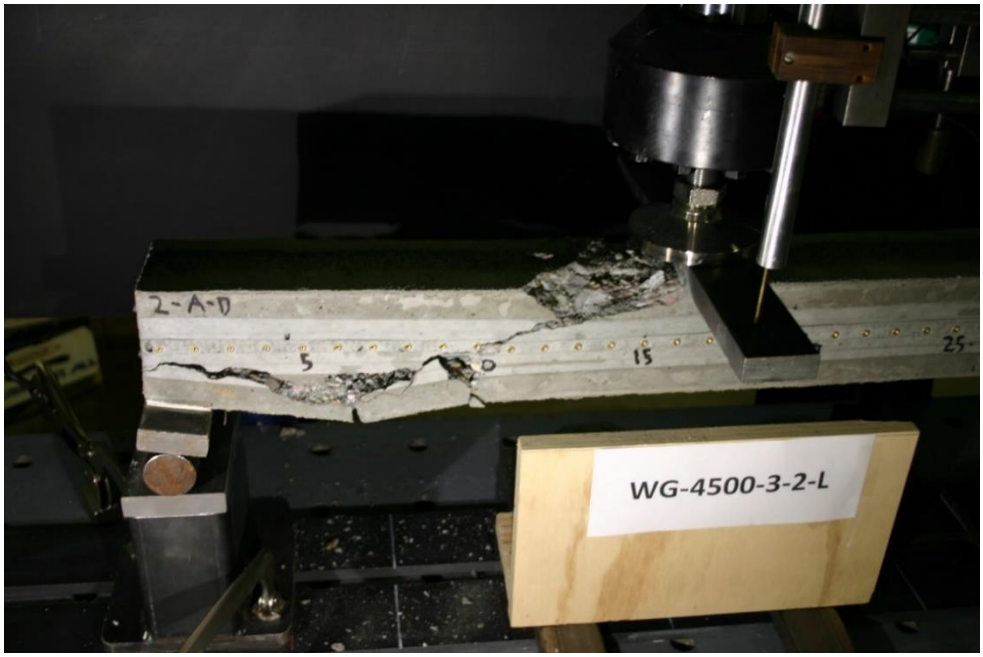


Figure 234 Picture of Failed Prism WG-4500-3-2-L

Beam Identification	WG-4500-3-2-S
Wire Type:	WG
Embedment Length:	9.5 in
Release Strength:	4500 psi
Slump:	3 in

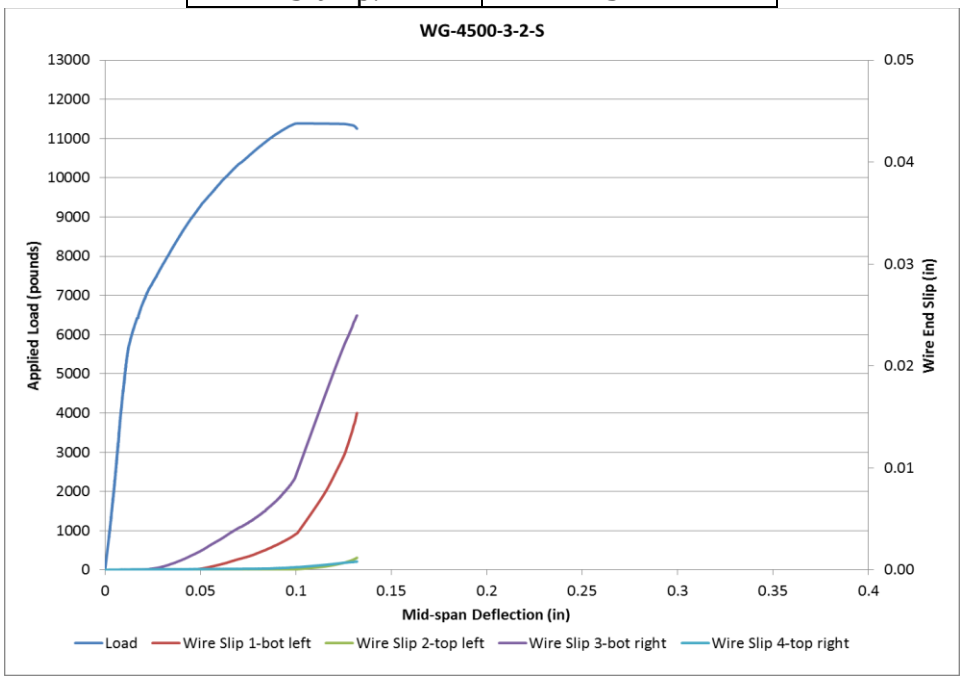


Figure 235Load Deflection and Wire End Slip WG-4500-3-2-S



Figure 236 Picture of Failed Prism WG-4500-3-2-S

Beam Identification	WH-4500-3-1-L
Wire Type:	WH
Embedment Length:	20 in
Release Strength:	4500 psi
Slump:	3 in

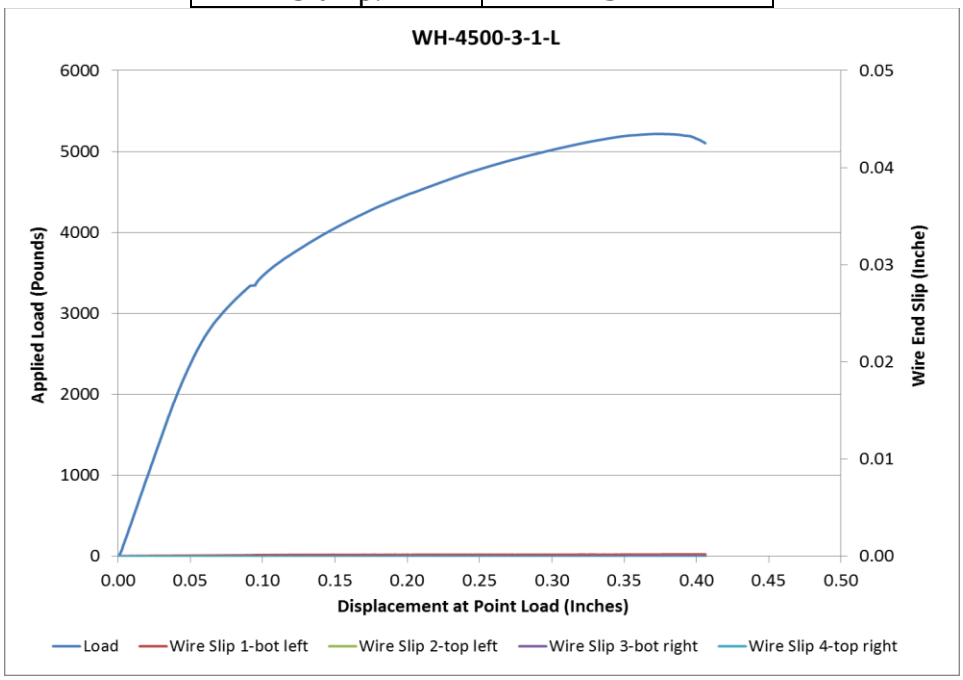


Figure 237 Load Deflection and Wire End Slip WH-4500-3-1-L

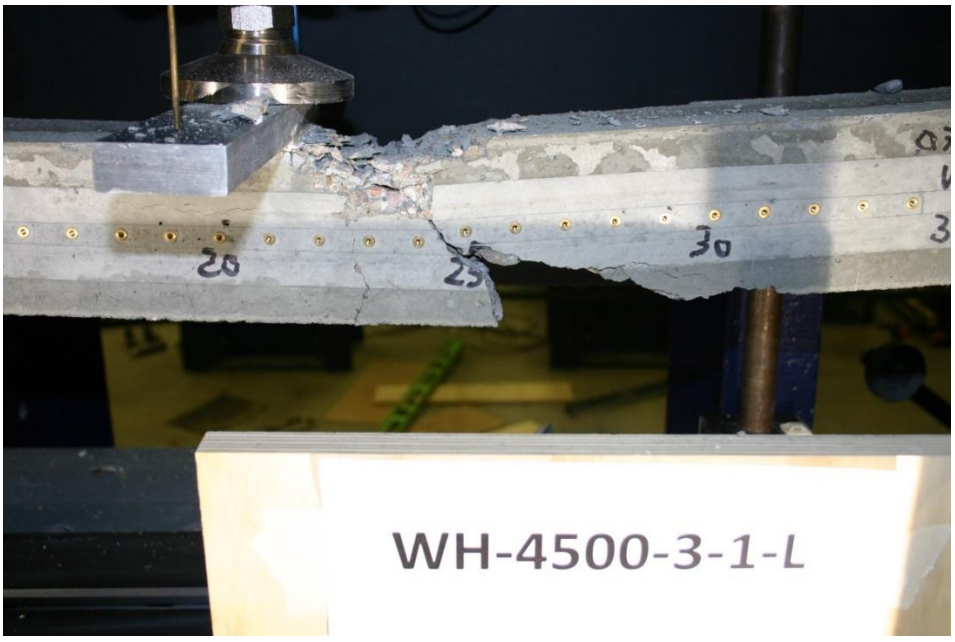


Figure 238 Picture of Failed Prism WH-4500-3-1-L

Beam Identification	WH-4500-3-1-S
Wire Type:	WH
Embedment Length:	13 in
Release Strength:	4500 psi
Slump:	3 in

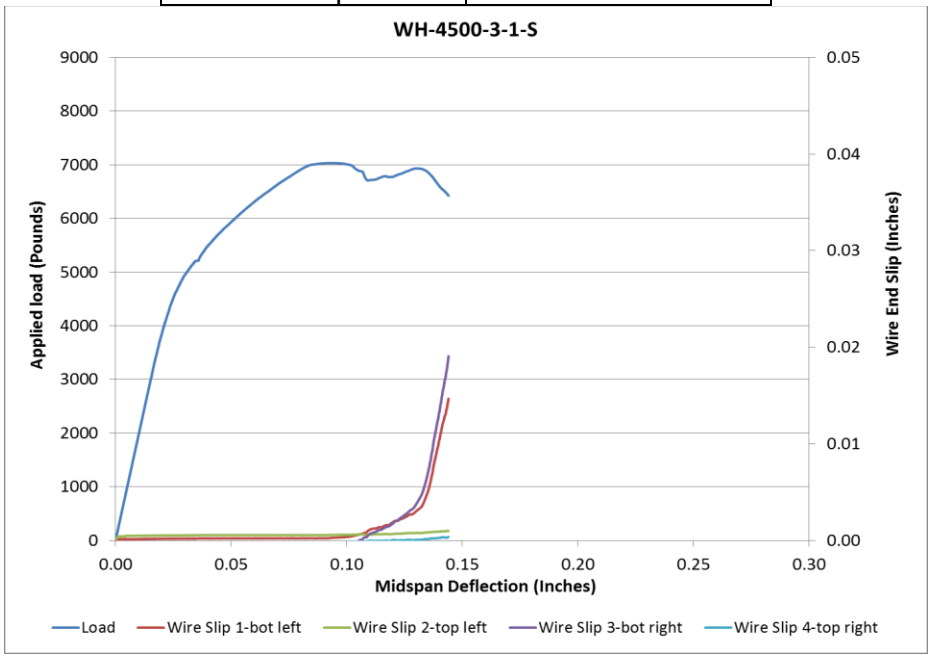
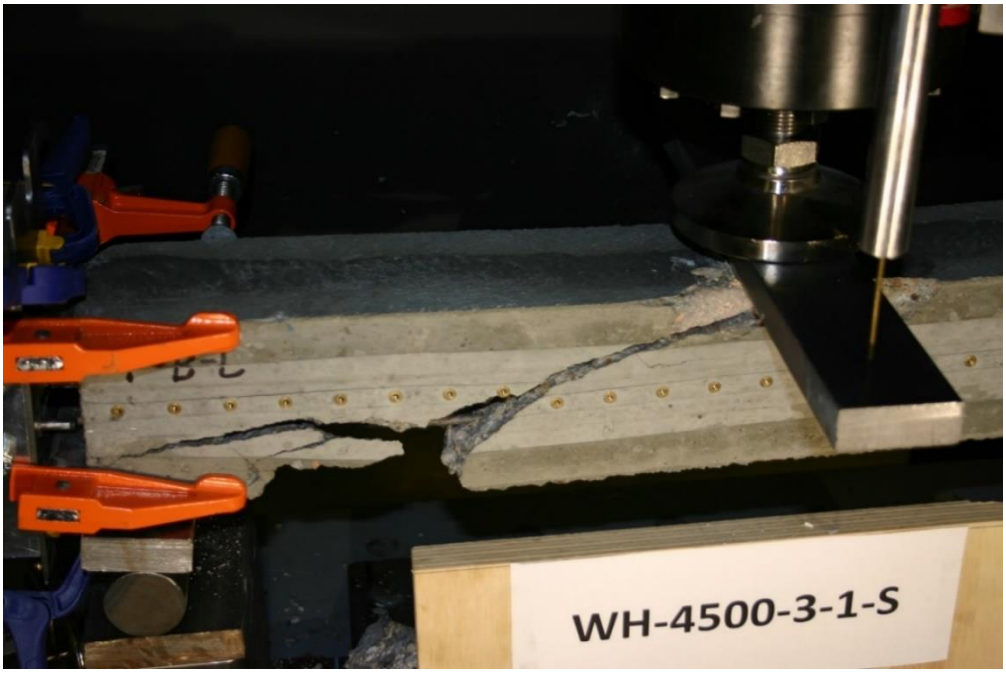


Figure 239 Load Deflection and Wire End Slip WH-4500-3-1-S



Picture of Failed Prism WH-4500-3-1-S

Beam Identification	WH-4500-3-2-L
Wire Type:	WH
Embedment Length:	16.5 in
Release Strength:	4500 psi
Slump:	3 in

Beam had defects and longitudinal cracks

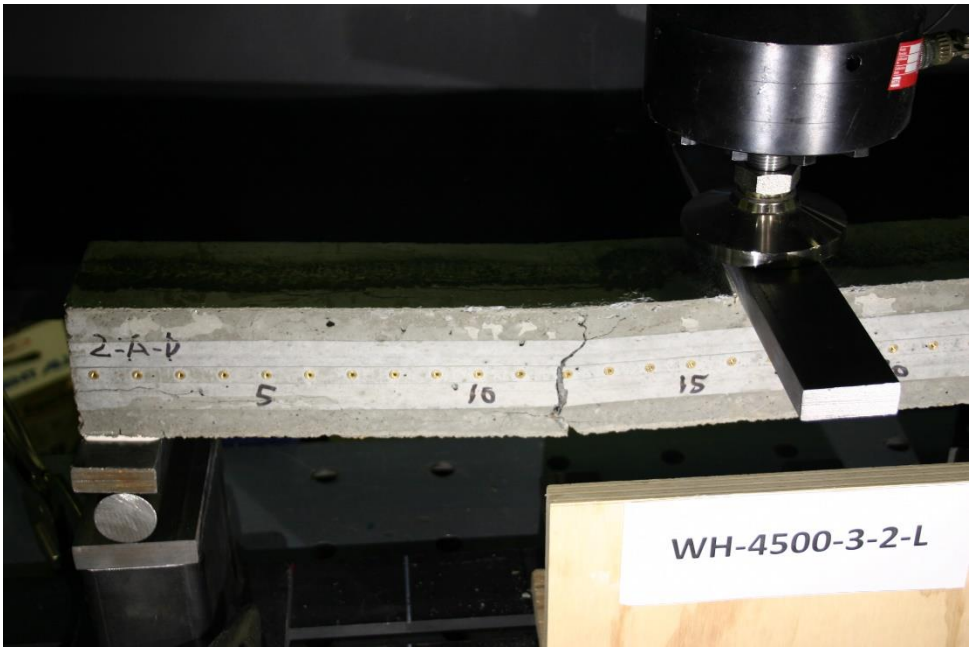


Figure 240 Picture of Failed Prism WH-4500-3-2-L

Beam Identification	WH-4500-3-2-S
Wire Type:	WH
Embedment Length:	9.5 in
Release Strength:	4500 psi
Slump:	3 in

Beam had defects and longitudinal cracks

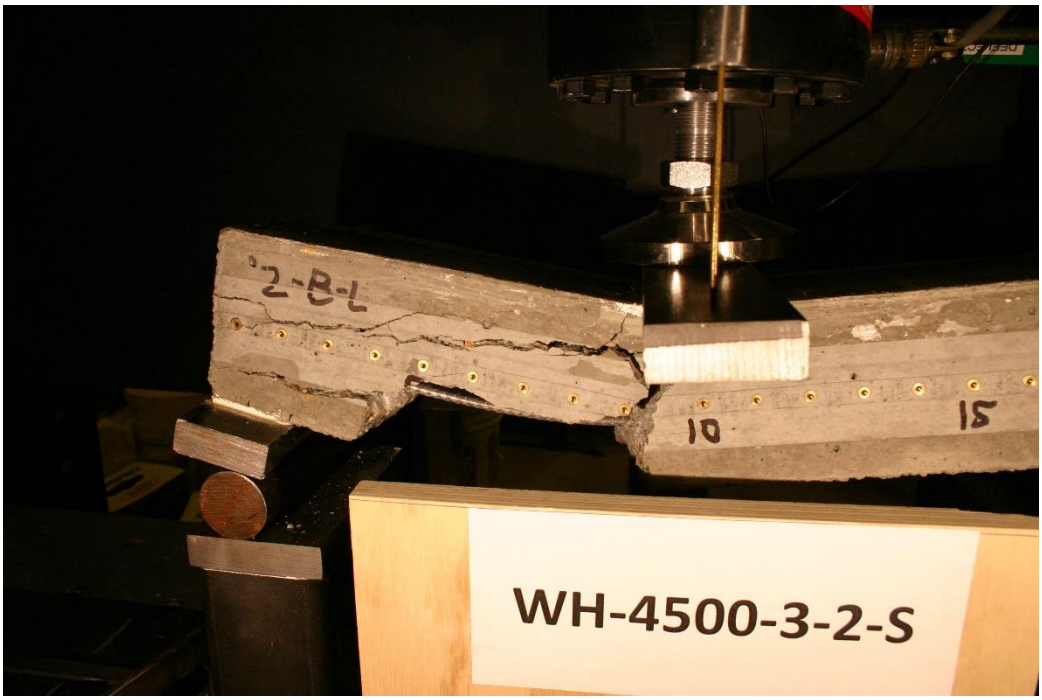


Figure 241 Picture of Failed Prism WH-4500-3-2-S

Beam Identification	WK-4500-3-1-L
Wire Type:	WK
Embedment Length:	20 in
Release Strength:	4500 psi
Slump:	3 in

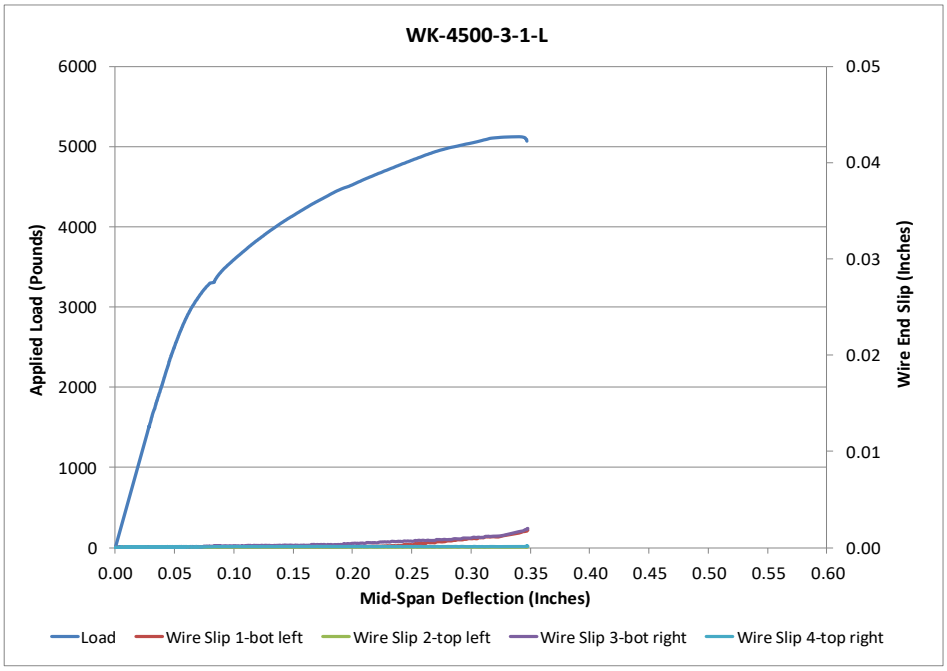


Figure 242 Load Deflection and Wire End Slip WK-4500-3-1-L

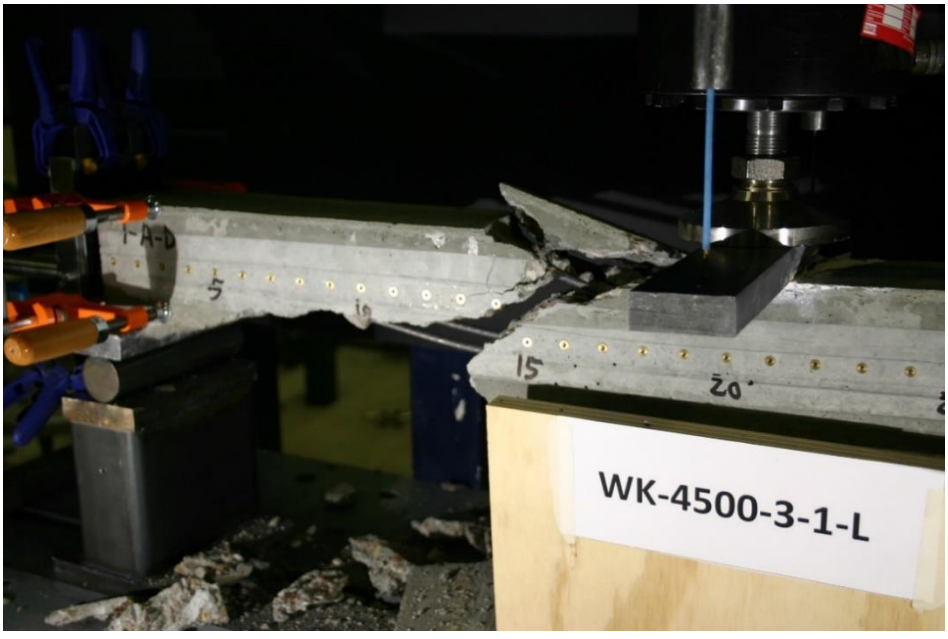


Figure 243 Picture of Failed Prism WK-4500-3-1-L

Beam Identification	WK-4500-3-1-S
Wire Type:	WK
Embedment Length:	13 in
Release Strength:	4500 psi
Slump:	3 in

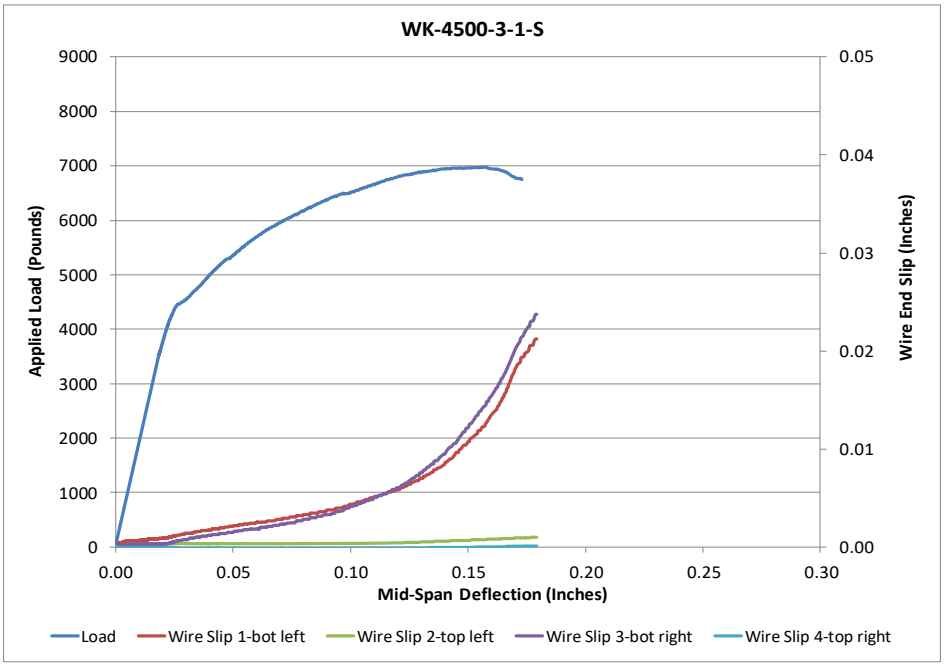


Figure 244 Load Deflection and Wire End Slip WK-4500-3-1-S



Figure 245 Picture of Failed Prism WK-4500-3-1-S

am Identification	WK-4500-3-2-L
Wire Type:	WK
Embedment Length:	16.5 in
Release Strength:	4500 psi
Slump:	3 in

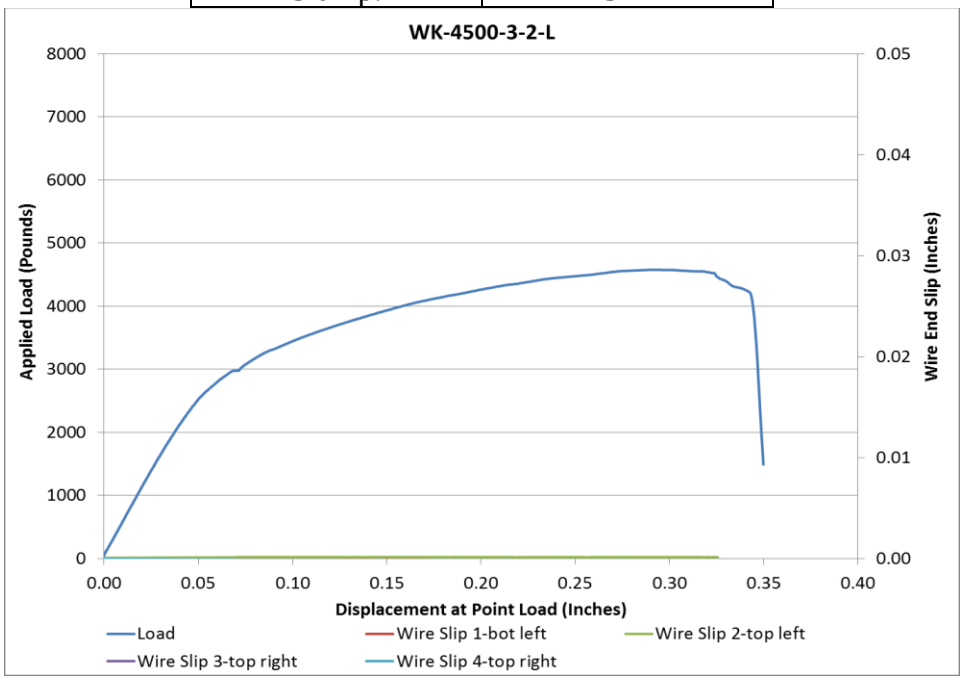


Figure 246 Load Deflection and Wire End Slip WK-4500-3-2-L



Figure 247 Picture of Failed Prism WK-4500-3-2-L

Beam Identification	WK-4500-3-2-S
Wire Type:	WK
Embedment Length:	9.5 in
Release Strength:	4500 psi
Slump:	3 in

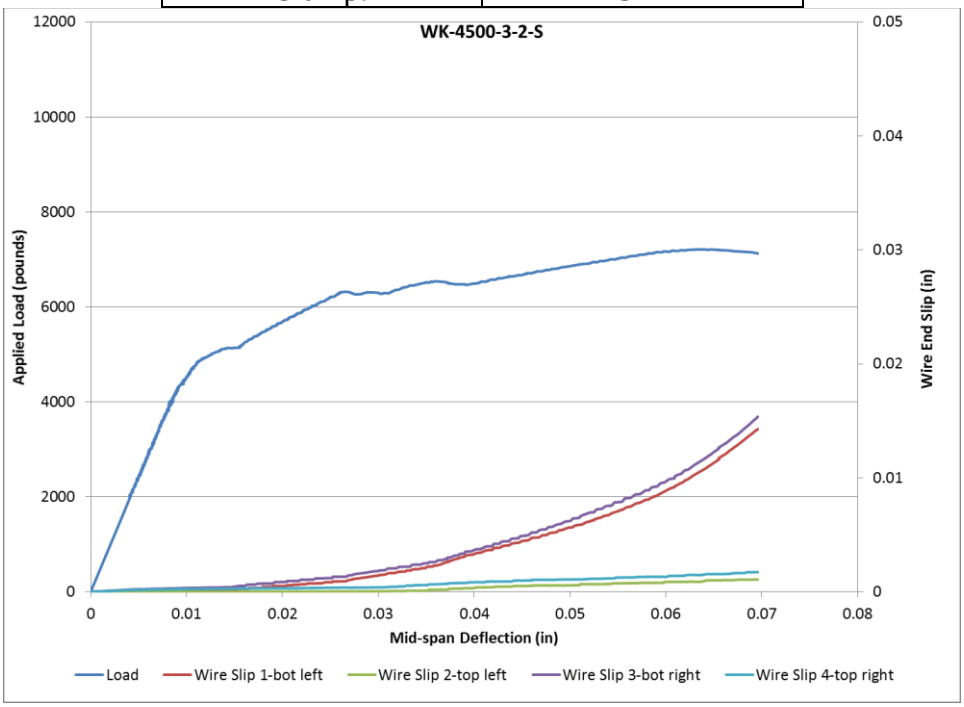


Figure 248 Load Deflection and Wire End Slip WK-4500-3-2-S

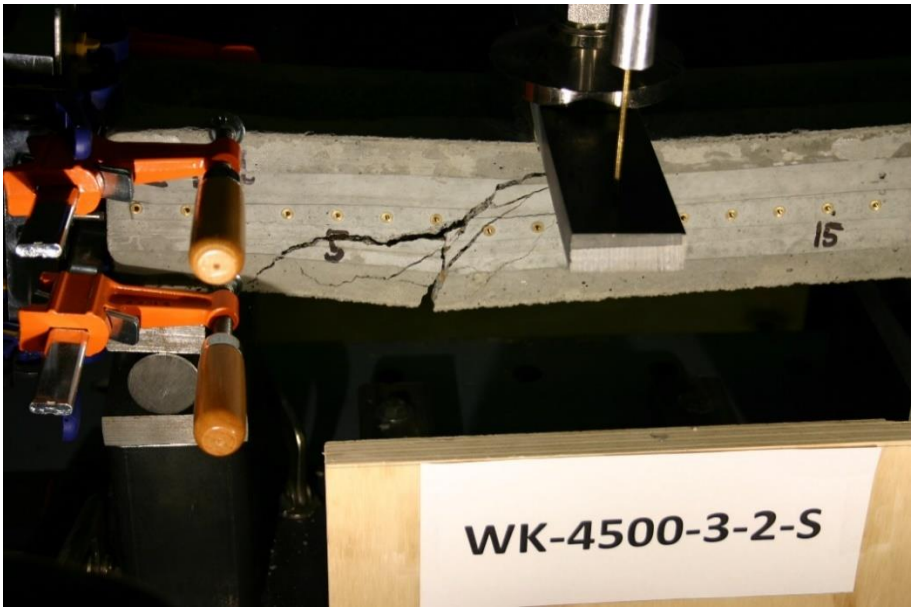


Figure 249 Picture of Failed Prism WK-4500-3-2-S

Prisms made with wires, 4500 psi concrete release strength and 9 in. slump

Beam Identification	WA-4500-9-1-L
Wire Type:	WA
Embedment Length:	20 in
Release Strength:	4500 psi
Slump:	9 in

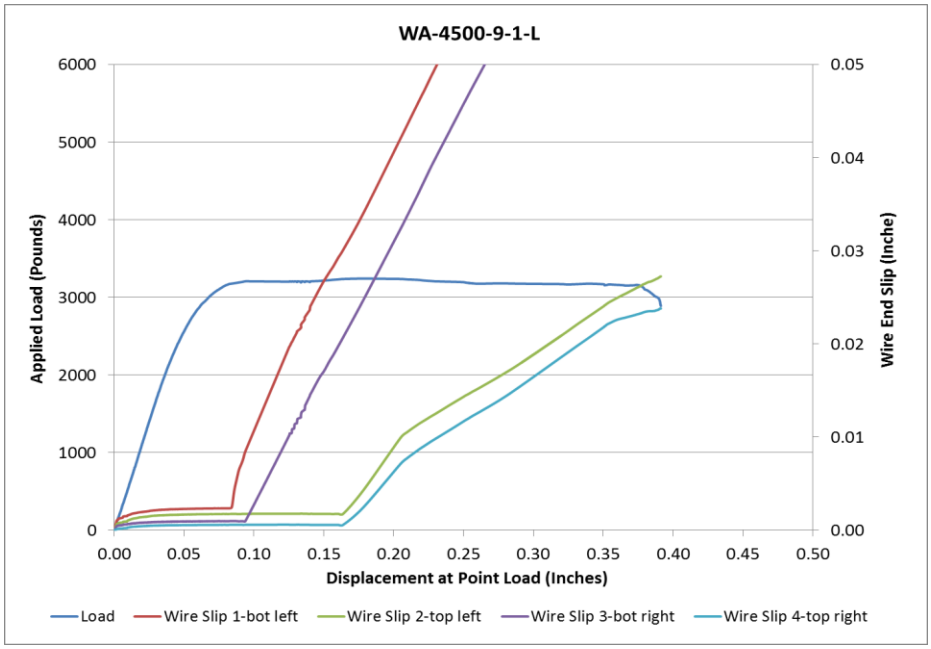


Figure 250 Figure 144 Load Deflection and Wire End Slip WA-4500-9-1-L

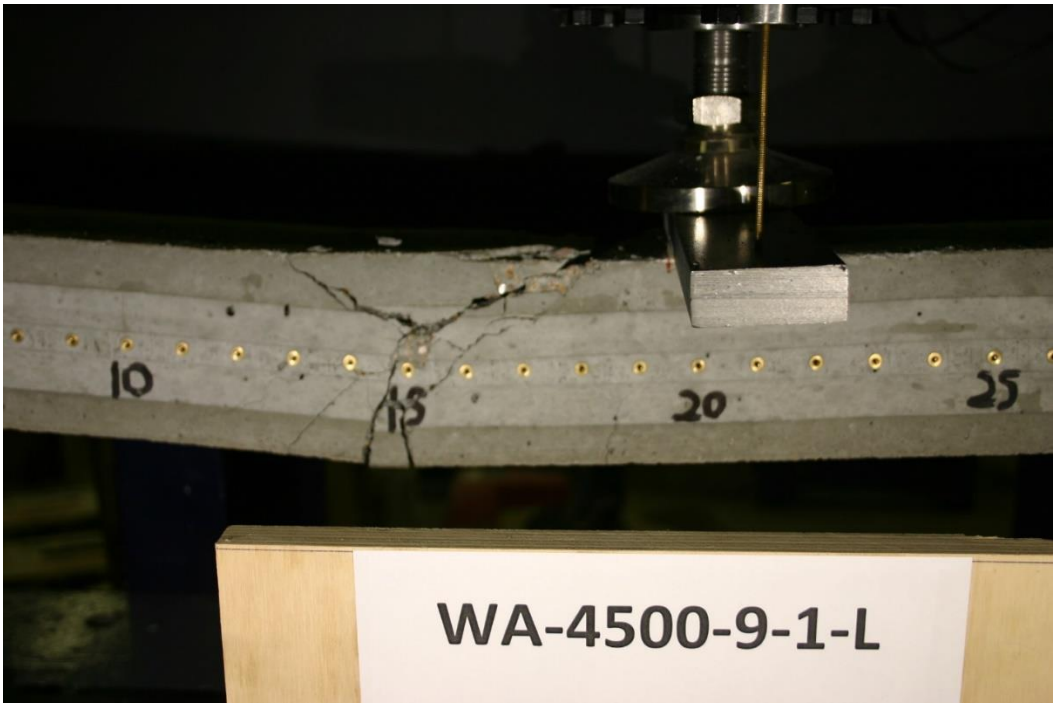


Figure 251 Picture of Failed Prism WA-4500-9-1-L

Beam Identification	WA-4500-9-1-S
Wire Type:	WA
Embedment Length:	13 in
Release Strength:	4500 psi
Slump:	9 in

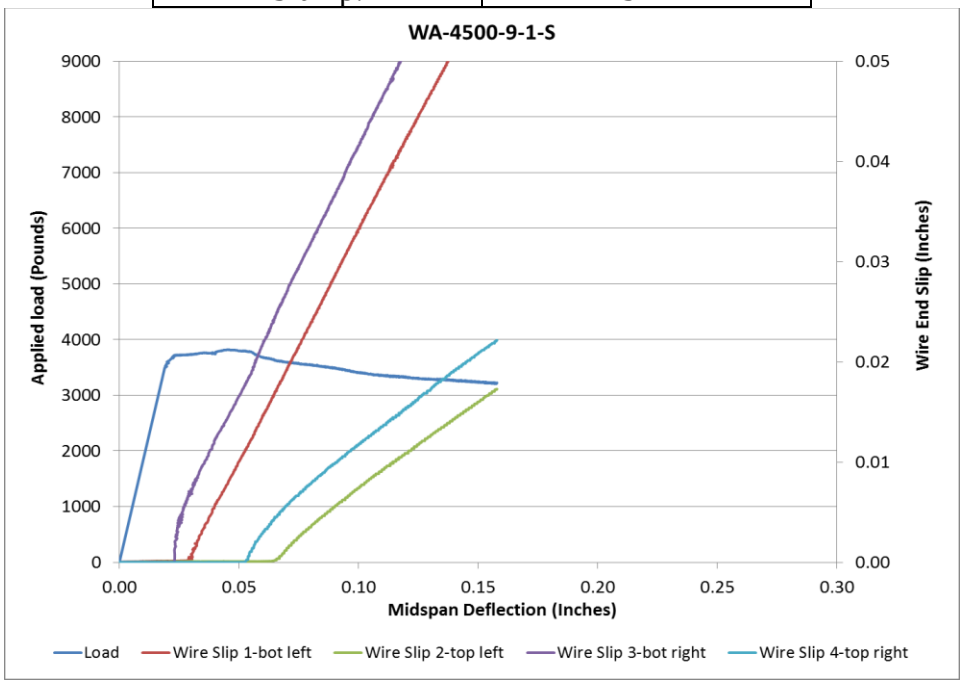


Figure 252 Load Deflection and Wire End Slip WA-4500-9-1-S



Figure 253 Picture of Failed Prism WA-4500-9-1-S

Beam Identification	WA-4500-9-2-L
Wire Type:	WA
Embedment Length:	16.5 in
Release Strength:	4500 psi
Slump:	9 in

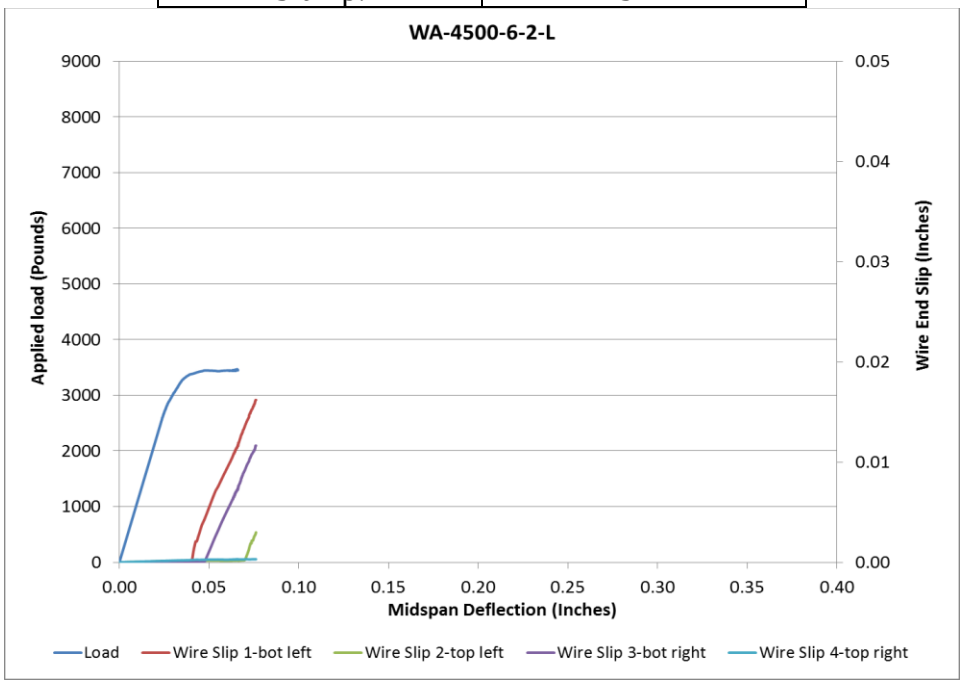


Figure 254 Load Deflection and Wire End Slip WA-4500-9-2-L

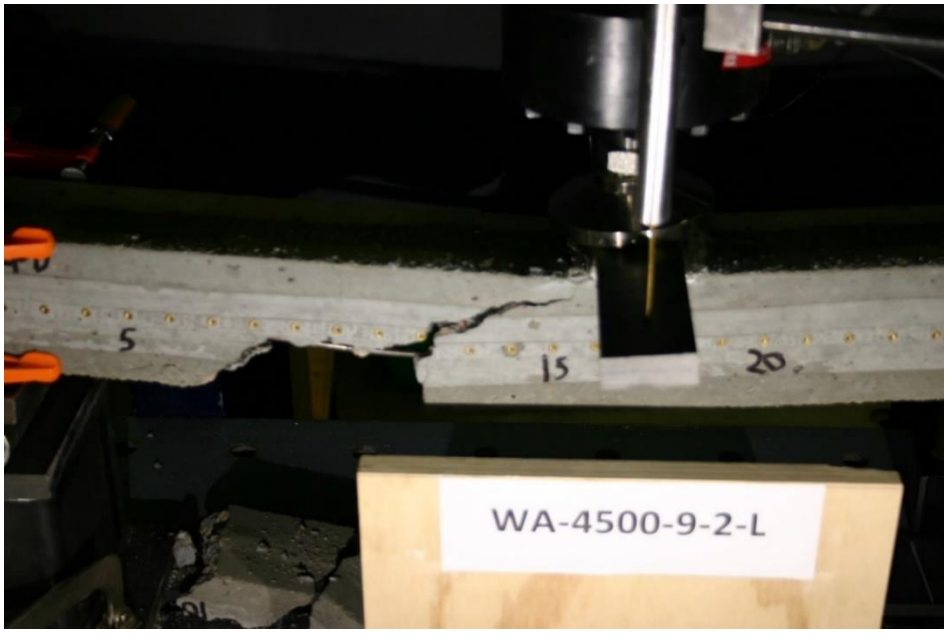


Figure 255 Picture of Failed Prism WA-4500-9-2-L

Beam Identification	WA-4500-9-2-S
Wire Type:	WA
Embedment Length:	9.5 in
Release Strength:	4500 psi
Slump:	9 in

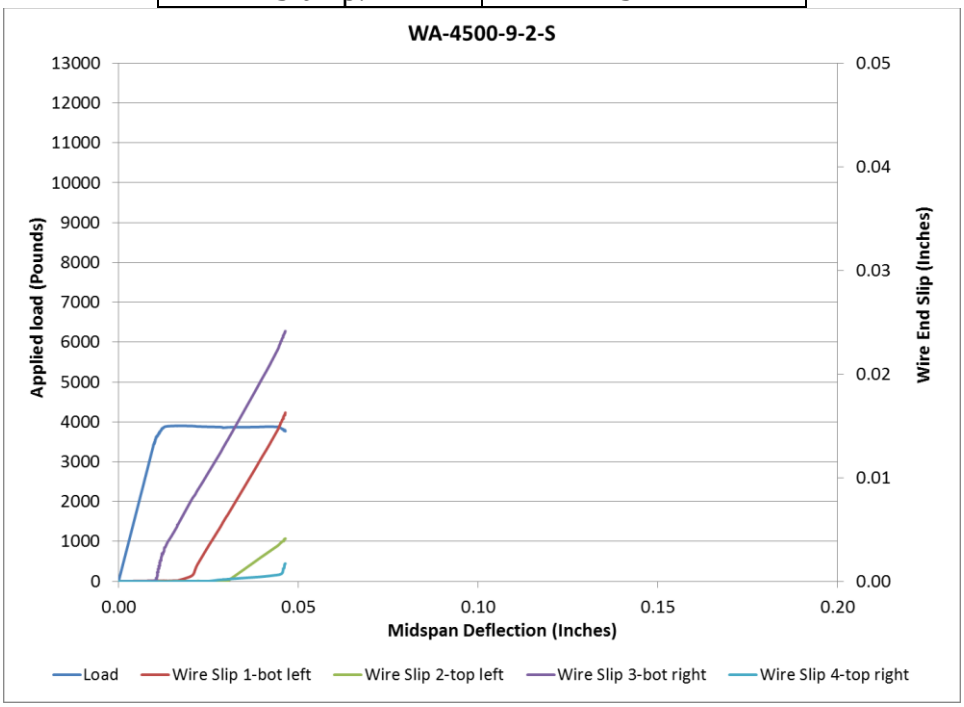


Figure 256 Load Deflection and Wire End Slip WA-4500-9-2-S

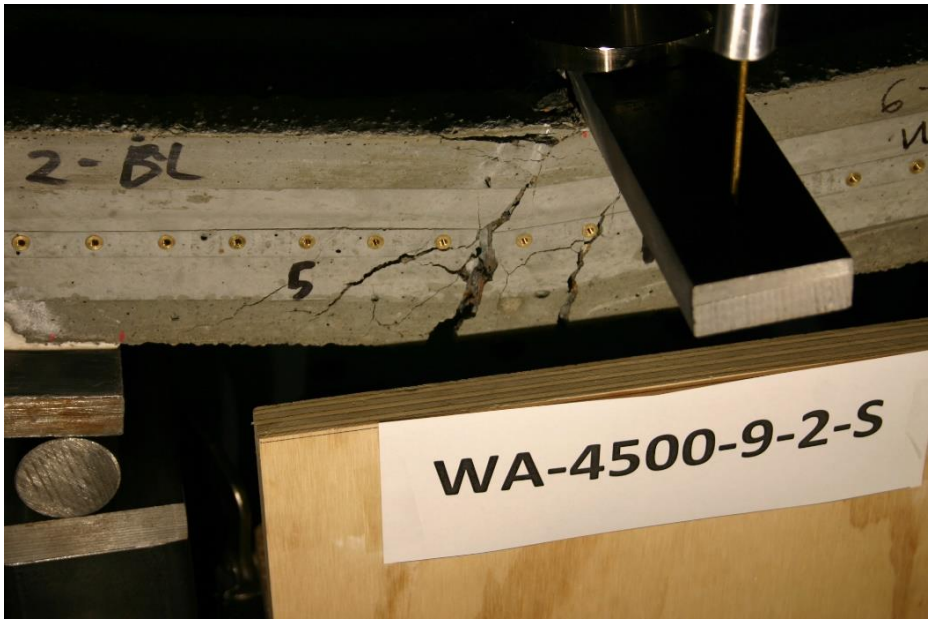


Figure 257 Picture of Failed Prism WA-4500-9-2-S

Beam Identification	WE-4500-9-1-L
Wire Type:	WE
Embedment Length:	20 in
Release Strength:	4500 psi
Slump:	9 in

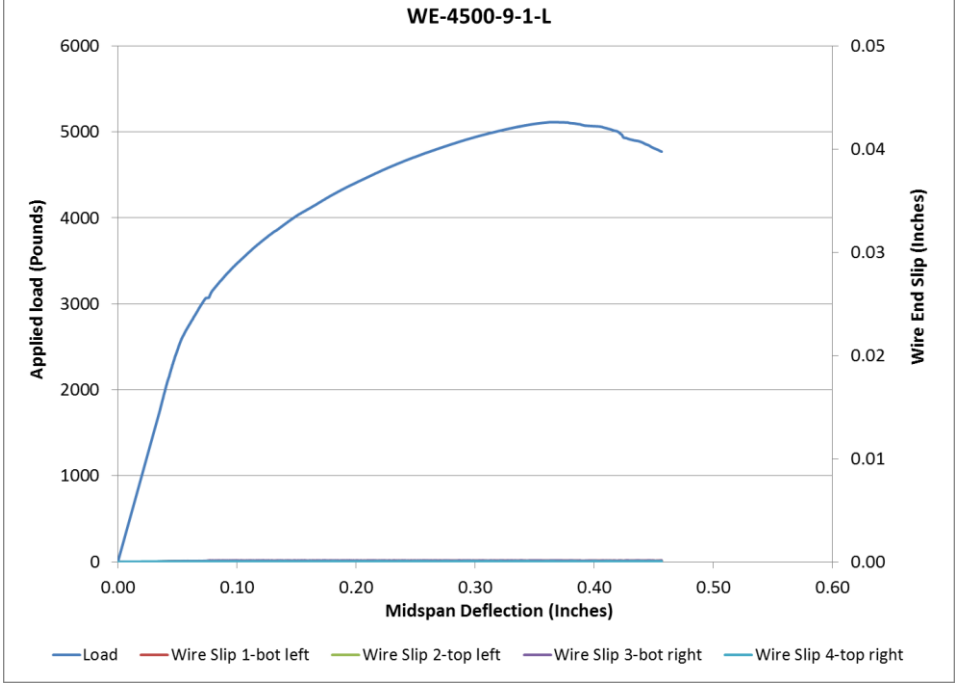


Figure 258 Load Deflection and Wire End Slip WE-4500-9-1-L



Figure 259 Picture of Failed Prism WE-4500-9-1-L

Beam Identification	WE-4500-9-1-S
Wire Type:	WE
Embedment Length:	13 in
Release Strength:	4500 psi
Slump:	9 in

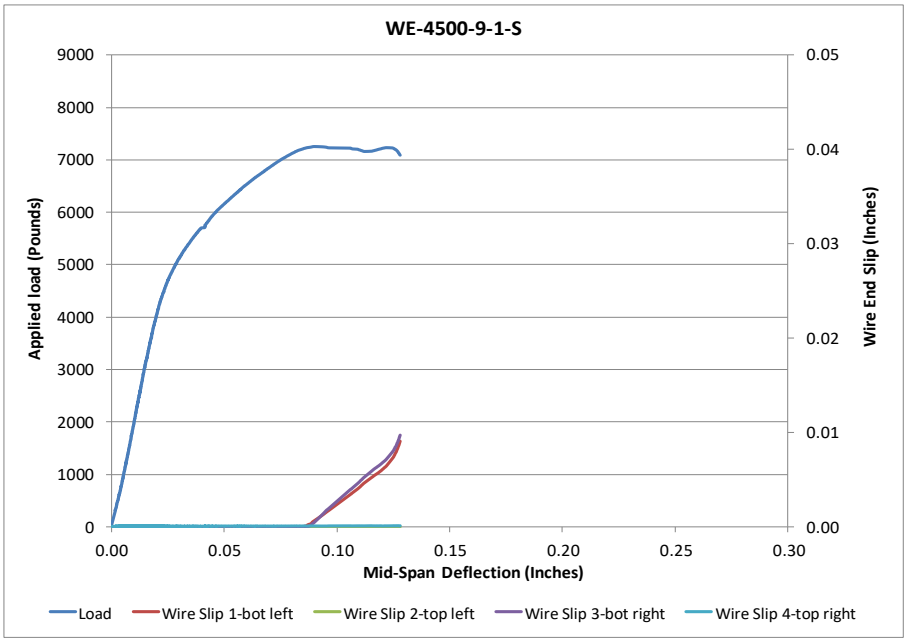


Figure 260 Load Deflection and Wire End Slip WE-4500-9-1-S

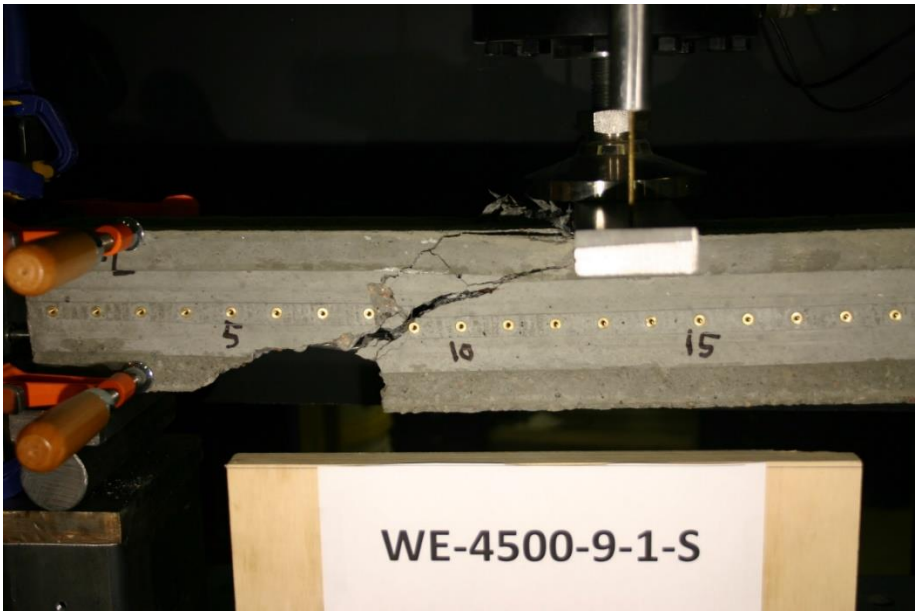


Figure 261 Picture of Failed Prism WE-4500-9-1-S

Beam Identification	WE-4500-9-2-L
Wire Type:	WE
Embedment Length:	16.5 in
Release Strength:	4500 psi
Slump:	9 in

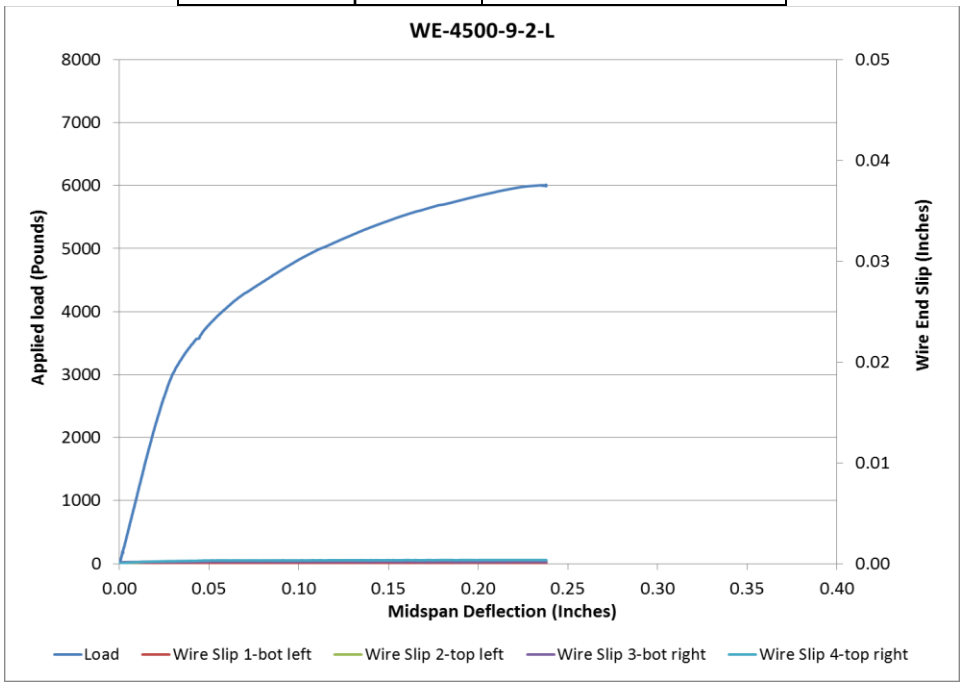


Figure 262 Load Deflection and Wire End Slip WE-4500-9-2-L

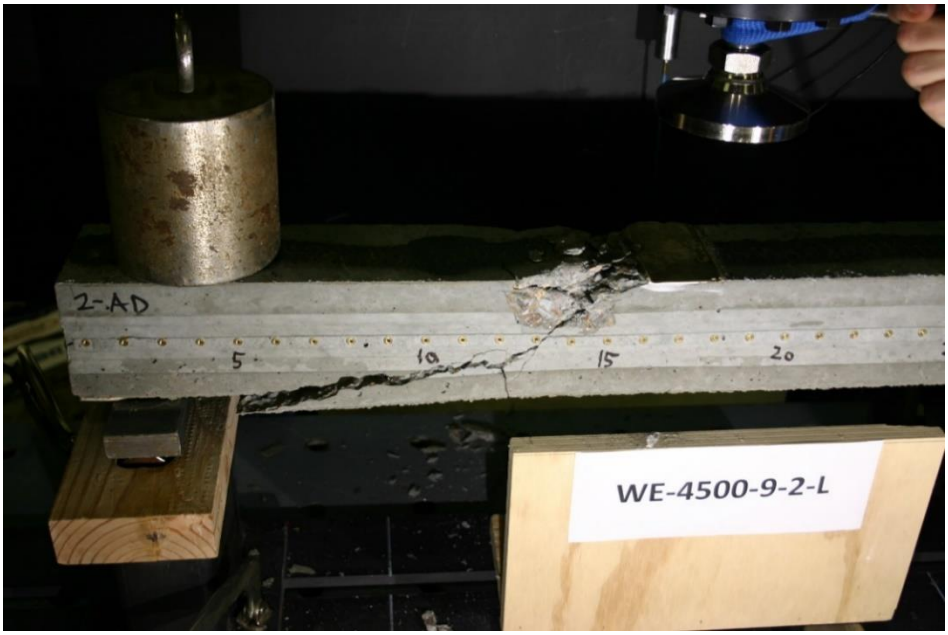


Figure 263 Picture of Failed Prism WE-4500-9-2-L

Beam Identification	WE-4500-9-2-S
Wire Type:	WE
Embedment Length:	9.5 in
Release Strength:	4500 psi
Slump:	9 in

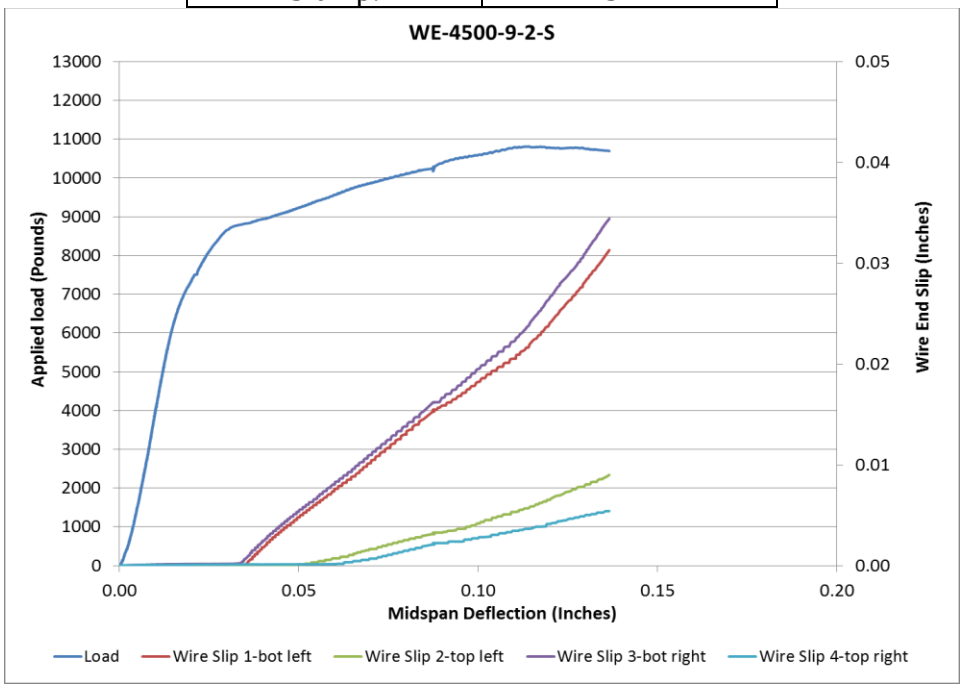


Figure 264 Load Deflection and Wire End Slip WE-4500-9-2-S



Figure 265 Picture of Failed Prism WE-4500-9-2-S

Beam Identification	WG-4500-9-1-L
Wire Type:	WG
Embedment Length:	20 in
Release Strength:	4500 psi
Slump:	9 in

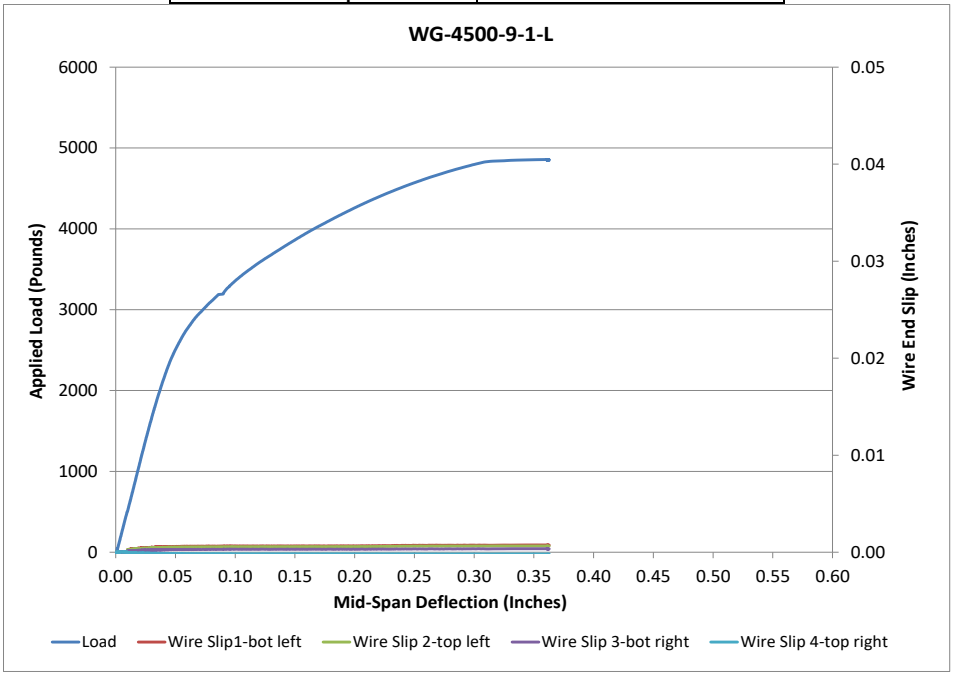


Figure 266 Load Deflection and Wire End Slip WG-4500-9-1-L



Figure 267 Picture of Failed Prism WG-4500-9-1-L

Beam Identification	WG-4500-9-1-S
Wire Type:	WG
Embedment Length:	13 in
Release Strength:	4500 psi
Slump:	in

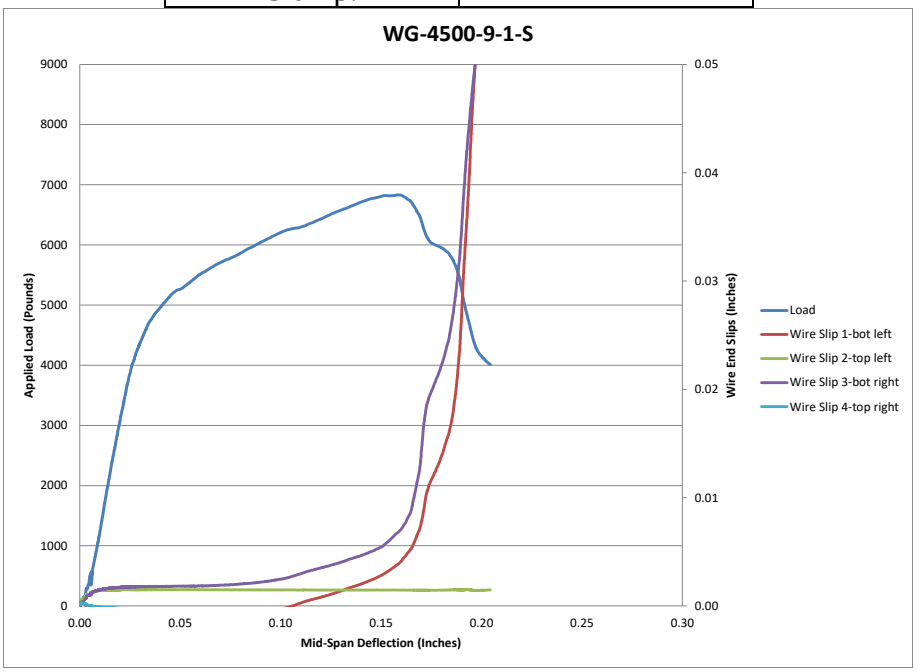


Figure 268 Load Deflection and Wire End Slip WG-4500-9-1-S



Figure 269 Picture of Failed Prism WG-4500-9-1-S

Beam Identification	WG-4500-9-2-L
Wire Type:	WG
Embedment Length:	16.5 in
Release Strength:	4500 psi
Slump:	9 in

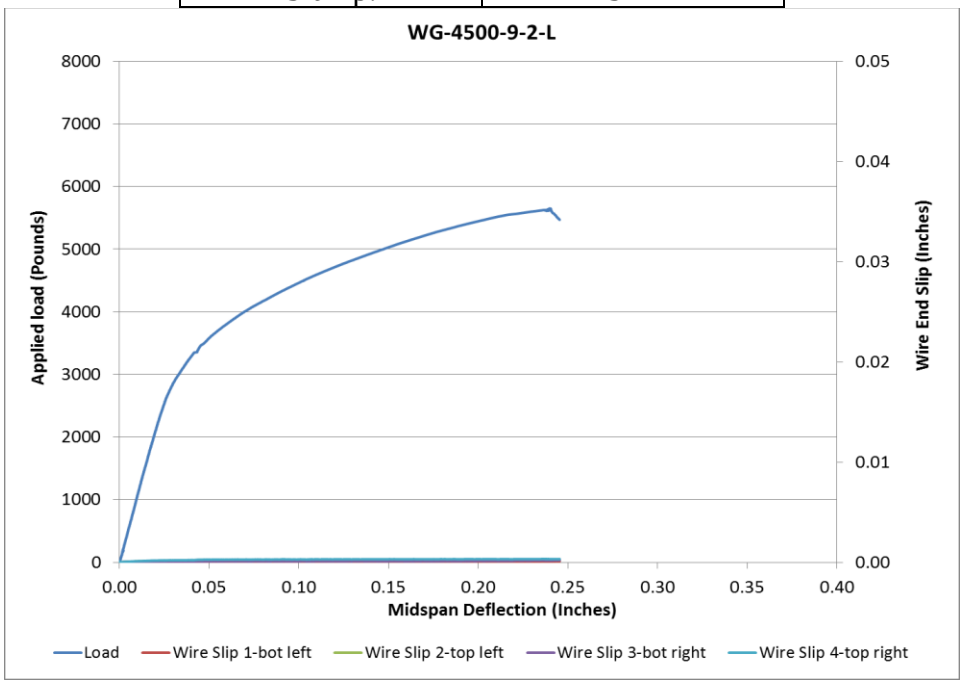


Figure 270 Load Deflection and Wire End Slip WG-4500-9-2-L



Figure 271 Picture of Failed Prism WG-4500-9-2-L

Beam Identification	WG-4500-9-2-S
Wire Type:	WG
Embedment Length:	9.5 in
Release Strength:	4500 psi
Slump:	9 in

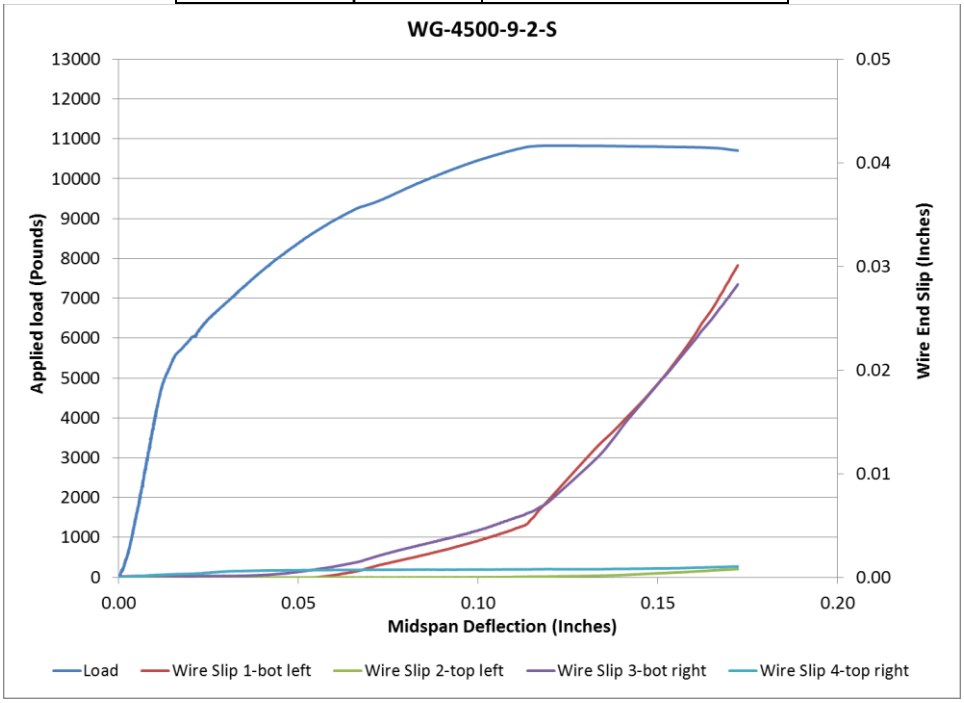


Figure 272 Load Deflection and Wire End Slip WG-4500-9-2-S



Figure 273 Picture of Failed Prism WG-4500-9-2-S

Beam Identification	WH-4500-9-1-L
Wire Type:	WH
Embedment Length:	20 in
Release Strength:	4500 psi
Slump:	9 in

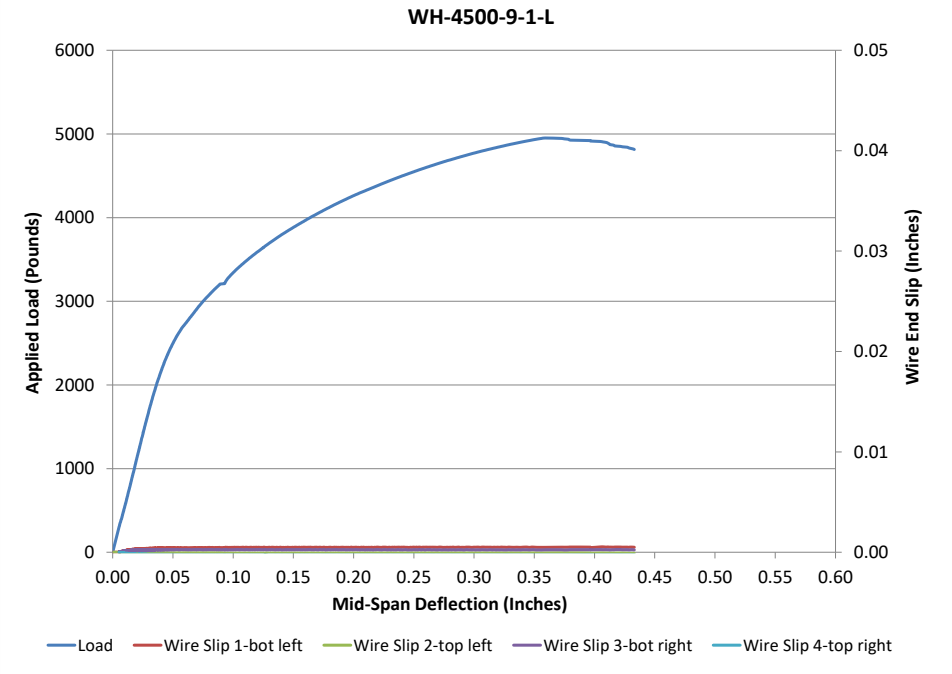


Figure 274 Load Deflection and Wire End Slip WH-4500-9-1-L

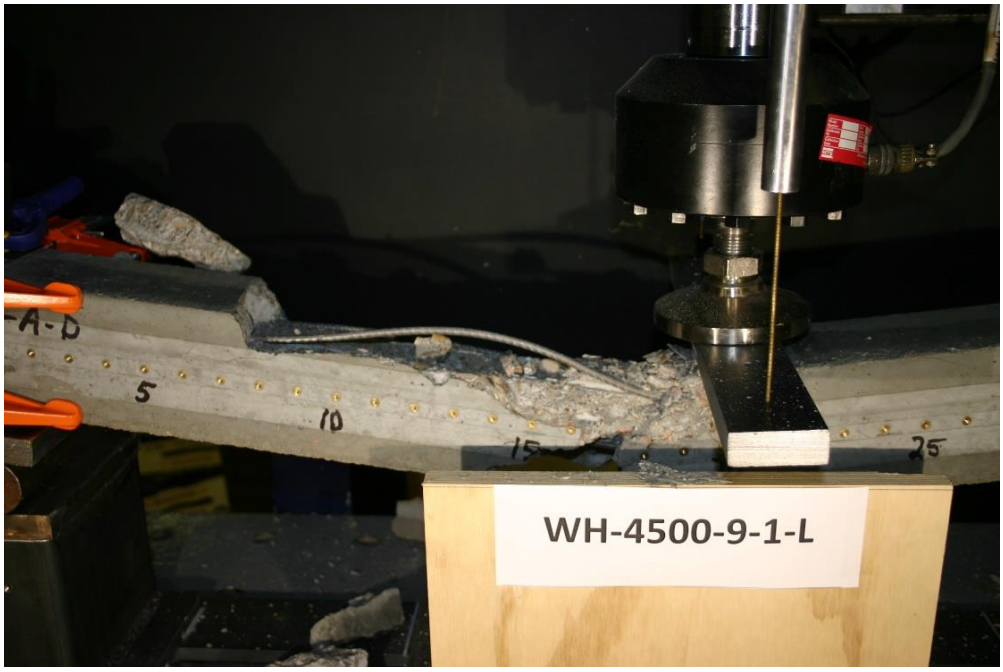


Figure 275 Picture of Failed Prism WH-4500-9-1-L

Beam Identification	WH-4500-9-1-S
Wire Type:	WH
Embedment Length:	13 in
Release Strength:	4500 psi
Slump:	9 in

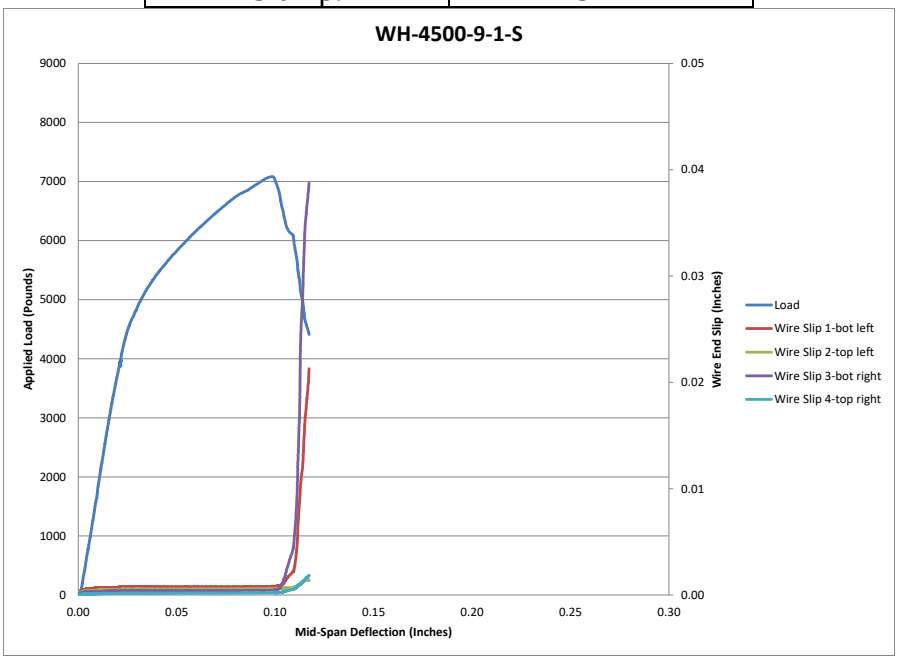


Figure 276 Load Deflection and Wire End Slip WH-4500-9-1-S

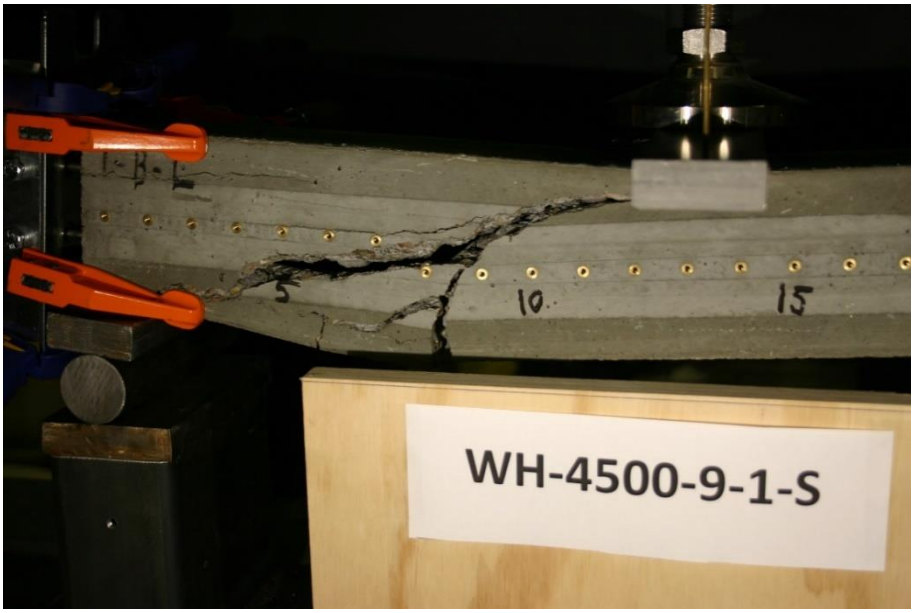


Figure 277 Picture of Failed Prism WH-4500-9-1-S

Beam Identification	WH-4500-9-2-L
Wire Type:	WH
Embedment Length:	16.5 in
Release Strength:	4500 psi
Slump:	9 in

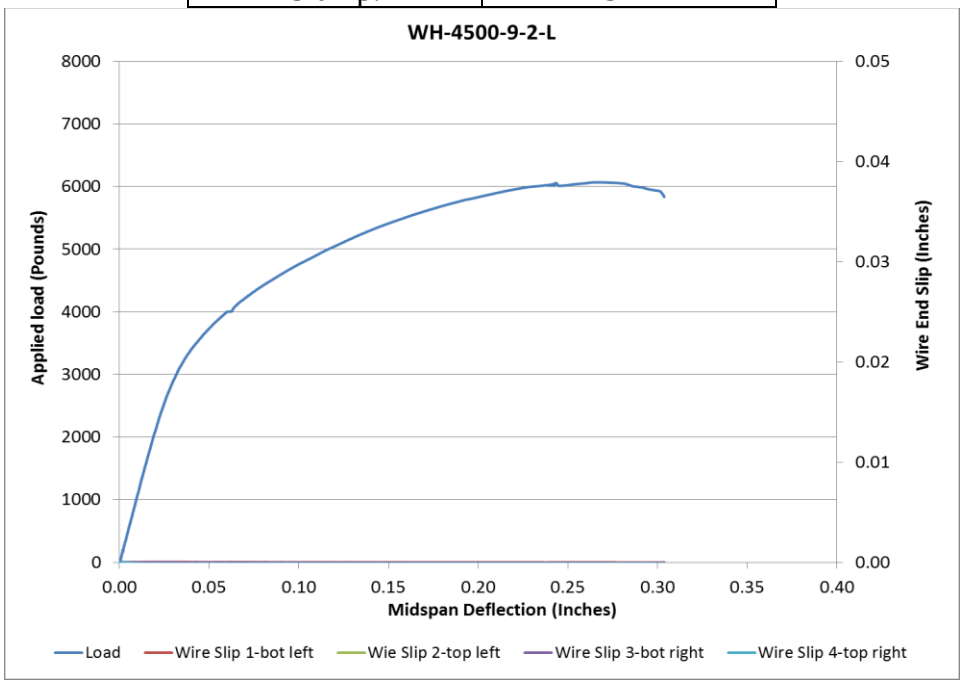


Figure 278 Load Deflection and Wire End Slip WH-4500-9-2-L

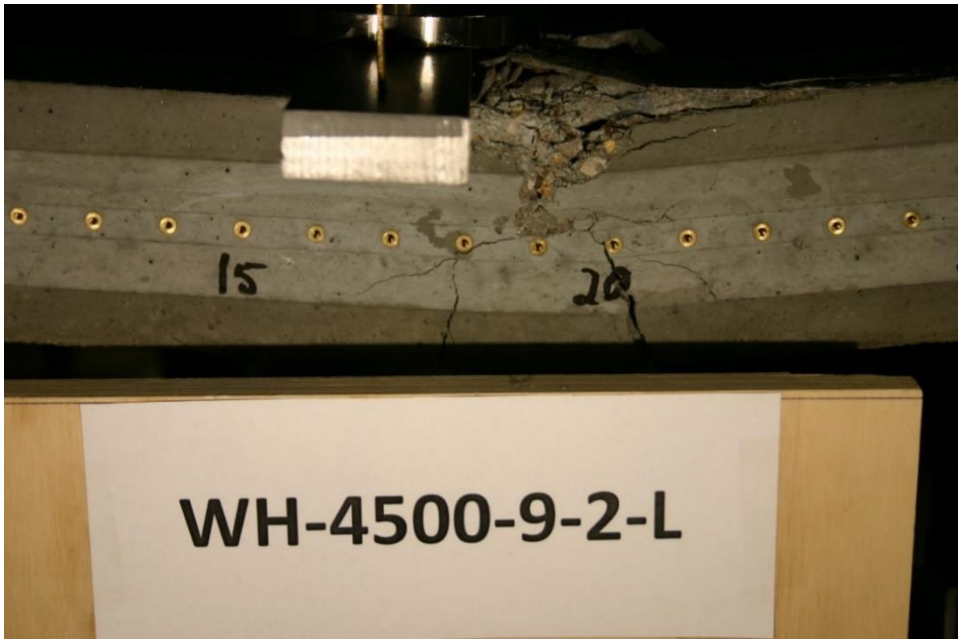


Figure 279 Picture of Failed Prism WH-4500-9-2-L

Beam Identification	WH-4500-9-2-S
Wire Type:	WH
Embedment Length:	9.5 in
Release Strength:	4500 psi
Slump:	9 in

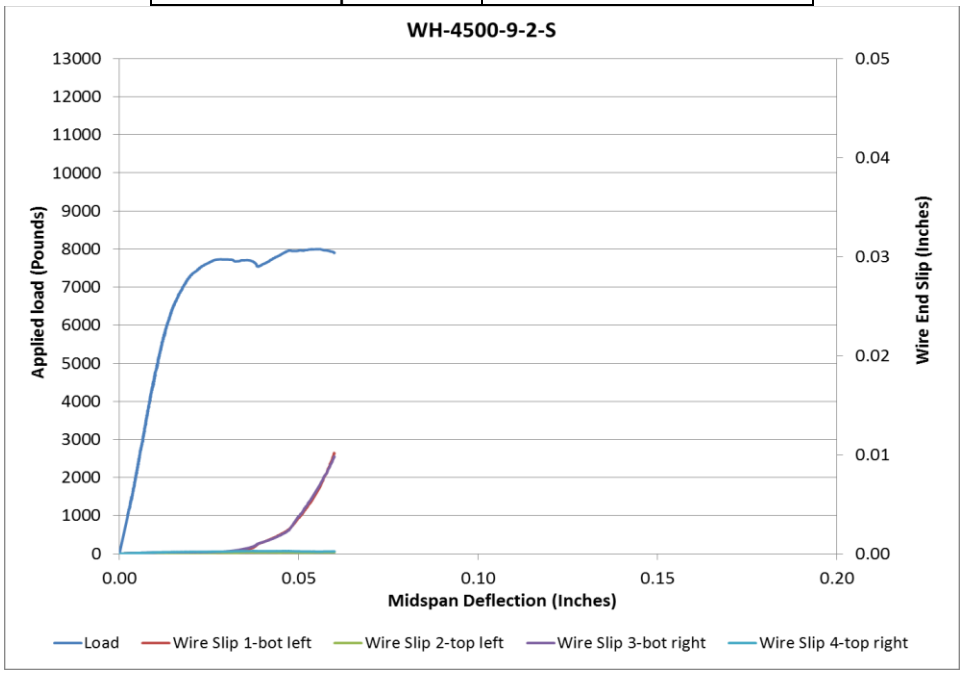


Figure 280 Load Deflection and Wire End Slip WH-4500-9-2-S

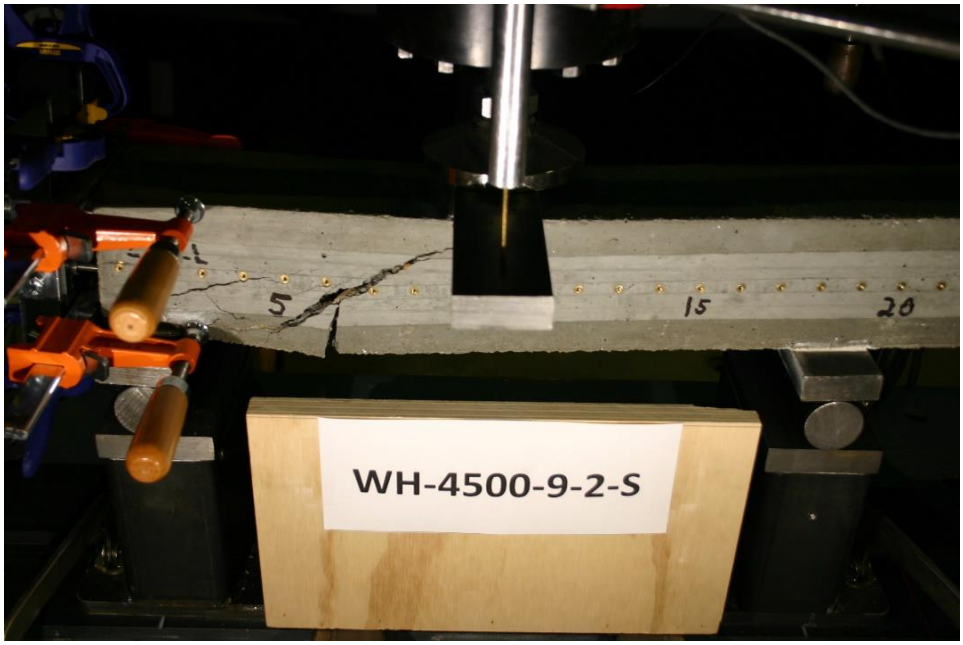


Figure 281 Picture of Failed Prism WH-4500-9-2-S

Beam Identification	WK-4500-9-1-L
Wire Type:	WK
Embedment Length:	20 in
Release Strength:	4500 psi
Slump:	9 in

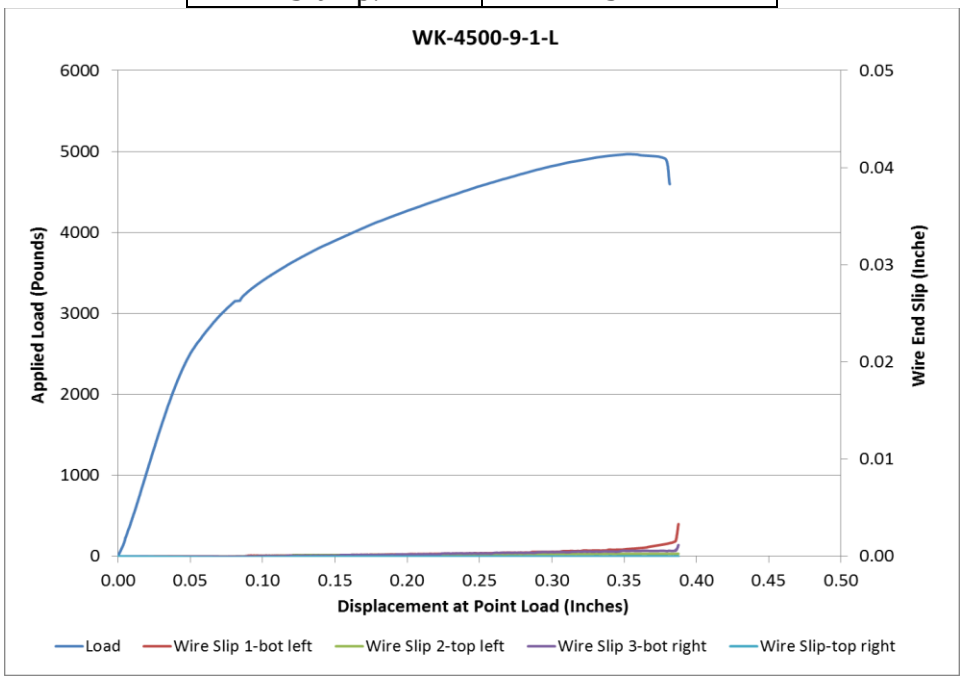


Figure 282 Load Deflection and Wire End Slip WK-4500-9-1-L



Figure 283 Picture of Failed Prism WK-4500-9-1-L

Beam Identification	WK-4500-9-1-S
Wire Type:	WK
Embedment Length:	13 in
Release Strength:	4500 psi
Slump:	9 in

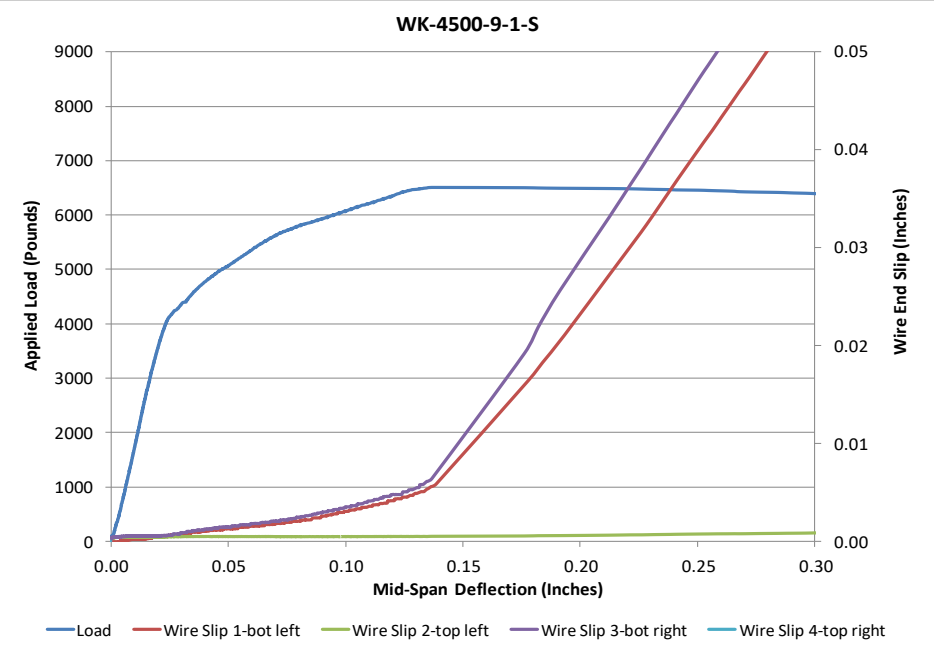


Figure 284 Load Deflection and Wire End Slip WK-4500-9-1-S

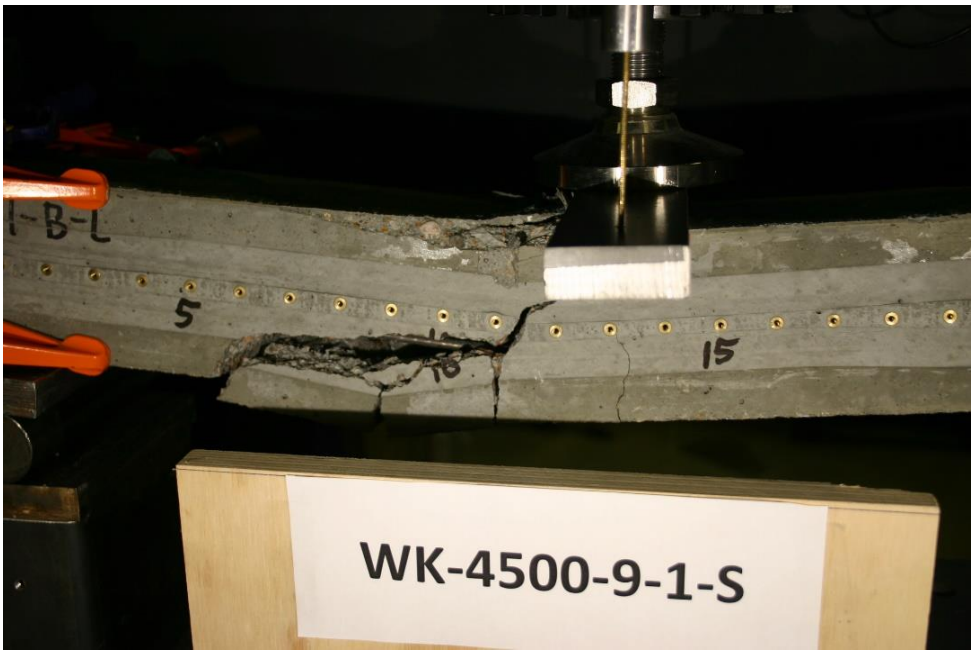


Figure 285 Picture of Failed Prism WK-4500-9-1-S

Beam Identification	WK-4500-9-2-L
Wire Type:	WK
Embedment Length:	16.5 in
Release Strength:	4500 psi
Slump:	9 in

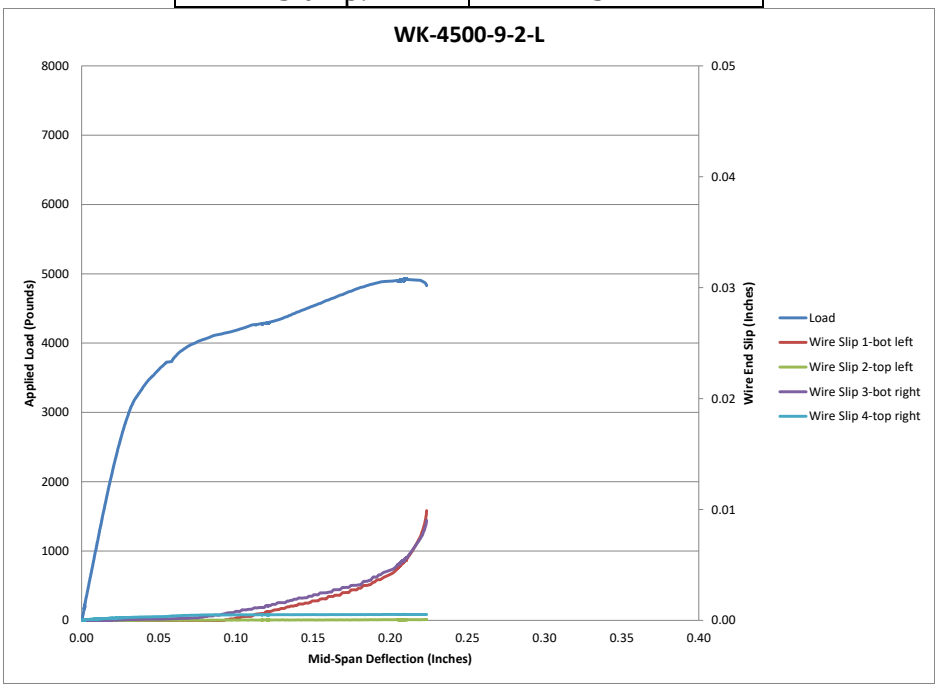


Figure 286 Load Deflection and Wire End Slip WK-4500-9-2-L

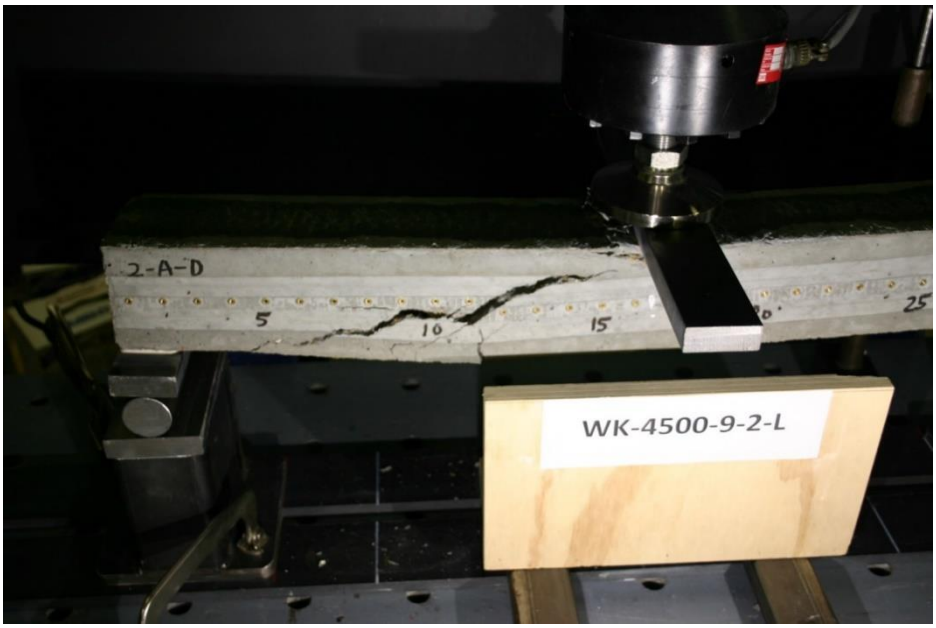


Figure 287 Picture of Failed Prism WK-4500-9-2-L

Beam Identification	WK-4500-9-2-S
Wire Type:	WK
Embedment Length:	9.5 in
Release Strength:	4500 psi
Slump:	9 in

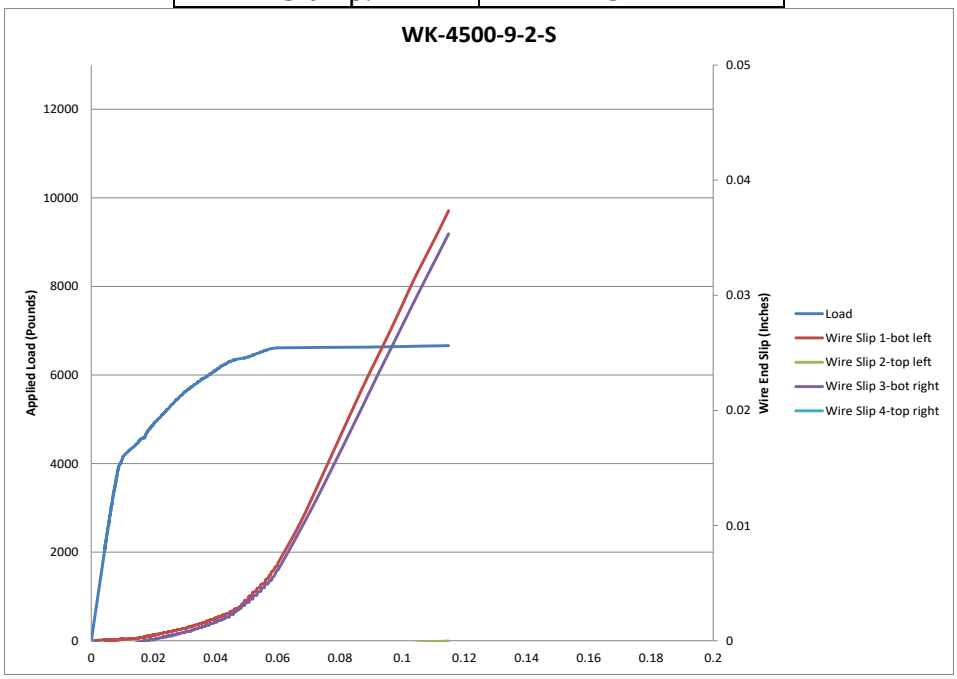


Figure 288 Load Deflection and Wire End Slip WK-4500-9-2-S

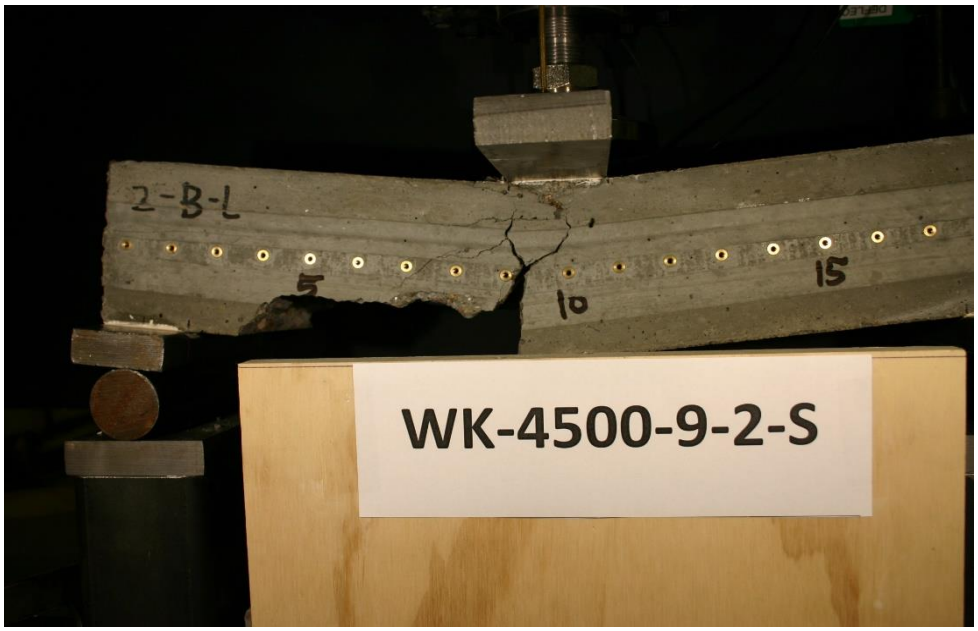


Figure 289 Picture of Failed Prism WK-4500-9-2-S

Prisms made with wires, 6000 psi concrete release strength and 6 in. slump

Beam Identification	WA-6000-6-1-L
Wire Type:	WA
Embedment Length:	20 in
Release Strength:	6000 psi
Slump:	6 in

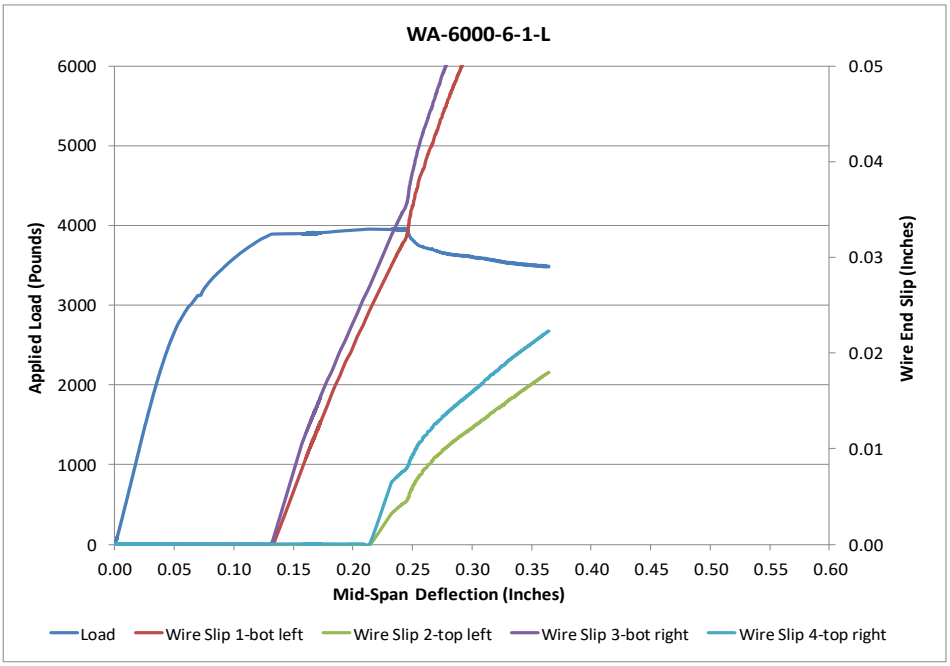


Figure 290 Load Deflection and Wire End Slip WA-6000-6-1-L

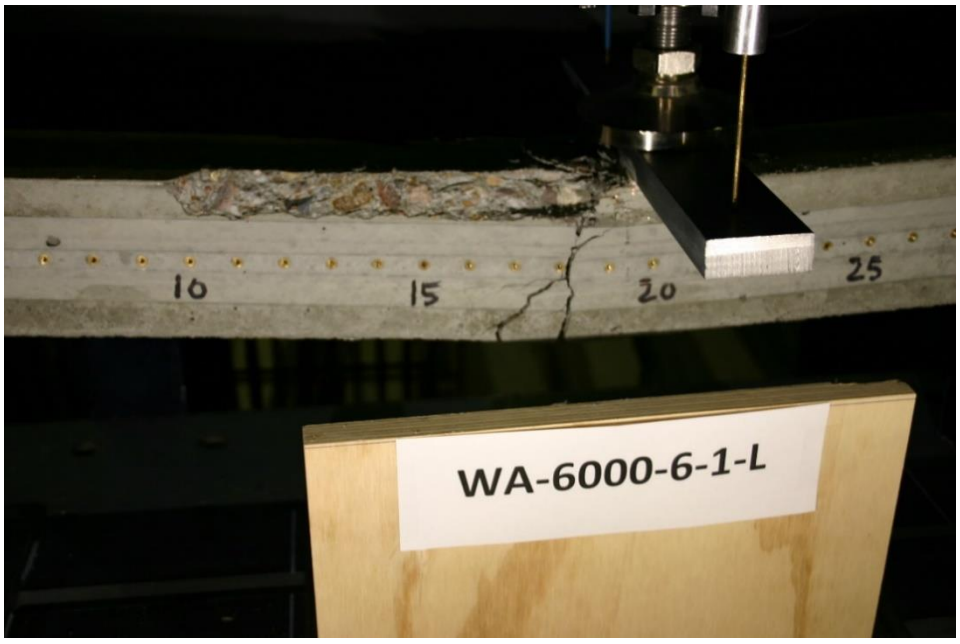


Figure 291 Picture of Failed Prism WA-6000-6-1-L

Beam Identification	WA-6000-6-1-S
Wire Type:	WA
Embedment Length:	13 in
Release Strength:	6000 psi
Slump:	6 in

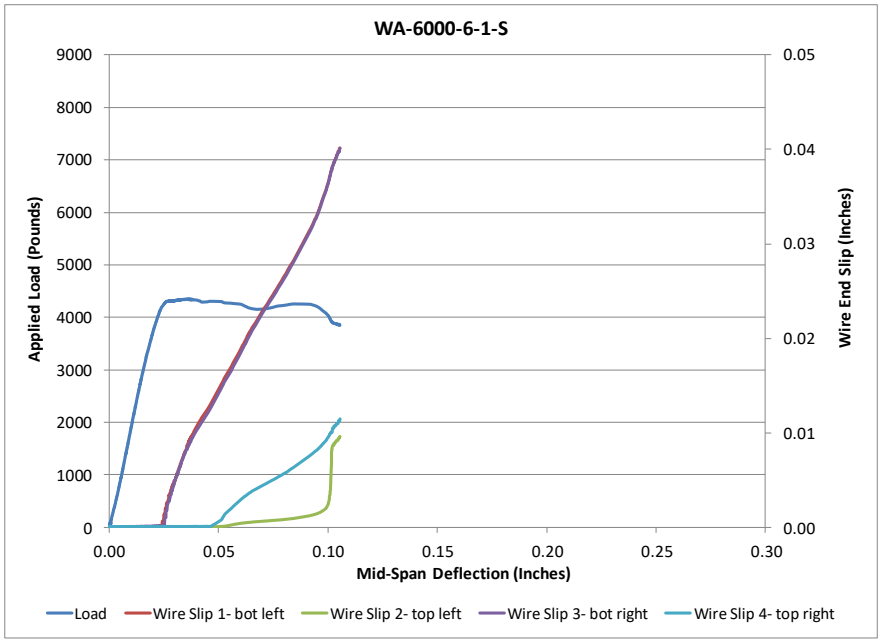


Figure 292 Load Deflection and Wire End Slip WA-6000-6-1-S

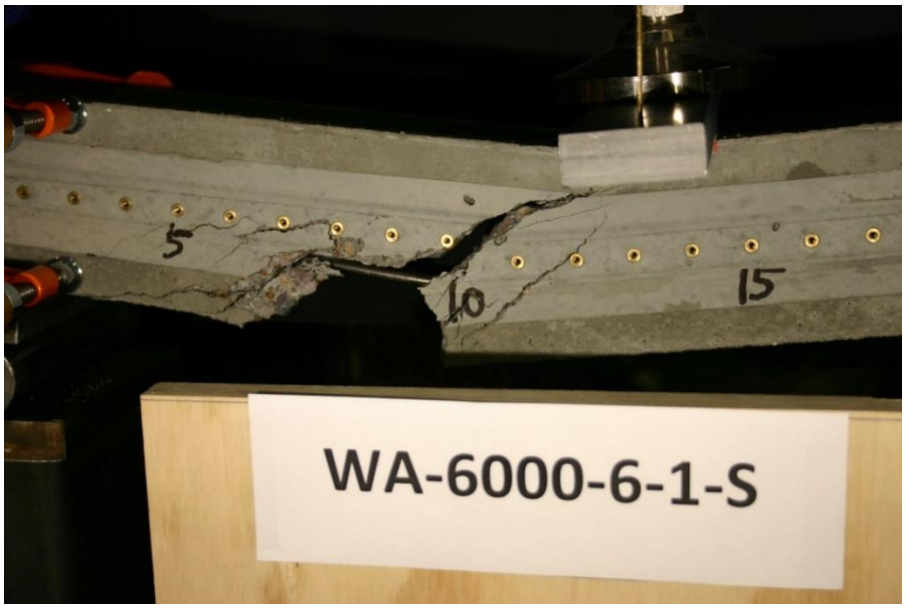


Figure 293 Picture of Failed Prism WA-6000-6-1-S

Beam Identification	WA-6000-6-2-L
Wire Type:	WA
Embedment Length:	16.5 in
Release Strength:	6000 psi
Slump:	6 in

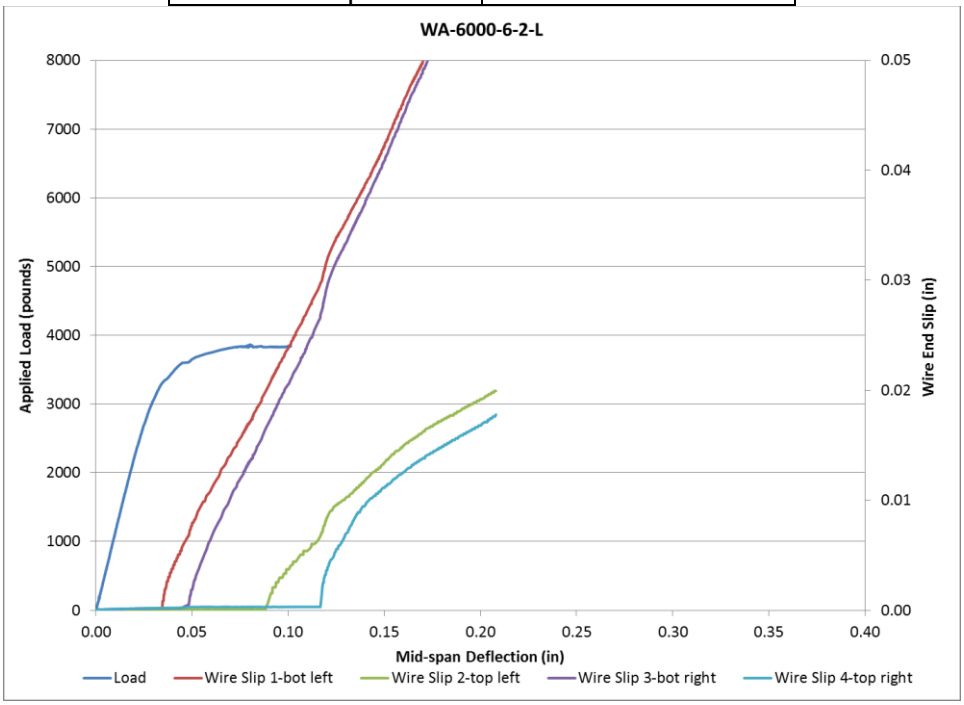


Figure 294 Load Deflection and Wire End Slip WA-6000-6-2-L



Figure 295 Picture of Failed Prism WA-6000-6-2-L

Beam Identification	WA-6000-6-2-S
Wire Type:	WA
Embedment Length:	9.5 in
Release Strength:	6000 psi
Slump:	6 in

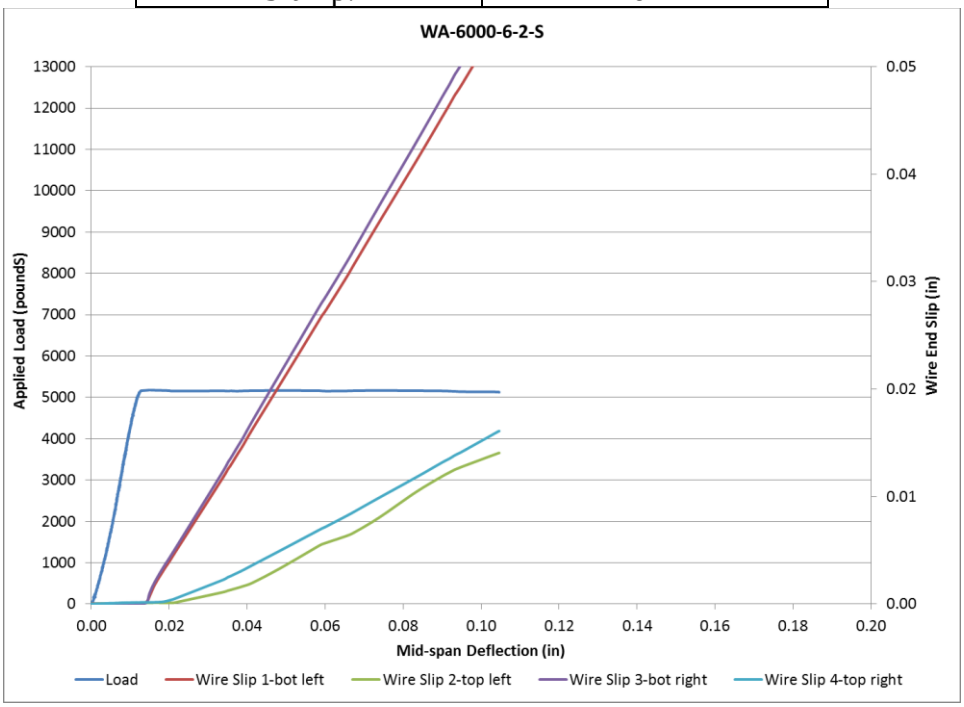


Figure 296 Load Deflection and Wire End Slip WA-6000-6-2-S

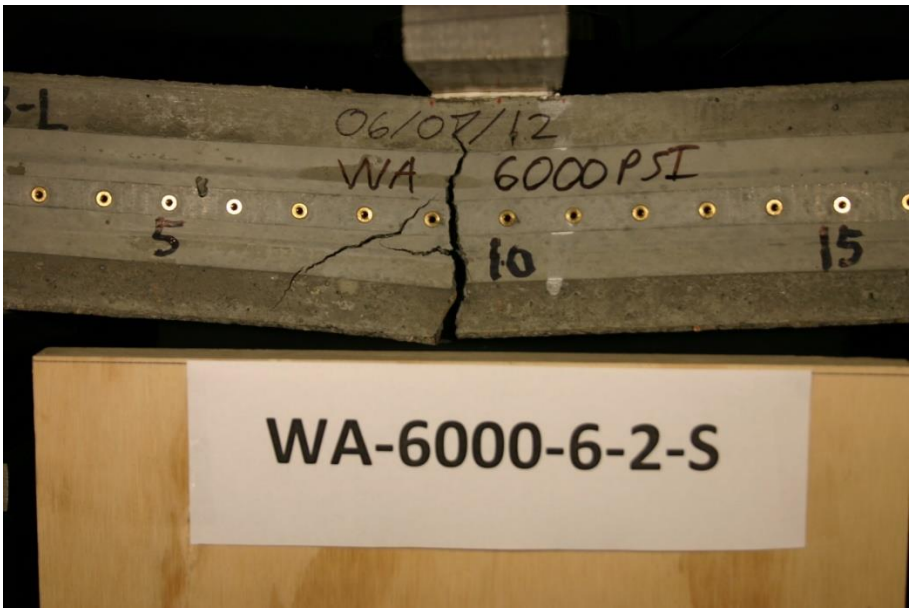


Figure 297 Picture of Failed Prism WA-6000-6-2-S

Beam Identification	WE-6000-6-1-L
Wire Type:	WE
Embedment Length:	20 in
Release Strength:	6000 psi
Slump:	6 in

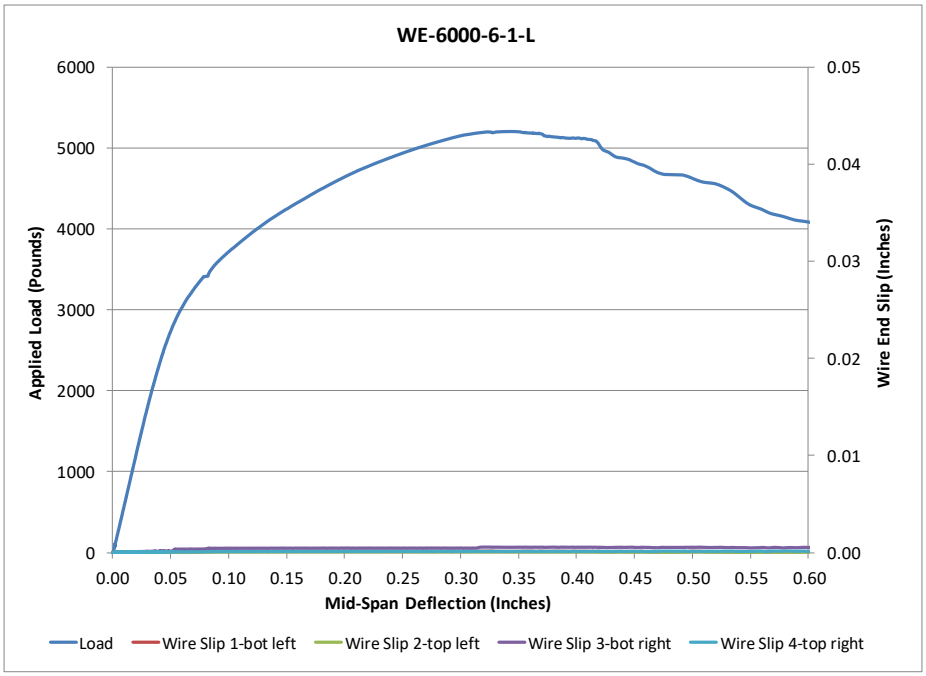


Figure 298 Load Deflection and Wire End Slip WE-6000-6-1-L

Beam Identification	WE-6000-6-1-S
Wire Type:	WE
Embedment Length:	13 in
Release Strength:	4500 psi
Slump:	6 in

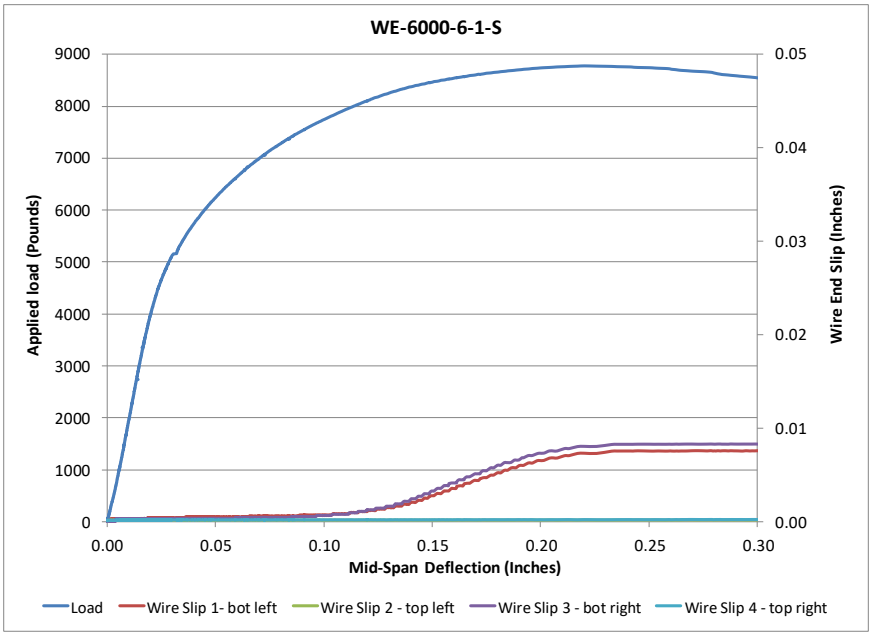


Figure 299 Load Deflection and Wire End Slip WE-6000-6-1-S

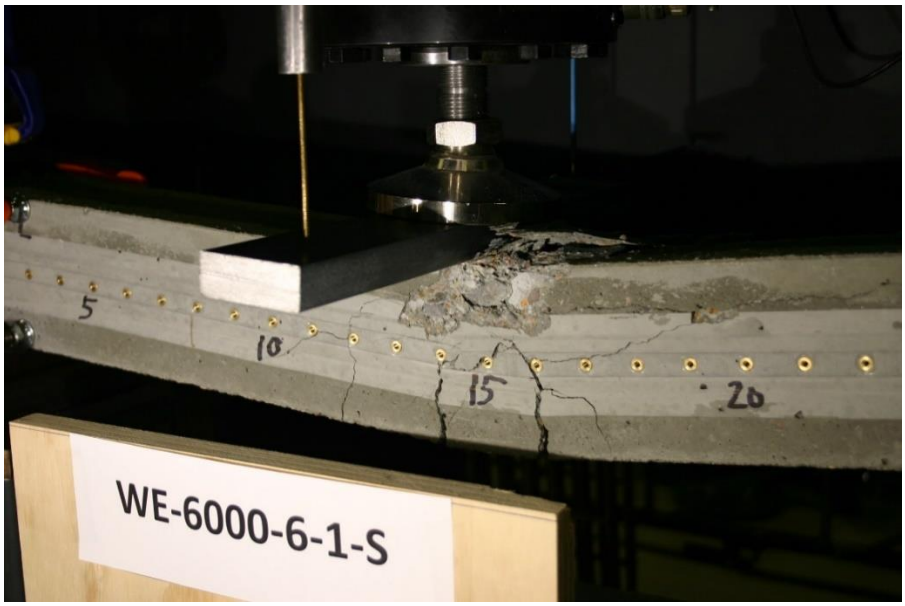


Figure 300 Picture of Failed Prism WE-6000-6-1-S

Beam Identification	WE-6000-6-2-L
Wire Type:	WE
Embedment Length:	16.5 in
Release Strength:	4500 psi
Slump:	6 in

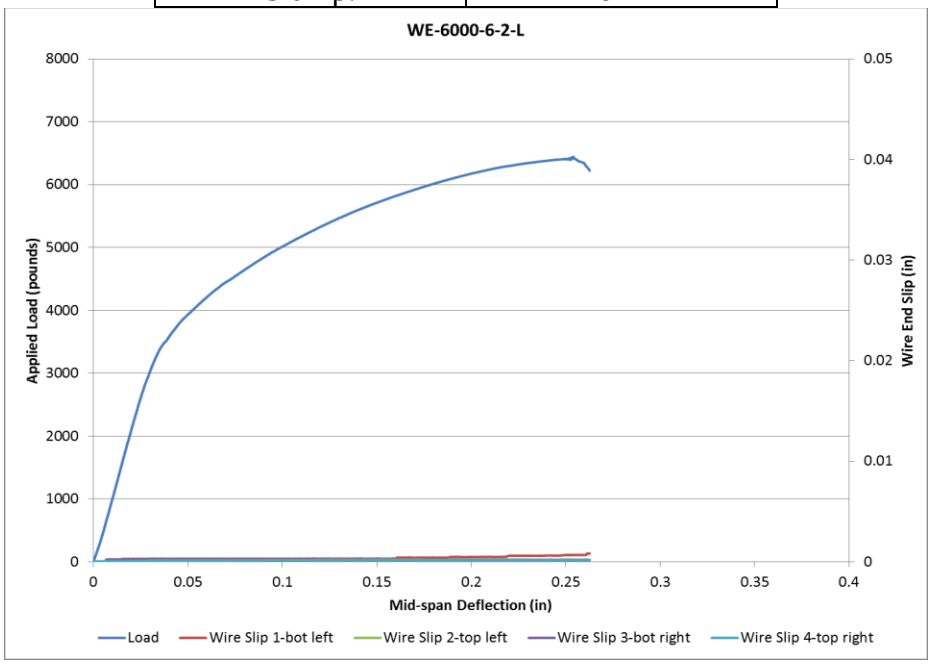


Figure 301 Load Deflection and Wire End Slip WE-6000-6-2-L



Figure 302 Picture of Failed Prism WE-6000-6-2-L

Beam Identification	WE-6000-6-2-S
Wire Type:	WE
Embedment Length:	9.5 in
Release Strength:	4500 psi
Slump:	6 in

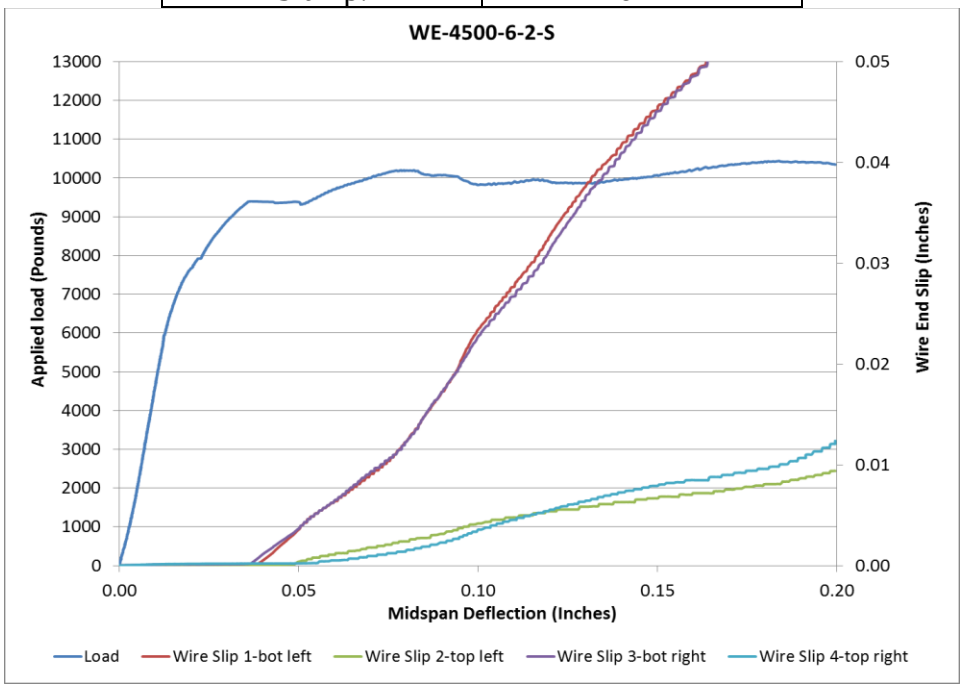


Figure 303 Load Deflection and Wire End Slip WE-6000-6-2-S

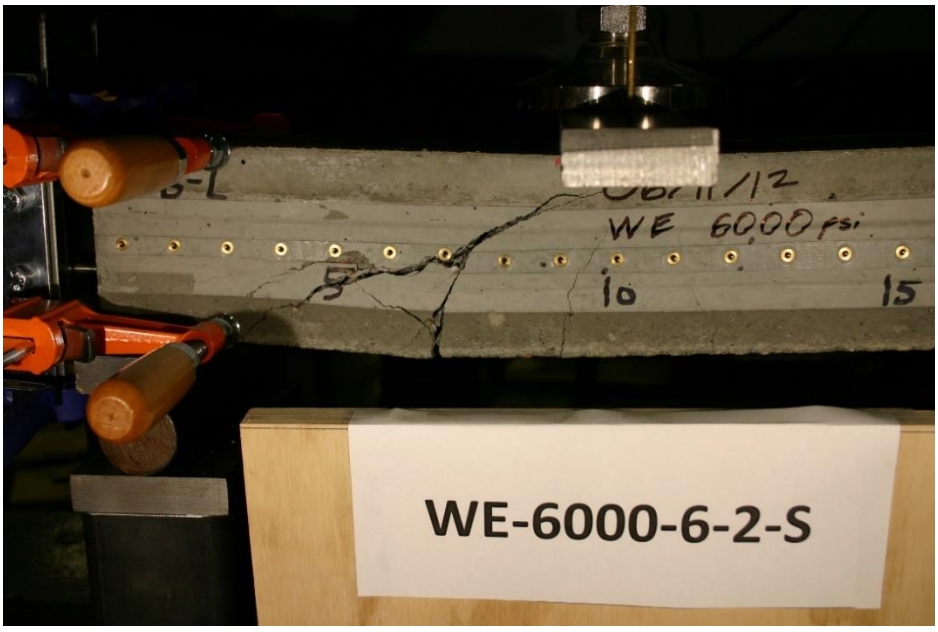


Figure 304 Picture of Failed Prism WE-6000-6-2-S

Beam Identification	WG-6000-6-1-L
Wire Type:	WG
Embedment Length:	20 in
Release Strength:	6000 psi
Slump:	6 in

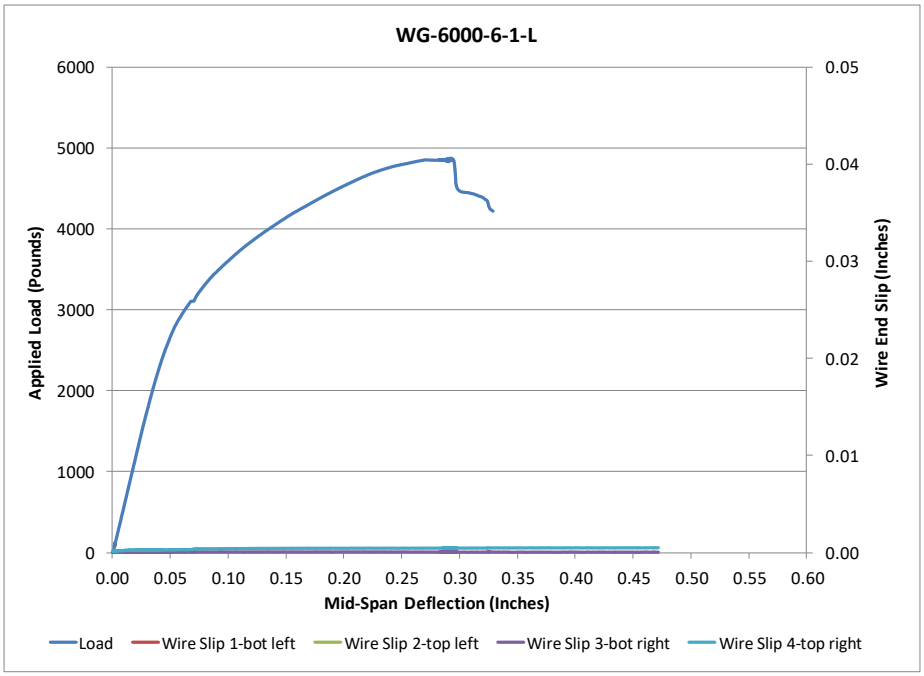


Figure 305 Load Deflection and Wire End Slip WG-6000-6-1-L

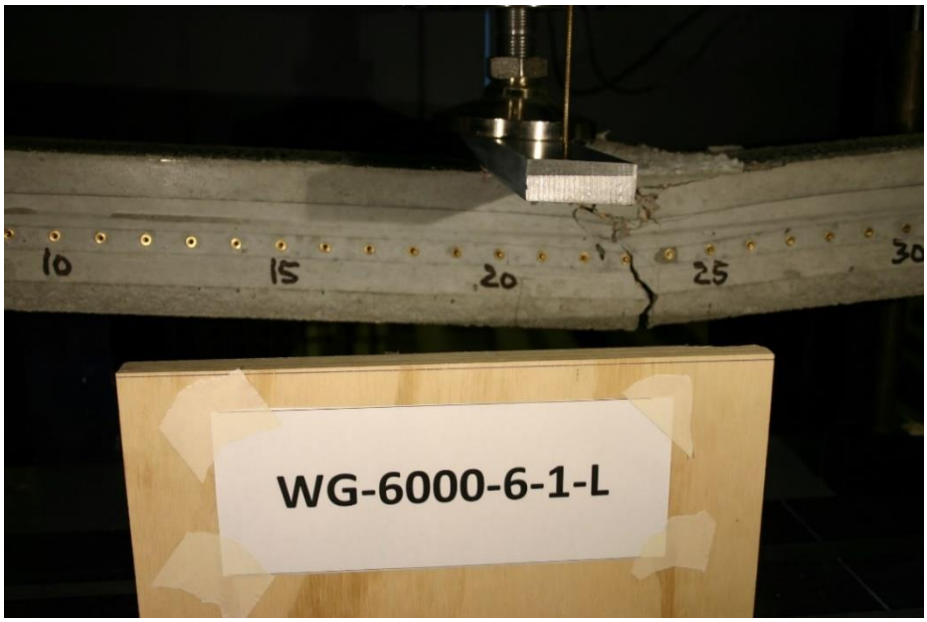


Figure 306 Picture of Failed Prism WG-6000-6-1-L

Beam Identification	WG-6000-6-1-S
Wire Type:	WG
Embedment Length:	13 in
Release Strength:	6000 psi
Slump:	6 in

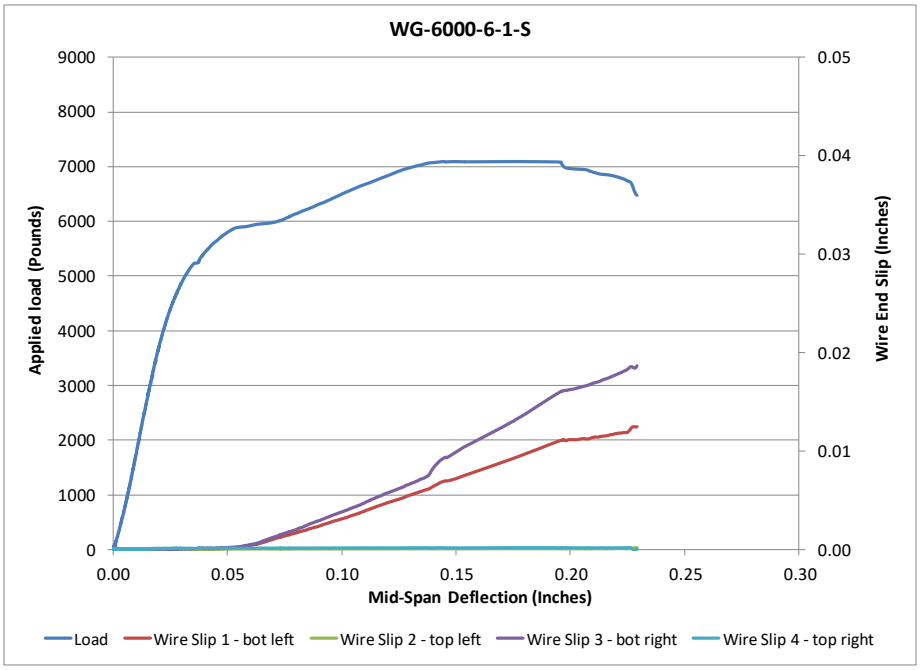


Figure 307 Load Deflection and Wire End Slip WG-6000-6-1-S

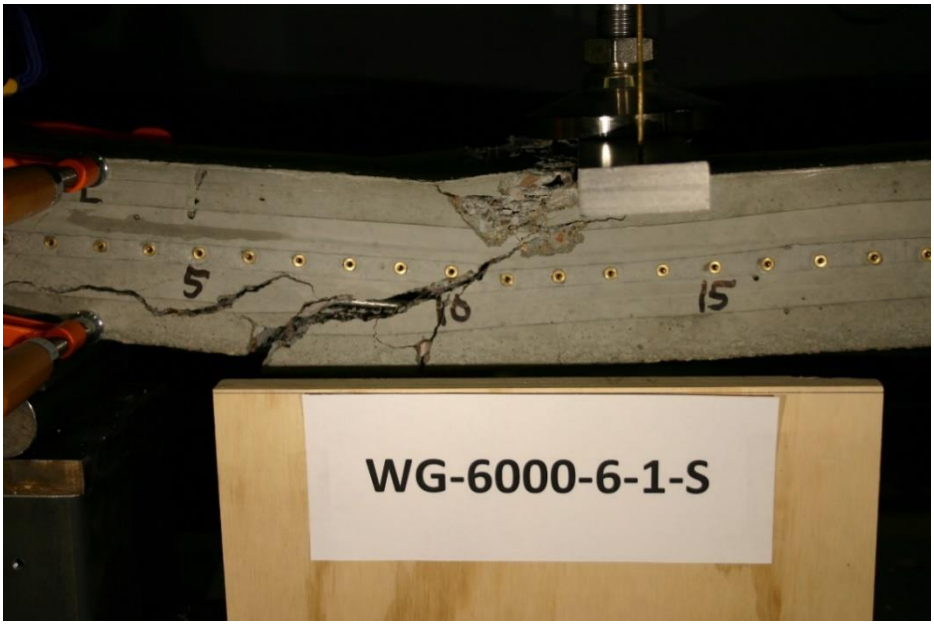


Figure 308 Picture of Failed Prism WG-6000-6-1-S

Beam Identification	WG-6000-6-2-L
Wire Type:	WG
Embedment Length:	16.5 in
Release Strength:	6000 psi
Slump:	6 in

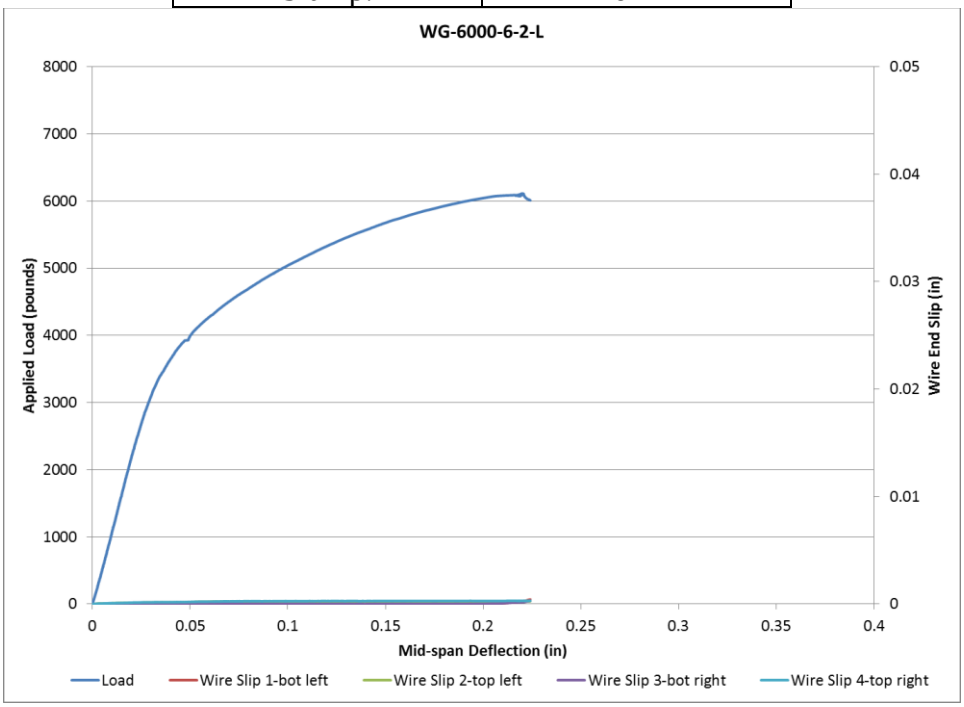


Figure 309 Load Deflection and Wire End Slip WG-6000-6-2-L



Figure 310 Picture of Failed Prism WG-6000-6-2-L

Beam Identification	WG-6000-6-2-S
Wire Type:	WG
Embedment Length:	9.5 in
Release Strength:	6000 psi
Slump:	6 in

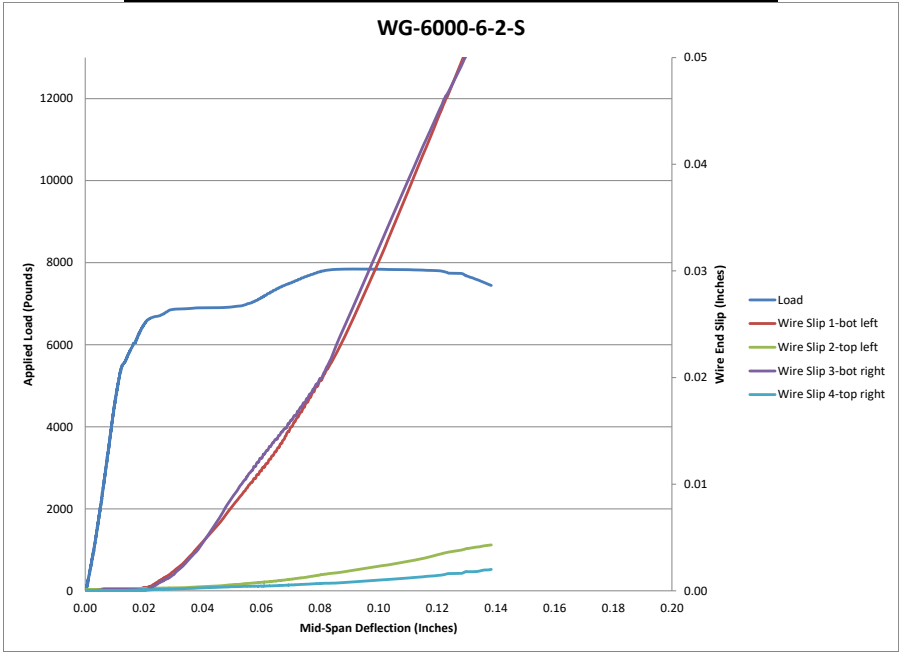


Figure 311 Load Deflection and Wire End Slip WG-6000-6-2-S



Figure 312 Picture of Failed Prism WG-6000-6-2-S

Beam Identification	WH-6000-6-1-L
Wire Type:	WH
Embedment Length:	20 in
Release Strength:	6000 psi
Slump:	6 in

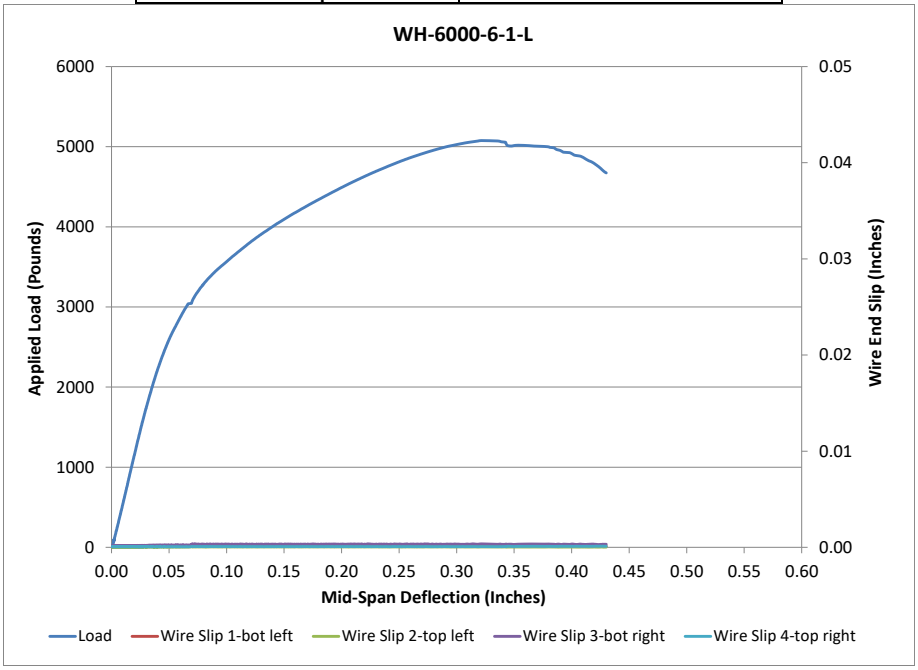


Figure 313 Load Deflection and Wire End Slip WH-6000-6-1-L

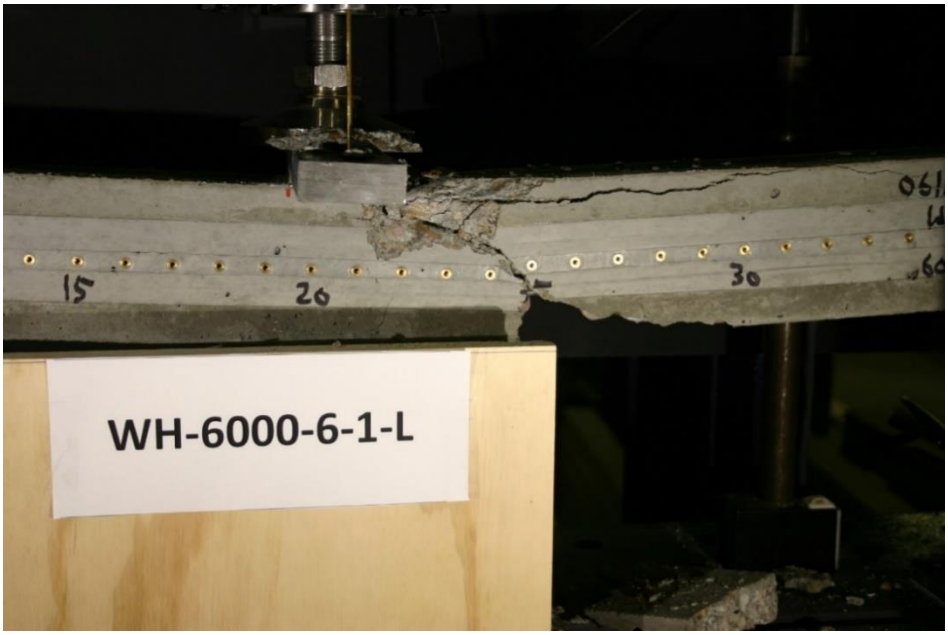


Figure 314 Picture of Failed Prism WH-6000-6-1-L

Beam Identification	WH-6000-6-1-S
Wire Type:	WH
Embedment Length:	13 in
Release Strength:	6000 psi
Slump:	6 in

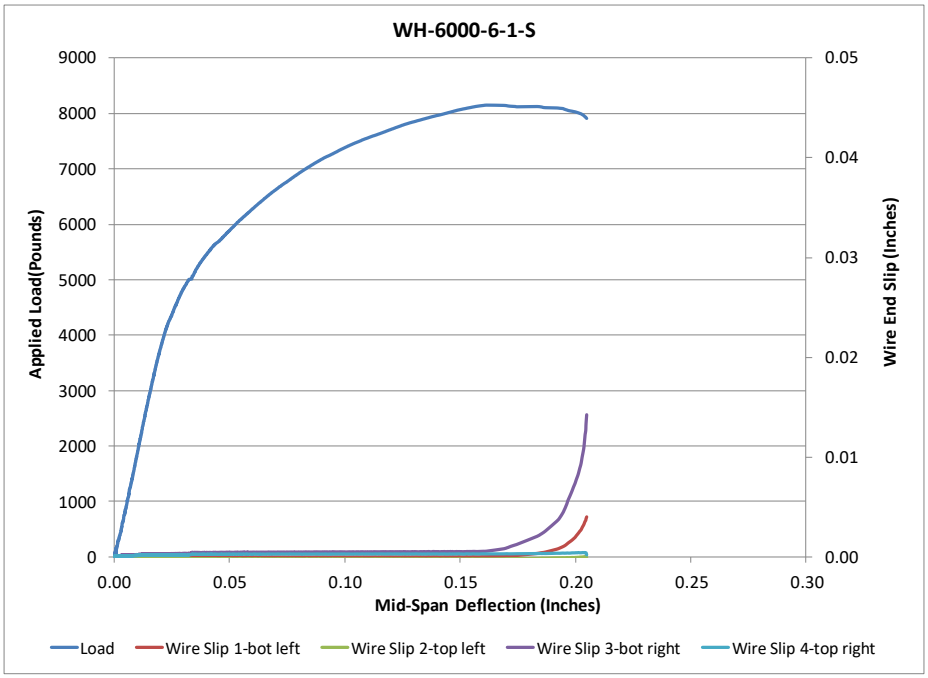


Figure 315 Load Deflection and Wire End Slip WH-6000-6-1-S

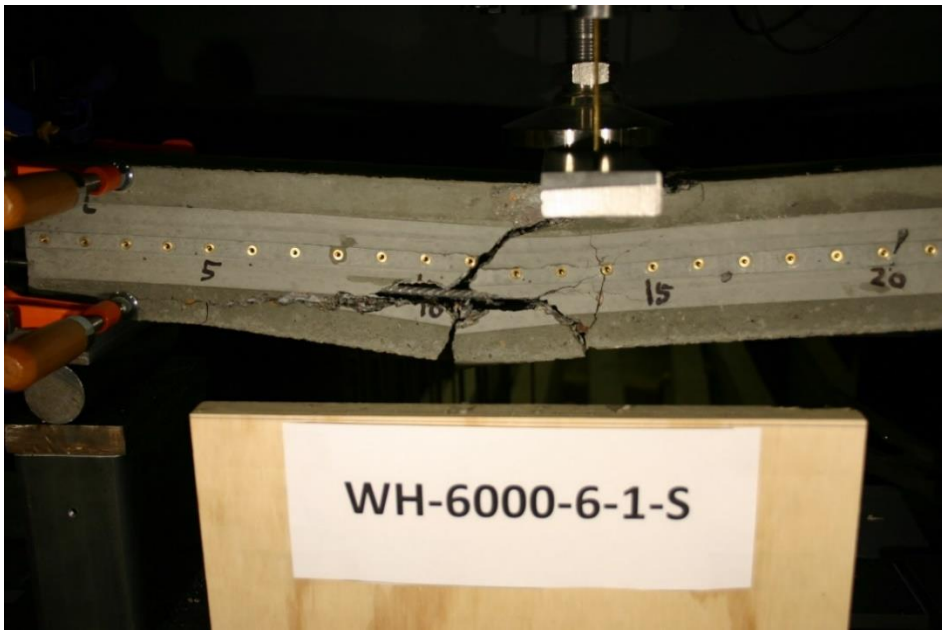


Figure 316 Picture of Failed Prism WH-6000-6-1-S

Beam Identification	WH-6000-6-2-L
Wire Type:	WH
Embedment Length:	16.5 in
Release Strength:	6000 psi
Slump:	6 in

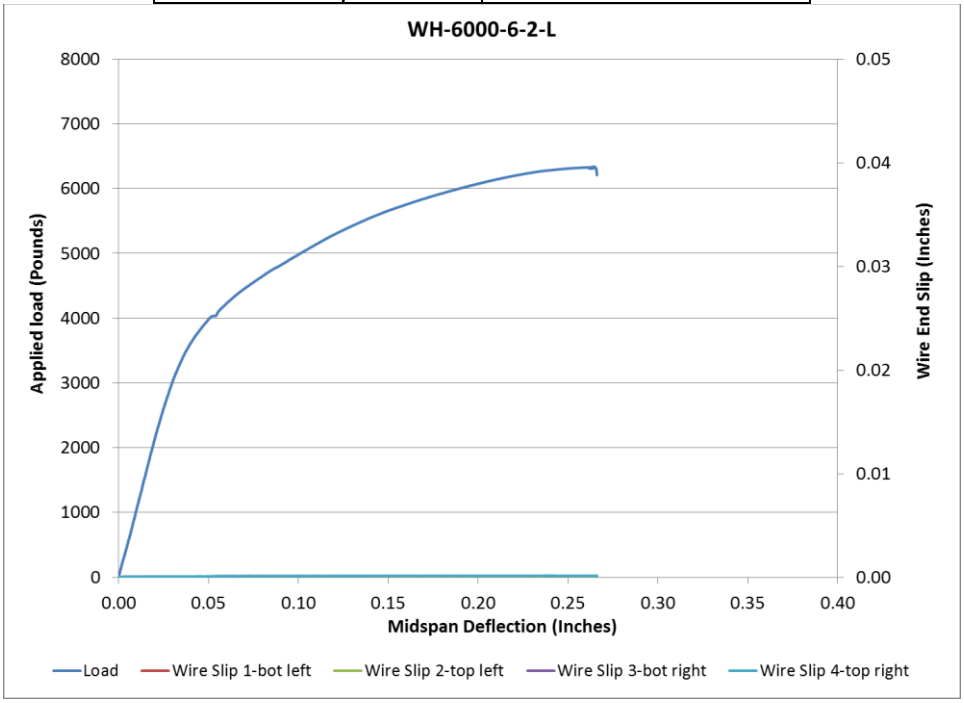


Figure 317 Load Deflection and Wire End Slip WH-6000-6-2-L

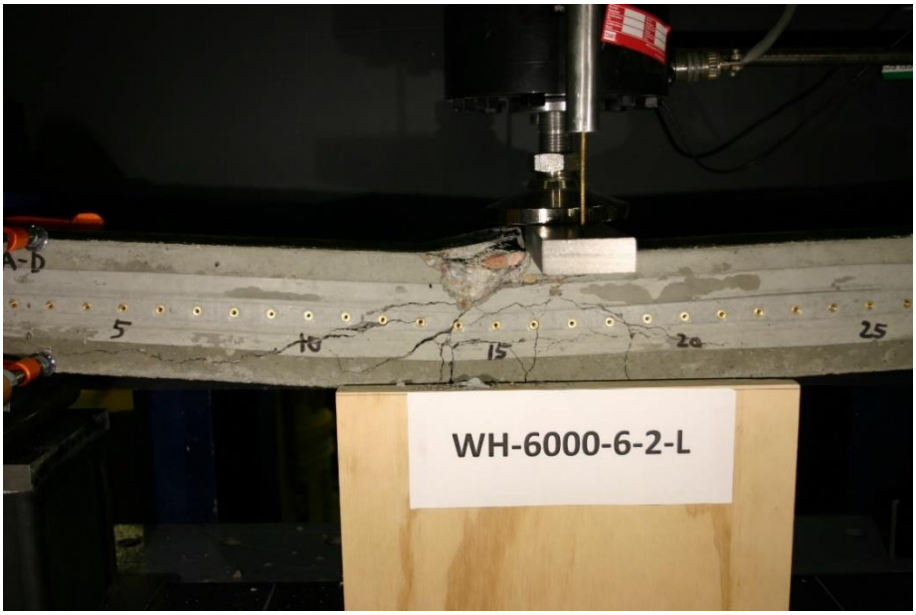


Figure 318 Picture of Failed Prism WH-6000-6-2-L

Beam Identification	WH-6000-6-2-S
Wire Type:	WH
Embedment Length:	9.5 in
Release Strength:	6000 psi
Slump:	6 in

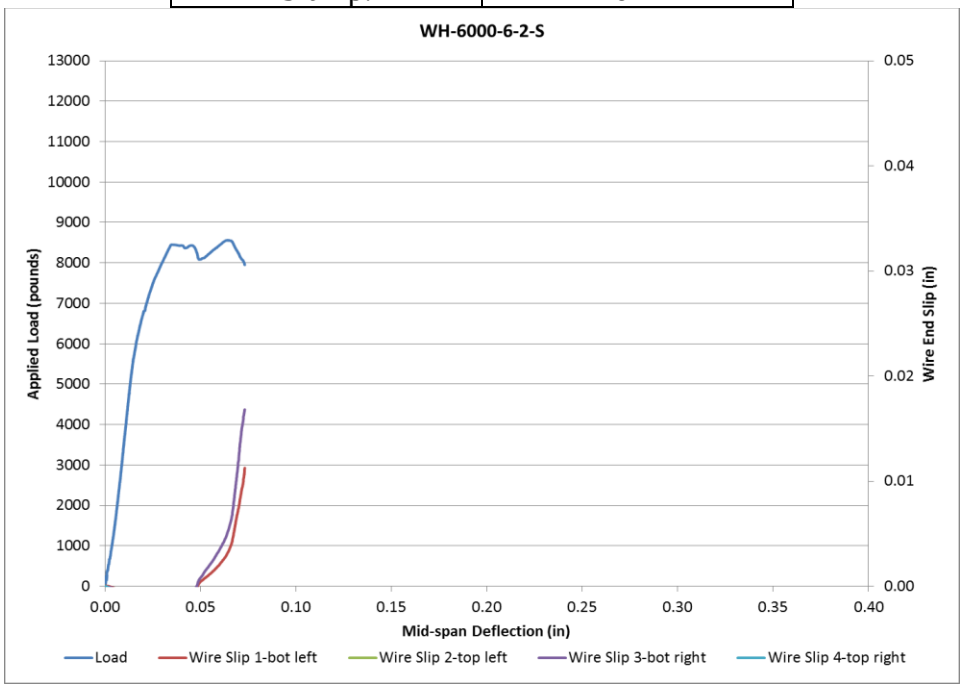


Figure 319 Load Deflection and Wire End Slip WH-6000-6-2-S



Figure 320 Picture of Failed Prism WH-6000-6-2-S

Beam Identification	WK-6000-6-1-L
Wire Type:	WK
Embedment Length:	20 in
Release Strength:	6000 psi
Slump:	6 in

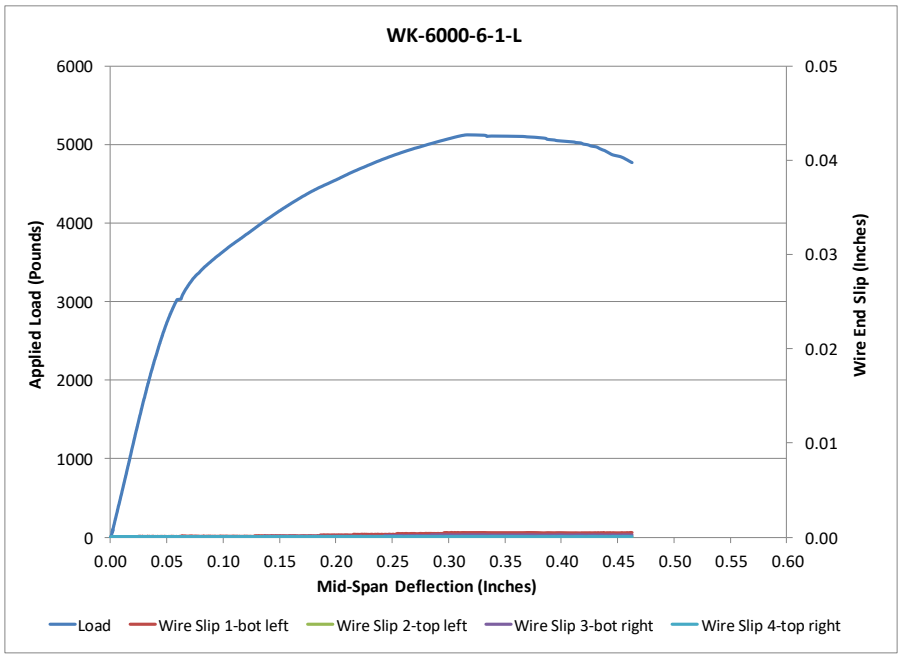


Figure 321 Load Deflection and Wire End Slip WK-6000-6-1-L

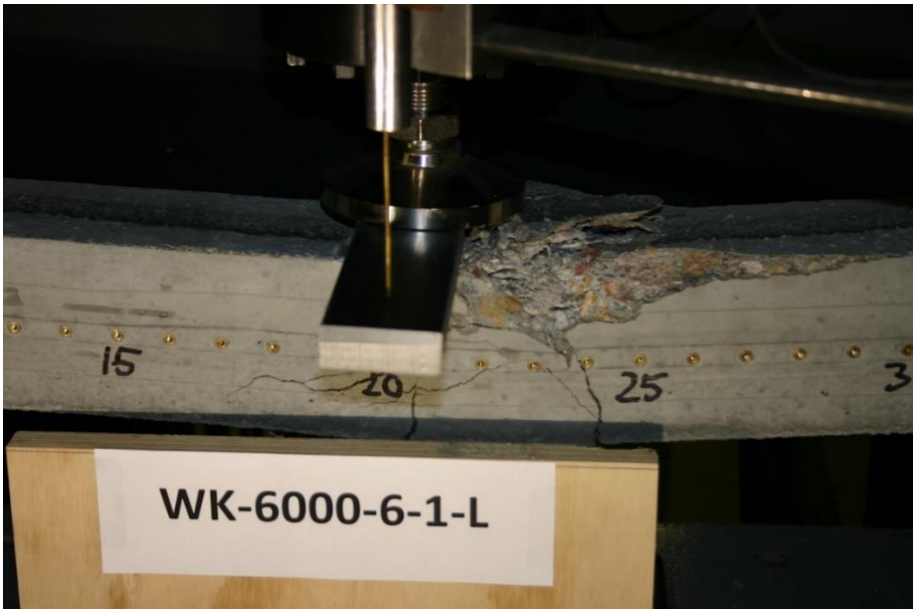


Figure 322 Picture of Failed Prism WK-6000-6-1-L

Beam Identification	WK-6000-6-1-S
Wire Type:	WK
Embedment Length:	13 in
Release Strength:	6000 psi
Slump:	6 in

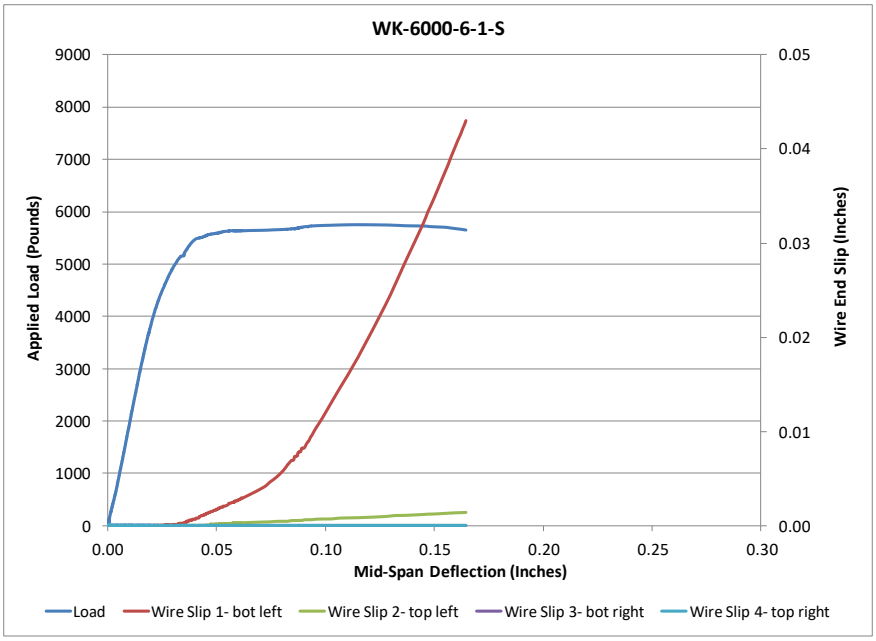


Figure 323 Load Deflection and Wire End Slip WK-6000-6-1-S



Figure 324 Picture of Failed Prism WK-6000-6-1-S

Beam Identification	WK-6000-6-2-L
Wire Type:	WK
Embedment Length:	16.5 in
Release Strength:	6000 psi
Slump:	6 in

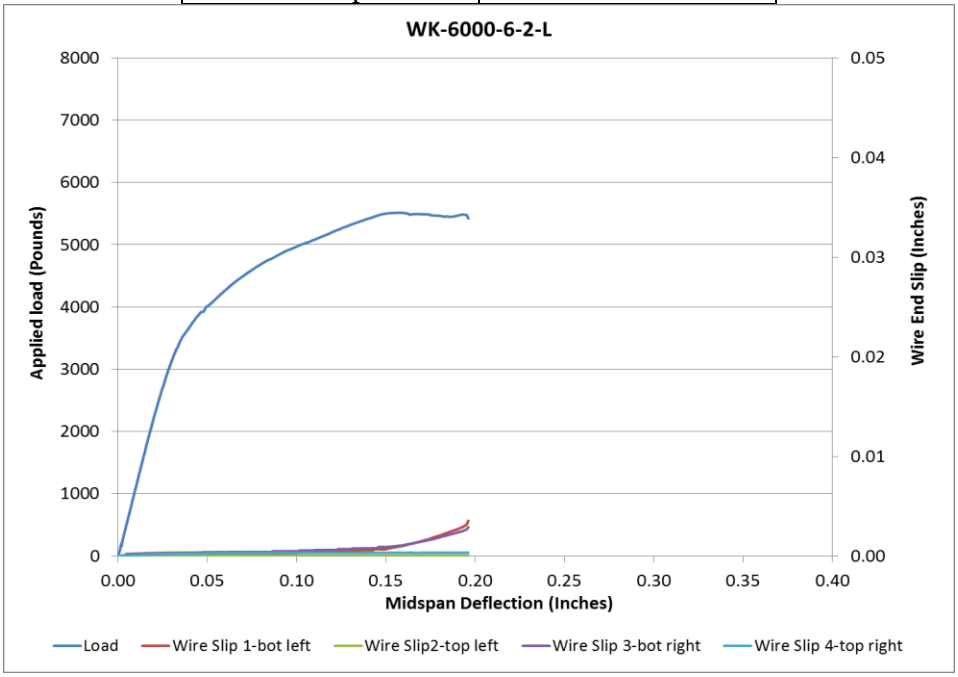


Figure 325 Load Deflection and Wire End Slip WK-6000-6-2-L

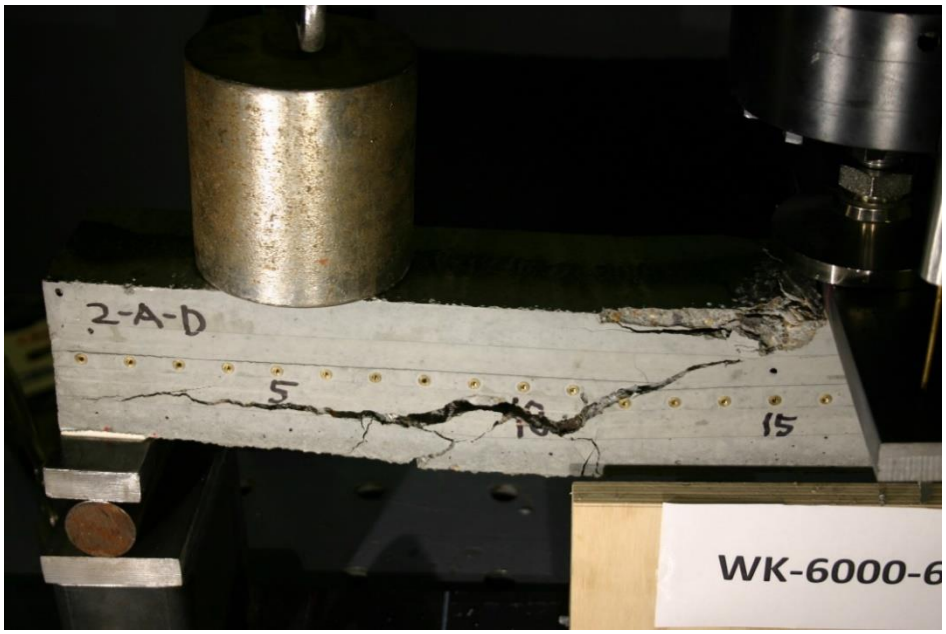


Figure 326 Picture of Failed Prism WK-6000-6-2-L

Beam Identification	WK-6000-6-2-S
Wire Type:	WK
Embedment Length:	9.5 in
Release Strength:	6000 psi
Slump:	6 in

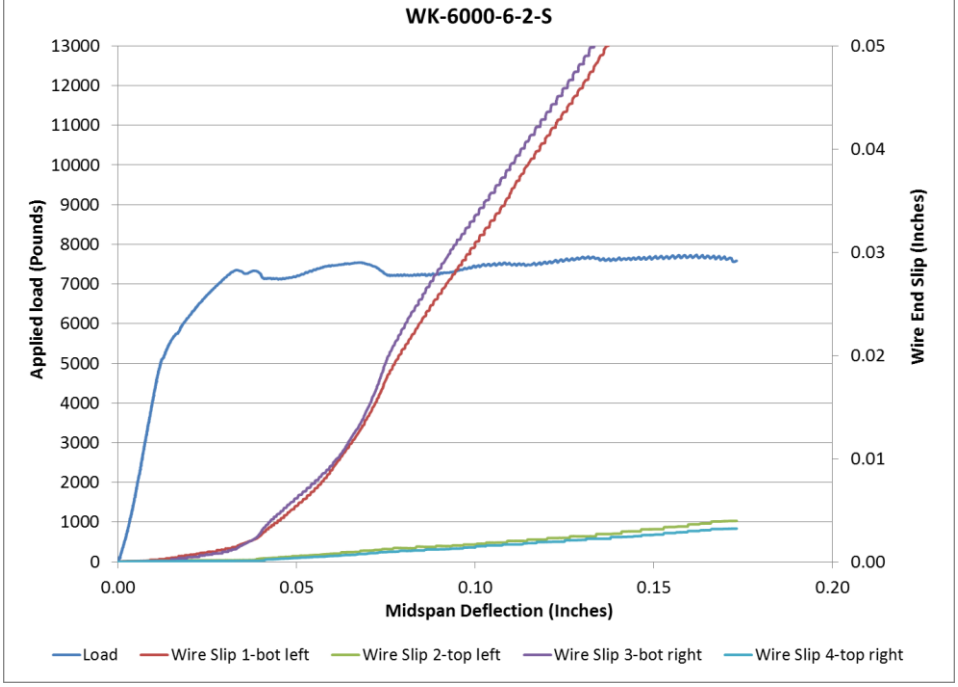


Figure 327 Load Deflection and Wire End Slip WK-6000-6-2-S

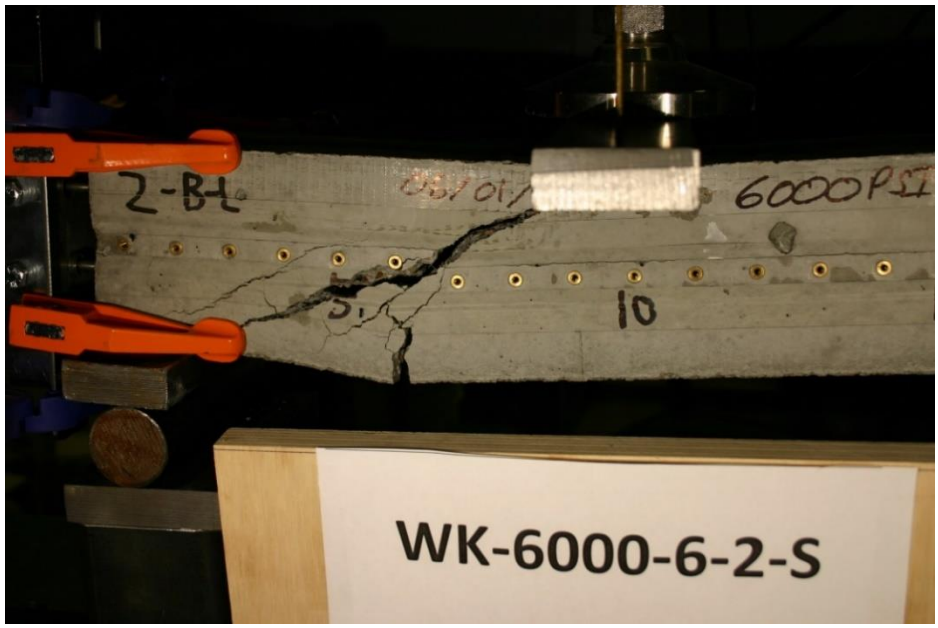


Figure 328 Picture of Failed Prism WK-6000-6-2-S

Prisms made with wires, 3500 psi concrete release strength and 6 in. slump

Beam Identification	WA-3500-6-1-L
Wire Type:	WA
Embedment Length:	20 in
Release Strength:	3500 psi
Slump:	6 in

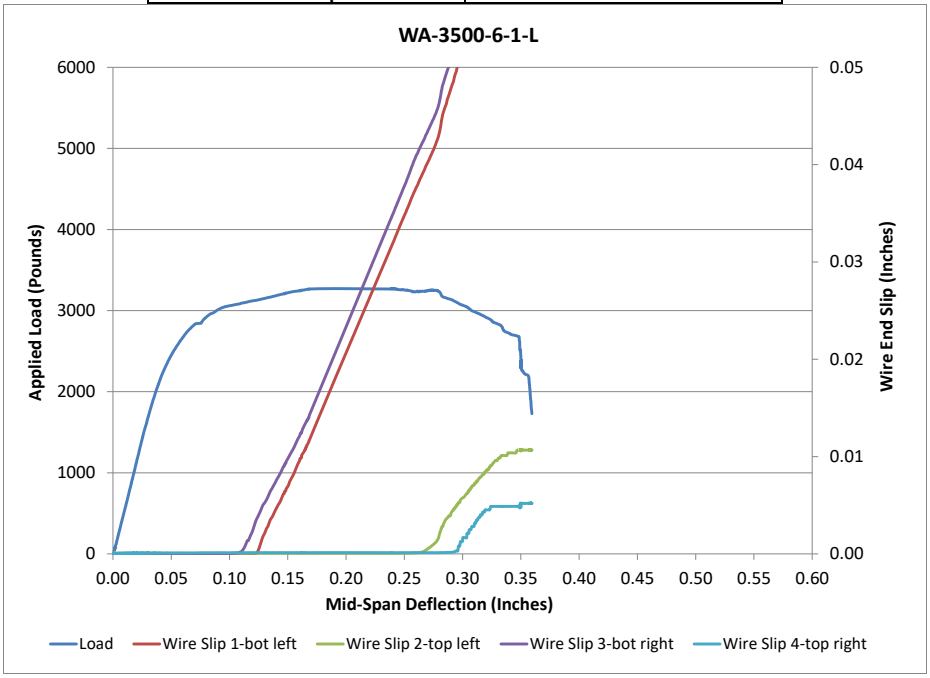


Figure 329 Load Deflection and Wire End Slip WA-3500-6-1-L

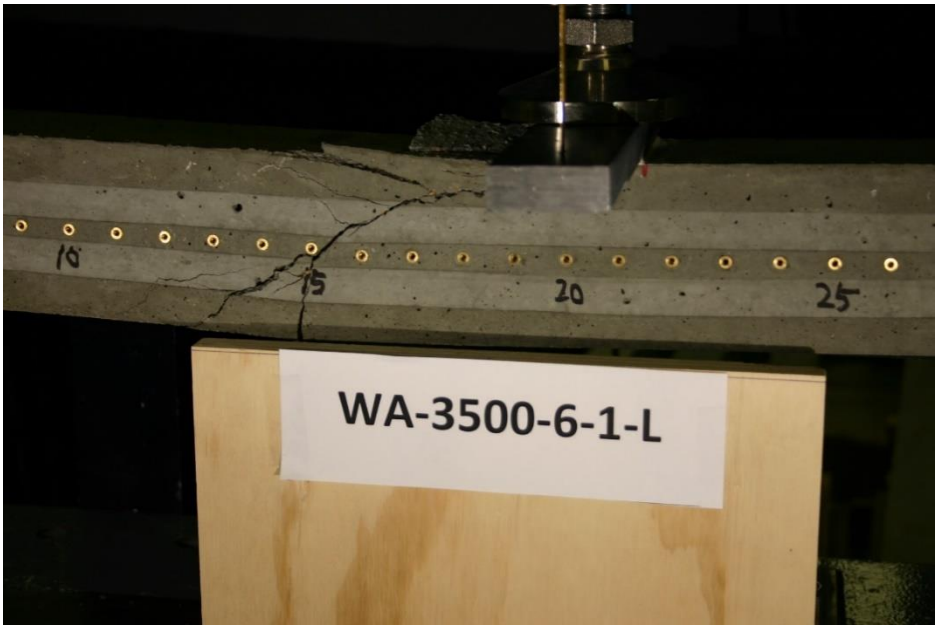


Figure 330 Picture of Failed Prism WA-3500-6-1-L

Beam Identification	WA-3500-6-1-S
Wire Type:	WA
Embedment Length:	13 in
Release Strength:	3500 psi
Slump:	6 in

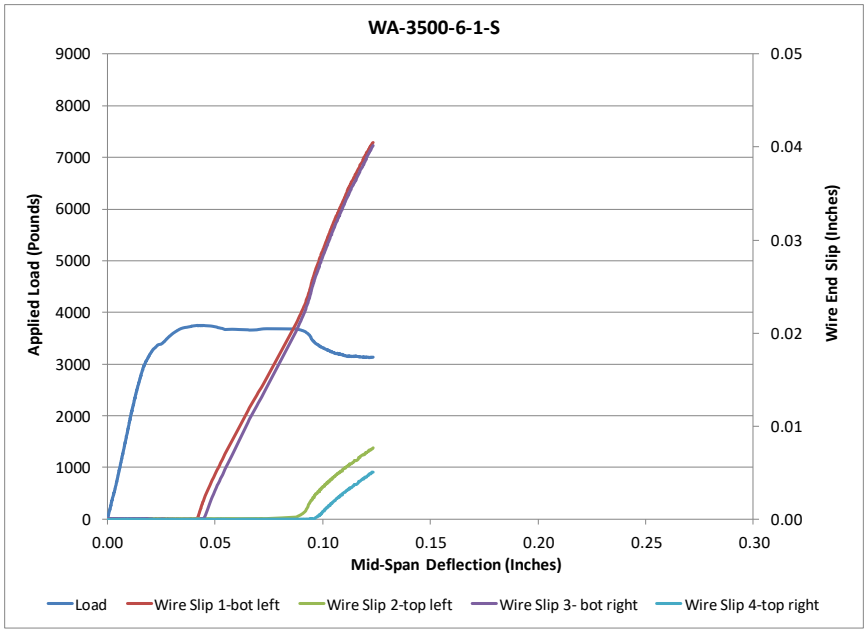


Figure 331 Load Deflection and Wire End Slip WA-3500-6-1-S

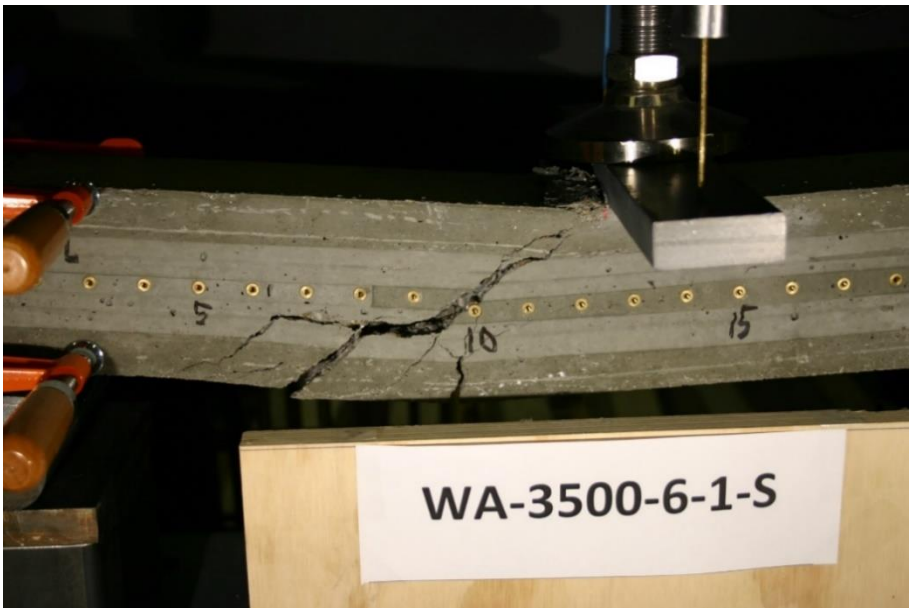


Figure 332 Picture of Failed Prism WA-3500-6-1-S

Beam Identification	WA-3500-6-2-L
Wire Type:	WA
Embedment Length:	16.5 in
Release Strength:	3500 psi
Slump:	6 in

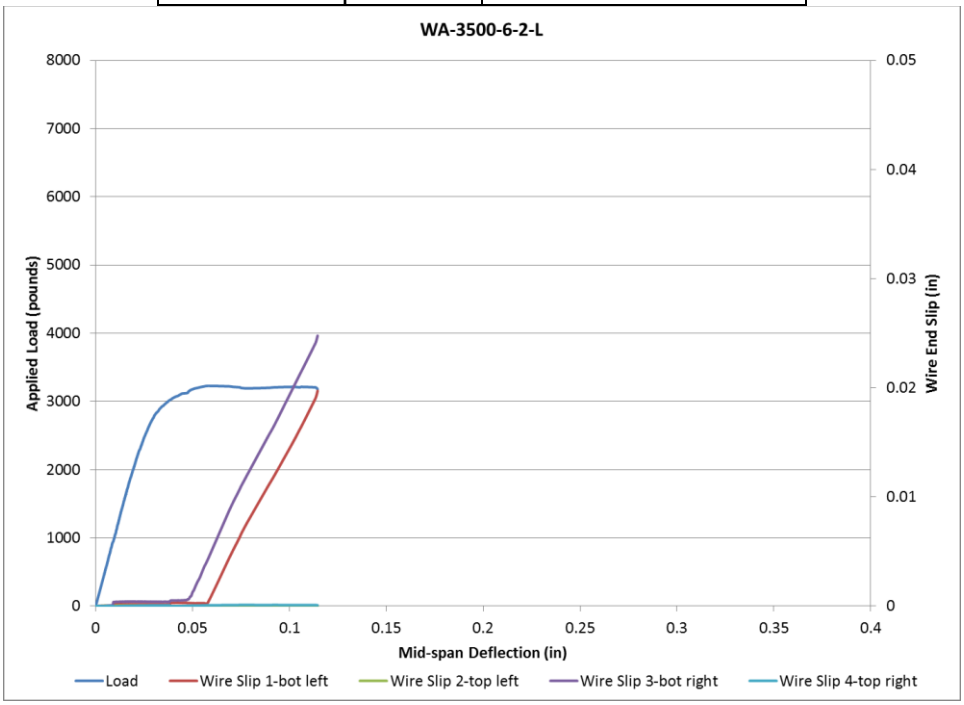


Figure 333 Load Deflection and Wire End Slip WA-3500-6-2-L

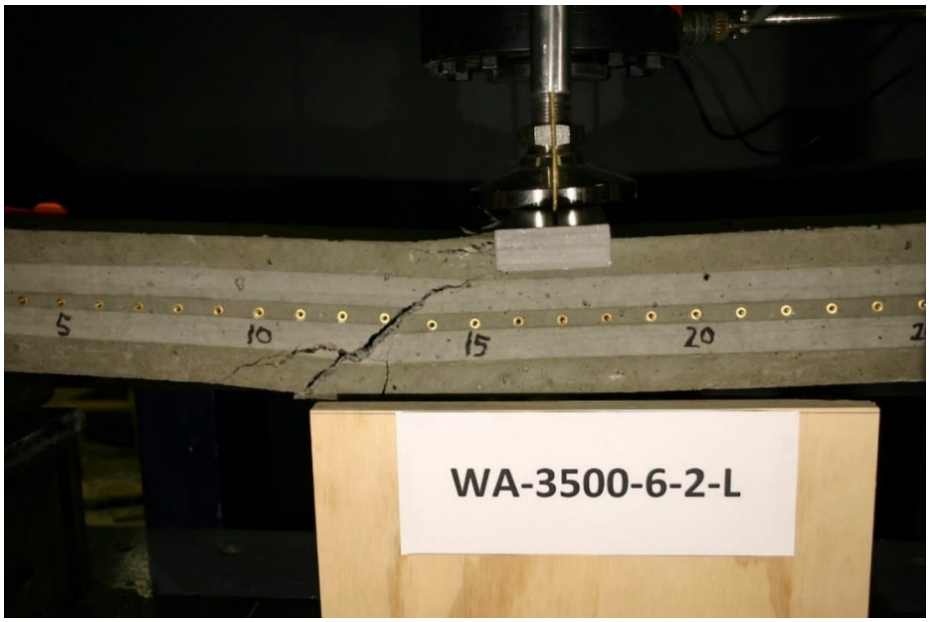


Figure 334 Picture of Failed Prism WA-3500-6-2-L

Beam Identification	WA-3500-6-2-S
Wire Type:	WA
Embedment Length:	9.5 in
Release Strength:	3500 psi
Slump:	6 in

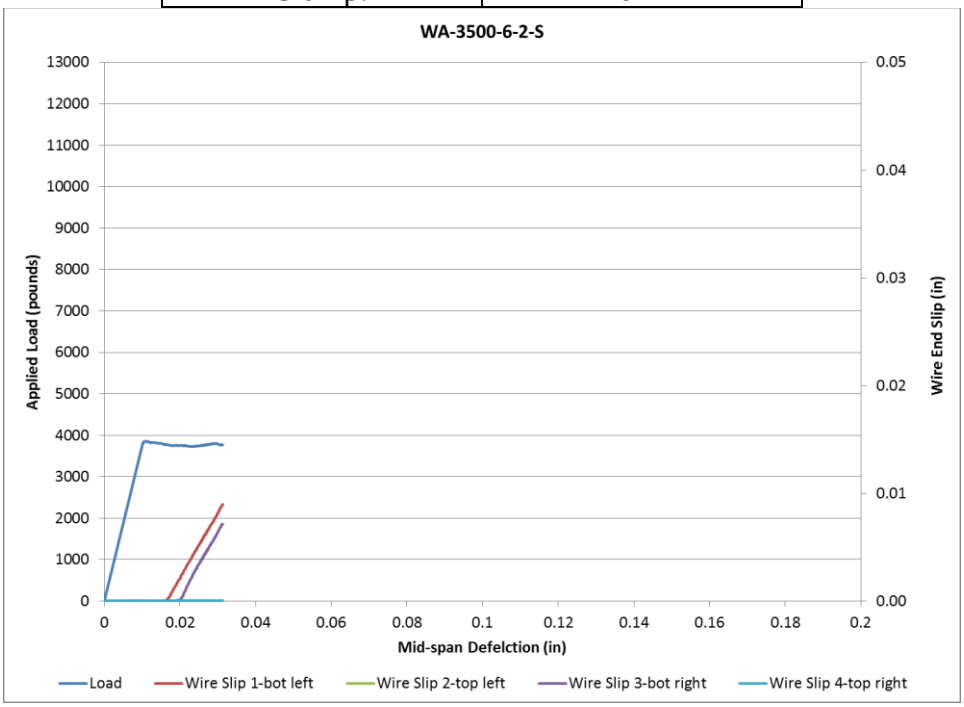


Figure 335 Load Deflection and Wire End Slip WA-3500-6-2-S

Beam Identification	WE-3500-6-1-L
Wire Type:	WE
Embedment Length:	20 in
Release Strength:	3500 psi
Slump:	6 in

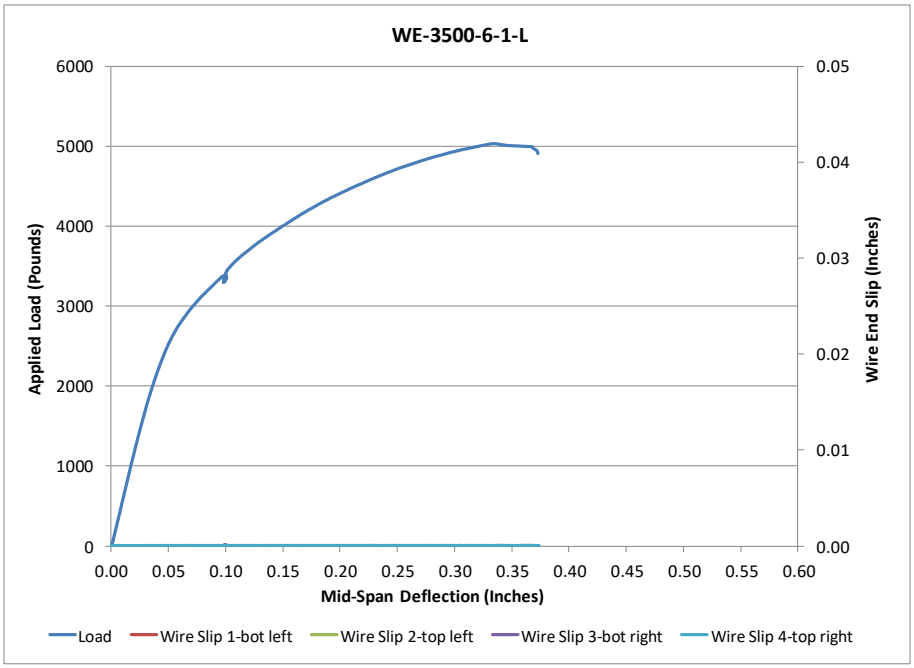


Figure 336 Load vs Deflection and Wire End Slip WE-3500-6-1-L



Figure 337 Picture of Failed Prism for WE-3500-6-1-L

Beam Identification	WE-3500-6-1-S
Wire Type:	WE
Embedment Length:	13 in
Release Strength:	4500 psi
Slump:	6 in

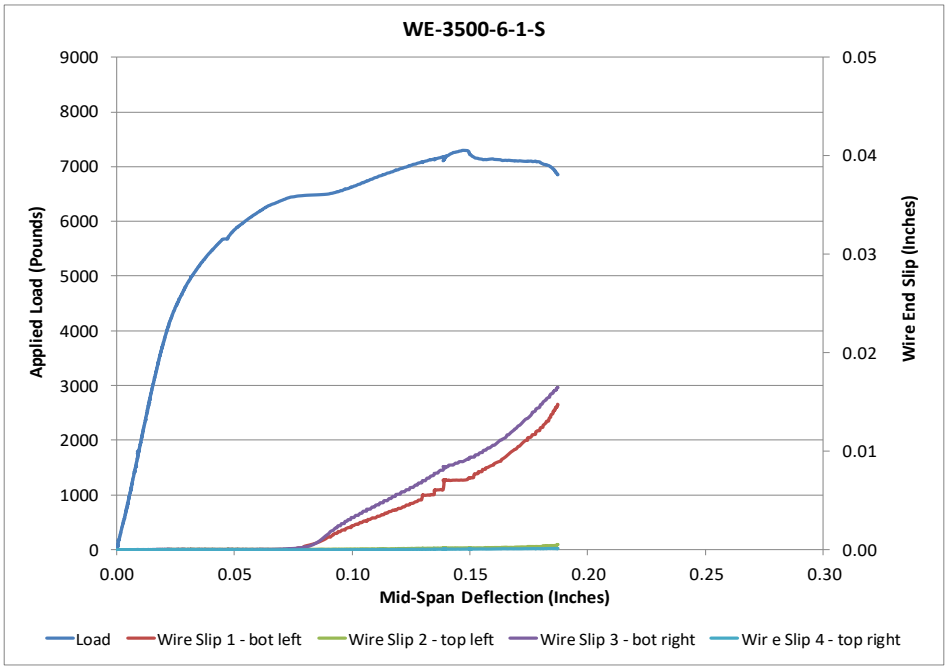


Figure 338 Load vs Deflection and Wire End Slip WE-3500-6-1-S

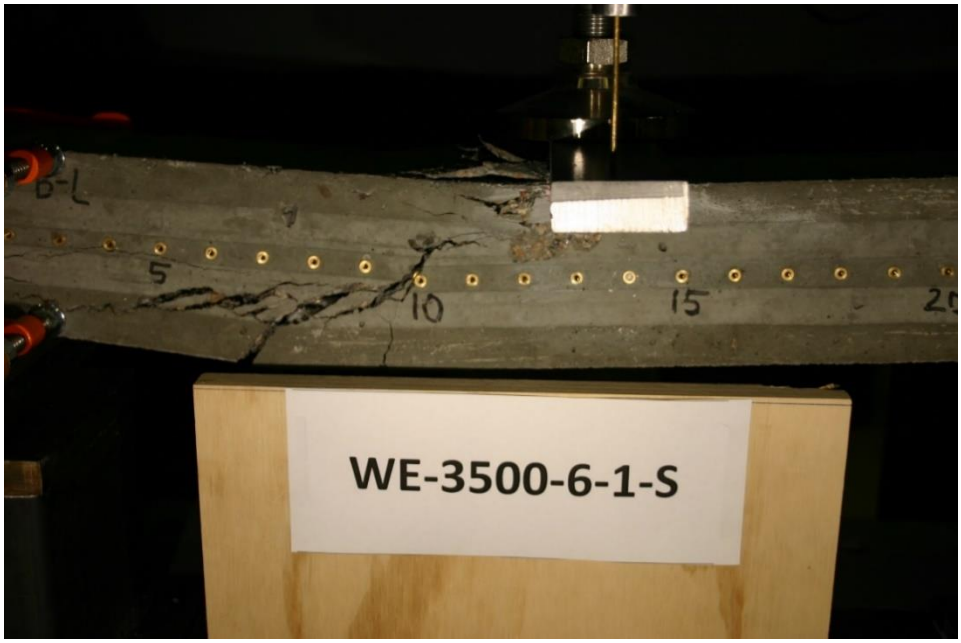


Figure 339 Picture of Failed Prism for WE-3500-6-1-S

Beam Identification	WE-3500-6-2-L
Wire Type:	WE
Embedment Length:	16.5 in
Release Strength:	4500 psi
Slump:	6 in

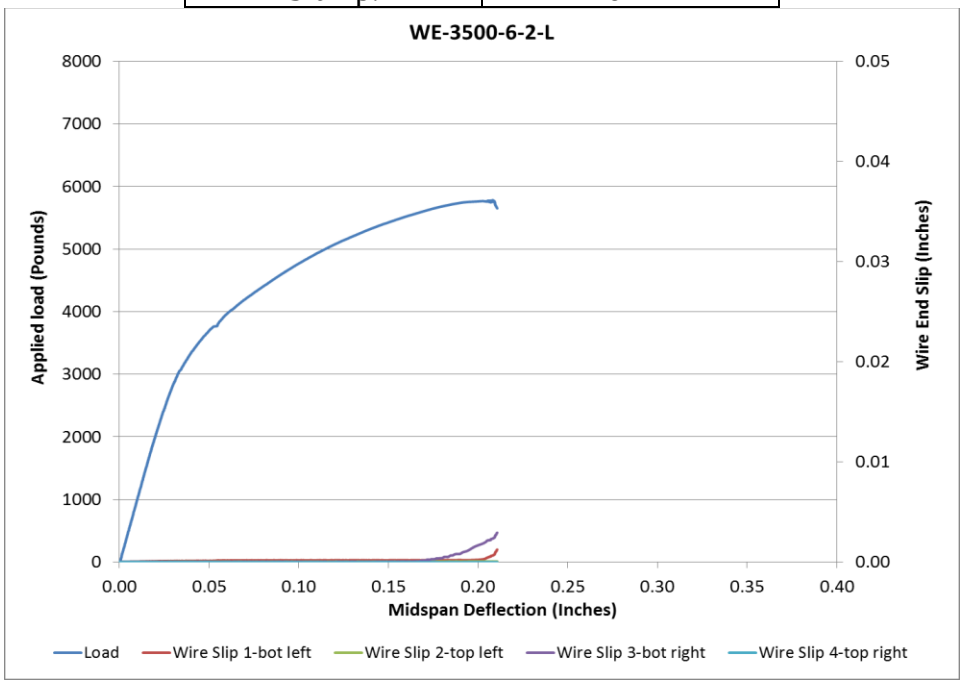


Figure 340 Load vs Deflection and Wire End Slip WE-3500-6-2-L

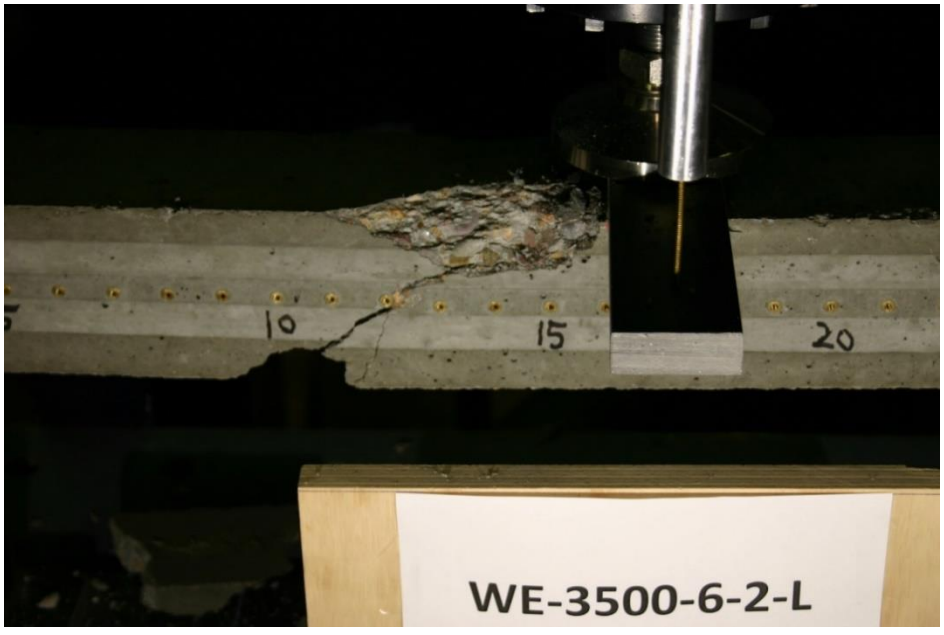


Figure 341 Picture of Failed Prism for WE-3500-6-2-L

Beam Identification	WE-3500-6-2-S
Wire Type:	WE
Embedment Length:	9.5 in
Release Strength:	4500 psi
Slump:	6 in

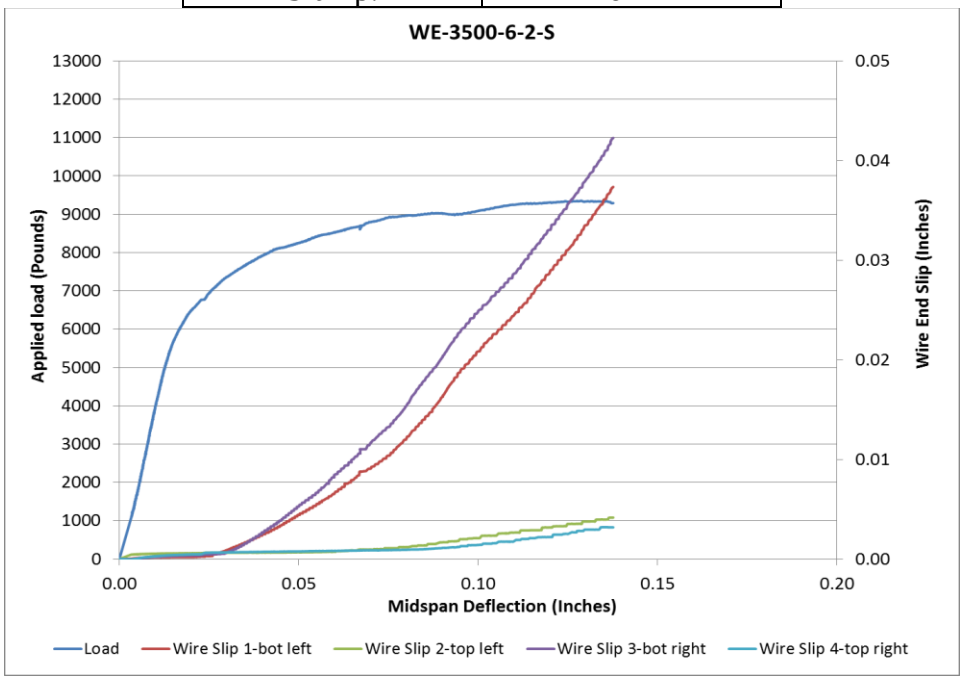


Figure 342 Load vs Deflection and Wire End Slip WE-3500-6-2-S

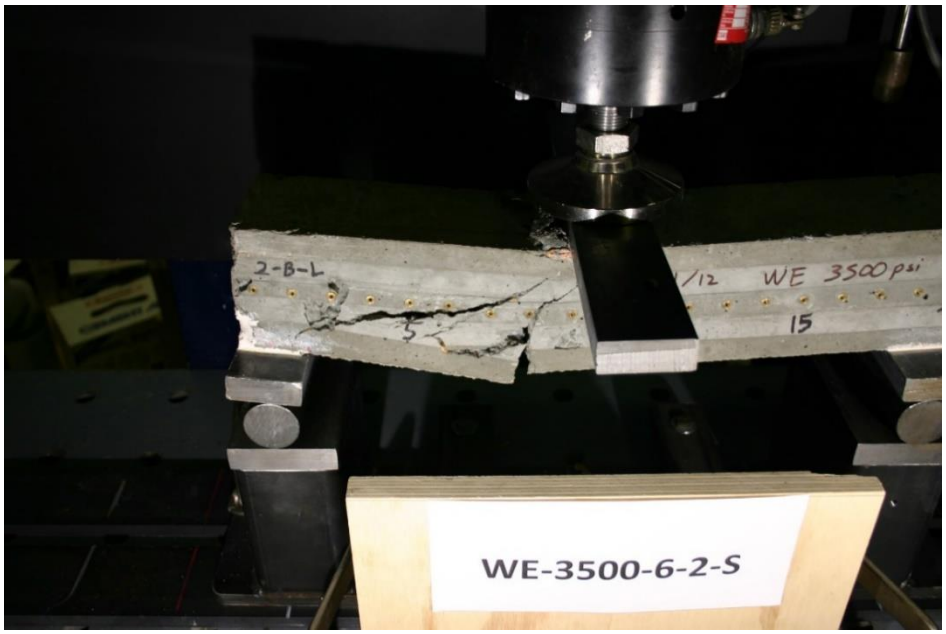


Figure 343 Picture of Failed Prism for WE-3500-6-2-S

Beam Identification	WG-3500-6-1-L
Wire Type:	WG
Embedment Length:	20 in
Release Strength:	3500 psi
Slump:	6 in

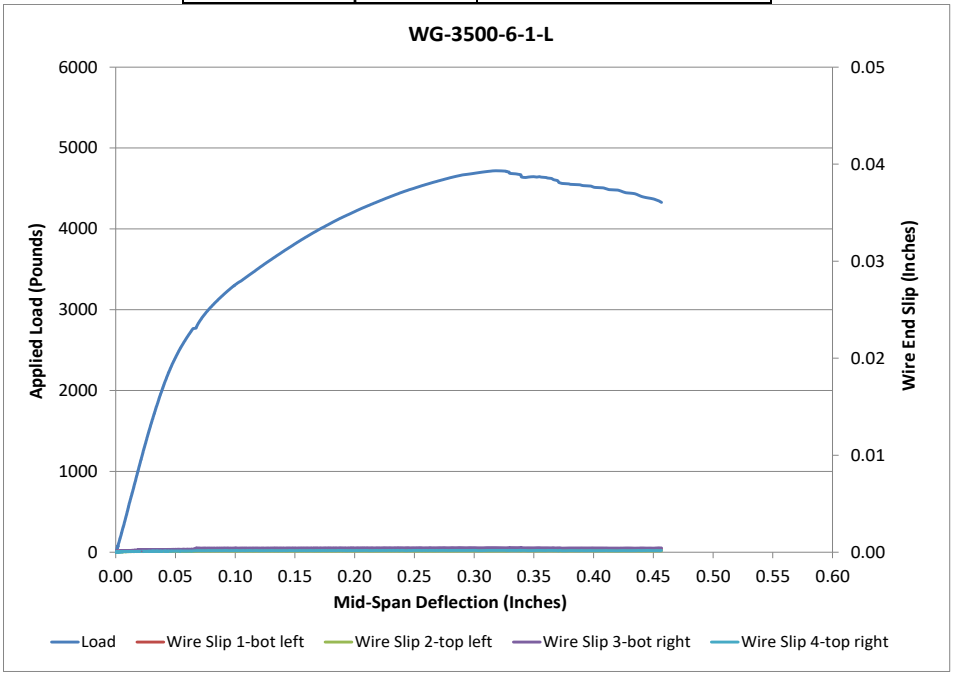


Figure 344 Load vs Deflection and Wire End Slip WG-3500-6-1-L



Figure 345 Picture of Failed Prism for WG-3500-6-1-L

Beam Identification	WG-3500-6-1-S
Wire Type:	WG
Embedment Length:	13 in
Release Strength:	3500 psi
Slump:	6 in

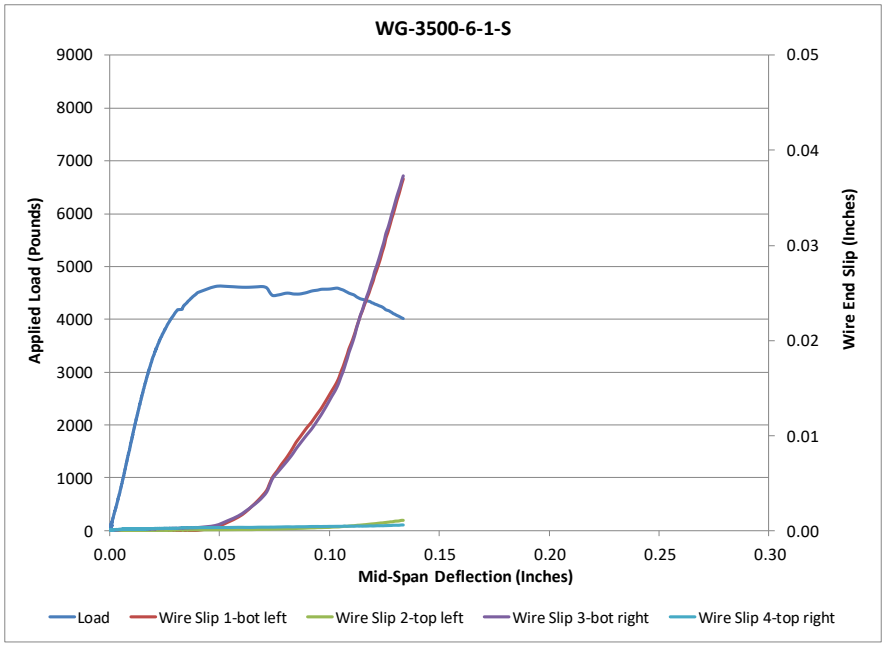


Figure 346 Load vs Deflection and Wire End Slip WG-3500-6-1-S

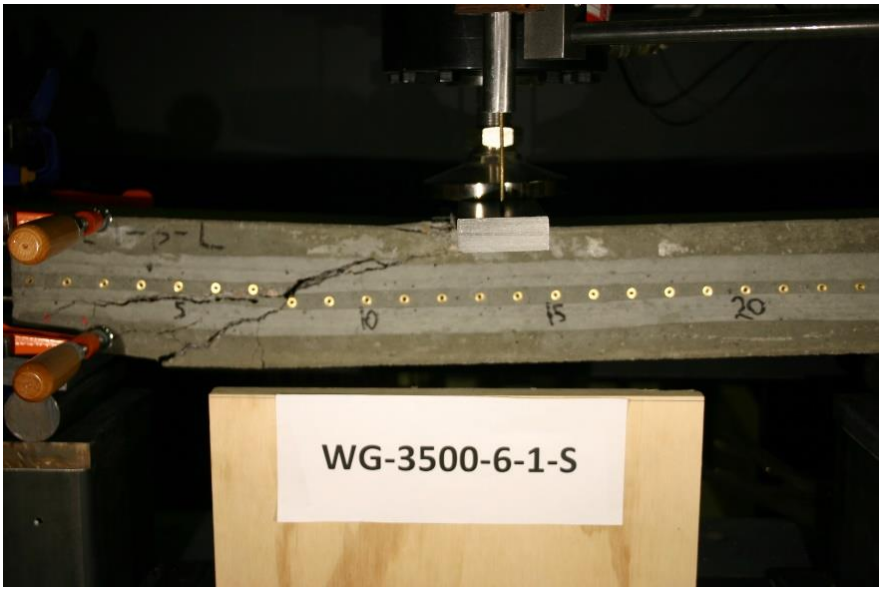
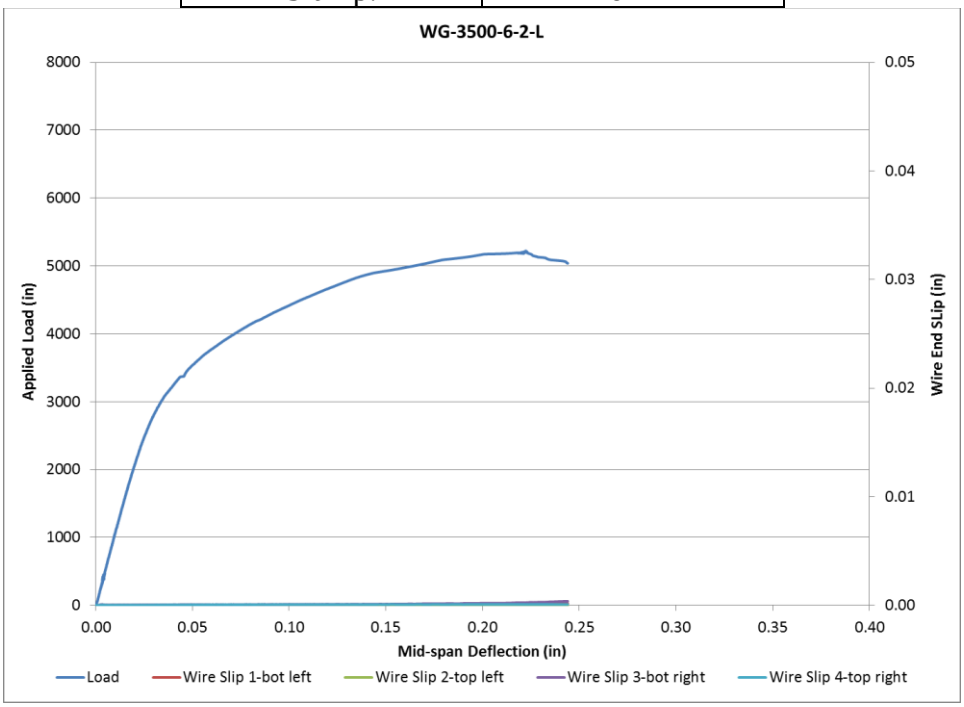


Figure 347 Picture of Failed Prism for WG-3500-6-1-S

Beam Identification	WG-3500-6-2-L
Wire Type:	WG
Embedment Length:	16.5 in
Release Strength:	3500 psi
Slump:	6 in



Load vs Deflection and Wire End Slip WG-3500-6-2-L

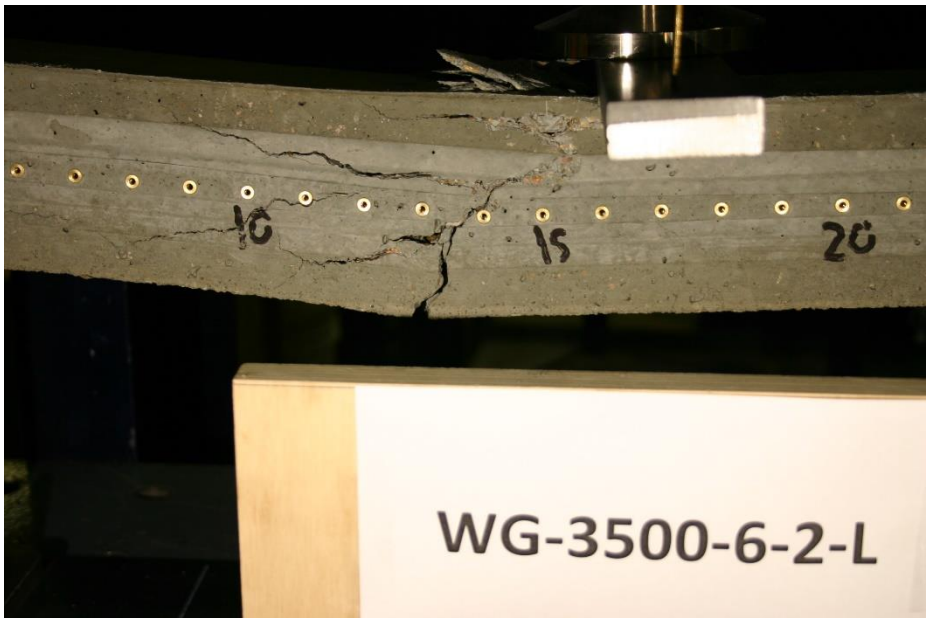


Figure 348 Picture of Failed Prism for WG-3500-6-2-L

Beam Identification	WG-3500-6-2-S
Wire Type:	WG
Embedment Length:	9.5 in
Release Strength:	3500 psi
Slump:	6 in

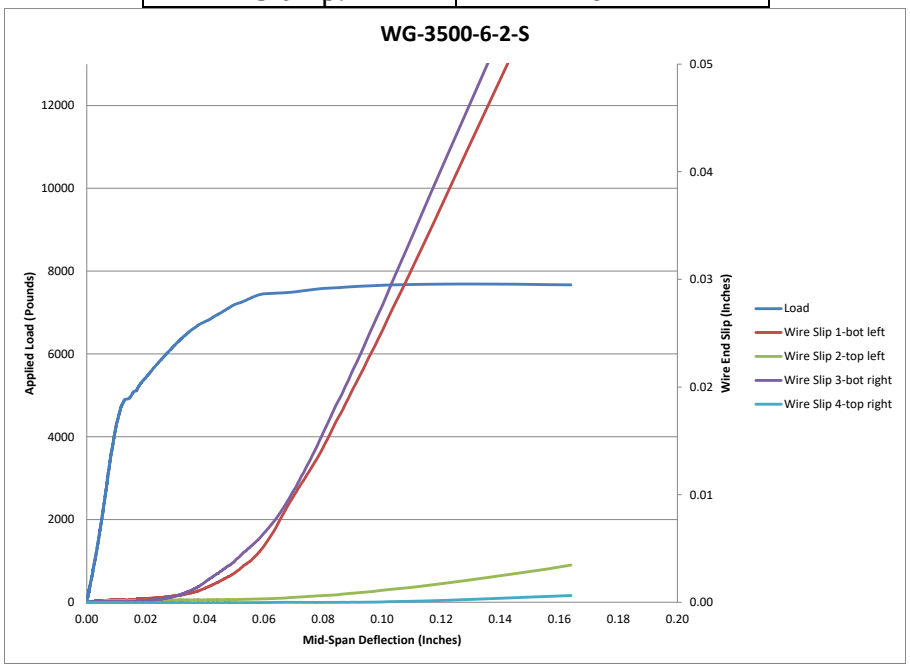


Figure 349 Load vs Deflection and Wire End Slip WG-3500-6-2-S



Figure 350 Picture of Failed Prism for WG-3500-6-2-S

Beam Identification	WH-3500-6-1-L
Wire Type:	WH
Embedment Length:	20 in
Release Strength:	3500 psi
Slump:	6 in

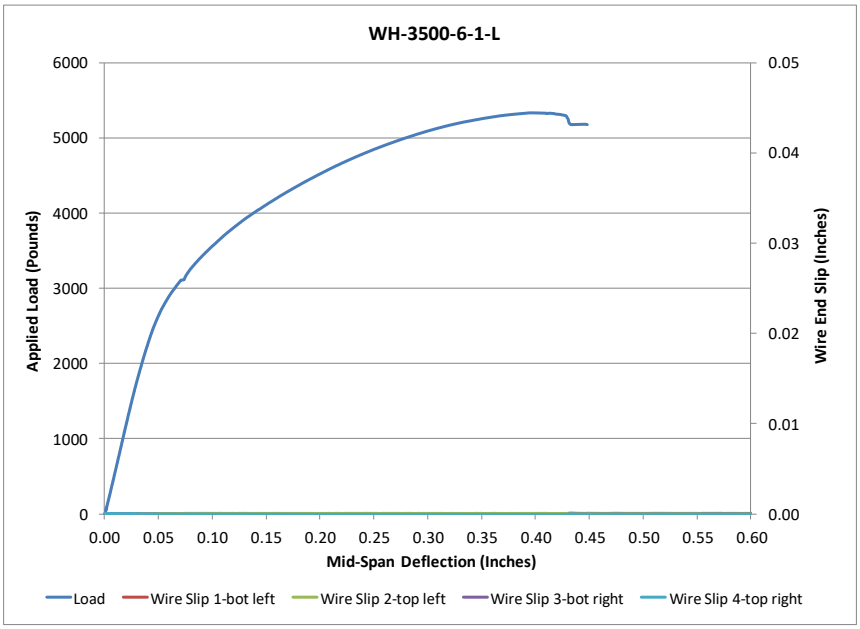


Figure 351 Load vs Deflection and Wire End Slip WH-3500-6-1-L

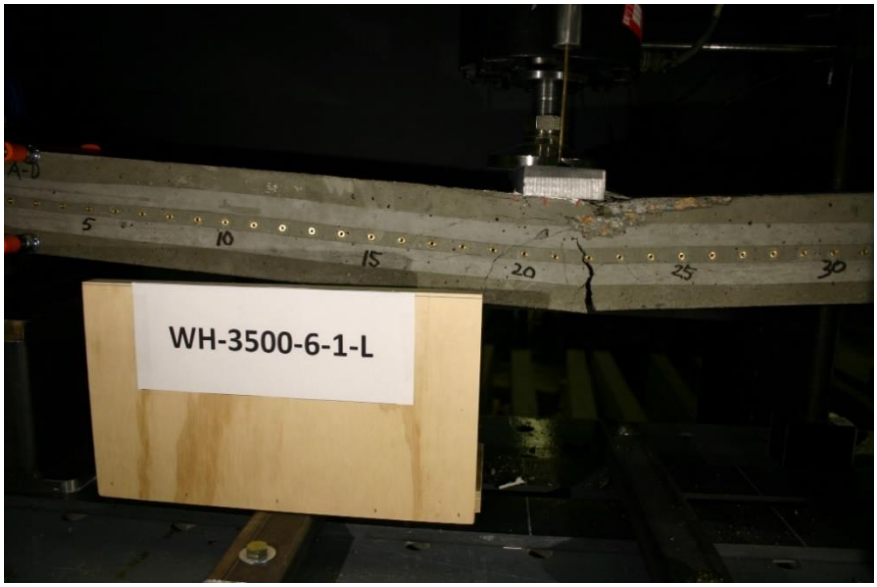


Figure 352 Picture of Failed Prism for WH-3500-6-1-L

Beam Identification	WH-3500-6-1-S
Wire Type:	WH
Embedment Length:	13 in
Release Strength:	3500 psi
Slump:	6 in

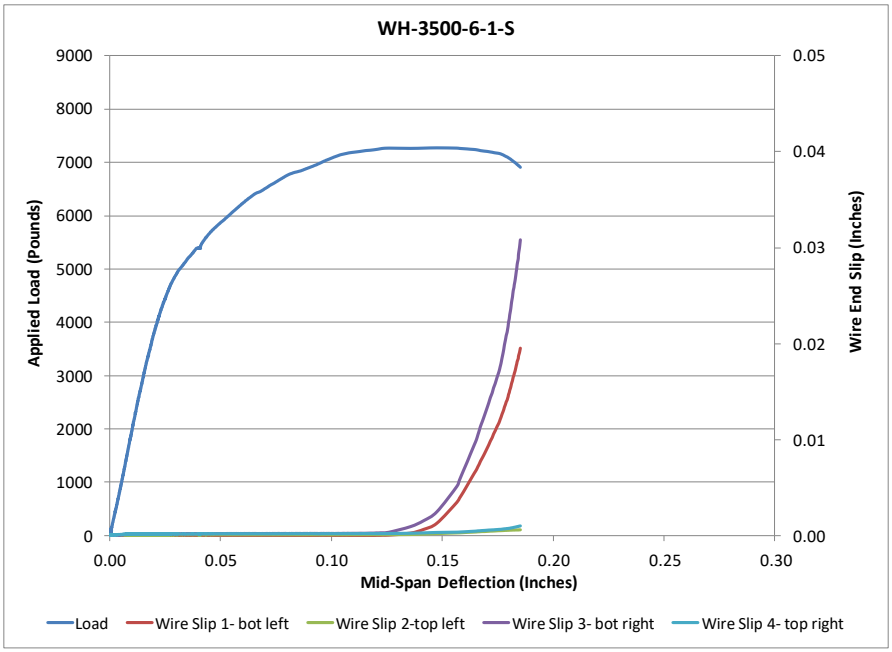


Figure 353 Load vs Deflection and Wire End Slip WH-3500-6-1-S

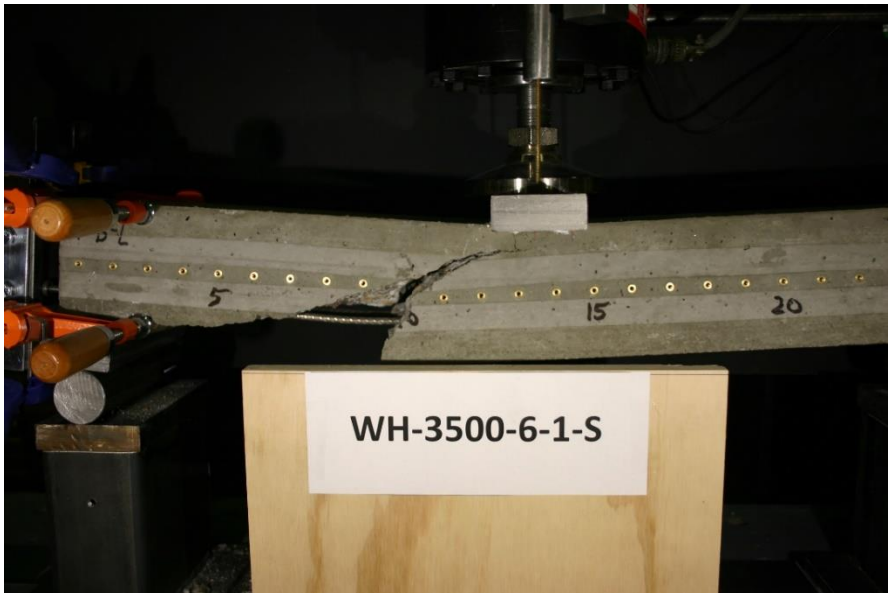


Figure 354 Picture of Failed Prism for WH-3500-6-1-S

Beam Identification	WH-3500-6-2-L
Wire Type:	WH
Embedment Length:	16.5 in
Release Strength:	3500 psi
Slump:	6 in

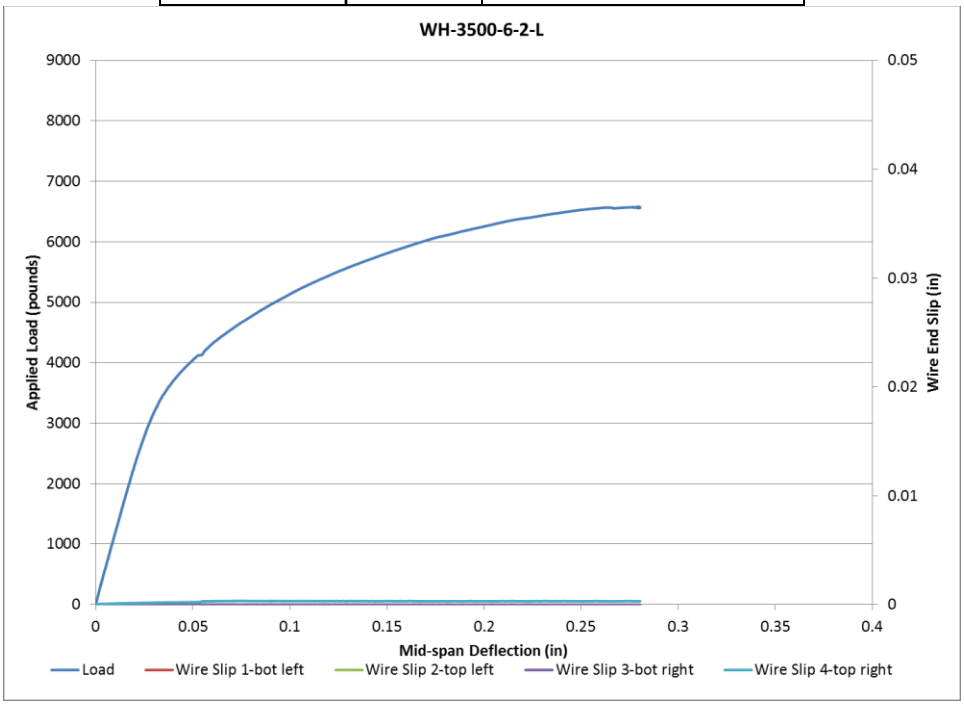


Figure 355 Load vs Deflection and Wire End Slip WH-3500-6-2-L

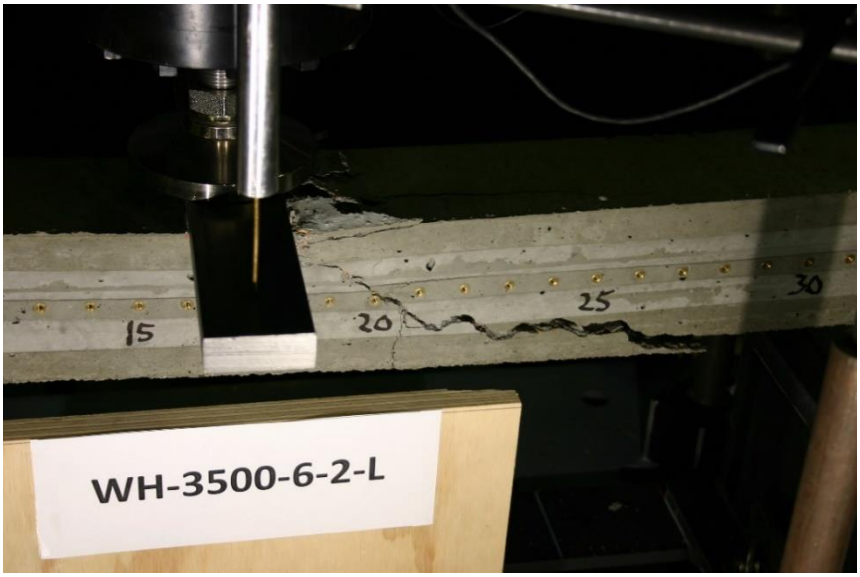


Figure 356 Picture of Failed Prism for WH-3500-6-2-L

Beam Identification	WH-3500-6-2-S
Wire Type:	WH
Embedment Length:	9.5 in
Release Strength:	3500 psi
Slump:	6 in

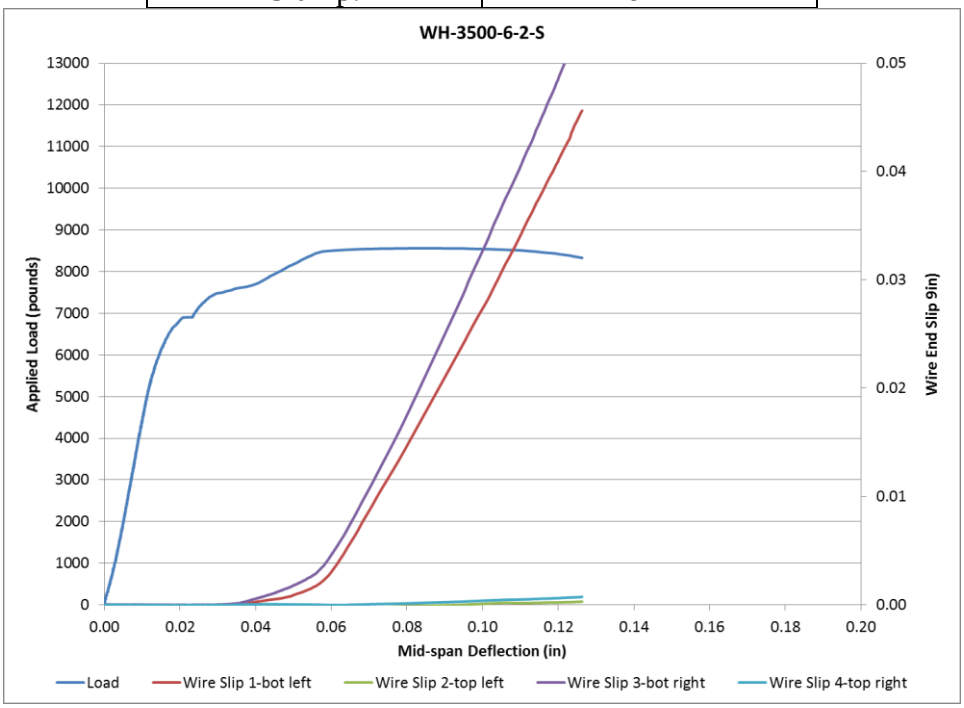


Figure 357 Load vs Deflection and Wire End Slip WH-3500-6-2-S

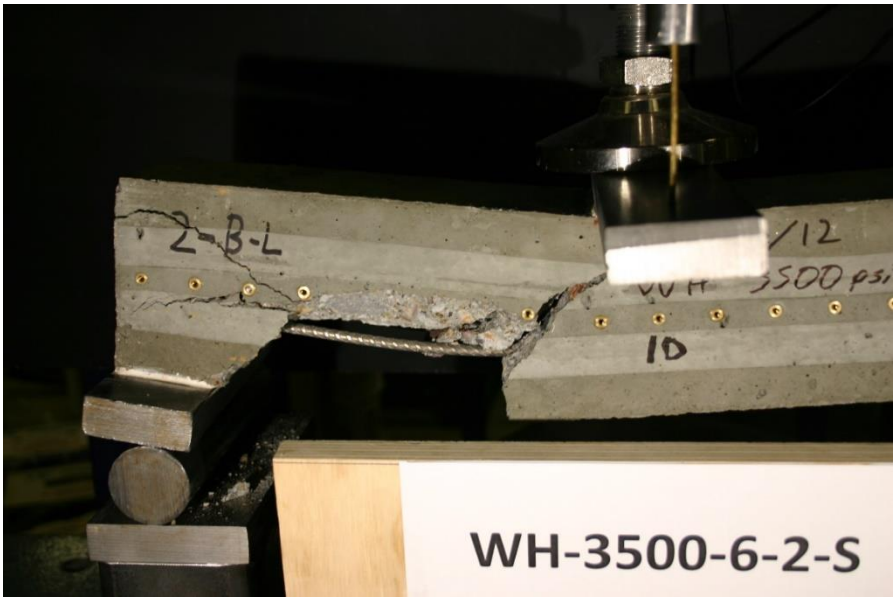


Figure 358 Picture of Failed Prism for WH-3500-6-2-S

Beam Identification	WK-3500-6-1-L
Wire Type:	WK
Embedment Length:	20 in
Release Strength:	3500 psi
Slump:	6 in

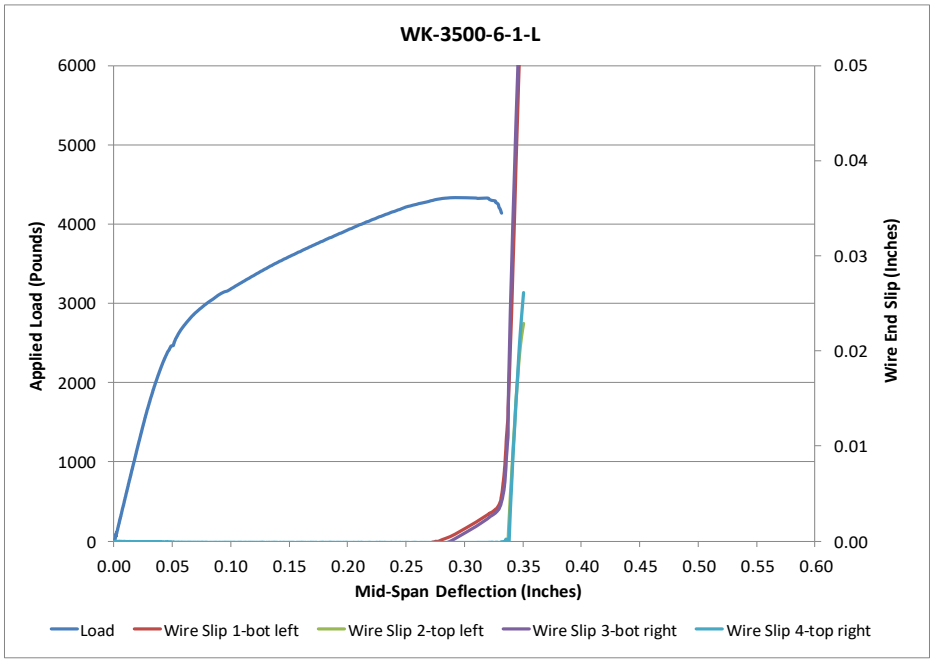


Figure 359 Load vs Deflection and Wire End Slip WK-3500-6-1-L

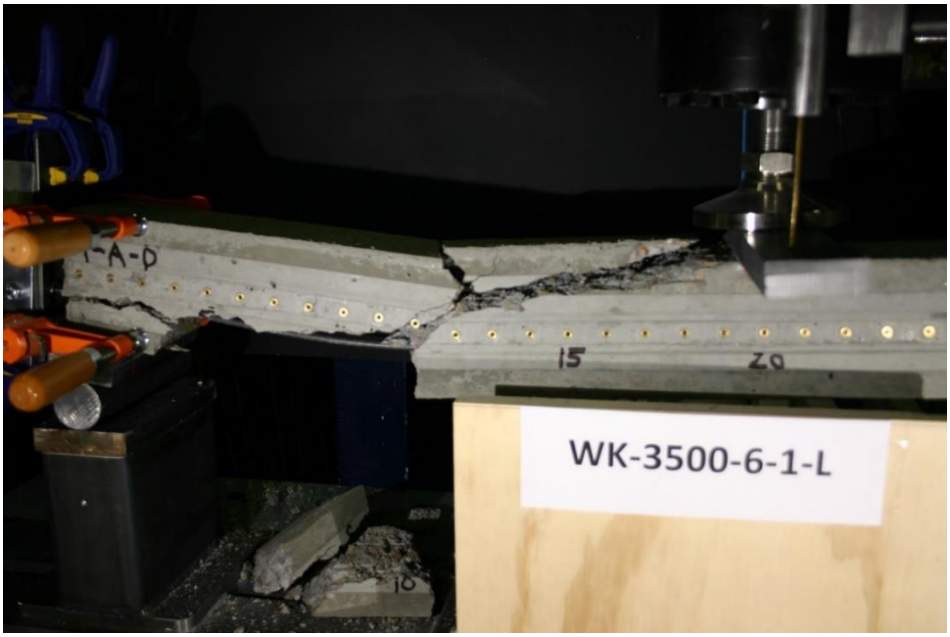


Figure 360 Picture of Failed Prism for WK-3500-6-1-L

Beam Identification	WK-3500-6-1-S
Wire Type:	WK
Embedment Length:	13 in
Release Strength:	3500 psi
Slump:	6 in

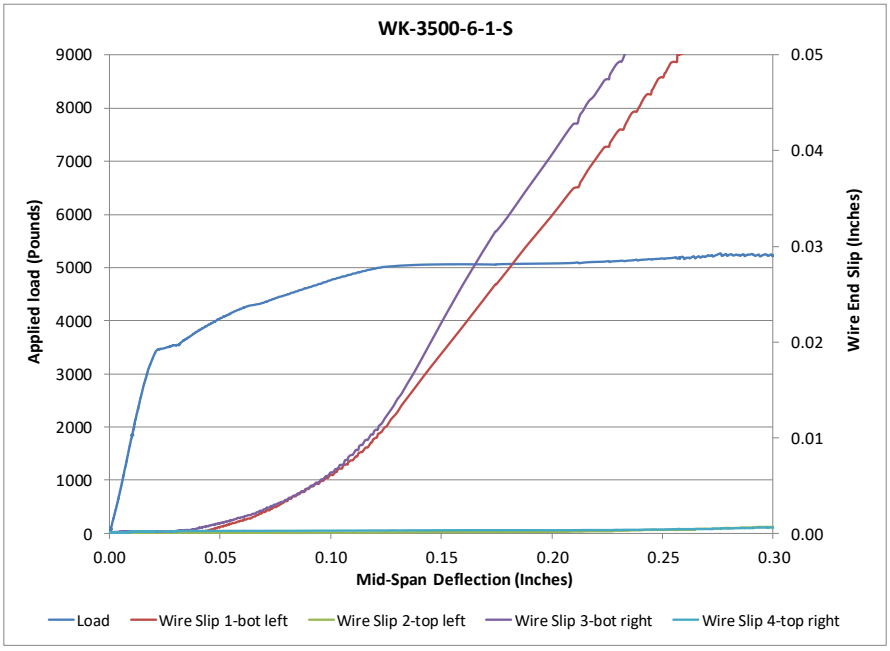


Figure 361 Load vs Deflection and Wire End Slip WK-3500-6-1-S

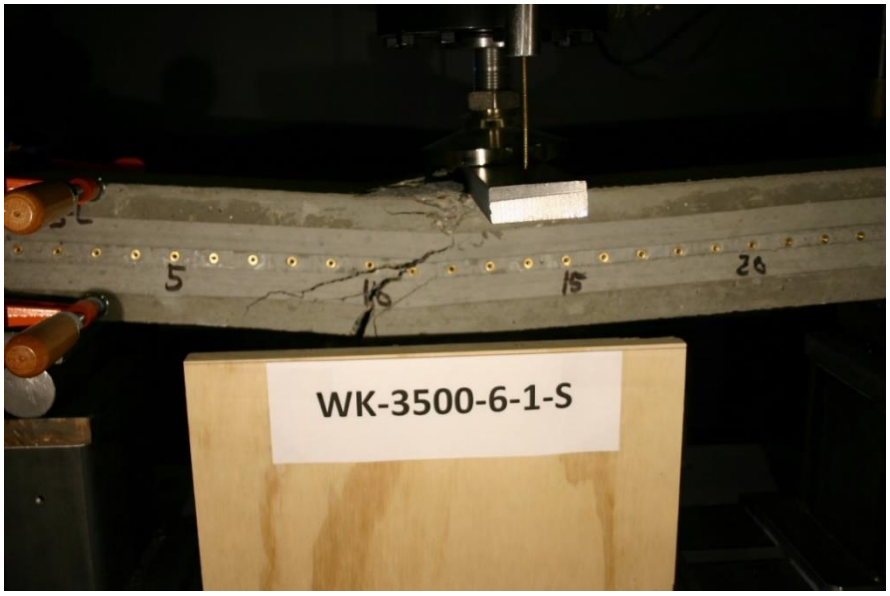


Figure 362 Picture of Failed Prism for WK-3500-6-1-S

Beam Identification	WK-3500-6-2-L
Wire Type:	WK
Embedment Length:	16.5 in
Release Strength:	3500 psi
Slump:	6 in

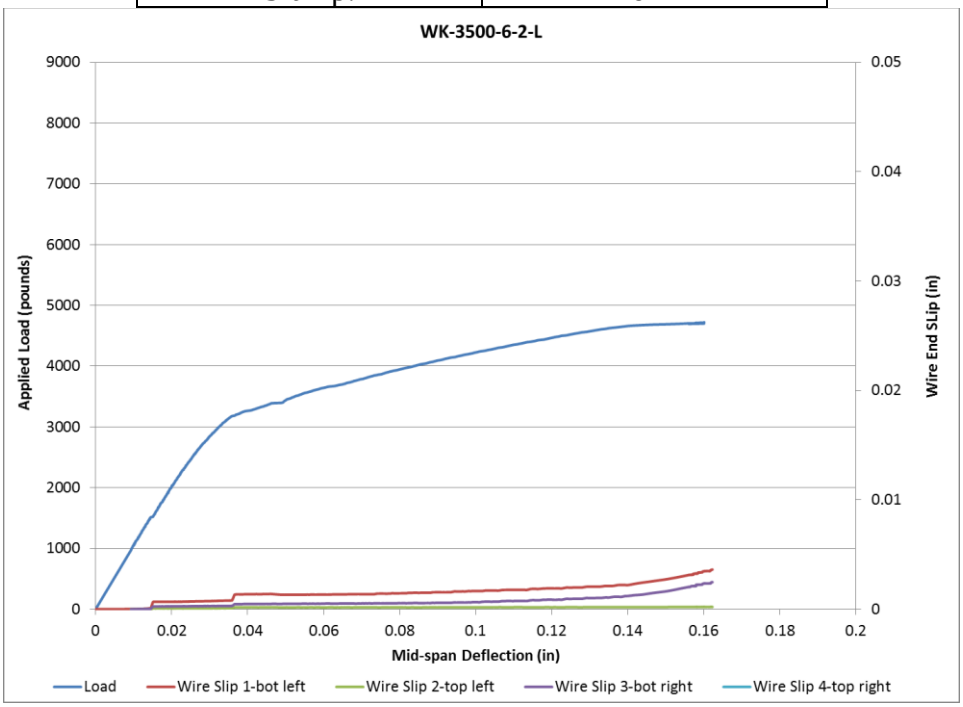


Figure 363 Load vs Deflection and Wire End Slip WK-3500-6-2-L

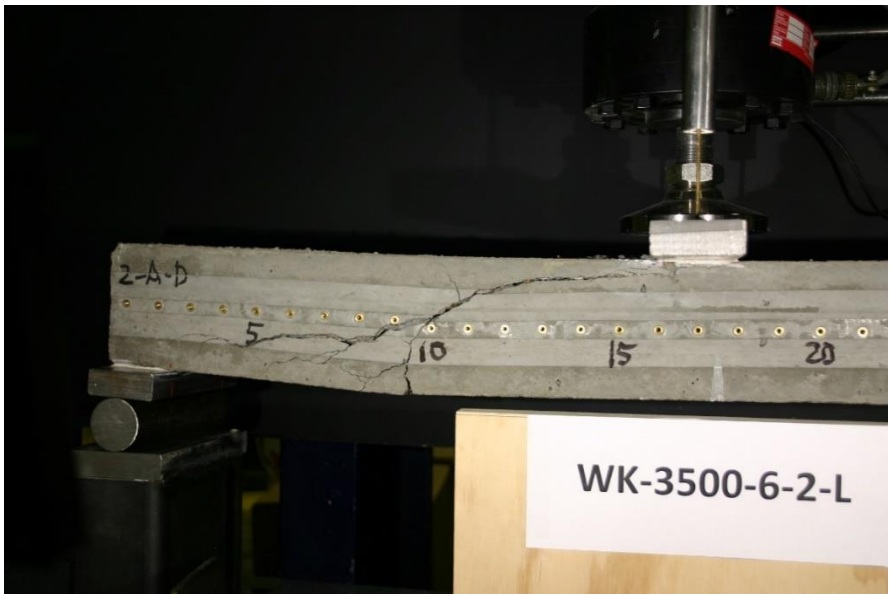


Figure 364 Picture of Failed Prism for WK-3500-6-2-L

Beam Identification	WK-3500-6-2-S
Wire Type:	WK
Embedment Length:	9.5 in
Release Strength:	3500 psi
Slump:	6 in

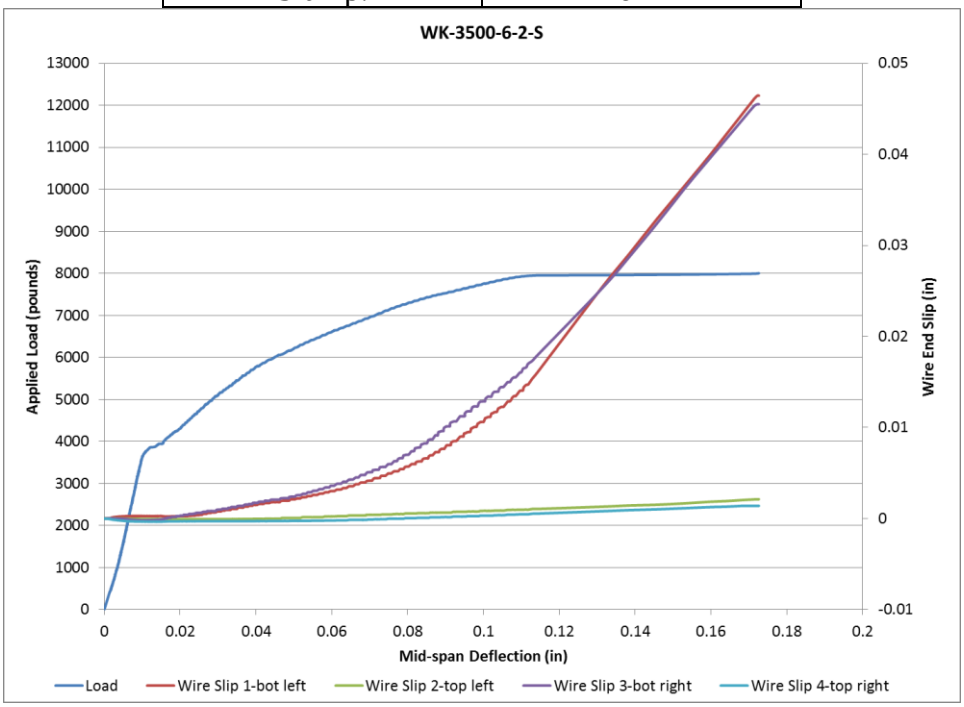


Figure 365 Load vs Deflection and Wire End Slip WK-3500-6-2-S

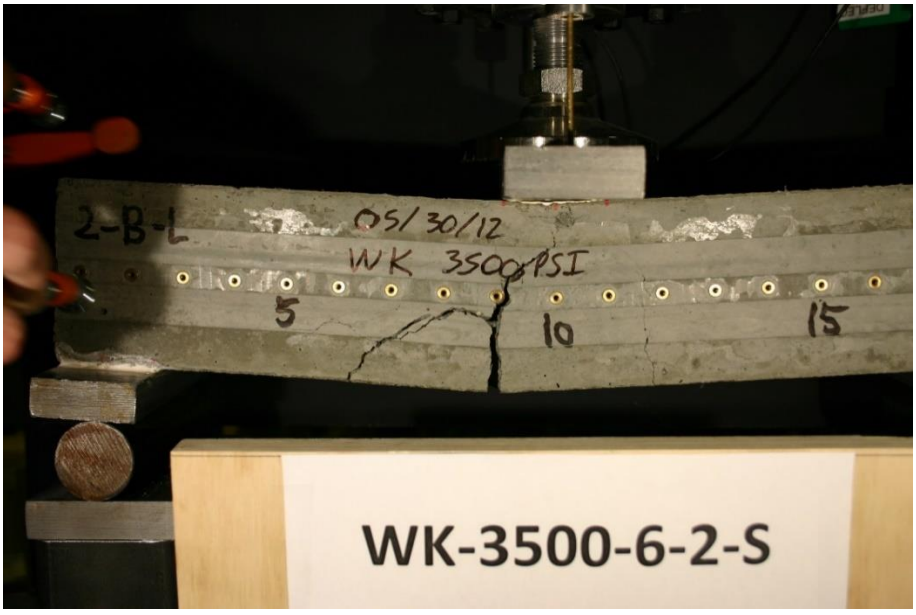


Figure 366 Picture of Failed Prism for WK-3500-6-2-S

Prisms made with strands, 4500 psi concrete release strength and 6 in. slump

Beam Identification	SA-4500-6-1-L
Wire Type:	SA
Embedment Length:	20 in
Release Strength:	4500 psi
Slump:	6 in

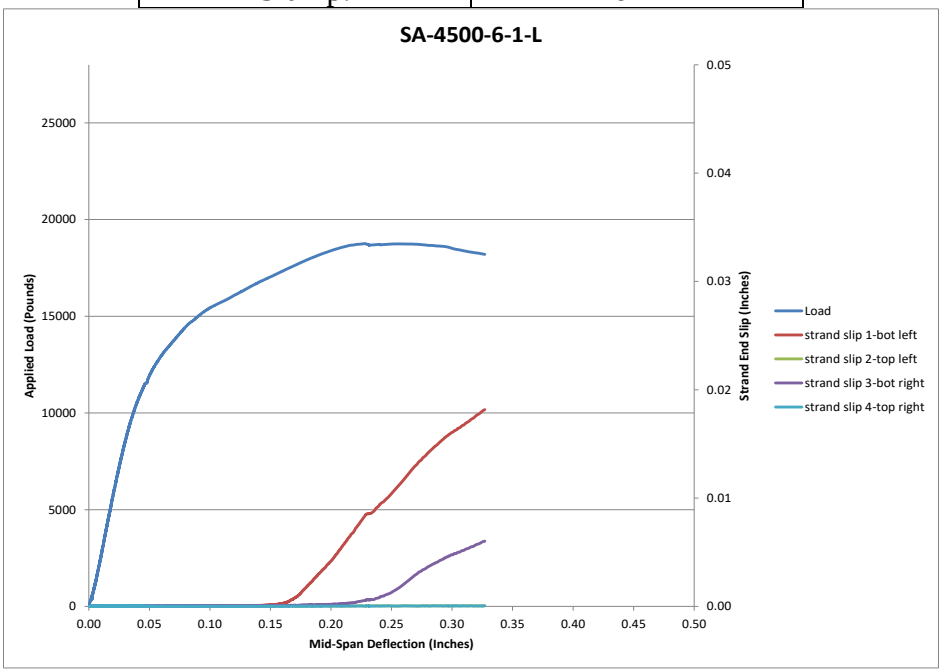


Figure 367 Load vs Deflection and Strand End Slip SA-4500-6-1-L



Figure 368 Picture of Failed Prism for SA-4500-6-1-L

Beam Identification	SA-4500-6-1-L-2nd
Wire Type:	SA
Embedment Length:	20 in
Release Strength:	4500 psi
Slump:	6 in

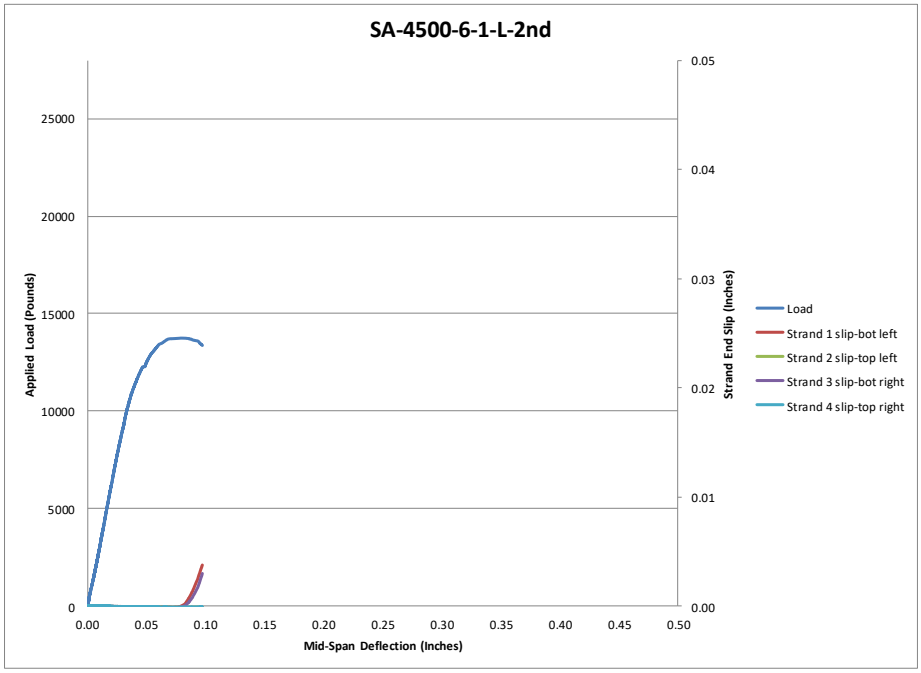


Figure 369 Load vs Deflection and Strand End Slip SA-4500-6-1-L-2nd



Figure 370 Picture of Failed Prism for SA-4500-6-1-L-2nd

Beam Identification	SA-4500-6-2-L
Wire Type:	SA
Embedment Length:	28 in
Release Strength:	4500 psi
Slump:	6 in

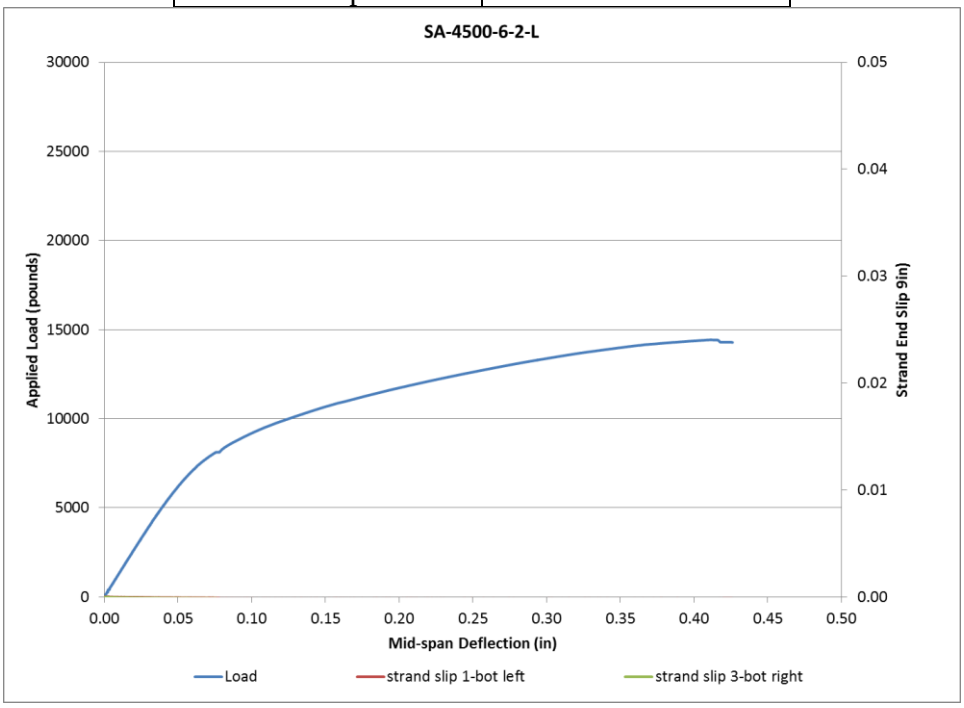


Figure 371 Load vs Deflection and Strand End Slip SA-4500-6-2-L

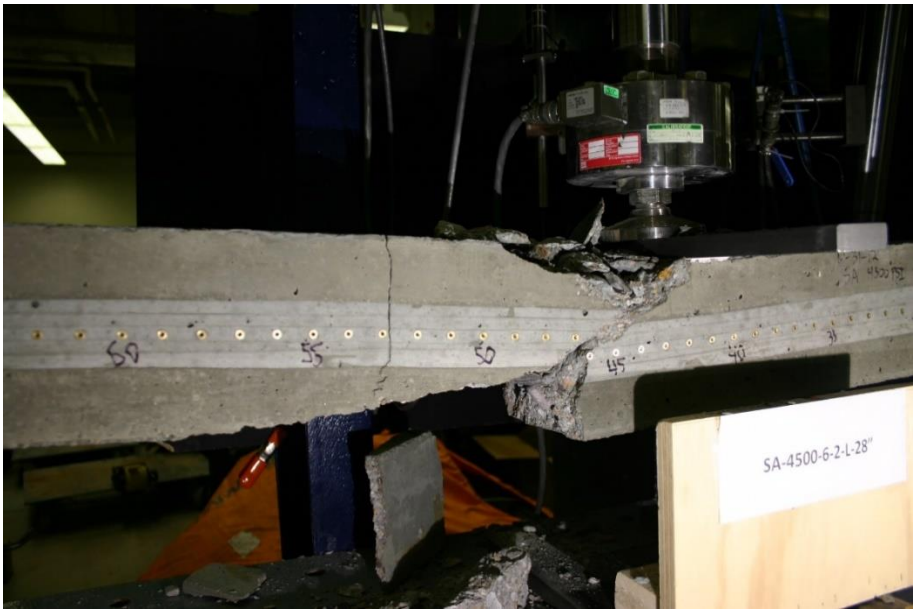


Figure 372 Picture of Failed Prism for SA-4500-6-2-L

Beam Identification	SA-4500-6-3-L
Wire Type:	SA
Embedment Length:	16.5 in
Release Strength:	4500 psi
Slump:	6 in

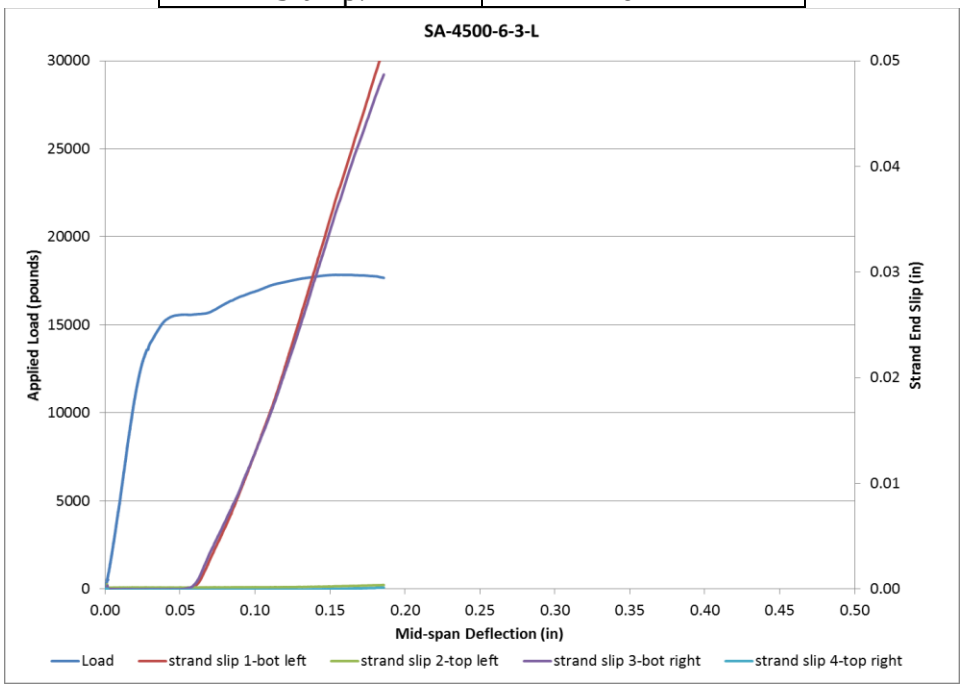


Figure 373 Load vs Deflection and Strand End Slip SA-4500-6-3-L



Figure 374 Picture of Failed Prism for SA-4500-6-3-L

Beam Identification	SA-4500-6-3-S
Wire Type:	SA
Embedment Length:	13 in
Release Strength:	4500 psi
Slump:	6 in

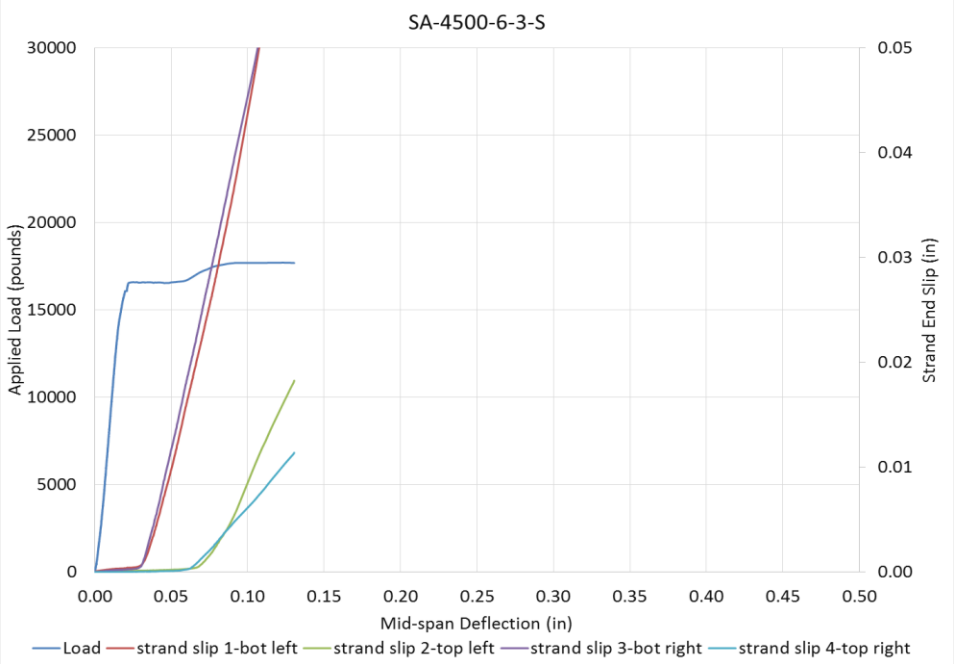


Figure 375 Load vs Deflection and Strand End Slip SA-4500-6-3-S



Figure 376 Picture of Failed Prism for SA-4500-6-3-S

Beam Identification	SB-4500-6-1-L
Wire Type:	SB
Embedment Length:	20 in
Release Strength:	4500 psi
Slump:	6 in

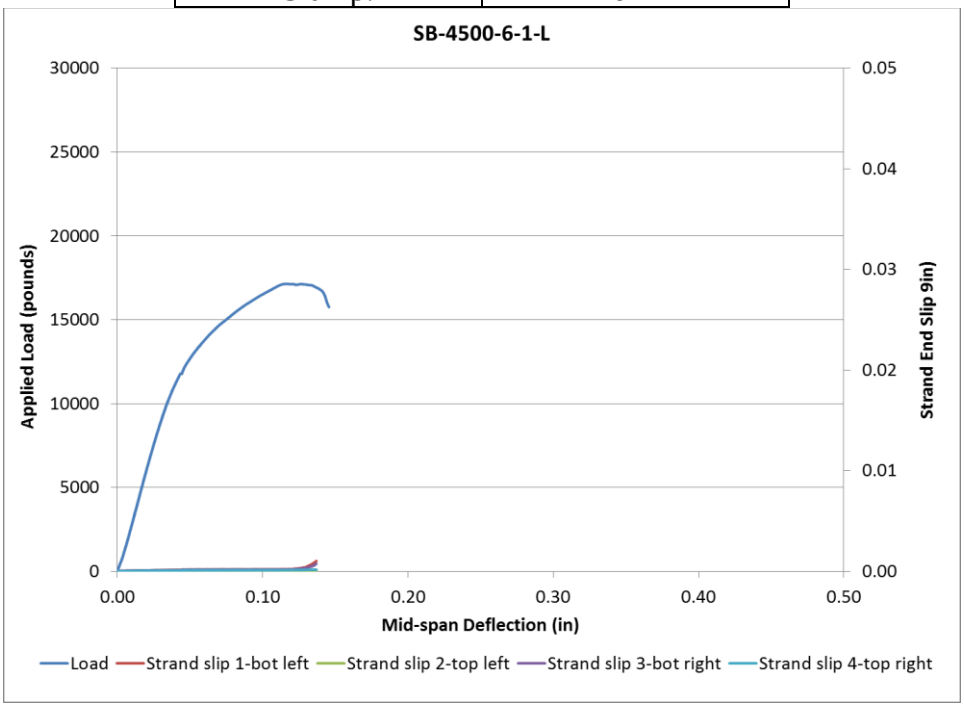


Figure 377 Load vs Deflection and Strand End Slip SB-4500-6-1-L



Figure 378 Picture of Failed Prism for SB-4500-6-1-L

Beam Identification	SB-4500-6-1-L-2nd
Wire Type:	SB
Embedment Length:	28 in
Release Strength:	4500 psi
Slump:	6 in

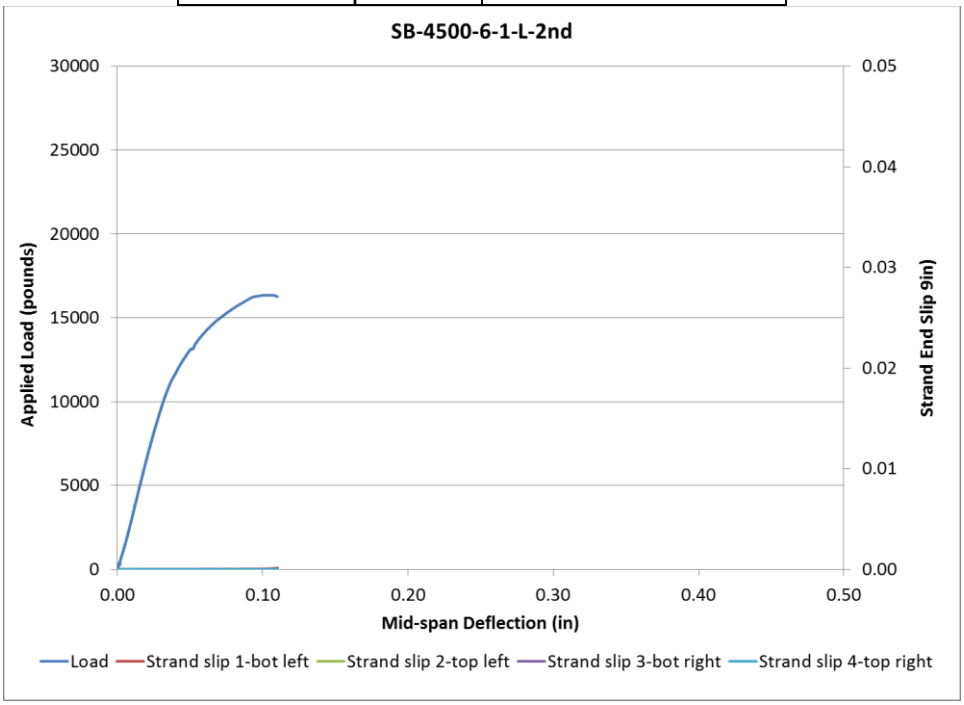


Figure 379 Load vs Deflection and Strand End Slip SB-4500-6-1-L-2nd



Figure 380 Picture of Failed Prism for SB-4500-6-1-L-2nd

Beam Identification	SB-4500-6-2-L
Wire Type:	SB
Embedment Length:	28 in
Release Strength:	4500 psi
Slump:	6 in

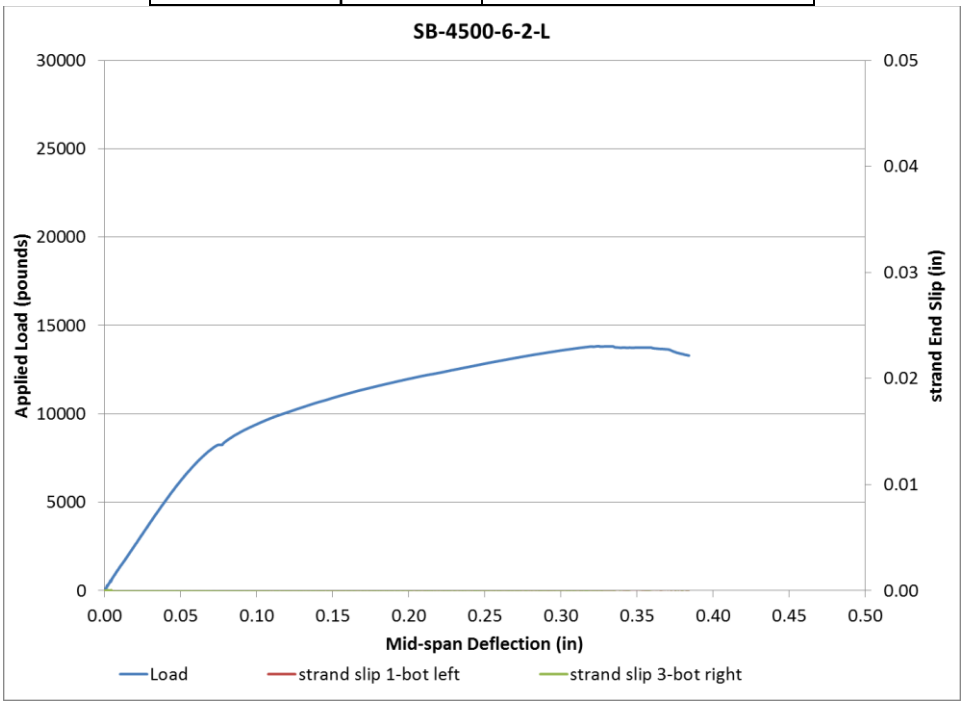


Figure 381 Load vs Deflection and Strand End Slip SB-4500-6-2-L

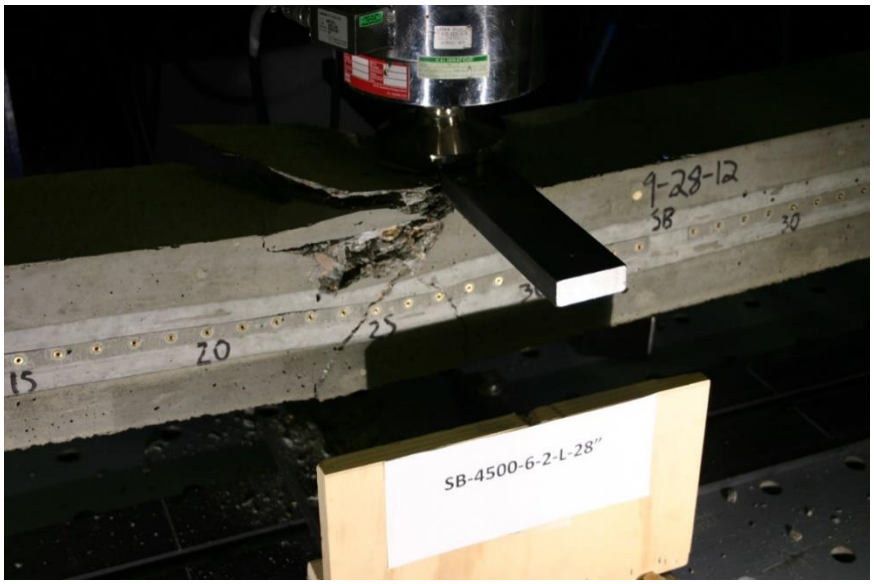


Figure 382 Picture of Failed Prism for SB-4500-6-2-L

Beam Identification	SB-4500-6-3-L
Wire Type:	SB
Embedment Length:	16.5 in
Release Strength:	4500 psi
Slump:	6 in

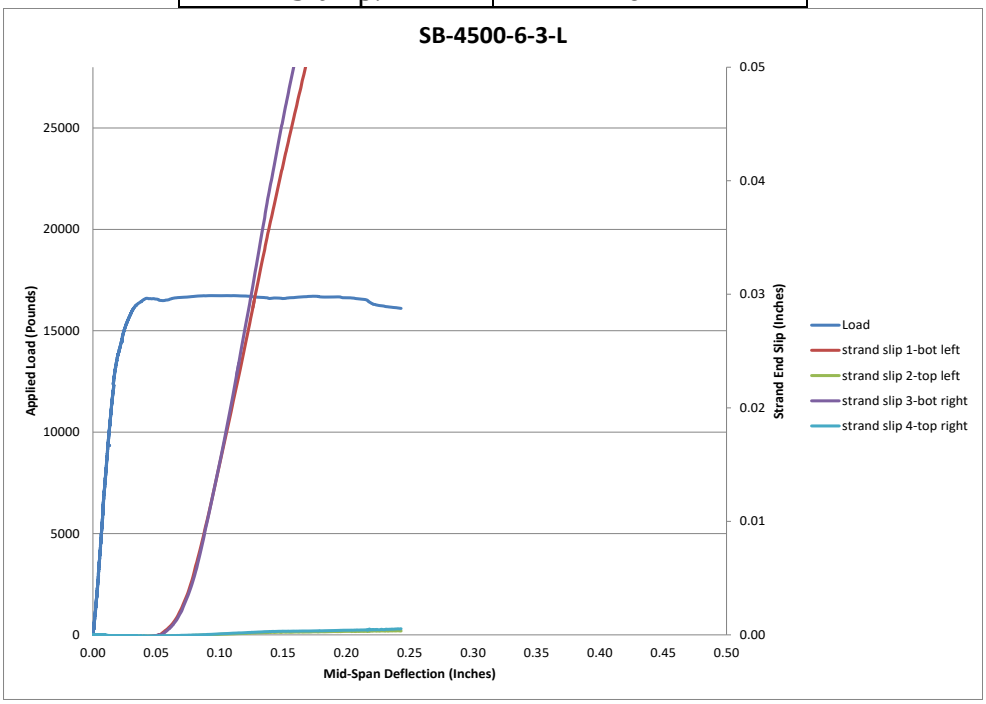


Figure 383 Load vs Deflection and Strand End Slip (SB-4500-6-3-L)



Figure 384 Picture of Failed Prism for SB-4500-6-3-L

Beam Identification	SB-4500-6-3-S
Wire Type:	SB
Embedment Length:	13 in
Release Strength:	4500 psi
Slump:	6 in

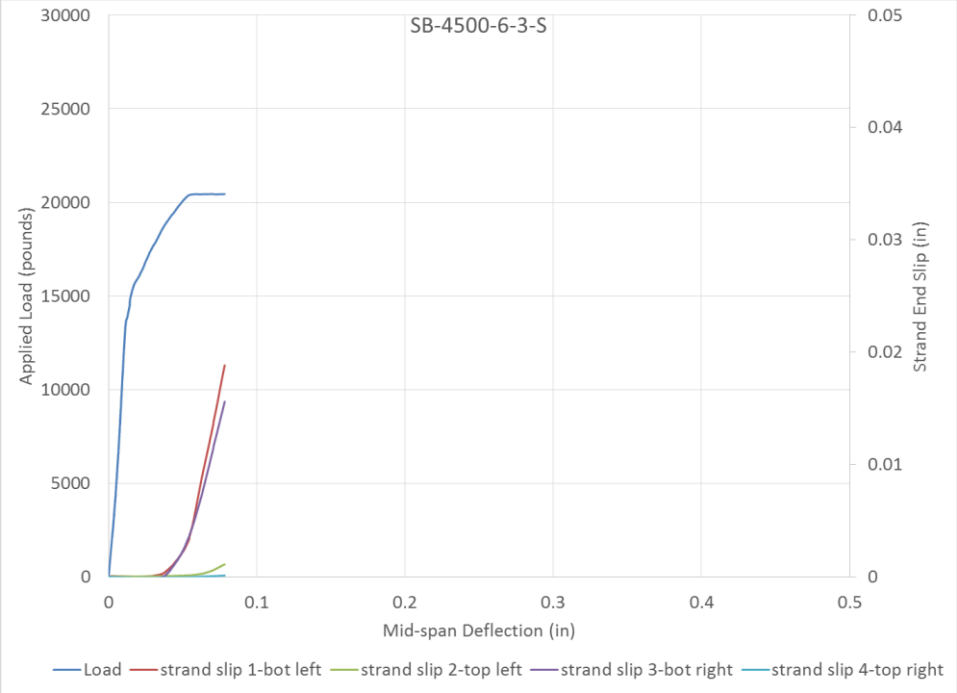


Figure 385 Load vs Deflection and Strand End Slip SB-4500-6-3-S



Figure 386 Picture of Failed Prism for SB-4500-6-3-S

Beam Identification	SD-4500-6-1-L
Wire Type:	SD
Embedment Length:	20 in
Release Strength:	4500 psi
Slump:	6 in

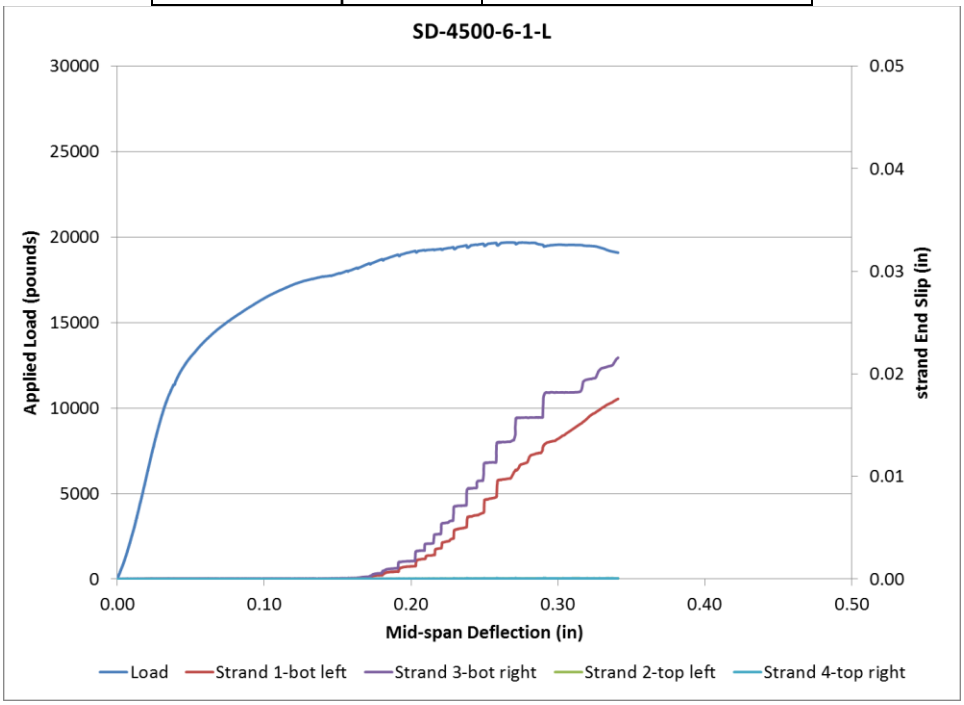


Figure 387 Load vs Deflection and Strand End Slip SD-4500-6-1-L

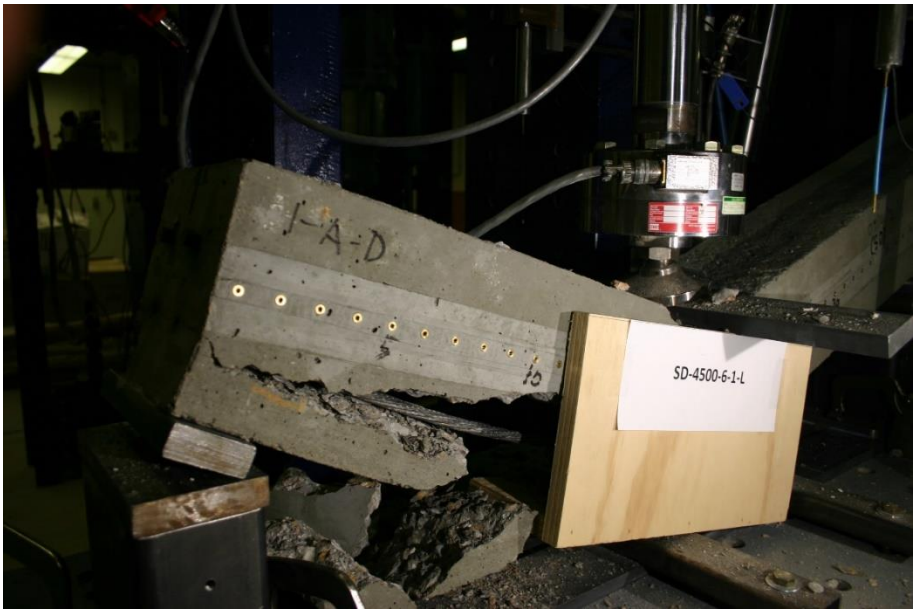


Figure 388 Picture of Failed Prism for SD-4500-6-1-L

Beam Identification	SD-4500-6-1-L-2nd
Wire Type:	SD
Embedment Length:	20 in
Release Strength:	4500 psi
Slump:	6 in

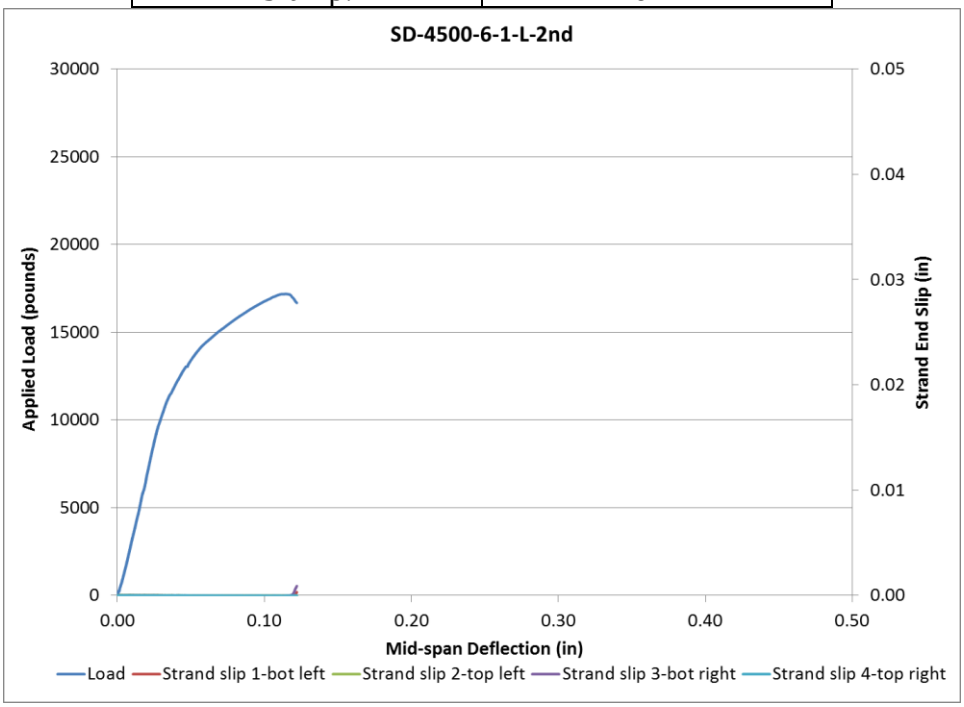


Figure 389 Load vs Deflection and Strand End Slip SD-4500-6-1-L-2nd

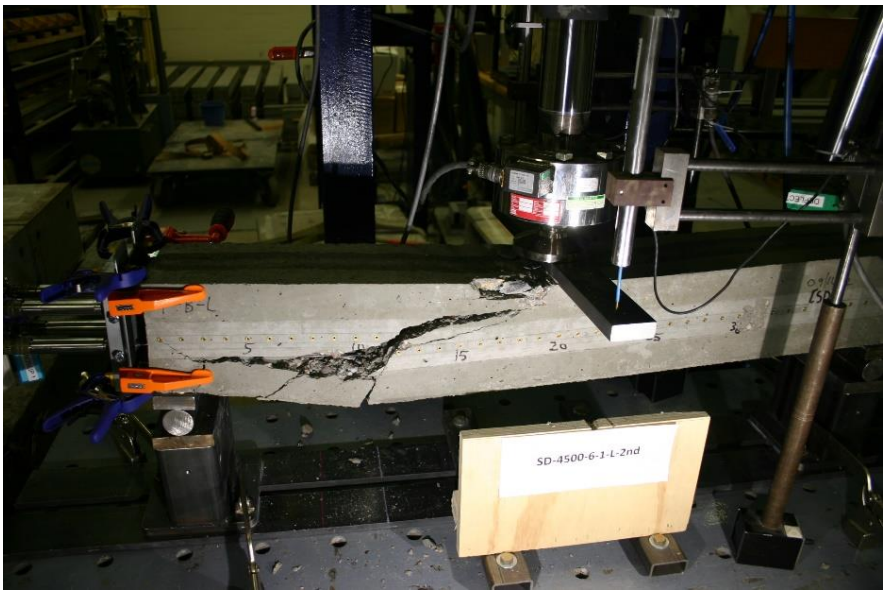


Figure 390 Picture of Failed Prism for SD-4500-6-1-L-2nd

Beam Identification	SD-4500-6-2-L
Wire Type:	SD
Embedment Length:	28 in
Release Strength:	4500 psi
Slump:	6 in

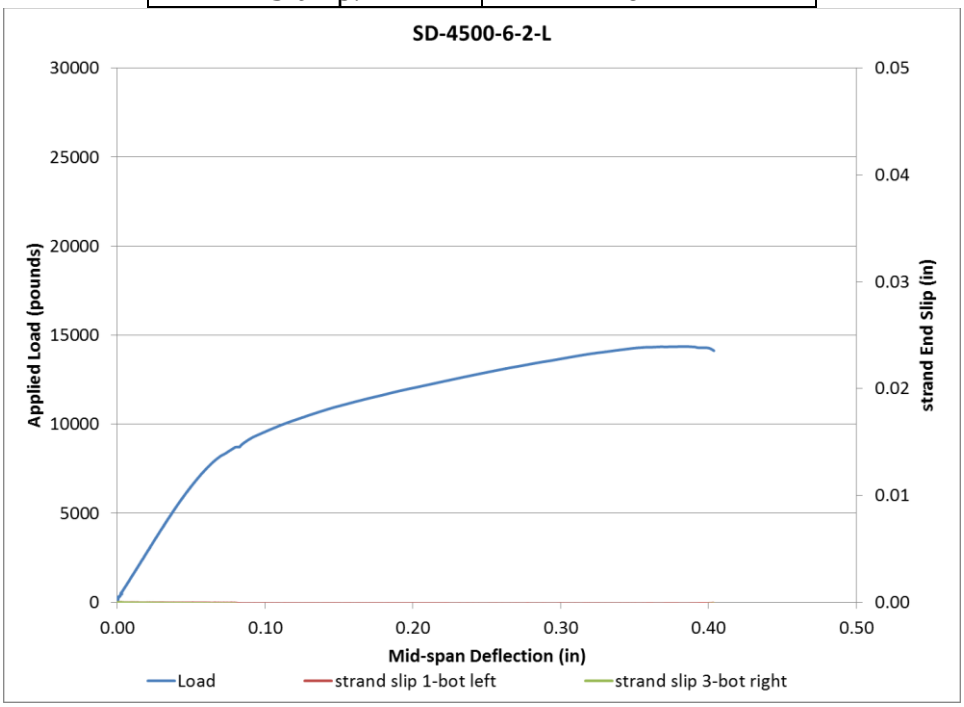


Figure 391 Load vs Deflection and Strand End Slip SD-4500-6-2-L

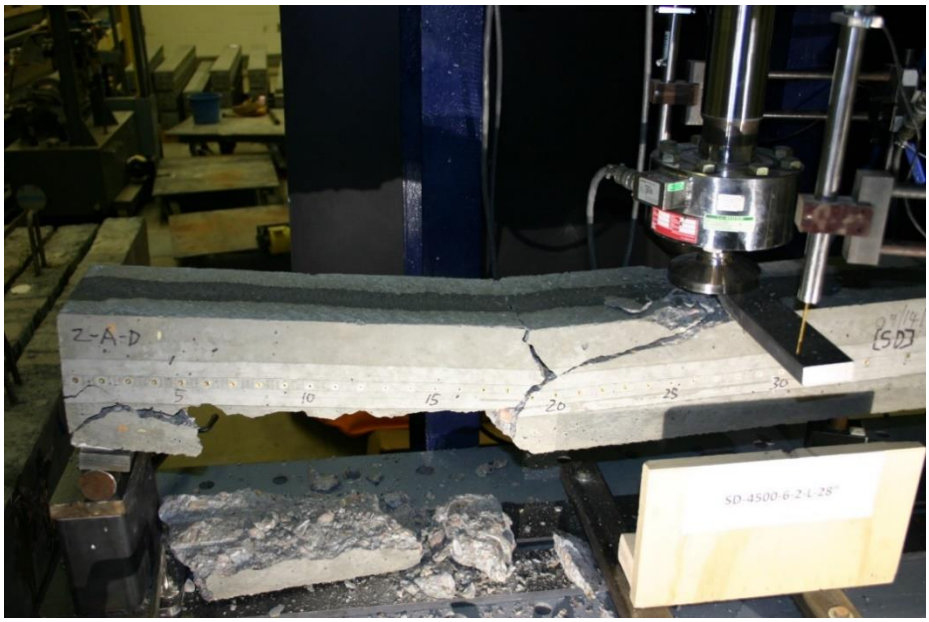


Figure 392 Picture of Failed Prism for SD-4500-6-2-L

Beam Identification	SD-4500-6-3-L
Wire Type:	SD
Embedment Length:	16.5 in
Release Strength:	4500 psi
Slump:	6 in

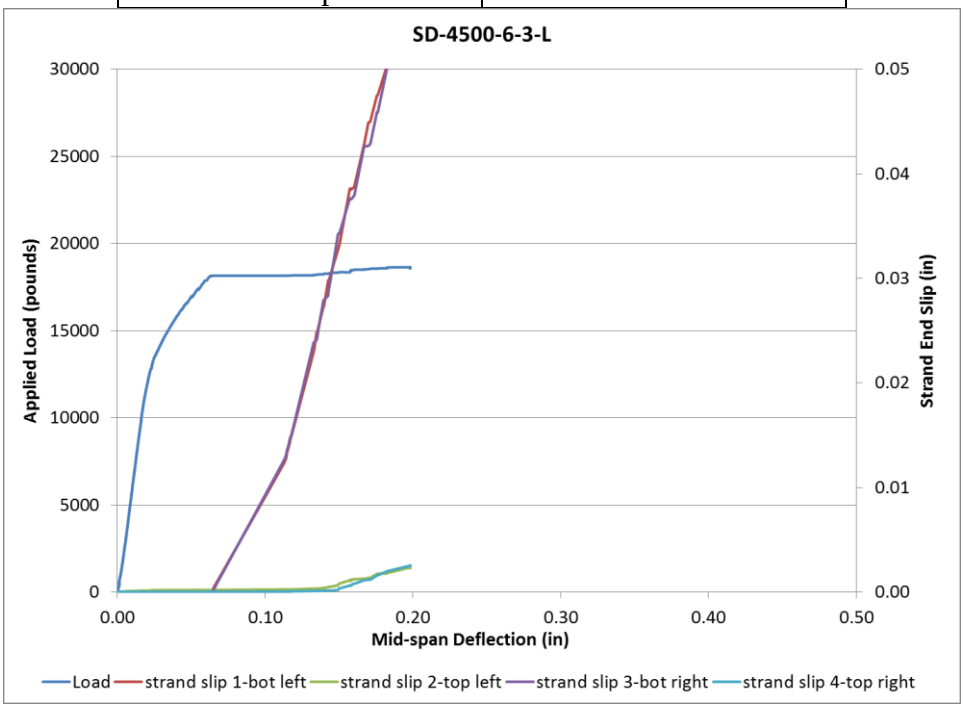


Figure 393 Load vs Deflection and Strand End Slip SD-4500-6-3-L



Figure 394 Picture of Failed Prism for SD-4500-6-3-L

Beam Identification	SD-4500-6-3-S
Wire Type:	SD
Embedment Length:	13 in
Release Strength:	4500 psi
Slump:	6 in

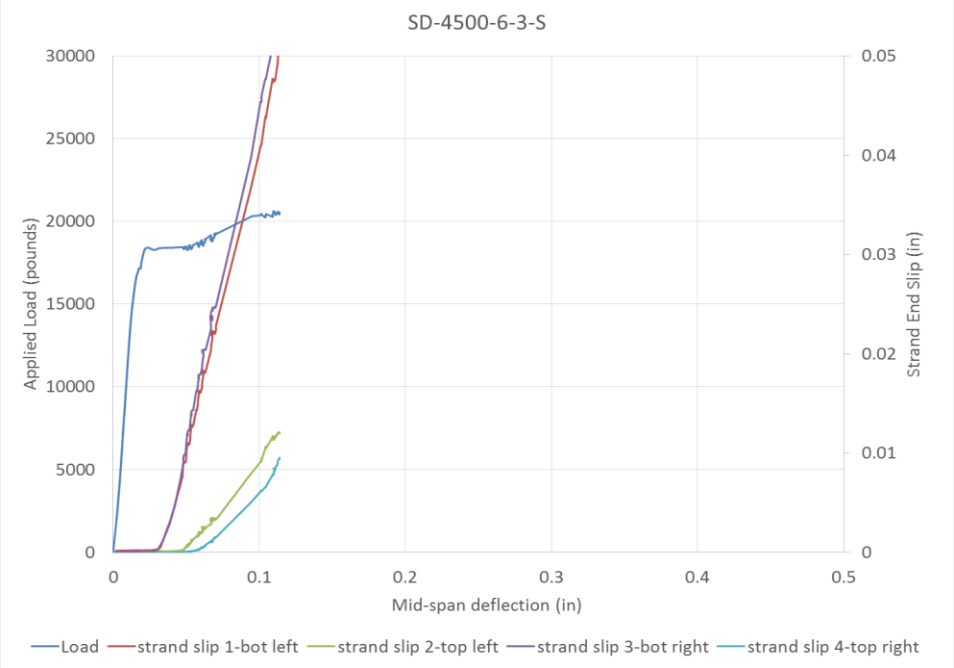


Figure 395 Load vs Deflection and Strand End Slip SD-4500-6-3-S



Figure 396 Picture of Failed Prism for SD-4500-6-3-S

Beam Identification	SE-4500-6-1-L
Wire Type:	SE
Embedment Length:	20 in
Release Strength:	4500 psi
Slump:	6 in

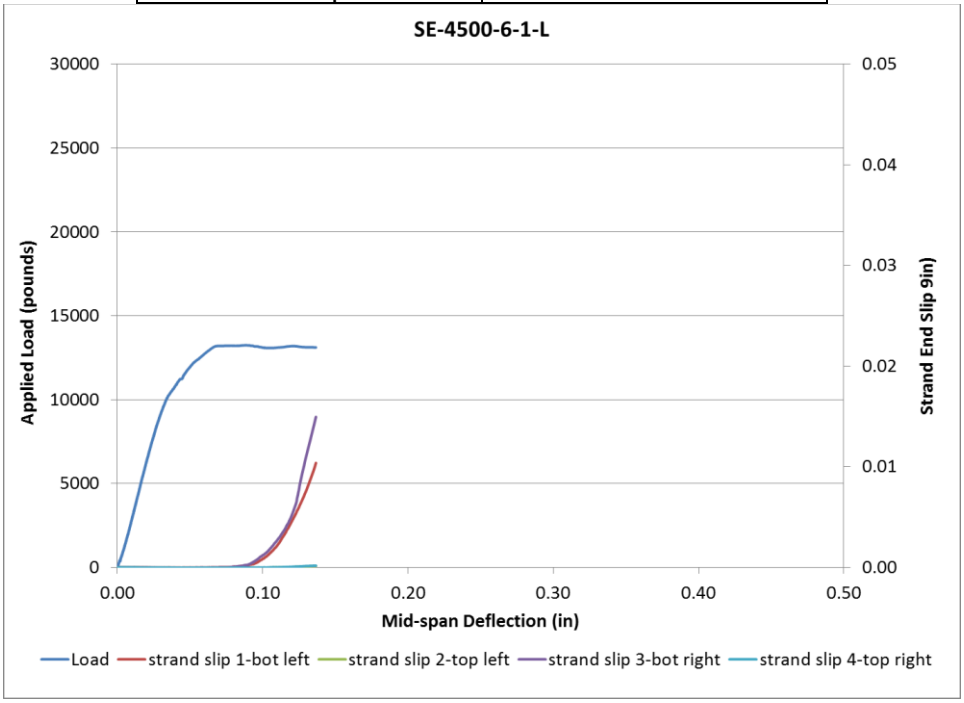


Figure 397 Load vs Deflection and Strand End Slip SE-4500-6-1-L

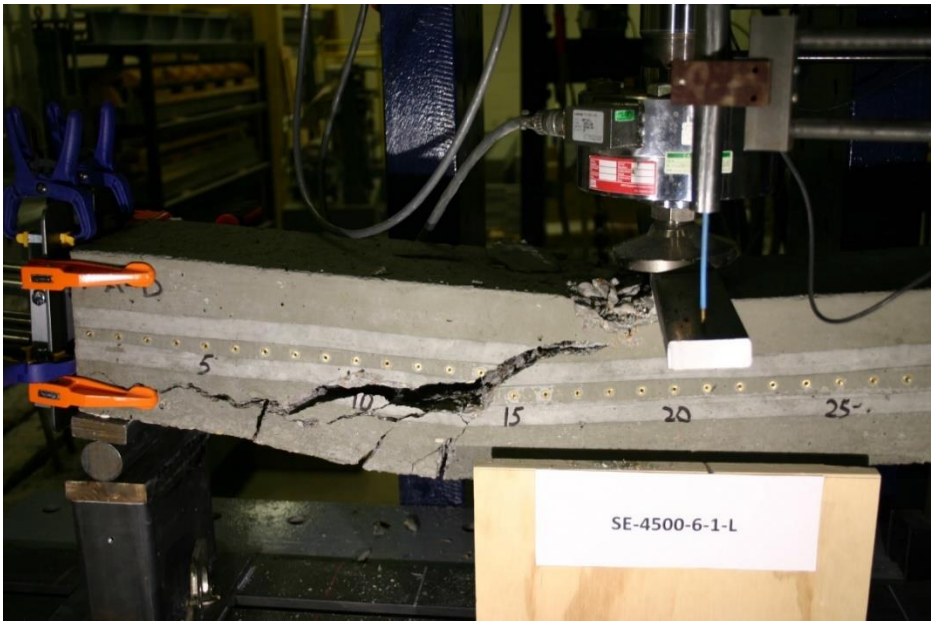


Figure 398 Picture of Failed Prism for SE-4500-6-1-L

Beam Identification	SE-4500-6-1-L-2nd
Wire Type:	SE
Embedment Length:	20 in
Release Strength:	4500 psi
Slump:	6 in

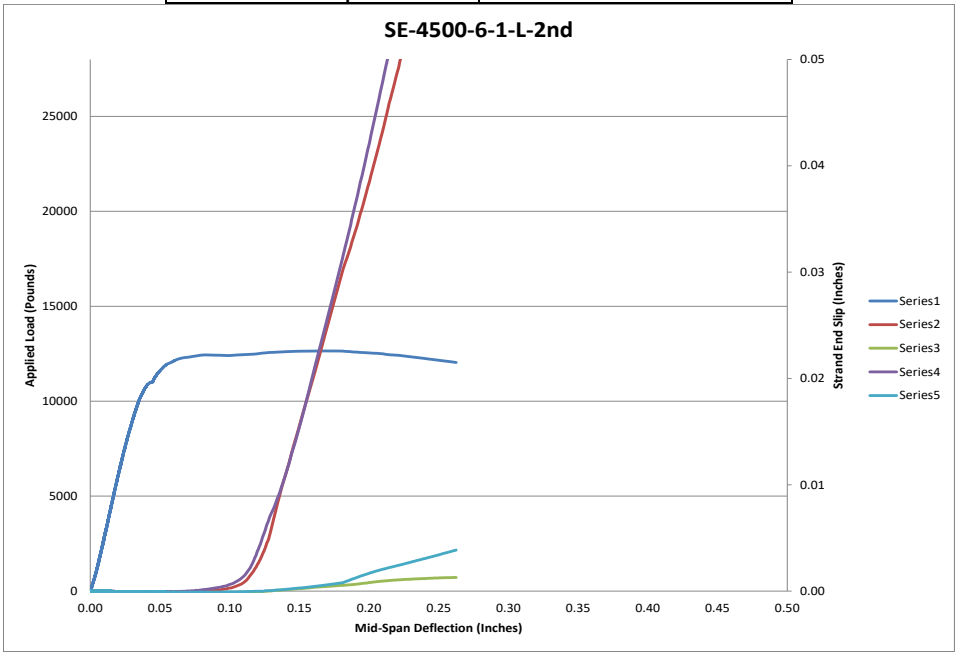


Figure 399 Load vs Deflection and Strand End Slip SE-4500-6-1-L-2nd



Figure 400 Picture of Failed Prism for SE-4500-6-1-L-2nd

Beam Identification	SE-4500-6-2-L
Wire Type:	SE
Embedment Length:	28 in
Release Strength:	4500 psi
Slump:	6 in

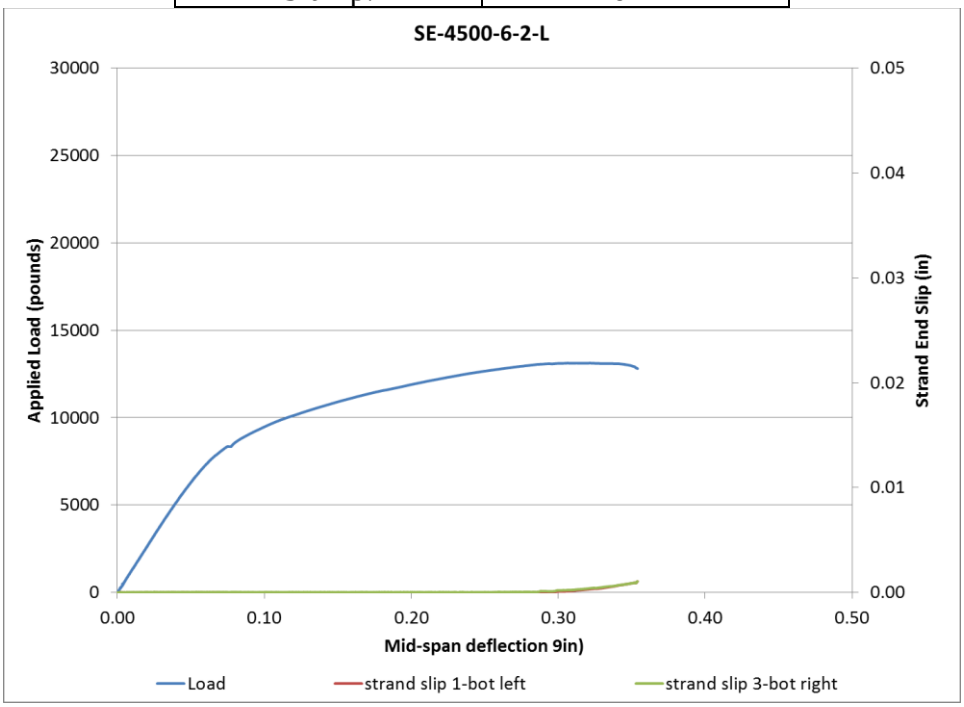


Figure 401 Load vs Deflection and Strand End Slip SE-4500-6-2-L

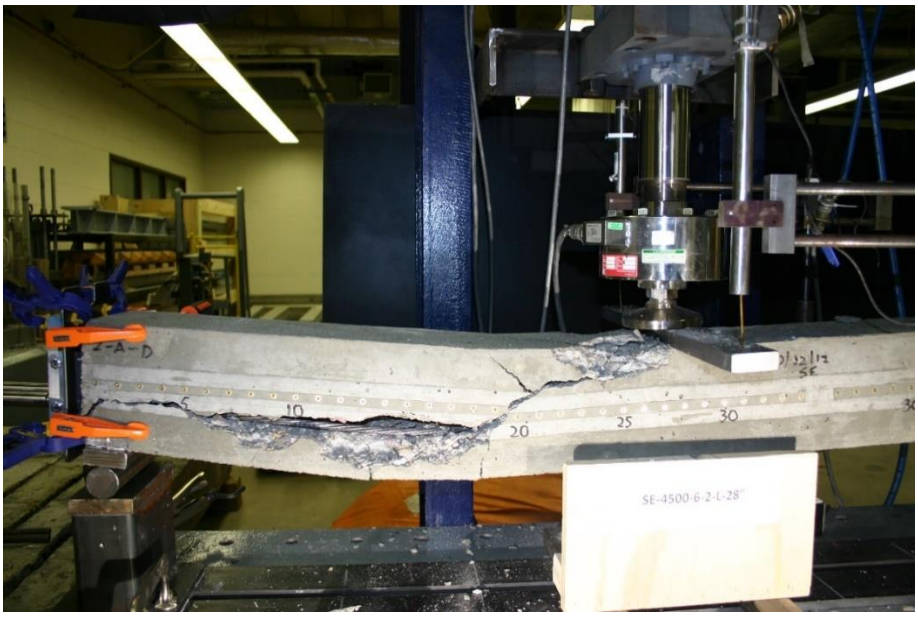


Figure 402 Picture of Failed Prism for SE-4500-6-2-L

Beam Identification	SE-4500-6-3-L
Wire Type:	SE
Embedment Length:	16.5 in
Release Strength:	4500 psi
Slump:	6 in

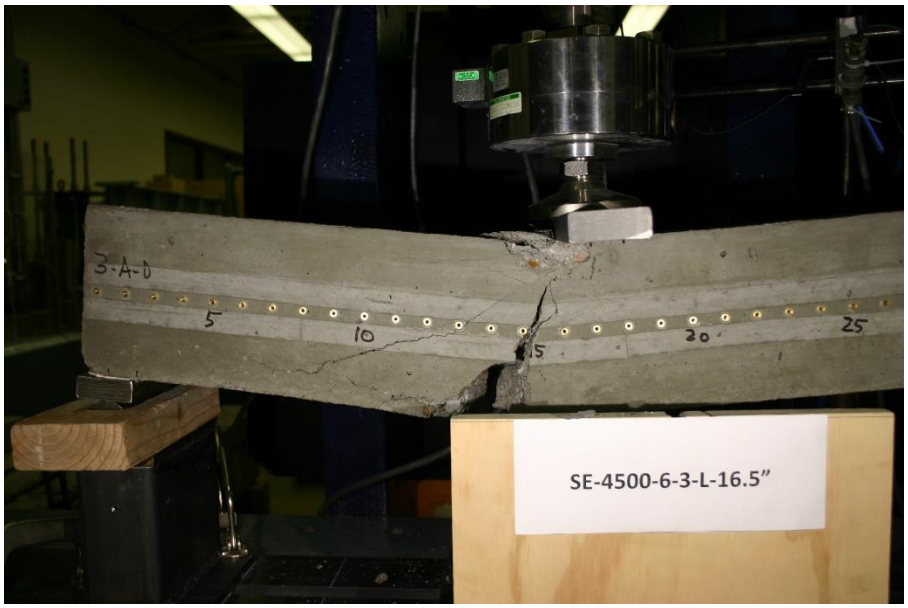


Figure 403 Picture of Failed Prism for SE-4500-6-3-L

Beam Identification	SE-4500-6-3-S
Wire Type:	SE
Embedment Length:	13 in
Release Strength:	4500 psi
Slump:	6 in

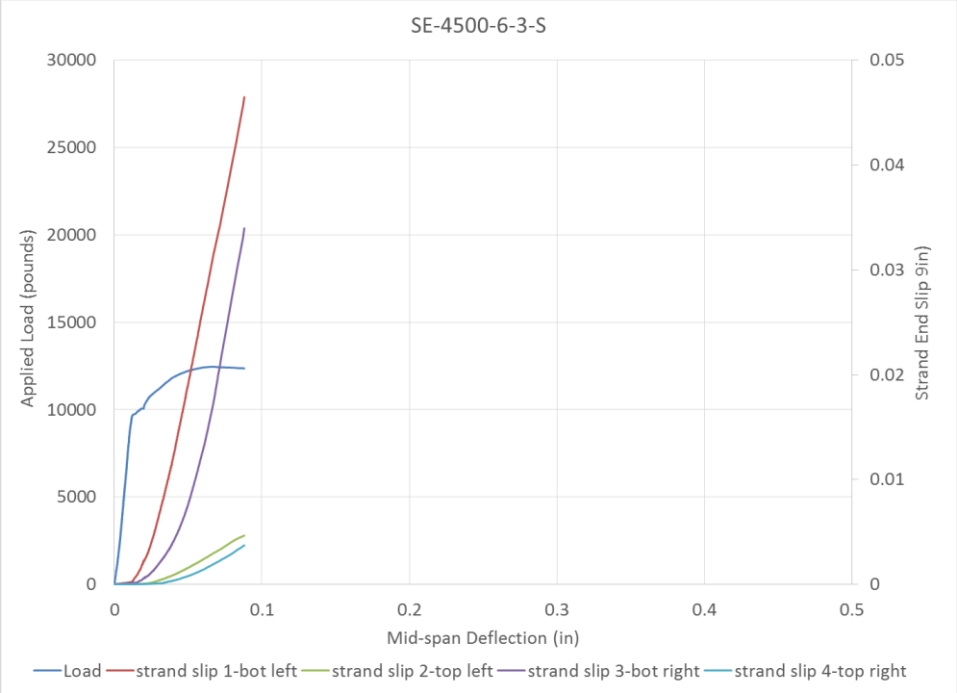


Figure 404 Load vs Deflection and Strand End Slip SE-4500-6-3-S



Figure 405 Picture of Failed Prism for SE-4500-6-3-S

Beam Identification	SF-4500-6-1-L
Wire Type:	SF
Embedment Length:	20 in
Release Strength:	4500 psi
Slump:	6 in

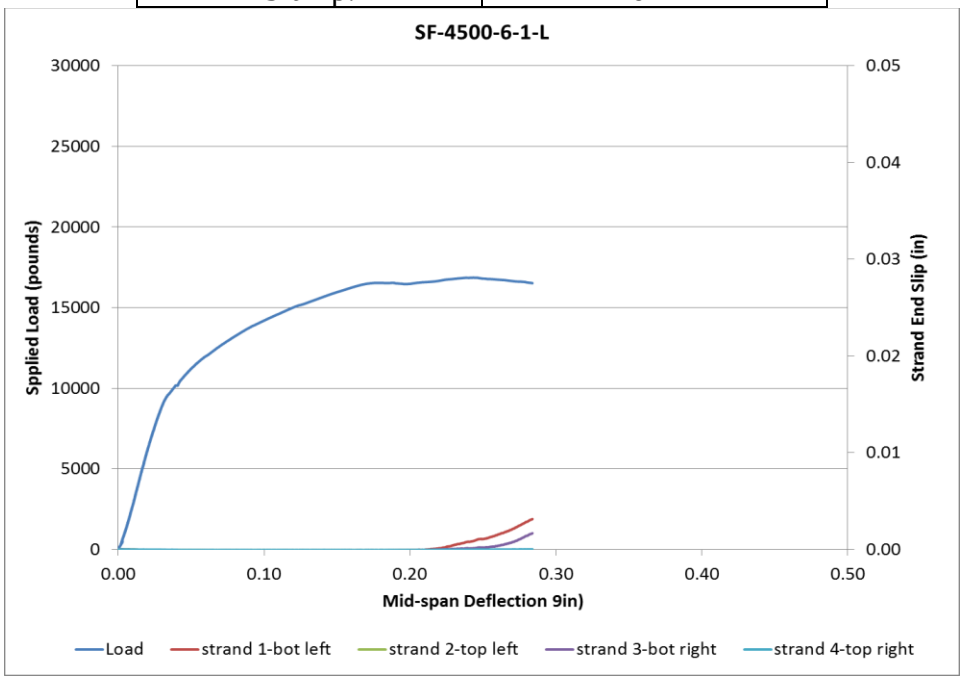


Figure 406 Load vs Deflection and Strand End Slip SF-4500-6-1-L



Figure 407 Picture of Failed Prism for SF-4500-6-1-L

Beam Identification	SF-4500-6-1-L-2nd
Wire Type:	SF
Embedment Length:	20 in
Release Strength:	4500 psi
Slump:	6 in

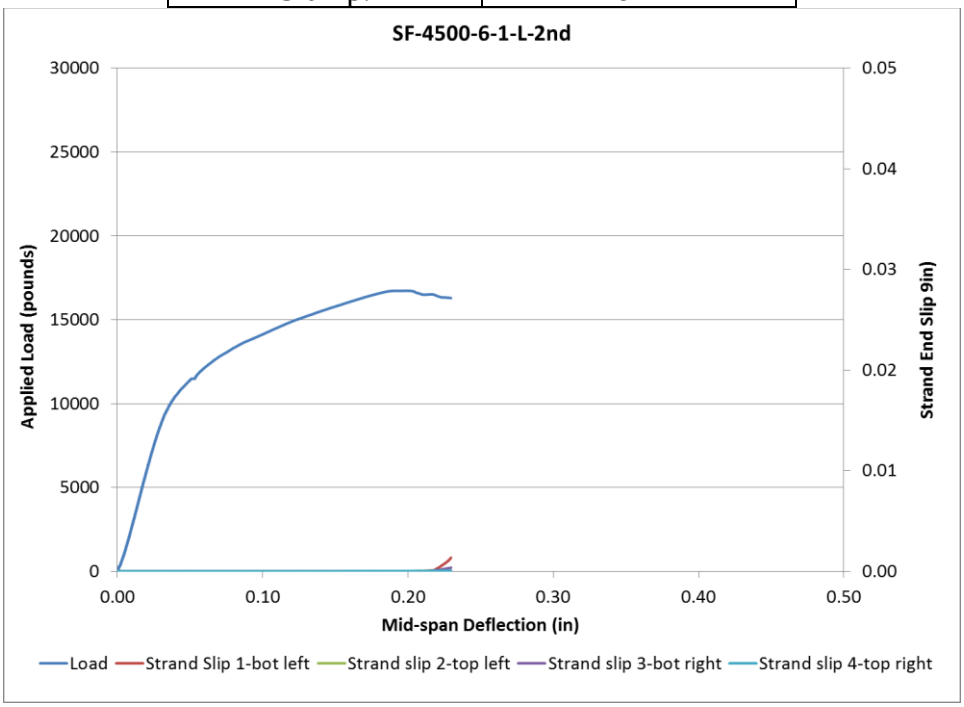


Figure 408 Load vs Deflection and Strand End Slip SF-4500-6-1-L-2nd

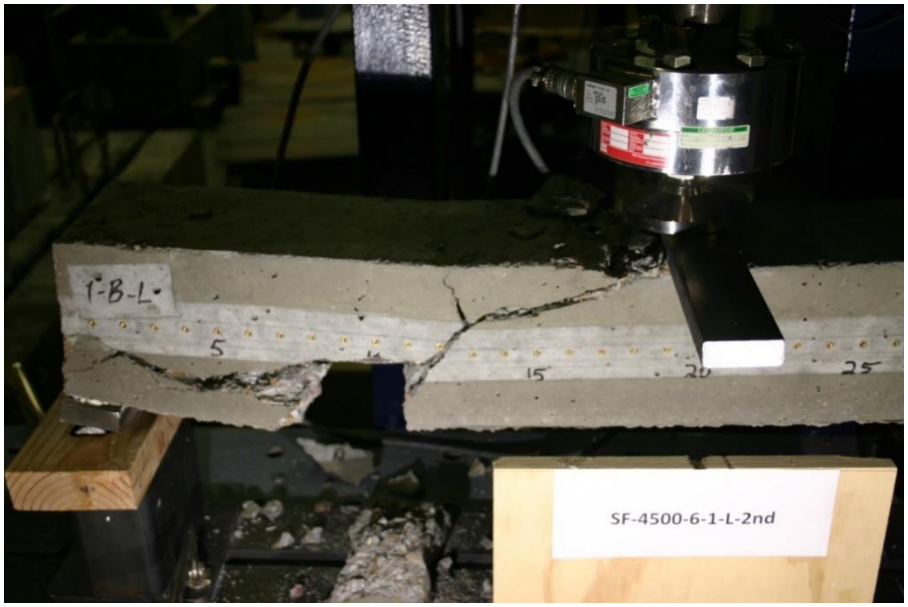


Figure 409 Picture of Failed Prism for SF-4500-6-1-L 2nd

Beam Identification	SF-4500-6-2-L
Wire Type:	SF
Embedment Length:	28 in
Release Strength:	4500 psi
Slump:	6 in

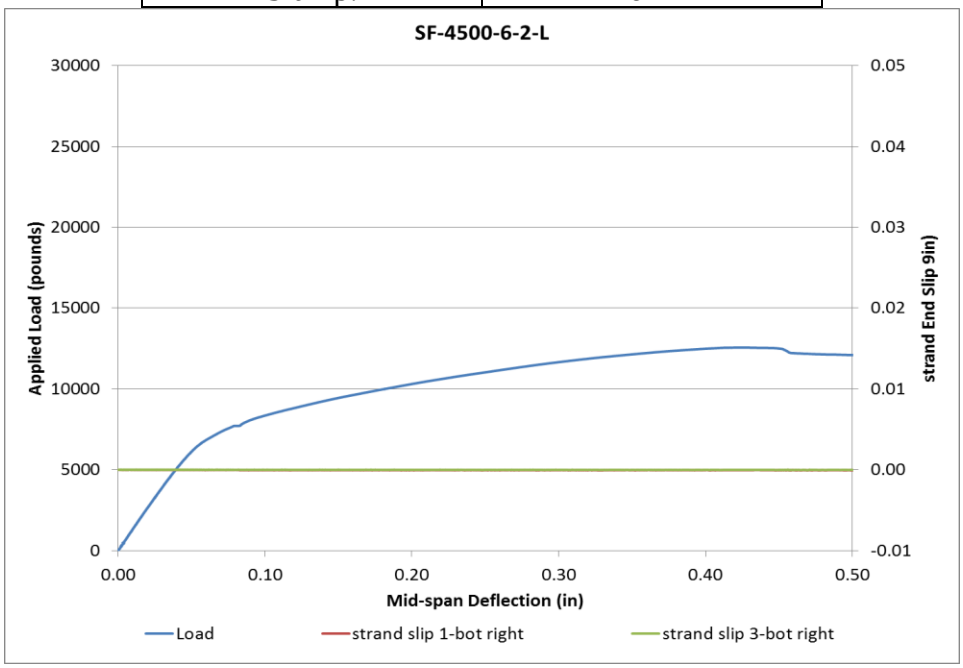


Figure 410 Load vs Deflection and Strand End Slip SF-4500-6-2-L

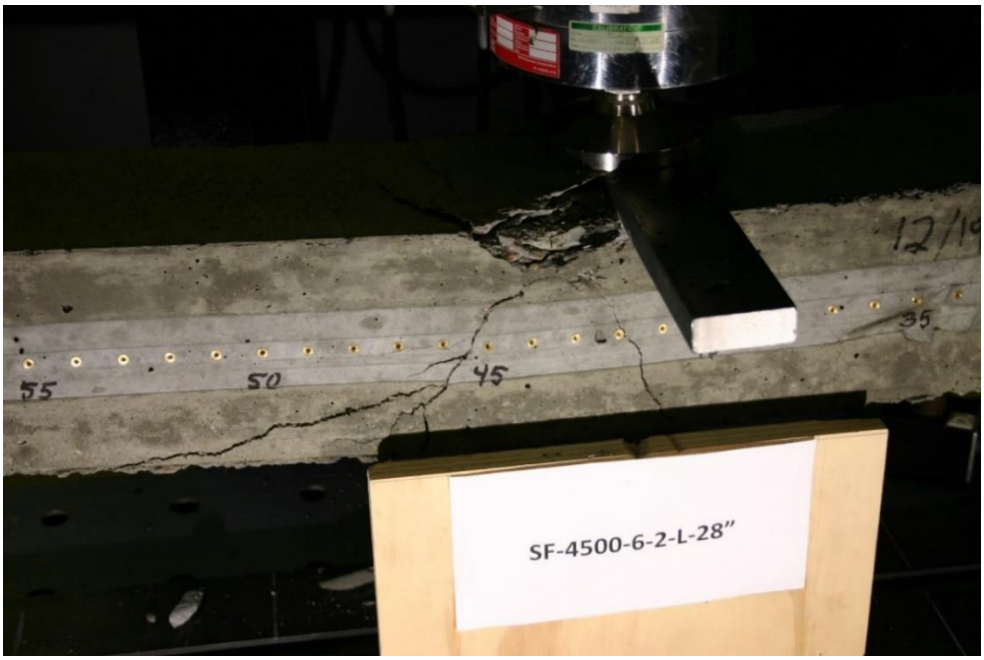


Figure 411 Picture of Failed Prism for SF-4500-6-2-L

Beam Identification	SF-4500-6-3-L
Wire Type:	SF
Embedment Length:	16.5 in
Release Strength:	4500 psi
Slump:	6 in

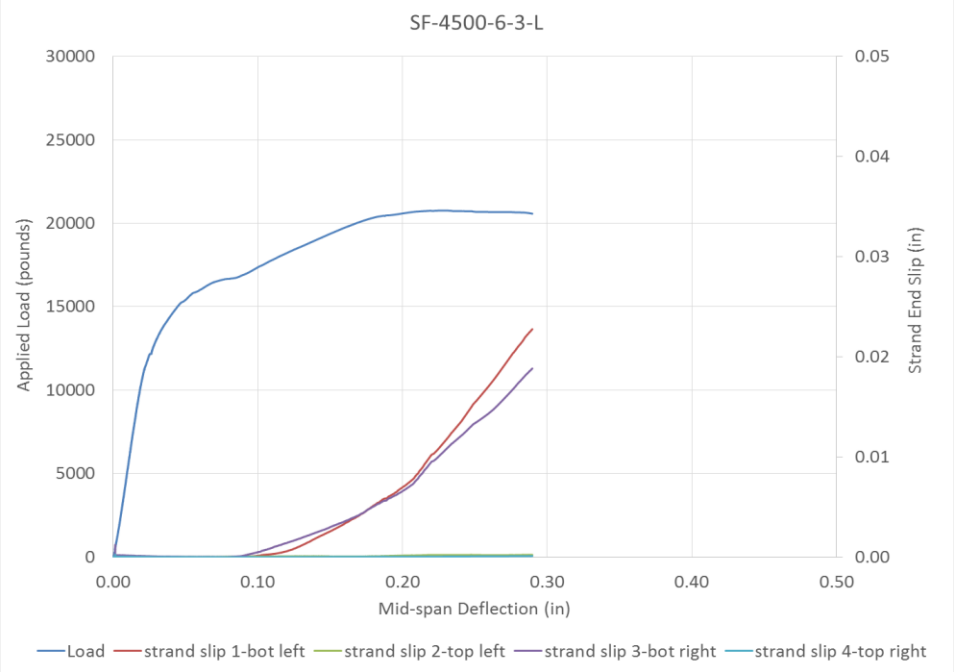


Figure 412 Load vs Deflection and Strand End Slip SF-4500-6-3-L



Figure 413 Picture of Failed Prism for SF-4500-6-3-L

Beam Identification	SF-4500-6-3-S
Wire Type:	SF
Embedment Length:	13 in
Release Strength:	4500 psi
Slump:	6 in

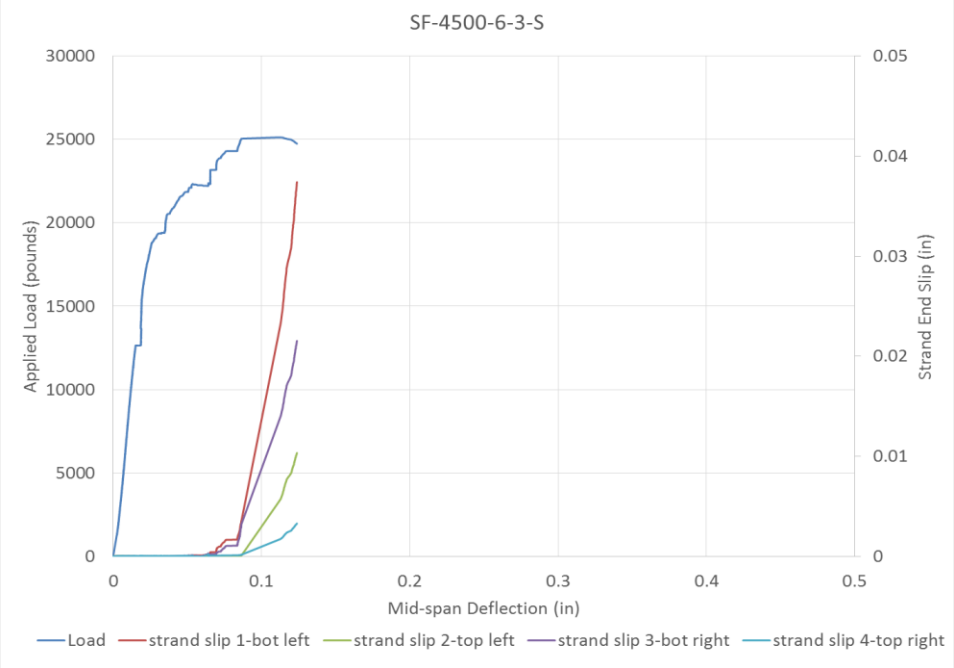


Figure 414 Load vs Deflection and Strand End Slip SF-4500-6-3-S

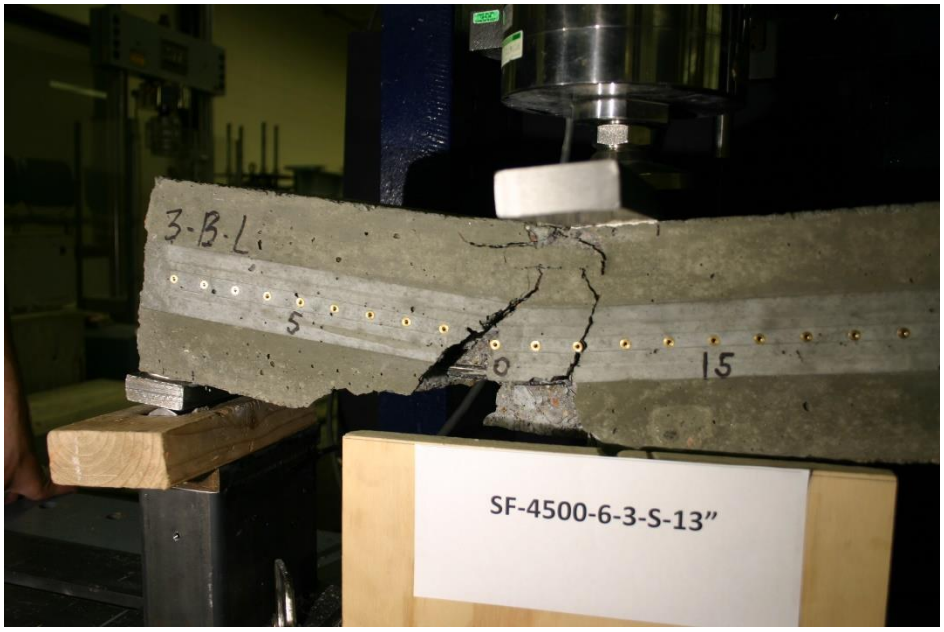


Figure 415 Picture of Failed Prism for SF-4500-6-3-S

Prisms made with strands, 3500 psi concrete release strength and 6 in. slump

Beam Identification	SA-3500-6-1-L
Wire Type:	SA
Embedment Length:	20 in
Release Strength:	3500 psi
Slump:	6 in

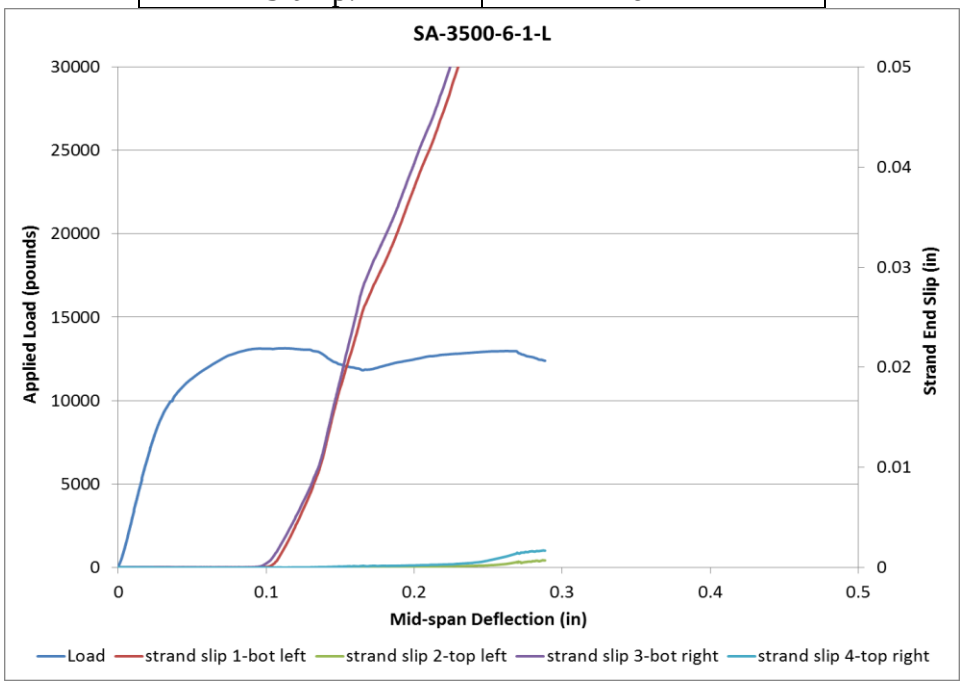


Figure 416 Load vs Deflection and Strand End Slip SA-3500-6-1-L

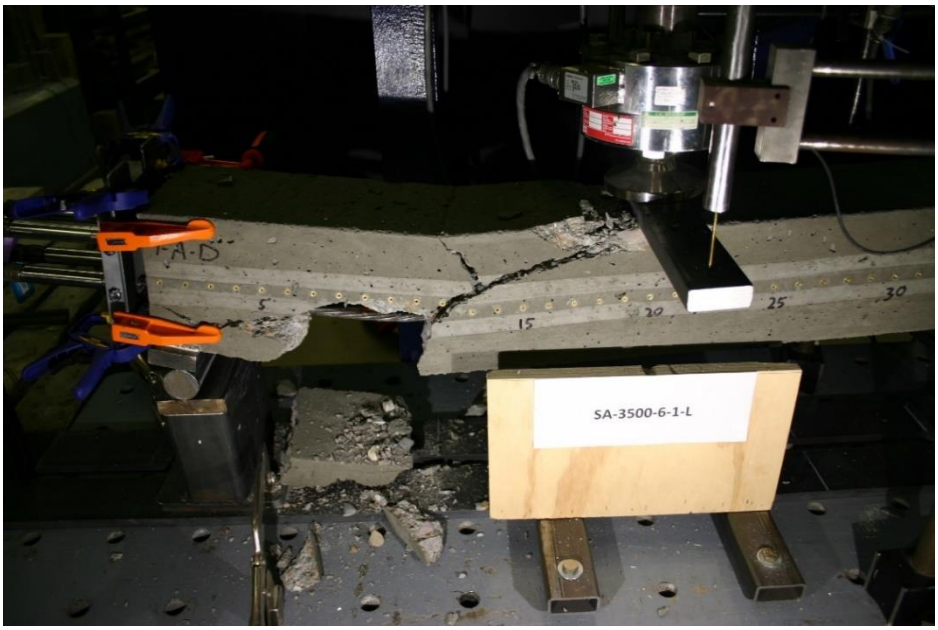
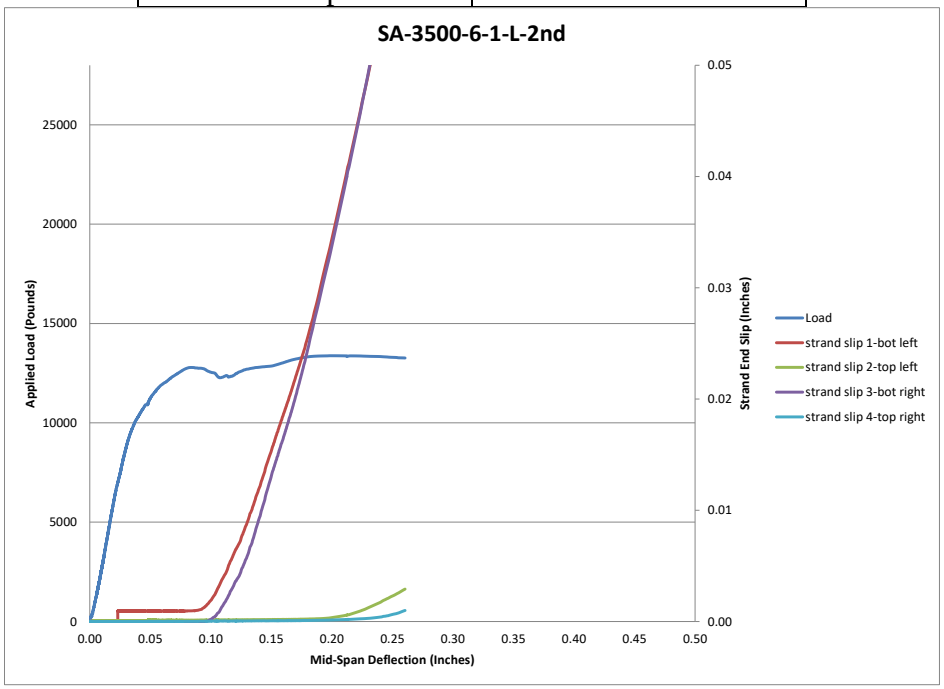


Figure 417 Picture of Failed Prism for SA-3500-6-1-L

Beam Identification	SA-3500-6-1-L-2nd
Wire Type:	SA
Embedment Length:	20 in
Release Strength:	3500 psi
Slump:	6 in



Load vs Deflection and Strand End Slip SA-3500-6-1-L-2nd



Figure 418 Picture of Failed Prism for SA-3500-6-1-L-2nd

Beam Identification	SA-3500-6-2-L
Wire Type:	SA
Embedment Length:	28 in
Release Strength:	3500 psi
Slump:	6 in

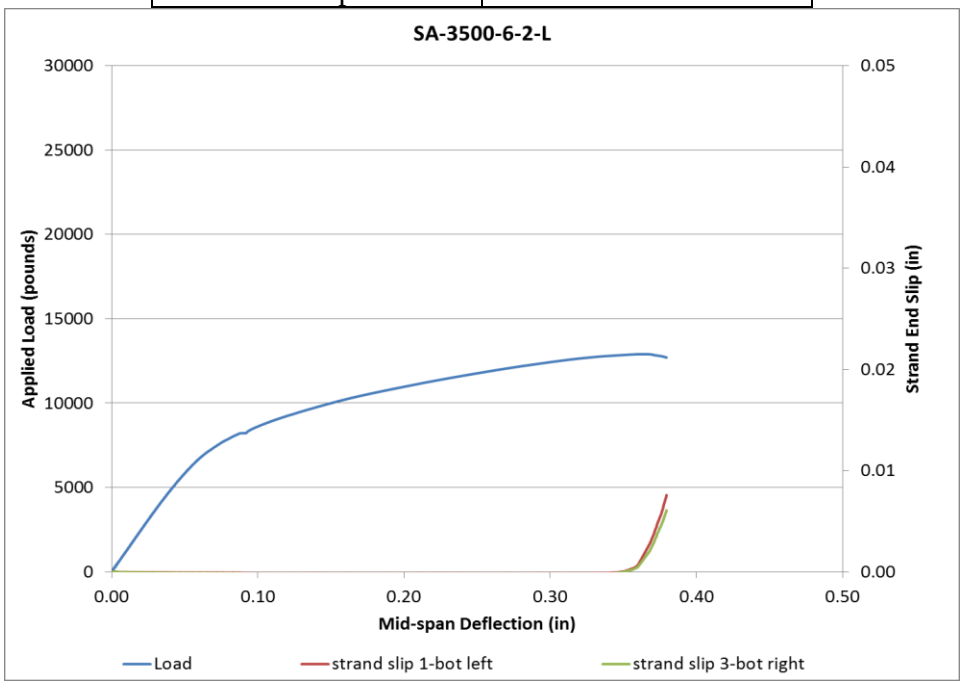


Figure 419 Load vs Deflection and Strand End Slip SA-3500-6-2-L

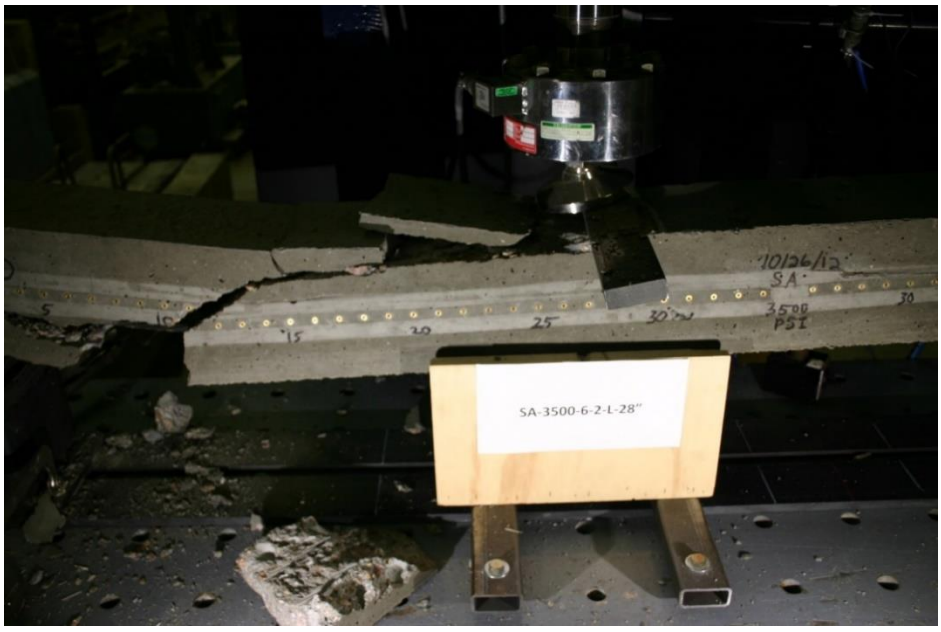


Figure 420 Picture of Failed Prism for SA-3500-6-2-L

Beam Identification	SA-3500-6-3-L
Wire Type:	SA
Embedment Length:	16.5 in
Release Strength:	3500 psi
Slump:	6 in

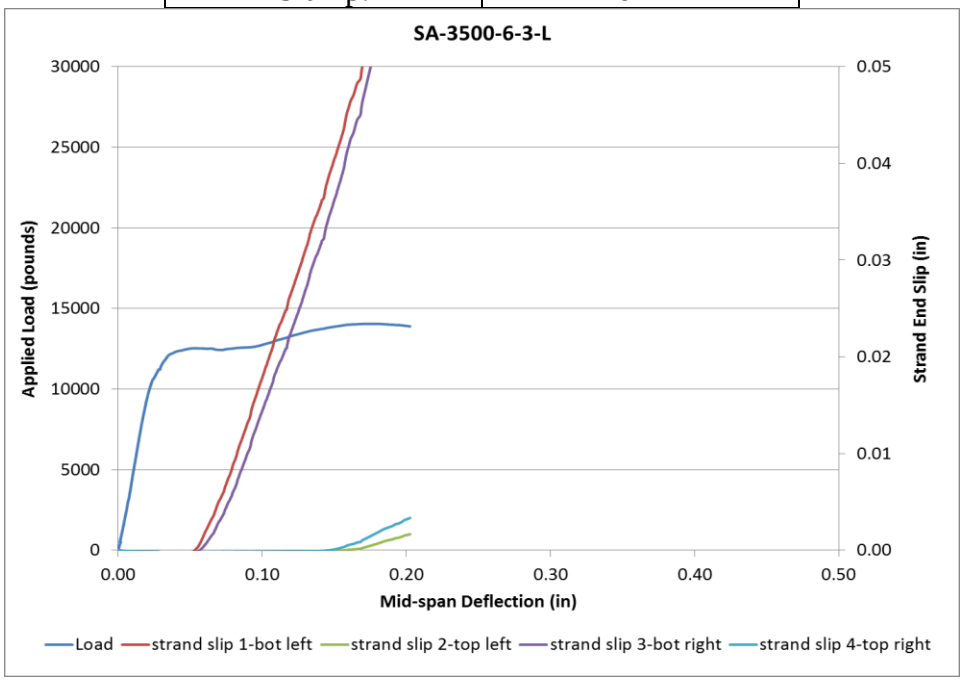


Figure 421 Load vs Deflection and Strand End Slip SA-3500-6-3-L

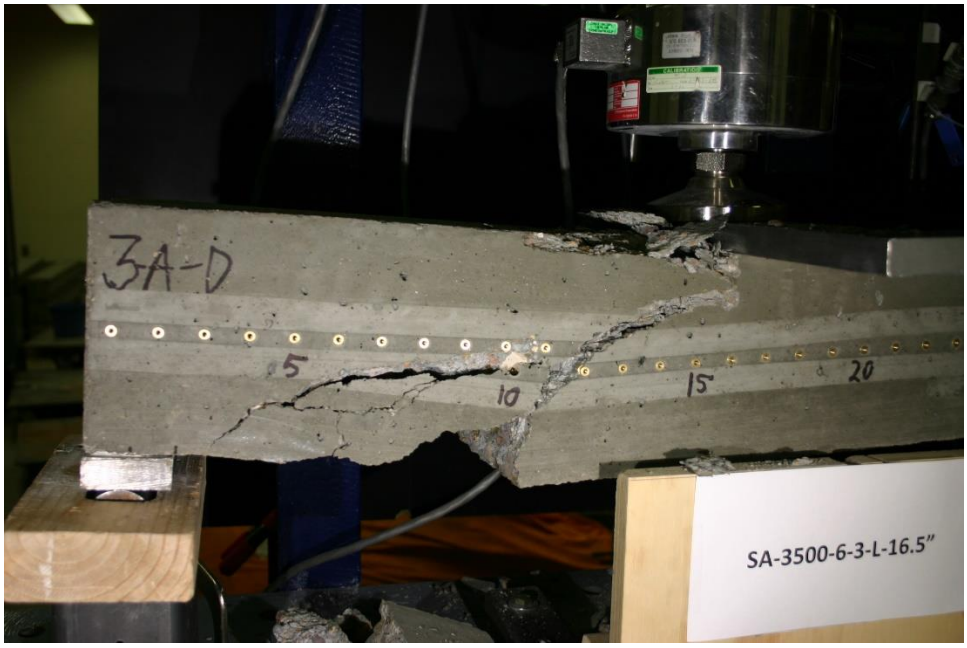


Figure 422 Picture of Failed Prism for SA-3500-6-3-L

Beam Identification	SA-3500-6-3-S
Wire Type:	SA
Embedment Length:	13 in
Release Strength:	3500 psi
Slump:	6 in

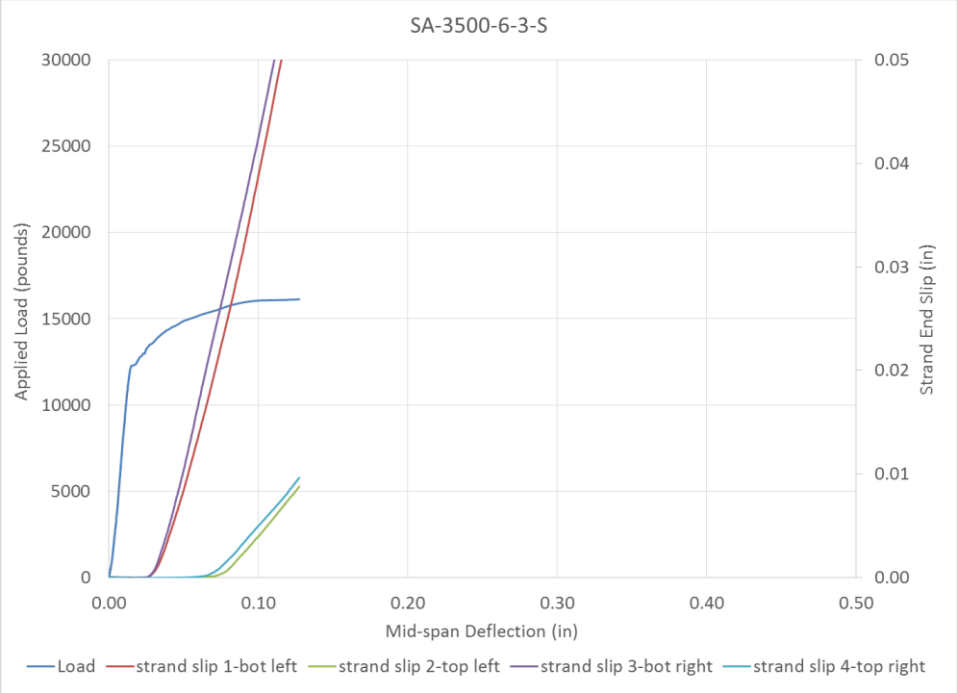


Figure 423 Load vs Deflection and Strand End Slip SA-3500-6-3-S



Figure 424 Picture of Failed Prism for SA-3500-6-3-S

Beam Identification	SD-3500-6-1-L
Wire Type:	SD
Embedment Length:	20 in
Release Strength:	3500 psi
Slump:	6 in

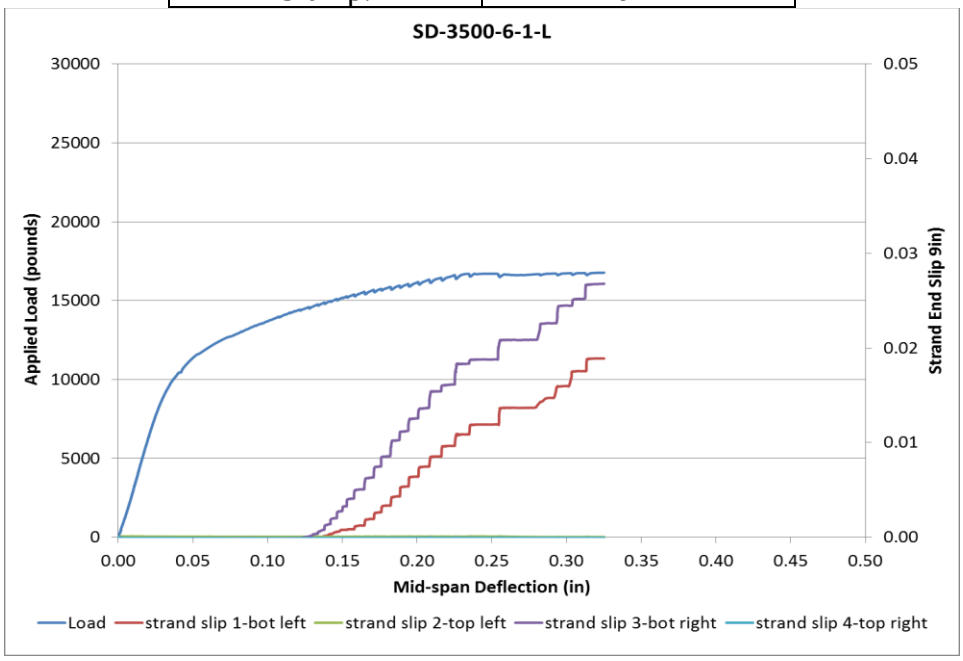


Figure 425 Load vs Deflection and Strand End Slip SD-3500-6-1-L

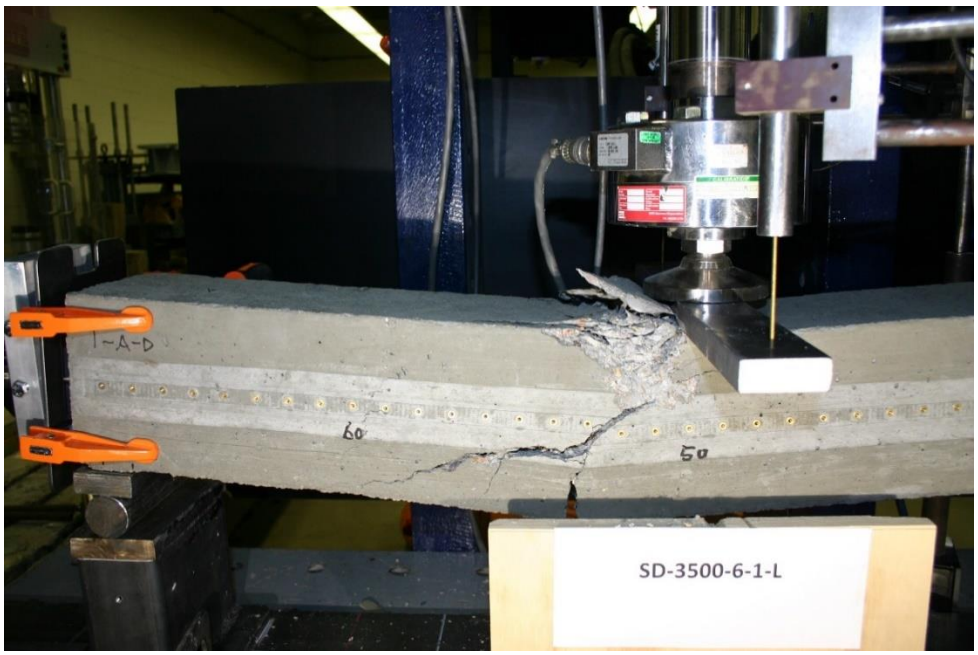


Figure 426 Picture of Failed Prism for SD-3500-6-1-L

Beam Identification	SD-3500-6-1-L-2nd
Wire Type:	SD
Embedment Length:	20 in
Release Strength:	3500 psi
Slump:	6 in

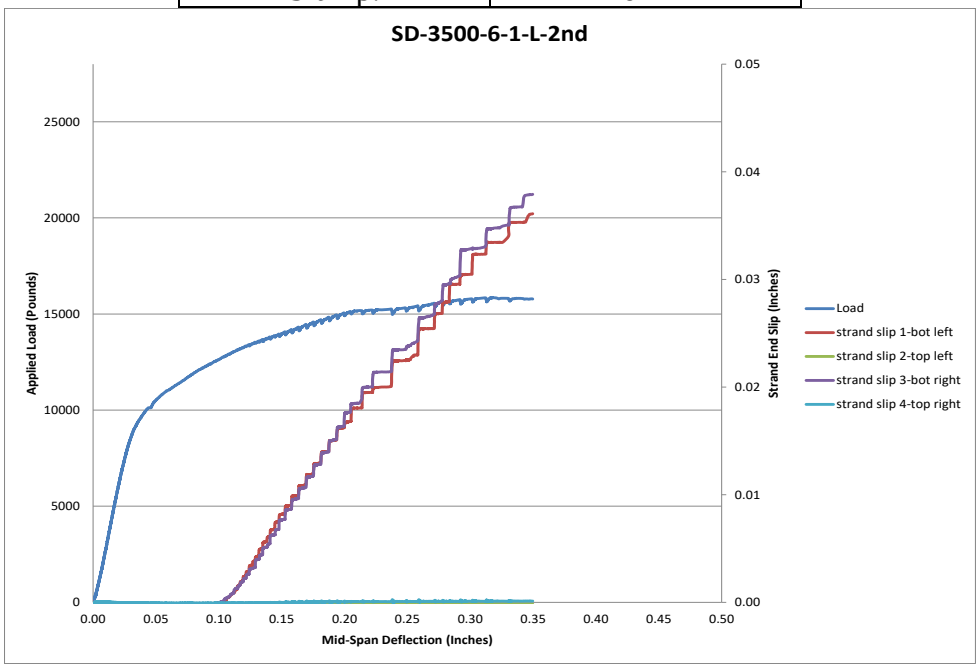


Figure 427 Load vs Deflection and Strand End Slip SD-3500-6-1-L-2nd

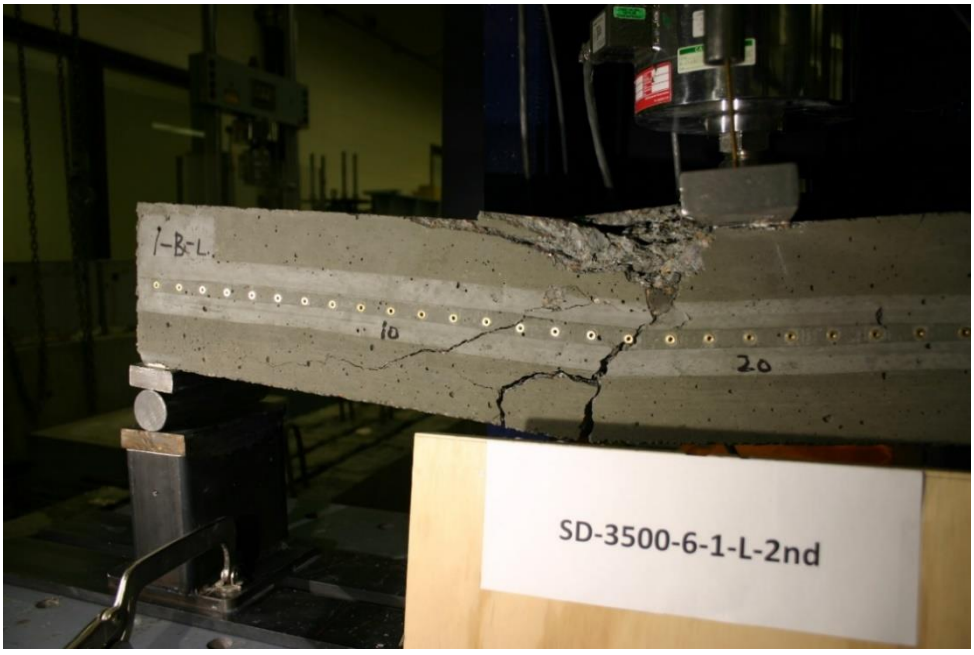


Figure 428 Picture of Failed Prism for SD-3500-6-1-L-2nd

Beam Identification	SD-3500-6-2-L
Wire Type:	SD
Embedment Length:	28 in
Release Strength:	3500 psi
Slump:	6 in

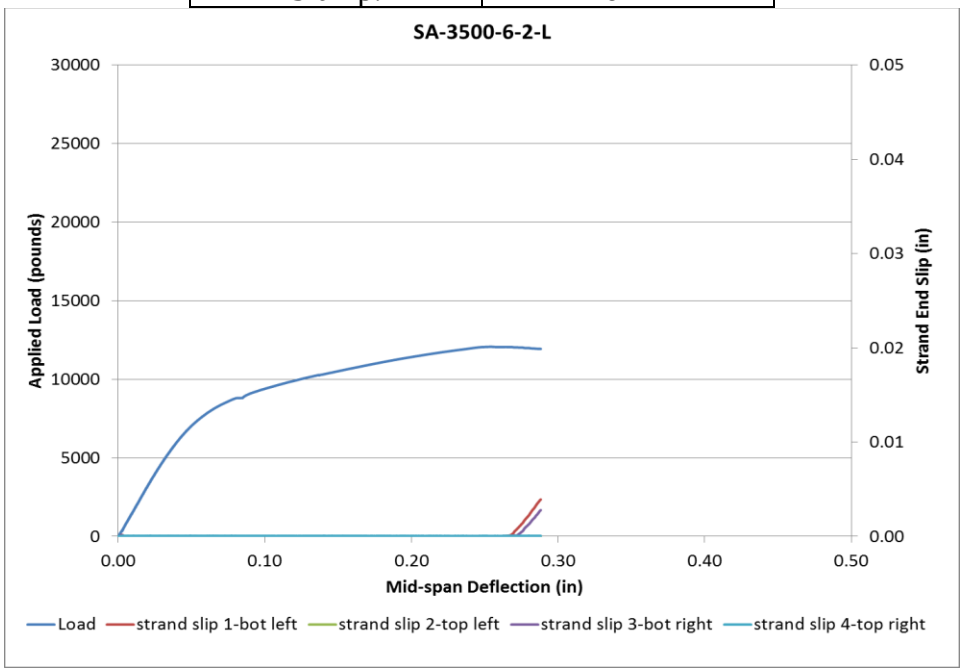


Figure 429 Load vs Deflection and Strand End Slip SA-3500-6-2-L

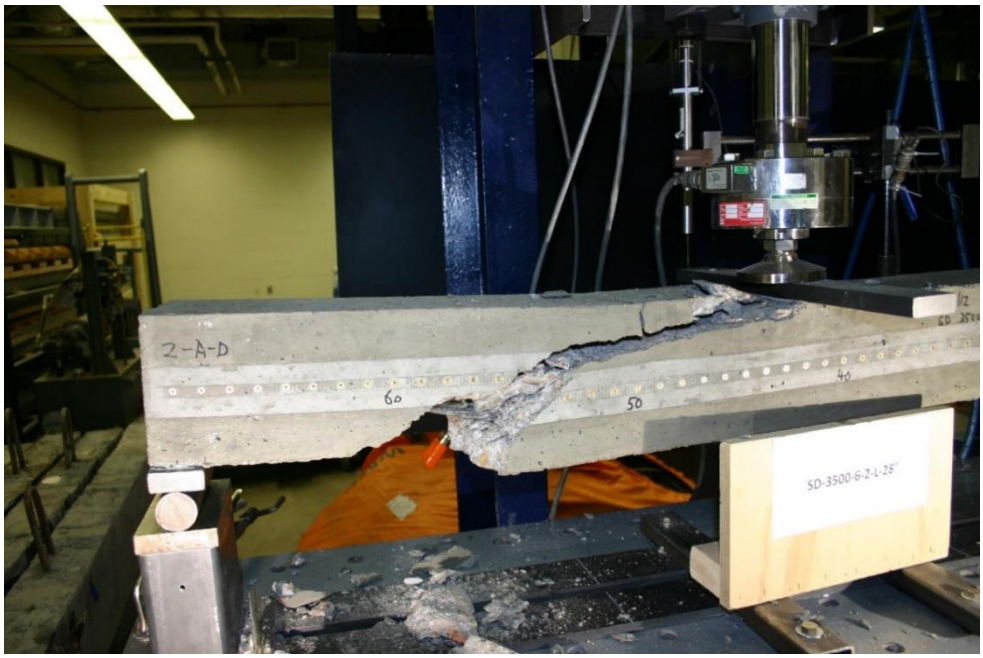


Figure 430 Picture of Failed Prism for SD-3500-6-2-L

Beam Identification	SD-3500-6-3-L
Wire Type:	SD
Embedment Length:	16.5 in
Release Strength:	3500 psi
Slump:	6 in

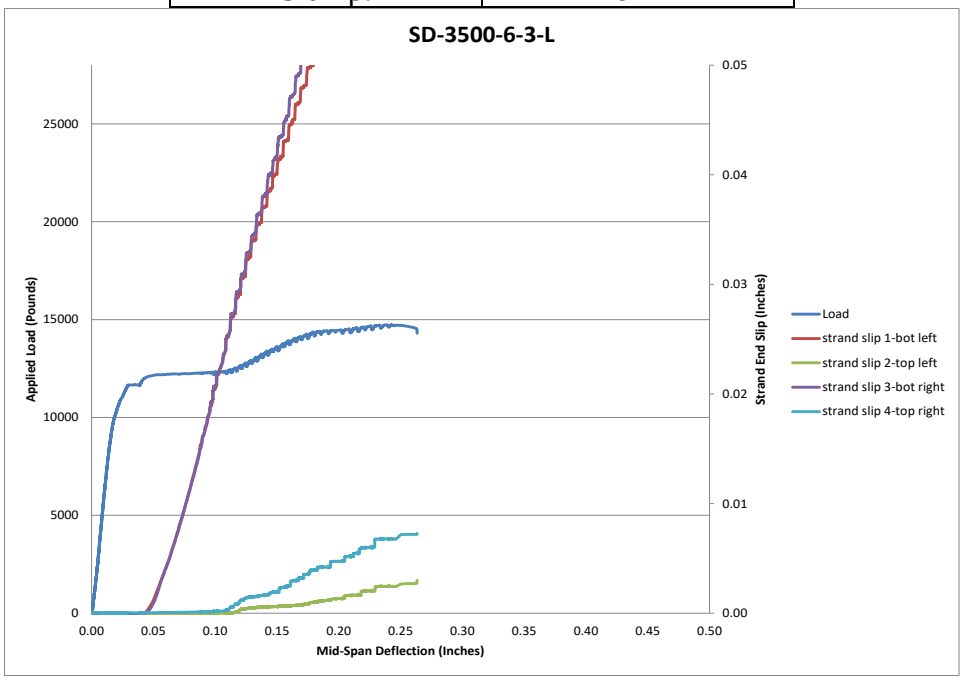


Figure 431vLoad vs Deflection and Strand End Slip SA-3500-6-3-L



Figure 432 Picture of Failed Prism for SD-3500-6-3-L

Beam Identification	SD-3500-6-3-S
Wire Type:	SD
Embedment Length:	13 in
Release Strength:	3500 psi
Slump:	6 in

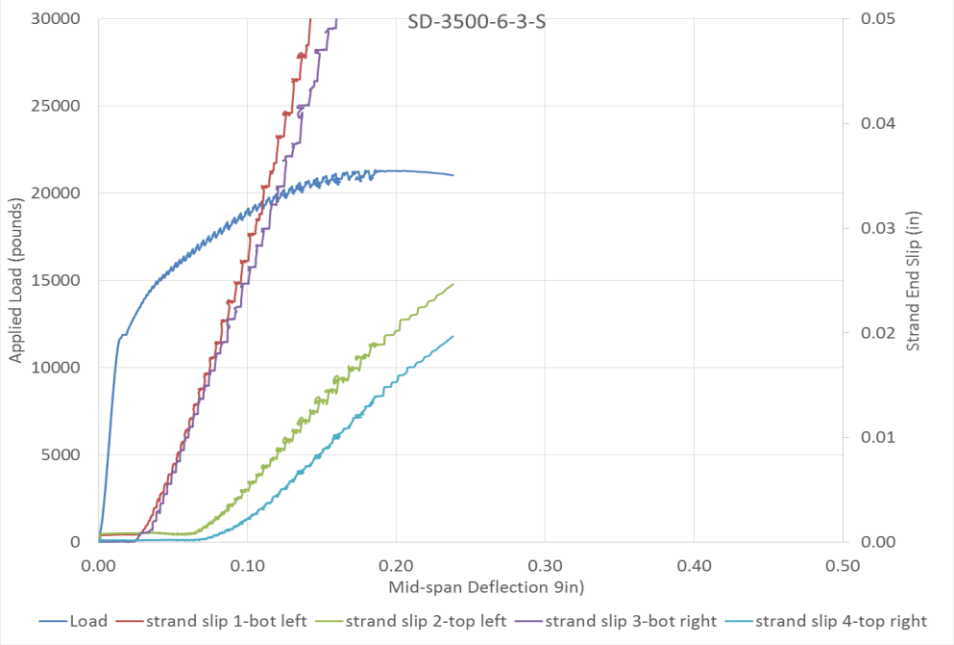


Figure 433 Load vs Deflection and Strand End Slip SD-3500-6-3-S



Figure 434 Picture of Failed Prism for SD-3500-6-3-S

Beam Identification	SE-3500-6-1-L
Wire Type:	SE
Embedment Length:	20 in
Release Strength:	3500 psi
Slump:	6 in

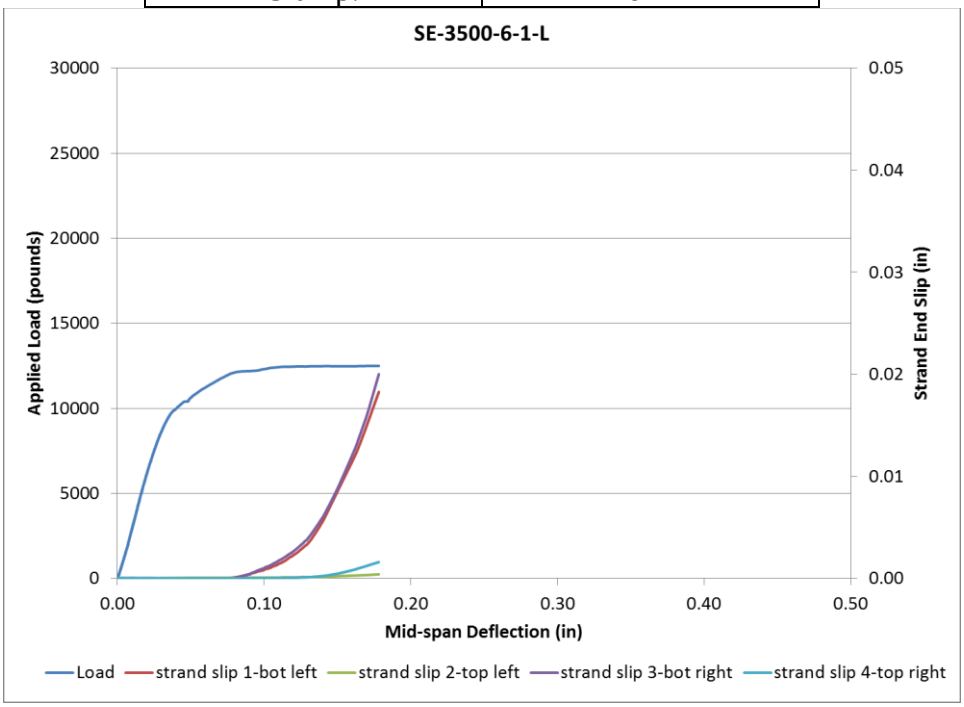


Figure 435 Load vs Deflection and Strand End Slip SE-3500-6-1-L

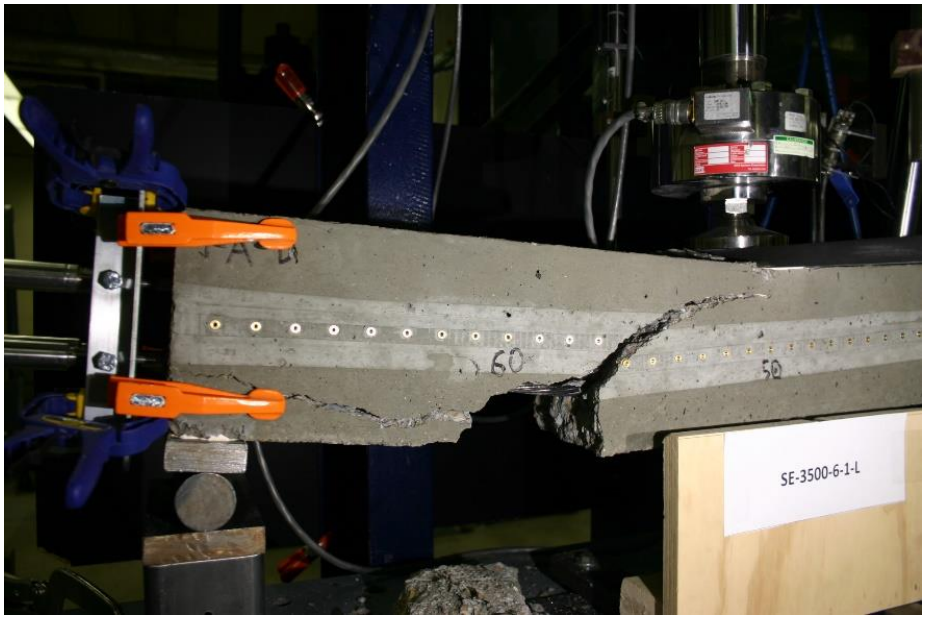


Figure 436 Picture of Failed Prism for SE-3500-6-1-L

Beam Identification	SE-3500-6-1-L-2nd
Wire Type:	SE
Embedment Length:	20 in
Release Strength:	3500 psi
Slump:	6 in

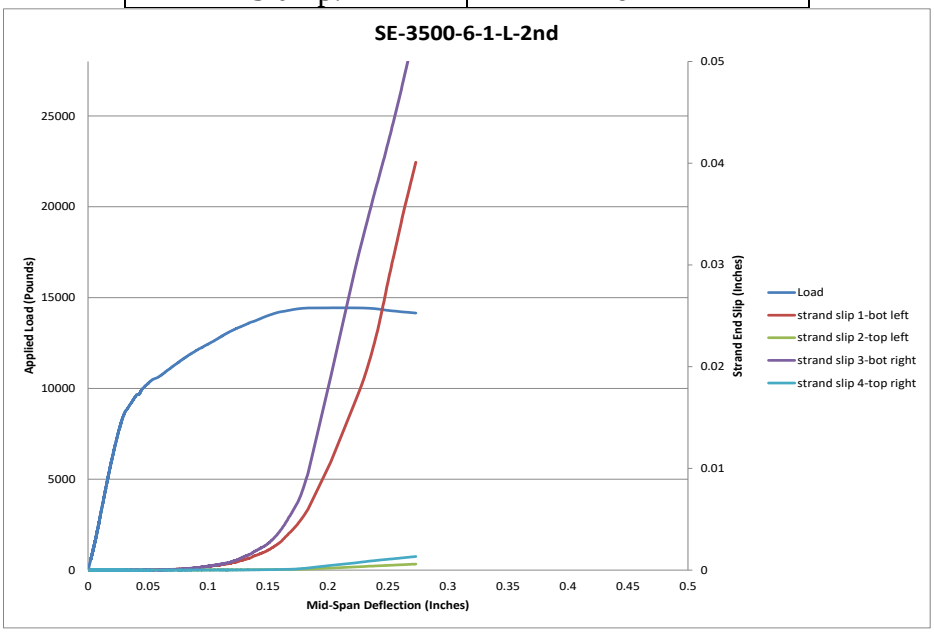


Figure 437 Load vs Deflection and Strand End Slip SE-3500-6-1-L-2nd



Figure 438 Picture of Failed Prism for SE-3500-6-1-L-2nd

Beam Identification	SE-3500-6-2-L
Wire Type:	SE
Embedment Length:	28 in
Release Strength:	3500 psi
Slump:	6 in

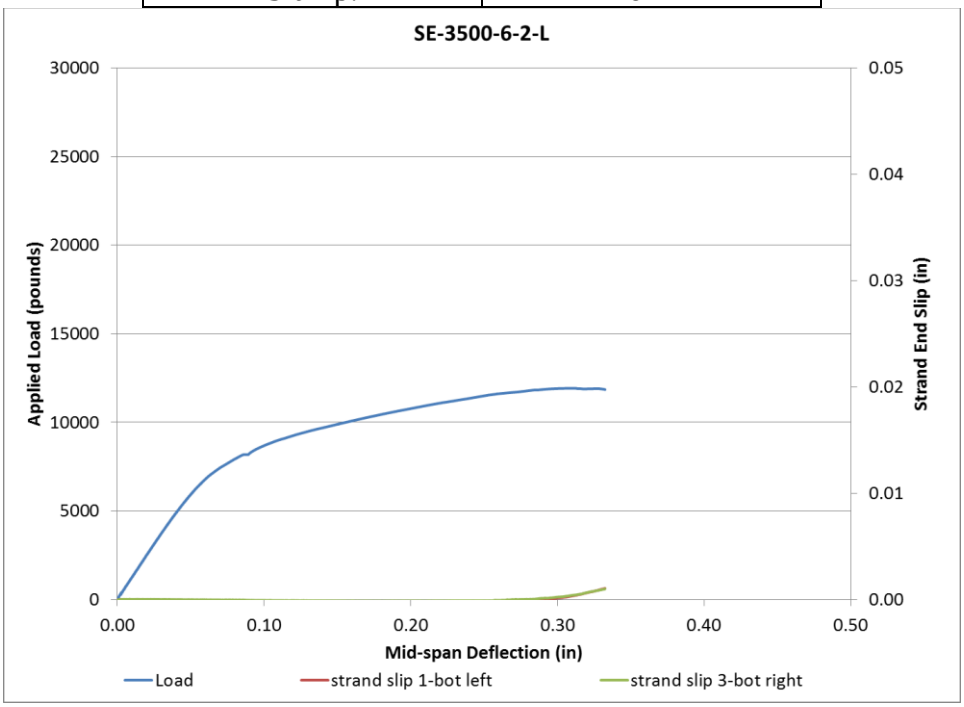


Figure 439 Load vs Deflection and Strand End Slip SE-3500-6-2-L



Figure 440 Picture of Failed Prism for SE-3500-6-2-L

Beam Identification	SE-3500-6-3-L
Wire Type:	SE
Embedment Length:	16.5 in
Release Strength:	3500 psi
Slump:	6 in

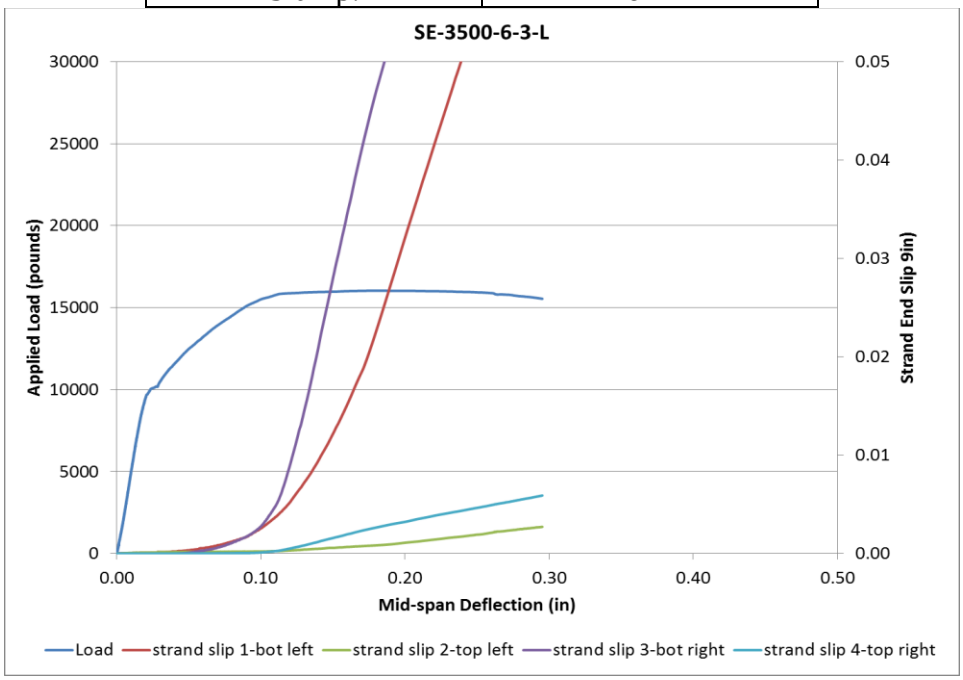


Figure 441 Load vs Deflection and Strand End Slip SE-3500-6-3-L

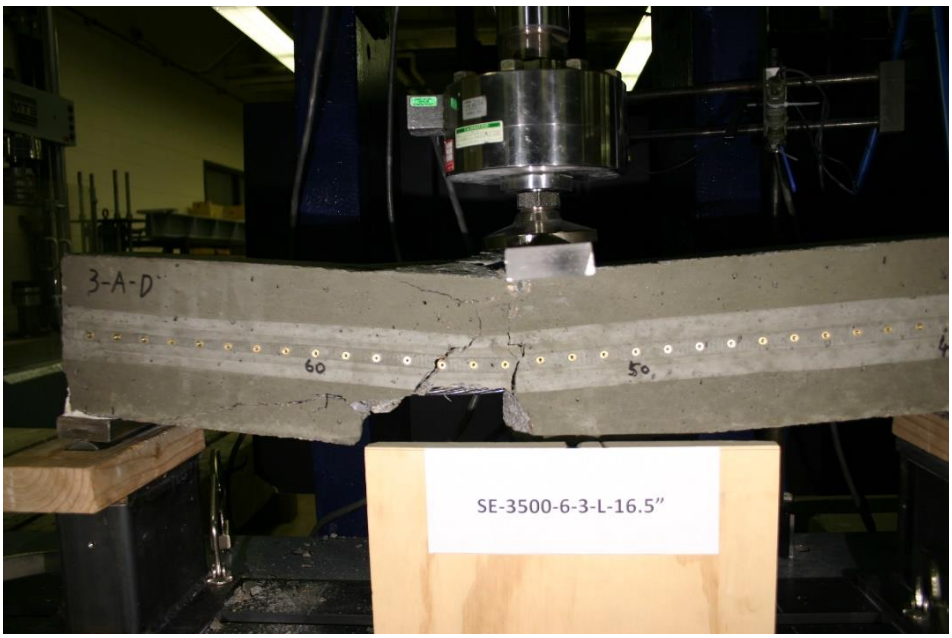


Figure 442 Figure 338 Picture of Failed Prism for SE-3500-6-3-L

Beam Identification	SE-3500-6-3-S
Wire Type:	SE
Embedment Length:	13 in
Release Strength:	3500 psi
Slump:	6 in

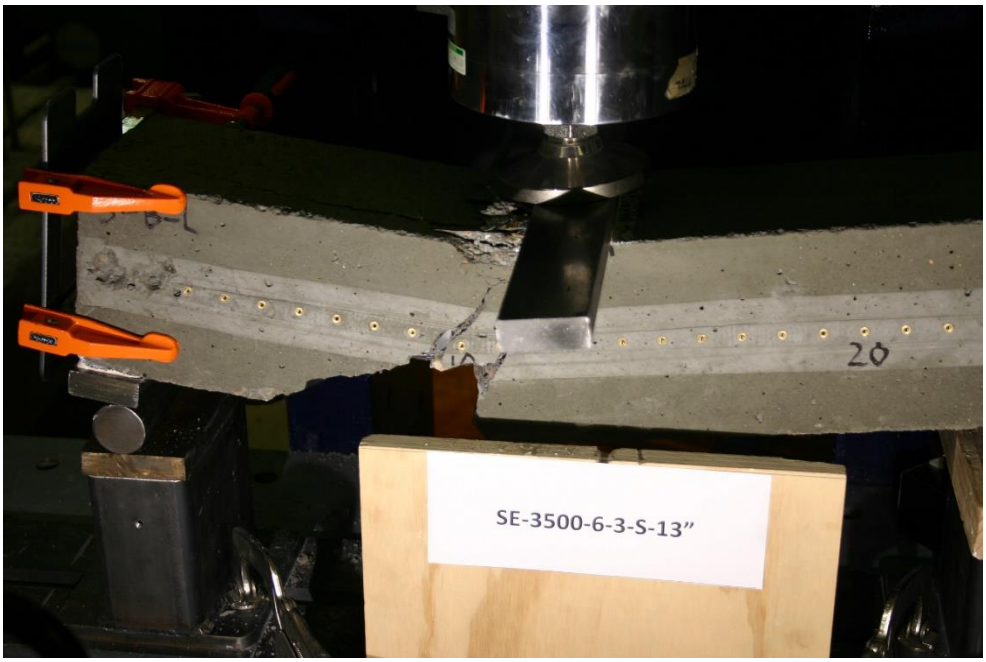


Figure 443 Picture of Failed Prism for SE-3500-6-3-S

Beam Identification	SF-3500-6-1-L
Wire Type:	SF
Embedment Length:	20 in
Release Strength:	3500 psi
Slump:	6 in

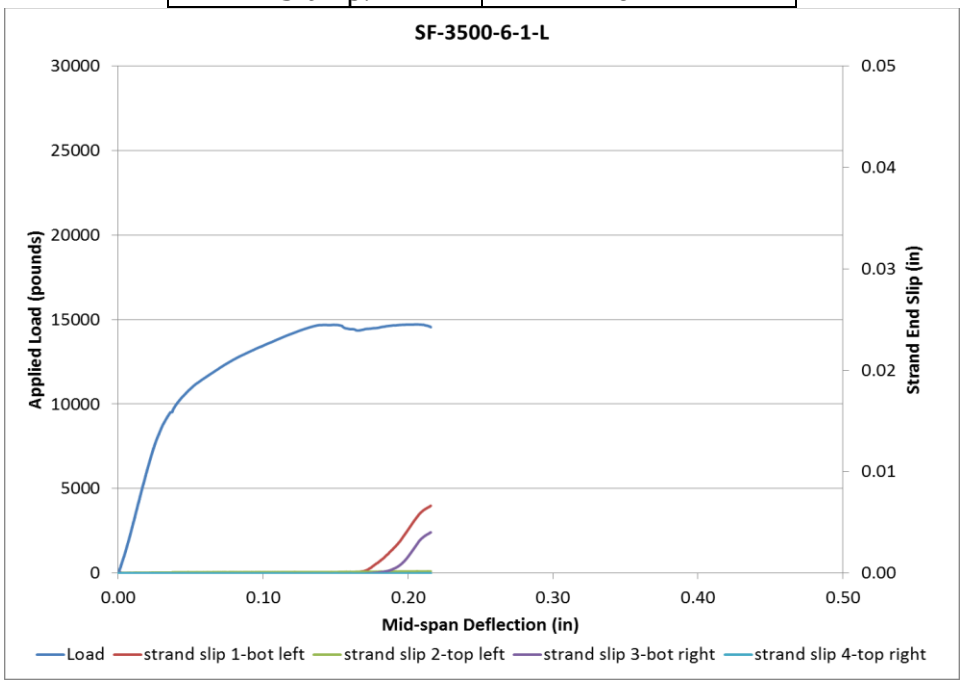


Figure 444 Load vs Deflection and Strand End Slip SF-3500-6-1-L



Figure 445 Picture of Failed Prism for SF-3500-6-1-L

Beam Identification	SF-3500-6-1-L-2nd
Wire Type:	SF
Embedment Length:	20 in
Release Strength:	3500 psi
Slump:	6 in

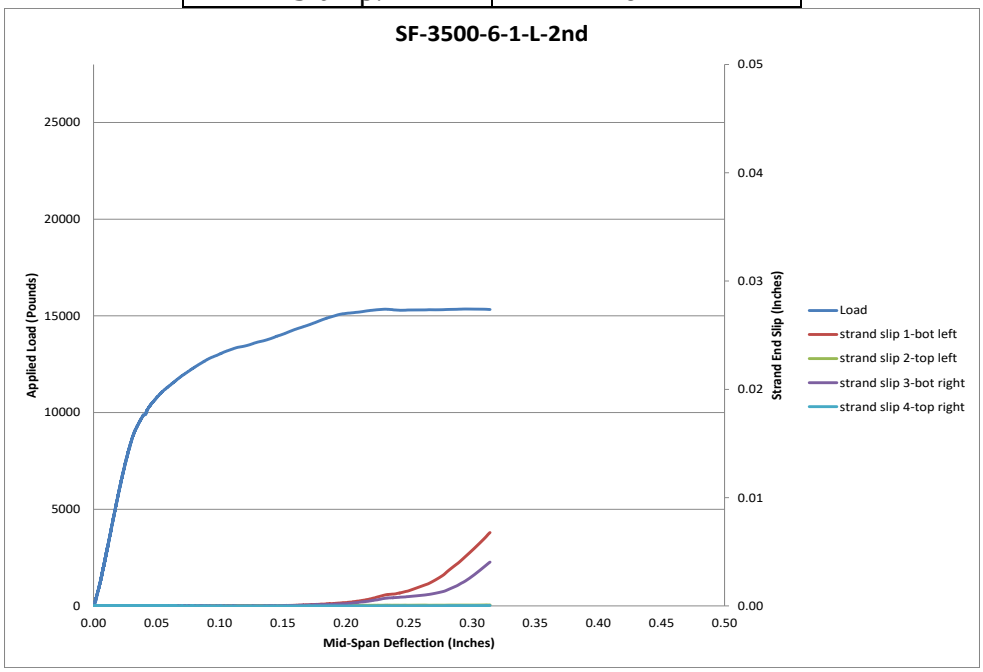


Figure 446 Load vs Deflection and Strand End Slip SF-3500-6-1-L-2nd



Figure 447 Picture of Failed Prism for SF-3500-6-1-L-2nd

Beam Identification	SF-3500-6-2-L
Wire Type:	SF
Embedment Length:	28 in
Release Strength:	3500 psi
Slump:	6 in

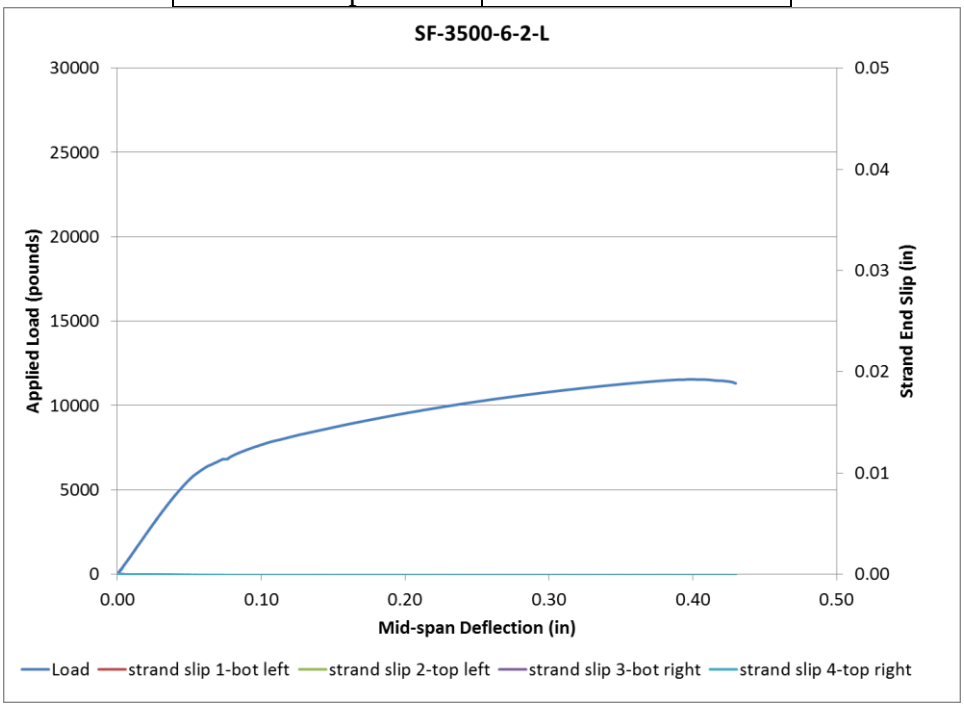


Figure 448 Load vs Deflection and Strand End Slip SF-3500-6-2-L



Figure 449 Picture of Failed Prism for SF-3500-6-2-L

Beam Identification	SF-3500-6-3-L
Wire Type:	SF
Embedment Length:	16.5 in
Release Strength:	3500 psi
Slump:	6 in

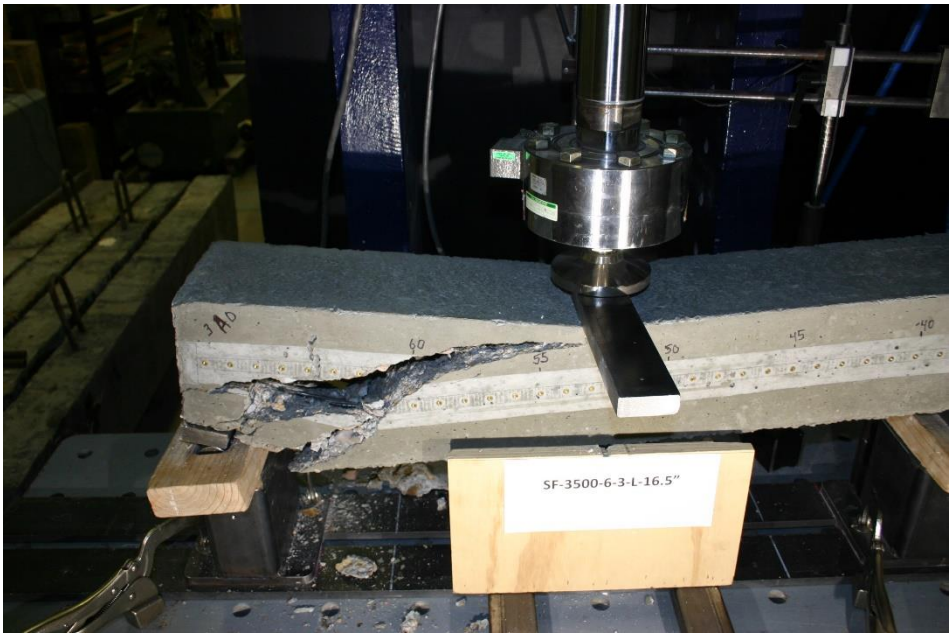


Figure 450 Picture of Failed Prism for SF-3500-6-3-L

Beam Identification	SF-3500-6-3-S
Wire Type:	SF
Embedment Length:	13 in
Release Strength:	3500 psi
Slump:	6 in

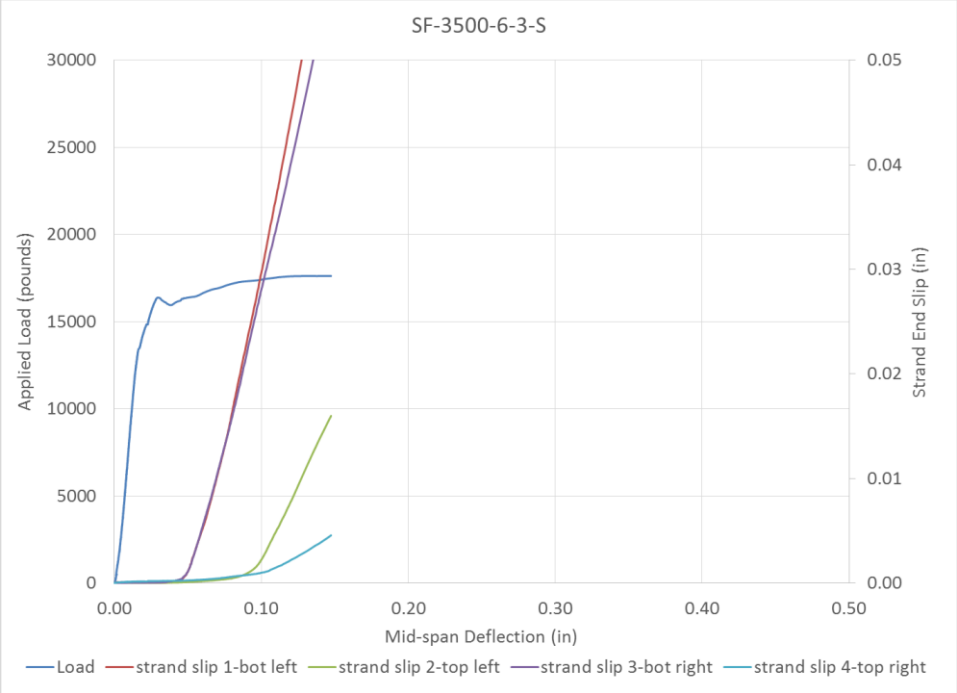


Figure 451 Load vs Deflection and Strand End Slip SF-3500-6-3-S



Figure 452 Picture of Failed Prism for SF-3500-6-3-S

Prisms made with strands, 6000 psi concrete release strength and 6 in. slump

Beam Identification	SA-6000-6-1-L
Wire Type:	SA
Embedment Length:	20 in
Release Strength:	6000 psi
Slump:	6 in

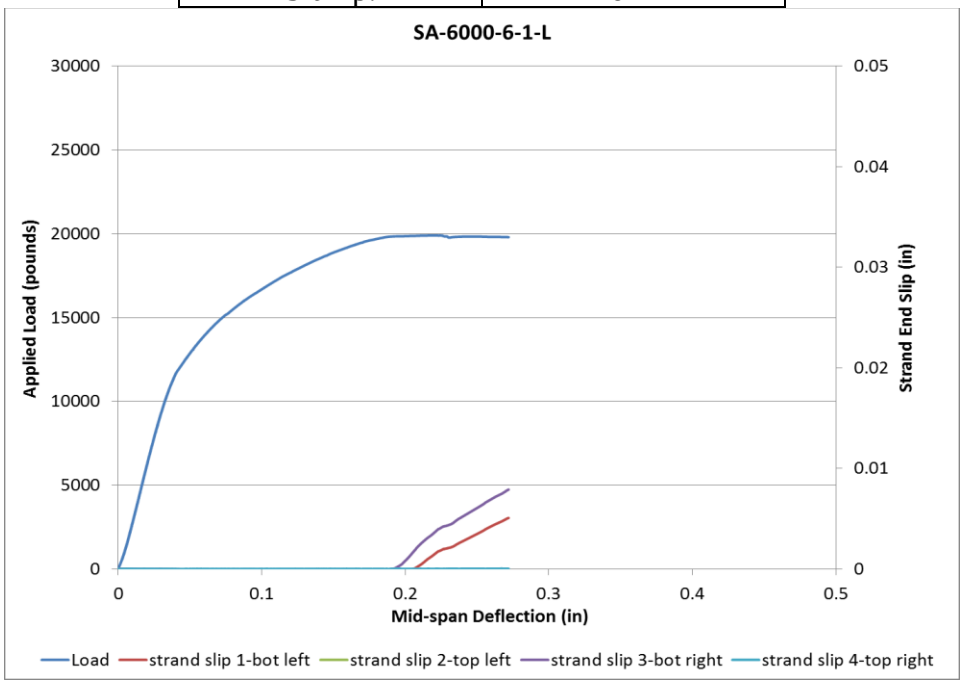


Figure 453 Load vs Deflection and Strand End Slip SA-6000-6-1-L



Figure 454 Picture of Failed Prism for SA-6000-6-1-L

Beam Identification	SA-6000-6-1-L-2nd
Wire Type:	SA
Embedment Length:	20 in
Release Strength:	6000 psi
Slump:	6 in

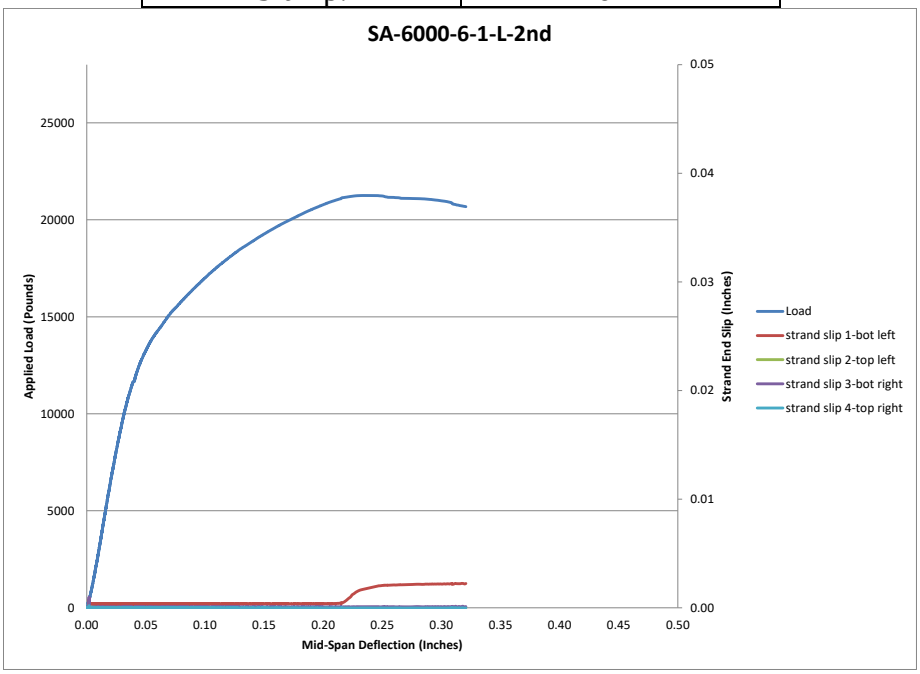


Figure 455 Load vs Deflection and Strand End Slip SA-6000-6-1-L-2nd



Figure 456 Picture of Failed Prism for SA-6000-6-1-L-2nd

Beam Identification	SA-6000-6-2-L
Wire Type:	SA
Embedment Length:	28 in
Release Strength:	6000 psi
Slump:	6 in

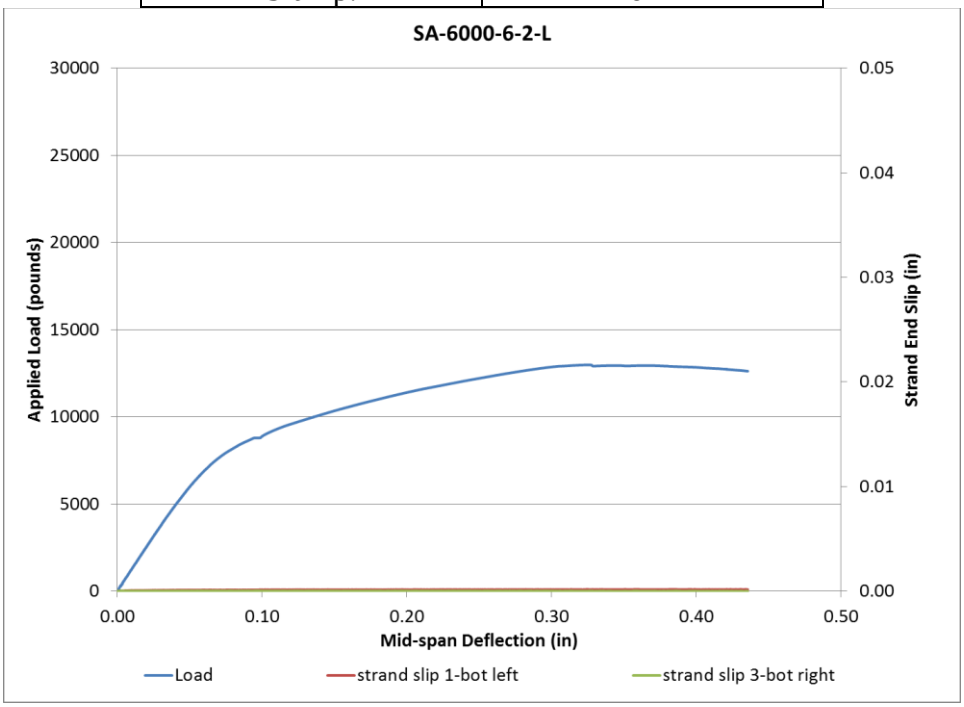


Figure 457 Load vs Deflection and Strand End Slip SA-6000-6-2-L

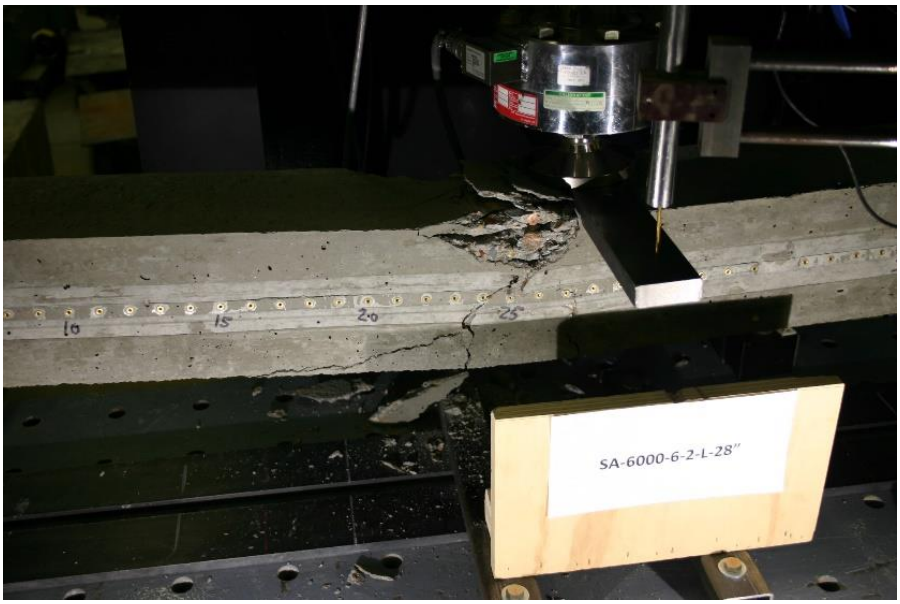


Figure 458 Picture of Failed Prism for SA-6000-6-2-L

Beam Identification	SA-6000-6-3-L
Wire Type:	SA
Embedment Length:	16.5 in
Release Strength:	6000 psi
Slump:	6 in

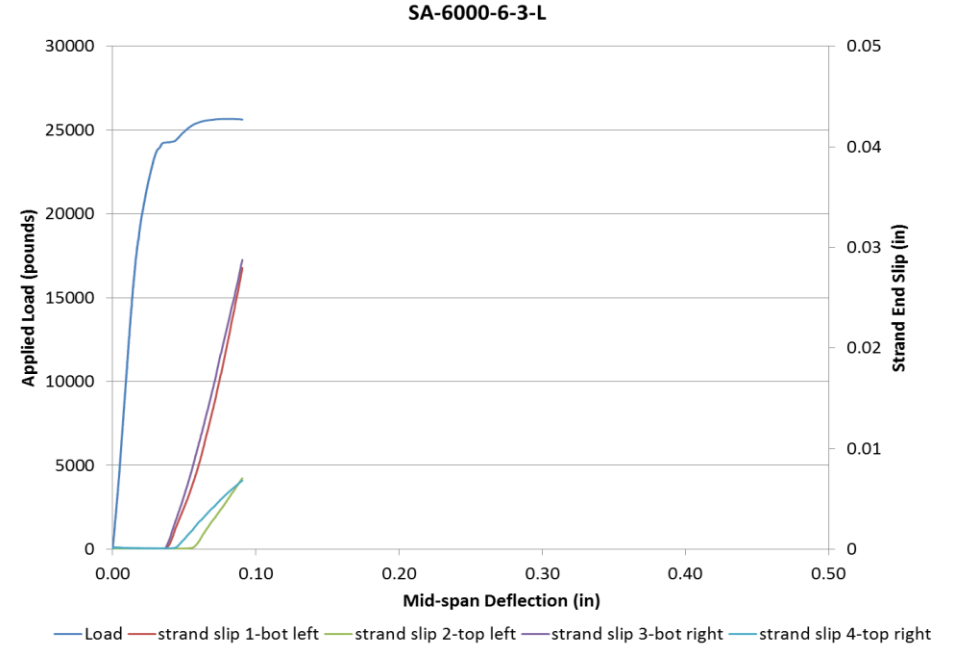


Figure 459 Load vs Deflection and Strand End Slip SA-6000-6-3-L



Figure 460 Picture of Failed Prism for SA-6000-6-3-L

Beam Identification	SA-6000-6-3-S
Wire Type:	SA
Embedment Length:	13 in
Release Strength:	6000 psi
Slump:	6 in

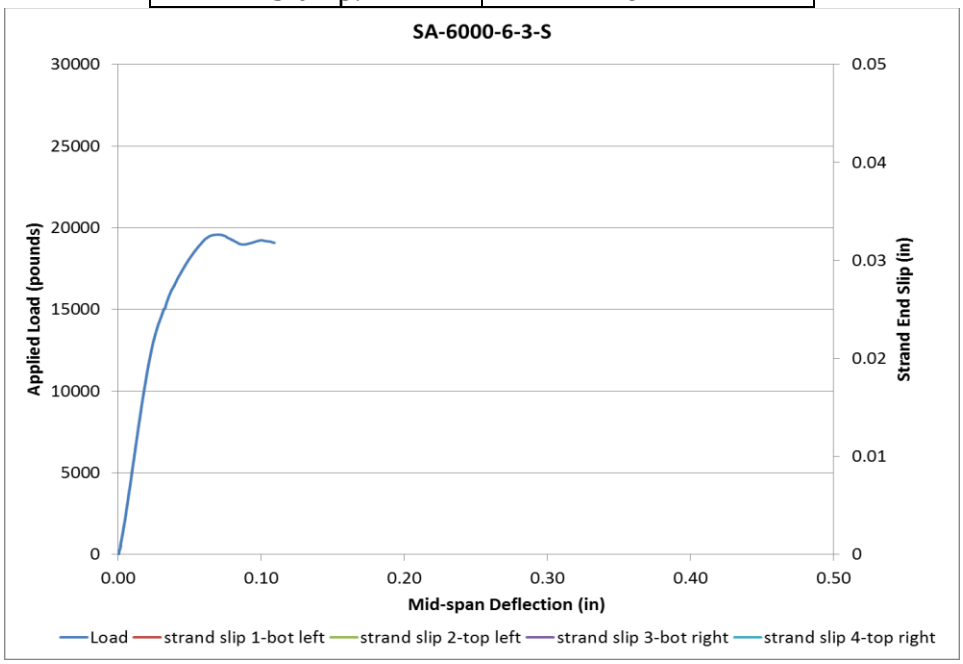


Figure 461 Load vs Deflection and Strand End Slip SA-6000-6-3-S



Figure 462 Picture of Failed Prism for SA-6000-6-3-S

Beam Identification	SD-6000-6-1-L
Wire Type:	SD
Embedment Length:	20 in
Release Strength:	6000 psi
Slump:	6 in

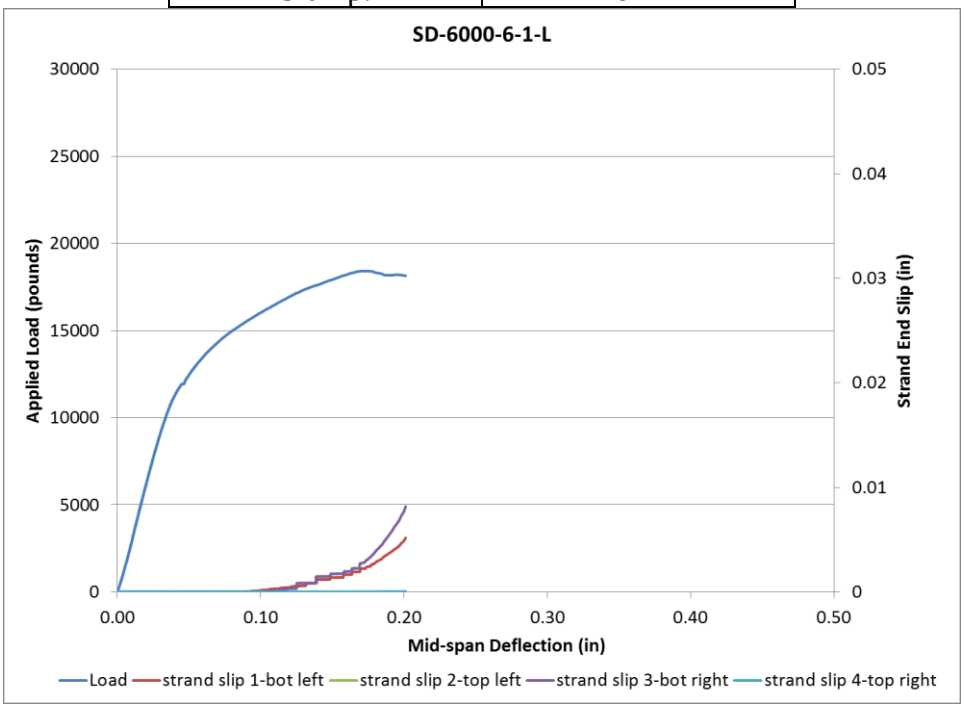


Figure 463 Load vs Deflection and Strand End Slip SD-6000-6-1-L

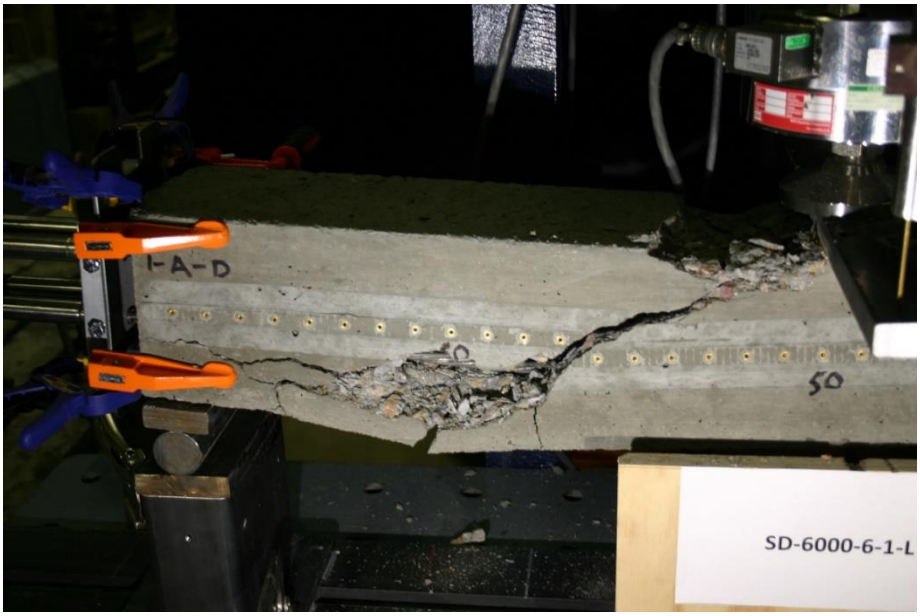


Figure 464 Picture of Failed Prism for SD-6000-6-1-L

Beam Identification	SD-6000-6-1-L-2nd
Wire Type:	SD
Embedment Length:	20 in
Release Strength:	6000 psi
Slump:	6 in

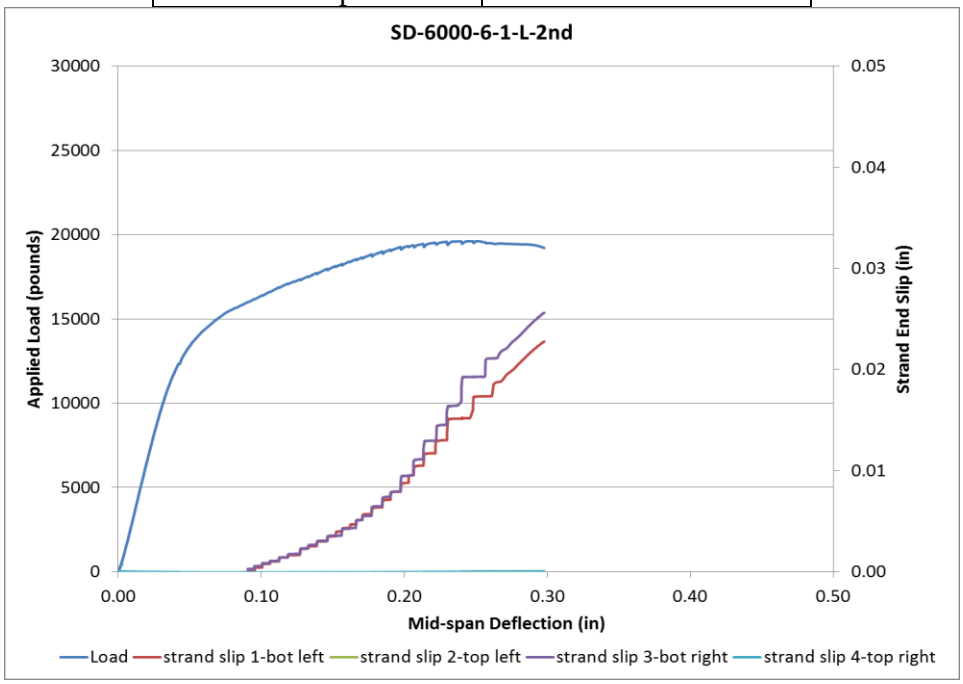


Figure 465 Load vs Deflection and Strand End Slip SD-6000-1-L-2nd

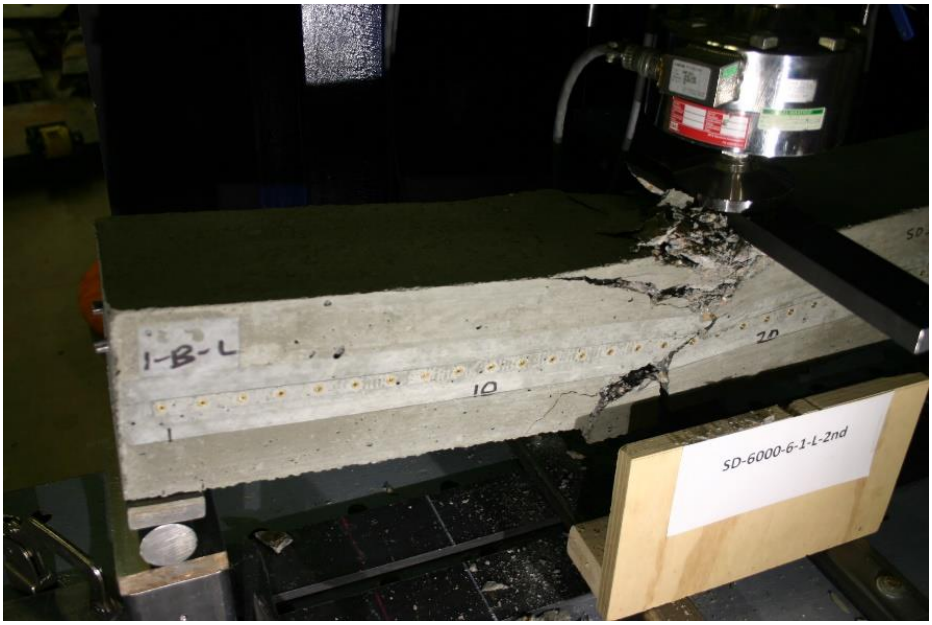


Figure 466 Picture of Failed Prism for SD-6000-6-1-L-2nd

Beam Identification	SD-6000-6-2-L
Wire Type:	SD
Embedment Length:	28 in
Release Strength:	6000 psi
Slump:	6 in

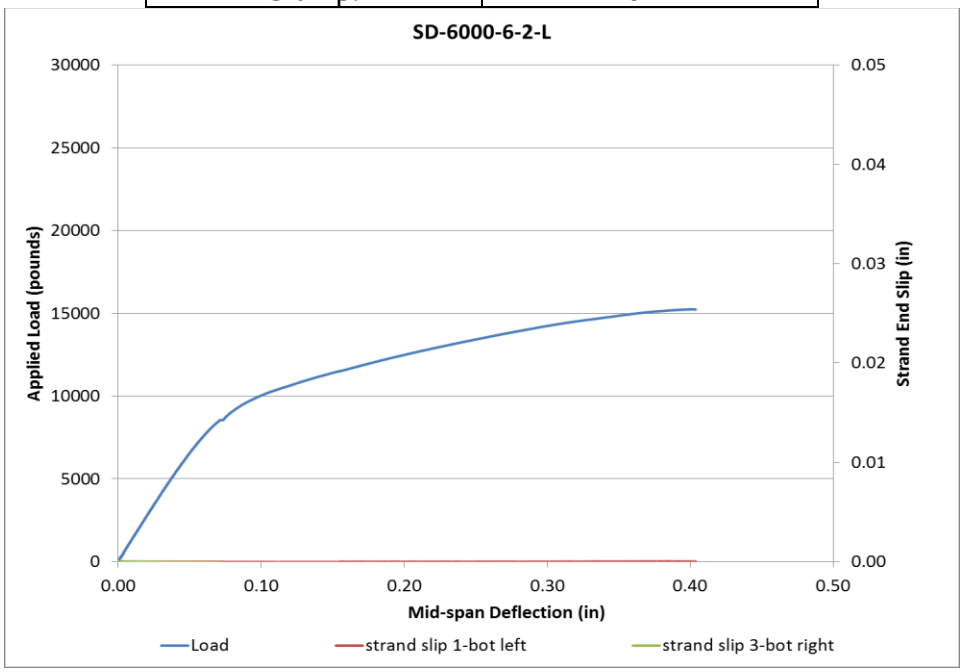


Figure 467 Load vs Deflection and Strand End Slip SD-6000-6-2-L



Figure 468 Picture of Failed Prism for SD-6000-6-2-L

Beam Identification	SD-6000-6-3-L
Wire Type:	SD
Embedment Length:	16.5 in
Release Strength:	6000 psi
Slump:	6 in

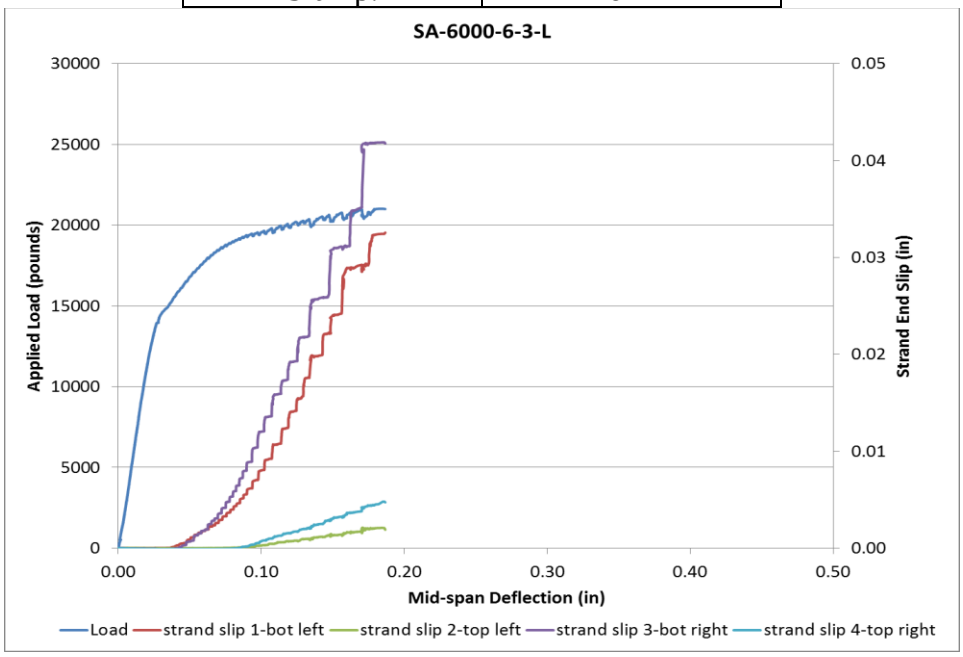


Figure 469 Load vs Deflection and Strand End Slip SA-6000-6-3-L



Figure 470 Picture of Failed Prism for SD-6000-6-3-L

Beam Identification	SD-6000-6-3-S
Wire Type:	SD
Embedment Length:	13 in
Release Strength:	6000 psi
Slump:	6 in

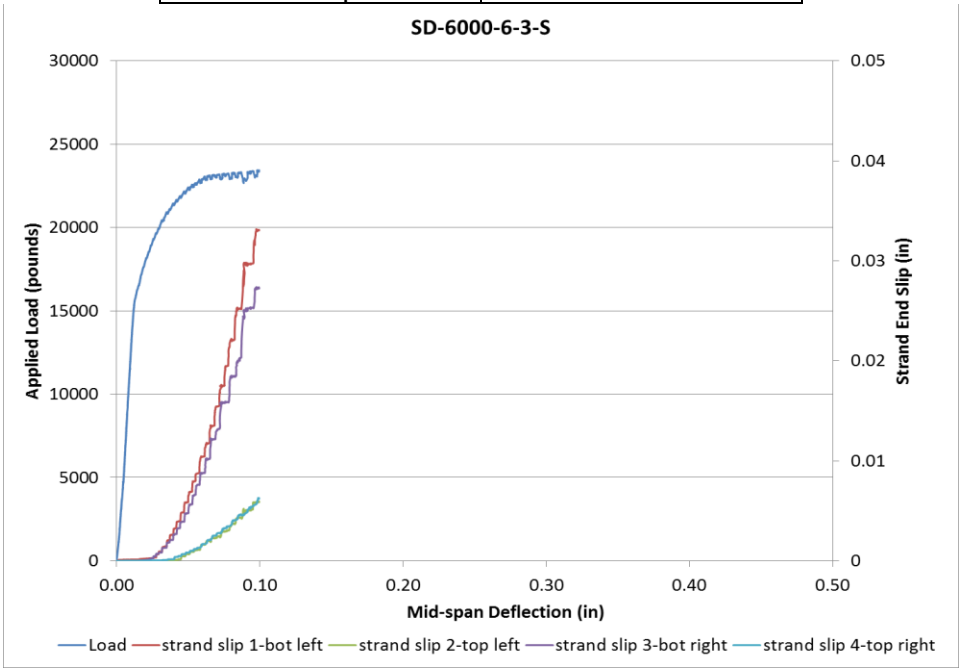


Figure 471 Load vs Deflection and Strand End Slip SD-6000-6-3-S



Figure 472 Picture of Failed Prism for SD-6000-6-3-S

Beam Identification	SE-6000-6-1-L
Wire Type:	SE
Embedment Length:	20 in
Release Strength:	6000 psi
Slump:	6 in

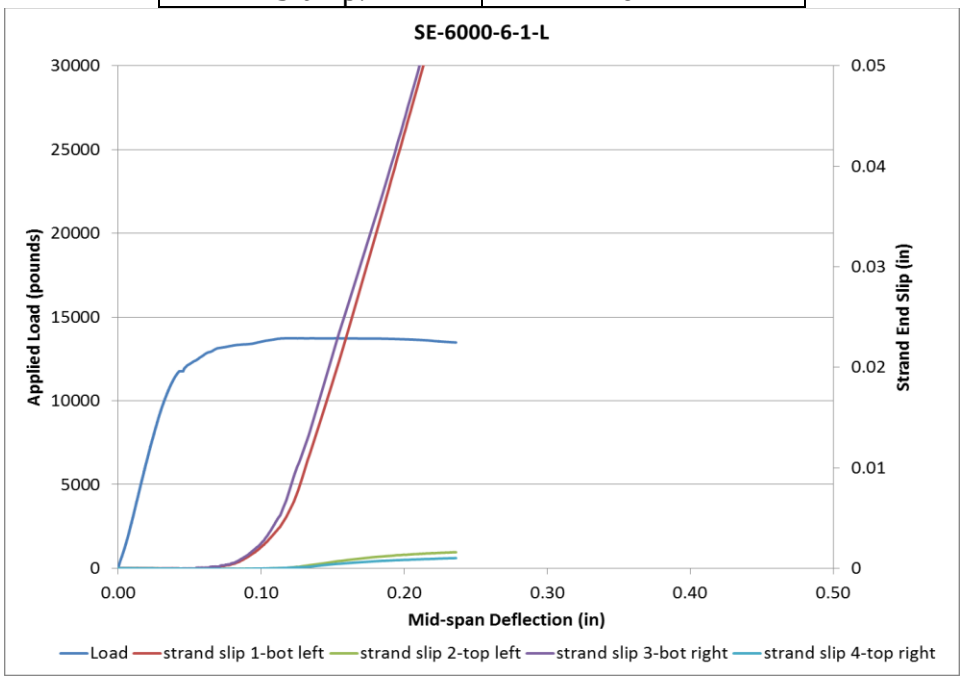


Figure 473 Load vs Deflection and Strand End Slip SE-6000-6-1-L



Figure 474 Picture of Failed Prism for SE-6000-6-1-L

Beam Identification	SE-6000-6-1-L-2nd
Wire Type:	SE
Embedment Length:	20 in
Release Strength:	6000 psi
Slump:	6 in

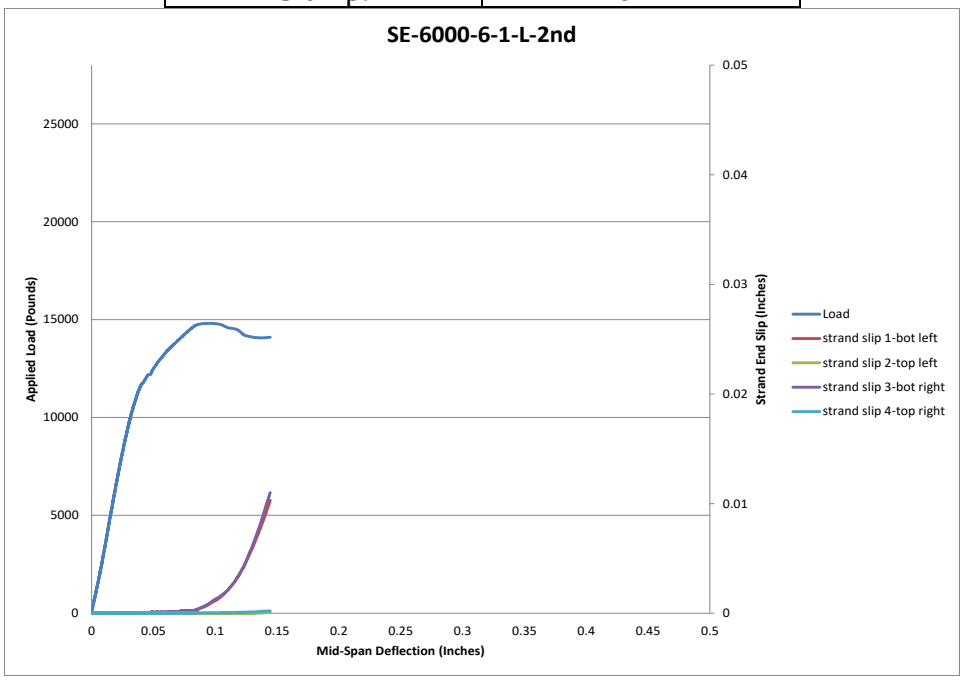
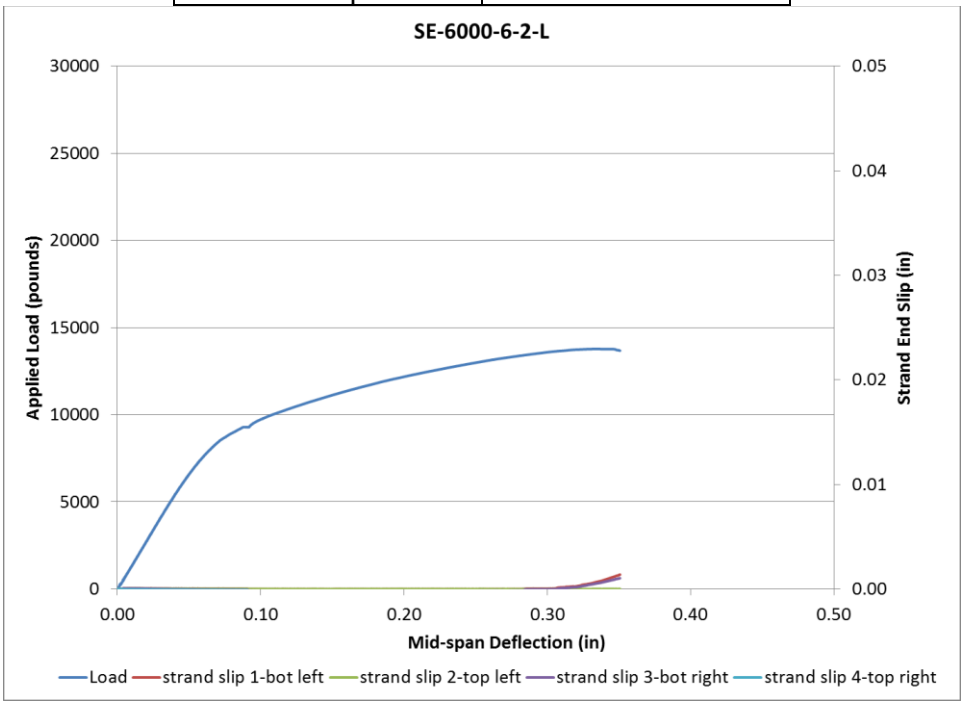


Figure 475 Load vs Deflection and Strand End Slip SE-6000-6-1-L-2nd



Figure 476 Picture of Failed Prism for SE-6000-6-1-L-2nd

Beam Identification	SE-6000-6-2-L
Wire Type:	SE
Embedment Length:	28 in
Release Strength:	6000 psi
Slump:	6 in



Load vs Deflection and Strand End Slip SE-6000-6-2-L



Figure 477 Picture of Failed Prism for SE-6000-6-2-L

Beam Identification	SE-6000-6-3-L
Wire Type:	SE
Embedment Length:	16.5 in
Release Strength:	6000 psi
Slump:	6 in

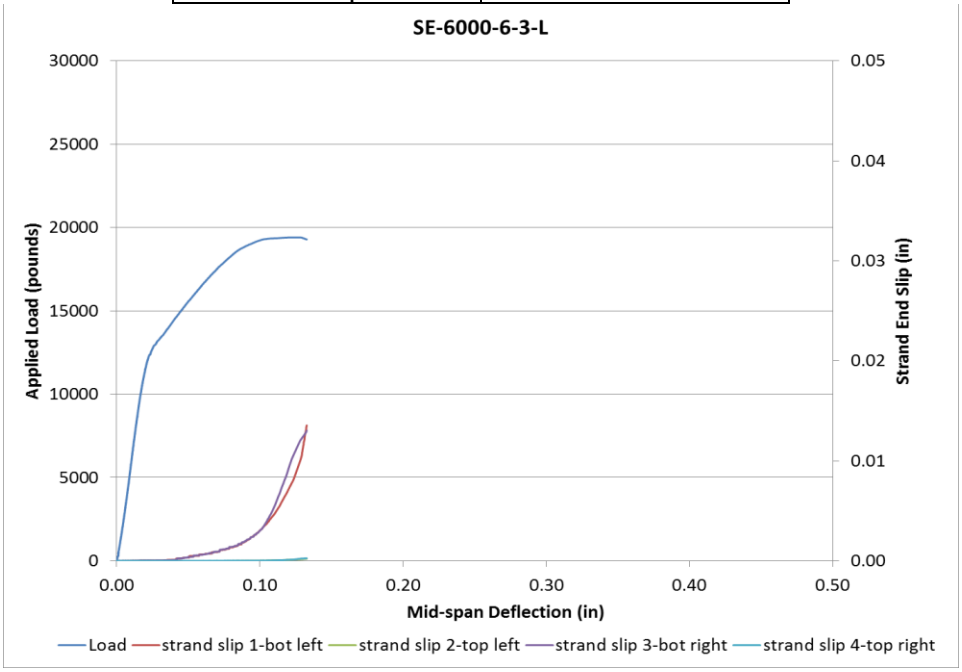


Figure 478 Load vs Deflection and Strand End Slip SE-6000-6-3-L



Figure 479 Picture of Failed Prism for SE-6000-6-3-L

Beam Identification	SE-6000-6-3-S
Wire Type:	SE
Embedment Length:	13 in
Release Strength:	6000 psi
Slump:	6 in

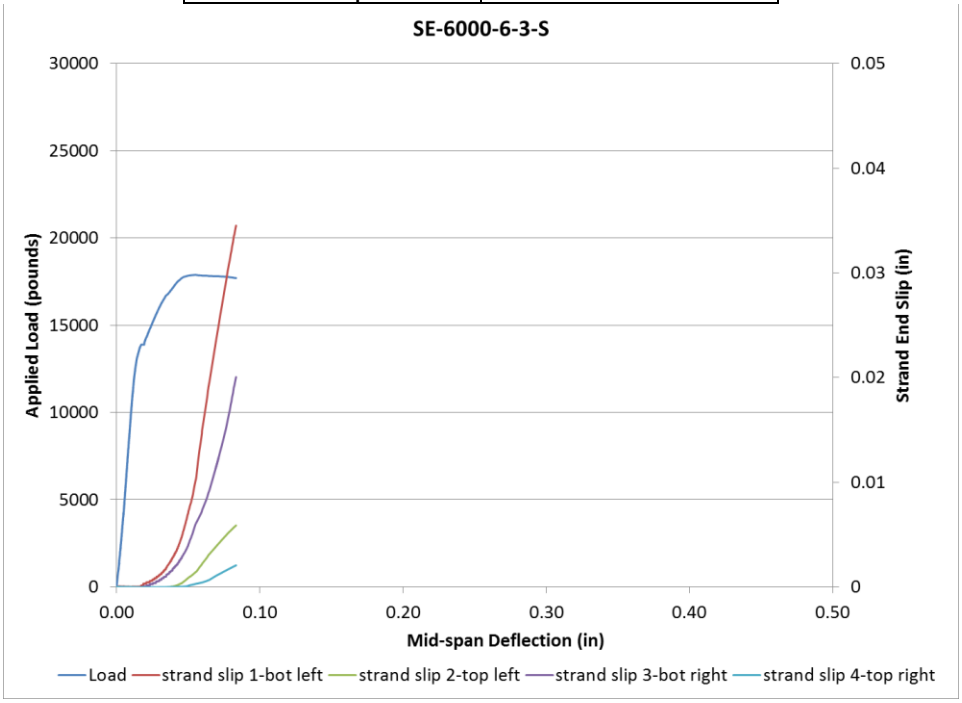


Figure 480 Load vs Deflection and Strand End Slip SE-6000-6-3-S



Figure 481 Picture of Failed Prism for SE-6000-6-3-S

Beam Identification	SF-6000-6-1-L
Wire Type:	SF
Embedment Length:	20 in
Release Strength:	6000 psi
Slump:	6 in

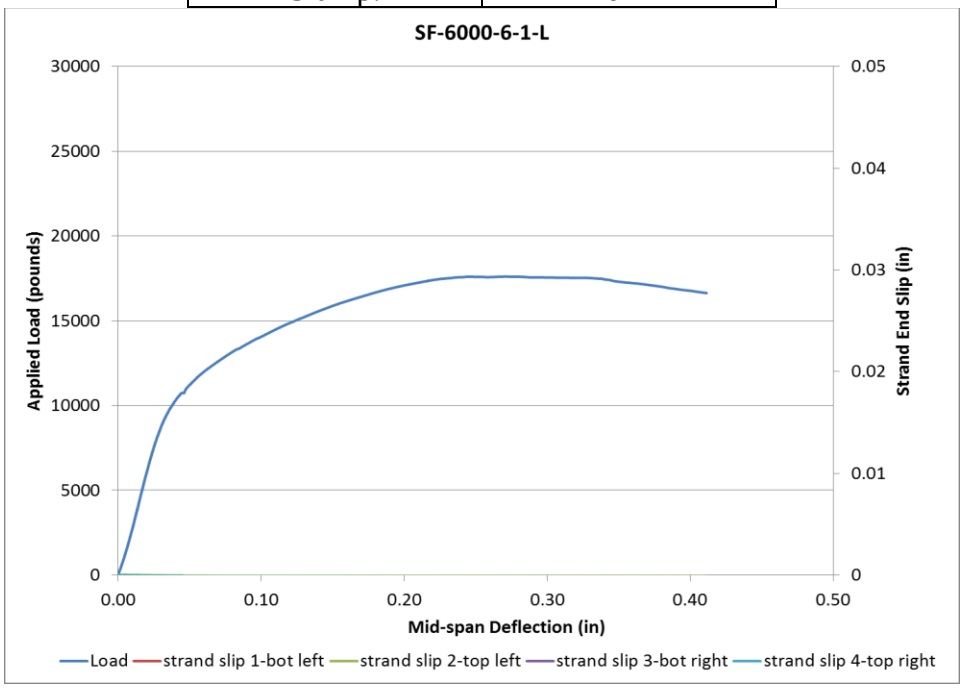


Figure 482 Load vs Deflection and Strand End Slip SF-6000-6-1-L



Figure 483 Picture of Failed Prism for SF-6000-6-1-L

Beam Identification	SF-6000-6-1-L-2nd
Wire Type:	SF
Embedment Length:	20 in
Release Strength:	6000 psi
Slump:	6 in

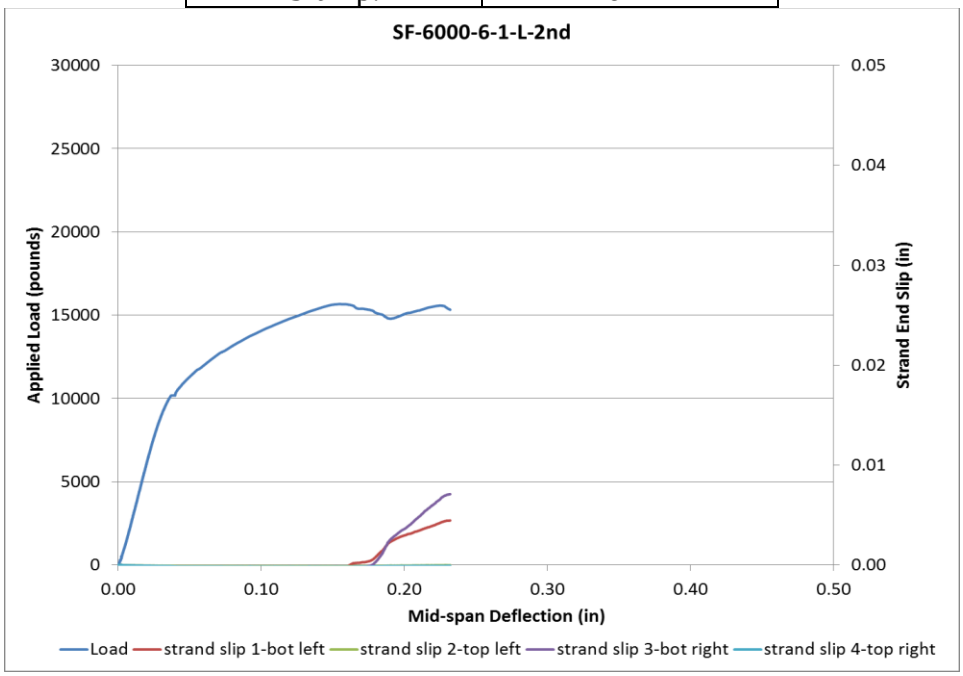


Figure 484 Load vs Deflection and Strand End Slip SF-6000-6-1-L-2nd



Figure 485 Picture of Failed Prism for SF-6000-6-1-L-2nd

Beam Identification	SF-6000-6-2-L
Wire Type:	SF
Embedment Length:	28 in
Release Strength:	6000 psi
Slump:	6 in

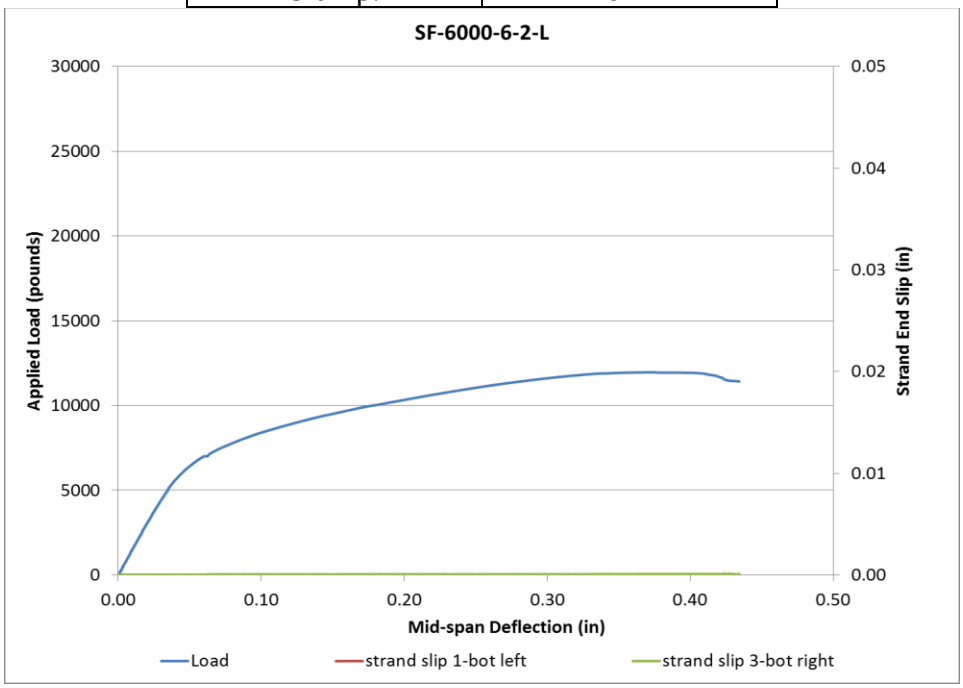


Figure 486 Load vs Deflection and Strand End Slip SF-6000-6-2-L

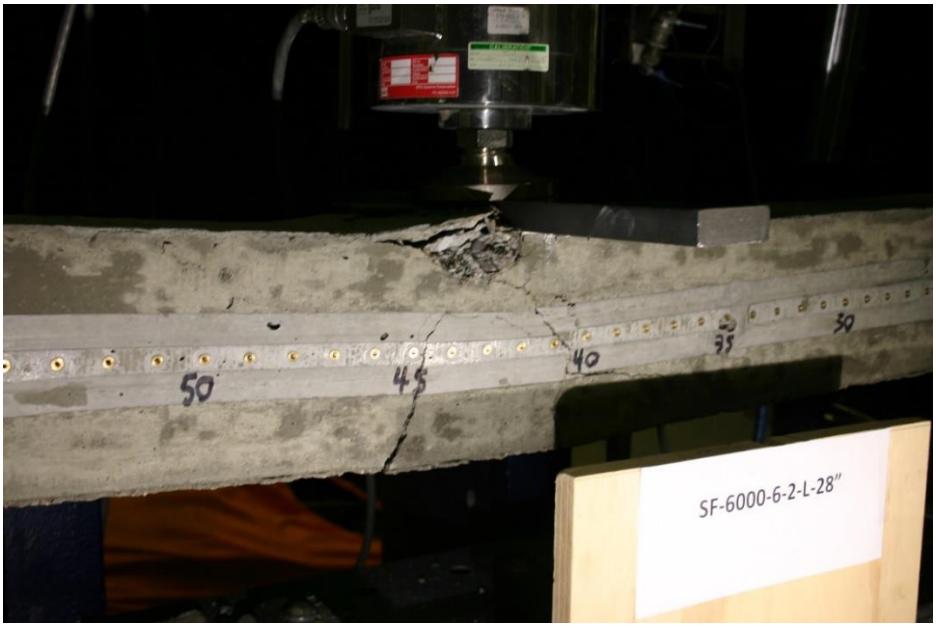


Figure 487 Picture of Failed Prism for SF-6000-6-2-L

Beam Identification	SF-6000-6-3-L
Wire Type:	SF
Embedment Length:	16.5 in
Release Strength:	6000 psi
Slump:	6 in

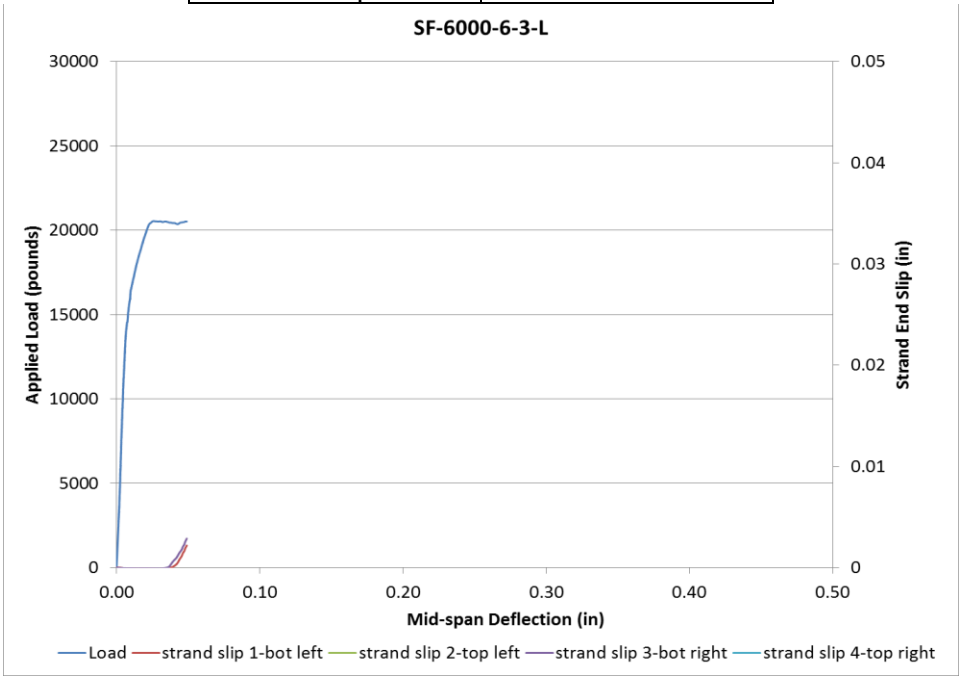


Figure 488 Load vs Deflection and Strand End Slip SF-6000-6-3-L



Figure 489 Picture of Failed Prism for SF-6000-6-3-L

Beam Identification	SF-6000-6-3-S
Wire Type:	SF
Embedment Length:	13 in
Release Strength:	6000 psi
Slump:	6 in



Figure 490 Picture of Failed Prism for SF-6000-6-3-S

Prisms made with wires, 4500 psi concrete release strength and 6 in. slump tested cyclically

Beam Identification	WA-4500-6-3-Cyclic Cracking
Wire Type:	WA
Embedment Length:	27 in
Release Strength:	4500 psi
Slump:	6 in

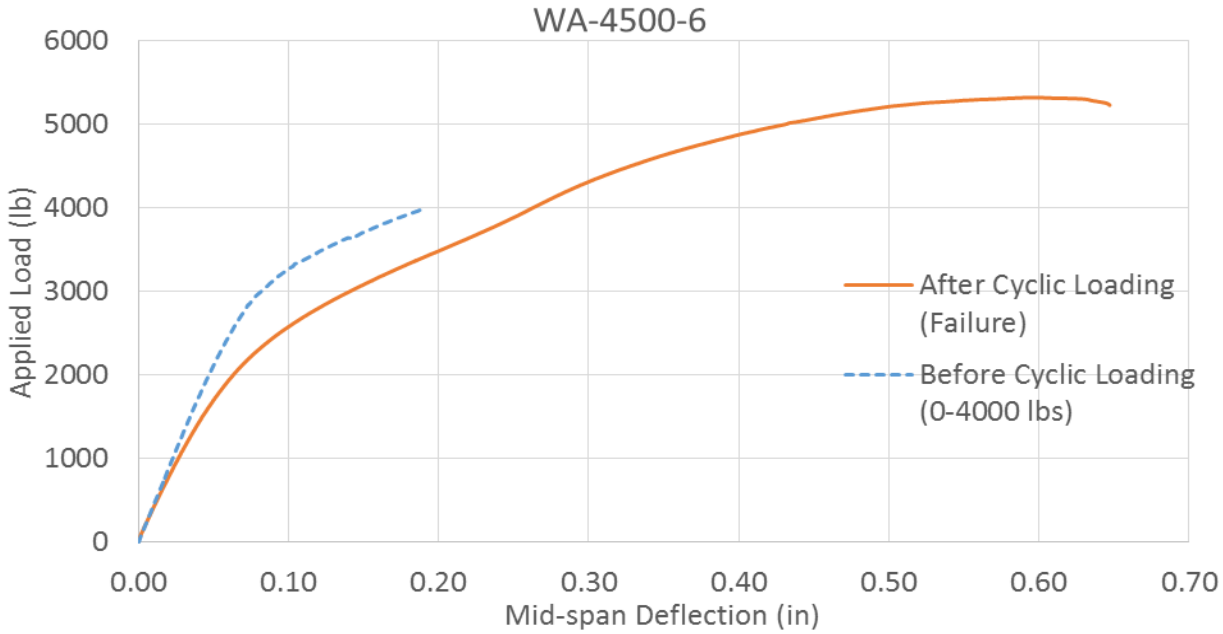


Figure 491 Load vs Deflection WA-4500-6

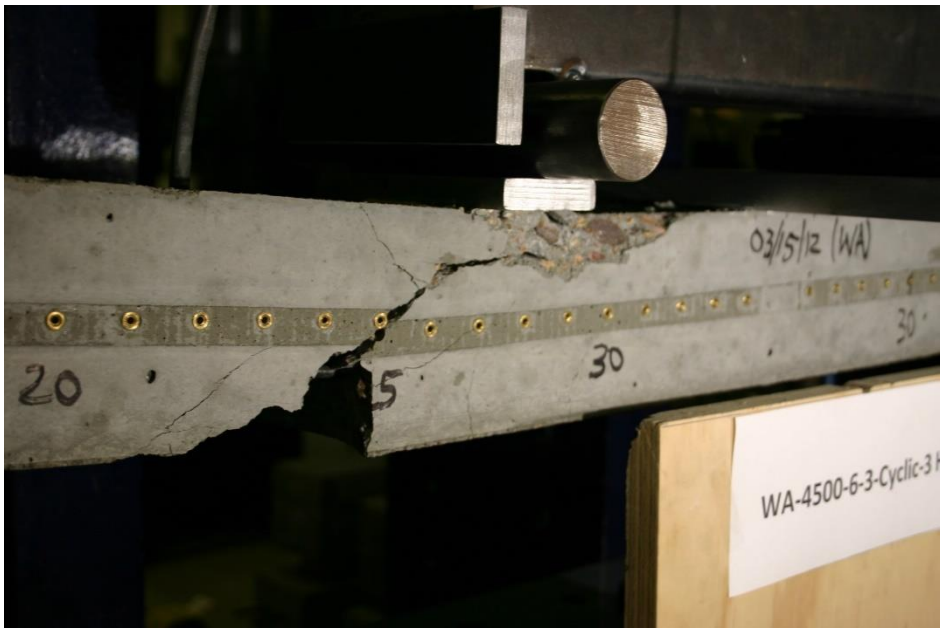


Figure 492 Picture of Failed Prism for WA-4500-6-3-Cyclic

Beam Identification	WB-4500-6-3-Cyclic Cracking
Wire Type:	WB
Embedment Length:	27 in
Release Strength:	4500 psi
Slump:	6 in

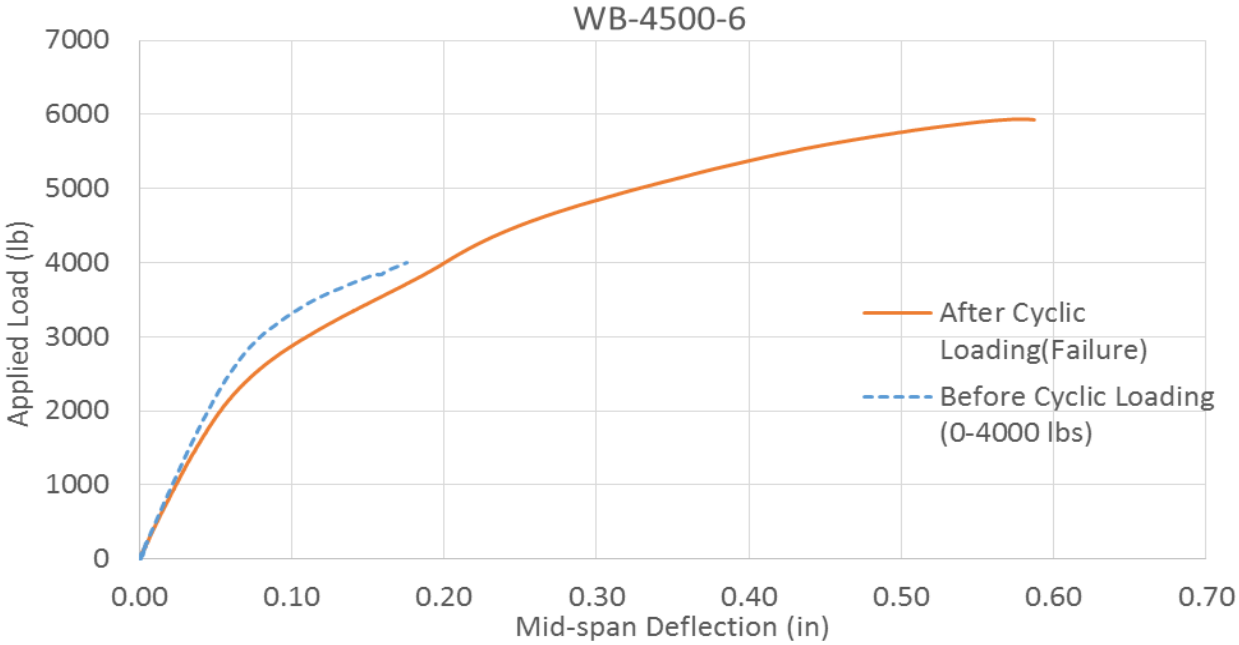


Figure 493 Load vs Deflection WB-4500-6

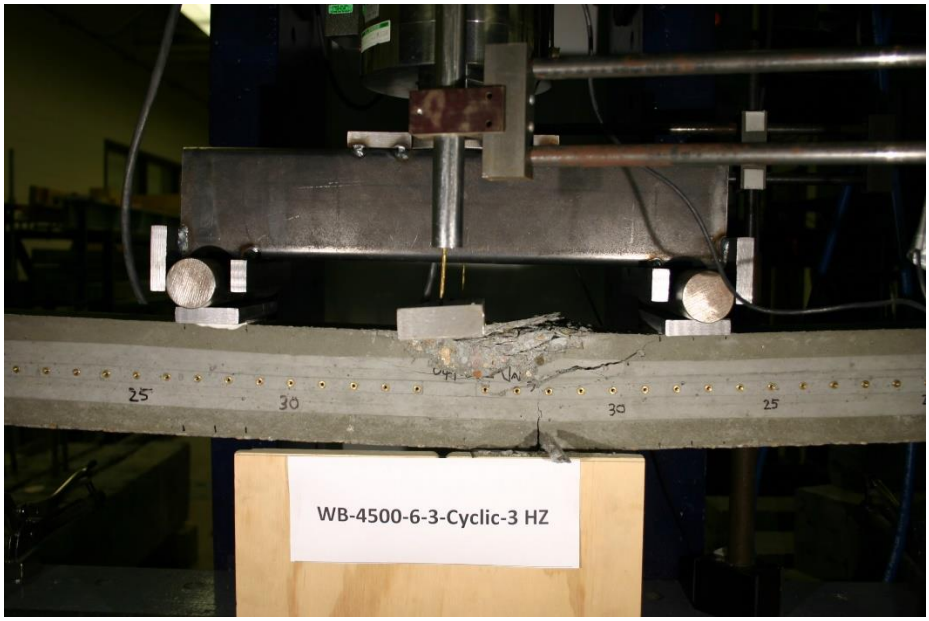


Figure 494 Picture of Failed Prism for WB-4500-6-3-Cyclic

Beam Identification	WC-4500-6-3-Cyclic Cracking
Wire Type:	WC
Embedment Length:	27 in
Release Strength:	4500 psi
Slump:	6 in

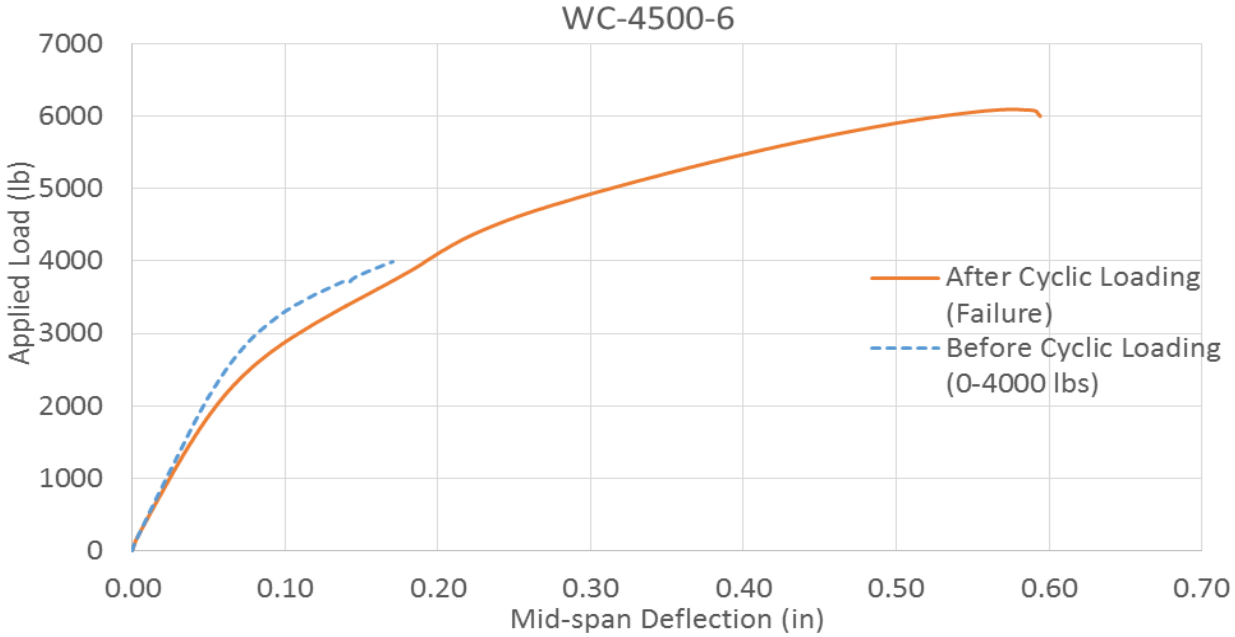


Figure 495 Load vs Deflection WC-4500-6

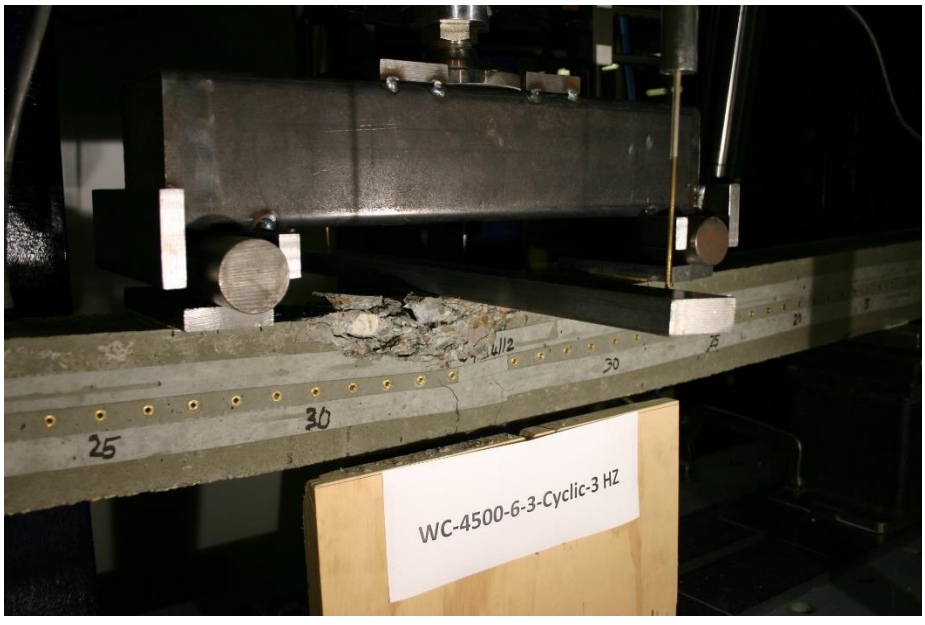


Figure 496 Picture of Failed Prism for WC-4500-6-3-Cyclic

Beam Identification	WD-4500-6-3-Cyclic Cracking
Wire Type:	WD
Embedment Length:	27 in
Release Strength:	4500 psi
Slump:	6 in

Failed under cyclic load



Figure 497 Picture of Failed Prism for WD-4500-6-3-Cyclic

Beam Identification	WE-4500-6-3-Cyclic Cracking
Wire Type:	WE
Embedment Length:	*
Release Strength:	4500 psi
Slump:	6 in

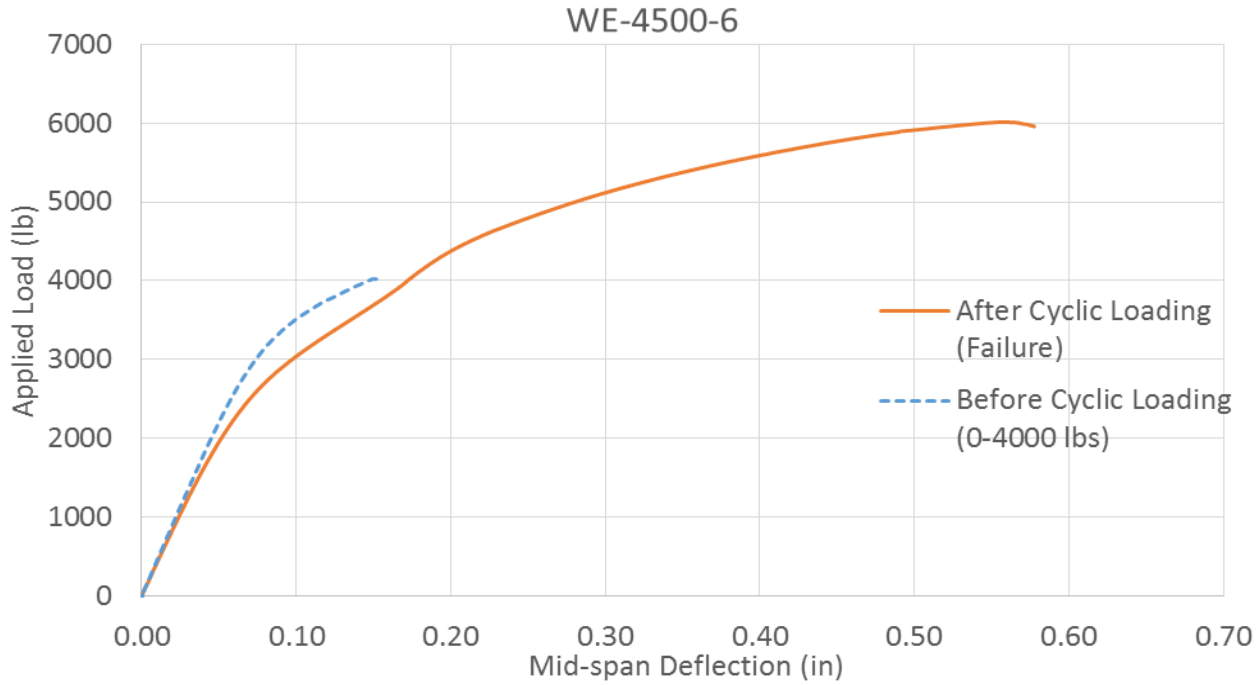


Figure 498 Load vs Deflection WE-4500-6



Figure 499 Picture of Failed Prism for WE-4500-6-3-Cyclic

Beam Identification	WF-4500-6-3-Cyclic Cracking
Wire Type:	WF
Embedment Length:	27
Release Strength:	4500 psi
Slump:	6 in

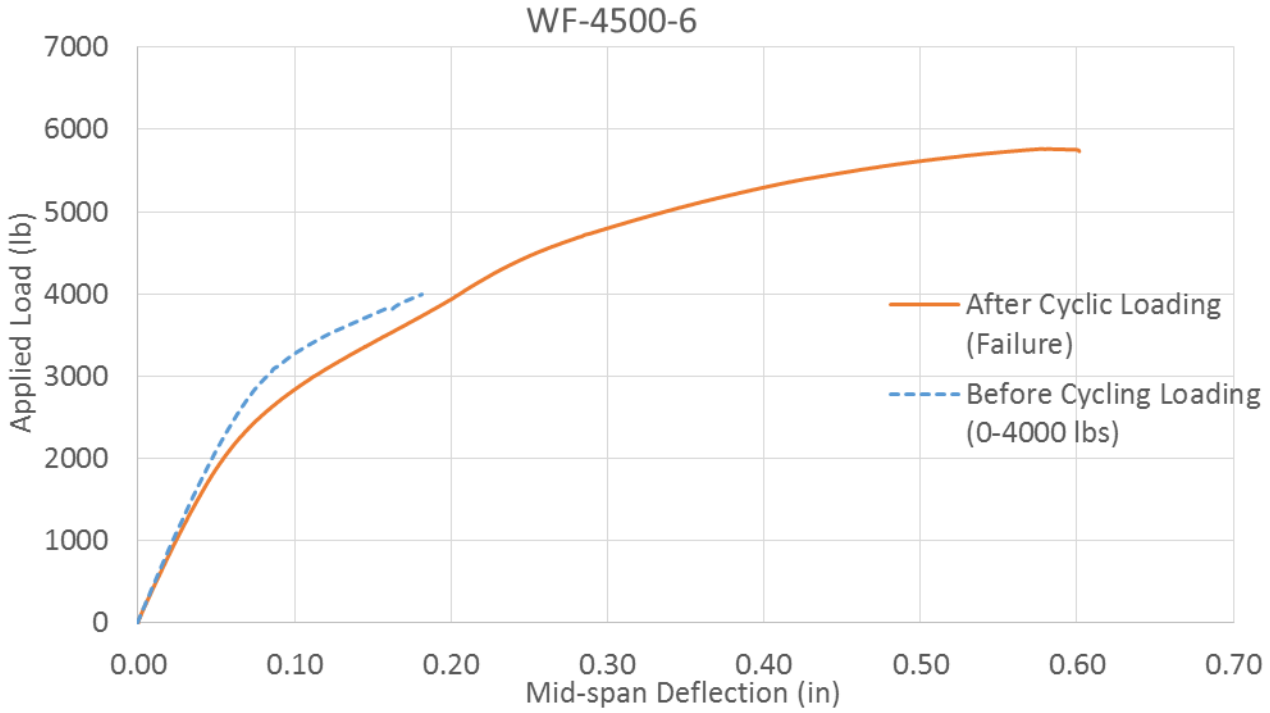


Figure 500 Load vs Deflection WF-4500-6

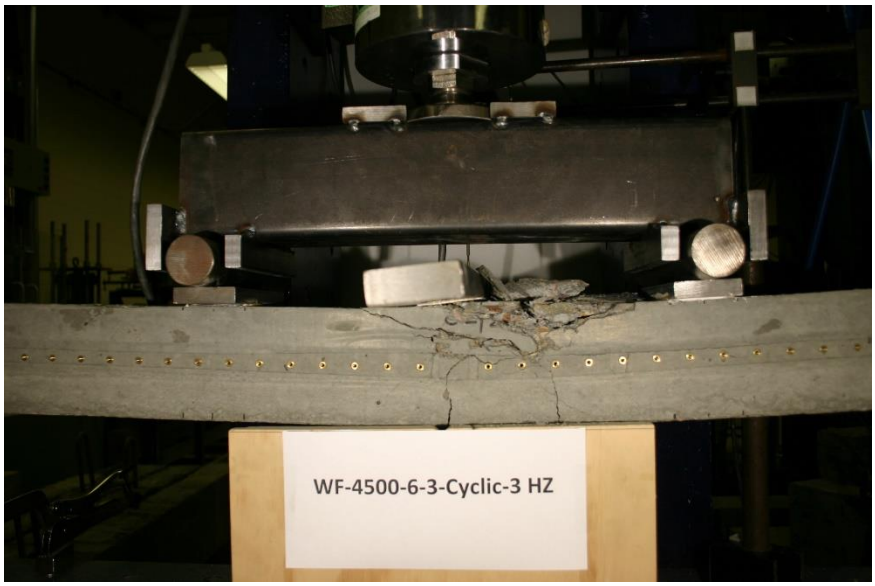


Figure 501 Picture of Failed Prism for WF-4500-6-3-Cyclic

Beam Identification	WG-4500-6-3-Cyclic Cracking
Wire Type:	WG
Embedment Length:	27
Release Strength:	4500 psi
Slump:	6 in

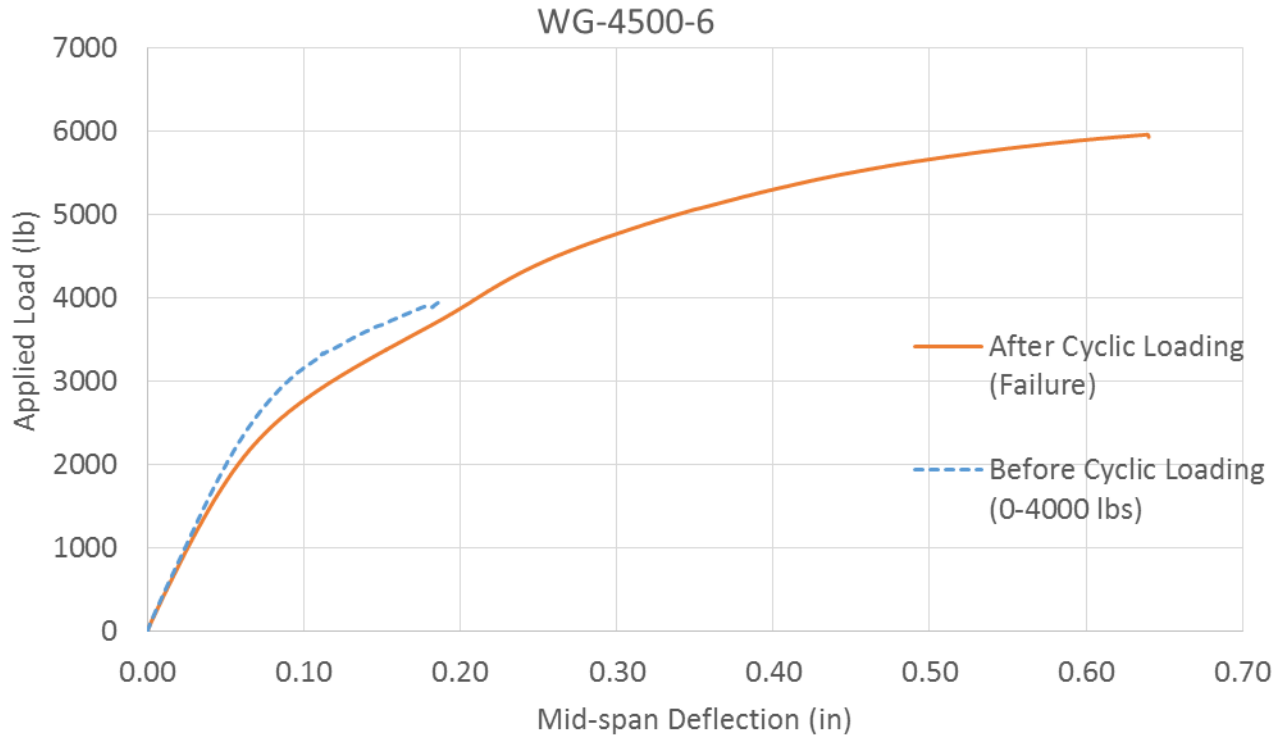


Figure 502 Load vs Deflection WG-4500-6



Figure 503 Picture of Failed Prism for WG-4500-6-3-Cyclic

Beam Identification	WH-4500-6-3-Cyclic Cracking
Wire Type:	WH
Embedment Length:	27 in
Release Strength:	4500 psi
Slump:	6 in

Failed under cyclic load

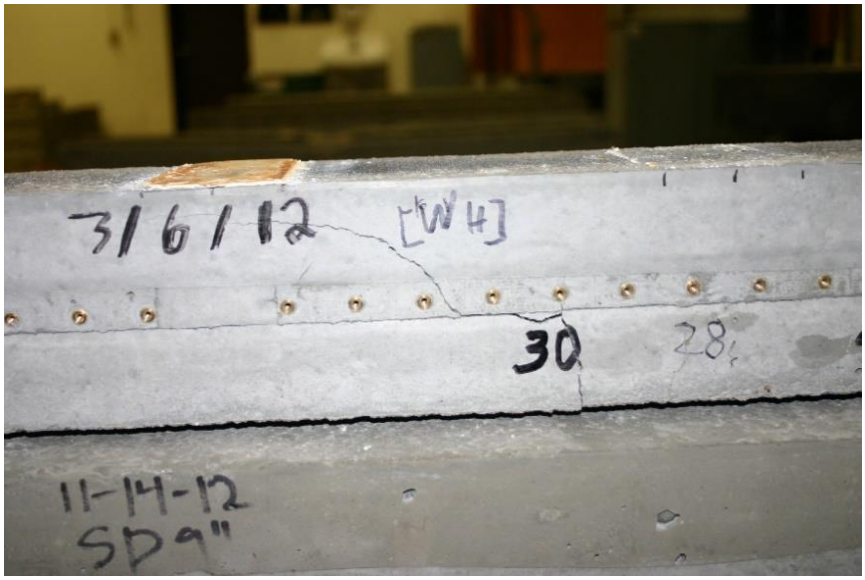


Figure 504 Picture of Failed Prism for WH-4500-6-3-Cyclic

Beam Identification	WI-4500-6-3-Cyclic Cracking
Wire Type:	WI
Embedment Length:	27 in
Release Strength:	4500 psi
Slump:	6 in

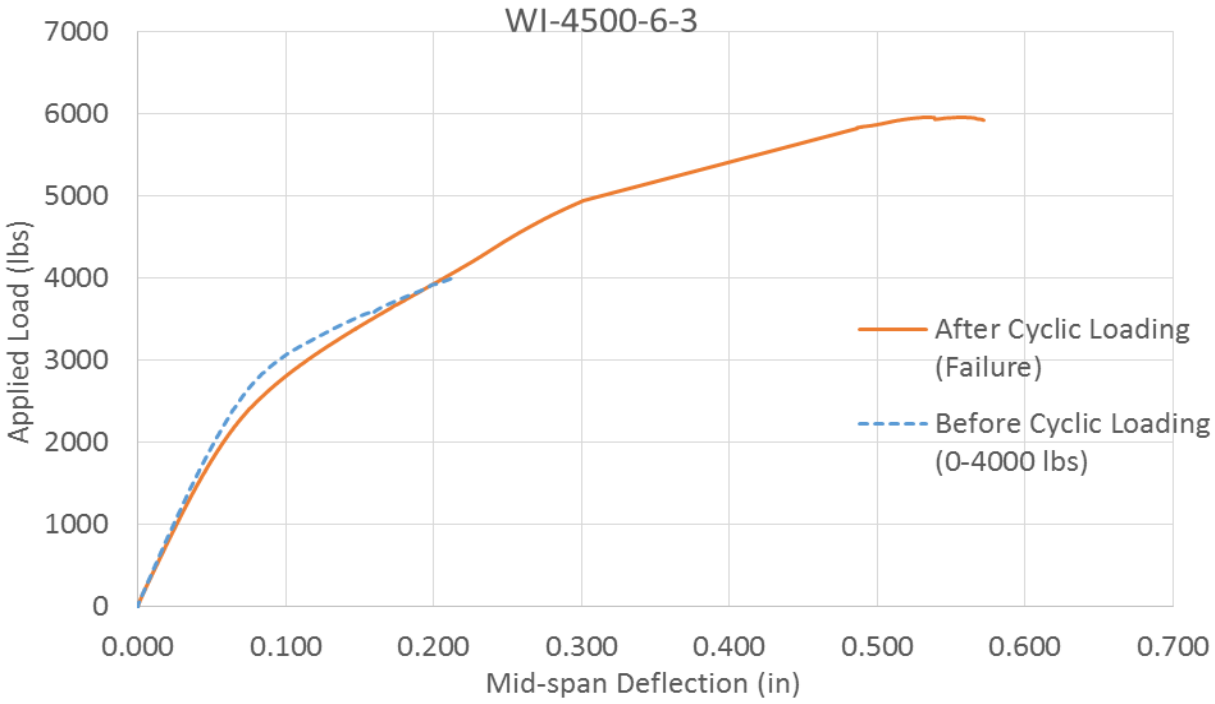


Figure 505 Load vs Deflection WI-4500-6



Figure 506 Picture of Failed Prism for WI-4500-6-3-Cyclic

Beam Identification	WJ-4500-6-3-Cyclic Cracking
Wire Type:	WJ
Embedment Length:	27 in
Release Strength:	4500 psi
Slump:	6 in

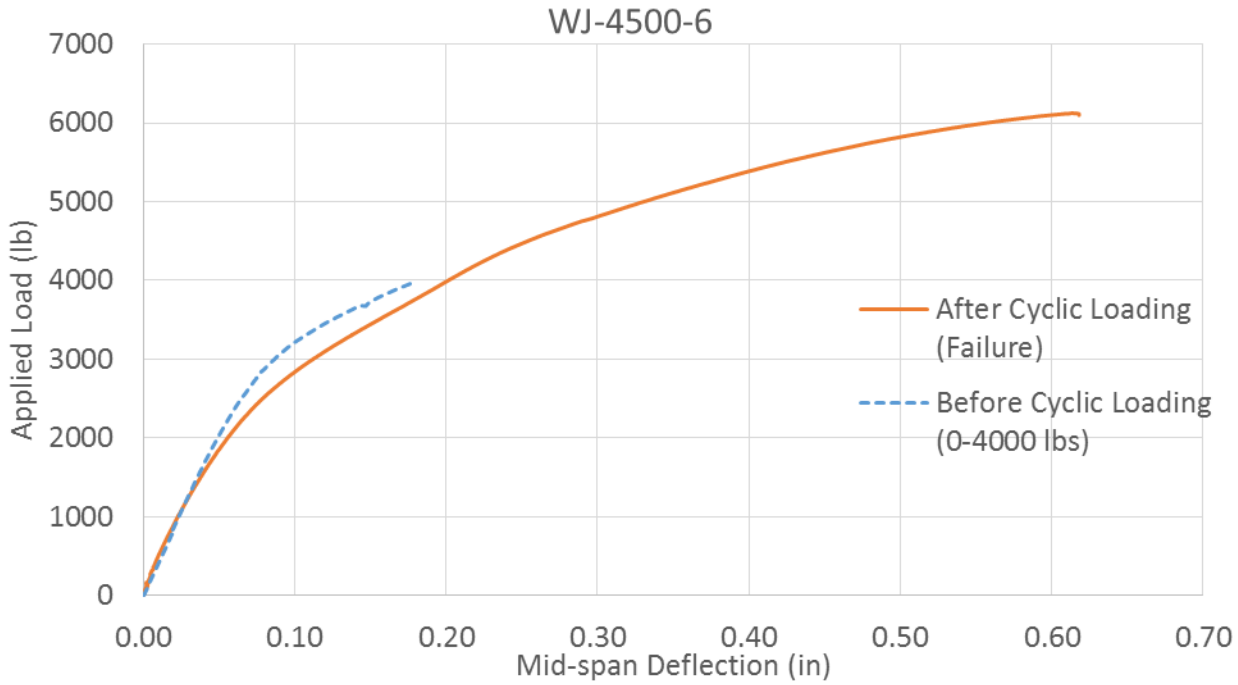


Figure 507 Load vs Deflection WJ-4500-6



Figure 508 Picture of Failed Prism for WJ-4500-6-3-Cyclic

Beam Identification	WK-4500-6-3-Cyclic Cracking
Wire Type:	WK
Embedment Length:	27 in
Release Strength:	4500 psi
Slump:	6 in

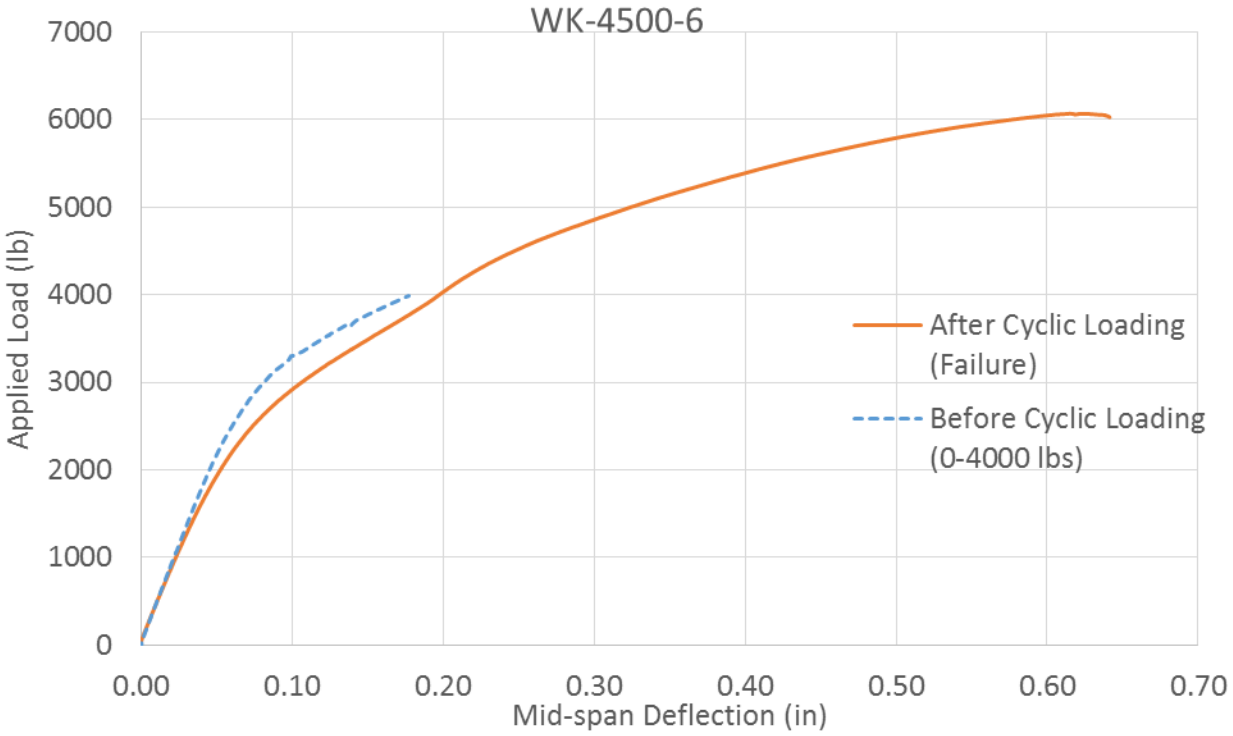


Figure 509 Load vs Deflection WK-4500-6

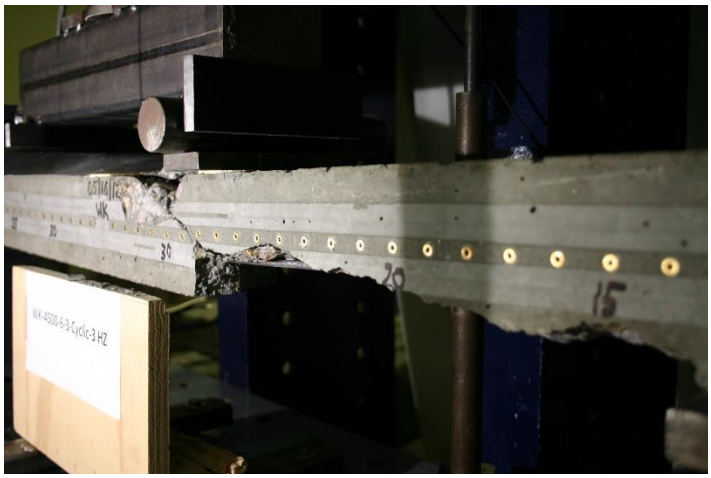


Figure 510 Picture of Failed Prism for WK-4500-6-3-Cyclic

Beam Identification	WL-4500-6-3-Cyclic Cracking
Wire Type:	WL
Embedment Length:	27 in
Release Strength:	4500 psi
Slump:	6 in

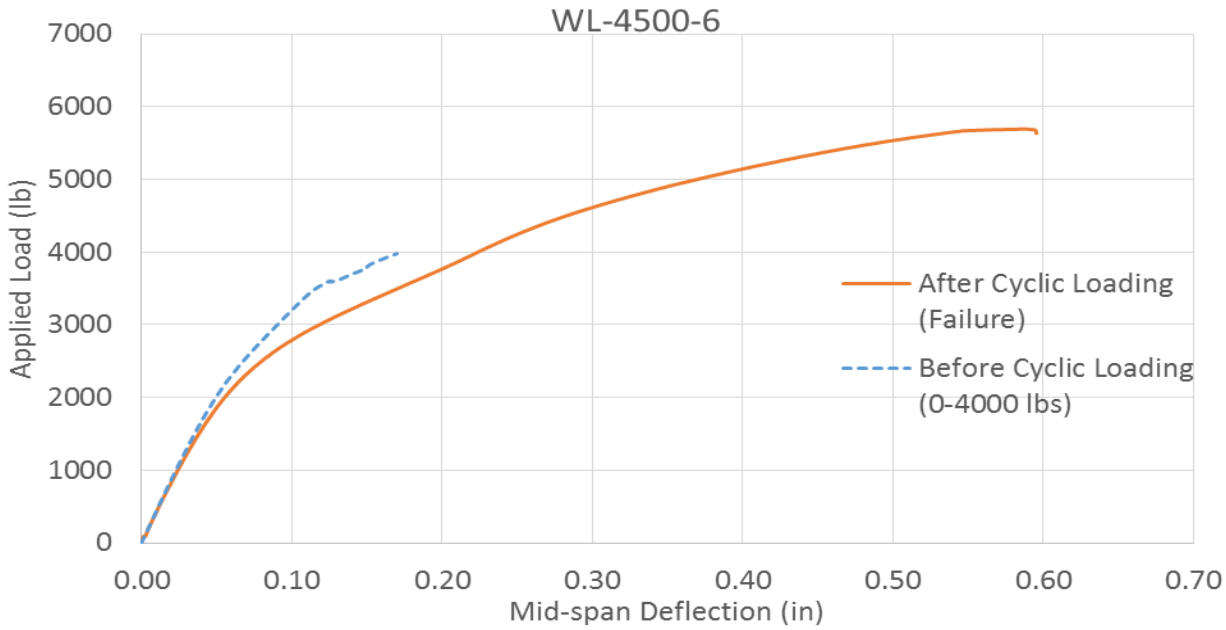


Figure 511 Load vs Deflection WL-4500-6

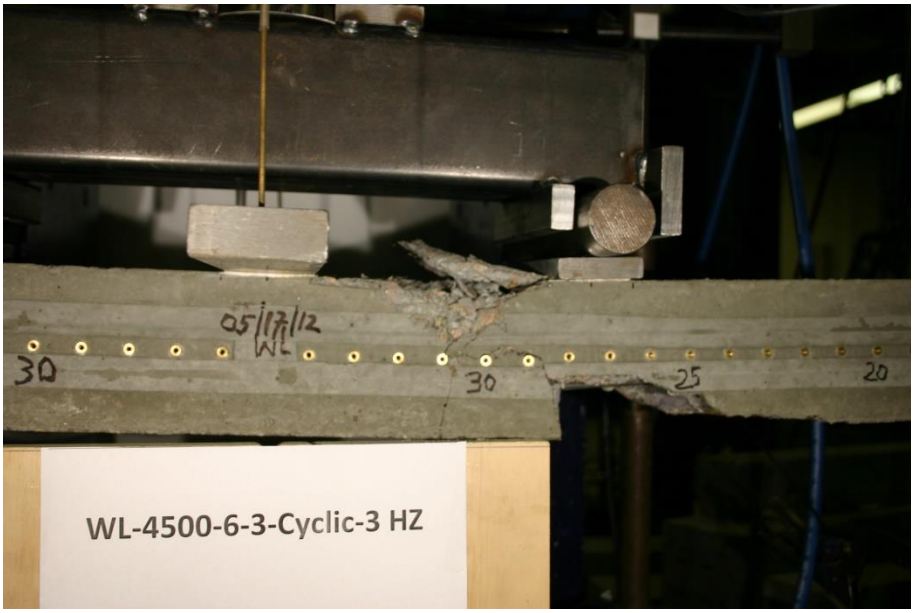


Figure 512 Picture of Failed Prism for WL-4500-6-3-Cyclic

Beam Identification	WM-4500-6-3-Cyclic Cracking
Wire Type:	WM
Embedment Length:	27 in
Release Strength:	4500 psi
Slump:	6 in

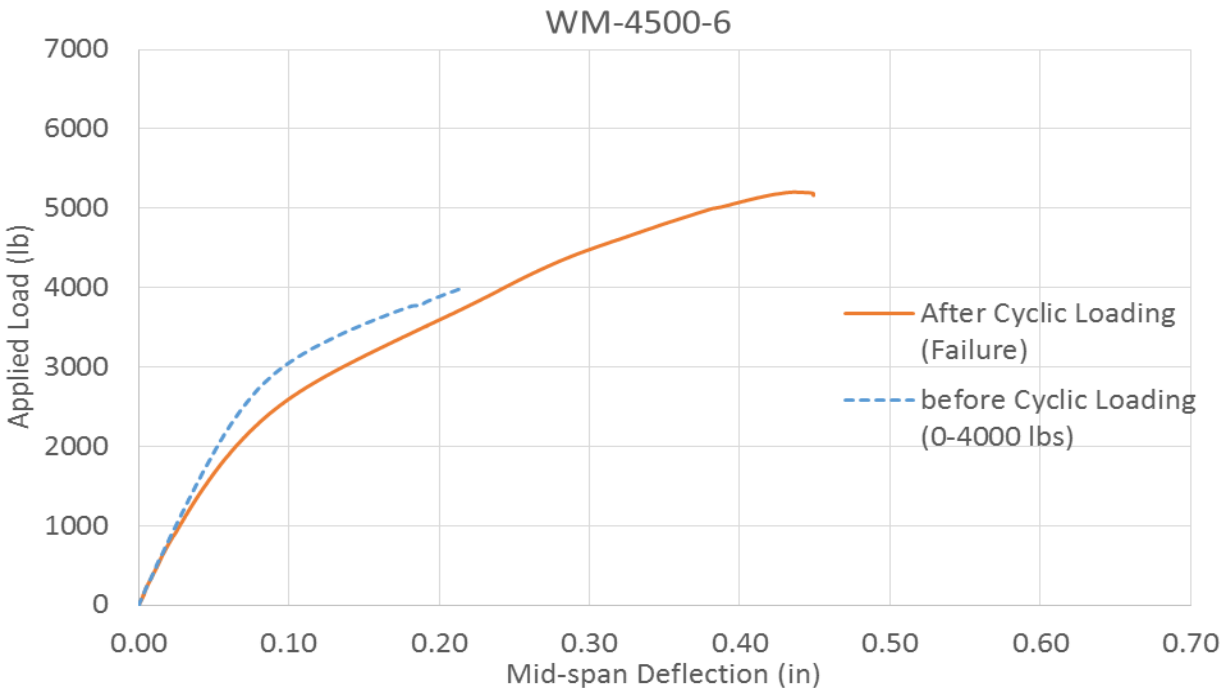


Figure 513 Load vs Deflection WM-4500-6



Figure 514 Picture of Failed Prism for WM-4500-6-3-Cyclic